Photoluminescence and Structural Evaluation of *O,O'* and *N,N'* bidentate ligands and its Re(I) Tricarbonyl Complexes

by

PHEELLO ISAAC NKOE

A thesis submitted to meet the requirements for the degree of

PHILOSOPHIAE DOCTOR

In the

DEPARTMENT OF CHEMISTRY
FACULTY OF NATURAL AND AGRICULTURAL SCIENCES

At the

UNIVERSITY OF THE FREE STATE

SUPERVISOR: DR. MARIETJIE SCHUTTE-SMITH
CO-SUPERVISOR: DR. ALICE BRINK

March 2021

ACKNOWLEDGEMENTS

First and foremost, I would like to thank God for giving me the strength and courage to complete this work. I am very blessed!

Prof André Roodt, it is a great honour to be known as one of your students. Thank you for giving me another opportunity to complete my PhD. I appreciate the opportunity.

Special thanks to Prof Deon Visser. Thank you for all your assistance, time and effort with the interpretations and understanding of the work. I appreciate your help a lot!

Dr Marietjie Schutte-Smith the best supervisor, I would like to gratefully thank you for your patience, understanding and your guidance. You are the best supervisor I could ask for. Thanks for not giving up on my throughout my studies!

Dr Alice Brink, thanks a lot for your encouragement and your support through tough times. I appreciate all the effort, time and support throughout my studies.

I would like to thank Prof R.E Kroon at the Department of Physics at the UFS for his effort and time spent on testing of the compounds.

A big thank you to the crystallographers for their time and help with the crystallographic part of this work.

Thanks to the Inorganic Chemistry group at the University of the Free State for being there for me when I needed you. Thanks you for sharing your knowledge and for your patience when having to review some of my chapters over and over again, without complains. All of you contributed to this study in some way and for that I thank you.

To my family, without your support, sacrifices, understanding, faith, love and continuous encouragement this would not be possible.

Contents

ABBREVIATIONS i

ABSTRACT iii

1 INTRODUCTION AND AIM 1

1.1 Applications of metals in medicine, Re(I) in particular 1

1.2 Aim of the study 5

2 LITERATURE STUDY OF RHENIUM CHEMISTRY AS APPLIED IN ANTI-CANCER AGENTS 8

2.1 Introduction 8

2.2 Background information of rhenium 9

2.3 Rhenium in nuclear medicine 10

2.3.1 Rhenium-188 11

2.3.2 Rhenium-186 12

2.4 The term radiopharmaceutical and its design 13

2.4.1 Important aspects influencing the design of radiopharmaceuticals 15

2.4.2 Choice of radionuclide and method of radiolabelling 15

2.5 *fac*-$[Re(CO)_3]^+$ in medicine 17

2.5.1 Introduction 17

2.5.2 *O,O'* Bidentate ligands 18

2.5.3 *N,N'* Bidentate ligands 24

2.6 Metal complexes in chemotherapy 29

2.6.1 Introduction to chemotherapy 29

2.6.2 Examples of rhenium(I) tricarbonyl complexes in chemotherapy 30

2.6.3 Metal complexes with *O,O'*- and *N,N'*- bidentate ligands in chemotherapy 33

2.7 The kinetics of *fac*-$[Re(CO)_3]^+$ type complexes 36

2.7.1 The water exchange of *fac*-$[M(CO)_3(H_2O)_3]^+$ 36

2.7.2 The substitution of water ligands in *fac*-$[M(CO)_3(H_2O)_3]^+$ 37

2.7.3 Substitution reactions in *fac*-$[Re(CO)_3(X)(L,L'\text{-Bid})]^n$ type complexes 39

2.8 Photoluminescence 47

2.8.1 Introduction 47

2.8.2 Fluorescence and phosphorescence 48

2.8.3 Photodynamic therapy 49

2.8.4 The application of β-hydroxyketone ligands in photoluminescence 51

2.8.5 Some examples of Re(I) tricarbonyl complexes with photoluminescent properties 56
2.9 Conclusion 63
3 SYNTHESIS OF LIGANDS AND RHENIUM(I) TRICARBONYL COMPLEXES 65
3.1 Introduction 65
3.2 Chemicals and apparatus used 69
3.3 Synthesis of *β*-hydroxyketone ligands 70
3.3.1 2,2,2-Trifluoro-1-(3-hydroxy-1H-inden-2-yl)ethan-1-one (TIFH) 70
3.3.2 2,2,2-Trifluoro-1-(3-hydroxy-1-methyl-1H-inden-2-yl)ethan-1-one (MeTIFH) 70
3.3.3 2,2,2-Trifluoro-1-(3-hydroxy-1-phenyl-1H-inden-2-yl)ethan-1-one (PhTIFH) 71
3.4 Synthesis of Rhenium compounds 72
3.4.1 Synthesis of *fac*-$[NEt_4]_2[Re(CO)_3(Br)_3]$ (ReAA) 72
3.4.2 *fac*-$[NEt_4][Re(CO)_3(Br)(TIF)]$ 72
3.4.3 *fac*-$[Re(CO)_3(MeOH)(TIF)]$ 73
3.4.4 *fac*-$[Re(CO)_3(TU)(TIF)]$ 73
3.4.5 *fac*-$[NEt_4][Re(CO)_3(NCS)(TIF)]$ 74
3.4.6 *fac*-$[Re(CO)_3(PCy_3)(TIF)]$ 74
3.4.7 *fac*-$[Re(CO)_3(H_2O)(TIF)]$ 75
3.4.8 *fac*-$[NEt_4][Re(CO)_3(Br)(MeTIF)]$ 75
3.4.9 *fac*-$[Re(CO)_3(MeOH)(MeTIF)]$ 76
3.4.10 *fac*-$[Re(CO)_3(TU)(MeTIF)]$ 76
3.4.11 *fac*-$[NEt_4][Re(CO)_3(NCS)(MeTIF)]$ 77
3.4.12 *fac*-$[Re(CO)_3(PCy_3)(MeTIF)]$ 77
3.4.13 *fac*-$[Re(CO)_3(H_2O)(MeTIF)]$ 78
3.4.14 *fac*-$[NEt_4][Re(CO)_3(Br)(PhTIF)]$ 78
3.4.15 *fac*-$[Re(CO)_3(H_2O)(PhTIF)]$ 79
3.4.16 *fac*-$[NEt_4][Re(CO)_3(Br)(3,5\text{-}DiMePh)]$ 79
3.4.17 *fac*-$[Re(CO)_3(H_2O)(3,5\text{-}DiMePh)]$ 80
3.4.18 *fac*-$[NEt_4][Re(CO)_3(Br)(MeDiPhPr)]$ 80
3.4.19 *fac*-$[Re(CO)_3(H_2O)(MeDiPhPr)]$ 80
3.4.20 *fac*-$[NEt_4][Re(CO)_3(Br)(BrDiPhPr)]$ 81
3.4.21 *fac*-$[Re(CO)_3(MeOH)(BrDiPhPr)]$ 81
3.4.22 *fac*-$[Re(CO)_3(TU)(BrDiPhPr)]$ 82
3.4.23 *fac*-$[NEt_4][Re(CO)_3(NCS)(BrDiPhPr)]$ 82
3.4.24 *fac*-$[Re(CO)_3(PPh_3)(BrDiPhPr)]$ 83

3.4.25 *fac*-[$Re(CO)_3(H_2O)(BrDiPhPr)$] 83
3.4.26 *fac*-[$Re(CO)_3(Br)(BAHY)$] 83
3.4.27 *fac*-[$Re(CO)_3(H_2O)(BAHY)][NO_3]$ 84
3.4.28 *fac*-[NEt_4][$Re(CO)_3(Br)(4\text{-}MeTPh)$] 84
3.4.29 *fac*-[$Re(CO)_3(MeOH)(4\text{-}MeTPh)$] 85
3.4.30 *fac*-[$Re(CO)_3(TU)(4\text{-}MeTPh)$] 85
3.4.31 *fac*-[NEt_4][$Re(CO)_3(NCS)(4\text{-}MeTPh)$] 85
3.4.32 *fac*-[$Re(CO)_3(PCy_3)(4\text{-}MeTPh)$] 86
3.4.33 *fac*-[$Re(CO)_3(H_2O)(4\text{-}MeTPh)$] 86
3.4.34 *fac*-[$Re(CO)_3(Br)(DiMePy)$] 87
3.4.35 *fac*-[$Re(CO)_3(MeOH)(DiMePy)][Br]$ 87
3.4.36 *fac*-[$Re(CO)_3(H_2O)(DiMePy)][NO_3]$ 87
3.4.37 *fac*-[$Re(CO)_3(Act)(DiMePy)][NO_3]$ 88
3.4.38 *fac*-[$Re(CO)_3(NO_3)(DiMePy)$] 88
3.4.39 *fac*-[$Re(CO)_3(TU)(DiMePy)][Br]$ 89
3.4.40 *fac*-[$Re(CO)_3(NCS)(DiMePy)$] 89
3.4.41 *fac*-[$Re(CO)_3(PCy_3)(DiMePy)][Br]$ 89
3.4.42 *fac*-[$Re(CO)_3(Br)(DiMeOPy)$] 90
3.4.43 *fac*-[$Re(CO)_3(MeOH)(DiMeOPy)][Br]$ 90
3.4.44 *fac*-[$Re(CO)_3(H_2O)(DiMeOPy)][NO_3]$ 91
3.4.45 *fac*-[$Re(CO)_3(Act)(DiMeOPy)][NO_3]$ 91
3.4.46 *fac*-[$Re(CO)_3(NO_3)(DiMeOPy)$] 91
3.4.47 *fac*-[$Re(CO)_3(TU)(DiMeOPy)][Br]$ 92
3.4.48 *fac*-[$Re(CO)_3(NCS)(DiMeOPy)$] 92
3.4.49 *fac*-[$Re(CO)_3(PCy_3)(DiMeOPy)][Br]$ 93
3.5 Discussion 93
4 X-RAY CRYSTALLOGRAPHIC STUDY OF A LIGAND AND RHENIUM(I) COMPOUNDS 99
4.1 Introduction 99
4.2 Experimental 100
4.3 Crystal structure of 4-MeTPh 103
4.4 Crystal structure of *fac*-[$Re(CO)_3(Br)(DiMePy)$] 107
4.5 Crystal structure of *fac*-[$Re(CO)_3(Act)(DiMePy)][NO_3]$ 112
4.6 Crystal structure of fac-[$Re(CO)_3(NO_3)(DiMePy)$] 118
4.7 Crystal structure of fac-[$Re(CO)_3Br(DiMeOPy)$] 122
4.8 Crystal structure of fac-[$Re(CO)_3(NO_3)(DiMeOPy)$] 128

4.9 Conclusion 135
5 Kinetic study of *fac*-[Re(CO)$_3$(MeOH)(*L,L'*-Bid)]^n type complexes 137
5.1 Introduction 137
5.2 Experimental procedures 140
5.2.1 General procedure 140
5.2.2 Treatment of data 140
5.3 Results and discussion 141
5.3.1 Reaction between *fac*-[Re(CO)$_3$(MeOH)(DiMePy)]$^+$ and entering ligands 144
5.3.2 Reaction between *fac*-[Re(CO)$_3$(MeOH)(DiMeOPy)]$^+$ and entering ligands 155
5.3.3 Reaction between *fac*-[Re(CO)$_3$(MeOH)(4-MeTPh)] and entering ligands 167
5.3.4 Reaction between *fac*-[Re(CO)$_3$(MeOH)(BrDiPhPr)] and entering ligands 178
5.3.5 Reaction between *fac*-[Re(CO)$_3$(MeOH)(TIF)] and entering ligands 190
5.3.6 Reaction between *fac*-[Re(CO)$_3$(MeOH)(MeTIF)] and entering ligands 202
5.4 Discussion 214
5.4.1 Rhenium(I) tricarbonyl complexes with *N,N'*-bidentate ligands 215
5.4.2 Rhenium(I) tricarbonyl complexes with *O,O'*-bidentate ligands 218
5.5 Conclusion 222
6 PHOTOLUMINESCENCE STUDY OF LIGANDS AND RHENIUM(I) TRICARBONYL COMPLEXES 225
6.1 Introduction 225
6.2 Experimental procedure 230
6.3 Solid state photoluminescence results and discussion 231
6.3.1 2,2,2-Trifluoro-1-(3-hydroxy-1H-inden-2-yl)ethan-1-one (TIFH) 232
6.3.2 *fac*-[Re(CO)$_3$(Br)(TIF)]$^-$ 233
6.3.3 *fac*-[Re(CO)$_3$(H$_2$O)(TIF)] 234
6.3.4 2,2,2-Trifluoro-1-(3-hydroxy-1-methyl-1H-inden-2-yl)ethan-1-one (MeTIFH) 235
6.3.5 *fac*-[Re(CO)$_3$(H$_2$O)(MeTIF)] 236
6.3.6 2,2,2-Trifluoro-1-(3-hydroxy-1-phenyl-1H-inden-2-yl)ethan-1-one (PhTIFH) 237
6.3.7 *fac*-[Re(CO)$_3$(Br)(PhTIF)]$^-$ 238
6.3.8 *fac*-[Re(CO)$_3$(H$_2$O)(PhTIF)] 239
6.3.9 *fac*-[Re(CO)$_3$(Br)(DiMePy)] 240
6.3.10 *fac*-[Re(CO)$_3$(H$_2$O)(DiMePy)]$^+$ 241
6.3.11 *fac*-[Re(CO)$_3$(MeOH)(DiMePy)]$^+$ 242
6.3.12 *fac*-[Re(CO)$_3$(TU)(DiMePy)]$^+$ 243
6.3.13 *fac*-[Re(CO)$_3$(NCS)(DiMePy)] 244

6.3.14 *fac*-[$Re(CO)_3(PCy_3)(DiMePy)]^+$ 245
6.3.15 *fac*-[$Re(CO)_3(Br)(DiMeOPy)$] 246
6.3.16 *fac*-[$Re(CO)_3(H_2O)(DiMeOPy)]^+$ 247
6.3.17 *fac*-[$Re(CO)_3(MeOH)(DiMeOPy)]^+$ 248
6.3.18 *fac*-[$Re(CO)_3(TU)(DiMeOPy)]^+$ 249
6.3.19 *fac*-[$Re(CO)_3(NCS)(DiMeOPy)$] 250
6.3.20 *fac*-[$Re(CO)_3(PCy_3)(DiMeOPy)]^+$ 251
6.3.21 *fac*-[$Re(CO)_3(Br)(4\text{-}MeTPh)]^-$ 252
6.3.22 *fac*-[$Re(CO)_3(H_2O)(4\text{-}MeTPh)$] 253
6.3.23 *fac*-[$Re(CO)_3(TU)(4\text{-}MeTPh)$] 254
6.3.24 *fac*-[$Re(CO)_3(NCS)(4\text{-}MeTPh)]^-$ 255
6.3.25 *fac*-[$Re(CO)_3(PCy_3)(4\text{-}MeTPh)$] 256
6.4 Solution state photoluminescence results and discussion 257
6.4.1 *fac*-[$Re(CO)_3(H_2O)(DiMePy)]^+$ 258
6.4.2 *fac*-[$Re(CO)_3(H_2O)(DiMeOPy)]^+$ 259
6.5 Conclusion 259
7 EVALUATION OF THIS STUDY 268
7.1 Results obtained 268
7.2 Future work 269
APPENDIX A 271
APPENDIX B 274
APPENDIX C 278
APPENDIX D 281
APPENDIX E 284
APPENDIX F 287
APPENDIX G 300
APPENDIX H 311
APPENDIX I 319
APPENDIX J 324
APPENDIX K 329
APPENDIX L 333
APPENDIX M 338

ABSTRACT

Despite the increase in research efforts, cancer remains amongst the leading causes of death worldwide. The survival rates vary with the type and stage of the tumour, including the sex, age and socioeconomic situation of each patient. Cancer treatment depends on the location, type and stage of the tumour, but the majority of patients undergo chemotherapy either as the main treatment or in combination with surgery or radiotherapy. Over 50 % of tumours are treated with platinum-based drugs alone or co-administered with other chemotherapeutic agents. In the past decades, many organometallic complexes have been confirmed as extremely promising anti-cancer drug candidates. Organometallic complexes provide structural and stereochemical variety, the possibility of rational ligand design and diverse mechanisms of action. The cytotoxicity of organometallic complexes and their potential are also reported in literature.

The potential cytotoxicity of rhenium(I) tricarbonyl complexes are evident from literature. The Rhenium(I) tricarbonyl core possesses intrinsic properties advantageous for the development of novel anti-cancer candidates. Rhenium(I) tricarbonyl complexes are good luminescence probes with long-lived emission states, high quantum yields, large Stokes shifts and emissions that can be tuned by varying the ligands.

One of the aims of this study was to investigate the ability of the synthesized *O,O'*-bidentate ligands and the chosen *N,N'*- and *O,O'*- bidentate ligands to coordinate to the *fac*-$[Re(CO)_3]^+$ core. The chosen ligands include: 2,2,2-trifluoro-1-(3-hydroxy-1H-inden-2-yl)ethan-1-one (TIFH), 2,2,2-trifluoro-1-(3-hydroxy-1-methyl-1H-inden-2-yl)ethan-1-one (MeTIFH), 2,2,2-trifluoro-1-(3-hydroxy-1-phenyl-1H-inden-2-yl)ethan-1-one (PhTIFH), 1,3-bis(3,5-dimethylphenyl)propane-1,3-dione (3,5-DiMePh), 2-methyl-1,3-diphenylpropane-1,3-dione (MeDiPhPr), 2-bromo-1,3-diphenylpropane-1,3-dione (BrDiPhPr), benzoic anhydride (BAHY), 1,3-bis(4-methoxyphenyl)propane-1,3-dione (4-MeTPh), 4,4'-dimethyl-2,2'-bipyridine (DiMePy) and 4,4'-dimethoxy-2,2'-bipyridine (DiMeOPy).

The ligands and complexes were characterized by IR, UV/Vis and NMR (^1H and ^{13}C). Crystal structures of the following were obtained: 4-MeTPh, *fac*-

[$Re(CO)_3(Br)(DiMePy)$], *fac*-[$Re(CO)_3(Act)(DiMePy)][NO_3]$, *fac*-[$Re(CO)_3(NO_3)(DiMePy)$], *fac*-[$Re(CO)_3(Br)(DiMeOPy)$], and *fac*-[$Re(CO)_3(NO_3)(DiMeOPy)$].

The lability and mechanism of substitution of the methanol ligands by simple monodentate nucleophiles were investigated by the methanol substitution reaction of *fac*-$[Re(CO)_3(MeOH)(DiMePy)]^+$, *fac*-$[Re(CO)_3(MeOH)(DiMeOPy)]^+$, *fac*-[$Re(CO)_3(MeOH)(4\text{-}MeTPh)$], *fac*-[$Re(CO)_3(MeOH)(BrDiPhPr)$], *fac*-[$Re(CO)_3(MeOH)(TIF)$] and *fac*-[$Re(CO)_3(MeOH)(MeTIF)$] with a variety of monodentate ligands (thiourea, sodium thiocyanate, triphenylphosphine or tricyclohexylphosphine and sodium bromide). A variation is seen in the $\Delta S^{\ddagger}$ values, ranging from small negative (-77 ± 4 $JK^{-1}mol^{-1}$) to small positive (94 ± 8 $JK^{-1}mol^{-1}$), pointing towards an interchange associative to an interchange dissociative type of activation. A large difference is mostly seen in the two $\Delta S^{\ddagger}$ values, calculated from the Eyring equation and the global fit, emphasizing the large errors in the $\Delta S^{\ddagger}$ values, highlighting the need for high pressure studies to unambiguously determine the mechanism of the reaction.

The photoluminescent properties of three ligand systems (TIFH, MeTIFH and PhTIFH) and twenty two Re(I) complexes were determined. The excitation wavelength of the synthesized bidentate ligands range from 534 nm to 650 nm and the emission wavelength range from 595 nm to 740 nm. The excitation wavelength of the Re(I) tricarbonyl complexes range from 285 nm to 705 nm and the emission wavelengths range from 450 nm to 740 nm. The Re(I) tricarbonyl complexes with bomido ligands in the sixth position yield higher quantum yields compared to the other Re(I) tricarbonyl complexes. The photoluminescent behaviour of *fac*-$[Re(CO)_3(H_2O)(DiMePy)]^+$ and *fac*-$[Re(CO)_3(H_2O)(DiMeOPy)]^+$ were further investigated in solution state. Both complexes were excited at 285 nm and gave rise to a maximum emission peak at 610 nm for *fac*-$[Re(CO)_3(H_2O)(DiMePy)]^+$ and 625 nm for *fac*-$[Re(CO)_3(H_2O)(DiMeOPy)]^+$. The solution state results (when compared to the solid state results), is red-shifted for both the aqua species; and the longer wavelength is potentially more appropriate for model PDT agents than the solid state results. The ligands and complexes investigated in this study gave good results with maximum excitation and emission wavelengths that are in the recommended range

of 534 nm to 705 nm and 595 nm to 740 nm respectively and can potentially be used as PDT agents, which should definitely be investigated further.

1 INTRODUCTION AND AIM

1.1 Applications of metals in medicine, Re(I) in particular

According to a new study on the analysis of cancer, where 32 cancer groups in 195 countries were investigated, cancer is the second leading cause of death after cardiovascular diseases with 8.7 million deaths globally.[1] In 2015, there were 114 091 new cancer cases and 58 237 deaths in total in South Africa. In 2019, cervical, lung and esophageal cancer were the three deadliest cancers in South Africa accounting for more than 1 900 deaths. [2]

Some of the cancer treatment methods used today are photodynamic therapy, radiotherapy, chemotherapy and surgery (which can be used on its own or in conjunction with one another), while the imaging methods include Scintigraphy, Positron Emission Tomography (PET) and Single Photon Emission Computed Tomography (SPECT).

Radiopharmaceuticals play a very important role in the field of medicine and is an essential component of the nuclear medicine practice.[3] Radiopharmaceuticals are drugs that contain a radioactive component for the treatment or diagnosis of diseases. The radioactive component acts as a tracking device or it can be used to destroy diseased cells in the body and exploit the pharmacological properties of radiopharmaceuticals and nuclear properties of the radionuclide. Now in routine, radiopharmaceuticals are used in clinical nuclear medicine for disease diagnosis in a variety of imaging protocols and treatments.[4] A variety of radiopharmaceuticals have

[1] Siegel, R.L., Miller, K.D., Jemal, A. *CA. Cancer J. Clin*. **70** (2020) 7-30.
[2] Alaouna, M., Hull, R., Penny, C., Dlamini, Z. *Clin. Exp. Gastroenterol.* **12** (2019) 157-177.
[3] Malvi,R., Bajpai., Jain. *Int.J Pharma & Bio Archi*. **3**(3) (2012) 487-492.
[4] Volkert, W.A., Hoffman, T.J. *Chem.Rev*. **99** (1999) 2269-2292.

been developed with different targeting mechanisms, routes and forms of administration.[5,6]

Photodynamic therapy (PDT) is a clinically approved, minimally invasive therapeutic procedure that can apply selective cytotoxic activity toward malignant cells. The procedure involves administration of a photosensitizing agent, followed by irradiation at a certain wavelength that corresponds to an absorbance band of the sensitizer. A series of events lead to direct tumour cell death, damage to the microvasculature, and induction of a local inflammatory reaction in the presence of oxygen. Clinical studies show that in particular early stage tumours, PDT can be curative.[7,8,9] It can prolong survival in patients with inoperable cancers and significantly improve quality of life. Minimal normal tissue toxicity, negligible systemic effects, greatly reduced long-term morbidity, lack of intrinsic or acquired resistance mechanisms, and excellent cosmetic as well as organ function-sparing effects of this treatment method makes it a valuable therapeutic option for combination treatments. PDT has the potential to be integrated into the mainstream of cancer treatment with a number of recent technological improvements.[10,11,12,13,14]

The fact that metal compounds are vital in medicine is undisputed, as can be judged by the use of compounds of bismuth (anti-ulcer), gold (anti-arthritic), antimony (anti-protozoal), silver (anti-microbial), iron (anti-malaria) and platinum (anti-cancer) in the treatment of different diseases.[15,16,17,18] Several compounds have received clinical

[5] Debnath, S., Babu, M.N., Kumar, G.V. *Pharma Times*. **48** (2016) 15-18.
[6] Prakash, D. Introduction to Nuclear Medicine. India Springer. (2014) 1-8.
[7] Agostinis, P., Berg, K., Cengel, K.A., Foster, T.H., Girotti, A.W., Gollnick, S.O., Hahn, S.M., Hamblin, M.R., Juzeniene, A., kessel, D., Korbelik, M., Moan, J., Mroz, P., Nowis, D., Piette, J., Wilson, B.C., Golab, J. *CA. Cancer J. Clin*. **61**(4) 250-281.
[8] Alsaab, H.O., Alghamdi, M.S., Alotaibi, A.S., Alzhrani, R.A., Alwuthaynani, F., Althobaiti, Y.S., Almaki, A.H., Sau, S., Iyer, A.K. *Cancer*. **12** (2020) 2793-2819.
[9] Yan, K., Zhang, Y., Mu, C., Xu, Q., Jing, X., Wang, D., Dang, D., Meng, L., Ma, J. *Theranostics*. **10**(16) (2020) 7287-7318.
[10] Agostinis, P., Berg, K., Cengel, K.A., Foster, T.H., Girotti, A.W., Gollnick, S.O., Hahn, S.M., Hamblin, M.R., Juzeniene, A., Kessel, D., Korbelik, M., Moan, J., Mroz, P., Nowis, D., Jacques, P.,Wilson, B.C., Golab, J. *CA Cancer. J. Clin.* **61** (2011) 250-281.
[11] Santos, A.F., de Almeida, D.R.Q., Terra, L.F., Baptista, M.S., Labriola, L. *J. Cancer Metastasis Treat.* **2** (2019) 25-45.
[12] Montaseri, H., Kruger, C.A., Abrahamse, H. *Int. J. Mol. Sci*. **21** (2020) 3358-3382.
[13] Rosenberg, S.A. *Nat. Rev. Clin. Oncol*. **11**(11) (2014) 630-632.
[14] De Freitas, L.M., Serafim, R.B., de Sousa, J.F., Moreira, T.F., Santos, C.T., Baviera, A.M., Valente, V., Soares, C.P. *BMC. Cancer*. **17** (2017) 123-135.
[15] Desoize, D. *Anticancer Res.* **24** (2004) 1529-1544.
[16] Kopf, P.-M., *Eur. J. Clin. Pharmacol*. **47** (1994) 1-16.
[17] Kasemodel, K., Roberts, K. *Proc. Okla. Acad. Sci*. **99** (2019) 106-113.
[18] Allardyce, C.S., Dyson, P.J. *Dalton Trans.* **45** (2016) 3201-3210.

approval and tetrapyrrole structures such as chlorins, porphyrins, phthalocyanines and bacteriochlorins with appropriate functionalization have been widely investigated in PDT.[19,20,21] Other molecular structures including the synthetic dyes classes like BODIPY (boron-dipyrromethene), phenothiazinium, squaraine, transition metal complexes, and natural products such as curcumin, hypericin and riboflavin have been investigated. [22,23,24] Targeted PDT uses photosensitizers conjugated to antibodies, peptides, proteins and other ligands with specific cellular receptors.[25]

The use of chemicals in order to inhibit malignant cell growth or to destroy the infectious agents of a disease such as micro-organisms without affecting the host cells is called chemotherapy.[26,27,28] The treatment is divided into two categories namely anti-cancer and antimicrobial chemotherapy. The drugs belonging to these categories, are different from other drugs as they are generally intended to inhibit the growth of malignant cells or kill the target organism and have no effect on the host cell.[29] Recently, efforts in this area have expanded to compounds of other third row transition metals, such as rhenium, osmium, and iridium.[30,31,32,33] Rhenium complexes, in particular, are rapidly gaining interest as anti-cancer agents because of its high stability, structural diversity, and rich spectroscopic properties.[34] Rhenium(I) tricarbonyl complexes reported by Knopf *et al.*[35] and Kozlov *et al*.[36] 2,2′-bipyridine,

[19] Mandal. A.K., Sahin, T., Liu, M., Lindsey, J.S., Bocian, D.F., Holten, D. *New J. Chem.* **40** (2016) 9684-9657.
[20] Singh, S., Aggarwal, A., Thompson, S., Tome, J. P.C., Zhu, X., Samaroo, D., Vinodu, M., Gao, R., Drain, C.M. *Bioconjug. Chem*. **21**(11) (2010) 2136-2146.
[21] Laville, I., Figueredo, T., Lock, B., Pigaglio, S., Maillard, P., Grierson, D.S., Croisy, A., Blais, J. *Bioorg Med Chem*. **11** (2003) 1643-1652.
[22] Wang, J., Boens, N., Jiao, L., Hao, E. *Org. Biomol. Chem.* **18** (2020) 4135-4156.
[23] Ulrich, G., Ziessel, R., Harriman, A. *Angew. Chem. Int. Ed*. **47** (2008) 1184-1201.
[24] Squeo, B.M., Gregoriou, V.G., Avgeropoulos, A., Baysec, S., Allard, S., Scherf, U., Chochos, C.L. *Prog. Polym. .Sci.* **71** (2017) 26-52.
[25] Abrahamse, H., Hamblin, M.R. *Biochem J.* **472**(4) 347-364.
[26] Knoepfler, P.S. *Stem cells*. **27**(5) (2009) 1050-1056.
[27] Alam, A., Farooq, U., Singh, R., Dubey, V.P., Kumar, S., Kumari, R., Naik, K.K., Dhar, K.L. *J. Tocxicol.* **2**(5) (2018) 1-6.
[28] Taniguchi, M., Lindsey, S. Chem. Rev. **2** (2017) 344-535.
[29] Drusano, G.L. Nat. Rev. *Microbiol*. **2**(4) (2004) 289-300.
[30] Gasser, G., Ott, I., Metzler-Nolte, N. *J. Med. Chem*. **54** (2011) 3-25.
[31] Zhang, P., Huang, H. *Dalton Trans*. **47** (2018) 14841-14854.
[32] Liu, Z., Sadler, P.J. *Acc. Chem. Res*. **47** (2014) 1174-1185.
[33] Konkankit, C.C., Marker, S.C., Knopf, K.M., Wilson, J.J. *Dalton Trans.**47*** (2018) 9934-9974.
[34] Lee, L.C.-C., Leung, K.-K., Lo, K.K.-W. *Dalton Trans*. **46** (2017) 16357-16380.
[35] Knopf, K.M., Murphy, B.L., MacMmillan, S.N., Baskin, J.M., Barr, M.P., Boros, E., Wilson, J.J. *J. Am. Chem. Soc*. **139**(40) (2017) 14302-14314.
[36] Kozlov, V.A., Churusova, S.G., Rybalkina, E.Y., Peregudov, A.S., Denisov, G.L., Aleksanyan, D.V. *INEOS OPEN*. **2**(5) (2019) 172-177.

4,4′-dimethyl-2,2′-bipyridine, 4,4′-dimethoxy-2,2′-bipyridine, dimethyl 2,2′-bipyridine-4,4′-dicarboxylate, 1,10-phenanthroline, 2,9-dimethyl-1,10-phenanthroline, or 4,7-diphenyl-1,10-phenanthroline, phenanthroline, diselenoether and β-carboline ligand were used as ligands where exhibit promising cytotoxic results.

Nuclear medicine imaging provides useful information that often cannot be found by using other imaging procedures and offers the potential to identify the disease in the early stages.[6,7] Scintigraphy provides scans of the structures inside the body and the areas where there are cancer cells inside the body. Scintigraphy is used to stage, diagnose and monitor diseases.[37] Single-photon emission computed tomography (SPECT) is where photons emitted from the radiotracer in the body are detected by the system as independent events, while two photons from the annihilation of positrons originally emitted from the radiotracer are the basis of image formations as these are detected by the system in coincidence. Positron emission tomography (PET) is the most advanced diagnostic imaging technology along with magnetic resonance imaging (MRI) and compute tomography (CT). PET techniques have a much higher sensitivity and resolution due to the autocollimation of 2 annihilation gamma photons. [38]

It is important for all researchers to investigate the kinetic behaviour of all potential drugs, in particular for characteristics and detail related to the synthetic procedure, the *in vivo* behaviour and stability, uptake and excretion from the body and the pharmacokinetic properties. It has been proven that slight changes in the bidentate ligands coordinated to the Re(I) core can have a considerable influence on the intimate mechanism of the reactions.[38] This is of significant interest to us, since this means that the behaviour of the drug can be modified and manipulated by changing and altering the bidentate ligand and the peripheral groups on the ligands.

Technetium and rhenium complexes, particularly the tricarbonyl synthon, are of interest to researchers because of its favourable properties:[39,40,41]

[37] Khalid, G., Yousef, M., Alfadi, M., Ali, W.M., Abdelazez, I., Wilson, A.B., Hassan, W. *Int. j. inf*. **4** (2017) 4716-4721.
[38] Piwowarska, H.-B., Spinska, A., Lwanowski, J., Tyczynska, A., Birkenfeld, B. *Pomeranian J Life Sci*. 65(3) (2019) 45-53.
[39] Payolla, F.B., Massabni, A.C., Orvig, C. *Ecletica Quimica*. **44** (2019) 11-19.
[40] Owen, J.O., Thomas, E., Menon, J., Gray, M., Skaripa-Koukelli, I., Gill, M.R., Wallington, S., Miller, R., Vallis, K., Carlisle, R. *J. Control. Release*. **319** (2020) 222-223.

- They displays a variety of coordination compounds in all oxidation states from -1 to +7.
- Technetium and rhenium based radiopharmaceuticals are typically in the +5 and +1 oxidation states due to considerable stability, and have shown reasonable biodistribution (pharmacokinetics) in medical imaging and therapeutic nuclear medicine compared to other oxidation states.
- Contains *fac*-$[M(CO)_3]^+$ which is small and compact, that allows for the labelling of biomolecules with a small molecular weight.
- *fac*-$[M(CO)_3]^+$ exhibits an octahedral low spin d^6 configuration which is kinetically inert leaving the other three *facial* sites open for substitution with a variety of functional groups including thiols, imines, phosphines and thioethers.

1.2 Aim of the study

In this study, the main objective was to synthesize rhenium(I) tricarbonyl complexes as model systems that can potentially be used as PDT agents and/or chemotherapeutic drugs; to fully characterize it in order to completely understand the chemical complexity of the complexes. The results will be compared to previous studies where *N,N'*- and *O,O'*-bidentate ligand systems were used to observe the difference in coordination behaviour, kinetic stability and reactivity. The photoluminescence and cytotoxicity will also be evaluated. The stepwise goals of this study are summarized below:

1. Synthesis of β-hydroxyketone bidentate ligand systems:
    - 2,2,2-Trifluoro-1-(3-hydroxy-1H-inden-2-yl)ethan-1-one (TIFH)
    - 2,2,2-Trifluoro-1-(3-hydroxy-1-methyl-1H-inden-2-yl)ethan-1-one (MeTIFH)
    - 2,2,2-Trifluoro-1-(3-hydroxy-1-phenyl-1H-inden-2-yl)ethan-1-one (PhTIFH)

[41] Orteca, G., Sinnes, J.P., Rubagotti, S., Lori, M., Capponi, P.C., Piel, M., Rosch, F., Ferrari, E., Asti, M. *J. Inorg. Biochem.* **204** (2020) 11034-11054.

These β-hydroxyketone bidentate ligand systems were chosen due to their potential photoluminescence properties and the possibility that they can be used as photodynamic and chemotherapeutic agents.

2. Synthesis of rhenium(I) tricarbonyl complexes of the type *fac*-$[Re(CO)_3(X)(O,O')]^n$ (n = 0, -1) and *fac*-$[Re(CO)_3(X)(N,N')]^n$ (n = +1, 0) with *O,O'*:

    - 1,3-Bis(3,5-dimethylphenyl)propane-1,3-dione (3,5-DiMePh)
    - 2-Methyl-1,3-diphenylpropane-1,3-dione (MeDiPhPr)
    - 2-Bromo-1,3-diphenylpropane-1,3-dione (BrDiPhPr)
    - Benzoic anhydride (BAHY)
    - 1,3-Bis(4-methoxyphenyl)propane-1,3-dione (4-MeTPh)
    - 2,2,2-Trifluoro-1-(3-hydroxy-1H-inden-2-yl)ethan-1-one (TIFH)
    - 2,2,2-Trifluoro-1-(3-hydroxy-1-methyl-1H-inden-2-yl)ethan-1-one (MeTIFH)
    - 2,2,2-Trifluoro-1-(3-hydroxy-1-phenyl-1H-inden-2-yl)ethan-1-one (PhTIFH)

    and *N,N'*-bidentate ligands:

    - 4,4'-Dimethyl-2,2'-bipyridine (DiMePy)
    - 4,4'-Dimethoxy-2,2'-bipyridine (DiMeOPy)

    and X:

    - Sodium bromide (Br^-)
    - Sodium thiocyande (NCS^-)
    - Thiourea (TU)
    - Tricyclohexylphosphine (PCy_3) or triphenylphosphine (PPh_3).

    The β-diketone *O,O'* bidentate ligands (3,5-DiMePh, MeDiPhPr, BrDiPhPr, BAHY and 4-MeTPh) were selected based on the different functionalities on the back bone with different electronic properties and steric effects and also its potential application as PDT (and chemotherapeutic for 4-MeTPh) agents. 4-MeTPh produces interesting luminescence characteristics as reported previously in literature.[42] The *O,O'* β-hydroxyketone bidentate ligands (TIFH, MeTIFH, PhTIFH) form 6 membered cyclic ring systems similar to the β-diketone ligands. The effects of the steric rigidity caused by the cyclopentene ring were of interest. These three ligands were synthesized with the aim to

[42] Zhang, G., Kim, S.H., Evans, R.E., Kim, B.H., Demas, J.N., Fraser, C.L. *J. Fluoresc*. **19** (2009) 881-889.

evaluate their photoluminescence properties and the effect the different functionalities on the back bone as well as the coordination to the metal core will have on these properties.

The chosen *N,N'*-bidentate ligands, DiMePy and DiMeOPy were selected based on their photoluminescence properties and possible use as chemotherapeutic agents, and to observe their behaviour when they are coordinated to the Re(I) tricarbonyl core and when the monodentate ligand in the 6th position of the Re(I) complex is varied.

The chosen monodentate ligands (X) Br^-, NCS^-, TU and PCy_3/PPh_3 were selected based on the difference in coordinating atom with particular focus on the effect it will have on the metal center which is evaluated during the kinetic studies. The different charges of the entering ligands will also be investigated.

3. Characterization of the ligands and complexes using various analytical techniques such as infrared spectroscopy (IR), ultraviolet–visible spectroscopy (UV/Vis), nuclear magnetic resonance (^{1}H NMR and ^{13}C NMR), and single crystal X-ray diffraction (XRD).
4. Preliminary determination of solid state photoluminescence properties of the ligands and the Re(I) tricarbonyl complexes and the determination of the quantum yields. Additionally, the preliminary determination of liquid state photolumincescence properties of *fac*-$[Re(CO)_3(H_2O)(DiMePy)]^+$ and *fac*-$[Re(CO)_3(H_2O)(DiMeOPy)]^+$ will be investigated. The liquid state results will be compared to the solid state photoluminescence results.
5. Evaluation of the mechanism of the substitution reactions of *fac*-$[Re(CO)_3(MeOH)(L,L'\text{-}Bid)]^n$ (*L,L'* = *N,N'* and *O,O'* type ligands, n = +1, 0) type complexes with different entering monodentate ligands (bromide ions (Br^-), thiocyanate ions (NCS^-), thiourea (TU), tricyclohexylphosphine (PCy_3) or triphenylphosphine (PPh_3)) by means of a kinetic study and the isolation and characterisation of the final products.
6. Cytotoxic evaluation of *N,N'*- and β-hydroxyketone ligands as well as 4-MeTPh, and their respective rhenium(I) tricarbonyl complexes.

2 LITERATURE STUDY OF RHENIUM CHEMISTRY AS APPLIED IN ANTI-CANCER AGENTS

2.1 Introduction

This study focuses on the development of model radiopharmaceutical and/or photodynamic therapy agents for the potential treatment and diagnosis of cancer. The use of organometallic complexes containing the radionuclides rhenium and technetium has proved to be highly effective towards the target disease of interest, namely cancer.[1,2,3] This is the general name for a large group of diseases that affect any part of the body through the creation of abnormal or unwanted cells. The term tumour is a lump or mass of tissue that may resemble swelling, but not all tumours are cancerous. The types of tumours are benign tumours that grow or spread at a very slow rate. If they are removed, they do not generally regrow and are considered not cancerous. They are unlikely to affect other parts of the body and are not harmful. If they press against blood vessels or nerves or if they trigger the over production of hormones such as the endocrine system they can cause pain. Premalignant tumours have significant potential to be malignant while malignant tumours can grow and spread throughout the body and it is considered cancerous. Cells grow uncontrollably and if they continue to grow and spread, this disease is life threatening. The cells grow quickly and easily spread throughout the body by a

[1] Gilles, G., Nils, M. *Chem. Bio*. **16** (2012) 84-91.
[2] Waziri, I., Umaru, U., Mohammed, I. *World J. Pharm*. **5** (2019) 28-35.
[3] Douglas, S.M., Kimberly, F., Brendon, E.C., Lynn, C.F., Brian, M.Z. *Dalton Trans*. **48** (2019) 14547-1456.

process called metastasizing.[4] The cells can invade or spread to nearby tissues through the blood to form more tumours from neighbouring cancerous sources.[5,6,7]

Worldwide, cancer receives considerable attention due to the increase in the number of deaths and its severity. Rhenium (Re) and technetium (Tc) have been considered as radionuclides due to the potential therapeutic nuclear medicine application of radionuclides Re-186 and Re-188 and the potential application of Tc-99m in medical diagnostic imaging.[8,9,10] The main focus of the project is based on rhenium as metal center.

2.2 Background information of rhenium

The chemistry of rhenium is the focal point of our potential anti-cancer drug development. An introduction into the history of rhenium will first be given.

At first, the investigators Henry Moseley and Dimitri Ivanovitch Mendeleev failed to discover the metal rhenium, because they were searching for the missing element in manganese ores based on the assumption that the missing element should look like the metal manganese with respect to its chemical properties. In June 1925, Ida Tacke Noddack and Walter Noddack utilized Moseley's technique to identify the unknown element (Re). With the help of Otto Berg, they managed to discover the new element in 1927 and they called it rhenium in honor of the River Rhein. A year after the discovery of rhenium, Ida Tacke Noddack managed to prepare the first gram of rhenium from 660 kg of molybdenit ore and was able to describe some properties of it.

Rhenium is element number 75 and in group VII and period VI on the periodic table. It is a transition metal and has the electron configuration [Xe]$4f^{14}5d^{5}6s^{2}$ and ground

[4] Siegel, R.L., Miller, K.D., Jemal, A. *Ca. Cancer. J. Clin*. **68** (2018) 7-30.
[5] Crowther, A.J., Liu, H. *Neuro-Oncology*. **16** (2014) 137-145.
[6] Waldum, H.L., Sandvik, A.K., Brenna, E., Fossmark, R., Qvigstad, G., Soga, J. *J. Exp. Clin. Cancer Res*. **27**(1) (2008) 70-74.
[7] Soga, J., Osaka, M., Suzuki, T., Aizawa, K., Suzuki, S., Ueki, K. *J. Exp. Clin. Cancer Res*. **14** (1995) 349-361.
[8] Gerber, T.I.A., Luzipo, D., Mayer, P. *J. Coord. Chem*. **57** (2004) 1345-1349.
[9] Abram, U., Alberto, R. *J. Braz. Chem. Soc*. **17** (2006) 1486-1500.
[10] Mukiza, J., Byamukama, E., Sezirahiga, L., Ngbolua, K.N., Ndebwanimana, V. *RMJ*. **75**(1) (2018) 14-22.

state level $^6S_{5/2}$. The oxidation states of rhenium range from -1 to +7. This metal has one of the highest melting points at 3180 ˚C. It has a boiling point ranging between 56300 ˚C and 59000 ˚C. The density of rhenium is 21.012 g.cm^{-3},[11] and it has a high specific gravity (21.4 g/mL) close to that of Os, Ir, and Pt.[11] Rhenium has properties similar to technetium (Tc) due to its position as the third row congener of Tc in group 7. Re and Tc are a coordinated match for both therapeutic and diagnostic applications in nuclear medicine. Rhenium is extensively used in nuclear medicine alongside technetium and is the primary focus of this research study. [12]

2.3 Rhenium in nuclear medicine

Nuclear medicine is the branch of medicine that deals with the use of radioactive materials in therapy and diagnosis. These radioactive materials are prepared in a suitable form for administration to the human-being either as a therapeutic agent or as a diagnostic agent for a specific disease. The radioactive material emits a type of radiation such as α, β or γ over a certain time, with a specific energy and tissue range. The use of radionuclides in nuclear medicine has been recognized across the world, with more than ten thousand medical facilities using radionuclides in nuclear medicine.[13]

The two radionuclides of rhenium that are important and have been used in nuclear medicine applications are Re-186 and Re-188.[14,15,16] The characteristics of these radionuclides are reported in Table **2-1**.

[11] Shabalin I.L. *Ultra-High Temperature Materials I. Spinger*. Manchester. New York. 2014.
[12] Baumester, J.E., Reinig, K.M., Barnes, C.L., Kelley, S.P., Jurisson, S.S. *Inorg. Chem*. **57**(20) (2018) 12920-12933.
[13] Mukiza, J., Byamukama, E., Sezirahiga, J., Ngbolua, K.N., Ndebwanimana, V. *Rwanda Med. J*. **75**(1) (2018) 14-22.
[14] Leddicotte, W.G. *The Radiochemistry of Rhenium*. National Research Council, Tennessee, 1961.
[15] Pillai, M.R.A., Dash, A., Knapp Jr, F.F. *Curr. Radiopharm*. **5** (2012) 228-243.
[16] Strominger, D., Hollander, J.M., Seaborg, G.T. *Rev. Mod. Phys*. **30** (1958) 585-904.

Table 2-1: Properties of Re-186 and Re-188 radionuclides.[14,15]

Radionuclide	^{186}Re	^{188}Re
Half-life ($t_{1/2}$)	89.4 hr	16.9 hr
Gamma Photon, KeV (%)	136 (9 %)	155 (15 %)
Tissue range (mm)	5	11
Direct Production Mode	^{185}Re (n,γ)^{186}Re	^{187}Re (n,γ)^{188}Re
Decay product	^{186}W (EC, 7.47 %) ^{186}Os (β^-, 92.43 %)	^{186}Os (β^-, 100 %)
Beta Particle, MeV (%)	1.069 (71 %) 0.932 (21.54 %) 0.581 (5.78 %) 0.459 (1.69 %)	2.120 (71.1 %) 1.965 (25.6 %) 1.487 (1.65 %)

2.3.1 Rhenium-188

Rhenium-188 (Re-188) is a high-energy β^- emitting radioisotope with a physical half-life of 16.9 hours and a maximum tissue penetration of 11 mm making it particularly suitable for treating larger sized tumours. It is one of the most attractive radionuclides for the use in therapeutic nuclear medicine and it has a low-abundant γ^- emission of 155 keV (15 %) that is sufficient for imaging and dosimetric calculations. The β^- emission has an average energy of 784 keV and a maximum energy of 2.12 MeV that is enough to penetrate and destroy the targeted unwanted tissues. It is also highly reproducible and available from a W-188/Re-188 generator. These characteristics make Re-188 an attractive therapeutic radionuclide for routine clinical use.[17,18]

Re-188 can be produced in a nuclear reactor or from a W-188/Re-188 generator. For the reactor production of Re-188, the first route is where metallic rhenium or oxide in natural abundance is targeted: Re-187 → Re-188 → Os-188 (stable). The second route is where the double neutron capture on the parent radionuclide W-186 forms W-188 and produce Re-188 via the decay of β^- particles (Scheme **2-1**).[19,20,21]

The production of Re-188 from a generator occurs in an alumina column containing W-188 as tungstic acid and Re-188 is eluted with saline. The W-188/Re-188 generator is very similar to the Mo-99/Tc-99m generator system. The

[17] Lyra, M.E., Andreou, M., Georgantzoglou, A., Kordolaimi, S., Lagopati, N., Ploussi, A., Salvara, A., Vamcaks, I.*Curr. Med. Imaging Rev*. **9** (2013) 51-75.
[18] Lepareur, N., Lacoeuille, F., Bouvry, C., Hindre, F., Garcion, E., Cherel, M., Noiret, N., Garin, E., Jr Knapp, F.F.R. *Front. Med*. **6** (2019) 132-152.
[19] Jeong, J.M., Knapp, F.F. *Semin. Nucl. Med*. **38** (2008) S19-S29.
[20] Vučina, J., Lukić, D. *Phys. Chem. and Tech.* **2** (2002) 235-243.
[21] Hsieh, B., Lin, W., Luo, T., Chen, K. *J. Radianal. Nucl. Chem.* **274** (2007) 569-573.

production process of W-188 results in a carrier-added W-188 production like Mo-99 that is produced from the fission of U-235. The absorption column of the W-188/Re-188 generator is bigger than that of the Mo-99/Tc-99m generator at the same radioactivity. The concentration method is used when a large amount of elution is required in order to elute Re-188 in a reasonable quantity.[22,23]

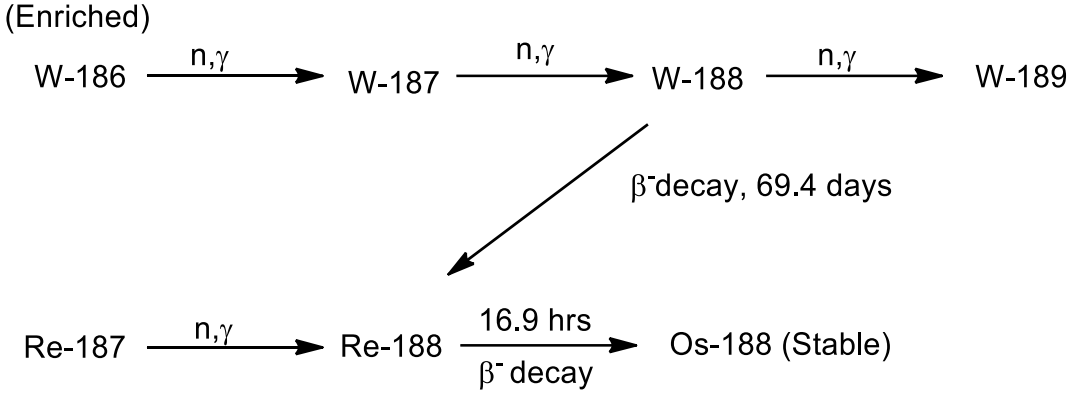

Scheme 2-1: The reactor production routes of rhenium-188.

2.3.2 Rhenium-186

Re-186 is a β^- emitting radioisotope with a half-life of 89.4 hours, which allows sufficient time for the synthesis and shipment of potential radiopharmaceuticals, and a maximum gamma photon energy of 136 KeV (9 %) and β^- energy of 1.069 MeV (71 %). The γ emission of 137 keV (9 %) is sufficient to enable molecular scintigraphy imaging during therapy and a bio-distribution assessment for patient-specific dosimetry calculations. The principal drawback of Re-186 in the receptor or radioimmunotherapy agent guided radiotherapy is the low specific activity resulting from the production method using the (n,γ) reaction in a nuclear reactor. This method for the production of Re-186 by the Re-185 (n,γ) Re-186 reaction in the reactor was developed by Knapp *et al*.[24] while the method based on the neutron bombardment of enriched aluminium perrhenate were developed by Ehrhardt *et al*.[25] The specific activity of Re-186 that can be produced in a reactor is about 558 Ci/mmol Re, which is considered marginal for radioimmunotherapy even though the thermal and

[22] Saha, G.B. *Fundamentals of Nuclear Pharmacy*, 6th Edition, Springer-Verlag, New York, (2010).
[23] Knapp, F.F., Callahan, A.P., Beets, A.L. *Appl. Radiat. Isot*. **45** (1994) 1123-1128.
[24] Knapp, F.F., Mirzadeh, S., Beets, A.L. *J. Radioanal. Nucl. Chem.* **205** (1996) 93-100.
[25] Ehrhardt, G.J., Blumer, M.E., Su, F.M., Vanderheyden, J.L., Fritzberg, A.R. *Appl. Radiat. Isot*. **48** (1997) 1-4.

epithermal neutron cross-section of Re-185 are high (106 and 1634 b). Due to only a handful of reactors with higher neutron fluxes operating in the world, methods of enhancing the specific activity of Re-186 by other means are desirable.[26,27,28,29]

2.4 The term radiopharmaceutical and its design

The term radiopharmaceutical refers to the medical formulation containing a radioisotope and an organic molecule, that are used in medical practices for diagnostic or therapeutic purposes. Different types of radioisotopes are used for various purposes in nuclear medicine. About 95 % of radiopharmaceuticals in use today are used for diagnostic purposes, while the rest are used in therapy.[30,31,32]

The radionuclide used is the visualization source for molecular imaging or the source of the cytotoxic dose in radiotherapy. The radiopharmaceuticals are classified based on their application as therapeutic and diagnostic agents, whereby β^- emitters are useful as therapeutic agents and γ emitters are useful as diagnostic agents. All radiopharmaceutical applications are based on nuclear medicine. Nuclear medicine based radiopharmaceuticals can be made up of four individual parts which are then linked: the radiometal (for example Y-90, Lu-177, Bi-213, Cu-67, In-111, Tc-99m, Re-186, Re-188),[33,34,35] a targeting biomolecule, the bifunctional chelating agent (BFCA) and a pharmacokinetic modifying linker as illustrated in Scheme **2-2**.

[26] Jia, W., Ehrhardt, G.J. *Radiochim Acta.* **79** (1997) 131-136.
[27] Eckerman, K.F., Bolch, W.E., Zankl, M., Petoussi-Henss, N. *Radiat. Prot. Dosim*. **127** (2007) 1-4.
[28] Bolch, W.E., Shah, A.P., Watchman, C.J. *Rad. Prot. Dos.* **127** (2007) 169-173.
[29] Moustapha, M.E., Ehrhardt, G.J., Smith, C.J., Szajek, L.P., Eckelman, W.C., Jurisson, S.S. *Nucl. Med. Biol*. **33** (2006) 81-89.
[30] Malvi, R., Bajpai, R., Jain, S. *Int. J. Pharm. Biol. Sci. Arch*. **3** (2005) 461-469.
[31] Saha, G.B., *Fundamentals of Nuclear Pharmacy*, 5th Edition, Springer-Verlag, New York, 2003.
[32] World Health Organization, Radiopharmaceuticals. 4th Edition, The International Pharmacopoeia. 2008.
[33] Guo, Z., Sandler, P.J. *Angew. Chem. Int. Ed. Engl*. **38**(11) (1999) 1512-1531.
[34] Lui. S. *Adv. Drug Deliv. Rev*. **60**(12) (2008) 1347-1370.
[35] Metzle-Nolte, N. *Angew. Chem. Int. Ed. Engl*. **40**(6) (2001) 1040-1043.

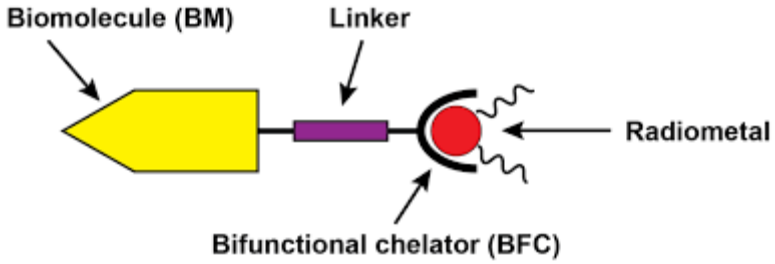

Scheme 2-2: Illustration of the individual parts of radiopharmaceuticals.[34]

One of the important requirements for the radiolabelling of biomolecules with metallic radionuclides is the use of a BFCA. The targeting biomolecules act as a carrier for the specific delivery of the radiometal. The selection of the radiometal depend on factors like the biodistribution of the radiometal used, the target tissue, the clearance rate of the radiometal complex from both non-target and target tissues as well as the half-life. The use of radioactive metals led to the development of different BFCA's that act as the cross linker between the carrier and the metallic radionuclide. In addition, a BFCA bears a functional group enabling the coordination to the carrier.[34] A variety of BFCA's with different donor atoms and chelator frameworks are required since the radiometals used in nuclear medicine vary significantly in their coordination chemistry depending on their oxidation state.

Ideally, the metal-ligand complexes must have high yields of ~99.5 % with high specific activities. The oxidation state and electronegativity play a key role in the development of metal-ligand complexes. One of the problems that might occur during the labelling of radiopharmaceuticals with radiometals is if the metal ion forms insoluble hydroxides at physiological pH. It is therefore very important that the BFCA stabilizes the radiometal. In order to prevent the release/dissociation of the radiometal from the complex and to avoid the accumulation in non-targeted organs, a high thermodynamic stability and a kinetic inertness of the radiopharmaceutical are required under physiological conditions.[36,37]

Nuclear medicine plays a vital role in the use of radiopharmaceuticals for the purpose of diagnosis and therapy. In diagnostic nuclear medicine, radiopharmaceuticals usually emit either gamma radiation or positrons; the half-lives of radionuclides for

[36] Hepperler, A., Froidevaux, S., Macke, H.R., Jermann, E., Behe, M., Powell, P., Hennig, M. *Chem. Eur. J*. **5**(7) (1999) 1974-1981.
[37] Ando, A., Ando, I., Hiraki, T., Hidada, K. *Int. J. Rad. Appl. Instrum. B*. **16**(1) (1989) 57-80.

imaging application usually range from minutes to a few hours. Low concentrations within the range of 10^{-6} to 10^{-8} M are not expected to have any pharmacological impact and are mostly used in diagnostic radiation. The main aims of diagnostic radiation are the detailed description of the morphologic structure of the tissue or organ and the testing of the physiological function through the accumulation of the radio-tracer.

In therapeutic radiopharmaceuticals, the agents are designed to convey therapeutic dosages of ionizing radiation to a specific infection site to cure the specific tumour, or for pain palliation. The ionizing radiation incites irreversible harm to atomic DNA by the reduction of double strand breaks, thereby hindering further distribution of these cells. The biological effect is obtained by the energy ingested from the radiation transmitted by the radionuclide. The radionuclide used for targeted therapy emits a particular radiation like beta, alpha or auger electron emission that have moderately short path lengths.[37]

2.4.1 Important aspects influencing the design of radiopharmaceuticals

During the development of new radiopharmaceuticals, there are some crucial factors that need to be considered such as the stability of the complex; it must be stable and its structure must not change, whether *in vivo* or *in vitro*.[32,29] The charge of the molecule determines the solubility of a chemical compound in various solvents as well as the site-specific biodistribution. All the compounds bind to some degree to the proteins (globulin or albumin) and these bindings are controlled by the coordinating site available (O-, S- and N-donor atoms), charge of the molecule, pH, nature of the protein and the anion concentration in the plasma. Abnormal tissue distribution or slow plasma clearance of the radiopharmaceutical cause a negative result in protein binding due to the poor uptake in the organs. When introducing new radiopharmaceuticals to the human body, a pH of approximately 7.4, which is similar to that of the blood, is needed. The majority of neutral drugs need to be protonated first because they are not soluble in saline. The quantity of each nuclide and reducing agent must be known and it is crucial that an adequate amount of chelating agent be added to get maximum labelling. The chemical properties of the nuclide and the

ligand must be known in order for the chosen nuclide to coordinate to the ligand in high purity.

2.4.2 Choice of radionuclide and method of radiolabelling

The choice of radionuclide is just as important as the choice of the targeting protein or peptide. The radiochemistry is crucial for the stable attachment of a given nuclide to a given protein or peptide and it is important to consider a variety of biological and pharmacological factors. These factors determine the selection of the most acceptable radionuclide for the considered application and the selection of the labelling method, that provide delivery of a high radiation dose to the malignant cells while sparing healthy tissues and organs.[22,38]

The most crucial requirement for a therapeutic radiopharmaceutical is the energy released during the decay of the nuclide. It should be deposited locally to ensure a low radiation or no dose to the healthy tissue and a high local radiation dose to the tumour cells. The general requirements of physical properties for a radionuclide to be used in therapy include the radio-catabolites to be eliminated from the body without too much accumulation in normal tissue. The radionuclide must be developed with a high amount of radioactivity and a desirable specific radioactivity. High-energy γ components is unsuitable at high abundances because it causes entire body irradiation, therefore imaging such as dosimetry and therapy monitoring are in favour of low abundance photons. Chemical properties of the radionuclide should enable high-yield labelling of proteins and a cost-effective way to produce the radionuclide. The radionuclide should emit a particular radiation such as alpha-particles (α), beta-particles (β^-) and Auger or conversion electrons to maintain cytotoxic actions and the best physical half-life seems to be 1 to 14 days according to *in vivo* pharmacokinetics.[18,38]

The radiolabelling method is the chemical reaction where the desired molecule reacts with the radionuclide to produce the radiotracer. These methods depend on the proposed studies. During the labelling process, the bifunctional approach and the

[38] Vladimir, T. *Targeted Radionuclide Tumour Therapy*. 4th Edition. Springer. New York. 2008. Pp 145-174.

intrinsic approach are the two primary methods used for the preparation of receptor specific targeting molecules.[39] Radiolabelling has grown significantly in various fields such as the medical and biochemical field. In the medical field, γ and β^- emitting radionuclides are used more often. γ Emitting radionuclides are restricted to *in vivo* imaging of different organs while β^- emitting radionuclides curtailed to therapeutic treatment and *in vitro* experiments.[39]

In the area of diagnosis, special devices are utilised to image the body and it depends on the type of examination required. The radiopharmaceuticals may be administered by injection, ingestion or inhalation to map, trace and identify the area of concern in a patient. The resulting radioactive emissions are captured by a device that allows the visualization of the area of interest with the help of a computer.

2.5 *fac*-$[Re(CO)_3]^+$ in medicine

2.5.1 Introduction

After the discovery of $[^{99m}Tc^{I}(MIBI)_6]^+$, where MIBI is 2-methoxy-2-methylpropylisocyanide,[40] much interest has been expressed in the radiopharmaceutical development of rhenium and technetium. Rhenium is kinetically more inert than technetium and is similar to technetium in physical properties, shape, formal charge, liphophilicity and size.[41,40] In 1984, Alberto and co-workers developed the aqueous synthetic procedure of *fac*-$[M(CO)_3(H_2O)_3]^+$ (M = Re, Tc).[32] This synthon (*fac*-$[M(CO)_3]^+$) meets the ideal requirements for the development of potential new radiopharmaceuticals such as high stability, low-spin electron configuration and a robust core. *fac*-$[M(CO)_3]^+$ has several other favourable properties such as being easily prepared from permetalates in aqueous-based kit formulations, has unique photo-physical properties allowing for its detection with its low luminescence when no ligands are coordinated, highly stable in air and water, also chemically inert because of its low spin d^6-configuration providing a convenient platform for drug development.

[39] Jeon, J. *Int. J. Mol. Sci*. **20** (2019) 2323-2340.
[40] Alberto, R., Schibli, R., Waibel, R., Schubiger, P.A. *Coord. Chem. Rev.* **190** (1984) 901-919.
[41] Jurisson, S., Berning, D., Jia, W., Ma D. *Chem. Rev*. **93** (1993) 1137-1156.

Labile solvent ligands in *fac*-$[M(CO)_3]^+$ can be substituted with a variety of functional groups such as phosphines, imines, thioesters and thiols. [42,43,44,45,46,47,48,49,50] It allows for the labelling of low molecular weight biomolecules due to its small size. The ease of preparation of *fac*-$[M(CO)_3(H_2O)_3]^+$ and *fac*-$[M(CO)_3(X)_3]^{2-}$ (where X = Cl^-/Br^-) is an additional attractive factor.[51,52,53,54,55]

In this project the β-diketone/β-hydroxyketone *O,O'* bidentate ligands and bipyridine *N,N'* bidentate ligands were selected based on their functionalization with different electronic properties and steric bulk. It is known from literature that the β-diketone/β-hydroxyketone and bipyridine bidentate ligands have excellent luminescent properties.[56,57,58] We therefore decided to use the selected β-diketone/β-hydroxyketone and bipyridine bidentate ligands to see the effect of the metal centre on the photoluminescence results; and also to monitor the effect these ligands have on the reactivity of the Re(I) tricarbonyl core. The β-hydroxyketone *O,O'* bidentate ligands form 6 membered cyclic ring systems similar to the β-diketone ligands, while bipyridine type ligands form 5 membered cyclic ring systems when they coordinate to the rhenium(I) tricarbonyl core. The following paragraphs will focus on previous work reported based on *O,O'* and *N,N'* type bidentate ligands as well as interesting Re(I) tricarbonyl research done in the last few years.

[42] Schutte, M., Kemp, G.,Visser, H.G., Roodt, A. *Inorg. Chem*. **50** (2011) 12486-12498.
[43] Brink. A., Visser, H.G., Roodt, A. *Inorg. Chem.* **52** (2013) 8950-8961.
[44] Fuks, L., Gniazdowska, E., Kozminski, P. *Polyhedron*. **29** (2010) 634-638.
[45] Booysen, I.N. PhD Thesis. Nelson Mandela Metropolitan University, Port Elizabeth, South Africa, 2009.
[46] Divya, V.D., Freire, R.O., Reddy, M.L.P. *Dalton Trans*. **40** (2011) 3257-3268.
[47] Werts, M.H.V., Duin, M.A., Hofstraat, J.W.,Verhoeven, J.W. *Chem. Commun*. **9** (1999) 799-800.
[48] Ballerstadt, R., Schultz, J.S. *Anal. Chem*. **72** (2000) 4185-4192.
[49] Tolosa, L., Gryczynski, I., Eichhorn, L.R., Dattelbaum, J.D., Castellano, F.N., Rao, G., Lakowicz, J.R. *Anal. Biochem*. **267** (1999) 114-120.
[50] Nagase, T., Shinkai, S., Hamachi, I. *Chem. Commun*. **39** (2001) 229-230.
[51] Jr Favale, J.M., Danilov, E.O., Yarnell, J.E., Castellano, F.N. *Inorg. Chem*. **58**(13) (2019) 8750-8762.
[52] Liang, H., Zheng-Yin, P., Wei-Wei, Q., Yi, L., Cai-Ping, T.M., Zong-Wan, M. *Dalton Trans*. **48** (2019) 4398-4405.
[53] Akabar, N., Chaturvedi, V., Shillito, G.E., Shwehr, B.J., Gordon, K.C., Huff, G.S., Sutton, J.J., Sobolev, A.N., Stagni, S., Nelson, D.J., Massi, M. *Dalton Trans*. 48 (2019) 15613-15625.
[54] Komreddy, V., Ensz, K., Nguyen, H., Rillema, D.P. *Inorganica Chim. Acta*. 511 (2020) 119815-119823.
[55] Delasoie, J., Pavic, A., Voutier, N., Vojnovic, S., Crochet, A., Nikodinovic-Runic, J., Zobi, F. *Eur. J. Med. Chem*. 204 (2020) 112583-112601.
[56] Li, J., Li, H., Yan, P., Chen, P., Hou, P., Hou, G., Li, G. *Inorg. Chem*. **51** (2012) 5050-5057.
[57] Yan,W., Yan, P., Hou, G., Li, H., Li, G. *Dalton Tans*. **42** (2013) 11537-11547.
[58] Constable, E.C., Housecroft, C.E. *Molecules*. **24** (2019) 3951-3989.

2.5.2 *O,O'* Bidentate ligands

The β-diketone type ligand systems are organic compounds that are widely known and have very interesting properties like an emitting layer to fabricate white organic light-emitting diodes (WOLED), turn-on sensors for detecting basic molecules hosted in nanozeolite, high sensitive temperature sensor and tow-photon sensitized luminescent probes for application in biological imaging based on its structure. [59,60,61] They exist as an equilibrium mixture of tautomeric keto and enol forms, but are strongly shifted towards the enol form because of the formation of the distinct resonance structure as a six membered ring.[62] Its equilibrium can be affected by numerous factors such as solvent polarity and the presence and properties of substituents. The capacity to form stable complexes with metals depends on the formation of the enol form as illustrated in Scheme **2-3**.[45,63] The *β*-diketone ligands are very important substrates in many chemical syntheses because of the two carbonyl groups that can be used as the starting material in the preparation of ketoimines, thioketones and various heterocyclic compounds like pyrimidine derivatives.[62]

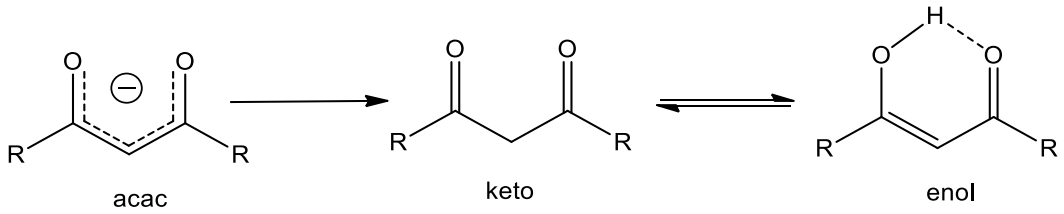

Scheme 2-3: The keto-enol equilibrium of acetylacetone and the acetylacetonato ion.[64]

The modification of the methylene group in a β-diketone ligand which involve the incorporation of a substituent, do not impact the activity of the resulting ligand in

[59] Lima, P.P., Paz, F.A.A., Brites, C.D.S., Quirino, W.G., Legnani, C., Costa, S.M. *Org. Electron*. **15** (2014) 798-808.
[60] Li, P., Zhang, Y., Wang, Y., Wang Y., Li, H. *Chem. Commun*. **50** (2014) 13680-13682.
[61] Hu, Z.-J., Tian, X.-H., Zhao, X.-H., Wang, P., Zhang, Q., Sun, P.-P. *Chem. Commun*. **47** (2011) 12467-12469.
[62] Urbaniak, W., Jurek, K., Witt, K., Gorączko, A. *Chemik*. **65** (4) (2011) 273-282.
[63] Benny, P.D., Fugat, G.A., Ganguly, T., Twamley, B., Bucar, D., MacGaillivray, L.R. *Inorg. Chim. Acta*. **365** (2011) 356-362.
[64] Okoye, N.C., Baumeister, J.E., Khosroshahi, F.N., Heather, M., Hennkens, M., Jurisson, S.S. *Radiochim. Acta*. **107**(2019) 1087-1120.

further reactions.[65,66,67] It is possible to incorporate substituents that can be further modified. For example, the polymerisation of unsaturated bonds which opens up many possibilities for the application of the ligands.

The β-diketone ligands and its complexes have been used in different fields such as the sciences and in industry. The ligands are usually used in polymer technology as substrates for the manufacturing of homogeneous and heterogeneous catalysts, polymerization catalysts (metal complexes) and substances that modify the properties of the resulting polymers (oxygen or UV resistance).[68] β-Diketone complexes containing transition metals are used as catalysts in reactions such as oxidation and epoxidation or olygomerisation. [69,62,70]

The β-diketone/β-hydroxyketone ligands are utilized as active pharmaceutical ingredients or cosmetic additives in healthcare that reduce the harmful effects of UV radiation on the skin. β-Diketone/β-hydroxyketone ligands are also important for chemical analysis used in sample concentration, air pollution monitoring and stationary phases in gas chromatography. In nuclear medicine, β-diketone/β-hydroxyketone ligands have many purposes such as an anti-asthmatic and lung disease drug, anti-ulcer and gastroprotective drugs and anti-diabetic agents.[62,71]

Triantis *et al*.[72] reported the neutral complexes *fac*-[$M(CO)_3(P)(O,O')$] and *cis-trans*-[$M(CO)_2(P)_2(O,O')$] where M = Re or Tc-99m, *O,O'* is deprotonated acetylacetone or curcumin and P is a phosphine ligand (triphenylphosphine or methyldiphenylphosphine) (Scheme **2-4**). The complexes were synthesized from the intermediate aqua complex *fac*-[$M(CO)_3(H_2O)(O,O')$]. At room temperature the phosphine ligand substitutes the H_2O molecule and form the neutral complex *fac*-[$Re(CO)_3(P)(O,O')$], but under reflux conditions further substitution of the CO trans to the phosphine ligand occurs and generate the new stable dicarbonyl bisphosphine complex *cis-trans*-[$Re(CO)_2(P)_2(O,O')$]. The monophosphine and

[65] Tsukahara, T., Nagaoka, K., Morikawa, K., Mawatari, K., Kitamori, T. *J Phys. Chem. B.* **119** (2015) 14750-14755.
[66] Isakova, V.G., Khlebnikova, T.S., Lakhvich, F.A. *Russ. Chem. Rev*. **79**(10) (2010) 849-879.
[67] Kljun, J., Turel, I. *Eur. J. Inorg. Chem*. **17** (2017) 1655-1666.
[68] Cullen, W.R., Wickenheiser, E.B. *Organomet. Chem*. **370** (1989) 141-154.
[69] Rao, C.D., Rase, H.F. *Ind. Eng. Chem. Prod. Rev. Dev*. **20** (1981) 95-97.
[70] Lewis, F.D., Miller, A.M., Salvi, S.G. *Inorg. Chem*. **34** (1995) 3173-3181.
[71] Haltiwanger , C., Wenzel, T.J., Williams, E.J., Seivers R.E. *Polyhedron*. **4**(3) (1985) 369-378.
[72] Triantis, C., Tsotakos, T., Tsoukalas, C., Sagnou, M., Raptopoulou, C., Terzis, A., Psycharis, V., Pelecanou, M., Pirmettis, I., Papadopoulos, M. *Inorg. Chem.* **52** (2013) 12995-13003.

bisphosphine complexes of curcumin show selective binding to β-amyloid plaques of Alzheimer's disease. The same type of complexes, *fac*-[^{99m}Tc(CO)$_3$(P)(*O,O'*)] and *cis-trans*-[^{99m}Tc(CO)$_2$(P)$_2$(*O,O'*)] were synthesized at Tc-99m tracer level, introducing new donor combinations for ^{99m}Tc. β-Diketone and phosphine ligands constitute a versatile ligand combination for Re(I) and ^{99m}Tc(I). The successful application of the multipotent curcumin as β-diketone ligand provided a solid example of the potential of this system.

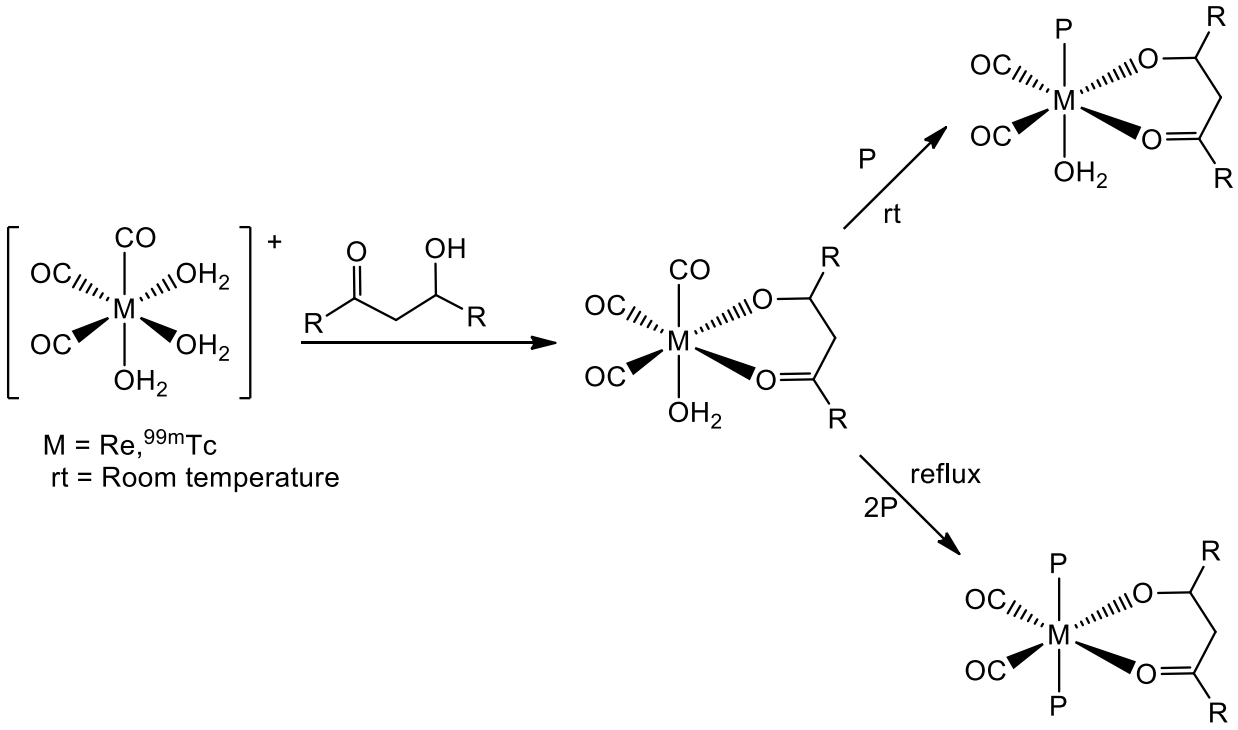

Scheme 2-4: Illustration of neutral complexes *fac*-[M(CO)$_3$(P)(*O,O'*)] and *cis-trans*-[M(CO)$_2$(P)$_2$(*O,O'*)] reported by Triantis *et al*.[72]

Sagnou *et al*.**[73]** also reported "2 + 1" complexes with the *fac*-[M(CO)$_3$]$^+$ (M = Re, Tc-99m) core coordinated to the β-diketone ligands acetylacetone and curcumin as *O,O'* donor bidentate ligands, but with imidazole or isocyanocyclohexane as monodentate ligands (Scheme **2-5**). The *fac*-[Re(CO$_3$)(H$_2$O)$_3$]$^+$ precursor was reacted with the β-diketone to generate the intermediate aqua complexes *fac*-[Re(CO)$_3$(H$_2$O)(*O,O'*)] followed by the substitution of the labile water molecule by the monodentate ligand. The chemistry was successfully transferred at Tc-99m tracer level. Due to the wide

73 Sagnou, M., Benaki, D., Triantis, C., Tsotakos, T., Psycharis, V., Raptopoulou, C.P., Pirmettis, I., Papadopoulos, M., Pelecanou, M. *Inorg. Chem.* **50** (2011) 1295-1303.

spectrum of pharmacological activity of curcumin, the curcumin complexes and intermediate aqua complexes bear potential for radiopharmaceutical applications. They were successfully tested for selective staining of β-amyloid plaques of Alzheimer's disease. The fact that the complexes maintain the affinity of the mother compound curcumin for β-amyloid plaque, prompts for further exploration for their chemistry and biological properties as radioimaging probes.

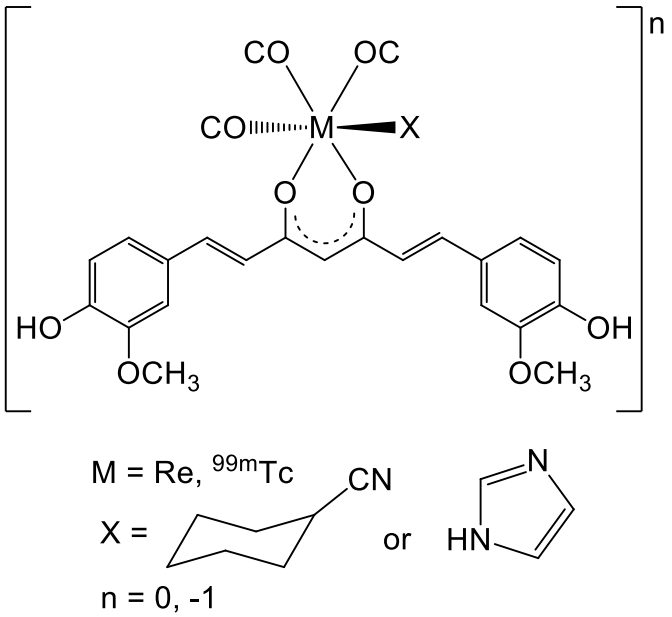

Scheme 2-5: Illustration of the "2 + 1" complexes synthesized by Sagnou *et al*.[73]

The recent study by Gantsho *et al*.**[74]** reported the Re(I) di- and tri-carbonyl complexes of the form *fac*-[$Re(CO)_3(X)$(*L,L'*-Bid)] and [$Re(CO)_2(X)_2$(*L,L'*-Bid)] (X = H_2O, MeOH, PPh_3, PTA, PCy_3 and L,L'-Bid = *O,O'* bidentate ligands (tropolone = TropH and 3-hydroxyflavone = FlavH) and *N,O* bidentate ligands (8-hydroxyquinoline = QuinH, 5,7-chloro-8-hydroxyquinoline = diCl-QuinH and quinoline-2,4-dicarboxylic acid = $QuinH_2$)). The toxicity of the complexes illustrated in Scheme **2-6** was evaluated and some complexes showed high cytotoxicity against human cervix adenocarcinoma (HeLa) cells and some degree of selectivity over non-cancerous cells.

[74] Gantsho, V.L., Dotou, M., Jakubaszek, M., Goud, B., Gasser, G., Visser, H.G., Schutte-Smith, M. *Dalton Trans*. **49** (2020) 35-46.

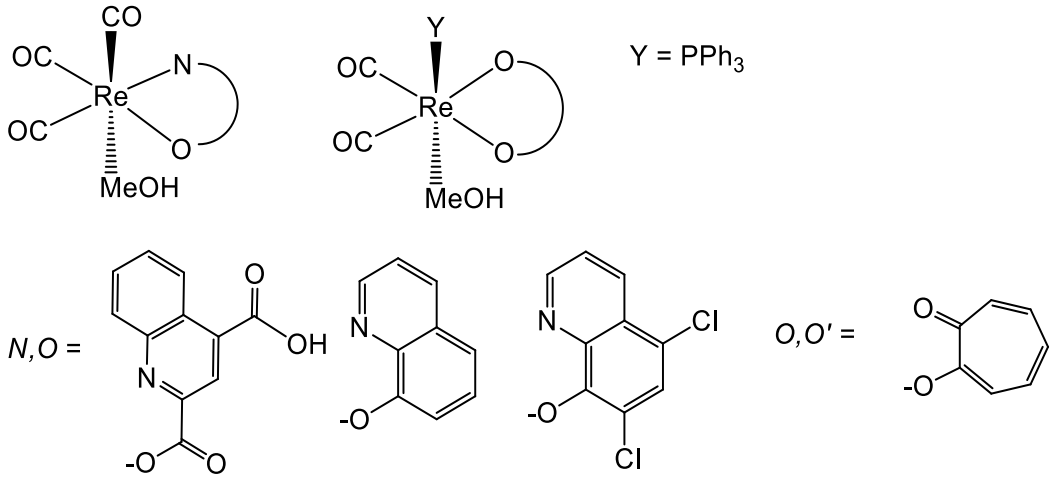

Scheme 2-6: Schematic representation of Re(I) di- and tri-carbonyl complexes synthesized by Gantsho *et al*.[74]

Schutte-Smith *et al*.**[75]** reported Re(I) tricarbonyl complexes of the form *fac*-$[Re(CO)_3(X)(Trop)]^n$ (where TropH = tropolone, X = pyridine (Py), 4-dimethylaminopyridine (DMAP), imidazole (Im), thiourea (TU), 1-methyl-2-thiourea (MeTU), bromide (Br^-) iodide (I^-) and n = 0, -1). A schematic representation of the complexes synthesized is presented in Scheme **2-7**. The methanol substitution reaction by a range of seven nucleophiles was investigated at variable temperatures, at ambient and high pressure. The kinetic results obtained are important in nuclear medicine and in particular to aspects related to synthesis, *in vivo* stability, uptake, excretion and general pharmacokinetics rates of the metabolized and parent radiopharmarceutical based on the *fac*-$[M(CO)_3(H_2O)_3]^+$ synthon (M = ^{186}Re(I), ^{188}Re(I) or ^{99m}Tc(I)). The kinetic results of this study will be discussed in paragraph 2.6.3.

75 Schutte-Smith, M., Roodt, A., Visser, H.G. *Dalton Trans*. **48** (2019) 9984-9997.

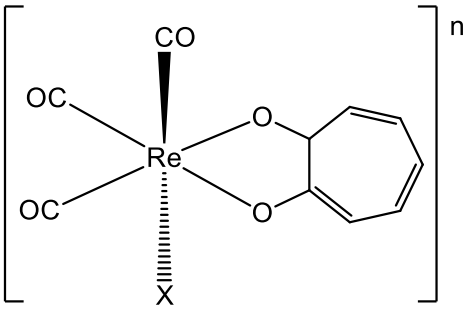

X = MeOH, Py, DMAP, Im, TU, $MeTU^-$, Br^-, I^-
n = 0, -1

Scheme 2-7: Schematic representation of the synthesized Re(I) tricarbonyl complexes by Schutte-Smith *et al*.[75]

2.5.3 *N,N'* Bidentate ligands

2,2'-Bipyridine, an *N,N'* bidentate ligand is an organic compound that has been used extensively in the complexation of metal ions. It is a neutral ligand that forms coordination complexes with many transition metals, that exhibit intense luminescence.[76] The general structure of bipyridine is illustrated in Scheme **2-8**; it is very easy to distinguish between the symmetrical bipyridine (2,2', 3,3' and 4,4') and asymmetrical ones (2,3', 2,4' and 3,4').[77,78,79]

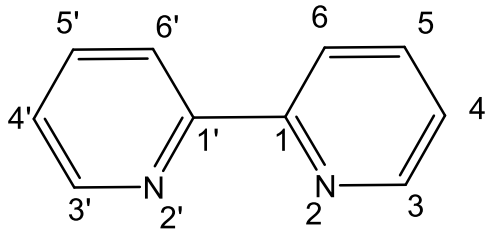

2,2'-Bipyridine

Scheme 2-8: Schematic representation of the bipyridine ligand system.[76]

[76] Kaes, C., Katz, A., Hosseini, M.W. *Chem Rev*. **100** (2000) 3553-3590.
[77] Jacob, P., Benowitz, N., Yu, L., Duan, M.J., Liang, G. *Addiction*. **92** (1997) 615-626.
[78] Schumacher, J.N., Green, C.R., Best, F.W., Newell, M.P. *J. Agric. Food Chem*. **25** (1977) 310-320.
[79] Foder, G.B., Colasanti, B. *In Alkaloids: Chemical and Biological Perspectives*, Pelletier, S. W. Ed., Wiley: New York, 1985; Vol.3, Chapter 1.

The 2,2'-bipyridine ligand system has been used in a variety of approaches dealing with structural coordination chemistry and functional systems based on the 2,2'-bipyridine metal complexes.[80,81,82]

A literature search resulted in quite a lot of rhenium(I) tricarbonyl complexes with *N,N'* bidentate ligands coordinated to it. Yang *et al*.[83] reported phosphorescent organometallic rhenium(I) tricarbonyl complexes with *N,N'* bidentate ligands (Scheme **2-9**) as mitochondria-targeted theranostic agents capable of inducing and tracking the therapeutic effect simultaneously. Some of the complexes are synthesised quickly and efficiently penetrate into A549 cells when localizing within mitochondria. Their cytotoxicity is superior to cisplatin against the cancer cells screened (HeLa, human pulmonary carcinoma; A549, human lung carcinoma; A549R, cisplatin-resistant cell line; LO2, human normal liver cell line). Some of the complexes contain a thiol-reactive chloromethylpyridyl moiety for mitochondrial immobilization and shows higher cytotoxicity and selectivity against cancer cells than other synthesised rhenium(I) complexes without mitochondria-immobilization properties. The reported mechanistic studies show that the complexes induce a cascade of mitochondria-dependent events including mitochondrial damage, mitochondrial respiration inhibition, reactive oxygen species elevation, cellular ATP depletion and caspase-dependent apoptosis. The excellent phosphorescent and O_2-sensitive life-times of the mitochondrial immobilized complexes can be utilized for real-time tracking of the morphological changes of mitochondria and mitochondrial respiration repression during therapy processes; accordingly reliable information for the understanding of anti-cancer mechanisms were obtained from this study.

[80] Fiorini, V., Ranieri, A.M., Muzzioli, S., Magee, K.D.M., Zacchini, S., Akabar, N., Stefan, A., Ogden, M.I., Massi, M., Stagni, S. *Dalton Trans*. **44** (2015) 20597-20608.
[81] Morimoto, T., Nakajima, T., Sawa, S., Nakanishi, R., Imori, D., Ishatani, O. *J. Am. Chem. Soc.* **135** (2013) 16825-16828.
[82] Yang, L., Ren, A.M., Feng, J.K., Liu, X.J., Ma, Y.G., Zhang, M., Liu, X.D., She, J.C., Zhang, H.X. *J. Phys. Chem*. A. **108** (2004) 6797-6808.
[83] Yang, J., Zhao, J., Cao, Q., Hao, L., Zhou, D., Zhenji, G., Ji, L.N., Mao, Z.W. *ACS Appl. Mater. Interfaces*. **9** (2017) 13900-13912.

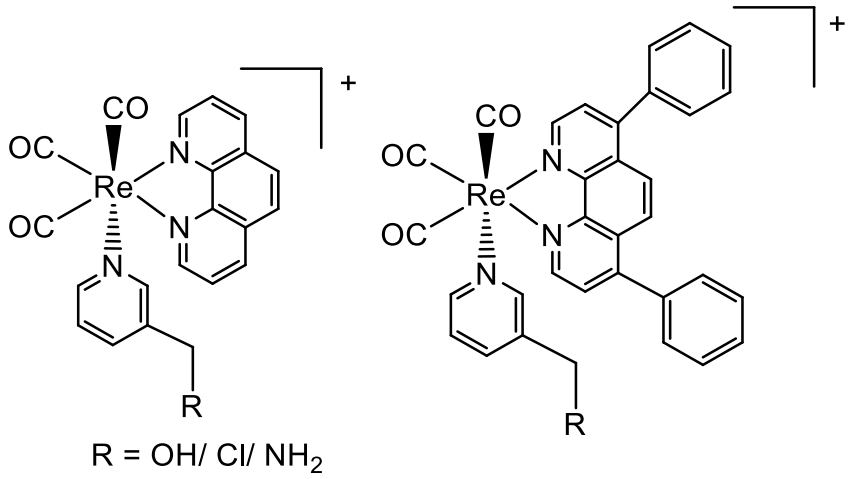

Scheme 2-9: The rhenium(I) tricarbonyl complexes with *N,N'* bidentate ligands synthesised by Yang *et al*.[83]

Bertrand *et al*.**[84]** also developed rhenium(I) complexes with ancillary ligands showing interesting luminescence quantum yields in acetonitrile and constitute valuable luminescence metal complexes in organic media. Some complexes show impressive enhancement of their luminescence properties relative to the other rhenium(I) tricarbonyl complexes. Very interesting preliminary cellular imaging studies in breast cancer cells reveal a strong increase in the luminescence signal in cells incubated with rhenium tricarbonyl complexes (Scheme **2-10**).

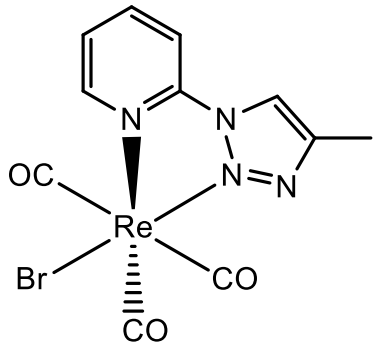

Scheme 2-10: A typical structure of the Re(I) complexes synthesized by Bertrand *et al*.[84]

84 Bertrand, H., Clede, S., Guillot, R., Lambert, F., Policar, C. *Inorg. Chem.* **53**(12) (2014) 6204-6223.

In 2016, Zhong *et al*.[85] reported a Re(I) tricarbonyl complex (Scheme **2-11**) with a strong visible light absorbing ability (624 nm, ε = 5.69 x 10^4 L/(mol cm)), long-lived triplet excited state (τ_T= 448.9 μs) and a moderate fluorescence quantum yield (Φ_F = 41.6 %). The photophysical properties of the complex was studied with steady state UV/Vis absorption, luminescence spectroscopy, nanosecond transient absorption spectroscopy and density functional theory (DFT) /time-dependent density functional theory (TDDFT) calculations. The synthesized complex were subjected to intracellular PDT and luminescence imaging studies. The results observed indicated low dark toxicity, but it is able to kill cancer cells on illumination with 635 nm light.

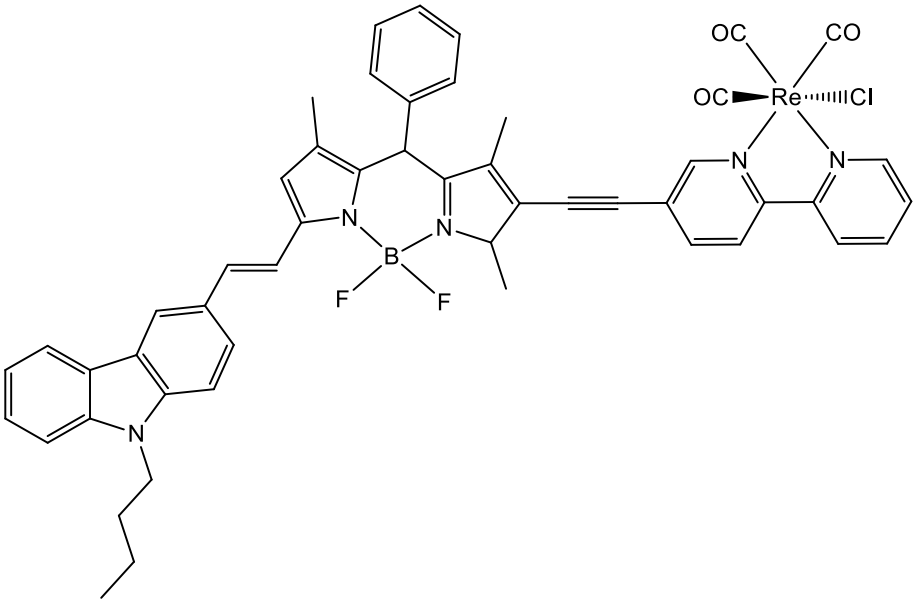

Scheme 2-11: Schematic representation of the Re(I) tricarbonyl complex synthesized by Zhong et al.,[85] **with a strong visible light absorbing ability.**

Marker *et al*.[86] reported fifteen water-soluble Re(I) tricarbonyl complexes of the form *fac*-[$Re(CO)_3$(X)(L,L'-Bid)] (where X = 1,3,5-triaza-7-phosphaadamantane (PTA), tris(hydroxymethyl)phosphine (THP), or 1,4-diacetyl-1,3,7-triaza-5-phosphabicylco[3.3.1]nonane (DAPTA), Scheme **2-12**). The Re(I) tricarbonyl complexes with coordinated THP and DAPTA ligands exhibit triplet-based luminescence in air-equilibrated aqueous solutions with quantum yields ranging from 3.4 to 11.5 %. These complexes also undergo photo-substitution of a CO ligand upon

[85] Zhong, F., Yuan, X., Zhao, J., Wang, Q. Chem. *Sci. China. Chem*. **54** (2016) 70-77.
[86] Marker, S.C., MacMillan, S.N., Zipfel, W.R., Li, Z., Ford, P.C., Wilson, J.J. *Inorg. Chem*. **57**(3) (2018) 1311-1331.

irradiation with 365 nm light with quantum yields ranging from 1.1 to 5.5 % and sensitise the formation of $^1O_2$ with quantum yields as high as 70 %. All complexes with PTA ligands are non-emissive and do not undergo photo-substitution upon irradiation with 365 nm light. These complexes were evaluated as photo-activated anti-cancer agents in human cervical (HeLa), ovarian (A2780), and cisplatin-resistant ovarian (A2780CP70) cancer cell lines. All complexes with THP and DAPTA ligands exhibited a cytotoxic response upon irradiation with minimal toxicity in the absence of light. However, complexes with DAPTA and 1,10-phenanthroline ligands gave rise to an IC_{50} value of 6 µM in HeLa cells upon irradiation, rendering it the most phototoxic compounds reported in this study.

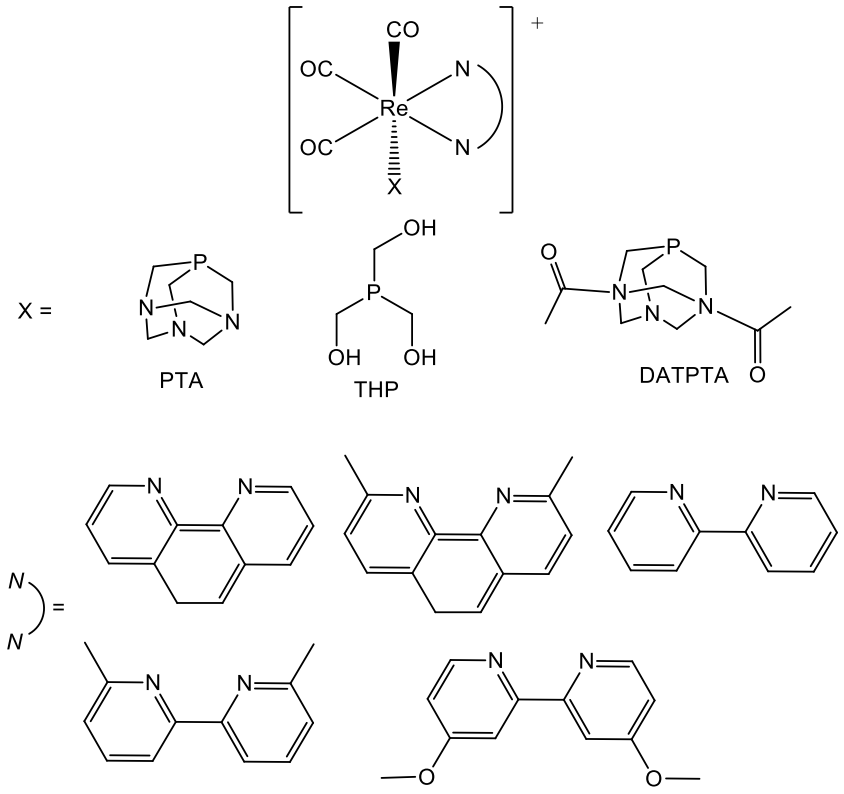

Scheme 2-12: Water-soluble Re(I) tricarbonyl complexes reported by Marker *et al*.[86]

The nature of the photo-induced cytoxicity of these compounds was explored in further detail and the data indicated that the phototoxic response may result from the release of both CO and the rhenium-containing photoproduct as well as the production of $^1O_2$.

2.6 Metal complexes in chemotherapy

2.6.1 Introduction to chemotherapy

In simple terms, chemotherapy is the treatment of cancer by using drugs that destroy cancer cells and has been known to control cancer.[87,88] It works by slowing or stopping the growth of cancer cells that grows and divides quickly.[87,88]

The well-known German chemist Paul Ehrlich developed a drug to treat infectious diseases in the early 1990s.[89] He coined the term 'chemotherapy' that is defined as the use of chemicals to treat diseases. While using the rabbit model for syphiliss, Paul Ehrlich developed arsenicals to treat infectious diseases.[90] He was also interested in the development of drugs to treat cancer, including aniline dyes and primitive alkylating agents.[90] However, Ehrlich was not optimistic about a chance for success. Until the 1960s, surgery and radiotherapy were the major forms of cancer therapy. The cure rates of these methods plateaued at about 33 % due to the presence of micro-metastases which was unacknowledged until then. New results revealed the possibility of combination chemotherapy to cure patients with various advanced cancers.[89] The latter observation opened many opportunities to apply drugs in conjunction with surgery or radiation treatments to deal with the problem of micro-metastases, the field of adjuvant chemotherapy, and was initially studied in breast cancer patients.[89]

Regarding the use of metals for the treatment of cancer, the platinum-based drugs carboplatin and cisplatin have some limitations.[91] These drugs induce toxic side effects and are susceptible to drug resistance.[92] The success of the platinum-based drugs has sparked interest in the development of new drug candidates containing metal centres. Complexes of ruthenium,[93] gold[94] and titanium[95] have been reported

[87] Knoepfler, P.S. *Stem Cells*. **27(5)** (2009) 1050-1056.
[88] Ferrara, N., Kerbel, R.S. *Nature*. **438** (2005) 967974.
[89] DeVita, V.T., Chu, E. *Cancer Res*. **68(21)** (2008) 8643-8653.
[90] Turk, J.L., Paul, E. *J. R. Soc. Med*. **87** (1994) 314-315.
[91] Kelland, L.R., Farrell, N.P. *Platinum-Based Drugs in Cancer Therapy*.1st edition. Eds. Human Press. New York. 2000.
[92] Martin, L.P., Hamilton, T.C., Schilder, R.J. *Clin. Cancer Res*. **14** (2008) 1291-1295.
[93] Zeng, L., Gupta, P., Chen, Y., Wang, E., Ji, L., Chao, H., Chen, Z.-S. *Chem. Soc. Rev*. **46** (2017) 5771-5804.

to exhibit anti-cancer activity via novel mechanisms of action. The potential of these metal complexes is exemplified by the current clinical trials of gold drug candidates such as auranofin and ruthenium drug candidates such as TLD-1433, NAMI-A and NKP-1339.[96] The effort in this area has expanded to the third row transition metals, such as rhenium (Re), osmium (Os) and iridium (Ir). Rhenium complexes have gained interest as anticancer agents due to its high stability, rich spectroscopic properties and structural diversity.[97] Many reports have illustrated its promising *in vitro* anti-cancer activity, nevertheless few studies show the potential efficacy of these complexes *in vivo*. The complexes containing the stable rhenium(I) tricarbonyl core have been extensively explored for both imaging and therapeutic applications among potential anti-cancer agents.[98,99,100]

2.6.2 Examples of rhenium(I) tricarbonyl complexes in chemotherapy

Knopf *et al*.[101] reported seven rhenium(I) tricarbonyl complexes of the type *fac*-[$Re(CO)_3(H_2O)$(*N,N'*-Bid)] (where *N,N'*-Bid = 2,2'-bipyridine (**8**), 4,4'-dimethyl-2,2'-bipyridine (**9**), 4,4'-dimethoxy-2,2'-bipyridine (**10**), 4,4'-dimethyl-2,2'-bipyridine-4,4-dicarboxylate (**11**), 1.10-phenanthroline (**12**), 2,9-dimethyl-1,10-phenanthroline (**13**) or 4,7-diphenyl-1,10-phenanthroline (**14**)) as illustrated in Scheme **2-13.**

[94] Zou, T., Lum, C.T., Lok, C.-N., Zhang, J.-J., Che, C.-M. *Chem. Soc. Rev.* **44** (2015) 8786-8801.
[95] Cini, M., Bradshaw, T.D., Woodward, S. *Chem. Soc. Rev*. **46** (2017) 1040-1051.
[96] Alessio, E. *Eur. J. Inorg. Chem*. **55** (2017) 1549-1560.
[97] Lee, L.C.-C., Leung, K.-K., Lo, K.K.-W. *Dalton Trans*. **46** (2017) 16357-16380.
[98] Trondl, R., Heffeter, P., Kowol, C.R., Jakupec, M.A., Berger, W., Keppler, B.K. *Chem. Sci*. **5** (2014) 2925-2932.
[99] Konkankit, C.C., Marker, S.C., Knoft, K.M., Wilson, J.J. *Dalton Trans*. **47** (2018) 9934-9974.
[100] Zhang, P., Huang, H. *Dalton Trans*. **47** (2018) 14841-14854.
[101] Knopf, K.M., Murphy, B.L., MacMillan, S.N., Baskin, J.M., Bar, M.P., Boros, E., Wilson, J. *J. Am. Chem. Soc*. **139** (2017) 14302-14314.

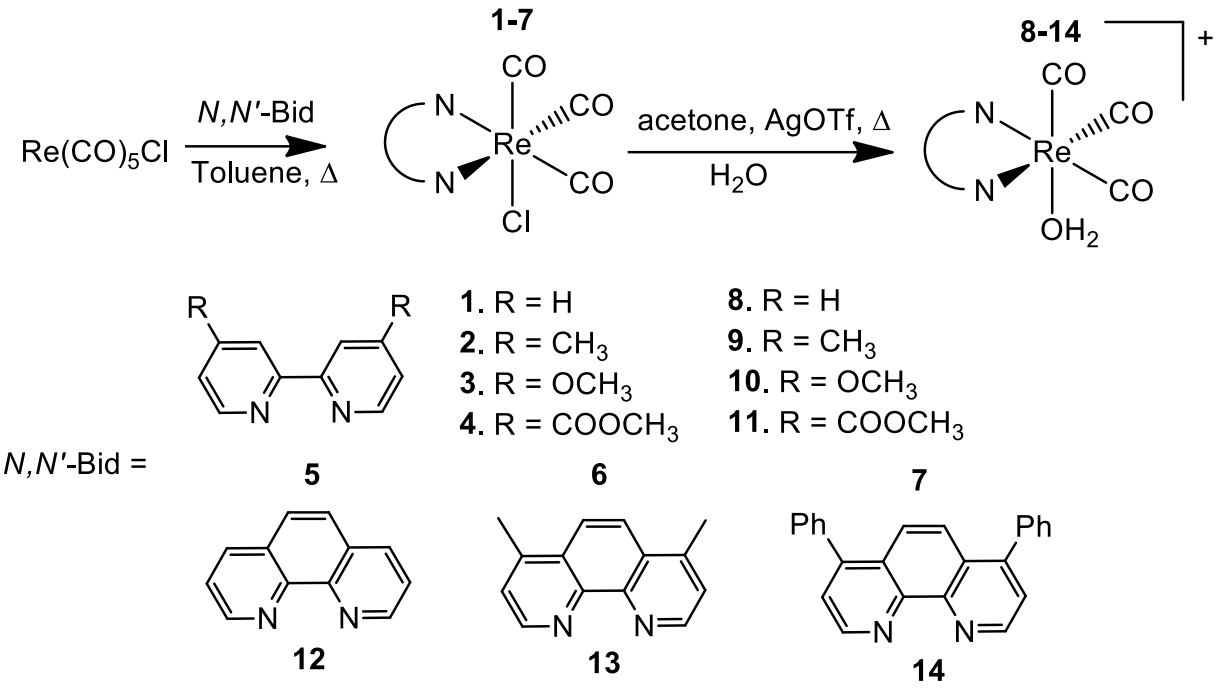

Scheme 2-13: Diimine rhenium(I) tricarbonyl complexes reported by Knopf *et al*.[101]

These complexes (with the exception of **11**) exhibit 50 % growth inhibitory concentration (IC_{50}) values that are less than 20 μM in HeLa cells and this indicates that all complexes represent a new potential class of anti-cancer agents. However, **9**, **10** and **13**, were found to be effective in the cisplatin-resistant, wild type cells, signifying that they circumvent cisplatin resistance. The mechanism of action of the most potent complex **13** was explored further by leveraging its intrinsic luminescent properties to determine the intracellular localization that **13** induces upon cell death without causing an increase in intracellular reactive oxygen species or depolarization of the mitochondrial membrane potential. The continuation of the studies revealed that the mode of cell death does not fall into one of the canonical categories such as apoptosis, paraptosis, necrosis and autophagy suggesting that a novel mode of action may be operative for this class of rhenium(I) tricarbonyl complexes. The *in vivo* biodistribution and metabolism of **13** and its ^{99m}Tc analogue (*fac*-[^{99m}Tc(CO)$_3$(H$_2$O)(*N,N'*-Bid)]) **13*** where *N,N'*-Bid = 2,9-dimethyl-1,10-phenanthroline) were also evaluated in naïve mode. **13** and **13*** exhibited comparable biodistribution profiles with both hepatic and renal excretion.[101] High-performance liquid chromatography inductively coupled plasma mass-spectrometry (HPLC-ICP-MS) analysis of mouse blood plasma and urine post-administration showed considerable metabolic stability of **6**, rendering this potent complex suitable for *in vivo* applications. This study illustrated the biological properties of rhenium(I) tricarbonyl complexes and

demonstrates their potential as promising theranostic anti-cancer agents that can circumvent cisplatin resistance.

Konkankit *et al*.[102] expanded on the work reported by Knopf *et al*[101]; *fac*-[Re(CO)$_3$(H$_2$O)(*N,N'*-Bid)] (**II**) (*N,N'*-Bid = 2,9-dimethyl-1,10-phenanthroline) (Scheme **2-14**) was further investigated to explore its aqueous speciation and anti-tumour activity. The cellular uptake of **II** was measured in wild-type (A2780) and cisplatin resistant (A2780CP70) ovarian cancer cells by inductively coupled plasma mass spectrometry and revealed similar uptake efficiency in both cell lines. In both cell lines, high accumulation was observed in the mitochondria contradicting prior fluorescence microscopy studies. The luminescence of **II** is dependent on the pH and coordination environment, making fluorescence microscopy unreliable for determining complex localization. Mice were used for the evaluation of *in vivo* anti-cancer activity bearing patient derived ovarian cancer tumour xenografts. It was found that **II** was capable of inhibiting tumour growth, providing further credibility for the use of these complexes as anti-cancer agents.

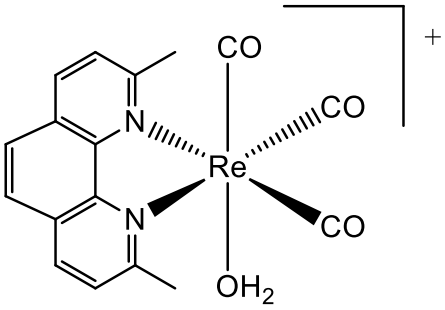

Scheme 2-14: The potent rhenium-based anticancer agent reported by Konkankit *et al.* [102]

Sovari *et al*.[103] reported a series of 3-arylcoumarin ligands and its respective *fac*-[Re(CO)$_3$(L)(bpy)] (L = 3-arylcoumarin monodentate, bpy = 2,2-bipyridine) and *fac*-[Re(CO)$_3$(Br)(*L,L'*-Bid)] (*L,L'*-Bid = 3-arylcoumarin bidentate) complexes and evaluated its anti-microbial efficacy. The 3-arylcoumarin ligands were virtually inactive against the human-associated pathogens with minimum inhibitory concentration of (MICs) > 150 µM but when coordinated to *fac*-[Re(CO)$_3$]$^+$, most of

[102] Konkankit, C.C., King, A.P., Knopf, K.M., Southhard, T.L., Wilson, J.J. *ACS Med. Chem. Lett*. **10** (2019) 822-827.
[103] Sovari, S.N., Vojnovic, S., Bogojevic, S.S., Crochet, A., Pavic, A., Nikodinovic, J.-R., Zobi, F. *Eur. J. Med. Chem*. **205** (2020) 112533-112549.

the resulting complexes showed a remarkable anti-bacterial potency. Some complexes exhibit activity in nano-molar concentration against Gram-positive pathogens such as staphylococcus aureus strains including methicillin resistant *S. Aureus (MRSA) and Enterococcus faecium.* The ligands do not have any effect on bacterial cell membrane potential but some potent complexes strongly interact with DNA and indicate it as a possible target for their mode of action. The *in vivo* studies in zebrafish models showed that the complexes with anti-staphylococcal/MRSA activity were non-toxic to the organism even at much higher doses of the corresponding MICs. The complexes increased the survival rate of infected fish up to 100 % in the zebrafish-MRSA and markedly reduced the bacterial burden. Furthermore, all rescued fish developed normally following the treatment with the metallic complexes.

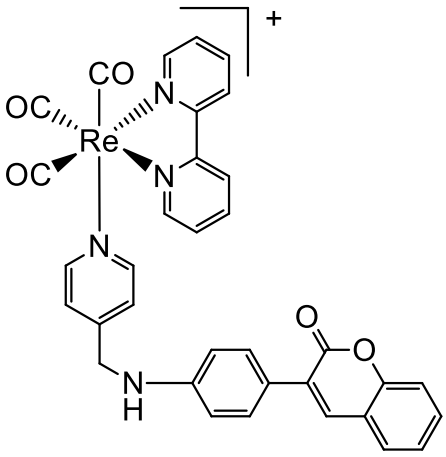

3-arylcoumarin as monodentate

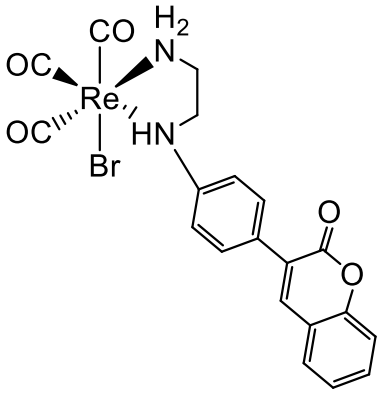

3-arylcoumarin as bidentate

Scheme 2-15: The 3-arylcoumarin ligands as mono- and bidentate ligands in the corresponding *fac*-$[Re(CO)_3]^+$ complexes reported by Sovari *et al*.[103]

2.6.3 Metal complexes with *O,O'*- and *N,N'*- bidentate ligands in chemotherapy

Karami *et al*.[104] reported a novel organometallic complex [Pd{(C,N)-$C_6H_4CH(CH_3)NH$}(CUR)] (CUR = 1,7-bis(4-hydroxy-3-methoxyphenyl)-1,6-heptadiene-3,5-dion) utilizing biologically active ligand (Scheme **2-16**). Fluorescence

[104] Karami, K., Rafiee, M., Lighvan, Z.H., Zakariazadeh, M., Faal, A.Y., Esmaeili, S.-A., Abbas, A.M.-B. *J. Mol. Struct*. **1154** (2018) 480-495.

spectroscopy demonstrates the affinity of [Pd{(C,N)-$C_6H_4CH(CH_3)NH$}(CUR)] for proteins, which exhibits a relatively high binding constant value (K_b) of 6.34 x 10^{-5}. UV/Vis spectroscopy, emission titration and helix melting methods used to study the interaction of [Pd{(C,N)-$C_6H_4CH(CH_3)NH$}(CUR)] with Calf thymus DNA (CT-DNA), showed that this complex bound to CT-DNA by intercalation and illustrated good cytotoxic activity against MCF-7 (human breast cancer) and JURKAT (human leukemia) cell lines whereas low cytotoxicity was observed against normal peripheral blood mononuclear cells.

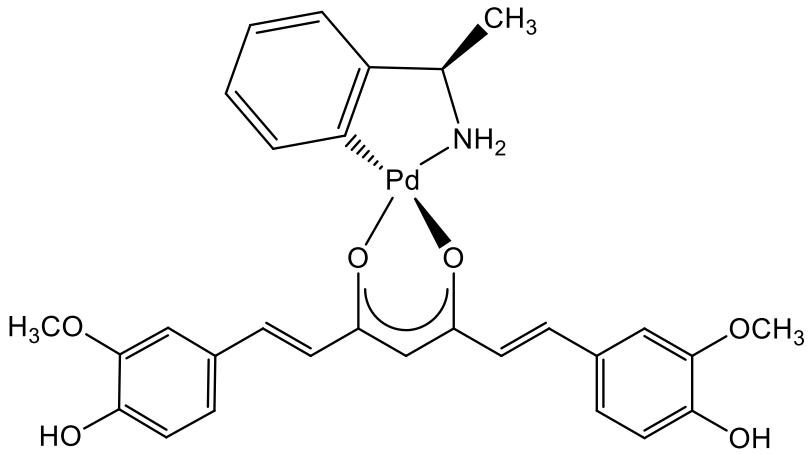

Scheme 2-16: The novel organometallic complex ([Pd{(C,N)-$C_6H_4CH(CH_3)NH$}(CUR)] reported by Karami *et al.* [104]

Paixao *et al*.[105] reported novel copper(II) complexes as illustrated in Scheme **2-17**. The cytotoxic activity of **1**, **2** and **3** in two tumour cell lines (Ehrlich tumour and sarcoma 180) and in a non-tumour cell line (myoblast C2C12) was evaluated and it was found that **3** exhibits good activity (IC_{50} Ehrlich = 15.75 µM and IC_{50} sarcoma 180 = 16.90 µM) and selectivity (SI > 4) in both tumour cell lines and also present good activity against Trypanosoma cruzi.

[105] Paizao, D.A., de Oliveira, B.C.A., Almeida, J.C., Sousa, L.M., Lopes, C.D., Carneiro, Z.A., Tezuka, D.Y., Clabijo, J.C.T., Ellena, J., Polloni, L., Machado, P.H.A., deAlbuquerque, S., de Oliveira, R.J., Guilardi, S., Guerra, W. *Inorg. Chim. Acta*. **499** (2020) 119164-119172.

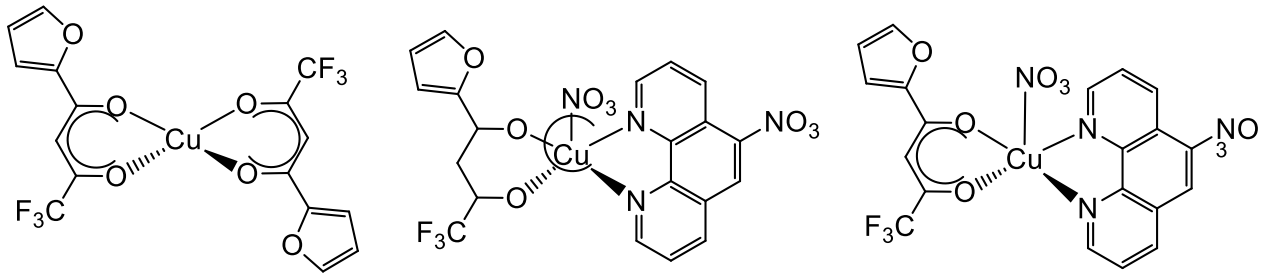

[Cu(tfa)$_2$] **1**

[Cu(tfa)(dmb)(NO$_3$)]•1.5H$_2$O **2**

[Cu(tfa)(nphen)(NO$_3$)] **3**

Scheme 2-17: Novel copper(II) complexes reported by Paixao *et al*.[105]

Abbas *et al.*[106] reported lanthanide(III) complexes (illustrated in Scheme **2-18**) of which the excited state life-time (s) and hydration number (q) were determined. The presence of three TTA (1,1,1-trifluoro-3-(2-theonyl)acetone) ligands in water inhibits non-radiative deactivation with life-times in the range of 0.306 - 0.445 ms. The calculated hydration number values (0.37 - 0.63) from the excited state life-time results show the absence of any bound H_2O molecules in the coordinatively saturated complexes (q < 1). Complexes **1** to **4** (Scheme **2-18**) were investigated for their biological interactions with DNA, protein and their DNA photo-cleavage activity. The binding constants with CT-DNA (K_b = 1.15 x 10^5 M^{-1} to 8.8 x 10^5 M^{-1}) and HSA (K_{HSA} = 6.5 x 10^5 M^{-1} to 8.1 x 10^5 M^{-1}) of **1** to **4** results in the significant affinity towards these biological targets. Incorporation of chalcone ligands containing anthracene or pyrene as a photosensitizing moiety in these complexes was effective in generating reactive oxygen species (ROS). **1** to **4** exhibit moderate photo-cleavage of supercoiled (SC)-DNA to its nicked circular (CN) form on exposure to UV-A light of 365 nm through the generation of singlet oxygen ($^1O_2$) and hydroxyl radicals (^cOH) under physiological conditions.

[106] Abbas, Z., Dasari, S., Patra, A.K. *RSC Adv*. **7** (2017) 44272-44281.

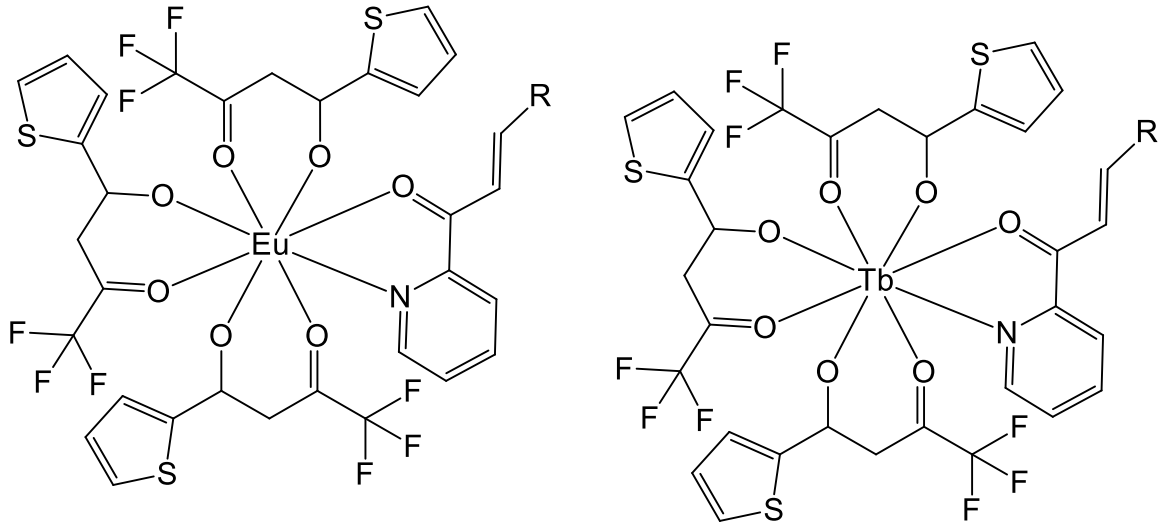

1: R = Antharacene
3: R = Pyrene

2: R = Antharacene
4: R = Pyrene

Scheme 2-18: The lanthanide(III) complexes reported by Abbas *et al*.[106]

2.7 The kinetics of *fac*-$[Re(CO)_3]^+$ type complexes

The tricarbonyl precursor *fac*-$[M(CO)_3(X)_3]^n$ (where M = Tc, Re; X = Br^-, H_2O; n = +1, -2) contain relatively stable carbonyl ligands and labile water or bromido ligands and it is because of these properties that complexes of the type *fac*-$[M(CO)_3(X)_3]^n$ are so attractive for application in nuclear medicine. The knowledge of the mechanism behind the substitution of these labile ligands can help to identify the complex's reactivity and stability.**[107]**

2.7.1 The water exchange of *fac*-$[M(CO)_3(H_2O)_3]^+$

Salignac and co-workers**[108]** reported the first thermodynamic and kinetic experimental data for the water exchange of *fac*-$[Re(CO)_3(H_2O)_3]^+$, where the water exchange rate constant for *fac*-$[Re(CO)_3(H_2O)_3]^+$ was calculated as k_{ex} = 6.3 ± 0.1 x 10^{-3} s^{-1}. The

107 Kluba, C.A., Mindt, T.L. *Molecules.* **18** (2013) 3206-3226.
108 Salignac, B., Grundler, P.V., Cayemittes, S., Frey, U., Scopelliti, R., Merbach, A. *Inorg. Chem*. **42** (2003) 3516-3522.

values for the activation parameters, $\Delta H^{\ddagger}$ = 90 ± 3 kJ mol^{-1} and $\Delta S^{\ddagger}$ = +14 ± 10 J K^{-1} mol^{-1} of *fac*-$[Re(CO)_3(H_2O)_3]^+$ suggested a dissociative activation mode for the water exchange process. At lower pH the only species in solution is *fac*-$[Re(CO)_3(H_2O)_3]^+$, but at a pH higher than 2.5, an acidity dependence was noted.

Grundler *et al*.[109] reported the water exchange of *fac*-$[Mn(CO)_3(H_2O)_3]^+$, *fac*-$[^{99m}Tc(CO)_3(H_2O)_3]^+$ and *fac*-$[Re(CO)_3(H_2O)_3]^+$ as shown in Table **2-2**, and observed that the water exchange rate decreases down group 7 from Mn to Tc and Re with water exchange rates of 23, 0.49 and 5.4 x 10^{-3} s^{-1}respectively.[109,110]

Table 2-2: Selected kinetic data for the water exchange of the aqua complexes *fac*-$[M(CO)_3(H_2O)_3]^+$ (M = Mn, Tc, Re).

	k_{ex} (s^{-1})	$\Delta S^{\ddagger}$ ($JK^{-1}mol^{-1}$)	$\Delta H^{\ddagger}$ (kJ mol^{-1})	$\Delta V^{\ddagger}$ ($cm^{-3}mol^{-1}$)	pK_a
***fac*-$[Mn(CO)_3(H_2O)_3]^+$**[109]	23	+24.4	72.5	+7.1	9-10
***fac*-$[Tc(CO)_3(H_2O)_3]^+$**[109]	0.49	+11.7	78.3	+3.8	-
***fac*-$[Re(CO)_3(H_2O)_3]^+$**[108,109]	6.3 x 10^{-3}, 5.4 x 10^{-3}	+14.5	90.3	-	7.5

2.7.2 The substitution of water ligands in *fac*-$[M(CO)_3(H_2O)_3]^+$

It is important to investigate the kinetic behaviour and mechanism of these *fac*-$[M(CO)_3(H_2O)_3]^+$ complexes with different ligands. During the preparation of a radiopharmaceutical, the complex formation reaction must be a complete and fast reaction, as the half-life of the radionuclide has a significant impact.

$$fac\text{-}[M(CO)_3(H_2O)_3]^+ + L \underset{k_{-1}}{\overset{k_1}{\rightleftharpoons}} fac\text{-}[M(CO)_3(H_2O)_2(L)]^n + H_2O \qquad K_1 = \frac{k_1}{k_{-1}}$$

$$fac\text{-}[M(CO)_3(H_2O)_2(L)]^n + L \underset{k_{-2}}{\overset{k_2}{\rightleftharpoons}} fac\text{-}[M(CO)_3(H_2O)(L)_2]^n + H_2O \qquad K_2 = \frac{k_2}{k_{-2}}$$

$$fac\text{-}[M(CO)_3(H_2O)(L_2)]^n + L \underset{k_{-3}}{\overset{k_3}{\rightleftharpoons}} fac\text{-}[M(CO)_3(L)_3]^n + H_2O \qquad K_3 = \frac{k_3}{k_{-3}}$$

Scheme 2-19: Proposed water substitution mechanism by monodentate ligands (M = Mn, Tc, Re).

[109] Grundler, P.V., Helm, L., Alberto, R., Merbach, A.E. *Inorg. Chem*. **45** (2006) 10378-10390.
[110] Grundler, P.V., Salignac, B., Cayemittes, S., Alberto, R., Merbach, A.E., *Inorg. Chem*. **43** (2004) 865-873.

The water molecules in *fac*-$[M(CO)_3(H_2O)_3]^+$ can be readily substituted by monodentate ligands. Scheme **2-16** above shows the kinetic mechanism of water molecules sequentially substituted by monodentate ligands with equilibrium constants K_i (i = 1, 2 and 3).

The equilibrium and rate constants for the water substitution reaction with varied entering ligands for *fac*-$[Re(CO)_3(H_2O)_3]^+$ as reported by Grundler *et al*.[110] is summarised in Table **2-3**.[110] A chemical 'attraction' of the metal for the S-binding ligands compared to the N-binding ligands is observed in the fast water substitution rate for the S-binding ligands compared to the N-binding ligands.

From Table **2-3,** the formation rate of *fac*-$[Re(CO)_3(H_2O)_3]^+$ from the reverse reaction rate constant (k_{-1}) can be seen and Grundler *et al*.[110] found that from Pyz to Br^-, k_{-1} increases in three orders of magnitude. The basic character and the change in nucleophilicity ability of each species, which is inversely related to each other, can explain this phenomenon. Br^- with a pk_a value of -4.7 (HBr) is the fastest leaving group compared to Pyz, which is the slowest leaving group with a pk_a value of 0.6 ($HPyz^+$). A plot of log k_{r1} vs log k_1 for the data reported by Grundler *et al*. yielded a slope of 0.73(6) which is not totally in agreement with the general principle of a linear free energy relationship, and therefore the mechanism proposed is much less indicative of a dissociative character, which would have yielded a slope of 1. These observations are confirmed by the substitution rate constant being close to the water exchange rate (k_{ex}), but there is a clear discrimination between nucleophiles (k_i) and it therefore indicates that the nucleophiles might coordinate to the Re(I) metal centre in an I_a transition state.

The activation volumes of the different reactions are positive for N-bonded ligands (Pyz, $\Delta V^{\ddagger}$ = +5.4 $cm^3\ mol^{-1}$) and negative for S-bonded ligands (THT, $\Delta V^{\ddagger}$ = -6.6 $cm^3\ mol^{-1}$; DMS, $\Delta V^{\ddagger}$ = -12 $cm^3\ mol^{-1}$). This disagrees with the previous results by Grundler *et al*.[110] and a changeover mechanism from an I_d (for the harder O- and N-donor ligands) to an I_a (for the softer S- and N-doner ligands) is concluded during the complex formation. Grundler *et al*.[110] observed that the rates of the substitution reactions are in the same order of magnitude as the water exchange rates and predicted a dissociation type mechanism in both cases. The kinetic data for the water substitution reactions for *fac*-$[M(CO)_3(H_2O)]^+$ (M = Mn, Tc, Re) by Grundler *et al*.[109,110]

with monodentate incoming ligands acetonitrile (CH_3CN), water (H_2O), dimethyl sulfide (DMS) and pyridine (Py) are reported in Table **2-3**.[109,110]

Table 2-3: The kinetic data for the water substitution reactions for *fac*-$[M(CO)_3(H_2O)_3]^+$ (where M = Mn, ^{99m}Tc and Re) at 25 ˚C.[109,110]

***fac*-$[Mn(CO)_3(H_2O)_3]^{+}$[109]**								
	CH_3CN	**H_2O**	**DMS**	**Pyz**	**THT**	**TU**	**Br^-**	**CF_3COO^-**
$K_1(M^{-1})$	4.5±0.2	-	25.2±0.5	-	-	-	-	-
$10^3k_{f,1}$ $(M^{-1}s^{-1})$	1 750±400	-	5340±2000	-	-	-	-	-
$10^3k_i'$ (s^{-1})	29 000	23 000±4000	89 000	-	-	-	-	-
$\Delta H_{f,1}^{\ddagger}$(kJ mol^{-1})	83.9±5	72.5±3	71.2±12	-	-	-	-	-
$\Delta S_{f,1}^{\ddagger}$(JK^{-1} mol^{-1})	+41.3±16	24.4±8	+8.1±38	-	-	-	-	-
$\Delta V_{f,1}^{\ddagger}$(cm^{-3} mol^{-1})	+4.2±1.2	+7.1±2.0	+11.3±0.6	-	-	-	-	-
***fac*-$[^{99m}Tc(CO)_3(H_2O)_3]^{+}$[109]**								
$K_1(M^{-1})$	2.9±0.1	-	14.9±0.1	-	-	-	-	-
$10^3k_{f,1}$ $(M^{-1}s^{-1})$	39.9±1	-	60.8±0.8	-	-	-	-	-
$10^5k_i'$ (s^{-1})	6.65	4.90±50	10.10	-	-	-	-	-
$\Delta H_{f,1}^{\ddagger}$(kJ mol^{-1})	77.8±8	78.3±1	70.6±3	-	-	-	-	-
$\Delta S_{f,1}^{\ddagger}$(JK^{-1} mol^{-1})	-10.0±27	+11.7±3	-31.1±10	-	-	-	-	-
$\Delta V_{f,1}^{\ddagger}$(cm^{-3} mol^{-1})	-	+3.8±2	-	-	-	-	-	-
***fac*-$[Re(CO)_3(H_2O)_3]^{+}$[109,110]**								
$K_1(M^{-1})$	4.8±0.5	-	8.3±0.1	237±15	41±1	160±8	0.7±0.3	0.82±0.02
$10^3k_{f,1}$ $(M^{-1}s^{-1})$	0.76±0.04	-	1.18 ± 0.06	1.06±0.05	1.28±0.07	2.49±0.09	1.6±0.3	0.81±0.01
10^5k_{-1} (s^{-1})	16	-	14.2	0.45	3.05	1.6	230	99
$10^5k_i'$ (s^{-1})	0.127	0.054±0.002	0.20	0.177	0.21	0.415	0.058	0.029
$\Delta H_{f,1}^{\ddagger}$(KJ mol^{-1})	98.6±3	90.3±2	-	-	-	-	-	-
$\Delta S_{f,1}^{\ddagger}$(JK^{-1} mol^{-1})	+26.6±10	+14.5±8	-	-	-	-	-	-
$\Delta V_{f,1}^{\ddagger}$(cm^{-3} mol^{-1})	-	-	-12±1	+5.4±1.5	-6.6±1	-	-	-

Pyz = pyrazine, DMS = dimethylsulfide, THT = tetrahydrothiophene, TU = thiourea, K_1 = equilibrium constant , $k_{f,1}$ = formation rate constant , k_{-1} = reverse reaction rate constant, k_i' = interchange rate constant , $\Delta H_{f,1}^{\ddagger}$ = enthalpy of activation , $\Delta S_{f,1}^{\ddagger}$ = entropy of activation, $\Delta V_{f,1}^{\ddagger}$ = volume of activation.

2.7.3 Substitution reactions in *fac*-$[Re(CO)_3(X)(L,L'\text{-Bid})]^n$ type complexes

The "2 + 1" ligand system is defined as a mixed ligand concept and is based on *fac*-$[M(CO)_3(X)_3]^n$ (M = Re, Tc, X = H_2O/MeOH, n = 0,+1) containing three stable CO monodentae ligands and three labile ligands that are substituted by one bidentate and one monodentate ligand.[111] The complexes of the type *fac*-$[Re(CO)_3(X)(L,L'\text{-Bid})]^n$ (*L,L'*-Bid = bidentate ligands, X = H_2O/MeOH, n = 0,+1) are considered as potential radiopharmaceuticals.[111]

[111] Abram, U., Alberto, R. *J. Braz. Chem. Soc*. **17**(8),(2006), 1486-1500.

In 2011, Schutte *et al*.[42] investigated a range of Re(I) tricarbonyl complexes and evaluated the reactivity by substituting the 6th position (H_2O/MeOH) by various incoming monodentate ligands. In this study it was confirmed that when dissolving the aqua complexes (*fac*-[$Re(CO)_3(H_2O)$(*L,L'*-Bid)] in methanol, the H_2O ligand is substituted with methanol to form the methanol complex (*fac*-[$Re(CO)_3$(MeOH)(*L,L'*-Bid)].

The complexes that were used in the metanol substitution kinetics were *fac*-[$Re(CO)_3$(MeOH)(*L,L'*-Bid)]^n (*L,L'*-Bid = 2,2'-bipyridine (Bipy), 1,10-phenanthroline (Phen), 2,4-dipicolinate (2,4-dPicoH), 2,4-diquinolinate (2,4-dQuinH), 2-picolinate (Pico), 2-Quinolinate (Quin), tribromotropolonate ($TropBr_3$), hydroxyflavonate (Flav), n = 0, +1). The monodentate ligands that were used as entering ligands were chloride (Cl^-), bromide (Br^-), iodide (I^-), pyridine (Py), meta-methylpyridine (*m*Mepy), para-methylpyridine (*p*Mepy), 1,3,5-triaza-7-phosphadamantane (PTA), imidazole (Im), 4-dimethylaminopyridine (DMAP), thiocyanate ions (NCS^-), thiourea (TU) and 1-methyl-2-thiourea (MeTU). The kinetic data obtained for the eight Re(I) tricarbonyl complexes are reported in Table **2-4**.

From the data in Table **2-4**, the k_1 values for the halides (Cl^-, Br^- and I^-) as the entering monodentate ligands are comparable for the reactions of *fac*-[$Re(CO)_3$(MeOH)(Bipy)]$^+$ and *fac*-[$Re(CO)_3$(MeOH)(Phen)]$^+$ and it was observed that these rate constants are 300 - 400 times faster than the values obtained for the neutral pyridine type ligands, 4 times faster than the value of PTA and twice as fast as the value obtained for MeTU. The higher affinity of the positively charged metal complex for the negatively charged entering halide ions indicate an associative mode of activation.

Table 2-4: The rate and equilibrium constants for the reaction between the Re(I) tricarbonyl complexes with various entering ligands by Schutte *et al*.[42]

Entering ligands	10^3k_1 ($M^{-1}s^{-1}$)	10^3k_{-1} (s^{-1})	10^3K_1[b] (M^{-1})	10^3k_1 ($M^{-1}s^{-1}$)	10^3k_{-1} (s^{-1})	10^3K_1[b] (M^{-1})
	***fac*-[Re(CO)$_3$(MeOH)(Bipy)]$^+$**			***fac*-[Re(CO)$_3$(MeOH)(Phen)]$^+$**		
Cl$^-$	17(2)	0.16(1)	100(11)	36(4)	0.41(3)	87(11)
Br$^-$	42(7)	0.65(1)	60(8)	50(3)	0.59(3)	84(7)
I$^-$	49(3)	0.68(1)	70(5)	53(1)	0.7(1)	76(11)
Py	0.096(1)	0.0012(1)	8.0(7)	0.064(3)	0.0058(4)	11(1)
***m*-Mepy**	0.025(1)	0.008(1)	3.0(4)	0.012(1)	0.0058(4)	11(1)
***p*-Mepy**	0.028(1)	0.00847(1)	5.0(2)	0.014(1)	0.0035(1)	4.0(3)
PTA	12.3(1)	0.12(2)	100(20)	7.9(1)	0.11(1)	70(9)
Metu	17.3(1)	0.011(1)	157(14)	13.7(1)	0.11(1)	120(11)
	***fac*-[Re(CO)$_3$(MeOH)(2,4-dPicoH)]**			***fac*-[Re(CO)$_3$(MeOH)(2,4-dQuinH)]**		
Br$^-$	15.7(2)	0.63(8)	25(3)	-	-	-
Py	1.641(8)	0.030(2)	21(1)	3.31(2)	0.051(7)	65(9)[c]
DMAP	3.21(4)	0.11(1)	29(3)	6.52(9)	0.025(3)	260(30)[d]
Pz	2.336(9)	0.016(3)	146(27)	-	-	-
Im	1.44(4)	0.070(5)	21(2)	-	-	-
	***fac*-[Re(CO)$_3$(MeOH)(Pico)]**			***fac*-[Re(CO)$_3$(MeOH)(Quin)]**		
Br$^-$	11.8(1)	0.8(1)	15(2)	29.6(3)	0.7(1)	42(6)
I$^-$	14(1)	0.64(1)	22(2)	28.0(1)	0.9(1)	31(4)
Py	1.6(1)	0.0084(1)	190(10)	3.9(1)	0.02(1)	195(97)
	***fac*-[Re(CO)$_3$(MeOH)(TropBr$_3$)]**			***fac*-[Re(CO)$_3$(MeOH)(Flav)]**		
Br$^-$	70.6(4)	4(1)	18(4)	$7.2(3)\times10^3$	$3.17(9)\times10^3$	2.5(2)
Py	20.3(7)	1.6(2)	12.2(2)[e]	$1.38(8)\times10^3$	0.3(1)	$4.6(1)\times10^3$
DMAP	34.5(7)	0.26(2)	133(11)[f]	$5.1(2)\times10^3$	0.16(4)	$3.2(8)\times10^3$

In the case of Py and *m*Mepy as entering monodentate ligands for the reaction of *fac*-[Re(CO)$_3$(MeOH)(Bipy)]$^+$ and *fac*-[Re(CO)$_3$(MeOH)(Phen)]$^+$, the more sterically hindered *m*Mepy reacted 4 - 6 times slower than its unsubstituted hindered counterpart. A similar observation was obtained for *p*Mepy. Salignac *et al*.**[108]** obtained a value of 1.6(3) $x10^{-3}$ $M^{-1}s^{-1}$ for the formation of *fac*-[Re(CO)$_3$(Br)(H$_2$O)$_2$] which is 20 to 30 times slower than the corresponding reactions of the Bipy and Phen complexes, indicating that the bidentate ligands activate the Re(I) metal center to a small extent. The rate of formation, k_1, for the reaction of *fac*-[Re(CO)$_3$(MeOH)(2,4-dPicoH)] with Br^- is 5 - 7 times faster than the reaction with the neutral ligands. The k_1 values decrease for Br^- > DMAP > Py, Pz, Im possibly due to the pk_a values of HBr, DMAP, imidazole, pyridine and pyrazole which are -4.7, 9.8, 6.99, 5.25 and 2.49 respectively. This points towards an associative activated mechanism and the

negative $\Delta S^{\ddagger}$ values for the reactions of *fac*-[Re(CO)$_3$(MeOH)(2,4-dPicoH)] suggests an I_a type mechanism. When comparing the cationic *N,N'*-bidentate complexes with the neutral *N,O*-bidentate complexes, an increase in the forward rate constant is observed for the Br^- entering ligand in the *N,N'*- bidentate complexes. The other entering ligands result in the opposite with a higher k_1 value for the *N,O*-bidentate complexes.

In the *O,O'*-bidentate complexes a large increase is observed from the reaction of Br^- with *fac*-[Re(CO)$_3$(MeOH)(TropBr$_3$)] to *fac*-[Re(CO)$_3$(MeOH)(Flav)]. This is due to the electrondrawing effects of the bromide atoms on the tribromotropolone ligand. The data for the neutral *O,O'*- and *N,O*-bidentate complexes tend to suggest an I_d mechanism while the cationic *N,N'*-complexes suggest and I_a mechanism. It is clear that the *O,O'*-bidentate complexes, particularly the flavone ligand, activate the rhenium metal centre more than the *N,O*- and *N,N'*-bidentate complexes. Overall, it was found that an increase in electron density on the rhenium metal centre increases the rate of the substitution reaction. However no definable conclusion could be made regarding the mechanism, with the uncertainties in the $\Delta S^{\ddagger}$ values making the *O,O'*-bidentate complexes comparable to the *N,N'*- and *N,O'*-bidentate complexes.

Schutte *et al*.[112] then reported the aqua substitution kinetics of *fac*-[Re(CO)$_3$(H$_2$O)(Trop)] (with TropH = tropolone) in aqueous medium. Thiocyanate was used as entering monodentate ligand. It was found that the substitution of H_2O by thiocyanate ions in aqueous medium is faster than the corresponding methanol substitution in methanol with one order of magnitude. This is indicative of an I_d activation mechanism where different leaving groups have an effect on the forward rate constant while, the reverse reaction rate constant, where NCS^- is the leaving group in both cases, are fairly similar.

Brink *et al*.[113,114] extended this study, where the methanol substitution in neutral *fac*-[Re(CO)$_3$(MeOH)(*N,O*-Bid)] complexes were investigated. Four different monodentate ligands pyridine (Py), 4-dimethylaminopyridine (DMAP), 3-chloropyridine (3-ClPy) and 4-picoline (4-Pic) were used as entering ligands. The rate constants for all the methanol substitution reactions between *fac*-

[112] Schutte, M., Roodt, A., Visser, H.G. *Inorg. Chem*. **51** (2012) 11996-12006.
[113] Brink, A., Visser, H.G., Roodt, A. *Inorg. Chem*. **52** (2013) 8950-8961.
[114] Brink, A., Visser, H.G., Roodt, A. *Inorg. Chem*. **53** (2014) 12480-12488.

[Re(CO)$_3$(MeOH)(Sal-*m*Tol)] (Sal-mTol = 2-(m-tolyliminomethyl)phenol) and the entering monodentate ligands are tabulated in Table **2-5**. When focusing on the pk_a of the entering monodentate ligands, the rate of the reaction of *fac*-[Re(CO)$_3$(MeOH)(Sal-mTol)] with the range of monodentate ligands decrease as the pk_a value increases: 3-ClPy < Py < 4-Pic < DMAP. The results are opposite to what was expected for an I_a mechanism. The positive value of $\Delta S^{\ddagger}$ as well as the non-linear rate plots suggested an I_d type mechanism.

Table 2-5: A summary of the rate constants of the methanol substitution reactions between *fac*-[Re(CO)$_3$(MeOH)(Sal-*m*Tol)] and different entering ligands at 25 ºC.[113,114]

Ligands	Py	DMAP	3-ClPy	4-Pic
k_1 (M^{-1} s^{-1})	1.29 (2)	-	2.33 (1)	1.27 (5)
k_{-1} (M^{-1} s^{-1})	0.019 (5)	-	0.026 (3)	0.05 (2)
K_1 (M^{-1})	67 (18)	-	91 (11)	25 (10)
pK_a	5.23	9.8	2.81	5.99

Brink *et al*. found that the rate constant (k_1) of the reaction between *fac*-[Re(CO)$_3$(MeOH)(Sal-mTol)] and pyridine are faster than the rate constants obtained by Schutte *et al*.[42] for other *N,O*-bidentate ligands as shown in Table **2-6**.

Table 2-6: A comparison of the k_1 rate constant values for various *N,O*-bidentate complexes with pyridine as entering ligand.

N,O-bidentate complexes	k_1 ($M^{-1}s^{-1}$)
***fac*-[Re(CO)$_3$(MeOH)(Sal-*m*Tol)]**[113]	1.29 (2)
***fac*-[Re(CO)$_3$(MeOH)(Sal-*p*Tol)]**[113]	1.393 (3)
***fac*-[Re(CO)$_3$(MeOH)(Sal-Ph)]**[113]	1.26 (2)
***fac*-[Re(CO)$_3$(MeOH)(Sal-3MeBu)]**[113]	1.79 (2)
***fac*-[Re(CO)$_3$(MeOH)(Sal-CylHexl)]**[113]	2.03 (6)
***fac*-[Re(CO)$_3$(MeOH)(Pico)]**[113]	1.6 (1)
***fac*-[Re(CO)$_3$(MeOH)(Quin)]**[42]	3.9 (1) x10^{-3}
***fac*-[Re(CO)$_3$(MeOH)(2,4-PicoH)]**[116]	1.641 (8) x10^{-3}
***fac*-[Re(CO)$_3$(MeOH)(2,4-Quin)]**[42]	3.31 (2) x10^{-3}

Sal-*m*Tol = 2-(m-Tolyliminomethyl)phenol; Sal-*p*Tol = 2-(o-Tolyliminomethyl)phenol; Quin = 2-quinolinate; Pico = 2-picolinate; Sal-Ph = 2-(phenyliminomethyl)phenol; Sal-3MeBu = 2-(3-Methylbutyliminomethyl)phenol; 2,4-PicoH = 2,4-dipicolinate; Sal-CylHexl = 2-(Cyclohexyliminomethyl)phenol; 2,4-Quin = 2,4-diquinolinate.

In 2019, Schutte-Smith *et al*.[75] expanded the work by investigating the methanol substitution reactions of *fac*-[Re(CO)$_3$(MeOH)(Trop)] (where TropH = tropolone) with a range of nucleophiles namely pyridine (Py), 4-dimethylaminopyridine (DMAP), imidazole (Im), thiourea (TU), 1-methyl-2-thiourea (MeTU), bromide (Br^-), and iodide (I^-) at variable temperatures and at ambient and high pressure. All the rate constants of the methanol substitution reactions are tabulated in Table **2-7**.

Table 2-7: Kinetic data and activation parameters for the methanol substitution in *fac*-[Re(CO)$_3$(MeOH)(Trop)] at 25˚C with different entering ligands at ambient[a] (eight ligands) and evelated pressures[b] (four ligands).

Ambient pressure					
		Entering ligands			
	P (MPa)	Br^-	I^-	DMAP	NCS^-
k_1 ($M^{-1}s^{-1}$)	[a]	0.505±0.004	0.765±0.002	0.341±0.002	0.268±0.002
k_{-1} (s^{-1})	[a]	0.477±0.001	0.674±0.001	0.0017±0.0001	0.004±0.0002
K_1 (M^{-1})	[a]	1.06±0.01	1.14±0.01	201±9	61±3
$\Delta H^{\neq}_{(k1)}$ (kJ mol^{-1})	[a]	76.1±0.6	75.3±0.9	61±2	62.2±2
$\Delta S^{\neq}_{(k1)}$ ($Jk^{-1}mol^{-1}$)	[a]	5±2	6±3	-47±7	-48±6
Elevated pressure					
	P[b] (MPa)	Br^-	I^-	DMAP	NCS^-
k_{obs}	0.6	(17.7±0.3) x10^{-3}	(11.3±0.7) x10^{-3}	(34.2±0.3) x10^{-3}	(42±1) x10^{-3}
	5	(17.2±0.4) x10^{-3}	(11.1±0.7) x10^{-3}	(33±2) x10^{-3}	(40.9±0.7) x10^{-3}
	10	(16.9±0.8) x10^{-3}	(10.7±0.3) x10^{-3}	(32±1) x10^{-3}	(38.9±0.6) x10^{-3}
	50	(14.5±0.9) x10^{-3}	(9.29±0.09) x10^{-3}	(28±1) x10^{-3}	(31.6±0.6) x10^{-3}
	80	(13.1±0.7) x10^{-3}	(8.1±0.2) x10^{-3}	(24.6±0.7)	(26.2±0.9) x10^{-3}
	100	(12.3±0.3) x10^{-3}	(7.55±0.7) x10^{-3}	(25.5±0.6)	(23.4±0.3) x10^{-3}
k_1 ($M^{-1}s^{-1}$)[c]		0.287±0.003	0.263±0.001	0.556±0.003	0.626±0.002
k_{-1} (s^{-1}) [c]		(0.46±0.09) x10^{-3}	(0.07±0.01) x10^{-3}	(0.95±0.01) x10^{-3}	(1.84±0.05) x10^{-3}
K_1 (M^{-1}) [c,d]		(6.2±1.2) x10^{-2}	(3.8±0.5) x10^{-3}	(5.9±0.6) x10^{-2}	(3.4±0.1) x10^{-2}
K_1 (M^{-1}) [c,e]		(1.0±0.3) x10^{-3}	(2.0±0.5) x10^{-3}	(3.7±0.4) x10^{-2}	(5.3±0.6) x10^{-2}
$\Delta H^{\neq}_{(k1)}$ (kJ mol^{-1}) [c]		61.8±0.7	64.7±0.9	58.0±0.7	59.0±0.4
$\Delta S^{\neq}_{(k1)}$ ($Jk^{-1}mol^{-1}$) [c]		-48±2	-39±3	-55±2	-51±1
$\Delta V^{\neq}_{(k1)}$(cm^3 mol^{-1})		9.0±0.2	10.1±0.2	10.0±0.3	14.3±0.3

[a] Ambient pressure; [b] Elevated pressure; [c] Calculated at 298 K and 0.101 MPa; [d] From kinetic data, $K_1 = k_1/k_{-1}$, [e] thermodynamically determined.

From the ambient pressure data, the forward rate constant, k_1, for eight different entering ligands differ by less than a factor of three and the solvolysis rate constant, k_{-1}, for these entering ligands differ by almost four orders of magnitude. This is a classic indication of a dissociative activation mechanism considering a general trend observed with respect to the ligand strength as manifested in the spectrochemical series, with the halides I^- and Br^- forming the weakest bond with the Re(I) metal centre and Py and DMAP the strongest bond.[42,115]

The overall possible substitution processes for the high-pressure kinetics study by Schutte-Smith *et al*.[75] is illustrated in Scheme **2-20**. The process is constructed to present an interchange activation with a transition state **b** or a pure dissociative activation through a formal intermediate **d**.

[115] Schutte, M., Visser, H.G., *Polyhedron*. **89** (2015) 122-128.

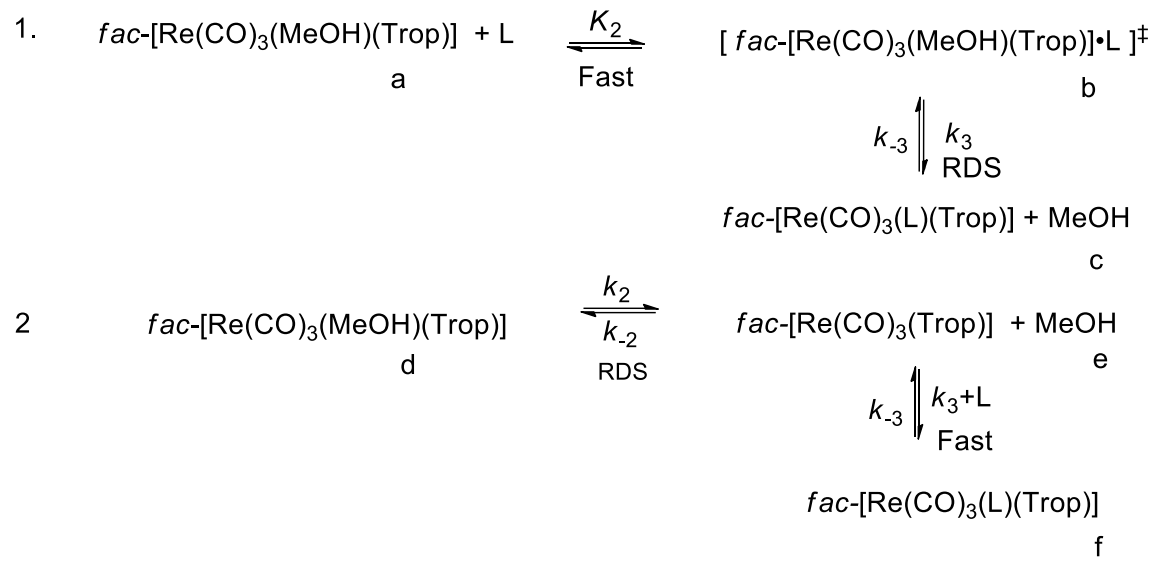

Scheme 2-20: Chemical reaction scheme representing two possibilities for the substitution of methanol from the *fac*-[Re(CO)$_3$(MeOH)(Trop)] complex.

The $\Delta V^{\neq}_{(k1)}$ values obtained in the four reactions during the study were all in the same range of 9 to 10 cm^{-3}mol^{-1}, except for 14.5±0.3 cm^{-3}mol^{-1} for the reaction with MeTU. This is expected in an interchange pathway since the pressure contribution to the preliminary outer sphere equilibrium (K_2 in Scheme **2-17**) is expected to be dependent on the relative partial molar volume of the entering ligand, however, in this case MeTU being some 10 -15 % larger than that of pyridine.

In Scheme **2-20**, the rate determining first step ($K_3 = k_3/k_{-3}$) wherein the dissociation of methanol dominates through formal intermediate **b** with a small or negligible entering ligand assistance, yield a variable option for the overarching methanol substitution process. The partial molar volume of methanol as the leaving group is larger (more than twice that of water: ca. 38 *vs* 18 cm^{3}mol^{-1}, respectively) and potentially implies a significant larger effect than water as a leaving group on the experimental activation volume due to changes in the first and second solvent coordination spheres. The corresponding reactions where water vs. methanol is being substituted are expected to show a progressive significant increase in the experimental volume of activation and it was not observed during that study.[112] An explanation for the smaller than expected experimental activation volume in a pure dissociative activation was reported to possibly be linked to the fact that the methyl group of the methanol molecule already penetrates the 2nd coordination sphere and that the dissociation thereof does not reflect its complete partial molar volume. However, this was considered speculative with only their current data at hand. In

spite of this, the seemingly "small" experimental volumes obtained were still relatively larger positives compared to other studies [+10 to 14 cm^3mol^{-1} vs +4 cm^3mol^{-1}]**[112]**. They concluded that there might be a larger drive in the *fac*-[$Re(CO)_3$(MeOH)(Trop)] complex towards a more dissociative character than the pure water system reported by Schutte-Smith *et al*.**[116]** and that a pure dissociative activation is indeed a very real option.

Table 2-8: The activation enthalpy and entropy data for a range of *fac*-[$Re(CO)_3$(MeOH)(L,L'-Bid)]^n type complexes. Enthalpy values ($\Delta H^{\neq}_{(k1)}$ kJ mol^{-1}) are followed by the entropy values, ($\Delta S^{\neq}_{(k1)}$ Jk^{-1} mol^{-1}).

Re-(*L,L'*-Bd)	Br^-	I^-	NCS^-	Py	Im	DMAP	TU	MeTU
Re-Phen[42]		70±1, -35±3						80±1, -9±1
Re-2,5-PicoH[115]	79.7±5, -15±2	77±1, -22±4	82.5±0.5, -19±2	82±1, -25±4	84±2, -19±6		70±1, -44±4	68±1, -49±4
Re-dPicoH[42]	80.8±0.6, -8±2			84±2, -19±4	85.2±0.7, -13±2	84.3±0.3, -10±1		
Re-Pico[42]		77±1, -19±3		84±1, -16±4				
Re-Isa[116]			87.7±0.7, -14±2	79.0±0.5, -13±2			78.9±0.5, -8±2	
Re-Flav[42]	52±5, -52±15			54±6, -60±21		84±4, -51±14		
Re-TropBr3[42]	63±6, -54±19			53±5, -102±17		69±4, -42±12		
Re-Trop[42,112]	76.1±0.6, 5±2	75.3±0.9 , 6±3	62±2, -48±6, 56.1±0.7, -49±2	64.7±0.9, -39±3	61.8±0.7, -48±2	61±2, -48±2	58.0±0.7, -55±2	59.0±0.4, -51±1
Re-Sal-*m*Tol[43]				92±2, 66±7		88±2, 53±6		
Re-Quin[116]								
	PTA	**PPh_3**	**PCy_3**					
Re-Trop[74]	72±2, -12±6	70±1, -16±5	67±2, -67±7					
Re-Flav[74]	51±3, -61±12	56±4, -39±13	49±2, -74(9)					

Re= *fac*-[$Re(CO)_3$(MeOH)]; Phen = 1,10-phenanthroline; 2,5-PicoH = pyridine-2-carboxylato-5-carboxylic acid, Pico = 2-picolinate; Isa = isatin; Flav = hydroxyflavonate; TropBr3 = tribromopolonate ; Trop = tropolone; Sal-*m*Tol = 2-(m-Tolyliminomethyl)phenol ; Quin = 2-quinolinate.

The activation parameter data of a range of kinetic studies of *fac*-[$Re(CO)_3$(MeOH)(L,L'-Bid)] type complexes have been combined and the data are summarized in Table **2-8**.

When comparing the activation enthalpy data ($\Delta H^{\ddagger}_{(k1)}$) in Table **2-8** of the different metal complexes with different entering mondentate ligands, it varies by 30 kJ mol^{-1}, from around 50 kJ mol^{-1} to just over 80 kJ mol^{-1}. The results obtained in Table **2-8** indicates a significant rate increase of almost four orders of magnitude activation from the neutral 1,10-phenanthroline to the most basic flavone and the tropolone.

[116] Schutte, M., Roodt, A., Visser, H.G. *Inorg. Chem*. **51**(21) (2012) 11996-12006.

Based on a different set of entering ligands (Br^-, I^-, NCS^-, Py, Im, DMAP, TU, MeTU, PTA, PPh_3, PCy_3) when changing the bidentate ligands in *fac*-[$Re(CO)_3$(MeOH)(L,L'-Bid)], results in a significant activation of the metal center and also relates to the electron donating ability of the bidentate ligands. The better the electron donor ligand, the faster the reaction, which is also indicative of a dissociative activation.

When comparing the activation entropy data ($\Delta S^{\ddagger}_{(k1)}$) in Table **2-8**, a fairly negative value of -102 $JK^{-1}mol^{-1}$ is obtained for the reaction of *fac*-[$Re(CO)_3$(MeOH)($TropBr_3$)] with pyridine as entering monodentate ligand; though with a very large e.s.d, to slightly positive values. The $\Delta S^{\neq}_{(k1)}$ values varying from ca -50 $JK^{-1}mol^{-1}$ to +6 $JK^{-1}mol^{-1}$ (*fac*-[$Re(CO)_3$(MeOH)(Flav)] with iodide as entering monodentate ligand) represented a better estimated range. However, this narrow range of the activation entropy values, although not convincing to indicate a specific activation, may hit at least at a similar type of activation for these substitution reactions over a broad range of bidentate ligand variables and corresponding reactivities.

2.8 Photoluminescence

2.8.1 Introduction

β-Diketone, β-hydroxyketone and bipyridine ligands are among the most important ligands for luminescence purposes due to their ability to form stable complexes and have strong absorption within a large wavelength range for its π-π* transition that sensitizes the luminescence of the metal ions.

In 1888, the German physicist and science historian Eilhard Wiedemann introduced the term “luminescenz” for all phenomena of light that are not caused by the rise in temperature, which is called incandescence. The definition of luminescence is the spontaneous emission of radiation from an electronically or vibrationally excited species not in thermal equilibrium with its environment.[117] The different types of luminescence are classified based on the excitation mode. Photoluminescence is the emission of light coming from the direct photo-excitation of the emitting species.

[117] Valeur, B., Berberan-Santos, M.N. *J. Chem. Educ*. **88** (2011) 731-738.

Phosphorescence, fluorescence and delayed fluorescence are a form of photoluminescence.[118,119,120] When photo-excitation takes place, electrons move to permissible excited states. When these electrons return to its equilibrium/ground states, the excess energy released can be in the form of emission of light. Following the absorption of light in materials is a valuable tool in many scientific and technological fields such as chemistry, biology, medicine, physics and material science. Many applications based on photoluminescence have been developed, namely forensics, optical brighteners, plasma screen phosphorescent labels, safety signs, fluorescence microscopy and fluorescent tubes.[121,122,123]

Mononuclear *fac*-Re(I) tricarbonyl complexes attracted many researcher's attention in nuclear medicine due to its ground and excited state properties, while the β-diketone and β-hydroxyketone *O,O'* bidentate ligands and bipyridine *N,N'* bidentate ligands also draw continuing attention to radiopharmaceuticals due to their photolumuniscence properties.

2.8.2 Fluorescence and phosphorescence

Fluorescence is the emission of light by a substance that has absorbed light or other electromagnetic radiation and it is a form of luminescence. The process where a fluorescence signal is reduced and phosphorescence is generated is called intersystem crossing while the quantum mechanical process that is responsible for intersystem crossing is spin-orbit coupling. The intersystem crossing explains the relaxation of the molecule from a singlet excited state to the triplet excited state (lower energy). The intersystem crossing rate is low, since the spin-orbit coupling is a weak effect. The relaxation from the triplet state to the singlet ground state requires

[118] Valeur, B. *From Well-Known to Underrated Applications of Fluorescence. In Fluorescence of Supermolecules, Polymers and Nanosystems; Springer Series on Fluorescence*, Vol. 4; Berberan-Santos, M.N., Ed.; Springer Verlag: Berlin, 2008.
[119] Braslavsky, S.E. *Pure Appl. Chem*. **79** (2007) 293- 65.
[120] Valeur, B. *Molecular Fluorescence. In Encyclopædia of Applied Spectroscopy*; Andrews, D., Ed.; Wiley-VCH: Weinheim, 2009; pp 477-532.
[121] Valeur, B. *Molecular Fluorescence: Principles and Applications*; Wiley-VCH: Weinheim, 2002.
[122] *Molecular Luminescence Spectroscopy*; Schulman, S. G., Ed.; Wiley Interscience: New York, 1993; Parts 1-3.
[123] Lakowicz, J.R. *Principles of Fluorescence Spectroscopy*, 3rd ed.; Springer: New York, 2006.

another change of multiplicity and has a very low rate. Radiative relaxation phosphorescence does occur due to spin-orbit coupling.[124,125]

Phosphorescence is the light energy produced by a type of chemical reaction where the excess chemical energy of the reactants is given off as light energy. The typical phosphorescence life-time is approximately microseconds to seconds. Phosphorescence has a larger stokes shift than fluorescence owing to the triple state having lower energy. Since the phosphorescence rate is often much lower than thermally activated non-radiative decay processes such as collisional quenching, phosphorescence is rarely observed in aqueous systems at physiological temperature. A number of protein conformation studies at cryogenic temperatures have utilized phosphorescence spectroscopy.[124,126] The quantum yield of a fluorophore is defined as the ratio of the number of emitted photons divided by the number of absorbed photons.[124,126]

2.8.3 Photodynamic therapy

2.8.3.1 Introduction

Hundred years ago, photodynamic therapy was discovered during a study of the interaction of fluorescent dyes on infusaria.[127,128] A German medical student in Munich named Oskar Raab discovered that the intense light applied to the dye resulted in the fast destruction of these microorganisms. Jesionek and von Tappeiner described the new light-based therapy formally and they coined the ablative process, “photodynamicsche winrkung”, best translated as the photodynamic reaction (PDR) and thereafter photodynamic therapy (PDT) was born. In the early 1900’s this process successfully treated a wide variety of cancer patients.[129,130] Regardless of this early successes, when PDR was discovered by Lipson *et al*.[130], PDT did not

[124] Becker, R.S. *Theory and interpretation of fluorescence and phosphorescence*. New York: Wiley Interscience. 1969.
[125] So, P.T., Dong, C.Y., Masters, B.R., Berland, K.M., Annu. *Rev. Biomed. Eng*. **02** (2000) 399-429.
[126] Huang, Y., Li, Z., Risinger, A.L., Enslow, B.T., Zeman, C.J., Gong, J., Yang, Y., Schanze, K.S. *PNAS*. **51** (2018) 1-6.
[127] Allison, R.R., Mota, H.C., Sibata, C.H. *Photodiagnosis. Photodyn. Ther.* **1** (2004) 263-277.
[128] Allison, R.R., Moghissi, K. *Clin Endosc*. **46**(1) (2013) 24-29.
[129] Von Tappeiner, H., Jensionek, A. *Munch Med. Wochenschr*. **47** (1903) 2042-2044.

achieve enough momentum and was lost for nearly 50 years.[130] Studies during 1950 – 1960 revealed the inter-related ability of a photosensitizing agent to fluoresce and demarcate tumours and not only tumour ablation.[131] Dougherty *et al.*[132] rediscovered PDT in 1998 while working with porphyrin compounds and recreated a suitable photosensitizing drug.

Photodynamic therapy abbreviated as PDT, is defined as a treatment that uses a drug called a photosensitizer (PS) and a particular type of light. When photosensitizers are exposed to a certain wavelength of light, they produce a form of oxygen that kills nearby cells. Photosensitizers are activated by the light of a specific wavelength; the wavelength determines the distance the light can travel into the body. Different photosensitizers and wavelengths of light are used to treat different areas of the body with PDT.[133,134,135]

During the process of cancer treatment, a photosensitizer is injected into the blood stream, absorbed into the blood by cells all over the body and stays in the cancer cells longer than it does in the normal cells. After a period of one to three days, the agent leaves the normal cells but remains in the cancer cells and the tumour is exposed to light. The remaining agent in the cancer cells absorbs the light and develops an active form of oxygen that kills nearby cancer cells. Fibre optic cables are used to deliver light to the areas inside the body by inserting it through an endoscope into the esophagus or lungs to treat cancer in these organs while a light source that have light-emitting diodes (LEDs) are used for surface tumours like skin cancer.

2.8.3.2 Clinical application of PDT

Photodynamic therapy is translated into a two-step procedure. 1st step (presensitisation): The Photosensitiser (PS) is administered systemically by intravenous injection; 2nd step (illumination): The presensitised tissue is exposed to a

[130] Lipson, R,L., Baldes, E. *J. Arch Dermatol.* **82** (1960) 517-520.
[131] Lipson, R.L., Baldes, E. *J. Arch Dermatol*. **82** (1960) 508-516.
[132] Dougherty, T.J., Gomer C.J., Henderson, B.W. *J. Nat Cancer Inst*. **90** (1998) 889-905.
[133] Dolmans, D.E., Fukumura, D., Jain, R.K. *Nat. Rev. Cancer*. **3**(5) (2003) 380–387.
[134] Dougherty, T.J., Gomer, C.J., Henderson, B.W.*J. Natl. Cancer Inst*. **90** (1998) 889-905.
[135] Vrouenraets, M.B., Visser, G.W., Snow, G.B., van Dongen, G.A. *Anticancer Res.* **23**(1B) (2003) 505-522.

specific light with a wavelength that matches the absorption band of the chemical or drug. The ensuing photodynamic reaction (PDR) is presented as necrotic destruction of the tissue under treatment. Clinicians can improve PDT by pointing the light at the target. As discussed, PDT is the interplay of the drug and the light, both of which can be manipulated to maximize the outcome in various clinical situations.[136]

2.8.4 The application of β-hydroxyketone ligands in photoluminescence

β-Hydroxyketone type ligands are among the most important ligands for luminescence purposes particularly when utilised in lanthanide complexes. Due to its ability to form stable compounds with Ln^{3+} ions and the fact that it has a strong absorption within a large wavelength range for its π-π* transition, it can sensitize the photoluminescence of the Ln^{3+} ions as an antenna and can be effectively transferred to the Ln^{3+} ions, resulting in higher efficiency emissions.[137] However, the *β*-hydroxyketone ligands contain high-energy oscillators such as N-H, C-H and O-H bonds that are able to quench the metal excited states non-radiatively, resulting in a shorter excited state life-time and lower photoluminescence intensities. This can be overcome by deuteration or halogenation of the ligands but requires significant synthetic endeavours.[137,138]

Significant research into the use of *β*-hydroxyketone bidentate ligands that have been coordinated to lanthanide metal centres are reported.[139,140,141,142] Raj *et at*.[143] reported very good photoluminescence results of europium(III) complexes containing 4,4,5,5,5-pentafluoro-1-(naphthalene-2-yl)pentane-1,3-dione (HPFNP) of general formula [Eu(PFNP).L] (where L = H_2O, 2,2'-bipyridine (bpy), 1,10-phenanthroline (phen), 4,7-diphenyl-1,10-1,10-phenanthroline (bath)) (Scheme **2-21**). At room temperature, the photoluminescence spectra of the complexes were composed of

[136] Allison, R.R., Moghissi. *Clin Endosc*. **46** (2013) 24-29.
[137] Kumar, R. *Int. J. Pharm. Sci. Rev. Res*. **45**(2) (2017) 182-186.
[138] Bader, C.A., Sorvina, A., Simpson, P.V., Wright, P.J., Stagni, S., Plush, S.E., Massi, M., Brooks, D.A. *FEBS Lett*. **590** (2016) 3051-3060.
[139] Ma, Y., Wang, Y. *Coord. Chem. Rev*. **254** (2010) 972-990.
[140] Carlos, L.D., Ferreira, R.A.S., de Zea Bermudez, V., Julian-Lopez, B., Escribano, P. *Chem. Soc. Rev*. **40**(2) (2011) 536-540.
[141] Dong, Y.,Yan, P., Zou, Z.,Yao, X., Hou, G., Li. G. *Dalton Trans*. **45** (2016) 9148-9157.
[142] Zhang, L., Li, H., Chen, P., Sun, W., Yan, P. *Chem. Res. Chin. Univ*. **32** (4) (2016) 534-538.
[143] Raj, D.B.A., Biju, S., Reddy, M.L.P. *Inorg. Chem*. **47** (2008) 8091-8100.

Eu^{3+} red emissions, assigned to the transition between the first excited state ($^5D_0$) and the multiplet ($^7F_{0\text{-}4}$). The results illustrated that the substitution of solvent molecules by bidentate nitrogen ligands in $[Eu(PFNP)_3].H_2O.EtOH$ greatly enhances the quantum yields and lifetime values.

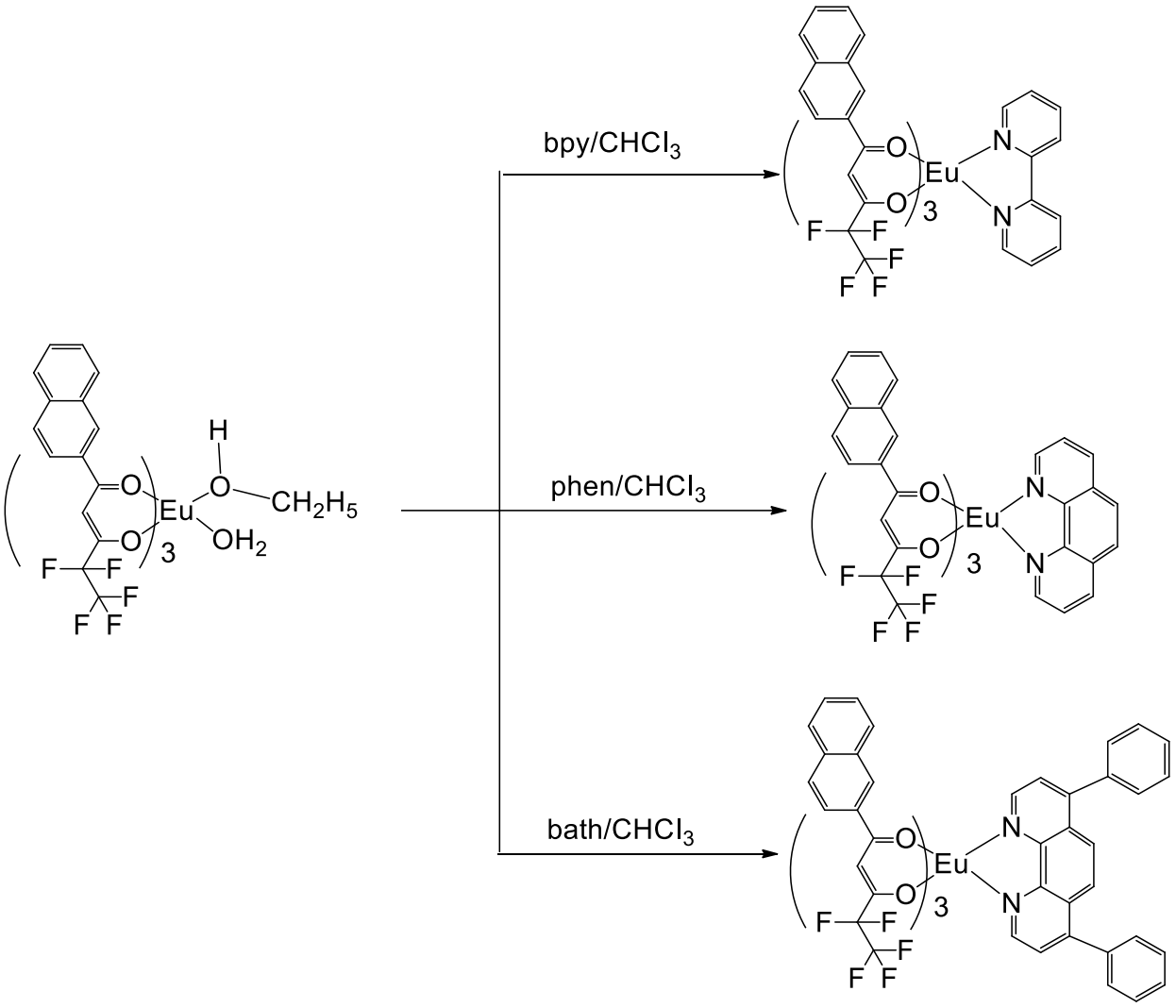

Scheme 2-21: Illustration of *β*-hydroxyketone bidentate ligands coordinated to europium as synthesized by Raj *et al*.[143]

Li *et al*.[144] reported lanthanide complexes of the type $[Ln(TIF)_3L]$ (where Ln = europium (Eu) or samarium (Sm), L = water (H_2O), 2,2'-bipyridine (bpy), 1,10-phenanthroline (phen) and 2-(2,2,2-trifluoroethyl)-1-indone (TIF). It was found that at room temperature photoluminescence spectra of the complexes in

[144] Li, J., Li, H., Yan, P., Chen, P., Hou, G., Li, G. *Inorg. Chem*. **51** (2012) 5050-5057.

Scheme **2-22** show strong characteristic emissions of the corresponding Eu^{3+} and Sm^{3+} ions.

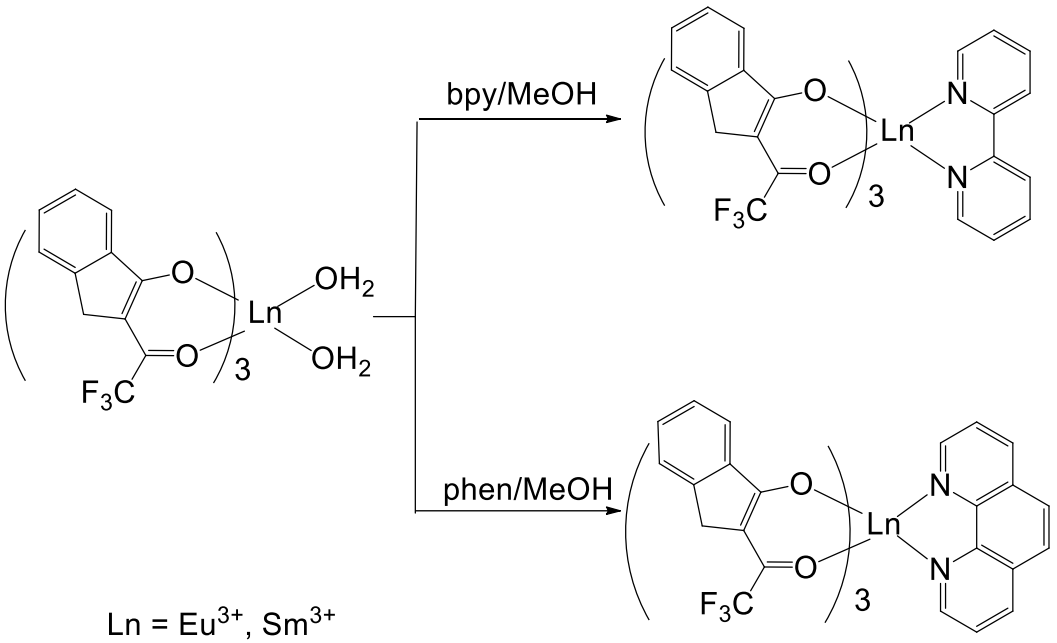

Scheme 2-22: Illustration of *β*-hydroxyketones bidentate ligands coordinated to eurapium and samarium as synthesized by Li *et al*.[144]

The substitution of the solvent molecules by nitrogen bidentate ligands essentially enhances the luminescence quantum yield and lifetimes of the complexes. Li and co-workers reported similar results to these where a methoxy group was substituted on the backbone of the *β*-hydroxyketone bidentate ligands (Scheme **2-23**).[145] The complexes in Scheme **2-20** show strong characteristic emissions of the corresponding Eu^{3+} and Sm^{3+} ions.

[145] Li, W., Yan, P., Hou, G., Li, H., Li, G. *Dalton Trans*. **42** (2013) 11537-11547.

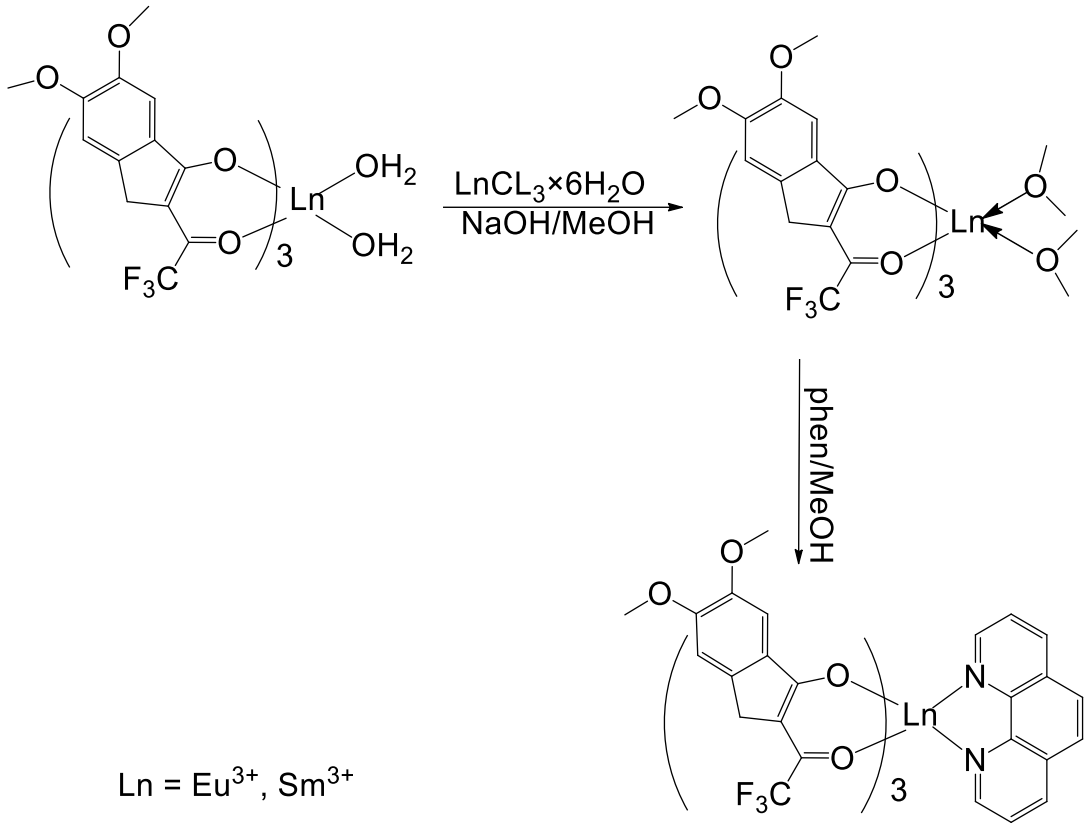

Scheme 2-23: Illustration of *β*-hydroxyketone bidentate ligands coordinated to eurapium and samarium as synthesized by Li *et al*.[145]

Kydonaki *et al*.**[146]** reported a range of Re(I) tricarbonyl complexes utilizing quinolone antimicrobial agents oxolic acid (Hoxo) and enrofloxacin (Herx) as bidentate ligands (Scheme **2-24**) and methanol, triphenylphosphine (PPh_3) and imidazole (Im) as monodentate ligands. UV spectroscopy studies as well as viscosity measurements suggest that these complexes possibly bind to calf-thymus (CT DNA) via intercalation. The complexes exhibited DNA-binding constants ranging from K_b = 8.61(±0.14) x 10^5 M^{-1} to K_b = 1.32 (±0.03) x 10^7 M^{-1}. Competitive studies utilizing ethidium bromide further support the possibility of DNA-interaction via intercalation. An enhanced inhibitory topoisomerase IIα activity of *fac*-[$Re(CO)_3$(MeOH)(erx)] compared to that of the free enrofloxacin ligand was observed, suggesting enhanced activity toward biological targets upon coordination of the quinoline moiety. The fluorescence emission spectroscopy investigation, of the interaction of the rhenium complexes with bovine and human serum albumin, showed binding constants

146 Kydonaki, T.E., Tsoukas, E., Mendes, F., Hatzidimitriou, A.G., Paulo, A., Papadopoulou, L.C., Papagiannopoulou, D., Psomas, G. *J. Inorg. Biochem*. **160** (2016) 94-105.

ranging from $K = 3.35 \times 10^3$ to $K = 6.41 \times 10^5$ M^{-1}. These results suggest optimal binding, transfer and release upon target arrival. The tracer complex *fac*-[^{99m}Tc(CO)$_3$(erx)(Im)] was synthesized and identified by comparative HPLC analysis along with the rhenium analogue. Preliminary studies in human K-562 erythroleukemia cells showed cellular uptake of the Tc-99m tracer with distribution primarily in the cytoplasm and the mitochondria, with some nuclear uptake. These preliminary results indicate that the quinolone Tc-99m/Re complexes show promise to be further evaluated as imaging or therapeutic agents.

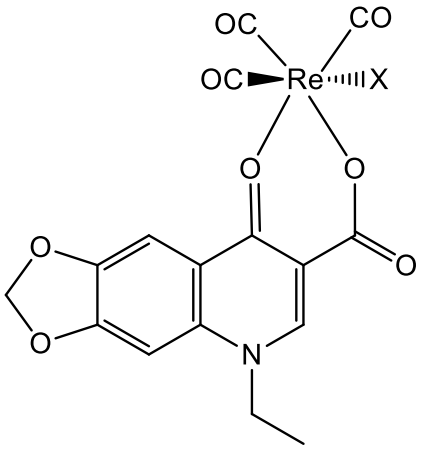

fac-[Re(CO)$_3$(X)(oxo)]
X = MeOH, Im, PPh$_3$

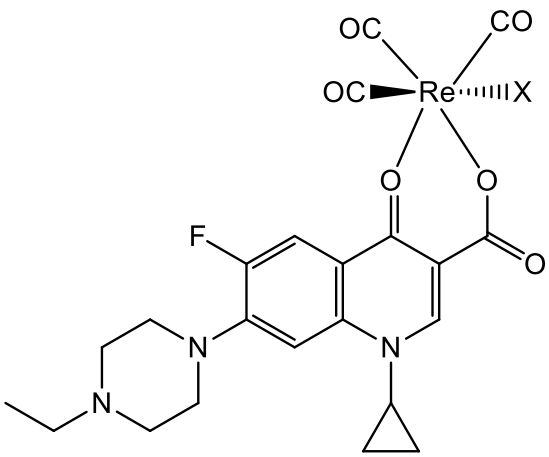

fac-[Re(CO)$_3$(X)(erx)]

Scheme 2-24: Complexes synthesized and evaluated by Kydonaki *et al*.[146]

Pagoni *et al*.**[147]** synthesized a series of Re(I) tricarbonyl complexes utilizing the quinolone antimicrobial agents enrofloxacin (Herx) and levofloxacin (Hlfx) (Scheme **2-25**) as bidentate ligands, methanol as the monodentate ligand and imidazole (Im) or pyridine (Py) as co-ligand. Similar results were obtained to that of Kydonaki *et al*.**[146]** The interactions of the rhenium complexes with bovine serum albumin were studied by fluorescence emission spectroscopy and the binding constants determined range from $K = 3.39 \times 10^4$ to $K = 1.17 \times 10^5$ M^{-1}. UV spectroscopy studies, viscosity studies as well as competitive studies with ethidium bromide were used to study the interaction of the rhenium complexes with CT DNA. The results of these studies suggested that intercalation is the most possible mode of

147 Pagon, C.-C., Xylourl, V.-S., Kalafas, G.C., Lazou, M., Bompola, G., Tsoukas, E., Papadopoulou, L.C., Psomas, G., Papaglannopoulou, D. *J, Biol. Inorg. Chem*. **24** (2019) 609-619.

action. The binding constants observed from these studies range from K_b = 1.58(±0.16) x 10^5 M^{-1} to K_b = 4.69 (±0.34) x 10^7 M^{-1}. The cytotoxicity of the Re(I) complexes against human K-562 erythroleukemia cells were found to be promising warranting the design of new Re(I) complexes of this type.

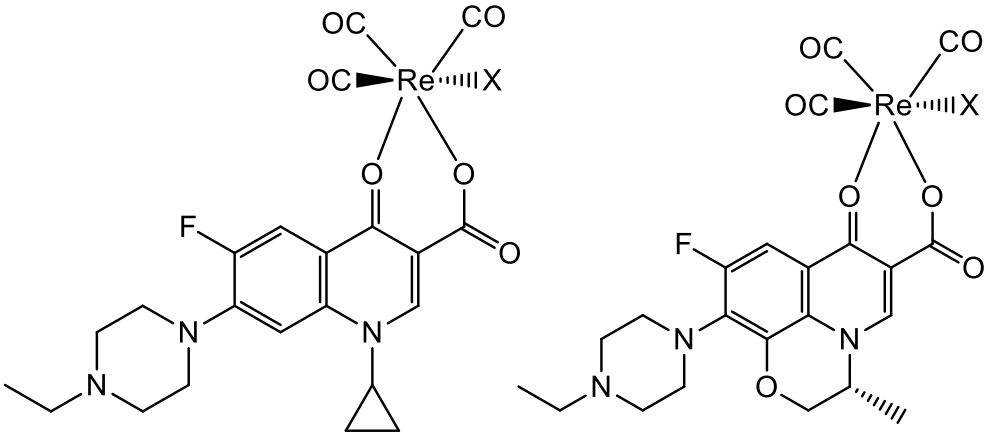

Scheme 2-25: Re(I) tricarbonyl complexes synthesized by Pagoni *et al*.[147]

2.8.5 Some examples of Re(I) tricarbonyl complexes with photoluminescent properties

Re(I) tricarbonyl complexes gained interest in fluorescence bioimaging due to its photophysical features. Cary *et al.*[148] reported the synthesis and fluorescence studies of boronic acid derivatives of rhenium bipyridine complexes for its potential use as glucose sensing molecules (illustrated in Scheme **2-26**). The fluorescence behaviour of the rhenium complexes was studied as a function of pH and exposure to various concentrations of glucose.

[148] Cary, D.R., Zaitseva, N.P., Gray, K., O'Day, K.E., Darrow, C.B., Lan, S.M., Peyser, T.A., Satcher, J.H., van Aantwerp. W.P., Nelsone, A.J., Reynolds, J.G. *Inorg. Chem*. **41** (2002) 1662-1669.

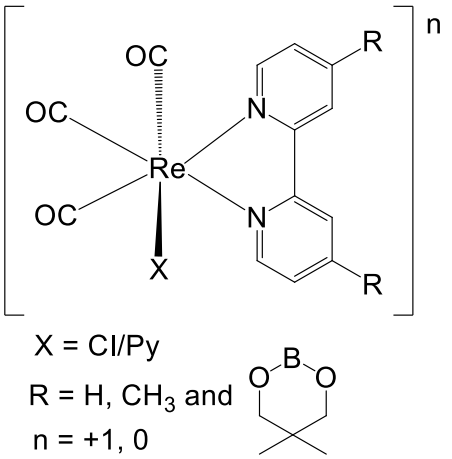

Scheme 2-26: Illustration of the rhenium complexes reported for potential use as glucose sensing molecules by Cary *et al*.[148]

Fluorescence quenching was observed at high pH as expected because of the photo-induced electron transfer (PET) signalling mechanism. Glucose testing showed a significant dependence on the solvent system used. The rhenium boronate complex exhibited a 55 % fluorescence intensity increase upon increasing the glucose concentration from 0 to 400 mg/dL in pure methanol. In 50 vol % methanol/phosphate buffered saline, none of the complexes showed a significant response in the glucose range of physiological interest.

Ramos *et al*.[149] reported the photophysical properties and preliminary time-dependent density function theory (DT-DFT) data of rhenium(I) polypyridyl compounds. *fac*-$[Re(CO)_3(L)(Am_2Phen)]^n$ (where Am_2Phen = 4,7-diamine-1,10-phenanthroline, L = Cl/ethyl isonicotinate and n = 0 or +1), provided insight on the excited-state deactivation through an unusual inversion between the two metal-to-ligand charge-transfer excited states. A schematic representation of the reported complexes is illustrated in Scheme **2-27**.

[149] Ramos, L.D., de Macedo, L.H., Gobo, N.R.S., de Oliveira, K.T., Cerchiaro, G., Frin, K.P.M. *Dalton Trans*. **46** (2020) 1-27.

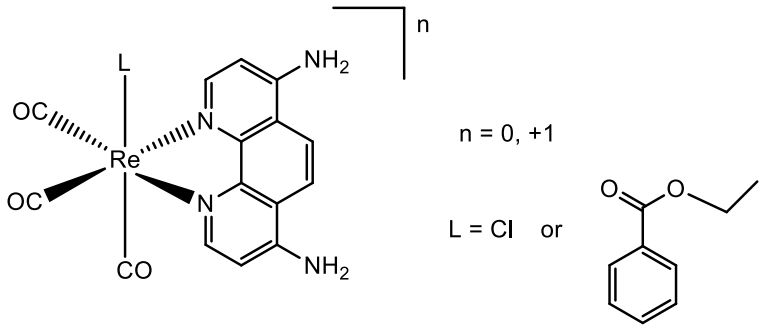

Scheme 2-27: Illustration of the structure of *fac*-$[Re(CO)_3(L)(Am_2Phen)]^{0/+}$ reported by Ramos *et al*.[149]

They investigated the cellular uptake using melanoma (SkMel-147 and SkMel-29) and breast cancer (MCF-7) cell lines and also looked into the bioactivity as well as the cell-killing mechanism and protein expression. The results exhibited a very strong broad absorption band around 300 nm to 400 nm that by preliminary TD-DFT corresponds to a mixture of $IL_{Am2Phen}$ and $MLCT_{Re\text{-}Am2Phen}$ transitions and a strong contribution by the charge transfer transition $MLCT_{Re\text{-}et\text{-}isonic}$ for *fac*-$[Re(CO)_3(Am_2Phen)(et\text{-}isonic)]^+$. The change from CI to et-isonic as monodentate ligand promoted a bathochromic shift of the emission maxima, a fast life-time, but a relatively low emission quantum yield in contrast to Re(I) polypyridyl complexes. The photophysical investigation of *fac*-$[Re(CO)_3(L)(et\text{-}isonic)_2]$ provided important information on the excited state manifold. The remarkable inversion of the lowest-lying excited state is taking place form the usually observed $MLCT_{Re\text{-}Am2Phen}$ to the unusual $MLCT_{Re\text{-}et\text{-}isonic}$. The positively charged complex has a higher lipophilicity than the negatively charged complex and the same trend was observed for the activity against cells without light.

Wahler *et al.*[150] introduced the first examples of rhenium(I) complexes with visible-light-induced *in-vitro* anticancer activity. Metallo-pyridocarbozole complexes, with improved chemical stability were demonstrated to induce apoptosis by the irradiation at wavelength $\lambda \geq 505$ nm.[150]

Gabr *et al*.[151] reported rhenium(I) tricarbonyl complexes coordinated to bis(pyridyl)- and bis(quinolyl) tetraarylethylene (TAE) ligands; the emission wavelengths of the complexes were influenced by the structural variation in the tetrarylethylene ligands,

[150] Wahler, K., Ludewig, A., Szabo, P., Harms, K., Meggers, E. *Eur. J. Inorg. Chem*. **5** (2014) 807-811.
[151] Gabr, M.T., Pigge, F.C. *Dalton. Trans*. **46** (2017) 15040-15047.

and several complexes exhibit aggregation-induced enhanced emission in aqueous solution. A significant enhancement were observed in luminescence intensity of rhenium(I) tricarbonyl complexes accompanied by the remarkable blue shift (~95 nm) upon specific binding to site II of human serum albumin (Scheme **2-28**).

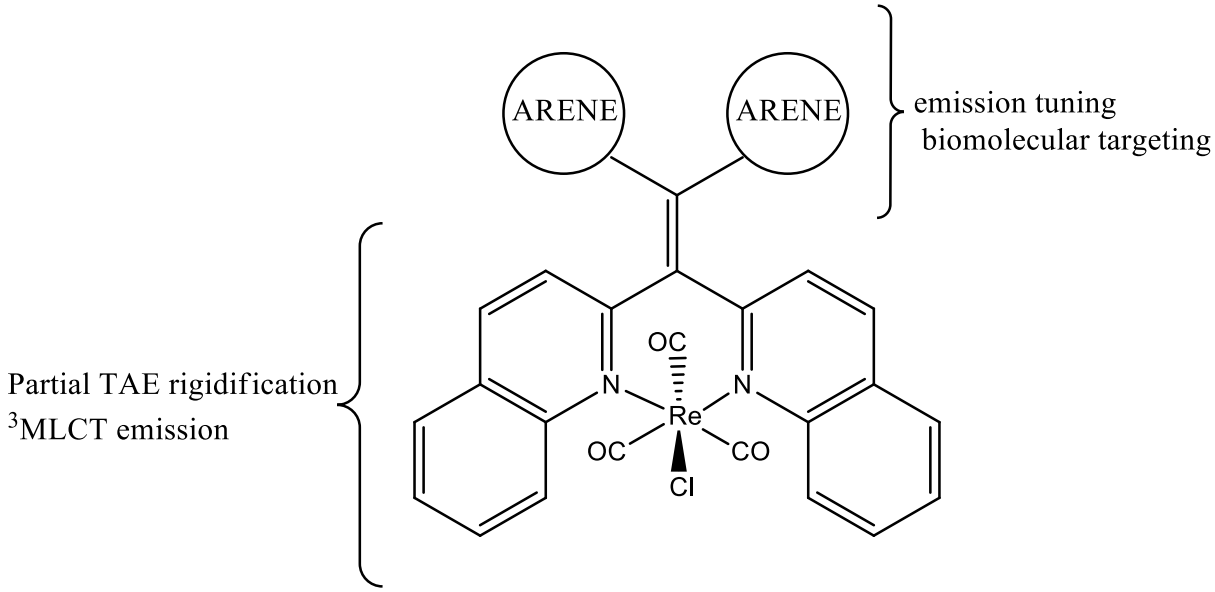

Scheme 2-28: Rhenium(I) tricarbonyl complexes with TAE-based ligands as described by Gabr *et al*.[151]

Langdon-Jones *et al*.[152] reported a range of biologically compatible, fluorescent rhenium-naphthalimide Re(I) tricarbonyl complexes. The fluorescent ligands are based on the N-functionalized, 4-amino-derived, 1,8-naphthalimide core and incorporate a dipicolyl amine binding unit to chelate Re(I). The bidentate ligands varied according to the nature of the alkylated imide as illustrated in Scheme **2-29**. These complexes are fluorescent in the visible region between 505 nm and 537 nm through a naphthalimide-localized intramolecular charge transfer with a corresponding fluorescent life-time of up to 9.8 ns. The complexes and ligands were investigated for their potential as imaging agents for human osteoarthritic cells and protistan fish parasite Spironudeus vortens using confocal fluorescence microscopy. The results illustrated that the specific nature of the naphthalimide serves to control the uptake and intercellular localization of the imaging agents. Significant differences

[152] Langdon-Jones, E.E., Symonds, N.O., Yate, S.E., Hayes, A.J., Lloyd, D., Williams, R., Coles, S.J., Horton, P.N., Pope, S.J.A. *Inorg. Chem*. **53** (2014) 3788-3797.

were observed between the free ligands and complexes, with Re(I) complexes of L2 showing the hydrogenosomal localization in Spironudeus vortens.

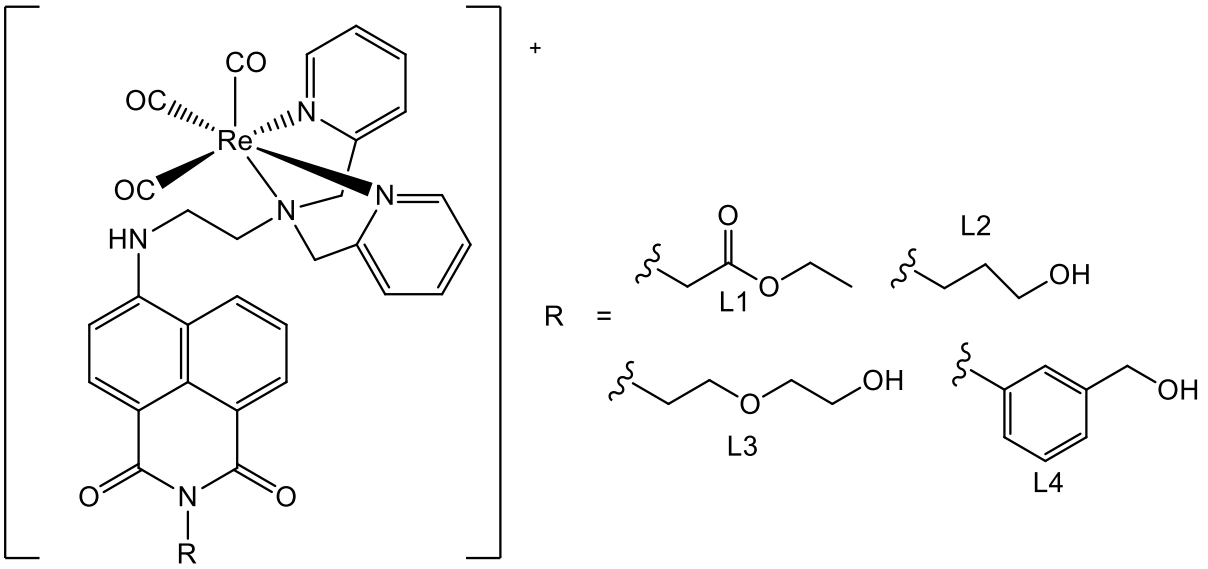

Scheme 2-29: Re(I) tricarbonyl complexes reported by Langdon-Jones *et al*.[152]

Leonidova *et al*.[153] reported the potential of two known *N,N'*-bis(quinolin) Re(I) tricarbonyl complex derivatives (Scheme **2-30**), namely Re(I) tricarbonyl [*N,N'*-bis(quinolin-2-ylmethyl)-aminol-4-butane-1-amine] (Re-NH_2) and Re(I) tricarbonyl [*N,N'*-bis(quinolin-2-ylmethyl)amino]-5-valeric acid (Re-COOH) as photodynamic therapy (PDT) photosensitizers. These two complexes have excellent singlet oxygen generators in a lipophilic environment with quantum yields of about 75 %. The selected ligands were functionalized to two types of peptides, namely a nuclear localization signal (NLS) and a derivate of the neuropeptide bombesin, to form Re-NLS and Re-Bombesin, respectively. The fluorescent microscopy on cervical cancer cells (HeLa) showed the conjugation of Re-COOH to NLS significantly enhanced the compound's accumulation into the cell nucleus and specifically into its nucleoli. The cytotoxicity of the Re(I) tricarbonyl complexes and their bioconjugates increased significantly upon light irradiation. Re-Bombesin was found to be at least 20-times more toxic after light irradiation. DNA photo-cleavage studies demonstrated that all the compounds damaged DNA *via* singlet oxygen and to a minor extent, superoxide production.

[153] Leonidova, A., Pierroz, V., Rubbiani, R., Heier, J., Ferrari, S., Gasser, G. *Dalton Trans*. **43** (2014) 4287-4294.

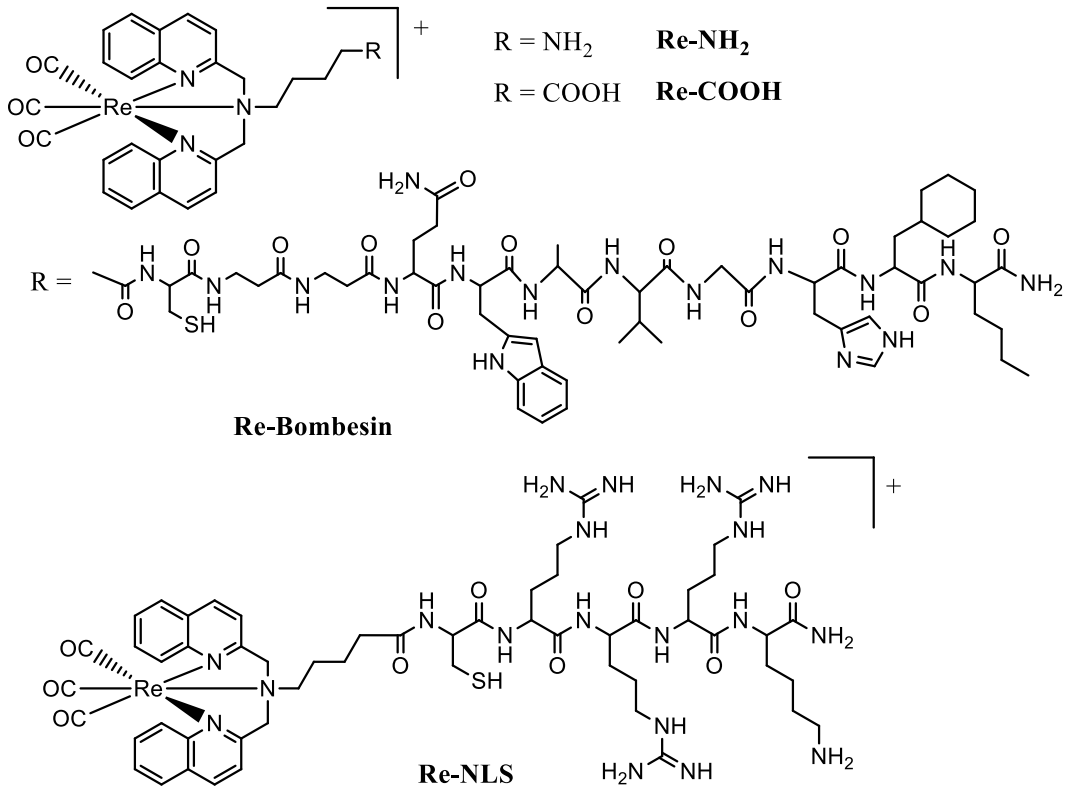

Scheme 2-30: The structure of Re(I) tricarbonyl complexes and their derivatives reported by Leonidova *et al*.[153]

Ranasinghe *et al*.[154] reported Re(I) tricarbonyl complexes containing a pyridyl triazine core as illustrated in Scheme **2-31**. The complexes displayed a weak absorption band in the visible region, which can be assigned to a metal to ligand charge transfer excitation and fluorescent emission lying in the range of 650 nm to 710 nm. The cytotoxicity assays of complexes **1**, **3** and **4** were carried out on both, plant cells (Allium cepa bulb cells) and rat peritoneal cells. The cells were stained using the maximum non-toxic concentration levels of the compounds, 20 mg mL^{-1} for **1** and **3** and 5 mg mL^{-1} for **4** and were observed under the epifluorence microscope. The results showed that the compounds concentrated in the nuclei region of both cell lines and showed red fluorescence upon excitation at 550 nm. All Re(I) tricarbonyl complexes showed a remarkable enhancement of fluorescence upon binding with cells. The visible range excitability demonstrates the possibility of using the new complexes in biological applications.

[154] Ranasinghe, K., Handunnetti, S., Perera, I.C., Perera, T. *Chem. Cent. J*. **10** (2016) 71-81.

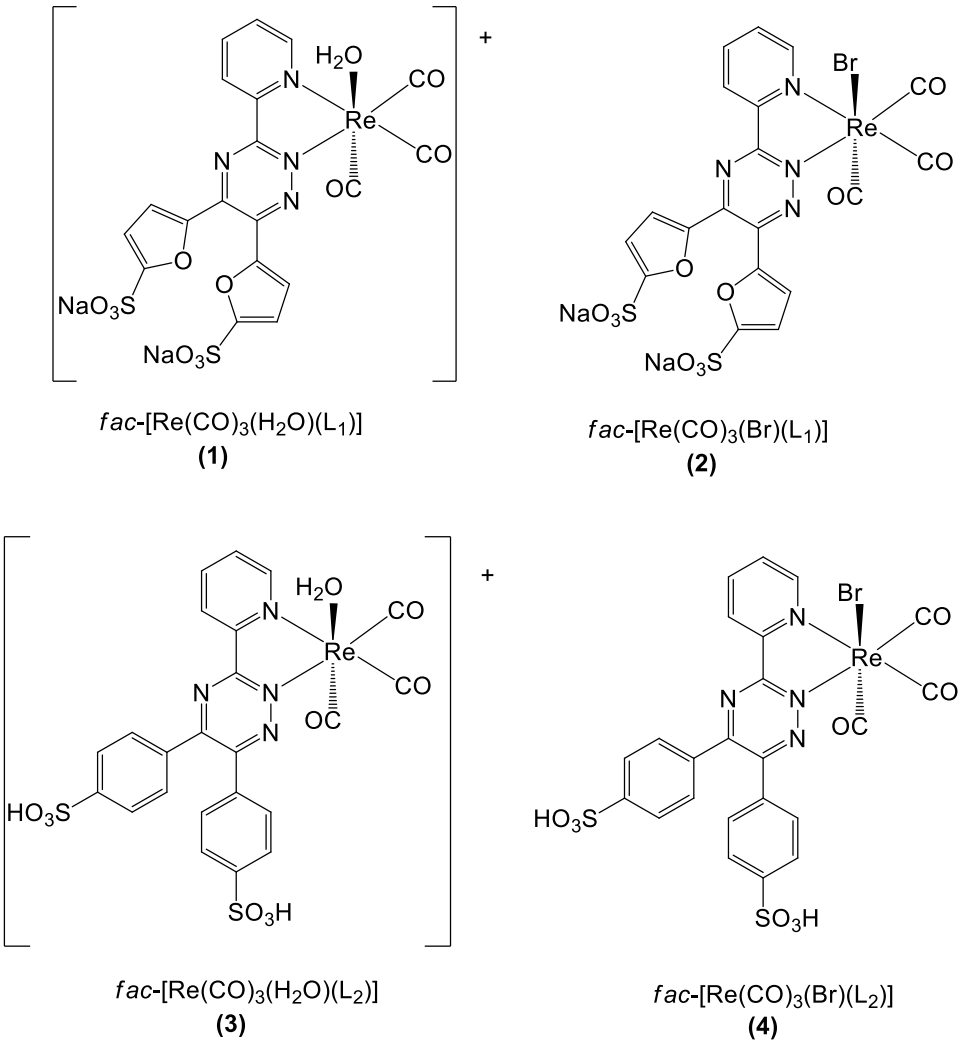

fac-[Re(CO)$_3$(H$_2$O)(L$_1$)]
(1)

fac-[Re(CO)$_3$(Br)(L$_1$)]
(2)

fac-[Re(CO)$_3$(H$_2$O)(L$_2$)]
(3)

fac-[Re(CO)$_3$(Br)(L$_2$)]
(4)

Scheme 2-31: Re(I) tricarbonyl complexes reported by Ranasinghe *et al.* [154]

Leonidova *et al*.[155] reported the Re organometallic complexes illustrated in Scheme **2-32**, that have shown anti-proliferative activity on cancer cell lines. A particular emphasis was placed on its cellular uptake and localization as well as its potential mechanism of action. Most of the compounds are potential anti-cancer agents with IC_{50} values reaching or exceeding the activity of cisplatin. The underlying mechanisms of toxicity are not always fully elucidated. The preparation of "hot" analogues of promising Re complexes to visualize their *in vivo* behaviour is an indispensable step and the most helpful tool to allow for the development of powerful and selective anti-cancer drugs.

[155] Leonidova, A., Gasser, G. *ACS Chem. Biol*. **9** (2014) 2180−2193.

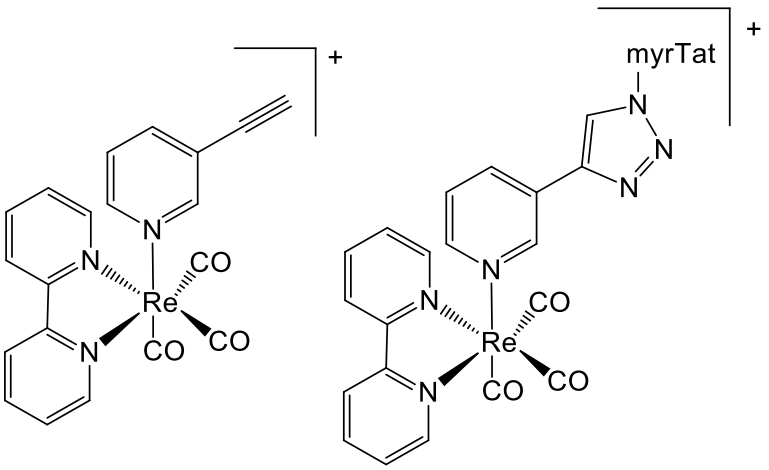

Scheme 2-32: Phototoxic Re(I) tricarbonyl complexes reported by Leonidova *et al*.[155]

2.9 Conclusion

The use of rhenium and technetium in medicine has been described, in particular the advantages of exploring the *fac*-$[M(CO)_3]^+$ core (M = Re and Tc) with its attractive synthetic possibilities. The reaction kinetic studies of the *fac*-$[M(CO)_3]^+$ core show that much is still unknown in understanding the mechanistic behaviour of these complexes. The photoluminescence of metal complexes is an exciting opportunity to combine the advantages of photodynamic therapy, induced by the coordinated ligands, with the chemotherapeutic advantages of the chosen ligand systems. To this end we have included the discussion of the *β*-hydroxyketone bidentate ligands as promising luminescence sensitizers on lanthanides ions, because of its rigid indanone group and trifluororinated alkyl group.[144,156] The isolation and structural characterization of the complexes containing *β*-hydroxyketone ligands demonstrate that the *β*-hydroxyketone ligands are effective sensitizers on luminescence and can effectively enhance the luminescence of the metal centre, quantum yield and lifetimes of selected metal ions.[144,156,157] Therefore these *O,O'*-bidentate ligands will be investigated further in this study with particular focus on its effect on the rhenium metal centre as potential PDT and chemotherapeutic agents.

The bipyridine type bidentate ligands are very good candidates for bioimaging probes because of their typically long-lived emission from triplet metal-to-ligand-charge-

[156] Li, W., Yan, P., Hou, G., Li, H., Li , G. *Dalton Trans*. **42** (2013) 11537-11547.
[157] Raj, D.B.A., Biju, S., Reddy . *Inorg. Chem*. **47** (2008) 8091- 8100.

transfer (^{3}MLCT) excited states.[78,79] The photophysical and bioimaging properties such as absorption/emission, cellular uptake/cytotoxicity and biomolecular specificity can be modulated through the variation of the coordinating ligands. The contributing effect of the monodentate ligand coordinated in the 6th position of the *fac*-[M(CO)$_3$]$^+$ core is of particular interest.

In Chapter 3 the synthetic procedure of the *β*-hydroxyketone bidentate ligands and its Re(I) tricarbonyl complexes as well as the *β*-diketone and bipyridine Re(I) complexes are described as potential anti-cancer agents (PDT and chemotherapy) and the characterization therefore by IR, UV/Vis and NMR (^{1}H and ^{13}C) are provided.

3 SYNTHESIS OF LIGANDS AND RHENIUM(I) TRICARBONYL COMPLEXES

3.1 Introduction

In the structure of any potential anti-cancer compound, the environment around the metal centre is very important in the design of the drug.[1] Most researchers find group 7 transition metal elements interesting due to their chemical and physical properties, especially Rhenium (Re) and Technetium (Tc). Alberto and co-workers synthesized *fac*-$[M(CO)_3(X)_3]^n$ (M = rhenium or technetium X = Br/H_2O, n = -2, +1) as a water soluble precursor utilised in the design of anti-cancer complexes which has been reviewed in numerous papers due to its advantageous chemical properties. [2,3,4,5] In *fac*-$[Re(CO)_3(X)_3]^n$, the three water/bromido molecules can easily be removed or substituted by a number of functional groups such as amines, phosphines, thiols and thioethers, but the *fac*-$[Re(CO)_3]^+$ core itself is chemically stable. Many Re(I) tricarbonyl complexes containing tridentate ligands with promising biological properties have been developed which are stable *in vivo*. The use of mixed ligands, such as a combination of a bidentate and a monodentate ligand also forms stable coordination complexes.[3] These mixed ligand systems are called the "2 + 1", "3 + 1", "3 + 2" and "4 + 1" approach,[6,7,8] and has been used in the design of multifunctional

[1] Alberto, R. *Eur. J. Inorg. Chem.* **1** (2009) 21-31.
[2] Alberto, R., Schibli, R., Egli, A., Schubiger, P.A., Herrmana, W.A., Artus, G., Abram, U., Kande, T.A. *J. Organomet. Chem.* **493** (1995) 119-127.
[3] Alberto, R., Egli, A., Abram, U., Hegetschweiler, K., Gramlich, V., Schubiger, P.A. *J. Chem. Soc. Dalton Trans.* **19** (1994) 2815-2820.
[4] Alberto, R., Schibli, R., Schubiger, A.P., Abram, U., Kaden,T.A. *Polyhedron.* **15**(7) (1996) 1079-1089.
[5] Leonidova, A., Gasser, G. *ACS Chem. Biol*. **9**(10) (2014) 2180-2193.
[6] Okoye, N.C., Baumeister, J.E., Khosroshahi, F.N., Heather, M., Hennkens, .M., Jurisson, S.S. *Radiochim. Acta*. **107** (2019) 767-1120.
[7] Schibli, R., Bella, R., Alberto, R., Garcia-Garayoa, E., Ortner, K., Ubram, U., Schubiger, P.A. *Bioconjugate Chem*. **11** (2000) 345-351.
[8] Mundwiler, S., Kunding, M., Ortner, K., Alberto, R. *Dalton Trans*. **9** (2004) 1320-1328.

therapeutic or imaging agents where the active moieties are coordinated to the metal complexes as well as in the design of dual imaging systems.[4,7,9,10,11]

In this study, one of the aims was to investigate the ability of the chosen *O,O'* and *N,N'* bidentate ligands to coordinate to *fac*-$[Re(CO)_3]^+$ and to explore its stability and kinetic behaviour towards incoming monodentate ligands at various concentrations and temperatures. The results will be compared to previous studies of Re(I) tricarbonyl complexes with *O,O'* and *N, N'* bidentate ligand systems in order to gain a better understanding of possible variations in coordination behaviour and a change in kinetic reactivity which could be induced by the different organic ligand systems.

From literature it is known that *N,N'* and *O,O'* β-hydroxyketone bidentate ligands as well as 1,3-bis(4-methoxyphenyl)propane-1,3-dione (4-MeTPh) and its complexes can be used as potential PDT and chemotherapeutic agents. For this purpose, the following ligands were used in this project and are listed in Table **3-1** together with the abbreviation, while the schematic representation of the ligands is given in Scheme **3-1**.

Table 3-1: List of the chosen ligand systems and the respective abbreviations.

Ligand name	**Abbreviation**
***O,O'* bidentate ligand systems**	
2,2,2-Trifluoro-1-(3-hydroxy-1H-inden-2-yl)ethan-1-one	TIFH
2,2,2-Trifluoro-1-(3-hydroxy-1-methyl-1H-inden-2-yl)ethan-1-one	MeTIFH
2,2,2-Trifluoro-1-(3-hydroxy-1-phenyl-1H-inden-2-yl)ethan-1-one	PhTIFH
1,3-Bis(3,5-dimethylphenyl)propane-1,3-dione	3,5-DiMePh
2-Methyl-1,3-diphenylpropane-1,3-dione	MeDiPhPr
2-Bromo-1,3-diphenylpropane-1,3-dione	BrDiPhPr
Benzoic anhydride	BAHY
1,3-Bis(4-methoxyphenyl)propane-1,3-dione	4-MeTPh
***N,N'* bidentate ligand systems**	
4,4'-Dimethyl-2,2'-bipyridine	DiMePy
4,4'-Dimethoxy-2,2'-bipyridine	DiMeOPy

[9] Abram, U., Alberto, R. *J. Braz. Chem. Soc*. **17**(8) (2006) 1486-1486.
[10] Okoye, N.C., Baumeiser, J.E., Khosroshahi, F.N., Hennkens, H.M., Jurisson, S.S. *Radiochim. Acta*. **107** (2019) 9-11.
[11] Fuks, L., Gniazdowska, E., Kozminski, P., Lyczko, M., Mieczkowski, J., Narbutt, *J. Appl. Radiat. Isot*. **68** (2010) 90-95.

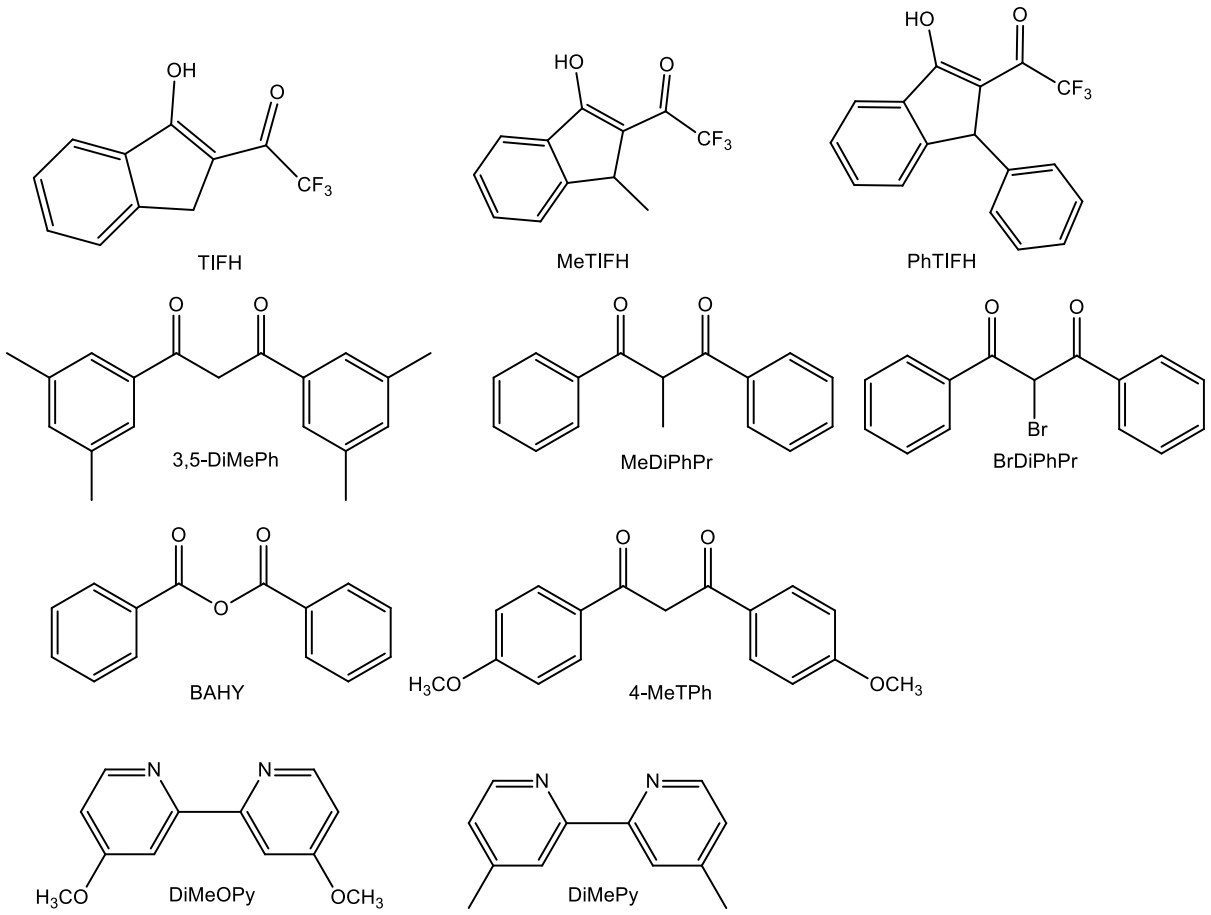

Scheme 3-1: Schematic illustration of the chosen ligand systems and the respective abbreviations.

The chosen *N,N'* bidentate ligands, 4,4'-dimethyl-2,2'-bipyridine (DiMePy) and 4,4'-dimethoxy-2,2'-bipyridine (DiMeOPy) were selected based on its chemical structure and potential photoluminescent and cytotoxic properties.[12,13,14,15,16,17] Our interest is also based on its behaviour when it is coordinated to the Re(I) tricarbonyl core and when exchanging the entering monodentate ligand in the 6th position (substitution of the bromido or aqua ligand). The β-diketone *O,O'* bidentate ligand systems (3,5-DiMePhH, MeDiPhPr, BrDiPhPr, BAHY and 4-MeTPh) were selected based on the different functional groups on the backbone with different electronic properties and steric bulk. It is known from literature that the β-hydroxyketone type *O,O'* bidentate

[12] Constable, E.C., Housecroft, C.E. *Molecules*. **24** (2019) 3951-3989.
[13] Wiederholt,K., McLaughlin, L.W. *Nucleic Acids Res. Spec. Pub*. **27**(12) (1999) 1487-2493.
[14] Fletcher, N. *J. Chem. Soc*., *Perkin Trans*. **1** (2002) 1831-1842.
[15] Liew, H.S., Mai, C.-W., Zulkefeli, M., Madheswaran, T., Kiew, L.V., Desuc, N., Low, M.L. *Molecules*. **25** (2020) 4176-4199.
[16] Banasinghe, K., Handunnetti, S., Perera, I.C., Perera, T. *Chem. Cent. J.* 1**0**(71) (2016) 1-10.
[17] Kozlov, V.A., Churusova, S.G., Rybalkina, E.Y., Peregudov, A.S., Denisov, G.L., Aleksanyan. D.V. *INEOS OPEN*. **2**(5) (2020) 172-177.

ligands have excellent luminescent and cytotoxic properties.[18,19,20,21,22] We therefore decided to synthesize three ligands (TIFH, MeTIFH and PhTIF) and its Re(I) tricarbonyl complexes in order to see the effect of the metal centre on the photoluminescence and cytotoxicity results, but also to see the effect these ligands have on the reactivity of the Re(I) tricarbonyl core. TIFH has been synthesized before by Li *et al*.[18] We resynthesized TIFH as well as two novel variations with a methyl and phenyl functional group on the backbone. These β-hydroxyketone *O,O'* bidentate ligands also form six membered cyclic ring systems similar to the β-diketone ligands. The effects of the different functional groups on the indanone backbone were of interest.

The following monodentate ligands were chosen for the methanol substitution reactions: sodium bromide (Br^-), sodium thiocyanate (NCS^-), tricyclohexylphosphine (PCy_3), triphenylphosphine (PPh_3) and thiourea (TU) were selected based on the different coordinating atoms and the possible different effects it will have on the metal centre. The kinetic end products were fully isolated and characterised. *fac*-[$Re(CO)_3$(Br)(DiMePy)], *fac*-[$Re(CO)_3$(Br)(DiMeOPy)], *fac*-[NEt_4][$Re(CO)_3$(Br)(4-MeTPh)], *fac*-[NEt_4][$Re(CO)_3$(Br)(BrDiPhPr)], *fac*-[NEt_4][$Re(CO)_3$(Br)(TIF)] and *fac*-[NEt_4][$Re(CO)_3$(Br)(MeTIF)] were dissolved in methanol and monitored with UV/Vis. It was found that after 24 hours the above mentioned complexes formed the methanol solvento species *fac*-[$Re(CO)_3$(MeOH)(DiMePy)]$^+$, *fac*-[$Re(CO)_3$(MeOH)(DiMeOPy)]$^+$, *fac*-[$Re(CO)_3$(MeOH)(4-MeTPh)], *fac*-[$Re(CO)_3$(MeOH)(BrDiPhPr)], *fac*-[$Re(CO)_3$(MeOH)(TIF)] and *fac*-[$Re(CO)_3$(MeOH)(MeTIF)]. The methanol species were all isolated and fully characterised. The kinetic end products of all the complexes were also isolated and characterised to prove the structure of the end products of the reactions observed on the UV/Vis. Single crystals of *fac*-[$Re(CO)_3$(Act)(DiMePy][NO_3], *fac*-[$Re(CO)_3$(NO_3)(DiMePy], *fac*-[$Re(CO)_3$(Act)(DiMeOPy][NO_3] and *fac*-[$Re(CO)_3$(NO_3)(DiMeOPy)] were isolated by chance. Thefore we resynthesized these complexes to confirm the synthetic procedure of the aqua, acetonato and nitrato complexes.

[18] Li, J., Li, H., Yan, P., Chen, P., Hou, G., Li, G. *Inorg Chem*. **51**(2012) 5050-5057.
[19] Li, W., Yan, P., Hou, G., Li, H., Li, G. *Dalton Trans*. 42 (2013) 11537-11547
[20] Raj, D.B.A., Reddy, L.P.M. *Inorg. Chem*. **47** (2008) 8091-8100.
[21] Sagnou, M., Benaki, D., Triantis, C., Tsotakos, T., Psycharis, V., Raptopoulous, C.P., Pirmettis, L., Papadopoulos, M., Pelecanou, M. *Inorg. Chem*. **50** (2011) 1295-1303.
[22] Prohl, M., Schubert, U.S., Weigand, W., Gottschaldt, M. *Coord. Chem. Rev.* **307** (2016) 32-41.

3.2 Chemicals and apparatus used

Unless stated otherwise, all the chemicals were purchased from Sigma-Aldrich, South Africa. Chemicals were used without any further purification and they were of reagent grade. Perrin's procedure was used to purify and dry all solvents.[23] All reactions that were air or moisture sensitive were performed under Schlenk line conditions. Rhenium pentacarbonyl bromide (98 %) was purchased from Strem Chemicals, Newburyport, US. The well-known procedure by Alberto *et al*. was used to prepare the precursor *fac*-$[NEt_4]_2[Re(CO)_3(Br)_3]$.[24] Nitric acid was used to adjust the pH during the synthesis of the aqua complexes.

All Nuclear Magnetic Resonance (NMR) spectra were recorded on a Bruker 300 MHz spectrometer (s = singlet, d = doublet, t = triplet and m = multiplet) using different deuterated solvents or samples spiked with different deuterated solvents; methanol (CD_3OD-d_4) with a chemical shift of 3.31, 4.87 and 49.3 ppm for proton and carbon NMR; dichloromethane-d_2 (CD_2Cl_2-d_2) with chemical shifts of 1.1, 5.32 and 53.5 ppm for proton and carbon NMR and dimethylsulfoxide-d_6 (DMSO-d_6) with chemical shifts of 2.50, 3.33 and 39.5 ppm for proton and carbon NMR. All the chemical shifts, δ, are reported in ppm (parts per million) using TMS (tetramethylsilane) as internal standard for ^{1}H NMR. Coupling constants, *J*, are reported in Hz. In some cases, the coordinated methanol's peak is hidden by the deuterated solvent used.

The infrared spectra (IR) of all the complexes were recorded at room temperature on a Bruker Tensor 27 Standard System or a Perkin Elmer BX II IR Spectrophotometer with a laser range of 4000 cm^{-1} to 370 cm^{-1} which is coupled to a computer. The IR Spectrometer was equipped with a temperature cell regulator accurate within 0.3 ºC. An ATR was used to characterize solid samples in Hertz (Hz). The UV/Vis spectra were recorded at room temperature on a Varian Cary 50 Conc UV/Visible Spectrophotometer, equipped with a Julabo F12mV temperature cell regulator accurate within 0.1 ºC in a 1.000 ± 0.001 cm quartz cuvette cell.

[23] Perrin, D.D., Armarego, W.L.F. *Purification of Laboratory Chemicals*, 5th Ed, Great Britain: Butterworth-Heinemann Publishers, 2003.
[24] Albert, R., Schibli, R., Waihle, R., Schubiger, P.A. *Coord. Chem. Rev*. **190** (1999) 190-192.

3.3 Synthesis of *β*-hydroxyketone ligands

A typical procedure of Claisen condensation was used to synthesize the β-hydroxyketone bidentate ligands, namely 2,2,2-trifluoro-1-(3-hydroxy-1H-inden-2-yl)ethan-1-one (TIFH), 2,2,2-trifluoro-1-(3-hydroxy-1-methyl-1H-inden-2-yl)ethan-1-one (MeTIFH) and 2,2,2-trifluoro-1-(3-hydroxy-1-phenyl-1H-inden-2-yl)ethan-1-one (PhTIFH).

3.3.1 2,2,2-Trifluoro-1-(3-hydroxy-1H-inden-2-yl)ethan-1-one (TIFH)

1-Indanone (980 mg, 7.41 mmol) and ethyl trifluoroacetate (1053 mg, 7.41 mmol) were added to THF (150 mL), and the solution was allowed to stir for 30 min at room temperature. To this solution, NaH (534 mg, 22.23 mmol) was added under an inert atmosphere and allowed to stir for 24 hours at room temperature. The resulting solution was quenched with water and acidified to pH 2 - 3 using hydrochloric acid (2 M solution). The suspension was extracted twice with CH_2Cl_2 (70 mL). The organic layer was dried over a drying agent (Na_2SO_4), and the solvent was evaporated leading to a maroon coloured oily product. The maroon oil was washed with hexane and left to evaporate forming a maroon crystalline product. Yield: 81 %, 1369 mg, 6.00 mmol.

UV/Vis: 280 nm, 350 nm, 580 nm, ε = 1129 $M^{-1}cm^{-1}$, 2087 $M^{-1}cm^{-1}$, 989 $M^{-1}cm^{-1}$.

IR (KBr, cm^{-1}): $\upsilon_{(C=O)}$ = 1667, $\upsilon_{(OH)}$ = 3440, $\upsilon_{(CF)}$= 1330, 1268, 1128, $\upsilon_{(CF_3)}$= 748.

^{1}H NMR (300.18 MHz, *DMSO-d$_6$*): δ (ppm) = 15.3 (s, 1H), 7.8 (d, *J* = 4.5 Hz, 1H), 7.6 (d, *J* = 4.5 Hz, 1H), 7.50 (d, *J* = 4.5 Hz, 1H), 7.4(t, *J* = 4.5 Hz, 1H), 4.9 (d, *J* = 4.8 Hz, 2H).

^{13}C NMR (75.48 MHz, *DMSO-d$_6$*): δ (ppm) = 178, 176, 174, 151, 148, 131, 127, 125, 121, 117, 99, 31.

3.3.2 2,2,2-Trifluoro-1-(3-hydroxy-1-methyl-1H-inden-2-yl)ethan-1-one (MeTIFH)

3-Methyl-1-indanone (980 mg, 6.70 mmol) and ethyl trifluoroacetate (951 mg, 6.70 mmol) were added to THF (150 mL), and the solution was allowed to stir for 30

min at room temperature. To this solution, NaH (480 mg, 20.10 mmol) was added under an inert atmosphere and allowed to stir for 24 hours at room temperature. The resulting solution was quenched with water and acidified to pH 2 - 3 using hydrochloric acid (2 M solution). The suspension was extracted twice with CH_2Cl_2 (70 mL). The organic layer was dried over a drying agent (Na_2SO_4), and the solvent was evaporated leading to a maroon coloured oily product. The maroon oil was washed with hexane and left to evaporate forming a maroon crystalline product. Yield: 86 %, 840 mg, 5.75 mmol.

UV/Vis: 350 nm, 525 nm , ε = 1311 $M^{-1}cm^{-1}$, 2268 $M^{-1}cm^{-1}$.

IR (KBr, cm^{-1}): $\nu_{(C=O)}$ = 1665, $\nu_{(OH)}$ = 3442, $\nu_{(CF)}$= 1326, 1265, 1127, $\nu_{(CF_3)}$= 748.

^{1}H NMR (300.18 MHz, *DMSO-d$_6$*): δ (ppm) = 16.1 (s, 1H), 7.9 (d, *J* = 3.9 Hz, 1H), 7.6 (d, *J* = 3.7 Hz, 1H), 7.4 (d, *J* = 3.9 Hz, 1H) 4.3 (d, *J* = 4.1 Hz, 1H), 3.4 (s, 3H).

^{13}C NMR (75.48 MHz, *DMSO-d$_6$*): δ (ppm) = 181, 176, 174, 148, 139, 126, 124, 123, 121, 116, 113, 31, 19.

3.3.3 2,2,2-Trifluoro-1-(3-hydroxy-1-phenyl-1H-inden-2-yl)ethan-1-one (PhTIFH)

3-Phenyl-1-indanone (980 mg, 4.71 mmol) and ethyl trifluoroacetate (665 mg, 4.71 mmol) were added to THF (40 mL), and the solution was allowed to stir for 30 min at room temperature. To this solution, NaH (339 mg, 14.13 mmol) was added under an inert atmosphere and allowed to stir for 24 hours at room temperature. The resulting solution was quenched with water and acidified to pH 2 - 3 using hydrochloric acid (2 M solution). The suspension was extracted twice with CH_2Cl_2 (20 mL). The organic layer was dried over Na_2SO_4, and the solvent was evaporated leading to a maroon coloured oily product. The maroon oil was dissolved in a small amount of methanol. The precipitate was filtered and weighed. Yield = 59 %, 850 mg, 2.80 mmol.

UV/Vis: 450 nm, 520 nm , ε = 1721 $M^{-1}cm^{-1}$, 2236 $M^{-1}cm^{-1}$.

IR (KBr, cm^{-1}): $\nu_{(C=O)}$ = 1671, $\nu_{(OH)}$ = 3446, $\nu_{(CF)}$= 1335, 1272, 1131, $\nu_{(CF_3)}$= 753.

^{1}H NMR (300.18 MHz, *DMSO-d$_6$*): δ (ppm) = 14.8 (s, 1H), 7.8 (d, *J* = 5.2 Hz, 1H), 7.6 (d, *J* = 5.2 Hz, 1H), 7.4 (t, *J* = 4.3 Hz, 1H), 7.3 (m, 4H), 7.1(d, *J* = 5.2 Hz, 2H), 5.1 (s, 1H).

^{13}C NMR (75.48 MHz, *DMSO-d$_6$*): δ (ppm) = 177, 172, 153, 148, 141, 136, 133, 130, 127, 125, 124, 123, 122, 120, 114, 100, 39.

3.4 Synthesis of Rhenium compounds

3.4.1 Synthesis of *fac*-[NEt$_4$]$_2$[Re(CO)$_3$(Br)$_3$] (ReAA)

$$ReBr(CO)_5 + 2(NEt_4)Br \xrightarrow{N_2,\text{diglyme}} fac\text{-}[NEt_4]_2[ReBr_3(CO)_3] + 2CO$$

Dried and grounded (NEt$_4$)Br (5.0 g, 24.0 mmol) was dissolved in 2,5,8-trioxanone diglyme (150 mL) under a dry nitrogen atmosphere and slurried in a preheated oil bath at a temperature of 80 ºC for 30 minutes. The system was evacuated and purged with nitrogen gas several times. Solid Re(CO)$_5$Br (5.0 g, 12.3 mmol) was added to the reaction mixture and stirred at 115 ºC for 16 hours. The reaction mixture was cooled down to room temperature and the precipitate was filtered off and dried. The precipitate was stirred in a small amount of cold ethanol for 5 minutes, filtered and washed with cold DCM. The product is slightly soluble in ethanol. Yield: 85 %, 8.0351 g, 10.5 mmol.

IR (KBr, cm^{-1}): $\nu_{Re(CO)}$ = 1995, 1846.

3.4.2 *fac*-[NEt$_4$][Re(CO)$_3$(Br)(TIF)]

ReAA (100 mg, 0.130 mmol) was dissolved in methanol (10 mL). 2,2,2-Trifluoro-1-(3-hydroxy-1H-inden-2-yl)ethan-1-one (29.6 mg, 0.130 mmol) was added to the reaction mixture and it was stirred at room temperature for 24 hours. The light orange product was collected by vacuum, washed with water and weighed. Yield: 89 %, 81.86 mg, 0.116 mmol.

UV/Vis: 348 nm, ε = 51123 M^{-1}cm^{-1}.

IR (KBr, cm^{-1}): $\nu_{Re(CO)}$ = 2015, 1882, $\nu_{(C=O)}$ = 1671, $\nu_{(CF)}$= 1334, 1272, 1130, $\nu_{(CF_3)}$= 750.

^{1}H NMR (300.18 MHz, DMSO-*d*$_6$): δ (ppm) = 7.5 (d, *J* = 4.7 Hz, 1H), 7.3 (d, *J* = 4.7 Hz, 1H), 7.1 (d, *J* = 4.7 Hz, 1H), 6.5 (d, *J* = 4.3 Hz, 1H), 4.2 (d, *J* = 4.2 Hz, 2H), 2.9 (q, 8H (NEt_4)), 1.1 (tt, 12H (NEt_4)).

^{13}C NMR (75.48 MHz, DMSO-*d*$_6$): δ (ppm) = 183, 179, 175, 150, 148, 132, 129, 127, 125, 117, 108, 51 (NEt_4), 28, 7 (NEt_4).

3.4.3 *fac*-[Re(CO)$_3$(MeOH)(TIF)]

fac-[NEt_4][$Re(CO)_3$(Br)(TIF)] (10.20 mg, 0.014 mmol) was dissolved in methanol (10 mL) and stirred for 7 hours at 35 ˚C. The light orange product was washed with water and the product filtered, washed with water and weighed. Yield: 83 %, 7.61 mg, 0.00115 mmol.

UV/Vis: 350 nm, ε = 54941 M^{-1}cm^{-1}.

IR (KBr, cm^{-1}): $\nu_{Re(CO)}$ = 2021, 1911, $\nu_{(C=O)}$ = 1674, $\nu_{(CF)}$= 1337, 1276, 1134, $\nu_{(CF_3)}$= 752.

^{1}H NMR (300.18 MHz, DMSO-*d*$_6$): δ (ppm) = 7.1 (d, *J* = 4.1 Hz, 1H), 7.0 (d, *J* = 4.2 Hz, 1H), 6.8 (d, *J* = 4.2 Hz, 1H), 5.8 (d, *J* = 4.0 Hz, 1H), 4.8 (d, *J* = 4.4 Hz, 2H).

^{13}C NMR (75.48 MHz, DMSO-*d*$_6$): δ (ppm) = 176, 172, 155, 146, 136, 133, 130, 129, 121, 113, 31.

3.4.4 *fac*-[Re(CO)$_3$(TU)(TIF)]

fac-[NEt_4][$Re(CO)_3$(Br)(TIF)] (10.21 mg, 0.014 mmol) was dissolved in methanol (10 mL) and stirred for 24 hours. Thiourea (1.10 mg, 0.014 mmol) was added to the stirring solution and left to stir for 2 hours at 35 ˚C. The solvent was evaporated, washed with water and the yellow product was weighed. Yield: 79 %, 6.4 mg, 0.011 mmol.

UV/Vis: 345 nm, ε = 50434 M^{-1}cm^{-1}.

IR (KBr, cm^{-1}): $\nu_{Re(CO)}$ = 2024, 1965, $\nu_{(C=O)}$ = 1658, $\nu_{(CF)}$= 1328, 1271, 1129, $\nu_{(CF_3)}$= 757.

^{1}H NMR (300.18 MHz, DMSO-*d*$_6$): δ (ppm) = 7.5 (d, *J* = 4.6 Hz, 2H), 7.3 (s, 4H), 6.9 (d, *J* = 4.3 Hz, 1H), 6.6 (d, *J* = 4.3 Hz, 1H), 4.2 (d, *J* = 4.5 Hz, 2H).

^{13}C NMR (75.48 MHz, DMSO-*d*$_6$): δ (ppm) = 182, 170, 167, 147, 143, 132, 130, 127, 124, 121, 110, 25.

3.4.5 *fac*-[NEt$_4$][Re(CO)$_3$(NCS)(TIF)]

fac-[NEt$_4$][Re(CO)$_3$(Br)(TIF)] (10.52 mg, 0.015 mmol) was dissolved in methanol and stirred for 24 hours. Sodium thiocyanate (1.22 mg, 0.015 mmol) was added to the stirring solution and left to stir for 4 hours at 35 ˚C. The solvent was evaporated and the yellow product was washed with water and weighed. Yield: 93 %, 7.8 mg, 0.014 mmol.

UV/Vis: 355 nm, ε = 574691 M^{-1}cm^{-1}.

IR (KBr, cm^{-1}): $\nu_{C=N}$ = 2245, $\nu_{Re(NCS)}$ = 2145, $\nu_{Re(CO)}$ = 2018, 1907, $\nu_{(C=O)}$ = 1681, $\nu_{(CF)}$= 1340, 1282, 1145, $\nu_{(CF_3)}$= 749.

^{1}H NMR (300.18 MHz, DMSO-*d*$_6$): δ (ppm) = 6.7 (d, *J* = 2.3 Hz, 1H), 6.5 (d, *J* = 2.4 Hz, 1H), 6.3 (d, *J* = 2.3 Hz, 1H), 6.1 (d, *J* = 2.4 Hz, 1H), 4.6 (d, *J* = 2.3 Hz, 2H).

^{13}C NMR (75.48 MHz, DMSO-*d*$_6$): δ (ppm) = 180, 177, 162, 144, 138, 133, 124, 123, 121, 113, 97, 35.

3.4.6 *fac*-[Re(CO)$_3$(PCy$_3$)(TIF)]

fac-[NEt$_4$][Re(CO)$_3$(Br)(TIF)] (10.41 mg, 0.015 mmol) was dissolved in methanol (10 mL) and stirred for 24 hours. Tricyclohexylphosphine (4.21 mg, 0.015 mmol) was added to the stirring solution and left to stir for 4 hours at 35 ˚C. The solvent was evaporated, washed with water and the yellow product was weighed. Yield: 74 %, 8.5 mg, 0.011 mmol.

UV/Vis: 350 nm, ε = 56311 M^{-1}cm^{-1}.

IR (KBr, cm^{-1}): $\nu_{Re(CO)}$ = 2021, 1904, $\nu_{(C=O)}$ = 1675, $\nu_{(CF)}$= 1334, 1278, 1140, $\nu_{(CF_3)}$= 746.

^{1}H NMR (300.18 MHz, DMSO-*d*$_6$): δ (ppm) = 7.1 (d, *J* = 3.5 Hz, 1H), 6.7 (d, *J* = 3.3 Hz, 1H), 6.4 (d, *J* = 4.5 Hz, 1H), 6.1 (d, *J* = 4.2 Hz, 1H), 5.8 (d, *J* = 3.8 Hz, 2H), 1.5-1.4 (m, 33 H).

^{13}C NMR (75.48 MHz, DMSO-*d*$_6$): δ (ppm) = 183, 179, 173, 168, 162, 144, 136, 120, 118, 110, 94, 68, 64, 54, 46, 35, 30.

3.4.7 *fac*-[Re(CO)$_3$(H$_2$O)(TIF)]

ReAA (100 mg, 0.130 mmol) was dissolved in H_2O at pH 2 (adjusted with HNO_3). Silver nitrate (66.2 mg, 0.390 mmol) was added to the solution and stirred for 24 hours at room temperature. The AgBr was filtered off. 2,2,2-Trifluoro-1-(3-hydroxy-1H-inden-2-yl)ethan-1-one (29.62 mg, 0.130 mmol) was added to the reaction mixture and it was stirred at room temperature for 24 hours. The orange precipitate was filtered and weighed. Yield: 89 %, 59.9 mg, 0.116 mmol.

UV/Vis: 348 nm, ε = 54591 $M^{-1}cm^{-1}$.

IR (KBr, cm^{-1}): $\nu_{Re(CO)}$ = 2040, 1971, $\nu_{(C=O)}$ = 1661, $\nu_{(CF)}$= 1331, 1268, 1131, $\nu_{(CF_3)}$= 752.

^{1}H NMR (300.18 MHz, *DMSO-d*$_6$): δ (ppm) = 7.9 (d, *J* = 4.5 Hz, 1H), 7.6 (t, *J* = 3.9 Hz, 1H), 7.3 (d, *J* = 3.9 Hz, 1H), 6.8 (t, *J* = 4.5 Hz, 1H), 4.7 (d, *J* = 4.8 Hz, 2H).

^{13}C NMR (75.48 MHz, *DMSO-d*$_6$): δ (ppm) = 177, 173, 142, 135, 134, 122, 120, 119, 111, 92, 23.

3.4.8 *fac*-[NEt$_4$][Re(CO)$_3$(Br)(MeTIF)]

ReAA (100 mg, 0.130 mmol) was dissolved in methanol (10 mL). 2,2,2-Trifluoro-1-(3-hydroxy-1-methyl-1H-inden-2-yl)ethan-1-one (31.48 mg, 0.130 mmol) was added to the reaction mixture and it was stirred at room temperature for 24 hours. The light orange product was collected by vacuum, washed with water and weighed. Yield: 84%, 78.5 mg, 0.11 mmol.

UV/Vis: 345 nm, 555 nm , ε = 51481 $M^{-1}cm^{-1}$, 47587 $M^{-1}cm^{-1}$.

IR (KBr, cm^{-1}): $\nu_{Re(CO)}$ = 2018, 1901, $\nu_{(C=O)}$ = 1651, $\nu_{(CF)}$= 1311, 1242, 1118, $\nu_{(CF_3)}$= 759.

^{1}H NMR (300.18 MHz, *DMSO-d$_6$*): δ (ppm) = 7.0 (m, 3H), 6.5 (d, *J* = 4.7 Hz, 1H), 3.4 (s, 1H), 2.8 (s, 3H), 2.3 (q, 8H (NEt_4)), 1.2 (tt, 12H (NEt_4)).

^{13}C NMR (75.48 MHz, *DMSO-d$_6$*): δ (ppm) = 174, 170, 146, 141, 132, 121, 118, 119, 114, 111, 109, 52(NEt_4), 25, 24 (NEt_4), 20.

3.4.9 *fac*-[Re(CO)$_3$(MeOH)(MeTIF)]

fac-[NEt_4][Re(CO)$_3$(Br)(MeTIF)] (10.60 mg, 0.015) was dissolved in methanol and stirred for 24 hours at temperature of 35 ˚C. The light yellow product was collected by vacuum, washed with water and weighed. Yield: 87 %, 6.8 mg, 0.013 mmol.

UV/Vis: 348 nm, ε = 55041 $M^{-1}cm^{-1}$.

IR (KBr, cm^{-1}): $\nu_{Re(CO)}$ = 2018, 1908, $\nu_{(C=O)}$ = 1680, $\nu_{(CF)}$= 1339, 1277, 1135, $\nu_{(CF_3)}$= 756.

^{1}H NMR (300.18 MHz, *DMSO-d$_6$*): δ (ppm) = 7.7 (d, *J* = 3.8 Hz, 2H), 7.4 (d, *J* = 3.8 Hz, 2H), 4.9 (d, *J* = 3.1 Hz, 1H), 2.8 (t, *J* = 2.7 Hz, 3H).

^{13}C NMR (75.48 MHz, *DMSO-d$_6$*): δ (ppm) = 177, 171, 140, 136, 133, 119, 117, 115, 111, 90, 31, 26.

3.4.10 *fac*-[Re(CO)$_3$(TU)(MeTIF)]

fac-[NEt_4][Re(CO)$_3$(Br)(MeTIF)] (10.14 mg, 0.013 mmol) was dissolved in methanol and stirred for 24 hours. Thiourea (0.97 mg, 0.013 mmol) was added to the stirring solution and left to stir for 4 hours at 35 ˚C. The light yellow product was collected by vacuum, washed with water and weighed. Yield: 82 %, 7.7 mg, 0.011 mmol.

UV/Vis: 345 nm, ε = 51771 $M^{-1}cm^{-1}$.

IR (KBr, cm^{-1}): $\nu_{Re(CO)}$= 2028, 1941 cm^{-1}, $\nu_{(C=O)}$ = 1675, $\nu_{(CF)}$= 1336, 1268, 1138, $\nu_{(CF_3)}$= 750.

^{1}H NMR (300.18 MHz, *DMSO-d$_6$*): δ (ppm) = 6.9 (d, *J* = 3.8 Hz, 2H), 6.7 (s, 4H), 6.5 (t, *J* = 3.8 Hz, 1H), 6.1 (d, *J* = 3.2 Hz, 1H), 5.7 (t, *J* = 3.8 Hz, 1H), 3.0 (d, *J* = 3.2 Hz, 3H).

^{13}C NMR (75.48 MHz, *DMSO-d$_6$*): δ (ppm) = 183, 181, 178, 152, 142, 137, 125, 120, 119, 114, 103, 36, 29.

3.4.11 *fac*-[NEt$_4$][Re(CO)$_3$(NCS)(MeTIF)]

fac-[NEt$_4$][Re(CO)$_3$(Br)(MeTIF)] (10.41 mg, 0.014 mmol) was dissolved in methanol and stirred for 24 hours. Sodium thiocyanate (1.14 mg, 0.014 mmol) was added to the stirring solution and left to stir for 4 hours at 35 ˚C. The light yellow product was collected by vacuum, washed with water and weighed. Yield: 83 %, 6.8 mg, 0.012 mmol.

UV/Vis: 345 nm, ε = 58149 M^{-1}cm^{-1}.

IR (KBr, cm^{-1}): $\nu_{C=N}$ = 2245, $\nu_{Re(NCS)}$ = 2150, $\nu_{Re(CO)}$ = 2104, 1914, $\nu_{(C=O)}$ = 1676, $\nu_{(CF)}$= 1335, 1279, 1138, $\nu_{(CF_3)}$= 761.

^{1}H NMR (300.18 MHz, *DMSO-d$_6$*): δ (ppm) = 7.4 (d, *J* = 2.1 Hz, 1H), 7.1 (t, *J* = 2.1 Hz, 1H), 6.5 (d, *J* = 2.7 Hz, 1H), 6.0 (t, *J* = 2.7 Hz, 1H), 3.5 (d, *J* = 2.6 Hz, 2H). 2.6 (q, 8H (NEt$_4$)), 1.2 (tt, 12H (NEt$_4$)).

^{13}C NMR (75.48 MHz, *DMSO-d$_6$*): δ (ppm) = 181, 178, 162, 152, 142, 137, 125, 120, 119, 114, 103, 51 (NEt$_4$), 36, 29, 27 (NEt$_4$).

3.4.12 *fac*-[Re(CO)$_3$(PCy$_3$)(MeTIF)]

fac-[NEt$_4$][Re(CO)$_3$(Br)(MeTIF)] (10.13 mg, 0.014 mmol) was dissolved in methanol and stirred for 24 hours. Tricyclohexylphosphine (3.94 mg, 0.014 mmol) was added to the stirring solution and left to stir for 4 hours at 35 ˚C. The light yellow product was collected by vacuum, washed with water and weighed. Yield: 71 %, 7.9 mg, 0.010 mmol.

UV/Vis: 320 nm, ε = 57394 M^{-1}cm^{-1}.

IR (KBr, cm^{-1}): $\nu_{Re(CO)}$ = 2026, 1914, $\nu_{(C=O)}$ = 1670, $\nu_{(CF)}$= 1341, 1282, 1141, $\nu_{(CF_3)}$= 748.

^{1}H NMR (300.18 MHz, *DMSO-d$_6$*): δ (ppm) = 8.5 (d, *J* = 4.7 Hz, 1H), 7.8 (d, *J* = 4.2 Hz, 1H), 7.1 (d, *J* = 2.7 Hz, 1H), 6.8 (t, *J* = 3.4.7 Hz, 1H), 4.5 (d, *J* = 3.7 Hz, 2H), 1.49 - 1.42 (m, 33H).

^{13}C NMR (75.48 MHz, *DMSO-d$_6$*): δ (ppm) = 177, 175, 158, 147, 135, 124, 123, 122, 117, 115, 113, 97, 68, 64, 54, 46, 41, 23.

3.4.13 *fac*-[Re(CO)$_3$(H$_2$O)(MeTIF)]

ReAA (100 mg, 0.130 mmol) was dissolved in H_2O at pH 2 (adjusted with HNO_3). Silver nitrate (66.2 mg, 0.390 mmol) was added to the solution and stirred for 24 hours at room temperature. The AgBr was filtered off. 2,2,2-Trifluoro-1-(3-hydroxy-1-methyl-1H-inden-2-yl)ethan-1-one (31.48 mg, 0.130 mmol) was added to the reaction mixture and it was stirred at room temperature for 24 hours. The orange precipitate was filtered and weighed. Yield: 80 %, 55.12 mg, 0.104 mmol.

UV/Vis: 353 nm, 530 nm, ε = 54851 $M^{-1}cm^{-1}$, 48019 $M^{-1}cm^{-1}$.
IR (KBr, cm^{-1}): $\nu_{Re(CO)}$ = 2039, 1967, $\nu_{(C=O)}$ = 1662, $\nu_{(CF)}$= 1319, 1253, 1127, $\nu_{(CF_3)}$= 743.
^{1}H NMR (300.18 MHz, *DMSO-d$_6$*): δ (ppm) = 7.4 (m, 3H), 7.0 (d, *J* = 3.7 Hz, 1H), 3.8 (s, 1H), 3.1 (s, 3H).
^{13}C NMR (75.48 MHz, *DMSO-d$_6$*): δ (ppm) = 178, 172, 143, 136, 124, 121, 120, 119, 115, 111, 28, 22.

3.4.14 *fac*-[NEt$_4$][Re(CO)$_3$(Br)(PhTIF)]

ReAA (100 mg, 0.130 mmol) was dissolved in methanol (10 mL). 2,2,2-Trifluoro-1-(3-hydroxy-1-phenyl-1H-inden-2-yl)ethan-1-one (39.5 mg, 0.130 mmol) was added to the reaction mixture and it was stirred at room temperature for 2 hours. The light yellow precipitate was filtered and weighed. Yield: 93 %, 94.74 mg, 0.121 mmol.

UV/Vis: 455 nm, 525 nm, ε = 61401, 58614 M^{-1} cm^{-1}.
IR (KBr, cm^{-1}): $\nu_{Re(CO)}$ = 2012, 1886, $\nu_{(C=O)}$ = 1678, $\nu_{(CF)}$= 1338, 1272, 1136, $\nu_{(CF_3)}$= 754.
^{1}H NMR (300.18 MHz, *DMSO-d$_6$*): δ (ppm) = 7.5 (d, *J* = 4.5 Hz, 1H), 7.0 (d, *J* = 4.6 Hz, 1H), 6.8 (t, *J* = 4.4 Hz, 1H), 6.6 (m, 4H), 6.4 (d, *J* = 4.2 Hz, 2H), 4.7 (s, 1H), 2.81 (q, 8H (NEt_4)), 1.08 (tt, 12H (NEt_4)).
^{13}C NMR (75.48 MHz, *DMSO-d$_6$*): δ (ppm) = 173, 169, 150, 143, 136, 130, 127, 125, 123, 120, 118, 117, 115, 113, 110, 98, 34, 51.33 (NEt_4), 7.04 (NEt_4).

3.4.15 *fac*-[Re(CO)$_3$(H$_2$O)(PhTIF)]

ReAA (100 mg, 0.130 mmol) was dissolved in H_2O at pH 2 (adjusted with HNO_3). Silver nitrate (66.2 mg, 0.390 mmol) was added to the solution and stirred for 24 hours at room temperature. The AgBr was filtered off. 2,2,2-Trifluoro-1-(3-hydroxy-1-phenyl-1H-inden-2-yl)ethan-1-one (39.5 mg, 0.130 mmol) was added to the reaction mixture and it was stirred at room temperature for 24 hours. The orange precipitate was filtered and weighed. Yield: 93 %, 63.8 mg, 0.120 mmol.

UV/Vis: 454 nm, 523 nm, ε = 63012, 59612 $M^{-1}cm^{-1}$.

IR (KBr, cm^{-1}): $\nu_{Re(CO)}$ = 2041, 1968, $\nu_{(C=O)}$ = 1676, $\nu_{(CF)}$= 1335, 1272, 1132, $\nu_{(CF_3)}$= 755.

^{1}H NMR (300.18 MHz, *DMSO-d$_6$*): δ (ppm) = 7.3 (d, *J* = 3.8 Hz, 1H), 7.0 (d, *J* = 3.8 Hz, 1H), 6.5 (t, *J* = 2.6 Hz, 1H), 6.2 (m, 4H), 5.8 (d, *J* = 2.6 Hz, 2H), 4.3 (s, 1H).

^{13}C NMR (75.48 MHz, *DMSO-d$_6$*): δ (ppm) = 175, 172, 163, 148, 139, 135, 133, 131, 130, 125, 125, 123, 121, 118, 115, 101, 41.

3.4.16 *fac*-[NEt$_4$][Re(CO)$_3$(Br)(3,5-DiMePh)]

ReAA (100 mg, 0.130 mmol) was dissolved in methanol (10 ml). 1,3-Bis(3,5-dimethylphenyl)propane-1,3-dione (36.5 mg, 0.130 mmol) was added to the reaction mixture and it was stirred at room temperature for 2 hours. The light yellow product was collected by vacuum, washed with water and weighed. Yield: 86 %, 70.5 mg, 0.112 mmol.

UV/Vis: 328 nm, ε = 61612 $M^{-1}cm^{-1}$.

IR (KBr, cm^{-1}): $\nu_{Re(CO)}$ = 2011, 1876.

^{1}H NMR (300.18 MHz, *CD$_2$Cl$_2$-d$_2$*): δ (ppm) = 7.65 (m, 4H), 7.25 (s, 2H), 6.88 (s, 1H), 2.43 (s, 12H), 2.28 (q, 8H (NEt_4)), 1.07(tt, 12H (NEt_4)).

^{13}C NMR (75.48 MHz, *CD$_2$Cl$_2$-d$_2$*): δ (ppm) = 183, 135, 131, 129, 123, 90, 52 (NEt_4), 26 (NEt_4), 17.

3.4.17 *fac*-[Re(CO)$_3$(H$_2$O)(3,5-DiMePh)]

ReAA (100 mg, 0.130 mmol) was dissolved in H_2O at pH 2 (adjusted with HNO_3). Silver nitrate (66.2 mg, 0.390 mmol) was added to the solution and stirred for 24 hours at room temperature. The AgBr was filtered off and 1,3-bis(3,5-dimethylphenyl)propane-1,3-dione (36.5 mg, 0.130 mmol) was added to the solution and stirred for 4 hours. The reaction mixture was filtered and the yellow precipitate was dried and weighed. Yield: 79 %, 72.9 mg, 0.103 mmol.

UV/Vis: 345 nm, ε = 62141 M^{-1} cm^{-1}.

IR (KBr, cm^{-1}): $\upsilon_{Re(CO)}$ = 2024, 1947.

^{1}H NMR (300.18 MHz, *DMSO-d$_6$*): δ (ppm) = 8.25 (m, 4H), 7.08 (s, 2H), 2.83 (s, 12H).

^{13}C NMR (75.48 MHz, *DMSO-d$_6$*): δ (ppm) = 185, 138, 135, 134, 124, 93, 21.

3.4.18 *fac*-[NEt$_4$][Re(CO)$_3$(Br)(MeDiPhPr)]

ReAA (100 mg, 0.130 mmol) was dissolved in methanol (10 ml). 2-Methyl-1,3-diphenylpropane-1,3-dione (30.9 mg, 0.130 mmol) was added to the reaction mixture and it was stirred at room temperature for 2 hours. The light yellow product was collected by vacuum, washed with water and weighed. Yield: 91%, 69.6 mg, 0.118 mmol.

UV/Vis: 319 nm, ε = 60514 $M^{-1}cm^{-1}$.

IR (KBr, cm^{-1}): $\upsilon_{Re(CO)}$ = 2017, 1859.

^{1}H NMR (300.18 MHz, *CD$_2$Cl$_2$-d$_2$*): δ (ppm) = 7.92 (m, 4H), 7.59 (m, 4H), 7.47 (m, 2H), 2.85 (q, 8H (NEt_4)) 1.70 (s, 3H), 1.12 (tt, 12H (NEt_4))

^{13}C NMR (**75.48 MHz, *CD$_2$Cl$_2$-d$_2$*)**: δ (ppm) = 165, 136, 134, 129, 128, 53 (NEt_4) 51, 29 (NEt_4), 14.

3.4.19 *fac*-[Re(CO)$_3$(H$_2$O)(MeDiPhPr)]

ReAA (100 mg, 0.130 mmol) was dissolved in H_2O at pH 2 (adjusted with HNO_3). Silver nitrate (66.2 mg, 0.390 mmol) was added to the solution and stirred for 24 hours at room temperature. The AgBr was filtered off. 2-Methyl-1,3-diphenylpropane-

1,3-dione (36.8 mg, 0.130 mmol) was added to the solution and stirred for 4 hours. The reaction mixture was filtered and the yellow precipitate was dried and weighed. Yield: 81 %, 70.4 mg, 0.105 mmol.

UV/Vis: 330 nm, ε = 64834 $M^{-1}cm^{-1}$.

IR (KBr, cm^{-1}): $\nu_{Re(CO)}$ = 2028, 1946.

^{1}H NMR (300.18 MHz, *DMSO-d$_6$*): δ (ppm) = 8.32 (m, 4H), 7.82 (m, 4H), 7.50 (m, 2H), 2.930 (s, 3H).

^{13}C NMR (75.48 MHz, *DMSO-d$_6$*): δ (ppm) = 189, 144, 141, 131, 121, 49, 18.

3.4.20 *fac*-[NEt$_4$][Re(CO)$_3$(Br)(BrDiPhPr)]

ReAA (100 mg, 0.130 mmol) was dissolved in methanol (10 ml). 2-Bromo-1,3-diphenylpropane-1,3-dione (39.4 mg, 0.130 mmol) was added to the reaction mixture and it was stirred at room temperature for 2 hours. The light yellow product was collected by vacuum, washed with water and weighed. Yield: 82 %, 69.6 mg, 0.107 mmol.

UV/Vis: 369 nm, ε = 61479 $M^{-1}cm^{-1}$.

IR (KBr, cm^{-1}): $\nu_{Re(CO)}$ = 2014, 1881.

^{1}H NMR (300.18 MHz, *CD$_2$Cl$_2$-d$_2$*): δ (ppm) = 7.97 - 7.88 (m, 4H), 7.67 – 7.59 (m, 4H), 7.47 (m, 2H), 2.65 (q, 8H (NEt_4)), 1.15 (tt, 12H (NEt_4)).

^{13}C NMR (75.48 MHz, *CD$_2$Cl$_2$-d$_2$*): δ (ppm) = 156, 128, 124, 129, 128, 54 (NEt_4) 51, 28 (NEt_4).

3.4.21 *fac*-[Re(CO)$_3$(MeOH)(BrDiPhPr)]

fac-[NEt_4][$Re(CO)_3$(Br)(BrDiPhPr)] (10.07 mg, 0.015 mmol) was dissolved in methanol and stirred for 24 hours at 35 ˚C. The solvent was evaporated and the yellow product was washed with water and weighed. Yield: 81 %, 7.3 mg, 0.012 mmol.

UV/Vis: 350 nm, ε = 60591 $M^{-1}cm^{-1}$.

IR (KBr, cm^{-1}): $\nu_{Re(CO)}$ = 2023, 1887.

^{1}H NMR (300.18 MHz, *DMSO-d$_6$*): δ (ppm) = 7.1 (d, *J* = 3.4 Hz, 4H), 6.7 (d, *J* = 3.1 Hz, 4H), 6.2 (d, *J* = 3.4 Hz, 2H), 3.2 (s, 3H).
^{13}C NMR (75.48 MHz, *DMSO-d$_6$*): δ (ppm) = 181, 176, 151, 141, 137, 119, 114, 76.

3.4.22 *fac*-[Re(CO)$_3$(TU)(BrDiPhPr)]

fac-[NEt$_4$][Re(CO)$_3$(Br)(BrDiPhPr)] (10.6 mg, 0.016 mmol) was dissolved in methanol and stirred for 24 hours. Thiourea (1.20 mg, 0.016 mmol) was added to the stirring solution and left to stir for 6 hours at 35 ˚C. The solvent was evaporated and the yellow product was washed with water and weighed. Yield: 74 %, 8.7 mg, 0.012 mmol.

UV/Vis: 343 nm, ε = 59896 M^{-1}cm^{-1}.
IR (KBr, cm^{-1}): $\upsilon_{Re(CO)}$ = 2021, 1912.
^{1}H NMR (300.18 MHz, *DMSO-d$_6$*): δ (ppm) = 7.1 (d, *J* = 3.5 Hz, 4H), 6.8 (d, *J* = 2.3 Hz, 2H), 6.6 (d, *J* = 2.3 Hz, 2H), 6.4 (t, *J* = 2.1 Hz, 4H), 6.1 (d, *J* = 1.6 Hz, 2H).
^{13}C NMR (75.48 MHz, *DMSO-d$_6$*): δ (ppm) = 182, 174, 171, 138, 135, 130, 114, 110, 81.

3.4.23 *fac*-[NEt$_4$][Re(CO)$_3$(NCS)(BrDiPhPr)]

fac-[NEt$_4$][Re(CO)$_3$(Br)(BrDiPhPr)] (10.01 mg, 0.015 mmol) was dissolved in methanol and stirred for 24 hours. Sodium thiocyanate (1.24 mg, 0.015 mmol) was added to the stirring solution and left to stir for 6 hours at 35 ˚C. The solvent was evaporated, washed with water and the yellow product was weighed. Yield: 99 %, 9.58 mg, 0.014 mmol.

UV/Vis: 350 nm, ε = 61581 M^{-1}cm^{-1}.
IR (KBr, cm^{-1}): $\upsilon_{C=N}$ = 2255, $\upsilon_{Re(NCS)}$ = 2151, $\upsilon_{Re(CO)}$ = 2013, 1897. $\upsilon_{(C=O)}$ = 1673, $\upsilon_{(CF)}$= 1328, 1298, 1125, $\upsilon_{(CF_3)}$= 754.
^{1}H NMR (300.18 MHz, *DMSO-d$_6$*): δ (ppm) = 7.4 (d, *J* = 4.1 Hz, 4H), 6.9 (t, *J* = 3.8 Hz, 2H), 6.4 (d, *J* = 2.5 Hz, 4H), 4.2 (d, *J* = 2.5 Hz, 1H), 2.76 (q, 8H (NEt$_4$)), 1.14 (tt, 12H (NEt$_4$)).
^{13}C NMR (75.48 MHz, *DMSO-d$_6$*): δ (ppm) = 179, 175, 141, 131, 126, 108, 101, 73, 52 (NEt$_4$), 25 (NEt$_4$).

3.4.24 *fac*-[Re(CO)$_3$(PPh$_3$)(BrDiPhPr)]

fac-[NEt$_4$][Re(CO)$_3$(Br)(BrDiPhPr)] (10.03 mg, 0.015 mmol) was dissolved in methanol and stirred for 24 hours. Triphenylphosphine (4.03 mg, 0.015 mmol) was added to the stirring solution and left to stir for 6 hours at 30 ˚C. The solvent was evaporated and the yellow product was weighed. Yield: 71 %, 9.8 mg, 0.0107 mmol.

UV/Vis: 350 nm, ε = 63897 $M^{-1}cm^{-1}$.

IR (KBr, cm^{-1}): $\nu_{Re(CO)}$ = 2021, 1923.

^{1}H NMR (300.18 MHz, *CD_2Cl_2-d_2*): δ (ppm) = 7.45 (d, *J* = 4.6 Hz, 4H), 7.43 (s, 2H), 7.40 (d, *J* = 4.6 Hz, 4H) 7.2 - 6.7 (m, 15H).

^{13}C NMR (75.48 MHz, *CD_2Cl_2-d_2*): δ (ppm) = 181, 178, 176, 175, 173, 170, 167,166, 165, 161,158, 157, 153, 151, 148, 145, 141, 140 139, 137, 136, 134, 133, 131, 113, 71.

3.4.25 *fac*-[Re(CO)$_3$(H$_2$O)(BrDiPhPr)]

ReAA (100 mg, 0.130 mmol) was dissolved in H_2O at pH 2 (adjusted with HNO_3). Silver nitrate (66.2 mg, 0.390 mmol) was added to the solution and stirred for 24 hours at room temperature. The AgBr was filtered off. 2-Bromo-1,3-diphenylpropane-1,3-dione (39.4 mg, 0.130 mmol) was added to the solution and stirred for 4 hours. The reaction mixture was filtered and the yellow product was weighted. Yield: 90 %, 76.4 mg, 0.117 mmol.

UV/Vis: 352 nm, ε = 61117 $M^{-1}cm^{-1}$.

IR (KBr, cm^{-1}): $\nu_{Re(CO)}$ = 2030, 1966.

^{1}H NMR (300.18 MHz, *CD_3OD-d_4*): δ (ppm) = 8.00 (*d*, *J* = 7.9 Hz, 4H), 7.63 (t, *J* = 7.0 Hz, 2H), 7.49 (t, *J* = 7.5 Hz, 4H).

^{13}C NMR (75.48 MHz, *CD_3OD-d_4*): δ (ppm) = 171, 135, 135, 130, 121, 53.

3.4.26 *fac*-[Re(CO)$_3$(Br)(BAHY)]

ReAA (100 mg, 0.130 mmol) was dissolved in methanol (3 ml). Benzoic anhydride (29.4 mg, 130 mmol) was dissolved in methanol (2 mL) and added to the rhenium solution. The mixture was stirred at room temperature for 2 hours. The light yellow

product was collected by vacuum, washed with water and weighed. Yield: 86 %, 64.6 mg, 0.112 mmol.

UV/Vis: 352 nm, ε = 61721 M^{-1} cm^{-1}.

IR (KBr, cm^{-1}): $\upsilon_{Re(CO)}$ = 2019, 1893.

^{1}H NMR (300.18 MHz, *DMSO-d_6*): δ (ppm) = 8.21 - 8.11 (m, 4H), 7.78 - 7.69 (m, 4H), 7.62 - 7.52 (m, 2H).

^{13}C NMR (75.48 MHz, *DMSO-d_6*): δ (ppm) = 162, 134, 133, 130, 130.

3.4.27 *fac*-[$Re(CO)_3(H_2O)(BAHY)][NO_3$]

ReAA (100 mg, 0.130 mmol) was dissolved in H_2O at pH 2 (adjusted with HNO_3). Silver nitrate (66.2 mg, 0.390 mmol) was added to the solution and stirred for 24 hours at room temperature. The AgBr was filtered off. Benzoic anhydride (29.4 mg, 0.130 mmol) was added to the solution and stirred for 4 hours. The precipitate was filtered and weighed. Yield: 90 %, 60.3 mg, 0.117 mmol.

UV/Vis: 352 nm, ε = 61949 $M^{-1}cm^{-1}$.

IR (KBr, cm^{-1}): $\upsilon_{Re(CO)}$ = 2030, 1966.

^{1}H NMR (300 MHz, *CD_3OD-d_4*): δ (ppm) = 7.95 (d, *J* = 7.4 Hz, 4H), 7.51 (t, *J* = 6.7 Hz, 2H), 7.39 (t, *J* = 6.9 Hz, 4H).

***^{13}*C NMR (75 MHz, *CD_3OD -d_4*)**: δ (ppm) = 169, 134, 131, 130, 129, 68.

3.4.28 *fac*-[NEt_4][$Re(CO)_3$(Br)(4-MeTPh)]

ReAA (100 mg, 0.130 mmol) was dissolved in methanol (10 ml). 1,3-Bis(4-methoxyphenyl)propane-1,3-dione (36.9 mg, 0.130 mmol) was added to the reaction mixture and it was stirred at room temperature for 2 hours. The yellow product was collected by vacuum, washed with water and weighed. Yield: 90 %, 74.2 mg, 0.117 mmol.

UV/Vis: 388 nm, ε = 62387 $M^{-1}cm^{-1}$.

IR (KBr, cm^{-1}): $\upsilon_{Re(CO)}$= 2017, 1900.

^{1}H NMR (300.18 MHz, *CD_2Cl_2-d_2*): δ (ppm) = 7.97 (d, *J* = 9.0 Hz, 4H), 6.99 (d, *J* = 8.9 Hz, 4H), 3.88 (s, 6H), 2.51 (q, 8H (NEt_4)), 1.10 (tt, 12H (NEt_4)).

^{13}C NMR (75.48 MHz, *CD_2Cl_2-d_2*): δ (ppm) = 154, 138, 129, 128, 113, 91, 55.

3.4.29 *fac*-[Re(CO)$_3$(MeOH)(4-MeTPh)]

fac-[NEt$_4$][Re(CO)$_3$(Br)(4-MeTPh)] (10.10 mg, 0.019 mmol) was dissolved in methanol and stirred for 24 hours at temperature of 35 ˚C. The yellow product was collected by vacuum. Yield: 91 %, 7.6 mg, 0.017 mmol.

UV/Vis: 345 ε = 62667 M^{-1} cm^{-1}.

IR (KBr, cm^{-1}): $\nu_{Re(CO)}$= 2018, 1937.

^{1}H NMR (300.18 MHz, *DMSO-d$_6$*): δ (ppm) = 7.9 (d, *J* = 7.1 Hz, 4H), 7.4 (d, *J* = 6.6 Hz, 4H), 4.6 (s, 6H).

^{13}C NMR (75.48 MHz, *DMSO-d$_6$*): δ (ppm) = 164, 142, 135, 129, 119, 96, 59.

3.4.30 *fac*-[Re(CO)$_3$(TU)(4-MeTPh)]

fac-[NEt$_4$][Re(CO)$_3$(Br)(4-MeTPh)] (10 mg, 0.016 mmol) was dissolved in methanol and stirred for 24 hours. Thiourea (1.22 mg, 0.016 mmol) was added to the stirring solution and left to stir for 2 hours at 30 ˚C. The yellow product was collected by vacuum, washed with water and weighed. Yield: 67 %, 7.6 mg, 0.011 mmol.

UV/Vis: 340 nm, ε = 63210 $M^{-1}cm^{-1}$.

IR (KBr, cm^{-1}): $\nu_{Re(CO)}$= 2018, 1937.

^{1}H NMR (300.18 MHz, *CD$_2$Cl$_2$-d$_2$*): δ (ppm) = 8.49 (s, 4H), 7.74 (d, *J* = 7.4 Hz, 4H), 6.74 (d, *J* = 6.6 Hz, 4H), 3.72 (s, 6H).

^{13}C NMR (75.48 MHz, *CD$_2$Cl$_2$-d$_2$*): δ (ppm) = 187, 183, 181, 160, 142, 128, 126, 111, 93, 52.

3.4.31 *fac*-[NEt$_4$][Re(CO)$_3$(NCS)(4-MeTPh)]

fac-[NEt$_4$][Re(CO)$_3$(Br)(4-MeTPh)] (10 mg, 0.016 mmol) was dissolved in methanol and stirred for 24 hours. Sodium thiocyanate (1.28 mg, 0.016 mmol) was added to the stirring solution and left to stir for 4 hours at 35 ˚C. The solvent was evaporated and the yellow product was washed with water and weighed. Yield: 98 %, 9.58 mg, 0.015 mmol.

UV/Vis: 338 nm, ε = 65036 $M^{-1}cm^{-1}$.

IR (KBr, cm^{-1}): $\nu_{C=N}$ = 2259, $\nu_{Re(NCS)}$ = 2153, $\nu_{Re(CO)}$ = 2017, 1895.

^{1}H NMR (300.18 MHz, *CD_2Cl_2-d_2*): δ (ppm) = 7.64 (d, *J* = 8.1 Hz, 4H), 6.85 (d, *J* =7.6 Hz, 4H), 3.76 (s, 6H), 2.64 (q, 8H (NEt_4)), 1.09 (tt, 12H (NEt_4)).

^{13}C NMR (75.48 MHz, *CD_2Cl_2-d_2*): δ (ppm) = 164, 155, 140, 131, 130, 116, 110, 54 51 (NEt_4), 31, 28 (NEt_4).

3.4.32 *fac*-[$Re(CO)_3(PCy_3)$(4-MeTPh)]

fac-[NEt_4][$Re(CO)_3$(Br)(4-MeTPh)] (10 mg, 0.016 mmol) was dissolved in methanol and stirred for 24 hours. Tricyclohexylphosphine (4.43 mg, 0.016 mmol) was added to the stirring solution and left to stir for 2 hours at 30 ˚C. The yellow product was collected by vacuum, washed with water and weighed. Yield: 56 %, 8.1 mg, 0.009 mmol.

UV/Vis: 340 nm, ε = 64910$M^{-1}cm^{-1}$.

IR (KBr, cm^{-1}): $\nu_{Re(CO)}$ = 2019, 1950.

^{1}H NMR (300.18 MHz, *CD_2Cl_2-d_2*): δ (ppm) = 7.95 (d, *J* = 9.2 Hz, 4H), 6.97 (d, *J* = 8.7 Hz, 4H), 3.85 (s, 6H), 1.37 - 1.33 (m, 33H).

^{13}C NMR (75.48 MHz, *CD_2Cl_2-d_2*): δ (ppm) = 157, 141, 133, 131, 113, 89, 55, 32, 28, 25, 23.

3.4.33 *fac*-[$Re(CO)_3(H_2O)$(4-MeTPh)]

ReAA (100 mg, 0.130 mmol) was dissolved in H_2O at pH 2 (adjusted with HNO_3). Silver nitrate (66.2 mg, 0.390 mmol) was added to the solution and stirred for 24 hours at room temperature. The AgBr was filtered off. 1,3-Bis(4-methoxyphenyl)propane-1,3-dione (36.9 mg, 0.130 mmol) was added to the solution and stirred for 4 hours. The reaction mixture was filtered. The yellow precipitate was dried and weighed. Yield: 87 %, 64.8 mg, 0.113 mmol.

UV/Vis: 360 nm, ε = 63809 M^{-1} cm^{-1}.

IR (KBr, cm^{-1}): $\nu_{Re(CO)}$ = 2036, 1980.

^{1}H NMR (300.18 MHz, *DMSO-d_6*): δ (ppm) = 8.07 (d, *J* = 9.0 Hz, 4H), 7.21 (d, *J* = 8.9 Hz, 4H), 4.88 (s, 6H).

^{13}C NMR (75.48 MHz, *DMSO-d$_6$*): δ (ppm) = 164, 142, 135, 129, 119, 96, 59.

3.4.34 *fac*-[Re(CO)$_3$(Br)(DiMePy)]

ReAA (100 mg, 0.130 mmol) was dissolved in methanol (10 mL). 4,4'-Dimethyl-2,2'-bipyridine (23.9 mg, 0.130 mmol) was added to the reaction mixture and it was stirred at room temperature for 2 hours. The yellow product was collected by vacuum and recrystallized from dichloromethane. Yield: 93 %, 64.6 mg, 0.121 mmol.

UV/Vis: 345 nm, ε = 46209 $M^{-1}cm^{-1}$.

IR (KBr, cm^{-1}): $\nu_{Re(CO)}$ = 2018, 1904.

^{1}H NMR (300.18 MHz, *DMSO-d$_6$*): δ (ppm) = 8.84 (d, *J* = 5.7 Hz, 2H), 8.62 (s, 2H), 7.57 (d, *J* = 5.7 Hz, 2H), 2.56 (s, 6H).

^{13}C NMR (75.48 MHz, *DMSO-d$_6$*): δ (ppm) = 155, 152, 152, 128, 125, 21.

3.4.35 *fac*-[Re(CO)$_3$(MeOH)(DiMePy)][Br]

fac-[Re(CO)$_3$(Br)(DiMePy)] (10.04 mg, 0.019 mmol) was dissolved in methanol and stirred for 24 hours at temperature of 35 ˚C. The yellow product was collected by vacuum. Yield: 82 %, 7.6 mg, 0.016 mmol.

UV/Vis: 360 nm, ε = 47130 M^{-1} cm^{-1}.

IR (KBr, cm^{-1}): $\nu_{Re(CO)}$ = 2022, 1924 cm^{-1}.

^{1}H NMR (300 MHz, *DMSO-d$_6$*): δ (ppm) = 8.7 (d, *J* = 4.5 Hz, 2H), 7.5 (s, 2H), 6.3 (d, *J* = 3.8 Hz, 2H), 4.13 (s, 6H).

^{13}C NMR (75 MHz, *DMSO-d$_6$*): δ (ppm) = 158, 156, 151, 147, 134, 35.

3.4.36 *fac*-[Re(CO)$_3$(H$_2$O)(DiMePy)][NO$_3$]

ReAA (100 mg, 0.130 mmol) was dissolved in H_2O at pH 2 (adjusted with HNO_3). Silver nitrate (66.2 mg, 0.390 mmol) was added to the solution and stirred for 24 hours at room temperature. The AgBr was filtered off. 4,4'-Dimethyl-2,2'-bipyridine (23.9 mg, 0.130 mmol) was added to the solution and stirred for 4 hours. The reaction mixture was filtered. The yellow precipitate was dried and weighed. Yield: 98 %, 68.2 mg, 0.127 mmol.

UV/Vis: 364 nm, ε = 47741 $M^{-1}cm^{-1}$.

IR (KBr, cm^{-1}): $\nu_{Re(CO)}$ = 2021, 1931.

^{1}H NMR (300.18 MHz, *DMSO-d$_6$*): δ (ppm) = 8.71 (d, *J* = 5.1 Hz, 2H), 8.56 (s, 2H), 7.34 (d, *J* = 5.1 Hz, 2H), 2.32 (s, 6H).

^{13}C NMR (75.48 MHz, *DMSO-d$_6$*): δ (ppm) = 158, 155, 153, 134, 132, 28.

3.4.37 *fac*-[Re(CO)$_3$(Act)(DiMePy)][NO$_3$]

ReAA (100 mg, 0.130 mmol) was dissolved in H_2O at pH 2 (adjusted with HNO_3). Silver nitrate (66.2 mg, 0.390 mmol) was added to the solution and stirred for 24 hours at room temperature. The AgBr was filtered off. 4,4'-Dimethyl-2,2'-bipyridine (23.9 mg, 0.130 mmol) was added to the solution and stirred for 4 hours. The reaction mixture was filtered. The yellow precipitate was dissolved in acetone and stirred for 2 hours. The light yellow product was collected by vacuum and recrystallized from acetone. Yield: 81 %, 60.5 mg, 0.105 mmol.

UV/Vis: 360 nm, ε = 47621 M^{-1} cm^{-1}.

IR (KBr, cm^{-1}): $\nu_{Re(CO)}$ = 2025, 1937.

^{1}H NMR (300.18 MHz, *DMSO-d$_6$*): δ (ppm) = 8.64 (d, *J* = 4.8 Hz, 2H), 7.61 (s, 2H), 6.58 (d, *J* = 4.8 Hz, 2H), 4.03 (s, 6H), 2.2, (s, 6H), 1.09 (s, 6H).

^{13}C NMR (75.48 MHz, *DMSO-d$_6$*): δ (ppm) = 158, 150, 148, 146, 126, 42, 29, 26,24.

3.4.38 *fac*-[Re(CO)$_3$(NO$_3$)(DiMePy)]

ReAA (100 mg, 0.130 mmol) was dissolved in methanol. Silver nitrate (66.2 mg, 0.390 mmol) was added to the solution and stirred for 24 hours at room temperature. The AgBr was filtered off. 4,4'-Dimethyl-2,2'-bipyridine (23.9 mg, 0.130 mmol) was added to the solution and stirred for 4 hours. An excess of $AgNO_3$ was added and stirred for 4 hours. The light yellow solution was left to crystallize. Yield: 71 %, 47.7 mg, 0.092 mmol.

UV/Vis: 364 nm, ε = 46612 M^{-1} cm^{-1}.

IR (KBr, cm^{-1}): $\nu_{Re(CO)}$ = 2027, 1936.

^{1}H NMR (300 MHz, *DMSO-d$_6$*): δ (ppm) = 8.81 (d, *J* = 5.6 Hz, 2H), 7.90 (s, 2H), 6.88 (d, *J* = 5.5 Hz, 2H), 4.48 (s, 6H).

^{13}C NMR (75 MHz, *DMSO-d$_6$*): δ (ppm) = 163, 154, 152, 149, 131, 27.

3.4.39 *fac*-[Re(CO)$_3$(TU)(DiMePy)][Br]

fac-[Re(CO)$_3$(Br)(DiMePy)] (10 mg, 0.019 mmol) was dissolved in methanol and stirred for 24 hours. Thiourea (1.42 mg, 0.019 mmol) was added to the stirring solution and left to stir for 4 hours at 35˚C. The yellow product was collected by vacuum and weighed. Yield: 59 %, 6.9 mg, 0.011 mmol.

UV/Vis: 355 nm, ε = 47351 M^{-1}cm^{-1}.

IR (KBr, cm^{-1}): $\upsilon_{Re(CO)}$ = 2023, 1926.

^{1}H NMR (300.18 MHz, *DMSO-d$_6$*): δ (ppm) = 8.80 (s, 4H), 8.76 (d, *J* = 5.4 Hz, 2H), 8.01 (s, 2H), 7.8 (d, *J* = 5.3 Hz, 2H), 7.5 (s, 4H) 7.31 (d, *J* = 5.3 Hz, 2H), 2.30 (s, 6H).

^{13}C NMR (75.48 MHz, *DMSO-d$_6$*): δ (ppm) = 186, 182, 161, 158, 156, 132, 31.

3.4.40 *fac*-[Re(CO)$_3$(NCS)(DiMePy)]

fac-[Re(CO)$_3$(Br)(DiMePy)] (10 mg, 0.019 mmol) was dissolved in methanol and stirred for 24 hours. Sodium thiocynate (1.51 mg, 0.019 mmol) was added to the stirring solution and left to stir for 4 hours at 35 ˚C. The yellow product was collected by vacuum, washed with water and weighed. Yield: 80 %, 9.05 mg, 0.015 mmol.

UV/Vis: 360 nm, ε = 47145 M^{-1}cm^{-1}.

IR (KBr, cm^{-1}): $\upsilon_{C=N}$ = 2257, $\upsilon_{Re(NCS)}$ = 2149, $\upsilon_{Re(CO)}$ = 2018, 1878.

^{1}H NMR (300.18 MHz, *DMSO-d$_6$*): δ (ppm) = 8.76 (d, *J* = 5.4 Hz, 2H), 8.01 (s, 2H), 7.31 (d, *J* = 5.3 Hz, 2H), 2.30 (s, 6H).

^{13}C NMR (75.48 MHz, *DMSO-d$_6$*): δ (ppm) = 159, 156, 155, 134, 125, 113, 28.

3.4.41 *fac*-[Re(CO)$_3$(PCy$_3$)(DiMePy)][Br]

fac-[Re(CO)$_3$(Br)(DiMePy)] (10 mg, 0.019 mmol) was dissolved in methanol and stirred for 24 hours. Tricyclohexylphosphine (5.244 mg, 0.019 mmol) was added to the stirring solution and left to stir for 2 hours at 30 ˚C. The yellow product was collected by vacuum and weighted. Yield: 56 %, 8.5 mg, 0.010 mmol.

UV/Vis: 362 nm, ε = 46004 M^{-1}cm^{-1}.

IR (KBr, cm^{-1}): $\upsilon_{Re(CO)}$ = 2021, 1924.

^{1}H NMR (300.18 MHz, *DMSO-d$_6$*): δ (ppm) = 8.78 (s, 4H), 8.72 (d, *J* = 5.4 Hz, 2H), 8.08 (s, 2H), 7.83 (d, *J* = 5.3 Hz, 2H), 7.28 (d, *J* = 5.3 Hz, 2H), 2.34 (s, 6H), 1.58 - 1.49 (m, 33H).

^{13}C NMR (75.48 MHz, *DMSO-d$_6$*): δ (ppm) = 161, 158, 156, 140, 132, 41, 38, 36, 32, 31, 28.

3.4.42 *fac*-[Re(CO)$_3$(Br)(DiMeOPy)]

ReAA (100 mg, 0.130 mmol) was dissolved in methanol (10 mL). 4,4'-Dimethoxy-2,2'-bipyridine (28.1 mg, 0.130 mmol) was added to the reaction mixture and it was stirred at room temperature for 2 hours. The yellow product was collected by vacuum and recrystallized from dichloromethane. Yield: 94 %, 69.0 mg, 0.122 mmol.

UV/Vis: 346 nm, ε = 46841 M^{-1}cm^{-1}.

IR (KBr, cm^{-1}): $\upsilon_{Re(CO)}$ = 2016, 1904.

^{1}H NMR (300.18 MHz, *DMSO-d$_6$*): δ (ppm) = 8.76 (d, *J* = 6.4 Hz, 2H), 8.33 (s, 2H), 7.30 (d, *J* = 6.4, 2.5 Hz, 2H), 4.06 (s, 6H).

^{13}C NMR (75.48 MHz, *DMSO-d$_6$*): δ (ppm) = 168, 157, 154, 113, 111, 57.

3.4.43 *fac*-[Re(CO)$_3$(MeOH)(DiMeOPy)][Br]

fac-[Re(CO)$_3$(Br)(DiMeOPy)] (10.03 mg, 0.018mmol) was dissolved in methanol and stirred for 24 hours at temperature of 35 ˚C. The yellow product was collected by vacuum and weight. Yield: 91 %, 8.5 mg, 0.016 mmol.

UV/Vis: 350 nm, ε = 47946 M^{-1}cm^{-1}.

IR (KBr, cm^{-1}): $\upsilon_{Re(CO)}$ = 2023, 1930.

^{1}H NMR (300.18 MHz, *DMSO-d$_6$*): δ (ppm) = 8.6 (d, *J* = 5.5 Hz, 2H), 8.1 (s, 2H), 7.0 (d, *J* = 4.2, 2.5 Hz, 2H), 3.8 (s, 6H).

^{13}C NMR (75.48 MHz, *DMSO-d$_6$*): δ (ppm) = 164, 152, 150, 109, 107, 53.

3.4.44 *fac*-[Re(CO)$_3$(H$_2$O)(DiMeOPy)][NO$_3$]

ReAA (100 mg, 0.130 mmol) was dissolved in H_2O at pH 2 (adjusted with HNO_3). Silver nitrate (66.2 mg, 0.390 mmol) was added to the solution and stirred for 24 hours at room temperature. The AgBr was filtered off. 4,4'-Dimethoxy-2,2'-bipyridine (28.1 mg, 0.130 mmol) was added to the solution and stirred for 4 hours. The reaction mixture was filtered. The yellow precipitate was dried and weighed. Yield: 77 %, 61.0 mg, 0.099 mmol.

UV/Vis: 360, ε = 47861 M^{-1} cm^{-1}.

IR (KBr, cm^{-1}): $\upsilon_{Re(CO)}$= 2025, 1943.

^{1}H NMR (300.18 MHz, *DMSO-d$_6$*): δ (ppm) = 8.79 (d, *J* = 6.4 Hz, 2H), 7.68 (s, 2H), 7.03 (d, *J* = 6.5 Hz, 2H), 4.03 (s, 6H).

^{13}C NMR (75.48 MHz, *DMSO-d$_6$*): δ (ppm) = 168, 157, 154, 112, 110, 54.

3.4.45 *fac*-[Re(CO)$_3$(Act)(DiMeOPy)][NO$_3$]

ReAA (100 mg, 0.130 mmol) was dissolved in H_2O at pH 2 (adjusted with HNO_3). Silver nitrate (66.2 mg, 0.390 mmol) was added to the solution and stirred for 24 hours at room temperature. The AgBr was filtered off. 4,4'-Dimethoxy-2,2'-bipyridine (28.1 mg, 0.130 mmol) was added to the solution and stirred for 4 hours. The reaction mixture was filtered. The yellow precipitate was dissolved in acetone and stirred for 2 hours. The light yellow product was collected by vacuum and recrystallized from acetone. Yield: 92 %, 71.0 mg, 0.120 mmol.

UV/Vis: 363 nm, ε = 47747 M^{-1} cm^{-1}.

IR (KBr, cm^{-1}): $\upsilon_{Re(CO)}$= 2022, 1963.

^{1}H NMR (300.18 MHz, *DMSO-d$_6$*): δ (ppm) = 7.61 (d, *J* = 4.4 Hz, 2H), 6.44 (s, 2H), 6.01 (d, *J* = 4.5 Hz, 2H), 3.88 (s, 6H), 1.4 (s, 6H).

^{13}C NMR (75.48 MHz, *DMSO-d$_6$*): δ (ppm) = 174, 162, 154, 136, 116, 64, 38.

3.4.46 *fac*-[Re(CO)$_3$(NO$_3$)(DiMeOPy)]

ReAA (100 mg, 0.130 mmol) was dissolved in methanol. Silver nitrate (66.2 mg, 0.390 mmol) was added to the solution and stirred for 24 hours at room temperature.

The AgBr was filtered off. 4,4'-Dimethoxy-2,2'-bipyridine (28.1 mg, 0.130 mmol) was added to the solution and stirred for 4 hours. An excess of $AgNO_3$ was added and stirred for 4 hours. The light yellow solution was left to crystallize. Yield: 78 %, 55.6 mg, 0.101 mmol.

UV/Vis: 365 nm, ε = 47210 M^{-1} cm^{-1}.

IR (KBr, cm^{-1}): $\nu_{Re(CO)}$= 2029, 1958.

^{1}H NMR (300.18 MHz, *DMSO-d$_6$*): δ (ppm) = 7.4 (d, *J* = 4.2 Hz, 2H), 6.2 (s, 2H), 6.0 (d, *J* = 4.1 Hz, 2H), 3.4 (s, 6H).

^{13}C NMR (75.48 MHz, *DMSO-d$_6$*): δ (ppm) = 174, 162, 154, 136, 116, 64.

3.4.47 *fac*-[Re(CO)$_3$(TU)(DiMeOPy)][Br]

fac-[Re(CO)$_3$(Br)(DiMeOPy)] (10 mg, 0.019 mmol) was dissolved in methanol and stirred for 24 hours. Thiourea (1.47 mg, 0.019 mmol) was added to the stirring solution and left to stir for 2 hours at 30 ˚C. The solvent was evaporated and the yellow product weighed. Yield: 79 %, 9.6 mg, 0.015 mmol.

UV/Vis: 353 nm, ε = 48137 $M^{-1}cm^{-1}$.

IR (KBr, cm^{-1}): $\nu_{Re(CO)}$ = 2017, 1941.

^{1}H NMR (300.18 MHz, *DMSO-d$_6$*): δ (ppm) = 8.8 (s, 4H), 8.8 (d, *J* = 5.6 Hz, 2H), 8.1 (s, 2H), 7.6 (s, 4H), 7.5 (d, *J* = 4.1, 1.8 Hz, 2H), 4.1 (s, 6H).

^{13}C NMR (75.48 MHz, *DMSO-d$_6$*): δ (ppm) = 187, 183, 170, 159, 158, 115, 113, 64.

3.4.48 *fac*-[Re(CO)$_3$(NCS)(DiMeOPy)]

fac-[Re(CO)$_3$(Br)(DiMeOPy)] (10 mg, 0.019 mmol) was dissolved in methanol and stirred for 24 hours. Sodium thiocyanate (1.56 mg, 0.019 mmol) was added to the stirring solution and left to stir for 2 hours at 30 ˚C. The solvent was evaporated and the yellow product was washed with water and weighed. Yield: 77 %, 8.0 mg, 0.015 mmol.

UV/Vis: 350 nm, ε = 47281 $M^{-1}cm^{-1}$.

IR (KBr, cm^{-1}): $\nu_{C=N}$ = 2241, $\nu_{Re(NCS)}$ = 2147, $\nu_{Re(CO)}$ = 2016, 1893.

^{1}H NMR (300.18 MHz, *DMSO-d$_6$*): δ (ppm) = 8.86 (d, *J* = 6.4 Hz, 2H), 8.42 (s, 2H), 7.34 (d, *J* = 6.1, 2.1 Hz, 2H), 4.06 (s, 6H).

^{13}C NMR (75.48 MHz, *DMSO-d$_6$*): δ (ppm) = 181, 172, 161, 157, 118, 116, 111, 63.

3.4.49 *fac*-[Re(CO)$_3$(PCy$_3$)(DiMeOPy)][Br]

fac-[Re(CO)$_3$(Br)(DiMeOPy)] (10 mg, 0.019 mmol) was dissolved in methanol and stirred for 24 hours. Tricyclohexylphosphine (5.24 mg, 0.019 mmol) was added to the stirring solution and left to stir for 2 hours at 30 ˚C. The solvent was evaporated and the yellow product weighed. Yield: 57 %, 8.9 mg, 0.011 mmol.

UV/Vis: 349 nm, ε = 46192 M^{-1}cm^{-1}.

IR (KBr, cm^{-1}): $\upsilon_{Re(CO)}$ = 2016, 1943.

^{1}H NMR (300.18 MHz, *DMSO-d$_6$*): δ (ppm) = 8.85 (s, 4H), 8.78 (d, *J* = 6.6 Hz, 2H), 8.14 (s, 2H), 7.41 (d, *J* = 3.9, 1.9 Hz, 2H), 4.11 (s, 6H), 1.46 - 1.39 (m, 33H).

^{13}C NMR (75.48 MHz, *DMSO-d$_6$*): δ (ppm) = 187, 170, 159, 158, 115, 115, 64, 33, 29, 27, 25.

3.5 Discussion

The aim of the study was to successfully synthesize three β-hydroxyketone ligands and to coordinate it to the Re(I) tricarbonyl core and also to synthesize the Re(I) tricarbonyl complexes of five *O,O'* β-diketone ligands and two *N,N'*-bidentate ligands. In addition we aimed to investigate the substitution behaviour of some of these Re(I) tricarbonyl complexes as well as the photoluminescence properties and potential cytotoxicity of selected ligands and complexes.

The Claisen condensation was used to synthesize the β-hydroxyketone ligands. The reaction between the precursor (ReAA) and *N,N'*- or *O,O'*-bidentate ligands were generally straight forward following the procedures described in literature.[1,24,25,26] ReAA and the bidentate ligands were dissolved in methanol as solvent and stirred for a specified amount of time to obtain the *fac*-[Re(CO)$_3$(Br)(*L,L'*-Bid)]^{n} (*L,L'*-Bid= *N,N"*-

[25] Schutte-Smith, M., Muller, T.J., Visser, H.G., Roodt, A. *Act Cryst*. **C69** (2013) 1467-1471.
[26] Brink, A., Visser, H.G., Roodt, A. *Polyhedron*. **52** (2013) 416-423.

or *O,O*'-bidentate ligand, n = -1, 0) type complexes. The bromido complexes were characterized fully and compared well to each other and to other reported complexes.[27,28,29] In the case of *fac*-$[Re(CO)_3(H_2O)(L,L'\text{-Bid})]^n$ (n = -1, 0) type complexes, the formation of the triaqua compound (*fac*-$[Re(CO)_3(H_2O)_3]^+$) was obtained after the precipitation of three equivalents of bromide (AgBr) by adding three equivalents of $AgNO_3$ to ReAA. The pH of the aqua solution was always adjusted to 2 to avoid the formation of polymeric species in solution (formation of Re-OH species at pH 4)[30]. The aqua complexes were characterized fully and it compared well with the bromido complexes and other reported aqua complexes.[31,32] The formation of the methanol complexes were obtained by stirring the *fac*-$[Re(CO)_3(Br)(L,L'\text{-Bid})]^n$ (*L,L'*-Bid = *N,N'*- or *O,O'*-bidentate ligand) (n = -1, 0) type complexes in methanol for several hours. The products were fully characterized and compared well with the bromido and aqua complexes.

The IR spectra of the synthesized TIFH, MeTIFH and PhTIFH ligands show a broad absorption peak in the region 3440 cm^{-1} to 3446 cm^{-1}, indicating the presence of the O-H bond and it was found to be similar to other β-hydroxyketone ligands in literature (TIFH, 5,6-DTIFH and HPFNP).[33,34,35] The carbonyl stretching frequencies of the TIFH, MeTIFH and PhTIFH ligands are in the range of 1665 - 1671 cm^{-1} which are also similar to the reported β-hydroxyketone ligands in the literature (TIFH, 5,6-DTIFH and HPFNP) with stretching frequencies from 1602 cm^{-1} to 1688 cm^{-1}. The stretching frequencies of C-F and CF_3 for the synthesized β-hydroxyketone ligands of 1665 cm^{-1} to 1688 cm^{-1} are in the normal range and correspond to the reported β-hydroxyketone ligands in literature (TIFH, 5,6-DTIFH and HPFNP) which range from 1602 cm^{-1} to 1680 cm^{-1}. When TIFH, MeTIFH and PhTIFH are coordinated to the Re(I) tricarbonyl core the broad absorption peak in the region 3440 cm^{-1} to 3446 cm^{-1} disappears and serves as confirmation of the coordination to the Re(I) tricarbonyl core in *fac*-$[Re(CO)_3(X)(L,L'\text{-Bid})]^n$ (where X = Br/MeOH/H_2O, *L,L*'-Bid =

[27] Schutte, M., Visser, H.G., Steyl, G. *Acta Cryst*. **E63** (2007) m3195-m3196.
[28] Walter, J.D., Jeffrey, R.D., Russell, H.S., Kristina, P.M., Scott, A.T.,Efram, G., Knight, D.A. *Inorg. Chem. Commun*. **83** (2017) 55-58.
[29] Kurtz, D.A., Dhakal, B., Donovan, E.S., Nichol, G.S., Felton, G.A.N., *Inorg. Chem. Commun*. **59** (2015) 80-83.
[30] Helm. L. *Coord. Chem. Rev*. **252** (2008) 2346-2361.
[31] Schutte, M,. Roodt, A., Visser, H.G. *Inorg. Chem*. 51(21) (2012) 11996-12006.
[32] Kokila, R., Shiroma, H., Inoka, C.P., Theshini, P. *Chem. Cent. J*. **10** (2016) 71-81.
[33] Li, W., Yan, P., Hou, G., Li, H.,Li.G. *Dalton Trans*. **42** (2013) 11537-11547.
[34] Li, J., Li, H., Yan, P., Chen, P., Hou, G., Li, G. *Inorg. Chem*. **51**(2012) 5050-5057.
[35] Raj, D.B.A., Biju, S., Reddy, M.L.P. *Inorg. Chem*. **47** (2008) 8091-8100.

TIF/MeTIF/PhTIF, n = -1, 0). Table **3-2** below summarises the stretching frequencies of the β-hydroxyketone ligands synthesized in this study as well as from literature for comparison reasons.

Table 3-2: The IR stretching frequencies (cm^{-1}) for the β-hydroxyketone ligands in literature and synthesized in this study.[33,34]

β-hydroxyketone ligands	O-H	$C=O_{Ligand}$	C-F	CF_3
TIFH[34]	3430	1688	1325, 1270, 1137	751
5,6-DTIFH[34]	3328	1680	1325, 1270, 1137	784
HPFNP[35]	3063	1602	1328, 1202, 1010	795
TIFH	3440	1667	1330, 1268, 1128	748
MeTIFH	3446	1671	1335, 1272, 1131	753
PhTIFH	3442	1665	1326, 1265, 1127	748

5,6-DTIFH = 5,6-dimethoxy-2(2,2,2-trifluoroethyl)-1-indone, HPFNP = 4,4,5,5,5-Pentafluoro-1-(naphthalen-2-yl)pentane-1,3-dione

The NMR spectra confirms the formation of the β-hydroxyketone ligands by showing a H-O peak in the normal range of 14.8 ppm to 16.1 ppm and the disappearance of the two protons in the β-position of the indanone. The disappearance of the protons on the β-position allows the ester enolate to coordinate.

The stretching frequencies of the Re(I) tricarbonyl complexes with the β-hydroxyketone ligands coordinated as bidentate ligands, are tabulated in Table **3-3**. It is clear that the methyl and phenyl group on the backbone of the β-hydroxyketone ligand do not have much influence on the stretching frequencies as indicated in Table **3-3**.

Table 3-3: The IR stretching frequencies (cm^{-1}) of C=O, C-F and CF_3 for the Re(I) tricarbonyl complexes with coordinated β-hydroxyketone ligands.

Re(I) tricarbonyl complexes	$C=O_{Ligand}$	C-F			CF_3
fac-[NEt_4][$Re(CO)_3(Br)$(TIF)]	1671	1334	1272	1130	750
fac-[$Re(CO)_3$(MeOH)(TIF)]	1674	1337	1276	1134	752
fac-[$Re(CO)_3$(TU)(TIF)]	1658	1328	1271	1129	757
fac-[NEt_4][$Re(CO)_3$(NCS)(TIF)]	1681	1340	1282	1145	749
fac-[$Re(CO)_3(PCy_3)$(TIF)]	1675	1334	1278	1140	746
fac-[$Re(CO)_3(H_2O)$(TIF)]	1661	1331	1268	1131	752
fac-[NEt_4][$Re(CO)_3$(Br)(MeTIF)]	1651	1311	1242	1118	759
fac-[$Re(CO)_3$(MeOH)(MeTIF)]	1680	1339	1277	1135	756
fac-[$Re(CO)_3$(TU)(MeTIF)]	1675	1336	1268	1138	750
fac-[NEt_4][$Re(CO)_3$(NCS)(MeTIF)]	1676	1335	1276	1138	761
fac-[$Re(CO)_3(PCy_3)$(MeTIF)]	1670	1341	1282	1141	748
fac-[$Re(CO)_3(H_2O)$(MeTIF)]	1662	1319	1253	1127	743
fac-[NEt_4][$Re(CO)_3$(Br)(PhTIF)]	1678	1338	1272	1136	754
fac-[$Re(CO)_3(H_2O)$(PhTIF)]	1676	1335	1272	1132	755

All the rhenium(I) tricarbonyl complexes were characterized by infrared spectroscopy which provides a good fingerprint by evaluating the CO stretching frequencies. Since the carbonyl group is permanently polarized, a well-defined absorption peak is found and any vibrational stretching of the bond influences the dipole moment. The bending frequencies require the least amount of energy compared to the corresponding stretching frequencies. The carbonyl stretching frequencies of the starting material *fac*-$[NEt_4]_2[Re(CO)_3(Br)_3]$ are 1996 and 1846 cm^{-1}. It is anticipated that electron donating ligands will increase the electron density on the Re(I) metal core as well as the backbonding from the carbonyl ligands and therefore will decrease the IR stretching frequency of the Re(I) complexes.

The molar absorption coefficient is a measure of how strongly a chemical species absorbs light at a particular wavelength. The molar absorption coefficients of all the Re(I) tricarbonyl complexes range between 46004 and 65036 $cm^{-1}M^{-1}$. It was observed that the molar absorption coefficients of the Re(I) tricarbonyl complexes with to *O,O'* bidentate ligands coordinated to the metal centre range between 50434 $cm^{-1}M^{-1}$ and 65036 $cm^{-1}M^{-1}$, while for Re(I) tricarbonyl complexes with coordinated *N,N'* bidentate ligand range between 46004 $cm^{-1}M^{-1}$ and 47946 $cm^{-1}M^{-1}$. It is clear that the molar absorption coefficients of the Re(I) tricarbonyl complexes follow the trend: Re-*N,N'* < Re-*O,O'*. No trend was observed as the monodentate ligand varies in a complex.

The carbonyl stretching frequencies as well as the molar absorption coefficient of the Re(I) tricarbonyl complexes are summarised in Table **3-4**.

Table 3-4: The Re-CO IR stretching frequencies v_{CO} and molar absorption coefficients (ε) of the synthesized Re(I) tricarbonyl complexes.

Complexes	Re-CO v_{CO} (cm^{-1})	ε ($cm^{-1}M^{-1}$)	Complexes	Re-CO v_{CO} (cm^{-1})	ε ($cm^{-1}M^{-1}$)
fac-[NEt_4][M(Br)(TIF)]	2015, 1882	51123	*fac*-[M(Br)(BAHY)]	2019, 1893	61721
fac-[M(MeOH)(TIF)]	2021, 1911	54941	*fac*-[M(H_2O)(BAHY)][NO_3]	2030, 1920	61949
fac-[M(TU)(TIF)]	2024, 1965	50434	*fac*-[NEt_4][M(Br)(4-MeTPh)]	2017, 1900	62387
fac-[NEt_4][M(NCS)(TIF)]	2018, 1907	57691	*fac*-[M(MeOH)(4-MeTPh)]	2018, 1937	62667
fac-[M(PCy_3)(TIF)]	2021, 1904	56311	*fac*-[M(TU)(4-MeTPh)]	2018, 1937	63210
fac-[M(H_2O)(TIF)]	2040, 1971	5459151481	*fac*-[NEt_4][M(NCS)(4-MeTPh)]	2017, 1895	65036
fac-[NEt_4][M(Br)(MeTIF)]	2018, 1901	51481, 47587	*fac*-[M(PCy_3)(4-MeTPh)]	2019, 1950	64910
fac-[M(MeOH)(MeTIF)]	2018, 1908	55041	*fac*-[M(H_2O)(4-MeTPh)]	2036, 1980	63809
fac-[M(TU)(MeTIF)]	2028, 1941	51771	*fac*-[M(Br)(DiMePy)]	2018, 1904	46209
fac-[NEt_4][M(NCS)(MeTIF)]	2010, 1914	58149	*fac*-[M(MeOH)(DiMePy)][Br]	2022, 1924	47130
fac-[M(PCy_3)(MeTIF)]	2026, 1914	57394	*fac*-[M(H_2O)(DiMePy)][NO_3]	2021, 1931	47741
fac-[M(H_2O)(MeTIF)]	2039, 1967	54851, 48019	*fac*-[M(Act)(DiMePy)[NO_3]	2025, 1937	47621
fac-[NEt_4][M(Br)(PhTIF)]	2012, 1886	61401, 58614	*fac*-[M(NO_3)(DiMePy)]	2027, 1936	46612
fac-[M(H_2O)(PhTIF)]	2041, 1968	63012, 59612	*fac*-[M(TU)(DiMePy)][Br]	2023, 1926	41351
fac-[NEt_4][M(Br)(3,5-DiMePh)]	2011, 1876	62141	*fac*-[M(NCS)(DiMePy)]	2018, 1878	47145
fac-[M(H_2O)(3,5-DiMePh)]	2024, 1947	62141	*fac*-[M(PCy_3)(DiMePy)][Br]	2021, 1924	46004
fac-[NEt_4][M(Br)(MeDiPhPr)]	2017,1859	60514	*fac*-[M(Br)(DiMeOPy)]	2016, 1904	46841
fac-[M(H_2O)(MeDiPhPr)]	2028, 1946	64834	*fac*-[M(MeOH)(DiMeOPy)][Br]	2023, 1930	47946
fac-[NEt_4][M(Br)(BrDiPhPr)]	2014,1881	61479	*fac*-[M(H_2O)(DiMeOPy)][NO_3]	2025, 1943	47861
fac-[(MeOH)(BrDiPhPr)]	2030,1887	60591	*fac*-[M(Act)(DiMeOPy)][NO_3]	2022, 1963	47747
fac-[M(TU)(BrDiPhPr)]	2021, 1912	59896	*fac*-[M(NO_3)(DiMeOPy)]	2029, 1958	47210
fac-[NEt_4][M(NCS)(BrDiPhPr)]	2013, 1897	61581	*fac*-[M(TU)(DiMeOPy)][Br]	2017, 1941	47137
fac-[M(PPh_3)(BrDiPhPr)]	2021, 1923	63897	*fac*-[M(NCS)(DiMeOPy)]	2016, 1893	47281
fac-[M(H_2O)(BrDiPhPr)]	2030, 1966	61117	*fac*-[M(PCy_3)(DiMeOPy)][Br]	2018, 1943	46182

M = $Re(CO)_3$

The general observations for *fac*-[$Re(CO)_3$(Br)(*L,L*'-Bid)]^n, *fac*-[$Re(CO)_3$(MeOH)(*L,L*'-Bid)] and *fac*-[$Re(CO)_3(H_2O)$(*L,L*'-Bid)] (where *L,L*'-Bid = *O,O'* or *N,N'*-bidentate ligand, n = -1, 0) type complexes indicate the following:

The bromido complexes generally have the lowest carbonyl stretching frequency values compared to the methanol and aqua complexes. This is due to the electron density that is donated to the metal centre, thereby increasing the electron density on the Re(I) metal centre. The expected trend that the *N,N'*-bidentate ligands will donate less electron density than the *O,O'*-bidentate ligands to the Re(I) metal centre is seen

in the generally higher stretching frequencies for the Re-*N,N'* complexes. There is a small change in carbonyl stretching frequency as the monodentate ligand is substituted by another ligand in the sixth position. If the Re(I) tricarbonyl complexes coordinated to TIFH, MeTIFH, BrDiPhPr, 4-MeTPh, DiMePy and DiMeOPy are compared and the respective aqua complexes are taken as reference, the Br^- and NCS^- complexes generally have the lowest CO stretching frequencies, followed by the TU complexes. No other noticeable trends were observed.

The Re-N stretching frequencies of the complexes with NCS^- coordinated in the sixth position *fac*-[NEt_4][$Re(CO)_3(NCS)(TIF)$], *fac*-[NEt_4][$Re(CO)_3(NCS)(MeTIF)$], *fac*-[NEt_4][$Re(CO)_3(NCS)(BrDiPhPr)$], *fac*-[NEt_4][$Re(CO)_3(NCS)(4\text{-}MeTPh)$], *fac*-[$Re(CO)_3(NCS)(DiMePy)$] and *fac*-[$Re(CO)_3(NCS)(DiMePy)$] ranges between 2145 cm^{-1} to 2153 cm^{-1}, which was found to be in the normal range of 2142 cm^{-1} and 2151 cm^{-1} compared to compounds in literature. [36,37,38]

The complexes, *fac*-[$Re(CO)_3(Br)(DiMePy)$], *fac*-[$Re(CO)_3(Act)(DiMePy)][NO_3$], *fac*-[$Re(CO)_3(NO_3)(DiMePy)$], *fac*-[$Re(CO)_3(Br)(DiMeOPy)$], *fac*-[$Re(CO)_3(Act)(DiMeOPy)][NO_3$] and *fac*-[$Re(CO)_3(NO_3)(DiMeOPy)$] and the ligand 4-MeTPh were fully characterized and suitable crystals for single crystal XRD was obtained. The crystal structures are discussed in chapter 4.

[36] Yumata, N.C., Habarurema,G., Mukiza, J., Gerber, T.I.A., Hosten, E., Taherkhani, F., Nahali, M. *Polyhedron*. 62 (2013) 89-103.
[37] Komreddy, V., Ensz, K., Nguyen, H., Rillema, D.P. *Inorg. Chim Acta*. **511** (2020) 119815-119823.
[38] Laramée-Milette, B.,Zaccheroni, N., Palomba, F., Hanan, G.S. *Chem. Eur. J*. **23** (2017) 6370-6379.

4 X-RAY CRYSTALLOGRAPHIC STUDY OF A LIGAND AND RHENIUM(I) COMPOUNDS

4.1 Introduction

X-ray crystallography is a technique used by chemists to determine the internal structure and bonding arrangements of molecules, including the structures of large complex molecules like protein and DNA. Several rhenium(I) tricarbonyl complexes with coordinated *O,O'* and *N,N'*-bidentate ligands and its crystal structures have been reported in literature.[1,2,3,4,5,6,7,8] This chapter describes the crystal structures of one *O,O'*-bidentate ligand, namely 1,3-bis(4-methoxyphenyl)propane-1,3-dione (4-MeTPh), and five rhenium(I) tricarbonyl complexes: three crystal structures with 4,4'-dimethyl-2,2'-bipyridine (DiMePy) as *N,N'*-bidentate ligand (with Br^-, acetone and NO_3^- as monodentate ligand in the 6th position) and two structures with 4,4'-dimethoxy-2,2'-bipyridine (DiMeOPy) as *N,N'*-bidentate ligand (with Br^- and NO_3^- as monodentate ligand in the 6th position). The choice of 4-MeTPh, DiMePy and DiMeOPy as bidentate ligands are discussed in detail in Chapter 3 but is mainly due to its photoluminescent properties and potential chemotherapeutic application.

[1] Alberto, R., Schibli, R., Waibel, R., Abram, U., Schubiger, A.P. *Coord. Chem. Rev.* **190-192** (1999) 901-919.
[2] Brink, A., Visser, H.G., Roodt, A. *Polyhedron*. **52** (2013) 416-423.
[3] Schutte-Smith, M., Muller, T.J., Visser, H.G., Roodt. A. *Act Cryst*. **C69** (2013) 1467-1471.
[4] Schutte-Smith, M., Roodt, A., Alberto, R., Twigge,T., Visser, H.G., Kirsten, L., Koen, R. *Act Cryst*. **C75** (2019) 2053-2269.
[5] Nkoe, P.I., Visser, H.G., Swart, C., Brink , A., Schutte-Smith, M. *Act Cryst*. **C74** (2018) 2053-2296.
[6] Carreno, A., Paez, D.-H., Zuniga, C., Ramirez, A.-O., Pizarro, N., Vega, A., Solis, E.-C., Rivera, M.M.-Z., Silva, A., Fuentes, J.A. *Dyes and Pigments*. **184** (2021) 108876-108890.
[7] Komreddy, V., Ensz, K., Nguyen, H., Rillema, D.P. *Inorg. Chim. Acta*. 511 (2020) 119815-119823.
[8] Bettes, J.W., Roth, P., Pattrick, C.A., Southam, H.M.,Roberto, M.L., Poole, R.K., Schatzschneider, U. *Metallomics*. **12** (2020) 1563-1576.

A schematic representation of the molecular structures of 1,3-bis(4-methoxyphenyl)propane-1,3-dione (4-MeTPh), *fac*-[Re(CO)$_3$(Br)(DiMePy)], *fac*-[Re(CO)$_3$(Act)(DiMePy)][NO$_3$], *fac*-[Re(CO)$_3$(NO$_3$)(DiMePy)], *fac*-[Re(CO)$_3$(Br)(DiMeOPy)] and *fac*-[Re(CO)$_3$(NO$_3$)(DiMeOPy)] is given in Scheme **4-1**. The crystallographic data and refinement parameters of the six crystal structures are summarised in Table **4-1** and Table **4-2**.

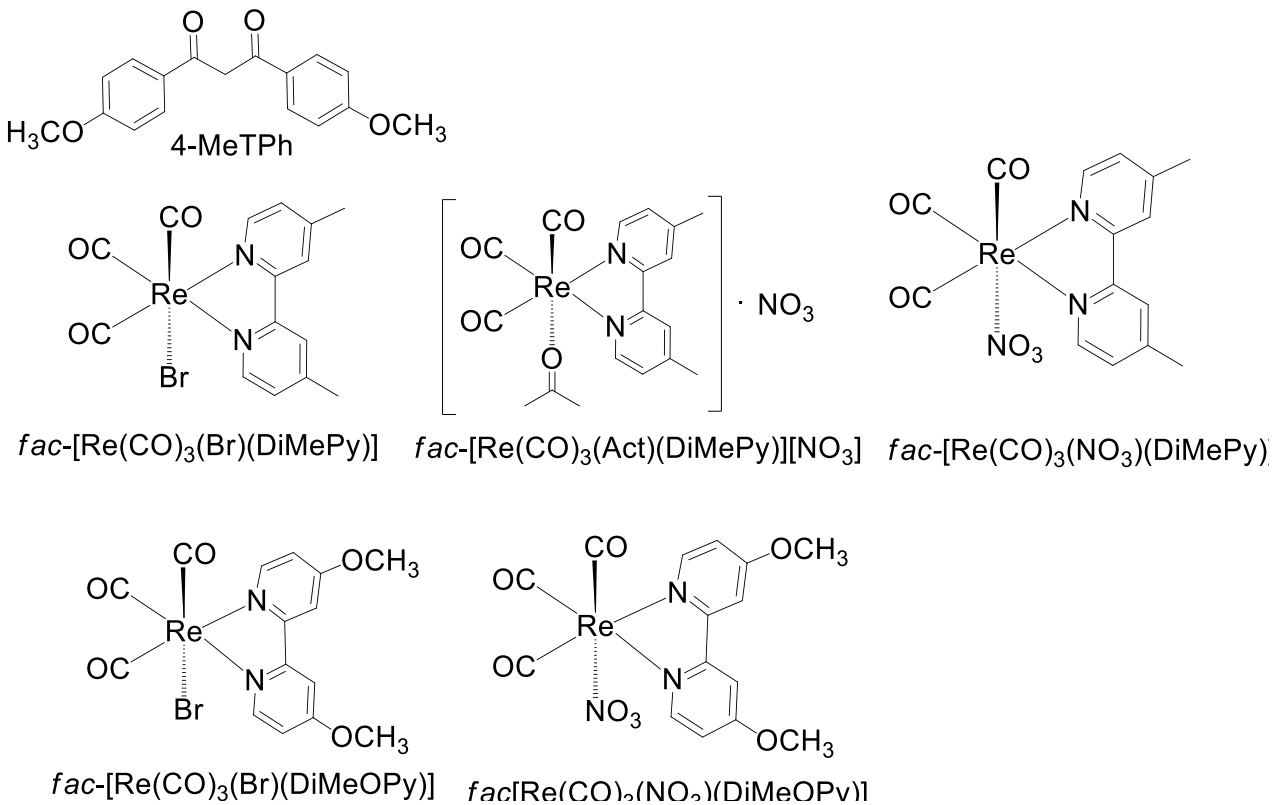

Scheme 4-1: An illustration of the six crystal structures reported in this chapter.

4.2 Experimental

A Bruker X8 ApexII 4K was used to collect the reflection data for the determination of single crystal structures. The apparatus was equipped with a wavelength of 0.71073 Å, graphite monochromated Mo Kα radiation with φ- and ω-scans at 100 K. The

Diamond software[9] was used for the molecular graphics. The SADABS software package[10] and multi-scan technique were used to obtain absorption corrections. SAINT-Plus[11] was used to perform the cell refinements and the data reduction was done with SAINT-Plus and XPREP[11]. SHELXL-97[12] and WingGX[13] were used for refinement and SIR-97[14] to solve the crystal structures. All the structures in this chapter are drawn with thermal ellipsoids at 50 % probability level. Non-hydrogen atoms were refined anisotropically. The methyl, methylene and aromatic hydrogen atoms were placed in geometrically idealized positions and constrained to ride on their parent atoms with C-H bond distances equal to 0.95 Å, 0.98 Å and 0.99 Å and U_{iso} (H) = 1.2U_{eq} (C) and 1.5U_{eq} (C) (for methyl and methylene). There is an indication of an unresolved solvent molecule within the unit cell as indicated by the elevated electron density peak in *fac*-[Re(CO)$_3$(Br)(DiMePy)] (4.48 and -3.12). The solvent has not been modelled as illustrated in the current structure as the structure and possible disorder is not fully understood.

[9] Brandenburg, K., Putz, H., DIAMOND, Release 3.0e, Crystal Impact GbR, Bonn, Germany, 2006.
[10] Bruker, SADABS, Version 2004/1, Bruker AXS Inc., Madison, Wisconsin, USA, 1998.
[11] Bruker, SAINT-Plus, Version 7.12 (including XPREP), Bruker AXS Inc., Madison, Wisconsin, USA, 2004.
[12] Sheldrick, G.M., SHELXL97, Program for the refinement of crystal structures, University of Göttingen, Germany, 1997.
[13] Farrugia, L.J., *J. Appl. Cryst*. **32** (1999) 837-838.
[14] Altomare, A., Burla, M.C., Camalli, M., Cascarano, G.L., Giacovazzo, C., Guagliardi, A., Moliterni, A.G.G., Polidori, G., Spagna, R., *J. Appl. Cryst*. **32** (1999) 115-119.

Table 4-1: Crystallographic data of 4-MeTPh, *fac*-[Re(CO)$_3$(Br)(DiMePy)] and *fac*-[Re(CO)$_3$(Act)(DiMePy)][NO$_3$].

Crystallographic data	4-MeTPh	Re-[(Br)(DiMePy)]	Re-[(Act)(DiMePy)][NO$_3$]
Emperical formula	$C_{17}H_{17}O_4$	$C_{15}H_{12}BrN_2O_3Re$	$C_{18}H_{18}N_3O_7Re$
Formula weight (g mol^{-1})	284.31	534.38	574.55
Crystal system	Monoclinic	Monoclinic	Monoclinic
Space group	*P*2$_1$/*c*	*P*2$_1$/*c*	*C*2/*c*
a (Å)	4.185(3)	15.306(2)	24.369(3)
b (Å)	10.358(7)	13.289(2)	12.122(15)
c (Å)	33.086(8)	7.687(1)	17.004(4)
α (º)	89.43(2)	90	90
β (º)	89.56(2)	97.299(7)	126.477(3)
$_\gamma$(º)	89.99(2)	90	90
Volume (Å^{-3})	1433(6)	1550(7)	4039(11)
Z	4	4	8
P_{calc} (g cm^{-3})	1.322	2.289	1.890
Crystal colour	Yellow	Yellow	Yellow
Crystal morphology	Needle	Cuboid	Cubic
Crystal size	0.103x0.126x0.385	0.091x0.099x0.248	0.190x0.258x0.463
μ (mm^{-1})	0.094	10.424	6.061
F (000)	604	1000	2224
θ range (º)	0.615 - 28.316	1.341 - 27.999	2.822 - 28.358
Index ranges	-5 ≤ h ≤ 5 -13 ≤ k ≤ 13 -43 ≤ l ≤ 41	-20 ≤ h ≤ 20 -17 ≤ k ≤ 17 -10 ≤ l ≤ 7	-32 ≤ h ≤ 32 -16 ≤ k ≤ 15 -22 ≤ l ≤ 22
Reflections collected	24270	35709	31488
Unique reflections	3467	3738	4857
Reflection with I>2σ	68918	35709	3620
R_{int}	0.0727	1.218	0.0736
Completeness to 2 theta (º, %)	25.42, 99.9 %	27.998, 99.9 %	28.358, 99.7 %
Data/ restraints/ parameters	3467 / 0 / 194	3738 / 0 / 199	4857 / 0 / 232
GooF	1.018	1.218	1.044
R[I>2σ(I)]	R_1= 0.0517 wR_2 = 0.1133	R_1= 0.0490 wR_2 = 0.1197	R_1= 0.0432 wR_2 = 0.1168
R(all data)	R_1= 0.1436 wR_2 = 0.1512	R_1= 0.0617 wR_2 = 0.1305	R_1= 0.0502 wR_2 = 0.1168
ρ_{max} and ρ_{min} (e.Å^{-3})	0.14 and -0.20	4.48 and -3.12	1.406 and -1.163

Re = *fac*-[Re(CO)$_3$]

Table 4-2: Crystallographic data of *fac*-[Re(CO)$_3$(NO$_3$)(DiMePy)], *fac*-[Re(CO)$_3$(Br)(DiMeOPy)] and *fac*-[Re(CO)$_3$(NO$_3$)(DiMePy)].

Crystallographic data	Re-[(NO$_3$)(DiMePy)]	Re-[(Br)(DiMeOPy)]	Re-[(NO$_3$)(DiMeOPy)]
Emperical formula	$C_{15}H_{12}N_3O_6Re$	$C_{15}H_{12}Br\ N_2O_5Re$	$C_{15}H_{12}N_3O_8Re$
Formula weight (g mol^{-1})	516.48	566.38	541.52
Crystal system	Monoclinic	Orthorhombic	Monoclinic
Space group	*P*2$_1$/*n*	*Pbcn*	*P*2$_1$/*n*
a (Å)	8.0498(6)	14.051(2)	10.546(1)
b (Å)	12.4089(10)	13.893(1)	10.984(1)
c (Å)	17.6719(14)	17.210(3)	15.674(2)
α (º)	90	90	90
β (º)	95.542(3)	90	98.306(4)
γ(º)	90	90	90
Volume (Å^{-3})	1757(4)	3389(1)	1797(5)
Z	4	8	4
P_{calc} (g cm^{-3})	1.775	2.240	2.002
Crystal colour	Yellow	Yellow	Yellow
Crystal morphology	Plate	Cuboid	Cuboid
Crystal size	0.033x0.063x0.225	0.097x0.177x0.278	0.184x0.186x0.219
μ (mm^{-1})	6.928	9.640	6.801
F (000)	896	2016	1040
θ range (º)	2.690 - 28.376	2.061 - 28.372	2.864 - 28.37
Index ranges	-10 ≤ h ≤ 10 -16 ≤ k ≤ 16 -23 ≤ l ≤ 23	-16 ≤ h ≤ 18 -14 ≤ k ≤ 18 22 ≤ h ≤ 22	-12 ≤ h ≤ 12 -14 ≤ k ≤ 14 -20 ≤ l ≤ 20
Reflections collected	28632	92205	19612
Unique reflections	4378	4208	4473
Reflection with I>2σ	3659	9291	8796
R_{int}	0.0686	0.0494	0.0523
Completeness to 2 theta (º, %)	25.242, 99.9	27.999, 99.9	25.242, 99.7
Data/ restraints/ parameters	4378 / 0 / 226	4055 / 0 / 217	4473 / 0 / 244
GooF	1.105	1.101	1.064
R[I>2σ(I)]	R_1= 0.0375 wR_2 = 0.0665	R_1= 0.0302 wR_2 = 0.0778	R_1= 0.0309 wR_2 = 0.0624
R(all data)	R_1= 0.0502 wR_2 = 0.0699	R_1= 0.0371 wR_2 = 0.0815	R_1= 0.0410 wR_2 = 0.0660
ρ_{max} and ρ_{min} (e.Å^{-3})	1.414 and -2.048	1.269 and -1.726	1.267 and -1.247

Re = *fac*-[Re(CO)$_3$]

4.3 Crystal structure of 4-MeTPh

The compound, 1,3-*bis*(4-methoxyphenyl)propane-1,3-dione (4-MeTPh), was obtained from a dichloromethane solution. It crystallized in the triclinic space group, $P\bar{1}$, with four molecules in the unit cell (Z = 4). The asymmetric unit contains two independent molecules. The molecular diagram of the crystal structure of 4-MeTPh is given below in Figure **4-1**, and a summary of the general crystal data of 4-MeTPh is given in Table **4-1**

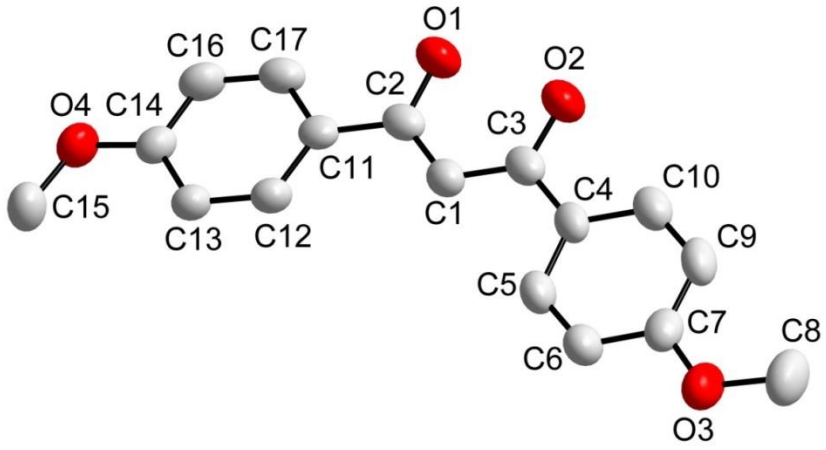

Figure 4-1: Molecular structure of 4-MeTPh. Hydrogen atoms are omitted for clarity. Displacement ellipsoids are drawn at 50 %.

Some bond distances and angles of 4-MeTPh were selected and are summarized in Table **4-3.**

Table 4-3: Selected bond distances and angles for the structure of 4-MeTPh.

Selected bond distances (Å)		Selected bond angles (°)	
O1-C2	1.297(2)	**C2-C1-C3**	122.0(2)
O2-C3	1.317(3)	**O1-C2-C1**	120.0(2)
C1-C2	1.403(4)	**O1-C2-C11**	116.6(3)
C1-C3	1.406(3)	**O2-C3-C1**	120.4(2)
C3-C4	1.469(6)	**O2-C3-C4**	115.5(4)
C2-C11	1.495(6)		

The crystal structure of 4-MeTPh is somewhat asymmetrical with the two reported carbonyl bond distances (C=O) of 1.297(2) Å and 1.317(3) Å being slightly different. 4-MeTPh was compared to similar *O,O'* β-diketone bidentate ligands reported in literature and the reported structures show similar asymmetry as indicated by the carbonyl bond distances (C=O) of 1.286(2) Å and 1.278(2) Å for 1,3-di(2-thenoyl)-1,3-propanedione and 1.268(2) Å and 1.297(3) Å for 1-phenyl-3-(2-thenoyl)-1,3-propanedione while 1.269(4) Å and 1.272(6) Å for 1,1,1-trifluoro-2,4-pentanedione is symmetrical within standard deviation as reported in literature. [15,16]

4-MeTPh is stabilized by two C-H…O intramolecular hydrogen bonding interactions. The bond distances, angles and symmetry operators are presented in Table **4-4**. The

[15] Conradie, M.M., Muller, A.J., Conradie, J. *Afr. J. Chem*. **61** (2008) 13-21.
[16] Dinh, T.-H., Nguyen, H.-H., Nguyen, M.-H. *Inorg. Chem. Commun*. **112** (2020) 107727-107732.

intramolecular hydrogen interactions contributing to the molecular packing of 4-MeTPh is illustrated in Figure **4-2**.

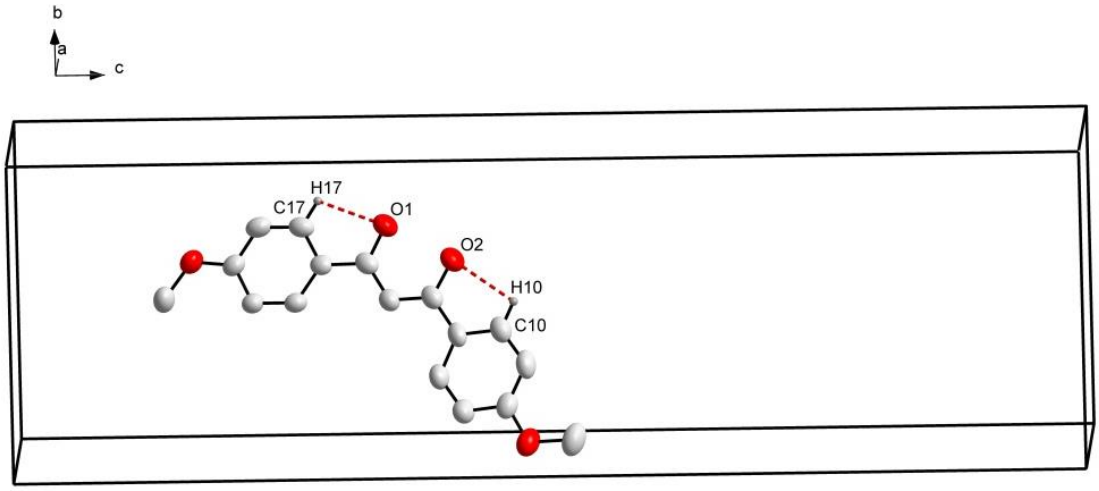

Figure 4-2: Intramolecular hydrogen bonding interactions observed in 4-MeTPh. The numbering of atoms not associated with the hydrogen interactions are omitted for clarity.

Table 4-4: Summary of the intramolecular hydrogen bonding interactions observed in 4-MeTPh. Bond distances and angles are reported in Å and º.

D-H…A	d(D-H)	d(H…A)	d(D…A)	D-H…A angle
C4-H4…O1[a]	0.93	2.49	2.804(6)	100
C12-H12…O12[a]	0.93	2.46	2.781(5)	101

Symmetry code, transformations used to generate equivalent atoms: [a] x, y, z.

The two benzene rings in 4-MeTPh are slightly displaced with a dihedral angle of 2.622(8) º between the planes through atoms O1..C1..C2..C11..C17..O4 and O2..C1..C3..C4..C10..O3 as illustrated in Figure **4-3**.

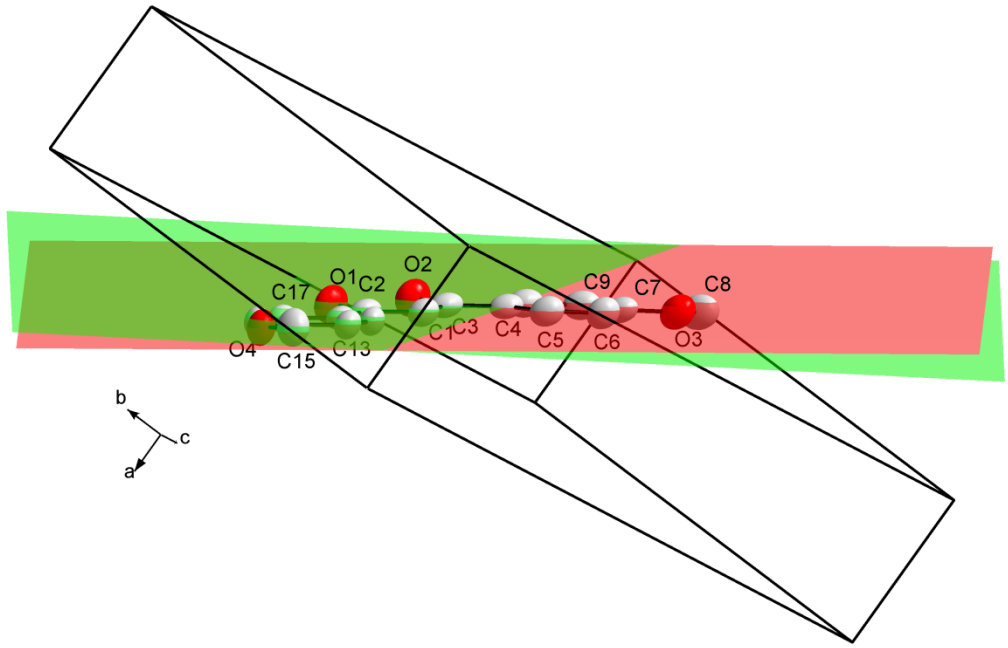

Figure 4-3: Illustration of the plane through O1..C1..C2..C11..C17..O4 (red plane) and O2..C1..C3..C4..C10..O3 (green plane) in the structure of 4-MeTPh with a dihedral angle of 2.622(8) º.

The molecules pack in a head-to-head fashion along the *c*-axis when viewed along the *bc*-plane as shown in Figure **4-4**.

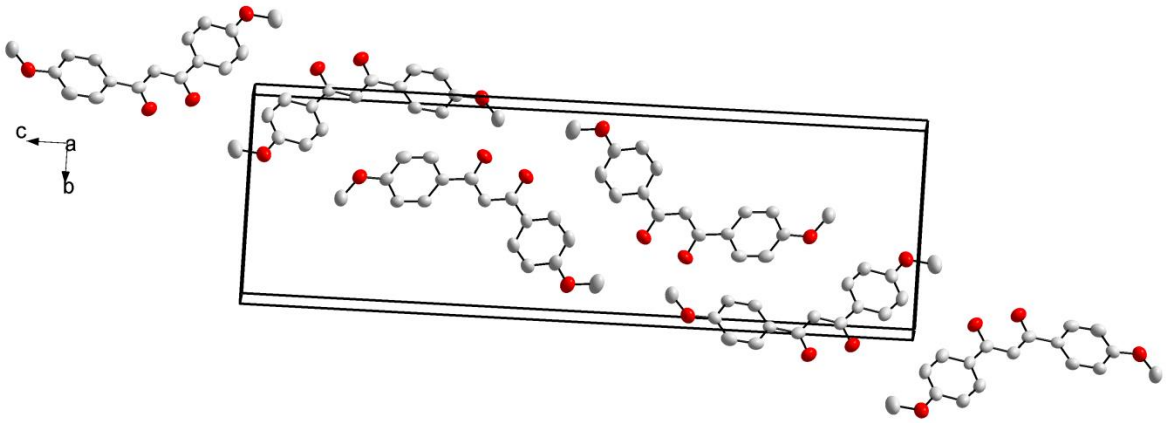

Figure 4-4: Molecular packing of 4-MeTPh in the unit cell viewed along the *bc*-plane. Hydrogen atoms and atom numbering were omitted for clarity.

4.4 Crystal structure of *fac*-[Re(CO)$_3$(Br)(DiMePy)]

fac-[Re(CO)$_3$(Br)(DiMePy)] was synthesized as described in Chapter 3. Yellow crystals were obtained from a methanol solution of the product. This compound crystallized in the monoclinic space group $P2_1/c$ with one neutral *fac*-[Re(CO)$_3$(Br)(DiMePy)] complex in the asymmetric unit (Z = 4). The Re atom has an octahedral coordination with three facially orientated carbonyl ligands, one bidentate 4,4'dimethyl-2,2'-bipyridine ligand and a bromido ligand. The molecular diagram of *fac*-[Re(CO)$_3$(Br)(DiMePy)] is given in Figure **4-5** below.

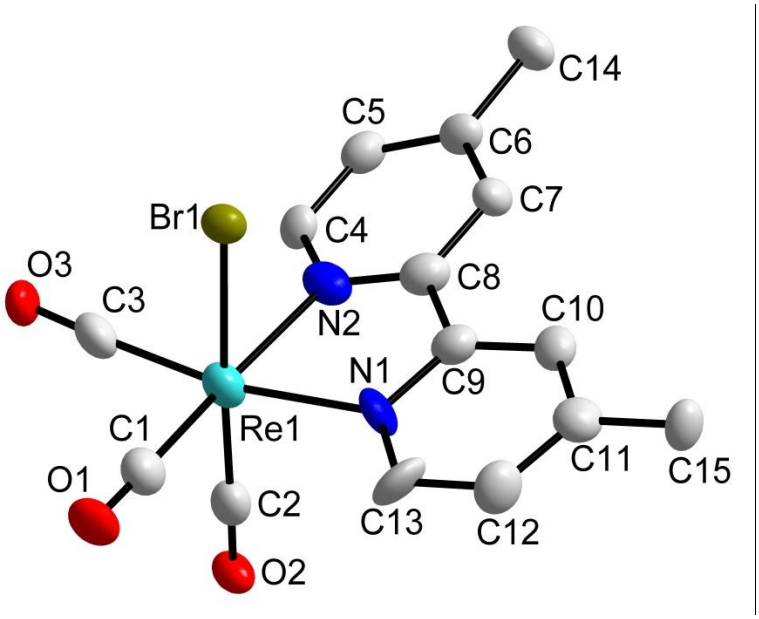

Figure 4-5: Molecular representation of the crystal structure of *fac*-[Re(CO)$_3$(Br)(DiMePy)]. Hydrogen atoms were omitted for clarity. Displacement ellipsoids are drawn at 50 %.

A summary of the general crystal data of *fac*-[Re(CO)$_3$(Br)(DiMePy)] is given in Table **4-1** and the molecular numbering scheme is shown in Figure **4-5**. Some bond distances and angles were selected and are summarized in Table **4-5**.

Table 4-5: Selected bond distances and angles for the structure of *fac*-[Re(CO)$_3$(Br)(DiMePy)].

Selected bond distances (Å)		Selected bond angles (º)	
Re-C1	1.938(14)	**N1-Re-N2**	75.2(4)
Re-C2	1.913(15)	**C1-Re-N1**	99.1(5)
Re-C3	1.936(15)	**C1-Re-N2**	173.1(5)
C1-O1	1.151(14)	**C2-Re-N1**	94.8(5)
C2-O2	1.138(14)	**C3-Re-N2**	96.1(5)
C3-O3	1.140(14)	**C2-Re-C3**	91.4(6)
Re-N1	2.175(10)		
Re-N2	2.187(10)		
Re-Br1	2.633(17)		

The bond distance from Re to the three carbonyl carbons (C1, C2 and C3) are all within the range of similar reported structures, varying from 1.913(15) Å to 1.938(14) Å.[17,18,19,20,21,22,23,24,25] The rhenium bromido distance is 2.633(17) Å, which is comparable to other reported bromido structures.[2,3,26] The rhenium to nitrogen bond distances, N1 and N2 of 2.175(10) Å and 2.187 (10) Á respectively are within normal range and are similar to other reported Re(I) tricarbonyl complexes with coordinated *N,N'*-bidentate ligands like *fac*-[Re(CO)$_3$(Cl)(dcbpy)], *fac*-[Re(CO)$_3$(MeCN)(dcbpy)]OTf, *fac*-[Re(CO)$_3$(py)(dcbpy)], *fac*-[Re(CO)$_3$(cpy)(dcbpy)]OTf and *fac*-[Re(CO)$_3$(Cl)(bcpbpy)] where (dcbpy = 4,4'-bis(4-cyanophenyl)-2,2'-bipyridyll and bcpbpy = 4,4'-bis[(*E*)-*2*-(4-cyanophenyl)vinyl]-2,2'-bipyridyl).[27,28,29,30,31,32] The small bite angle, N1-Re1-N2, of 75.287(11) º confirms the distorted octahedral geometry with the angles 99.1(5) º for C1-Re1-N1, 96.1(5) º for C3-Re1-N2 and 95.0(5) º for C2-Re1-N2 being the largest deviations from 90 º. The 'linear' angle C1-Re1-N2 of 173.1(5) º also deviates significantly from 180 º. All these

[17] Schutte, M., Visser, H.G., Brink, A. *Act Cryst*. **E65** (2009) m1757-m1576.
[18] Schutte, M., Visser, H.G. *Act Cryst*. **E64** (2008) m1226-m1227.
[19] Schutte, M., Visser, H.G., Steyl, G. *Act Cryst*. **E63** (2007) m3195-m3196.
[20] Makris, G., Karagiorgou, O., Papagiannopoulor, D., Papagiannopoulor, A., Raptopoulou, C.P., Terzis, A., Pyscharis, V., Pelecanou, M., Pirmettis, I., Papadopoulos, M.S. *Eur. J. Inorg. Chem*. **19** (2012) 3132-3139.
[21] Mokolokolo, P.P., Frei, A., Tsosane, M.S., Kama, D.V., Schutte-Smith, M., Brink, A., Visser, H.G., Meola, G., Alberto, R., Roodt, A. *Inorg. Chim. Acta*. **471** (2018) 249-256.
[22] Manicum, A., Alexander, O., Schutte-Smith, M., Visser, H.G., Roodt, A. *Z. Kristallogr. NCS.* **232(6)** (2017) 957-959.
[23] Brasey, T., Buryak, A., Scopelliti, R., Severin, K. *Eur. J. Inorg. Chem*. **5** (2004) 964-967.
[24] Nkoe, P.I., Koen, R., Brink, A., Schutte-Smith, M. *Z. Kristallogr. NCS*. **231(2)** (2016) 461-464.
[25] Brink, A., Visser, H.G., Roodt, A. *Polyhedron.* **52** (2013) 416-423.
[26] Schutte, M., Visser, H.G., Roodt, R. *Act Cryst.* **E66** (2010) m859-m860.
[27] Coleman, A., Brennan, C., Vos, J.G., Pryce, M.T. *Coord. Chem. Rev.* **252** (2008) 2585-2595.
[28] Lo, K.M., Louie, M., Zhang, K.Y. *Coord. Chem. Rev.* **254** (2010) 2603-2622.
[29] Cuestsa, L., Gerbino, D.C., Hevia, E., Morales,D., Clemente, M.E.N., Perez, J., Riera, L., Riera, V., Miguel, D., del Rio, I. Garcia-Granda. *Chem. Eur. J*. **10** (2004) 1765-1777.
[30] Hallett, A.J., Pope, S.J.A. *Inorg. Chem. Commun*. **14** (2011) 1606-1608.
[31] Carreno, A., Gacitua, M., Schott, E., Zarate,X., Manriquez, J.M., Preite, M., Ladeira, S., Castel, A., Pizarro, N., Veg, A., Chavez, I., Arrattia-Perez, R. *New. J. Chem*. **39** (2015) 5725-5734.
[32] Smieja, J.M., Kubiak, C.P. *Inorg. Chem*. **49** (2010) 9283-9289.

bond distances and angles were compared to similar reported structures and were found to be in good agreement.[17,18,19] A dihedral angle of 13.916(1) º was calculated between the planes through Re1, C1, O1, C3, O3, N1, N2 and N1,C4-C13, N2 as illustrated in Figure **4-6**. The bidentate ligand 'bends' significantly away from the axial carbonyl ligand and towards the monodentate ligand (Br^-).

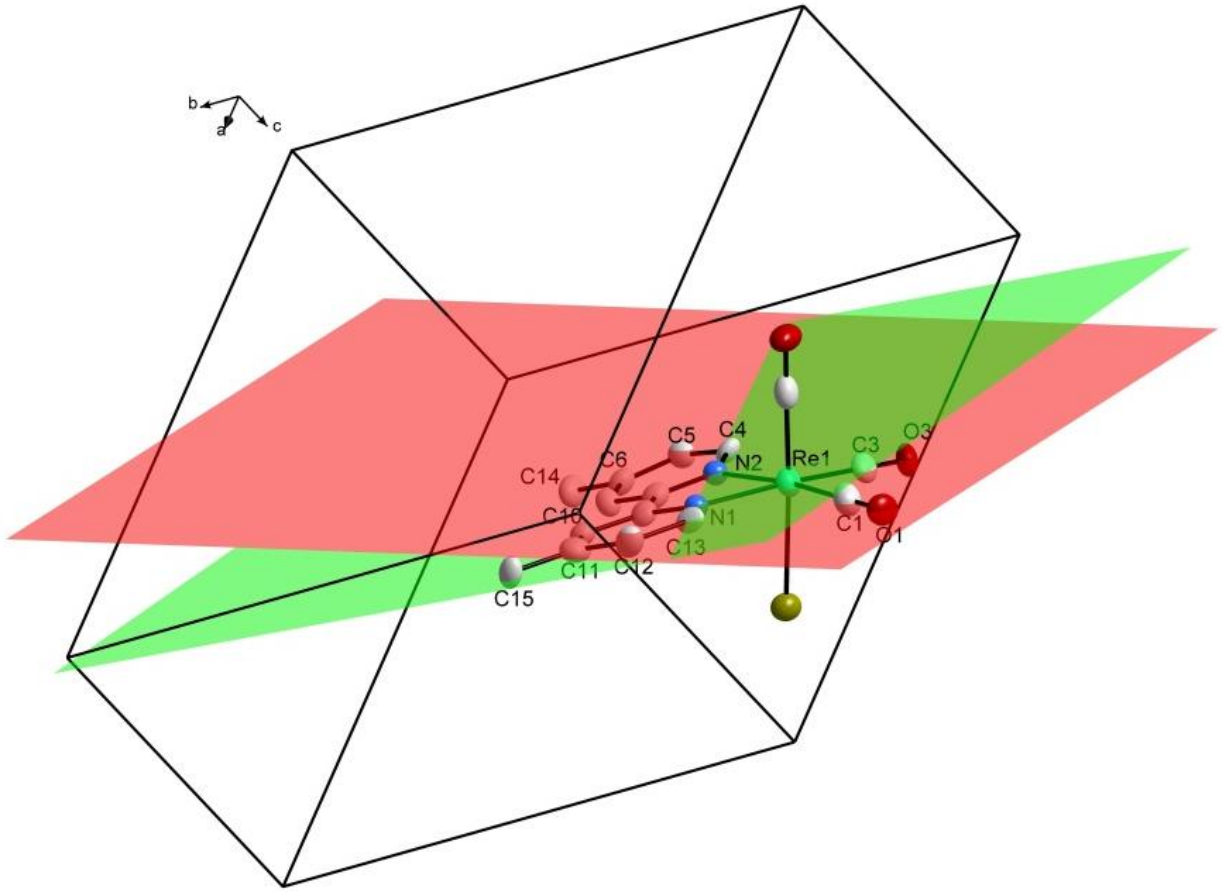

Figure 4-6: Illustration of the dihedral angle of 13.916(1) º between the planes through Re..C1..O1..C3..O3..N1..N2 (red plane) and N1..C4..C13..N2 (green plane). Hydrogen atoms were omitted for clarity.

The crystal structure of *fac*-[$Re(CO)_3$(Br)(DiMePy)] is stabilized by two intermolecular (one C-H…O and one C-H…Br) hydrogen bonding interactions. The bonding distances, angles and symmetry operators are presented in Table **4-6**. These intermolecular hydrogen bonding interactions contributing to the molecular packing of *fac*-[$Re(CO)_3$(Br)(DiMePy)] is illustrated in Figure **4-7** and viewed along the *bc*-plane.

Table 4-6: Summary of the intermolecular hydrogen bonding interactions observed in *fac*-[Re(CO)$_3$(Br)(DiMePy)]. Bond distances and angles are reported in Å and º respectively.

D-H…A	d(D-H)	d(H…A)	d(D…A)	D-H…A angle
C5-H5…O3[a]	0.93	2.54	3.393(17)	153
C7-H7…Br1[b]	0.93	2.84	3.744(12)	164

Symmetry code, transformations used to generate equivalent atoms: [a]1-x, ½+y, -½-z; [b]x, $\frac{3}{2}$-y, ½+z.

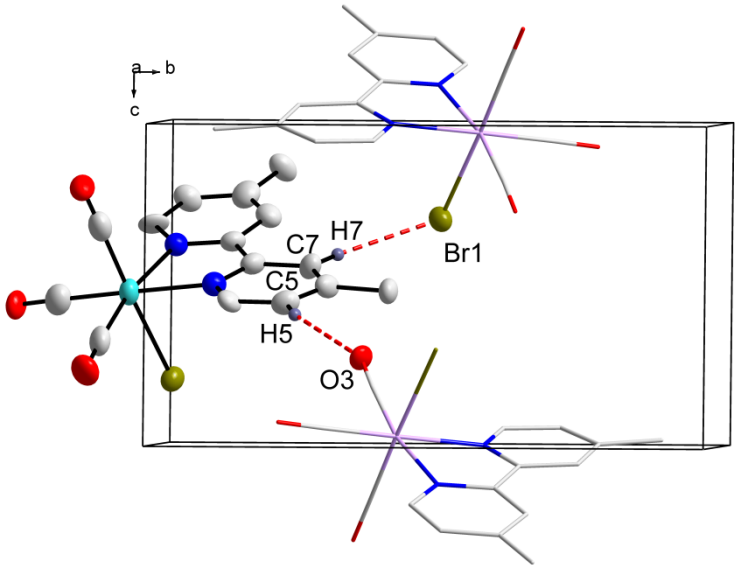

Figure 4-7: Hydrogen bonding interactions observed in *fac*-[Re(CO)$_3$(Br)(DiMePy)] when viewed along the *bc*-plane. Hydrogen atoms and numbering of atoms not associated with the hydrogen interations were omitted for clarity.

fac-[Re(CO)$_3$(Br)(DiMePy)] further experience lattice stability reinforcement via C-H…π and C-X…π molecular interactions, as indicated in Table **4-7**. Two Br…π interactions (one intermolecular and one intramolecular) and one intermolecular H…π interaction are observed in *fac*-[Re(CO)$_3$(Br)(DiMePy)]. The bromide to centroid Cg1 and Cg2 distances are reported as 2.914(4) Å (strong interaction) and 3.955(6) Å (weak interaction) respectively, as illustrated in Figure **4-8**. The hydrogen to centroid (Cg1) distance is reported as 2.97(2) Å and is considered as another strong interaction (illustrated in Figure **4-8**).

Table 4-7: Summary of the π-interactions observed in the structure of *fac*-[Re(CO)$_3$(Br)(DiMePy)].

Y-X(I)	Res(I) → Cg(J)	X…Cg (Å)	Y-X…Cg (º)	Y…Cg (Å)
Re1-Br1[a]	[1] → Cg1	2.914(4)	39	1.858
Re1-Br1[b]	[1] → Cg2	3.955(6)	151	6.387
C14-H14C	[1] → Cg1	2.97(2)	130	3.673

Symmetry code, transformations used to generate equivalent atoms: [a] x, y, z; [b] x, y, -1+z; Cg1; [c] x, $\frac{3}{2}$-y, -½+z; Cg1= centroid atoms of Re1-N1-C9-C8-N2; Cg2 = N1-C9-C10-C11-C12-C13.

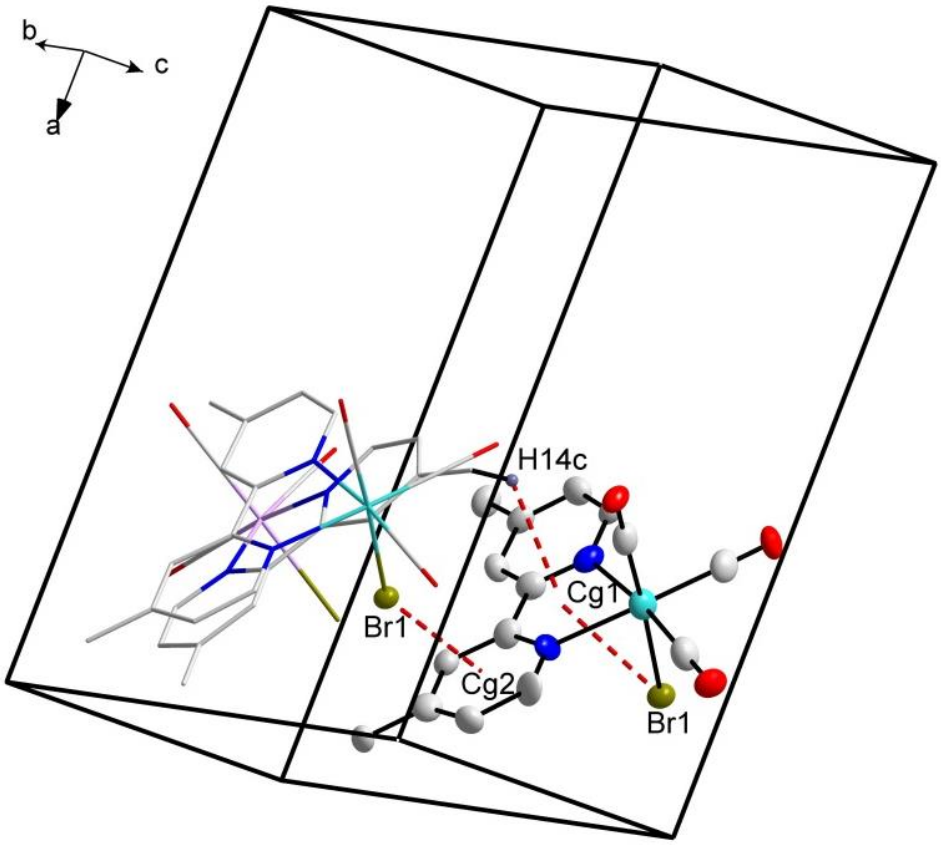

Figure 4-8: Illustration of the π-interactions observed in the structure of *fac*-[Re(CO)$_3$(Br)(DiMePy)]. Hydrogen atoms and numbering of certain atoms were omitted for clarity.

fac-[Re(CO)$_3$(Br)(DiMePy)] pack in a head-to-tail fashion in 'column-like' structures across the *ac*-plane as illustrated in Figure **4-9**.

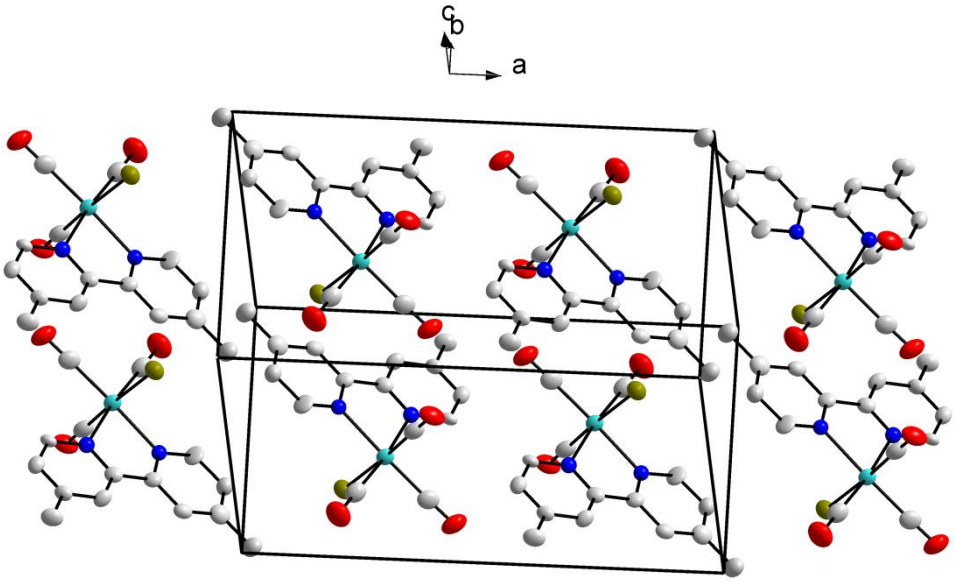

Figure 4-9: Molecular packing of *fac*-[Re(CO)$_3$(Br)(DiMePy)] in the unit cell, when viewed along the *ab*-plane. Hydrogen atoms are omitted for clarity.

4.5 Crystal structure of *fac*-[Re(CO)$_3$(Act)(DiMePy)][NO$_3$]

fac-[Re(CO)$_3$(Act)(DiMePy)][NO$_3$] was synthesized as described in chapter 3. The yellow crystals were obtained from an acetone solution of the product. *fac*-[Re(CO)$_3$(Act)(DiMePy)][NO$_3$] crystallized in the monoclinic space group *C2/c* with one cationic *fac*-[Re(CO)$_3$(Act)(DiMePy)]$^+$ complex and one NO$_3^-$ counter ion in the asymmetric unit (Z = 8). The Re atom is octahedrally surrounded by three facially orientated carbonyl ligands, one bidentate 4,4'dimethyl-2,2'-bipyridine ligand and an acetone ligand. The charge of the complex is balanced by the nitrate counter ion. The molecular structure of *fac*-[Re(CO)$_3$(Act)(DiMePy)][NO$_3$] is given in Figure **4-10** below.

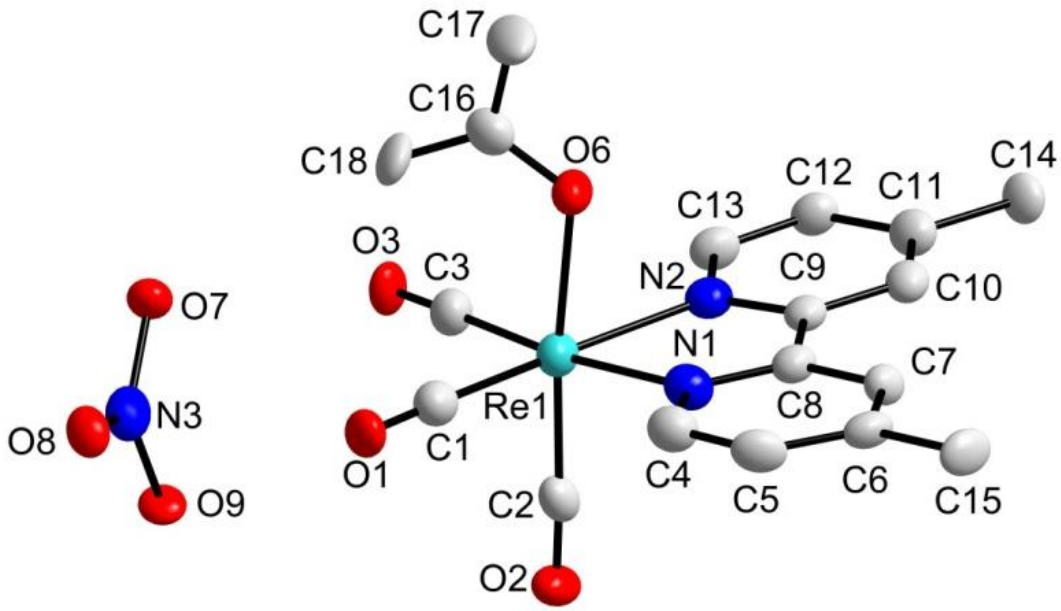

Figure 4-10: Molecular representation of the crystal structure of *fac*-[Re(CO)$_3$(Act)(DiMePy)][NO$_3$] with the atom numbering scheme indicated. Hydrogen atoms are omitted for clarity. Displacement ellipsoids are drawn at 50 %.

The general crystal data of *fac*-[Re(CO)$_3$(Act)(DiMePy)][NO$_3$] is given in Table **4-1** and the numbering scheme of *fac*-[Re(CO)$_3$(Act)(DiMePy)][NO$_3$] is shown in Figure **4-10**. Selected bond distances and angles of the structure of *fac*-[Re(CO)$_3$(Act)(DiMePy)][NO$_3$] are summarized in Table **4-8.**

Table 4-8: Selected bond distances and angles of the structure of *fac*-[Re(CO)$_3$(Act)(DiMePy)][NO$_3$].

Selected bond lengths (Å)		**Selected bond angles (º)**	
Re-C1	1.920(6)	**N2-Re-N1**	74.8(16)
Re-C2	1.899(9)	**C1-Re-N1**	97.0(2)
Re-C3	1.929(6)	**C3-Re-N2**	99.4(2)
C1-O1	1.137(10)	**C1-Re-O6**	95.9(2)
C2-O2	1.149(8)	**C3-Re-O6**	95.8(2)
C3-O3	1.138(8)	**C2-Re-O6**	174.6(18)
Re-O6	2.134(4)		
Re-N1	2.170(4)		
Re-N2	2.165(1)		

The bond distance from Re to the three carbonyl carbons (C1, C2 and C3) are all within normal range and vary from 1.899(9) Å to 1929(6) Å.[17-26] The distance between rhenium and the acetone oxygen (O6) is 2.134(4) Å and compare well to other Re(I) tricarbonyl complexes with an acetone ligand coordinated in the 6th position (2.187(5)

Å[33] and 2.151(8) Å[34]). The rhenium to nitrogen bond distances, N1 and N2 are 2.170(4) Å and 2.165(1) Å respectively, similar to *fac*-[Re(CO)$_3$(Br)(DiMePy)] reported in Paragraph 4.4 and other comparable reported structures.[27,28,35,36] The small bite angle, N1-Re-N2, of 74.8(16)º is also within range of *fac*-[Re(CO)$_3$(Br)(DiMePy)] (Paragraph 4.4) and other reported structures.[27,28,29,30,31,32] The angles 97.0(2) º for C1-Re-N1, 99.4(2) º for C3-Re-N2, and 95.8(2) º for C3-Re-O6 all significantly deviate from 90 º. The 'linear' angle C2-Re-O6 of 174.6(18) º also deviate quite significantly from 180 º. This results in a distorted octahedral coordination sphere. All the angles and bond distances were compared to similar reported structures and were found to be in good agreement.[34,35,37] A very small dihedral angle of 0.498(9) º is calculated between the plane through Re, C1, O1, C3, O3, N1, N2 and N1, C4-C13, N2 and is illustrated in Figure **4-11**. This confirms that the bidentate ligand is almost 'planar' with regards to the plane through Re, C1, O1, C3, O3, N1, N2 and almost don't 'bend' away from the axial carbonyl ligand. The 'bending' of the bidentate ligand is much less than in the case of *fac*-[Re(CO)$_3$(Br)(DiMePy)] where the bidentate ligand 'bends' away from the carbonyl ligand with a dihedral angle of 13.916(1) º.

[33] Hevia, E., Perez, J., Riera, V. *Inorg. Chem.* **41** (2002) 4673-4679.
[34] Chin, R.M., Barrera, J., Dubois, R.H., Helberg, L.E., Sabat, M., Bartucz, T.Y., Lough, A.J., Morris, R.H., Harman, W.D. *Inorg. Chem*. **36** (1997) 3553-3558.
[35] Hatcher, L.E. *CrystEngComm*. **20** (2018) 5990-5997.
[36] Hevia, E., Perez, J., Riera, V. *Inorg. Chem*. **41** (2002) 4673-4679.
[37] Velmurugan, G., Ramamoorthi, B.K., Venuvanalingam P. *Phys. Chem*. **16** (2014) 21157-21171.

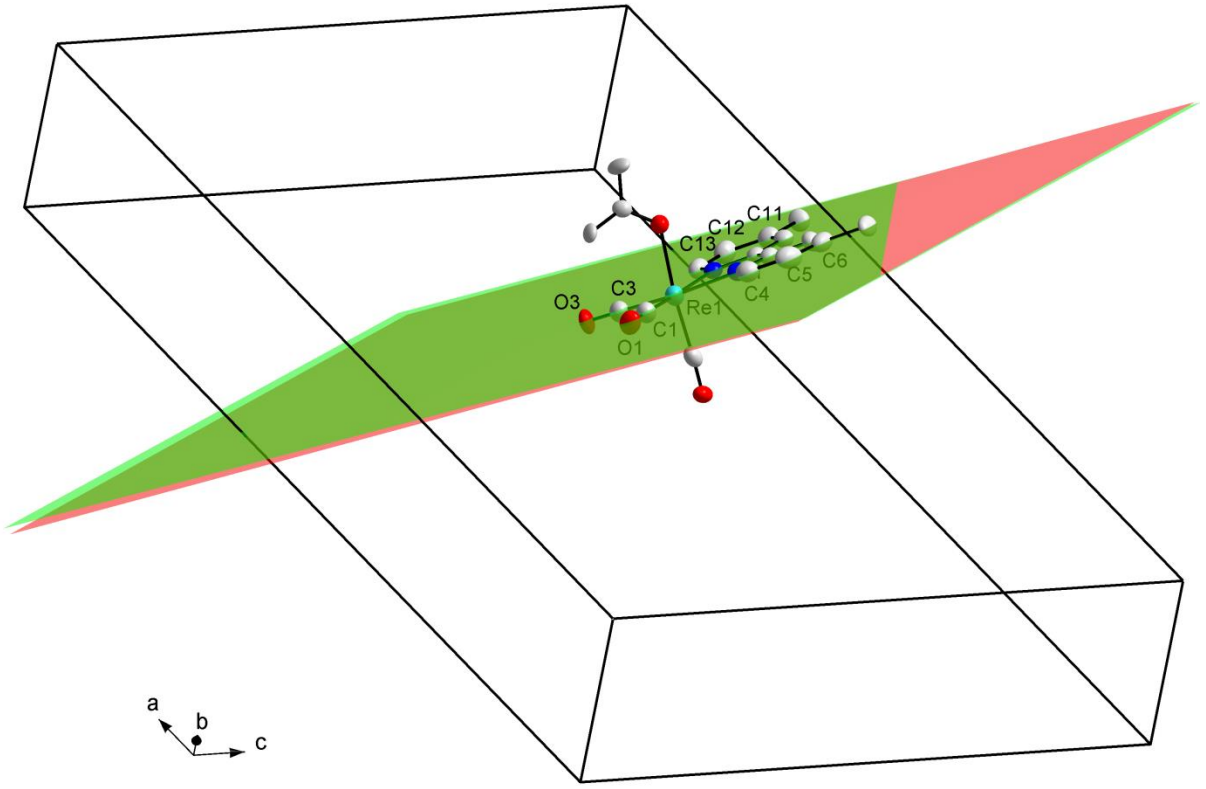

Figure 4-11: Illustration of the dihedral angle of 0.498(9) º between the planes through Re..C1..O1..C3..O3..N1..N2 (red plane) and N1..C4..C13..N2 (green plane). Hydrogen atoms were omitted for clarity.

The crystal structure of *fac*-[Re(CO)$_3$(Act)(DiMePy)][NO$_3$] is stabilized by two intermolecular C-H…O hydrogen bonding interactions. The bonding distances, angles and symmetry operators are presented in Table **4-9**. These intermolecular hydrogen bonding interactions, contributing to the molecular packing of *fac*-[Re(CO)$_3$(Act)(DiMePy)][NO$_3$], is illustrated in Figure **4-12**.

Table 4-9: Summary of the hydrogen bonding interaction distances (Å) and angles (º) observed in the structure of *fac*-[Re(CO)$_3$(Act)(DiMePy)][NO$_3$].

D-H…A	d(D-H) (Å)	d(H…A) (Å)	d(D…A) (Å)	D-H…A angle (º)
C5-H5…O8[a]	0.95	2.47	3.343(10)	153
C7-H7…O6[b]	0.95	2.54	3.317(7)	139

Symmetry code, transformations used to generate equivalent atoms: [a] ½+x,- ½+ y, z; [b] ½-x, ½y,-z.

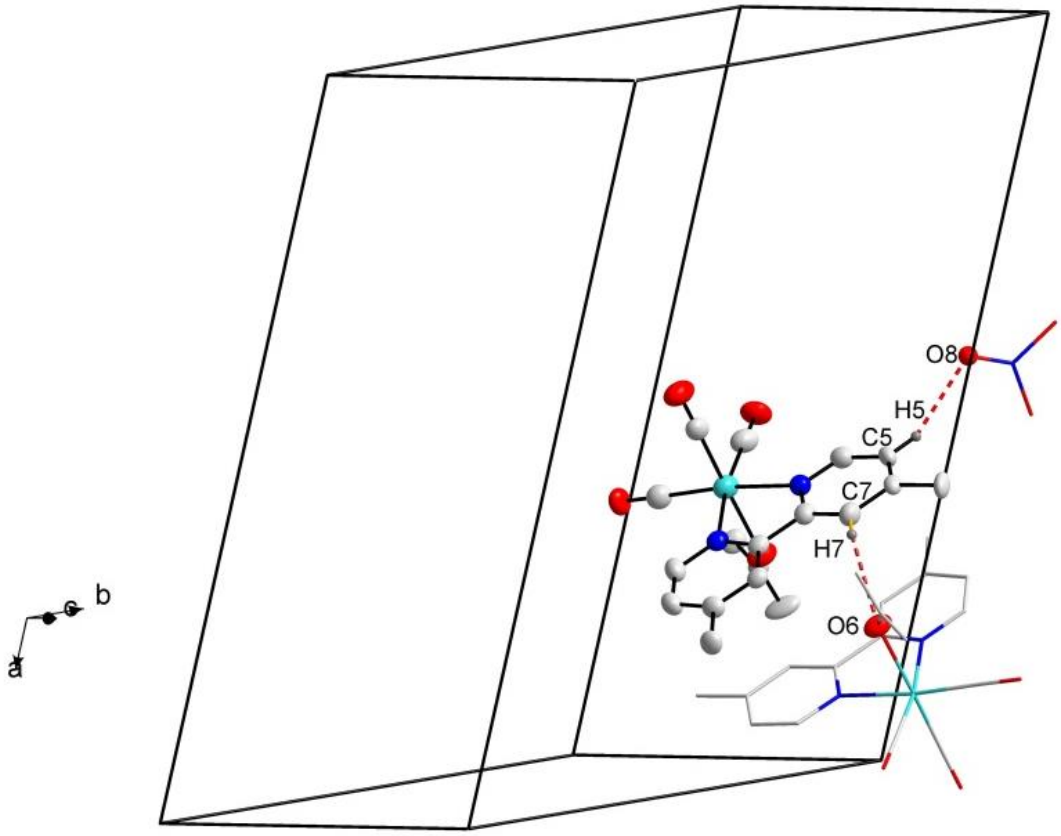

Figure 4-12: Hydrogen bonding interactions observed in the structure of *fac*-[Re(CO)$_3$(Act)(DiMePy)][NO$_3$] when viewed along the *ab*-plane. Hydrogen atoms not taking part in the interactions and numbering for certain atoms were omitted of clarity.

fac-[Re(CO)$_3$(Act)(DiMePy)][NO$_3$] further experience lattice stability reinforcement via a π-ring molecular interaction, as indicated in Table **4-10**. The weak intermolecular O…π interaction observed in *fac*-[Re(CO)$_3$(Act)(DiMePy)][NO$_3$] has a reported centroid (Cg1) to O2 distance of 3.913(9) Å and is illustrated in Figure **4-13**.

Table 4-10: A summary of the intermolecular π-ring interaction observed in the structure of *fac*-[Re(CO)$_3$(Act)(DiMePy)][NO$_3$].

Y-X(I)	Res(I) → Cg(J)	X…Cg (Å)	Y-X…Cg (°)	Y…Cg (Å)
C2-O2	[1] → Cg1	3.180(9)	122	3.913(9)

Symmetry code, transformations used to generate equivalent atoms: [a] 1-x, y, ½-z Cg1 = centroid atoms of Re1-N1-C9-C8-N2.

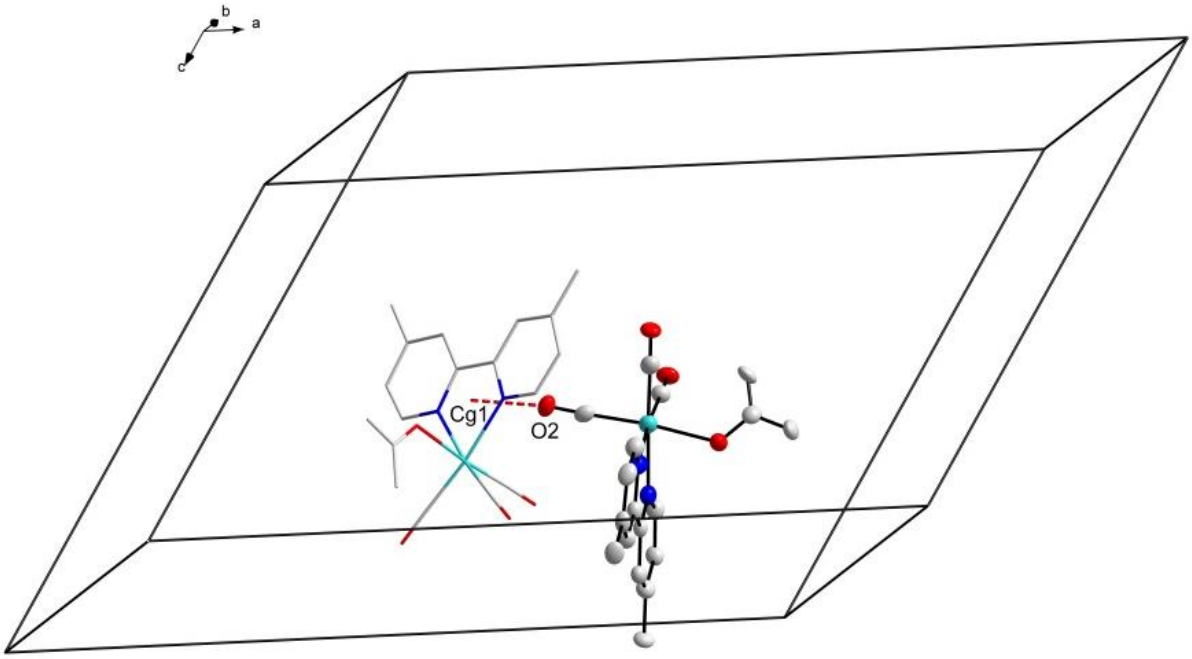

Figure 4-13: intermolecular π-ring interaction observed in the structure of *fac*-[Re(CO)$_3$(Br)(DiMePy)], viewed along the *ac*-plane. Hydrogen atoms and numbering of certain atoms were omitted for clarity.

The molecules pack in a head-to-head fashion, diagonally in 'column-like' structures across the *ab*-plane, as illustrated in Figure **4-14.**

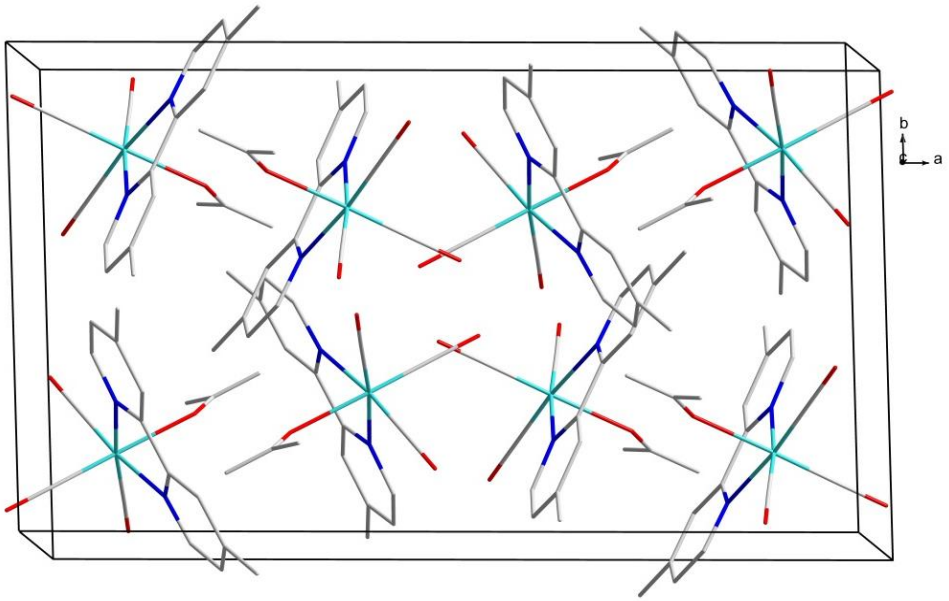

Figure 4-14: Molecular packing of *fac*-[Re(CO)$_3$(Act)(DiMePy)][NO$_3$] in the unit cell, viewed along the *ab*-plane. Hydrogen atoms and counter ions are omitted for clarity.

4.6 Crystal structure of fac-[Re(CO)$_3$(NO$_3$)(DiMePy)]

fac-[Re(CO)$_3$(NO$_3$)(DiMePy)] was synthesized as described in Chapter 3. The yellow crystals were obtained from a methanol solution of the product. The compound crystallized in the monoclinic space group $P2_1/n$ with one neutral *fac*-[Re(CO)$_3$(NO$_3$)(DiMePy)] in the asymmetric unit (Z = 4). The Re atom is octahedrally surrounded by three facially orientated carbonyl ligands, one bidentate 4,4'dimethyl-2,2'-bipyridine ligand and a nitrate ligand. The molecular structure of *fac*-[Re(CO)$_3$(NO$_3$)(DiMePy)] is given in Figure **4-15** below.

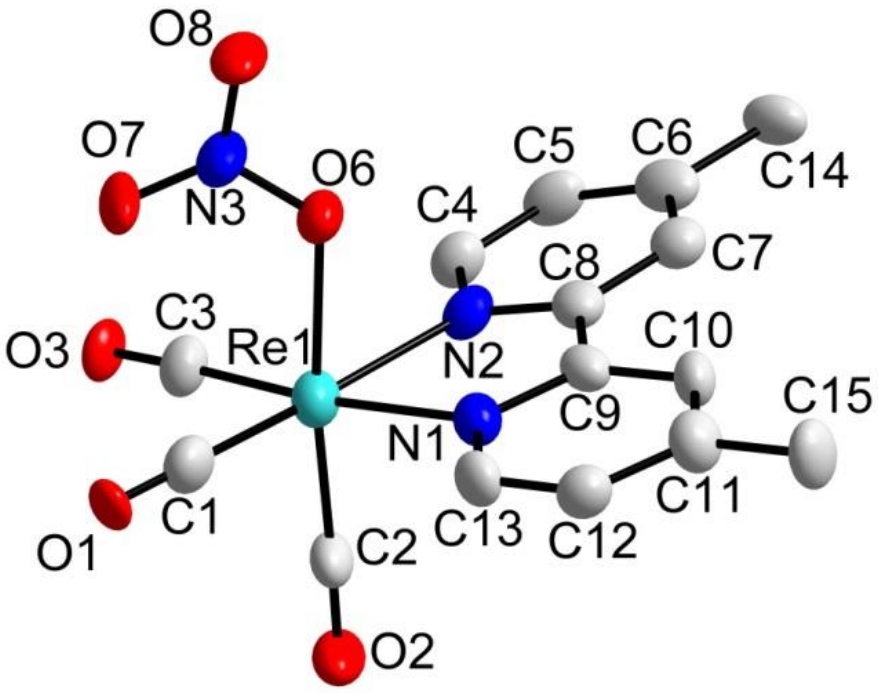

Figure 4-15: Molecular representation of the crystal structure of *fac*-[Re(CO)$_3$(NO$_3$)(DiMePy)]. Hydrogen atoms are omitted for clarity. Displacement ellipsoids are drawn at 50 %.

A summary of the general crystal data of *fac*-[Re(CO)$_3$(NO$_3$)(DiMePy)] is given in Table **4-2**. Some bond distances and angles were selected and are summarized in Table **4-11**.

Table 4-11: Selected bond distances and angles for the structure of *fac*-[Re(CO)$_3$(NO$_3$)(DiMePy)].

Selected bond lengths (Å)		Selected bond angles (º)	
Re-C1	1.913(6)	**N2-Re-N1**	74.73(16)
Re-C2	1.889(6)	**C1-Re-N1**	100.4(2)
Re-C3	1.919(6)	**C3-Re-N2**	98.8(2)
C1-O1	1.161(9)	**C1-Re-O6**	95.6(2)
C2-O2	1.155(9)	**C3-Re-O6**	97.0(2)
C3-O3	1.159(9)	**C2-Re-O6**	173.4(2)
Re-O6	2.156(4)		
Re-N1	2.170(4)		
Re-N2	2.159(9)		

The bond distance from Re to the three carbonyl carbons (C1, C2 and C3) are within normal range of similar reported structures, varying from 1.889(6) Å to 1.919(6) Å.[17-25] The distance between rhenium and the nitrate oxygen (O6) is 2.156(4) Å, which is comparable to *fac*-[Re(CO)$_3$(Act)(DiMePy)][NO$_3$] for a Re-O single bond and other structures with a nitrate ligand coordinated to Re(I).[37,35,38] The rhenium to nitrogen bond distances, N1 and N2 are 2.170(4) Å and 2.159(9) Å respectively, which are similar to *fac*-[Re(CO)$_3$(Br)(DiMePy)] and *fac*-[Re(CO)$_3$(Act)(DiMePy)][NO$_3$] (paragraph 4.4 and 4.5) and other reported structures (*fac*-[Re(CO)$_3$(Cl)(dcbpy)], *fac*-[Re(CO)$_3$(MeCN)(dcbpy)]OTf, *fac*-[Re(CO)$_3$(py)(dcbpy)], *fac*-[Re(CO)$_3$(cpy)(dcbpy)]OTf and *fac*-[Re(CO)$_3$(Cl)(bcpbpy)] where (dcbpy = 4,4'-bis(4-cyanophenyl)-2,2'-bipyridyll and bcpbpy = 4,4'-bis[(*E)-2*-(4-cyanophenyl)vinyl]-2,2'-bipyridyl)).[27-29] The small bite angle, N1-Re-N2, of 74.73(16) º is within range with *fac*-[Re(CO)$_3$(Br)(DiMePy)], *fac*-[Re(CO)$_3$(Act)(DiMePy)][NO$_3$] and similar compounds. The angles 100.4(2) º for C1-Re-N1, 98.8(17) º for C3-Re-N2 and 97.0(3) º for C3-Re-O6 all significantly deviate from 90 º. The 'linear' angle C2-Re-O6 of 173.4(2) º also deviates quite significantly from 180 º and confirms the distorted octahedral coordination sphere. All the bond distances and angles were compared to similar reported structures and were found to be in agreement.[17,18,19] A dihedral angle of 6.264(15) º was calculated between the plane through Re..C1..O1..C3..O3..N1..N2 and N1..C4..C13..N2 and is illustrated in Figure **4-16** The bidentate ligand 'bends' slightly away from the axial carbonyl ligand and towards the monodentate ligand (NO_3^-), but not as much as in the case of *fac*-[Re(CO)$_3$(Br)(DiMePy)] where a dihedral angle of 13.916(1) º was calculated, but significantly more that in the case of *fac*-[Re(CO)$_3$(Act)(DiMePy)][NO$_3$] where a dihedral angle of 0.498(9) º was calculated.

[38] Dominguez, S.E., Albores, P., Fagalde, F. *Polyhedron*. **67** (2014) 471-480.

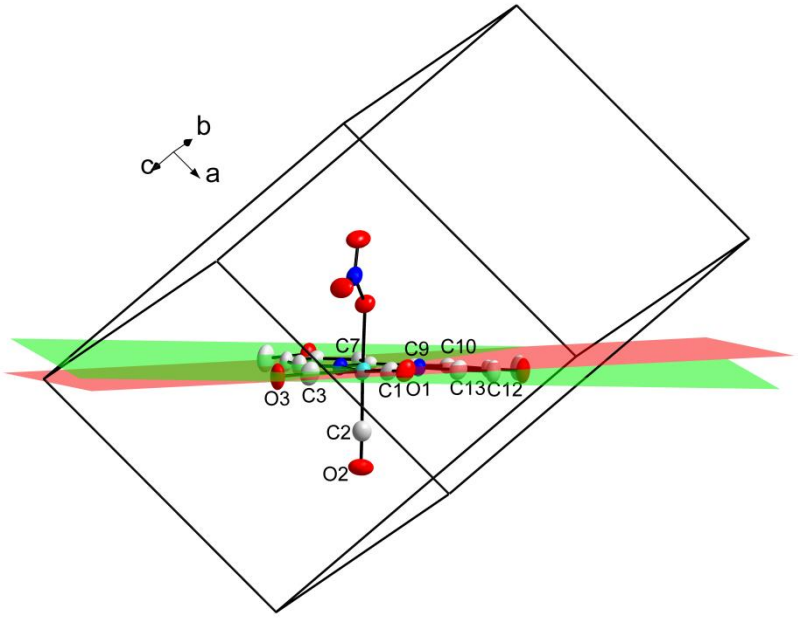

Figure 4-16: Illustration of the dihedral angle of 6.264(15) ° between the planes through Re..C1..O1..C3..O3..N1..N2 (red plane) and N1..C4..C13..N2 (green plane). Hydrogen atoms were omitted for clarity.

The crystal structure of *fac*-[Re(CO)$_3$(NO$_3$)(DiMePy)] is stabilized by five intermolecular C-H…O hydrogen bonding interactions. The bonding distances, angles and symmetry operators are presented in Table **4-12**. These intermolecular hydrogen bonding interactions, contributing to the molecular packing of *fac*-[Re(CO)$_3$(NO$_3$)(DiMePy)], is illustrated in Figure **4-17**.

Table 4-12: Summary of the hydrogen bonding interaction distances (Å) and angles (º) observed in *fac*-[Re(CO)$_3$(NO$_3$)(DiMePy)].

D-H…A	d(D-H)	d(H…A)	d(D…A)	D-H…A angle
C5-H5…O1[a]	0.95	2.56	3.352(8)	141
C7-H7…O6[b]	0.95	2.56	3.425(6)	151
C12-H12…O7[c]	0.95	2.55	3.165(8)	123
C15-H15B…O2[d]	0.98	2.46	3.230(8)	135
C15-H15C…O1[e]	0.98	2.53	3.460(9)	158

Symmetry code, transformations used to generate equivalent atoms: [a] $\frac{3}{2}$-x,-½-y,½-z; [b] 2-x,-y,-z; [c] $\frac{5}{2}$+x,-½-y,-½+z; [d] ½+x,-½-y,-½+z; ½+x, ½+y,-½+z.

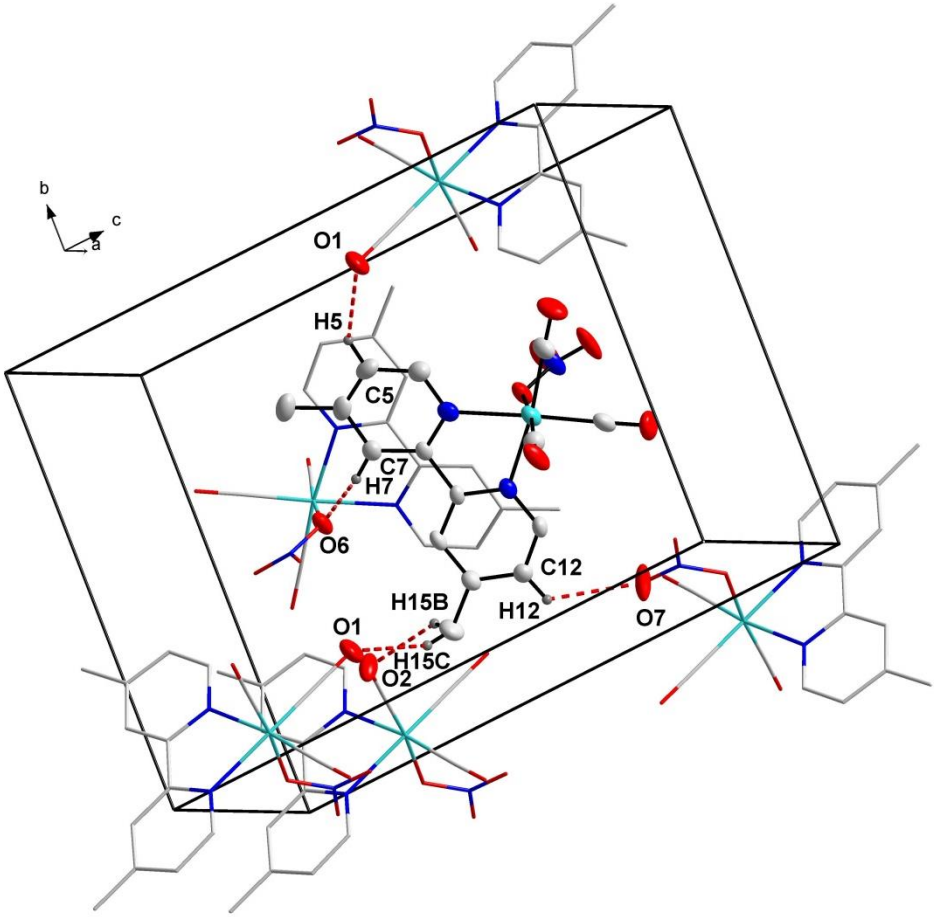

Figure 4-17: Hydrogen bonding interactions observed in the structure of *fac*-[Re(CO)$_3$(NO$_3$)(DiMePy)]. Hydrogen atoms not taking part in the interactions and numbering for certain atoms were omitted for clarity.

fac-[Re(CO)$_3$(NO$_3$)(DiMePy)] pack in a head-to-head fashion in alternating layers, diagonally across the *ac*-plane as illustrated in Figure **4-18.**

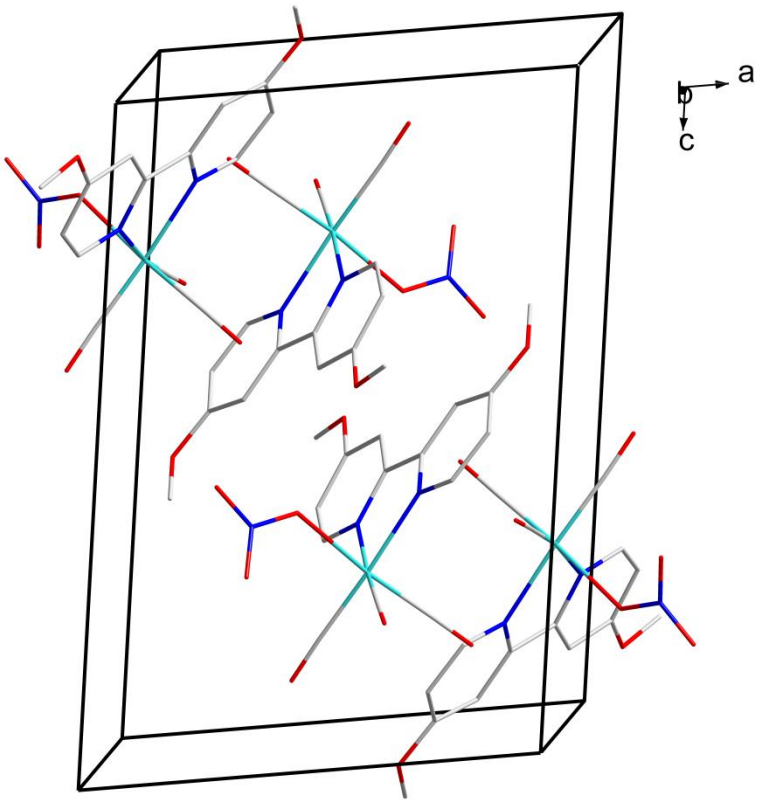

Figure 4-18: Molecular packing of *fac*-[Re(CO)$_3$(NO$_3$)(DiMePy)] in the unit cell, when viewed along the *ac*-plane. Hydrogen atoms are omitted for clarity.

4.7 Crystal structure of fac-[Re(CO)$_3$Br(DiMeOPy)]

fac-[Re(CO)$_3$(Br)(DiMeOPy)] was synthesized as described in Chapter 3. The yellow crystals were obtained from a methanol solution of the product. This compound crystallized in the orthorhombic space group, *Pbcn,* with one neutral *fac*-[Re(CO)$_3$(Br)(DiMeOPy)] complex in the asymmetric unit (Z = 8). The Re atom has octahedral coordination with three facially orientated carbonyl ligands, one bidentate 4,4'dimethoxy-2,2'-bipyridine ligand and a bromido ligand. The molecular structure of *fac*-[Re(CO)$_3$(Br)(DiMeOPy)] is given in Figure **4-19**.

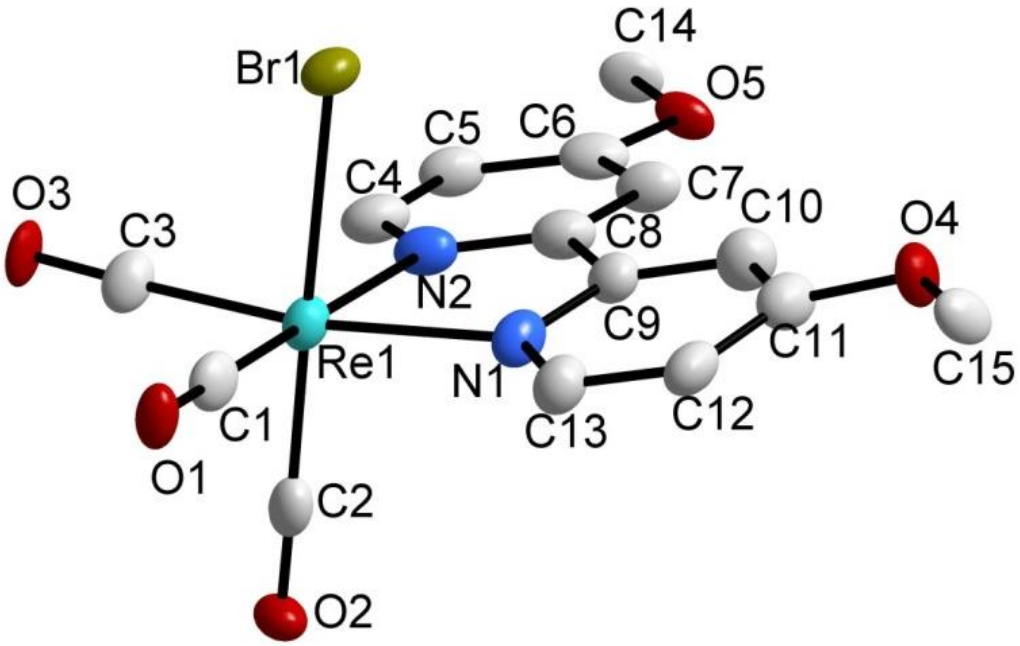

Figure 4-19: Molecular representation of the crystal structure of *fac*-[Re(CO)$_3$(Br)(DiMeOPy)]. Hydrogen atoms were omitted for clarity. Displacement ellipsoids are drawn at 50 %.

A summary of the general crystal data of *fac*-[Re(CO)$_3$(Br)(DiMeOPy)] is given in Table **4-2** Some bond distances and angles were selected and are summarized in Table **4-13**.

Table 4-13: Selected bond distances and angles for the structure of *fac*-[Re(CO)$_3$(Br)(DiMeOPy)].

Selected bond distances (Å)		Selected bond angles (°)	
Re-C1	1.926(8)	**N2-Re-N1**	74.7(2)
Re-C2	1.909(9)	**C1-Re-N1**	100.3(3)
Re-C3	1.927(8)	**C2-Re-N1**	96.5(3)
C1-O1	1.152(7)	**C3-Re-N2**	97.5(3)
C2-O2	1.154(7)	**C1-Re-C3**	87.2(3)
C3-O3	1.144(7)	**C1-Re-C2**	88.8(3)
Re-Br1	2.619(6)	**C1-Re-Br1**	91.6(2)
Re-N1	2.184(6)	**C2-Re-Br1**	179.1(2)
Re-N2	2.179(6)		

The bond distances from Re to the three carbonyl carbons (C1, C2 and C3) are all within the range of similar reported structures, varying from 1.909(9) Å to 1.927(8) Å.[17-26] The rhenium metal to bromido distance is 2.619(6) Å, which is comparable to *fac*-[Re(CO)$_3$(Br)(DiMePy)] and other related structures.[2,3,26] The rhenium to nitrogen bond distances, N1 and N2, are reported as 2.184(6) Å and 2.179(6) Å respectively, which are also similar to *fac*-[Re(CO)$_3$(Br)(DiMePy)],

fac-[Re(CO)$_3$(Act)(DiMePy)][NO$_3$], *fac*-[Re(CO)$_3$(NO$_3$)(DiMePy)] (reported earlier) and other reported structures with *N,N'*-bidentate ligands.[27-32] The small bite angle (N1-Re-N2) of 74.7(2) º confirms that distorted octahedral geometry; angles 100.3(3) º for C1-Re-N1, 97.5(3) º for C3-Re-N2, 96.5(3) º for C2-Re-N1 and 94.1(3) º for C2-Re-N2 also deviates significantly from 90 º. All angles and bonds in *fac*-[Re(CO)$_3$(Br)(DiMeOPy)] were found to be in range with other similar structures.[17,18,19,21] A dihedral angle of 12.988(4) º is calculated between the plane through Re..C1..O1..C3..O3..N1..N2 and N1..C4..C13..N2 and is illustrated in Figure **4-20**. The bidentate ligand also 'bends' away from the axial carbonyl ligand and towards the monodentate ligand (Br^-), but slightly less than what was seen in *fac*-[Re(CO)$_3$(Br)(DiMePy)] which had a dihedral angle of 13.913(1) º.

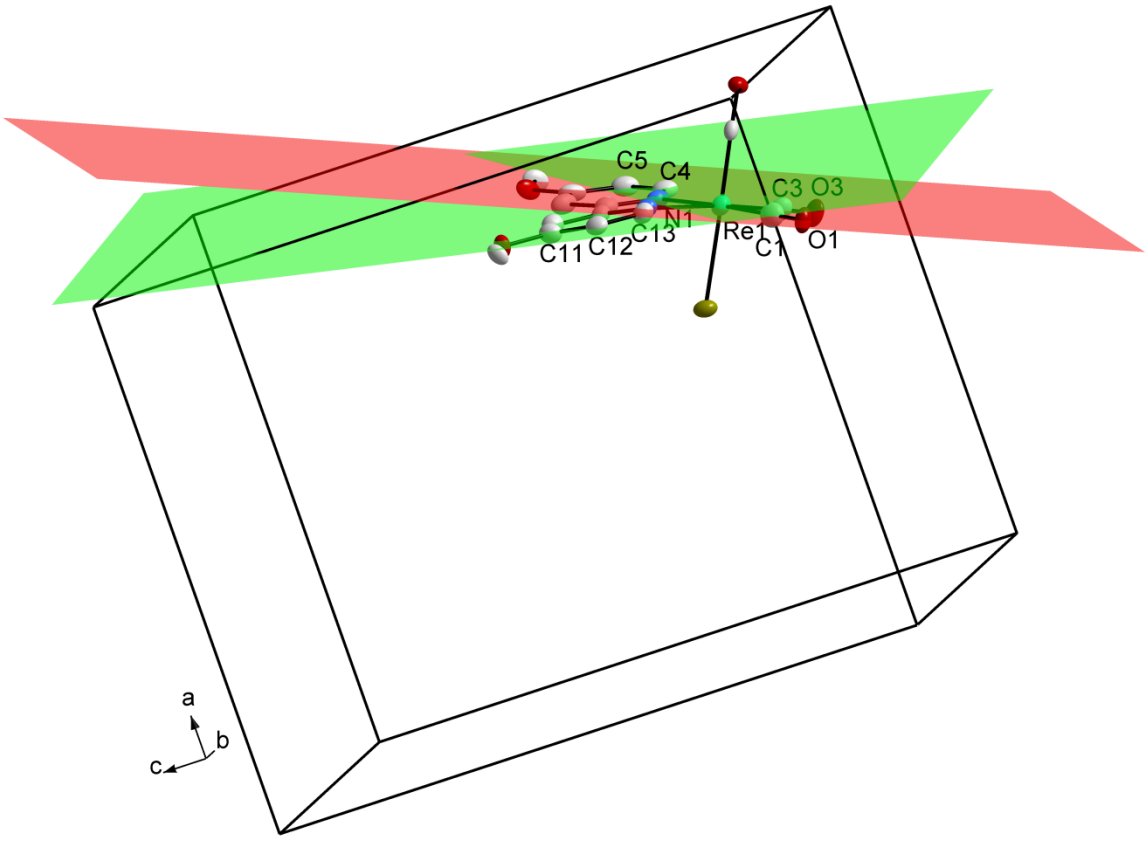

Figure 4-20: Illustration of the dihedral angle of 12.988(4) º between the planes through Re..C1..O1..C3..O3..N1..N2 (red plane) and N1..C4..C13..N2 (green plane). Hydrogen atoms were omitted for clarity.

The crystal structure of *fac*-[Re(CO)$_3$(Br)(DiMeOPy)] is stabilized by three (two C-H…O and one C-H…Br) intermolecular hydrogen bonding interactions. The interaction distances, angles and symmetry operators are presented in Table **4-14**. These

intermolecular hydrogen bonding interactions contributing to the molecular packing of *fac*-[Re(CO)$_3$(Br)(DiMeOPy)] is illustrated in Figure **4-21**.

Table 4-14: Summary of the hydrogen bonding distances (Å) and angles (º) observed in *fac*-[Re(CO)$_3$(Br)(DiMeOPy)].

D-H…A	d(D-H)	d(H…A)	d(D…A)	D-H…A angle
C7-H7…O2[a]	0.93	2.58	3.430(11)	152
C12-H12…Br1[b]	0.93	2.87	3.779(7)	167
C14-H12B…O1[c]	0.96	2.54	3.325(13)	139

Symmetry code, transformations used to generate equivalent atoms: [a] -x, y, ½-z; [b] ½-x, -½+y, z; [c] ½-x, ½-y, -½+z

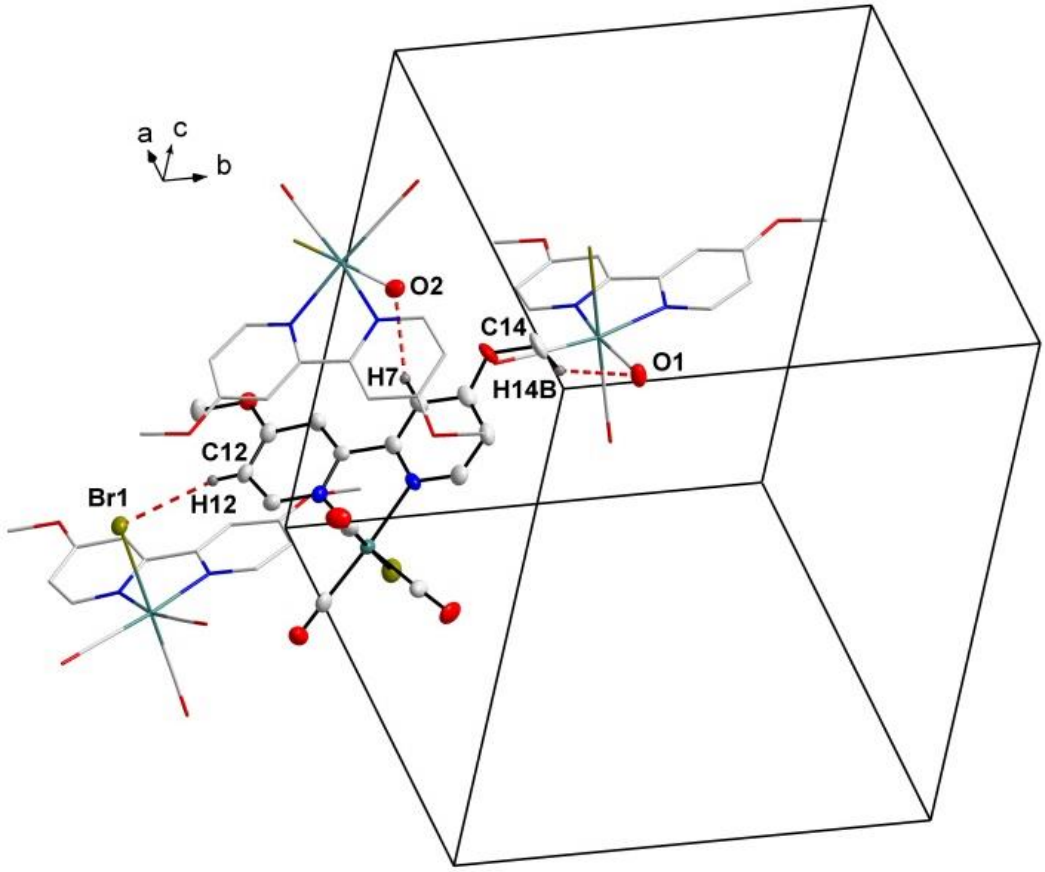

Figure 4-21: Hydrogen bonding interactions observed in the structure of *fac*-[Re(CO)$_3$(Br)(DiMeOPy)]. Hydrogen atoms not taking part in the interactions and atom numbering were omitted for clarity.

fac-[Re(CO)$_3$(Br)(DiMeOPy)] experience lattice stability reinforcement via a Br…π molecular interaction, as summarized in Table **4-15**. The bromide to centroid (Cg1) distance is reported as 2.947(18) Å and is illustrated in Figure **4-22**.

Table 4-15: The intramolecular π-ring interaction observed in the structure of *fac*-[Re(CO)$_3$(Br)(DiMeOPy)] (Å, º).

Y-X(I)	Res(I) → Cg(J)	X…Cg	Y-X…Cg	Y…Cg
Re1-Br1	[1] → Cg1	2.947(18)	38.7	1.871(2)

Symmetry code, transformations used to generate equivalent atoms: [a] x, y, z Cg1 = centroid atoms of Re1-N1-C9-C8-N2.

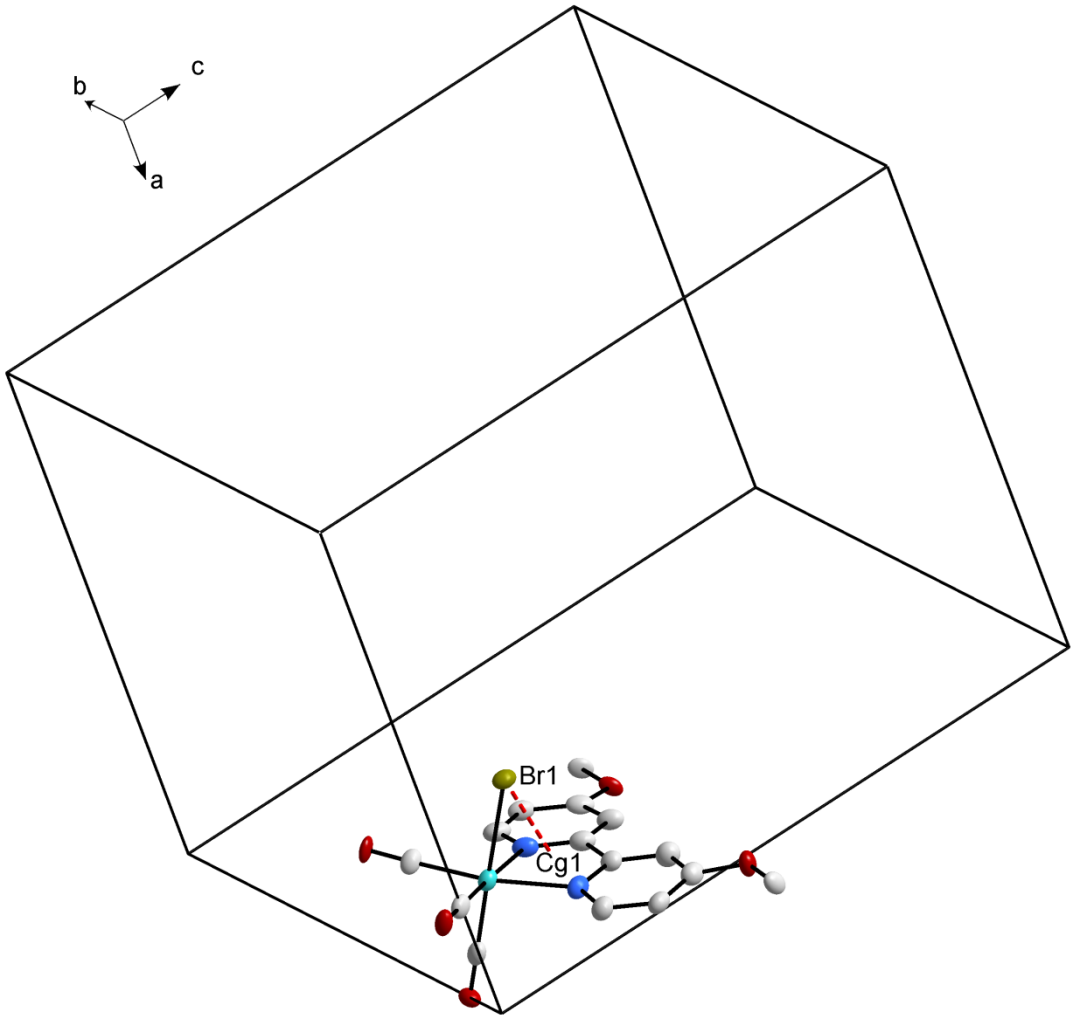

Figure 4-22: Br…π interaction observed in the structure of *fac*-[Re(CO)$_3$(Br)(DiMeOPy)]. Hydrogen atoms and numbering of certain atoms were omitted for clarity.

Infinite 1D-chains are formed with base vector [010]. These supermolecular chains are formed through an O…O interaction linking the molecules together. This interaction clearly contributes to the array of the molecules in the asymmetric unit cell as illustrated in Figure **4-23** which exhibit an interesting packing format.

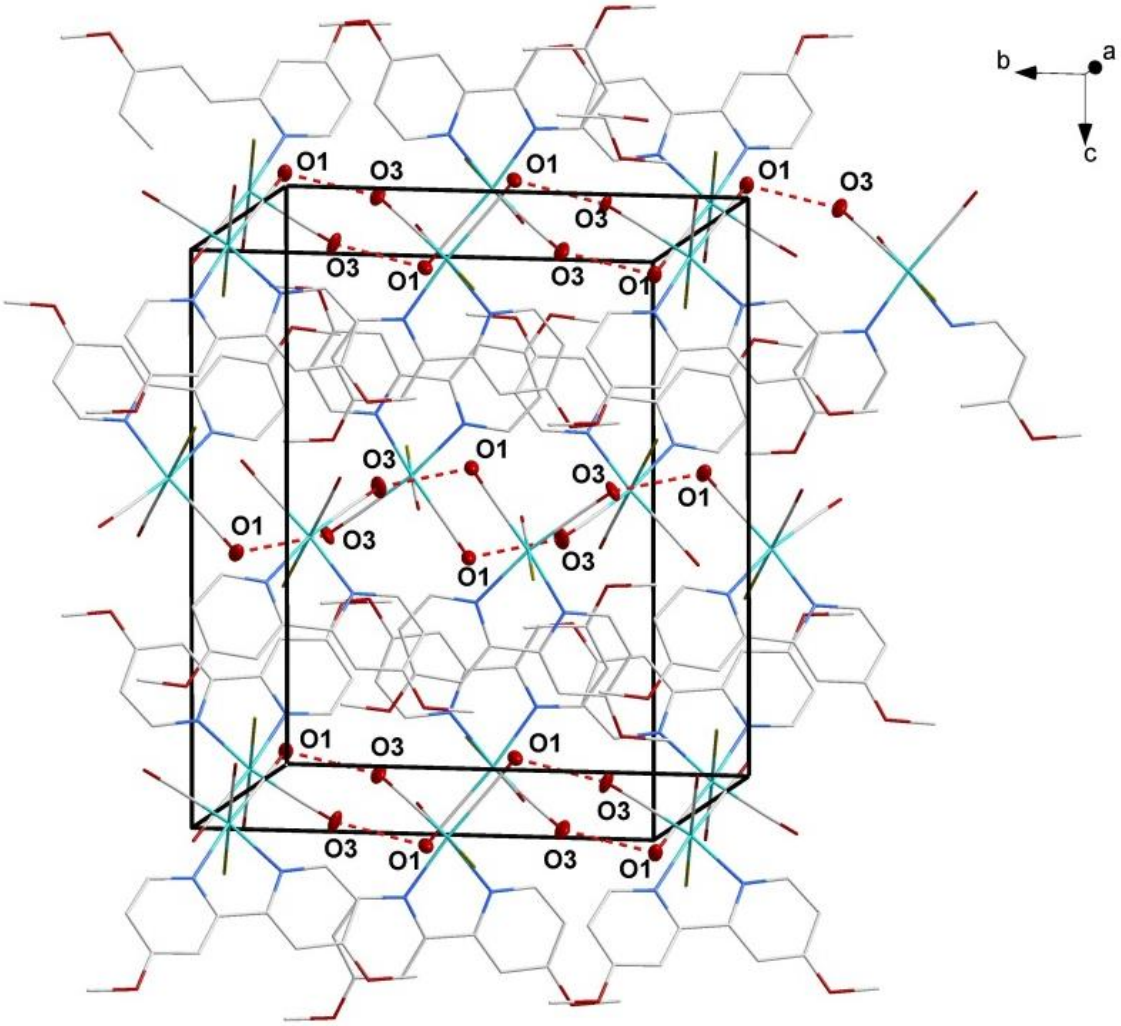

Figure 4-23: The infinite 1D-chains of *fac*-[Re(CO)$_3$(Br)(DiMeOPy)] along [010] in the unit cell.

The molecules pack in a head-to-head fashion in column-like structures, diagonally when viewd along the *ac*-plane (illustrated in Figure **4-24)**.

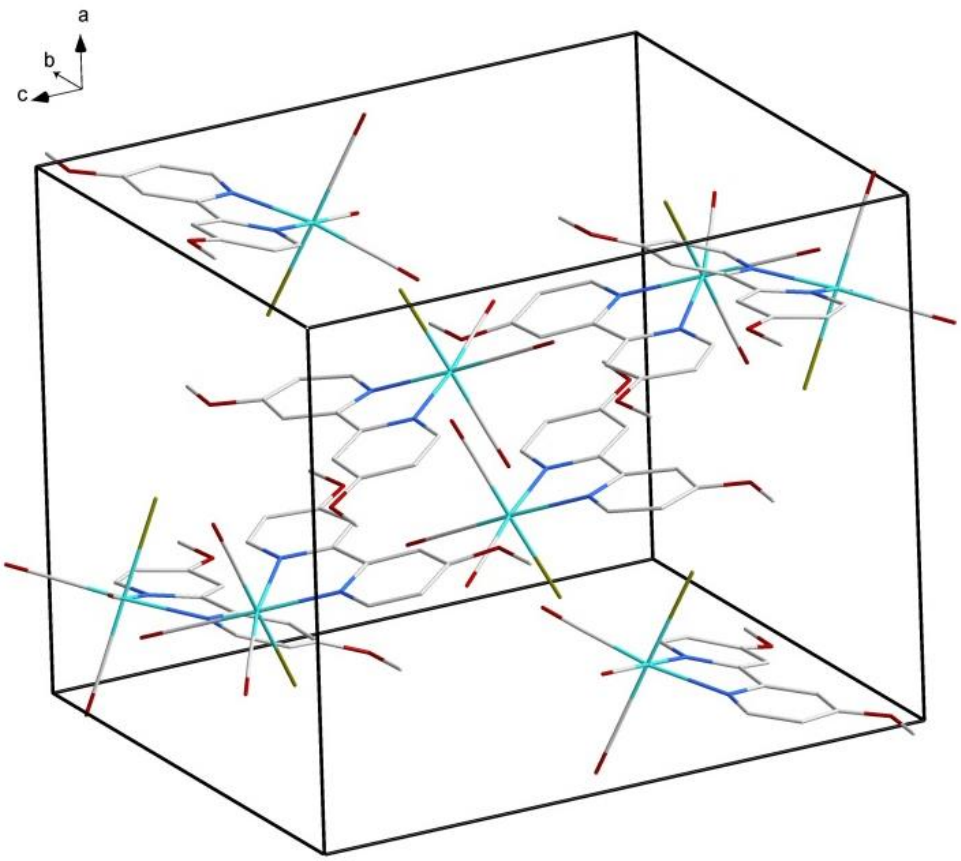

Figure 4-24: Molecular packing of *fac*-[Re(CO)$_3$(Br)(DiMeOPy)] in the unit cell, when viewed along the *ac*-plane. Hydrogen atoms are omitted for clarity.

4.8 Crystal structure of fac-[Re(CO)$_3$(NO$_3$)(DiMeOPy)]

fac-[Re(CO)$_3$(NO$_3$)(DiMeOPy)] was synthesized as described in chapter 3. The yellow crystals were obtained from a methanol solution of the product. The compound crystallized in the monoclinic space group $P2_1/c$ with one neutral *fac*-[Re(CO)$_3$(NO$_3$)(DiMeOPy)] complex in the asymmetric unit (Z = 4). The Re atom has octahedral coordination with three facially orientated carbonyl ligands, one bidentate 4,4'dimethoxy-2,2'-bipyridine ligand and a nitrate ligand. The molecular structure of *fac*-[Re(CO)$_3$(NO$_3$)(DiMeOPy)] is given in Figure **4-25**.

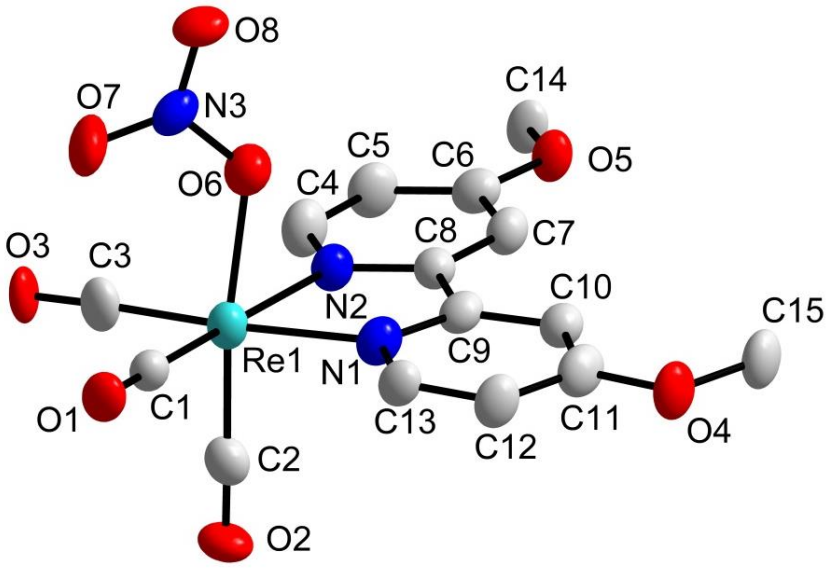

Figure 4-25: Molecular representation of the crystal structure of *fac*-[Re(CO)$_3$(NO$_3$)(DiMeOPy)]. Hydrogen atoms are omitted for clarity. Displacement ellipsoids are drawn at 50 %.

A summary of the general crystal data of *fac*-[Re(CO)$_3$(NO$_3$)(DiMeOPy)] is given in Table **4-2** and the molecular numbering scheme is shown in Figure **4-25**. Some bond distances and angles were selected and are summarized in Table **4-16**.

Table 4-16: Selected bond distances and angles for the structure of *fac*-[Re(CO)$_3$(NO$_3$)(DiMeOPy)].

Selected bond lengths (Å)		Selected bond angles (º)	
Re-C1	1.908(5)	**N2-Re-N1**	74.82(13)
Re-C2	1.898(6)	**C1-Re-N1**	98.05(17)
Re-C3	1.906(6)	**C3-Re-N2**	99.46(17)
C1-O1	1.142(5)	**C1-Re-O6**	95.22(17)
C2-O2	1.145(6)	**C3-Re-O6**	97.34(19)
C3-O3	1.159(6)	**C2-Re-O6**	172.75(16)
Re-O6	2.161(3)		
Re-N1	2.163(4)		
Re-N2	2.165(3)		

The bond distance from Re to the three carbonyl carbons (C1, C2 and C3) are all within normal range and similar to reported structures, varying from 1.898(6) Å to 1.908(5) Å.[17-26] The distance between rhenium and the nitrate oxygen (O6) is 2.161(3) Å, which is comparable to *fac*-[Re(CO)$_3$(NO$_3$)(DiMePy)] and other reported structures ([Re(CO)$_2$(Br)$_2$(NO$_3$)(NO)], [Re(CO)$_3$(NO$_3$)(PB)Au(dppm-H)Au]$_2$, where PB = 2-(2'-pyridyl)benzimidazole, dppm-H = 2,2'-

bis(diphenylphosphinomethane).[27-32,39,40] The rhenium to nitrogen bond distances, N1 and N2 are 2.163(4) Å and 2.165(3) Å respectively, which are similar to *fac*-$[Re(CO)_3(Br)(DiMePy)]$, *fac*-$[Re(CO)_3(Act)(DiMePy)][NO_3]$, *fac*-$[Re(CO)_3(NO_3)(DiMeOPy)]$, *fac*-$[Re(CO)_3(Br)(DiMeOPy)]$ and other reported structures.[27-29] The small bite angle, N1-Re-N2, of 74.82(13) º is within range with *fac*-$[Re(CO)_3(Br)(DiMePy)]$, *fac*-$[Re(CO)_3(Act)(DiMePy)][NO_3]$, *fac*-$[Re(CO)_3(NO_3)(DiMeOPy)]$, *fac*-$[Re(CO)_3(Br)(DiMeOPy)]$ and similar compounds, illustrating the distorted octahedral coordination sphere. The angles 98.05(17) º for C1-Re-N1, 99.46(17) º for C3-Re-N2 and 97.34(3) º for C3-Re-O6 all significantly deviate from 90 º. The 'linear' angle C2-Re-O6 of 172.75(16) º also deviate significantly from 180 º which confirms the distortion of the octahedral geometry. All the angles and bond distance were compared to similar reported structures and were found to be in good agreement.[17,18,19] A dihedral angle of 4.190(16) º is calculated between the plane through Re..C1..O1..C3..O3..N1..N2 and N1..C4..C13..N2 and is illustrated in Figure **4-26**. The bidentate ligand slightly 'bends' away from the axial carbonyl ligand and towards the monodentate ligand (NO_3^-), but not as much as in the case of *fac*-$[Re(CO)_3(Br)(DiMeOPy)]$ where a dihedral angle of 12.988(4) º were calculated between the same two planes.

[39] Schibli, R., Marti, N., Maurer, P., Spingler, B., Lehaire, M.-L., Gramlich, V., Barnes, C.L. *Inorg. Chem*. **44** (2005) 683-690.

[40] Tzeng, B.-C., Chen, B.-S., Chen, C.-K., Chang, Y.-P., Tzeng, W.-C., Lin, T.-Y., Lee, G.-H., Chou, P.-T., Fu, Y.F., Chang, H.-H. *Inorg. Chem*. **50** (2011) 5379-5388.

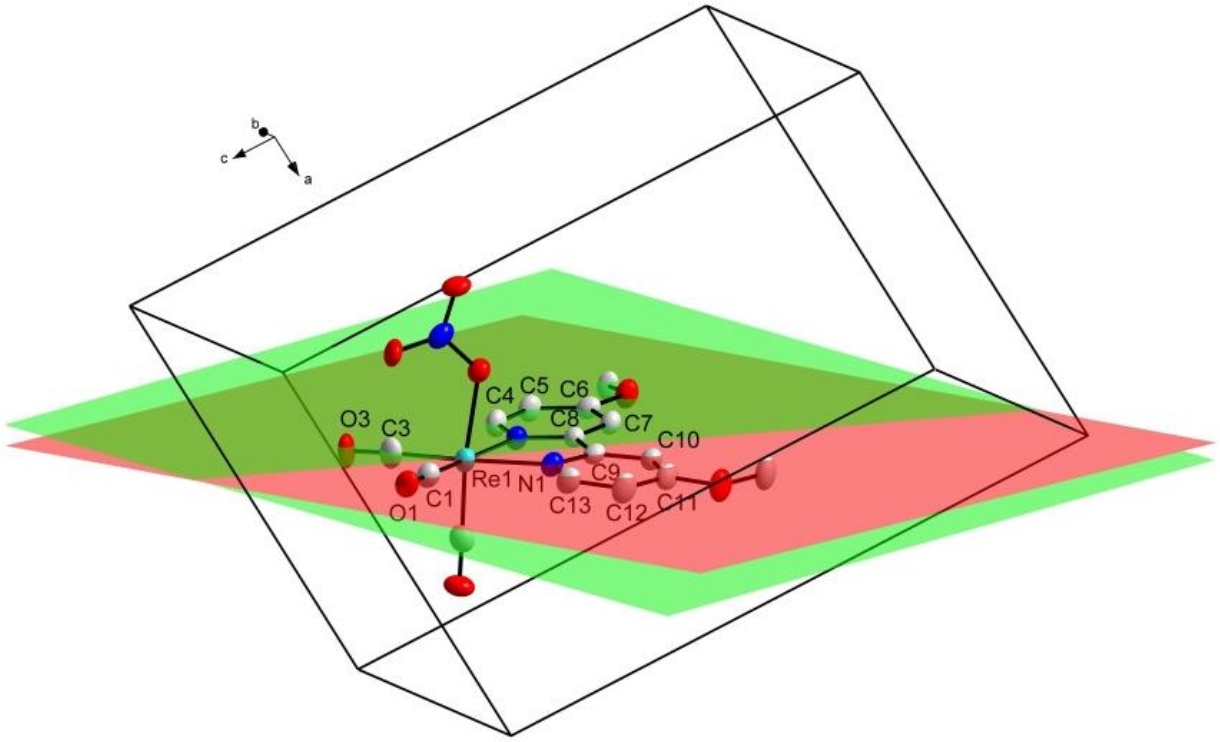

Figure 4-26: Illustration of the dihedral angle of 4.190(16) º between the planes through Re..C1..O1..C3..O3..N1..N2 (red plane) and N1..C4..C13..N2 (green plane). Hydrogen atoms were omitted for clarity.

The crystal structure of *fac*-[Re(CO)$_3$(NO$_3$)(DiMeOPy)] is stabilized by three C-H…O intermolecular hydrogen bonding interactions. The bonding distances, angles and symmetry operators are presented in Table **4-17**. These intermolecular hydrogen bonding interactions, contributing to the molecular packing of *fac*-[Re(CO)$_3$(NO$_3$)(DiMeOPy)], is illustrated in Figure **4-27**.

Table 4-17: Summary of the hydrogen bonding interaction distances (Å) and angles (º) observed in *fac*-[Re(CO)$_3$(NO$_3$)(DiMeOPy)].

D-H…A	d(D-H)	d(H…A)	d(D…A)	D-H…A angle
C7-H7…O6[a]	0.95	2.48	3.337(6)	150
C14-H14B…O3[b]	0.98	2.41	3.386(8)	174
C15-H15A…O1	0.98	2.56	3.412(7)	145

Symmetry code, transformations used to generate equivalent atoms: [a] -x,-y,-z; [b] -½-x, ½+y, ½-z; [c] ½+x,- ½-y,-½+z

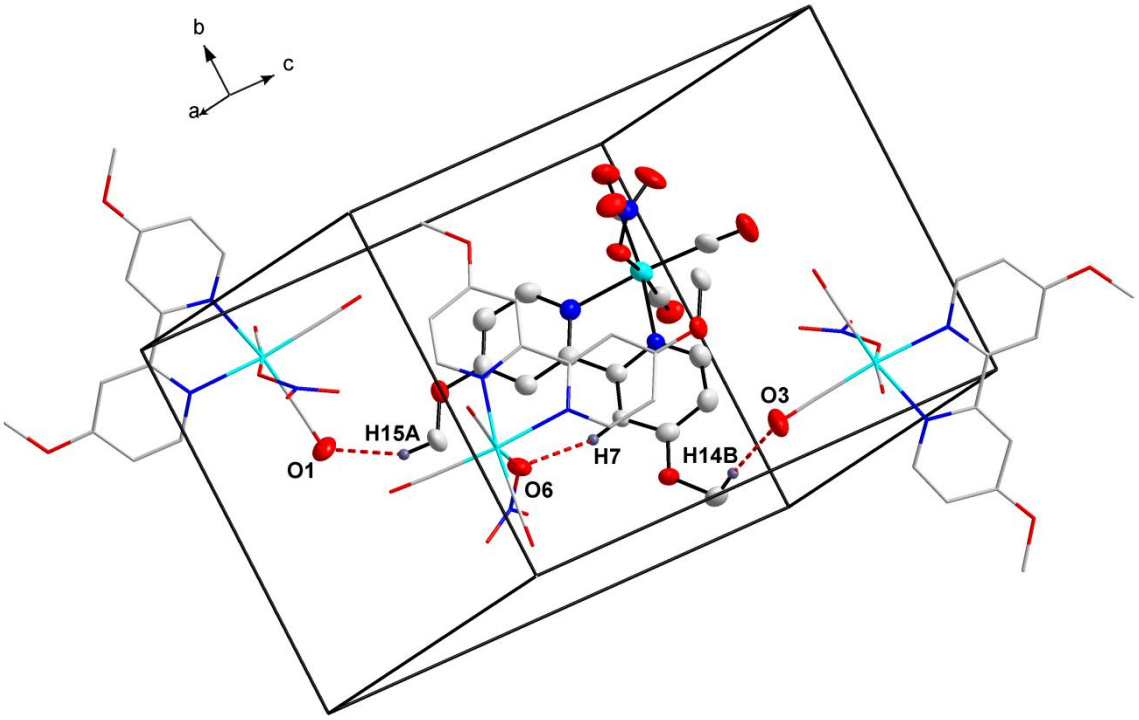

Figure 4-27: Hydrogen bonding interactions observed in the structure of *fac*-[Re(CO)$_3$(NO$_3$)(DiMeOPy)]. Hydrogen atoms not taking part in the interactions and numbering of certain atoms were omitted for clarity.

fac-[Re(CO)$_3$(Br)(DiMeOPy)] further experience lattice stability reinforcement via two O…π molecular interactions, as indicated in Table **4-18**. The oxygen to the centroid Cg1 and Cg2 distances are reported as 3.176(8) Å and 3.383(9) Å respectively and is illustrated in Figure **4-28**.

Table 4-18: The intermolecular O…π interactions observed in the structure of *fac*-[Re(CO)$_3$(NO$_3$)(DiMeOPy)] (Å, º).

Y-X(I)	Res(I) → Cg(J)	X…Cg	Y-X…Cg	Y…Cg
C1-O1 [a]	[1] → Cg1	3.176(8)	134	4.048
C1-O1 [a]	[1] → Cg2	3.383(9)	156	4.448

Symmetry code, transformations used to generate equivalent atoms: [a] ½-x, -½+y, ½-z; Cg1 = centroid atoms of Re1-N1-C9-C8-N2; Cg1 = N1-C9-C10-C11-C12-C13.

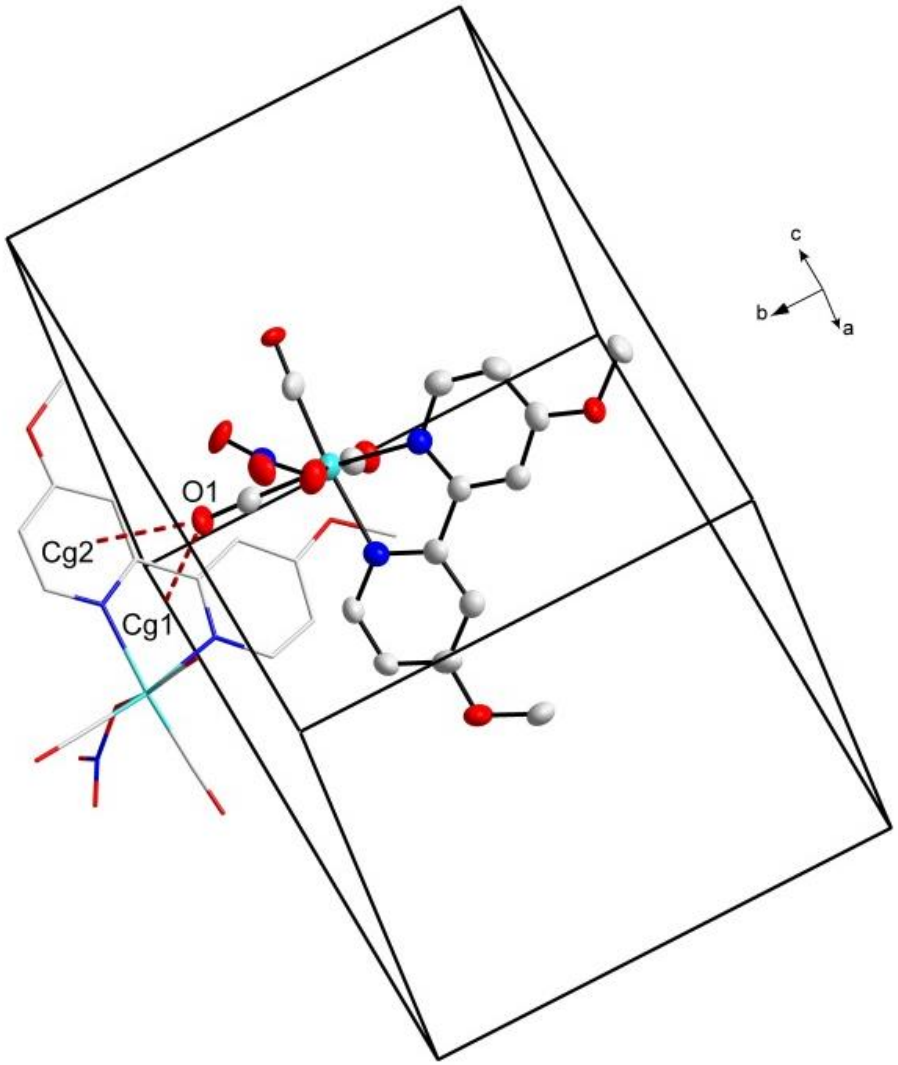

Figure 4-28: O…π interactions observed in the structure of *fac*-[Re(CO)$_3$(NO$_3$)(DiMeOPy)]. Hydrogen atoms and numbering of certain atoms were omitted for clarity.

An infinite 1D-chain is formed with base vector [010] through a O…C interaction linking the molecules together. These interactions clearly contribute to the array of the molecules in the unit cell which exhibit an interesting packing format as illustrated in Figure **4-29**.

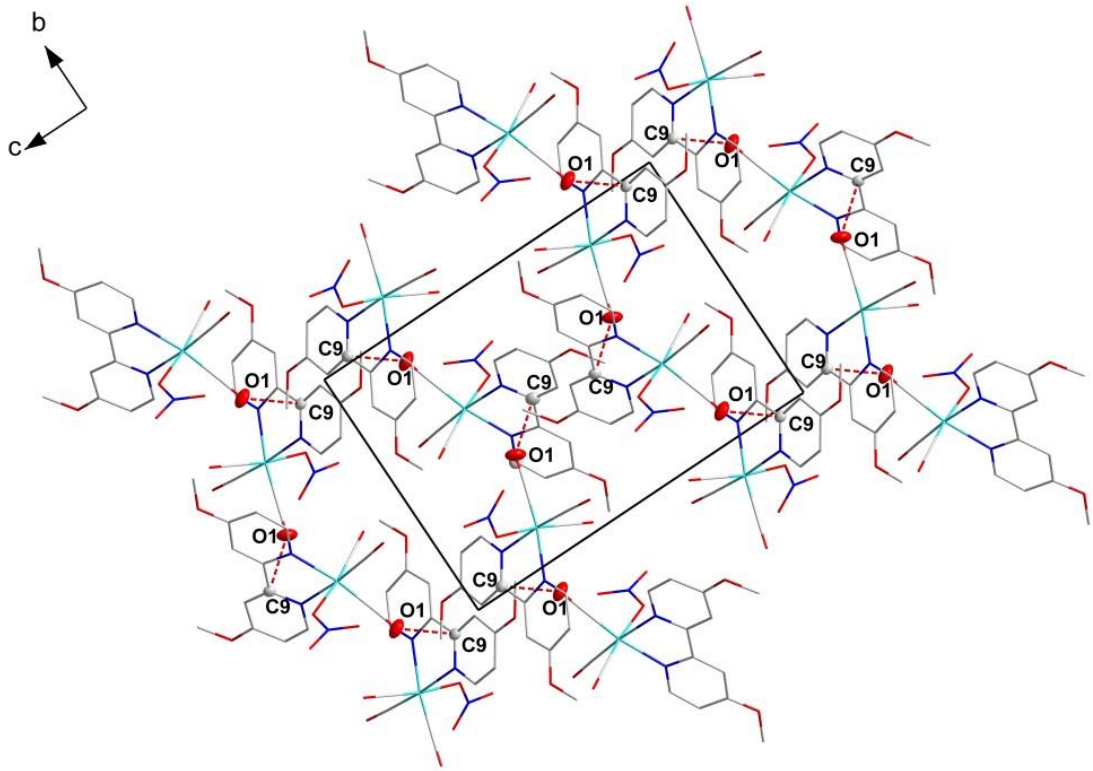

Figure 4-29: The infinite 1D-chain observed in the structure of *fac*-[Re(CO)$_3$(NO$_3$)(DiMeOPy)] with base vector [010].

The molecules pack in a head-to-head fashion in 'column-like' structures diagonally across the *bc*-plane as illustrated in Figure **4-30**.

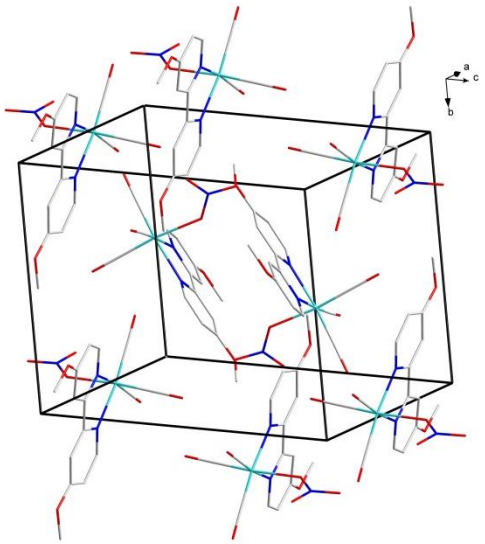

Figure 4-30: Molecular packing of *fac*-[Re(CO)$_3$(NO$_3$)(DiMeOPy)] in the unit cell, viewed along the *bc*-plane. Hydrogen atoms are omitted for clarity.

4.9 Conclusion

In this chapter, one ligand and five rhenium(I) tricarbonyl structures are reported namely 1,3-bis(4-methoxyphenyl)propane-1,3-dione (4-MeTPh) and the rhenium(I) tricarbonyl complexes *fac*-[Re(CO)$_3$(Br)(DiMePy)], *fac*-[Re(CO)$_3$(Act)(DiMePy)][NO$_3$], *fac*-[Re(CO)$_3$(NO$_3$)(DiMePy)], *fac*-[Re(CO)$_3$(Br)(DiMeOPy)] and *fac*-[Re(CO)$_3$(NO$_3$)(DiMeOPy)]. In Table **4-19**, selected bond distances and angles of the five rhenium structures are summarized for comparative reasons. The Re-N1 and Re-N2 distance refer to the rhenium-bidentate ligand distances. The X in the Re-X distance represents the various monodentate ligands in the sixth axial position. The bite angle N1-Re-N2 and the C3-Re-N1 angle are also included in the summary in Table **4-19**.

Table 4-19: Summary of selected bond distances and angles of the five Re(I) tricarbonyl crystal structures reported.

Crystal structures	Re-C1,C2,C3 (Å)	Re-N1 (Å)	Re-N2 (Å)	Re-X (Å)	N1-Re-N2 (˚)	C3-Re-N1 (˚)
***fac*-[Re(CO)$_3$(Br)(DiMePy)]**	1.938(14), 1.923(15), 1.936(15)	2.175(10)	2.187(10)	2.633(17)	75.2(4)	173.1(5)
***fac*-[Re(CO)$_3$(Act)(DiMePy)][NO$_3$]**	1.920(6), 1.899(9), 1.929(6)	2.170(4)	2.170(4)	2.157(4)	74.8(16)	174.6(18)
***fac*- [Re(CO)$_3$(NO$_3$)(DiMePy)]**	1.913(6), 1.889(6), 1.919(6)	2.170(4)	2.170(4)	2.156(4)	74.73(16)	173.4(2)
***fac*-[Re(CO)$_3$(Br)(DiMeOPy)]**	1.926(8), 1.909(9), 1.927(8)	2.184(6)	2.179(6)	2.619(9)	74.7(2)	179.1(2)
***fac*-[Re(CO)$_3$(NO$_3$)(DiMeOPy)]**	1.908(5), 1.898(6), 1.906(6)	2.163(4)	2.165(3)	2.161(3)	74.8(13)	172.7(16)

All the rhenium tricarbonyl distances are within the normal range and vary from 1.889(6) Å to 1.938(14) Å in the 5 Re(I) complexes. The rhenium nitrogen distances (to the bidentate ligands) are all similar and range from 2.163(4) Å to 2.187(10) Å and they compare well to other reported structures.[27-32]

The rhenium bromido distances are by far the longest as expected and are reported as 2.633(17) Å and 2.619(9) Å for *fac*-[Re(CO)$_3$(Br)(DiMePy)] and *fac*-[Re(CO)$_3$(Br)(DiMeOPy)]. The rhenium acetone distance and rhenium nitrate distance is similar at 2.157(4) Å and 2.156(4) Å, 2.161(3) Å.

The bite angles (N1-Re-N2) of the five structures are found to be very similar to each other. The linear angles (C3-Re-N1) were found to range from 172.7(16) º to 179.1(2) º which deviates significantly from the ideal 180 º with *fac*-[$Re(CO)_3(Br)(DiMeOPy)$] being the only structure with C3-Re-N1 bond angle close to linearity (179.1(2) º). All the complexes however indicate a distorted octahedral geometry.

Table **4-20** summarises the dihedral angles (between the plane through Re..C1..O1..C3..O3..N1..N2 and N1..C4..C13..N2) of *fac*-[$Re(CO)_3(Br)(DiMePy)$], *fac*-[$Re(CO)_3(Act)(DiMePy)][NO_3]$, *fac*-[$Re(CO)_3(NO_3)(DiMePy)$], *fac*-[$Re(CO)_3(Br)(DiMeOPy)$] and *fac*-[$Re(CO)_3(NO_3)(DiMeOPy)$]. The following trend of dihedral angles is observed for *fac*-[$Re(CO)_3(X)(DiMePy)]^n$ (X = Br^-, Acetone, NO_3^-; n = +1, 0); *fac*-[$Re(CO)_3(Br)(DiMePy)$] > *fac*-[$Re(CO)_3(NO_3)(DiMePy)$] > *fac*-[$Re(CO)_3(Act)(DiMePy)][NO_3]$. The same observation is seen for *fac*-[$Re(CO)_3(X)(DiMeOPy)]^n$ (X = Br^-, NO_3^-; n = +1, 0); *fac*-[$Re(CO)_3(Br)(DiMeOPy)$] > *fac*-[$Re(CO)_3(NO_3)(DiMeOPy)$].

Table 4-20: Summary of the dihedral angles (between the plane through Re..C1..O1..C3..O3..N1..N2 and N1..C4..C13..N2) of *fac*-$[Re(CO)_3(X)(DiMePy)]^n$ and *fac*-$[Re(CO)_3(X)(DiMeOPy)]^n$ (Å) (X = Br^-, Acetone, NO_3^-; n = +1, 0)

X	*fac*-$[Re(CO)_3(X)(DiMePy)]^n$	*fac*-$[Re(CO)_3(X)(DiMeOPy)]^n$
Br^-	13.916(1)	12.988(4)
Acetone	0.498(9)	-
NO_3	6.264(15)	4.190(16)

fac-[$Re(CO)_3(Br)(DiMePy)$] and *fac*-[$Re(CO)_3(Br)(DiMeOPy)$] were further investigated and the preliminary photoluminescence with different monodentate ligands (MeOH, H_2O, TU, Br^-, NCS^- and PCy_3) were evaluated. In addition the following ligands and rhenium(I) tricarbonyl complexes, namely TIFH, MeTIFH, PhTIFH, *fac*-[$Re(CO)_3(X)(TIF)$], *fac*-[$Re(CO)_3(Br)(MeTIF)$], *fac*-[$Re(CO)_3(H_2O)(MeTIF)$],, *fac*-[$Re(CO)_3(Br)(PhTIF)$], *fac*-[$Re(CO)_3(H_2O)(PhTIF)$], *fac*-[$Re(CO)_3(X)(DiMePy)]^n$, *fac*-[$Re(CO)_3(X)(DiMePy)]^n$ and *fac*-[$Re(CO)_3(X)(MeTPh)]^n$ (where X = Br, MeOH, H_2O, TU, NCS^- PCy_3, PPh_3 and n = +1, 0) were also investigated for their possible photoluminescence potential.

5 Kinetic study of *fac*-[Re(CO)$_3$(MeOH)(*L,L'*-Bid)]^n type complexes

5.1 Introduction

Chemical kinetics, also known as reaction kinetics is the determination of the rates of chemical processes, the effect of different variables and the mechanism of chemical reactions. The substitution kinetics of *fac*-[Re(CO)$_3$(H$_2$O)$_3$]$^+$ has been reported before.[1,2,3] Salignac *et al*. reported the water exchange process of *fac*-[Re(CO)$_3$(H$_2$O)$_3$]$^+$ by utilising ^{17}O NMR. [1] The acid dependency of the rate constant k_{obs} was investigated and it was found that k_{ex}^{298} = (6.3 ± 0.1) x 10^{-3} s^{-1} and k_{OH}^{298} = 2.7 ± 1 s^{-1}, for the water exchange rate constants of *fac*-[Re(CO)$_3$(H$_2$O)$_3$]$^+$ and the monohydroxo species (*fac*-[Re(CO)$_3$(OH)(H$_2$O)$_2$]) respectively. The kinetic contribution of *fac*-[Re(CO)$_3$(OH)(H$_2$O)$_2$] was significant only at [H$^+$] < 3 x 10^{-3} M; at higher [H$^+$] concentrations, the kinetic investigation is unambiguously conducted on *fac*-[Re(CO)$_3$(H$_2$O)$_3$]$^+$. The activation parameters $\Delta S^{\ddagger}$ and $\Delta H^{\ddagger}$ were determined as +14 ± 10 JK^{-1}mol^{-1} and 90 ± 3 kJmol^{-1} which gives an indication of a dissociative activation mode for the water exchange process.

The water substitution reaction of *fac*-[Re(CO)$_3$(H$_2$O)$_3$]$^+$ was followed by ^{1}H/^{13}C/^{19}F/^{17}O NMR with different ligands (Br$^-$, TFA = trifluoroacetate, CH$_3$N, phen = 1,10-phenanthroline, bipy = 2,2'-bipyridyl, DMS = dimethylsulfide, TU = thiourea) in order to support this assumption.[1] The calculated interchange rate constant for each ligand K_i (1.3 x 10^{-3} s^{-1} (phen) < 1.5 x 10^{-3} s^{-1} (bipy) < 2.9 x 10^{-3} s^{-1}

[1] Salignac, B., Grundler, P.V., Cayemittes, S., Frey, U., Scopelliti, R., Merbach, A.E. *Inorg. Chem*. **42** (2003) 3516-3526.
[2] Grundler, P.V., Salignac, B., Cayemittes, S., Alberto, R., Merbach, A.E. *Inorg. Chem*. **43** (2004) 865-873.
[3] Grundler, P.V., Helm, L., Alberto, R., Merbach, A.E. *Inorg. Chem*. **45**(25) (2006) 10378-10390.

(TFA) < 5.8 x 10^{-3} s^{-1} (Br^-) < 12.7 x 10^{-3} s^{-1} (CH_3CN) < 25.3 x 10^{-3} s^{-1} (DMS) < 41.5 x 10^{-3} s^{-1} (TU)) was in the same order as the water exchange rate constant k_{ex} with the S donor ligands being slightly more reactive. The results obtained are indicative of an I_d mechanism for water exchange and complex formation, since a larger variation of interchange rate constants were expected for an associatively activated mechanism.

Grundler *et al*.[2] studied the reaction between *fac*-$[Re(CO)_3(H_2O)_3]^+$ and different donor ligands (N, O and S) by ^1H NMR. The rate and equilibrium constants were in accord with previous results.[1] The calculated interchange rate constant k_i increases from the hard O and N donors to the softer S donors as illustrated in the following series: TFA (trifluoroacetate) < Br^- < CH_3CN < Pyz (pyrazine) < THT (tetrahydrothiophene) < DMS (dimethylsulfide) < TU (thiourea). However, the interchange rate constant values, k_i, remained close to that of the water exchange reaction of *fac*-$[Re(CO)_3(H_2O)_3]^+$ (k_{ex} = 6.3 x 10^{-3} s^{-1}). An I_d mechanism was assigned and the possibility of a slight deviation towards an associatively activated mechanism with the S donor ligands was suggested. The determination of activation volumes by high-pressure NMR revealed the ambivalent character of *fac*-$[Re(CO)_3(H_2O)_3]^+$ towards water substitution with a gradual change over of the reaction mechanism from a dissociative activated (I_d) for the hard O and N donor ligands, to an associatively activated mechanism (I_a) for the softer S donor ligands.[2]

In 2006, Grundler *et al*.[3] reported the water substitution kinetics of *fac*-$[M(CO)_3(H_2O)_3]^+$ (M = Mn, Re, Tc) by ^1H NMR using acetonitrile (CH_3N) and dimethylsulfide (DMS) as the entering ligands. It was found that the water substitution and complex formation with hard and soft donor ligands of *fac*-$[M(CO)_3(H_2O)_3]^+$ (M = Mn, Re, Tc) had a small dependence on the nature of the entering ligand, but were strongly dependent on the metal centre. The results proved that the manganese metal centre is more reactive than the technetium metal centre which in turn is faster than the rhenium metal centre.

Kemp *et al*.[4] reported the aqua substitution kinetics of Re(I) tricarbonyl complexes of the type *fac*-$[Re(CO)_3(H_2O)(N,N'\text{-Bid})]^+$ and *fac*-$[Re(CO)_3(H_2O)(N,O'\text{-Bid})]$ (where *N,N"*-Bid and *N,O*-Bid are bidentate ligands) using different monodentate ligands.

[4] Kemp, G. PhD Thesis. University of Johannesburg. South Africa. 2006.

This study was expanded by Schutte *et al*.[5] by introducing Re(I) tricarbonyl complexes of the type *fac*-[Re(CO)$_3$(MeOH)(*N,N"*-Bid)]^n, *fac*-[Re(CO)$_3$(MeOH)(*N,O*'-Bid)]^n and *fac*-[Re(CO)$_3$(MeOH)(*O,O"*-Bid)]^n (n = +1, 0) and using a range of different monodentate ligands. The coordination compounds were in many cases isolated as the aqua complexes; these were all converted to the corresponding methanol complexes upon dissolution in methanol for the kinetic experiments. It was observed that the rhenium tricarbonyl complexes coordinated to the *O,O'*-bidentate ligands reacted faster than the complexes with the *N,O*- and *N,N'*-bidentate ligands. Overall, the following reactivity trend was observed: *N,N'* < *N,O* < *O,O'*. The substitution reaction of these complexes was suggested to occur *via* an interchange mechanism, ranging from I_a for the cationic *N,N'*-Bid complexes to I_d for the *N,O*- and *O,O'*-Bid complexes.

In this study, the methanol substitution kinetics of *fac*-[Re(CO)$_3$(MeOH)(*L,L'*-Bid)]^n type complexes (where *L,L'*-Bid = *N,N'*- and *O,O'*-bidentate ligands, n = +1, 0) was investigated, with the use of different monodentate ligands (thiourea (TU), thiocyanate (NCS^-), triphenylphosphine (PPh_3) or tricyclohexylphosphine (PCy_3) and bromide (Br^-)) as entering ligand in the sixth position as illustrated in Scheme **5-1**.

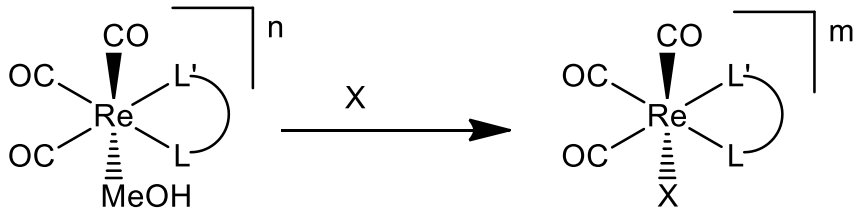

X = TU, NCS^-, PCy_3 or PPh_3, Br^-

L,L'-Bid = *N,N'*- and *O,O'*-bidentate ligands

n = +1, 0

m = +1, 0, -1

Scheme 5-1: Simplified schematic representation of the methanol substitution reactions of *fac*-[Re(CO)$_3$(MeOH)(*L,L'*-Bid)]^n.

[5] Schutte, M., Kemp, G., Visser, H.G., Roodt, A. *Inorg. Chem*. **50** (2011) 12486-12498.

5.2 Experimental procedures

5.2.1 General procedure

All the chemicals and reagents used in the procedures were of analytical grade. Kinetic reaction measurements were carried out on a Varian Cary 50 Conc UV/Visible spectrophotometer. A circulating water bath was used to maintain the temperature and the temperature was kept within ± 0.1 ˚C. The programs used to analyse the data were Microsoft Office Excel 2003[6] and Scientist Micromath, Version 2.01.[7] The individual data points represent the actual experimental data and the solid lines represent the least squares fit of the data. *Pseudo* first-order conditions were used for all kinetic measurements with the ligand in excess in each case. All the *fac*-$[Re(CO)_3(MeOH)(L,L'\text{-Bid})]^n$ complexes were found to be stable in methanol after 24 hours.

5.2.2 Treatment of data

Integrating and incorporating the Beer-Lambert law equation (Equation **1**), results in Equation **2** which is used for evaluating the absorbance change *vs* time in *pseudo* first-order reactions, where A = absorbance, ε = molar absorptivity, c = solution concentration, l = length of path travelled by the light, A_0 = initial absorbance, A_∞= final absorbance, A_t = total absorbance and k_{obs} = observed rate constant.

$$A = \varepsilon c l \qquad \text{Equation } \mathbf{1}$$

$$A_t = A_\infty - (A_\infty - A_0)^{k_{obs}t} \qquad \text{Equation } \mathbf{2}$$

The least-squares fit of absorbance *vs* time for the first-order reaction is used to obtain the *pseudo* first-order rate constant, k_{obs}. Equation **2** was used to fit all the kinetic reaction measurements performed in the study. The rate constants were calculated and are reported in Appendix G. The Eyring equation (Equation **3**) as well

[6] Microsoft Office Professional Edition 2003 Copyright © 1985 – 2003 Microsoft Corporation.
[7] MicroMath Scientist for Windows, Version 2.01, Copyright © 1986 – 1995, MicroMath, Inc.

as a global fit (Equation **4**) were used to determine the activation parameters; standard entropy change of activation ($\Delta S^{\ddagger}$) and standard enthalpy change of activation ($\Delta H^{\ddagger}$).

$$\mathrm{In}\frac{k}{\mathrm{T}} = \mathrm{In}\left(\frac{\mathrm{K_B}}{\mathrm{h}}\right) - \frac{\Delta \mathrm{H}^*}{\mathrm{RT}} + \frac{\Delta \mathrm{S}^*}{\mathrm{R}} \qquad \text{Equation } \mathbf{3}$$

Plotting $\mathrm{In}\left(\frac{k}{T}\right)$ *vs* $\frac{1}{T}$ results in a straight line with a slope of $(-\frac{\Delta \mathrm{H}^*}{\mathrm{T}})$ and an intercept of $(\mathrm{In}\left(\frac{\mathrm{K_B}}{\mathrm{h}}\right) + \frac{\Delta S^*}{\mathrm{R}})$, where K_B is Boltzmann constant and h is Planck's constant. Equation **4** below represents the global fit equation.

$$(k_{1\,\mathrm{obs}}) = k_1[\mathrm{X}] + k_{11} \qquad \text{Equation } \mathbf{4}$$

Where $k_1 = \left(\left(\frac{\mathrm{K_B}}{\mathrm{h}}\right)\mathrm{X}\,(\mathrm{T}+273.15)\mathrm{X}\,\mathrm{e}^{\left(\frac{\mathrm{S_1}}{\mathrm{R}}\right)}\right)\mathrm{X}\,(\mathrm{e}^{(\frac{(\mathrm{H_1\ X\ 1000})}{\mathrm{R\ X\ (273.15+T)}})})$ and

$k_{11} = \left(\left(\frac{\mathrm{K_B}}{\mathrm{h}}\right)\mathrm{X}\,(\mathrm{T}+273.15)\mathrm{X}\,\mathrm{e}^{\left(\frac{\mathrm{S_2}}{\mathrm{R}}\right)}\right)\mathrm{X}\,(\mathrm{e}^{(\frac{(\mathrm{H_2\ X\ 1000})}{\mathrm{R\ X\ (273.15+T)}})})$.

The equilibrium constants for all the reactions were calculated kinetically (Equation **5**) as well as thermodynamically (Equation **6**). The thermodynamically calculated K_1 for all the reaction are tabulated, but is illustrated for only one reaction per complex in the following Paragraphs.

$$K_1 = \frac{k_1}{k_{-1}} \qquad \text{Equation } \mathbf{5}$$

$$\mathrm{A_{obs}} = \frac{\mathrm{A_M} + \mathrm{A_{ML}}K_1[\mathrm{X}]}{1 + K_1[\mathrm{X}]} \qquad \text{Equation } \mathbf{6}$$

A_M and A_{ML} are the observed absorbance of *fac*-$[Re(CO)_3(MeOH)(L,L'\text{-Bid})]^n$ and *fac*-$[Re(CO)_3(X)(L,L'\text{-Bid})]^m$ (X = monodentate entering ligand, n = +1, 0; m = +1, 0, -1), A_{obs} is the observed absorbance and [X] is the concentration of the entering monodentate ligand.

5.3 Results and discussion

The methanol substitution reaction of *fac*-$[Re(CO)_3(MeOH)(DiMePy)]^+$, *fac*-$[Re(CO)_3(MeOH)(DiMeOPy)]^+$, *fac*-$[Re(CO)_3(MeOH)(4\text{-MeTPh})]$, *fac*-$[Re(CO)_3(MeOH)(BrDiPhPr)]$, *fac*-$[Re(CO)_3(MeOH)(TIF)]$ and

fac-[Re(CO)$_3$(MeOH)(MeTIF)] (where DiMePy = 4,4'-dimethyl-2,2'-bipyridine, DiMeOPy = 4,4'-dimethoxy-2,2'-bipyridine, 4-MeTPh = 1,3-bis(4-methoxyphenyl)propane-1,3-dione), BrDiPhPr = 2-bromo-1,3-diphenylpropane-1,3-dione, TIFH = 2,2,2-trifluoro-1-(3-hydroxy-1H-inden-2-yl)ethan-1-one, MeTIFH = 2,2,2-trifluoro-1-(3-hydroxy-1-methyl-1H-inden-2-yl)ethan-1-one), illustrated in Scheme **5-2**, was conducted where the coordinated MeOH was substituted by the following monodentate ligands: thiourea (TU), thiocyanate (NCS^-), triphenylphosphine (PPh_3) or tricyclohexylphosphine (PCy_3) and bromide (Br^-).

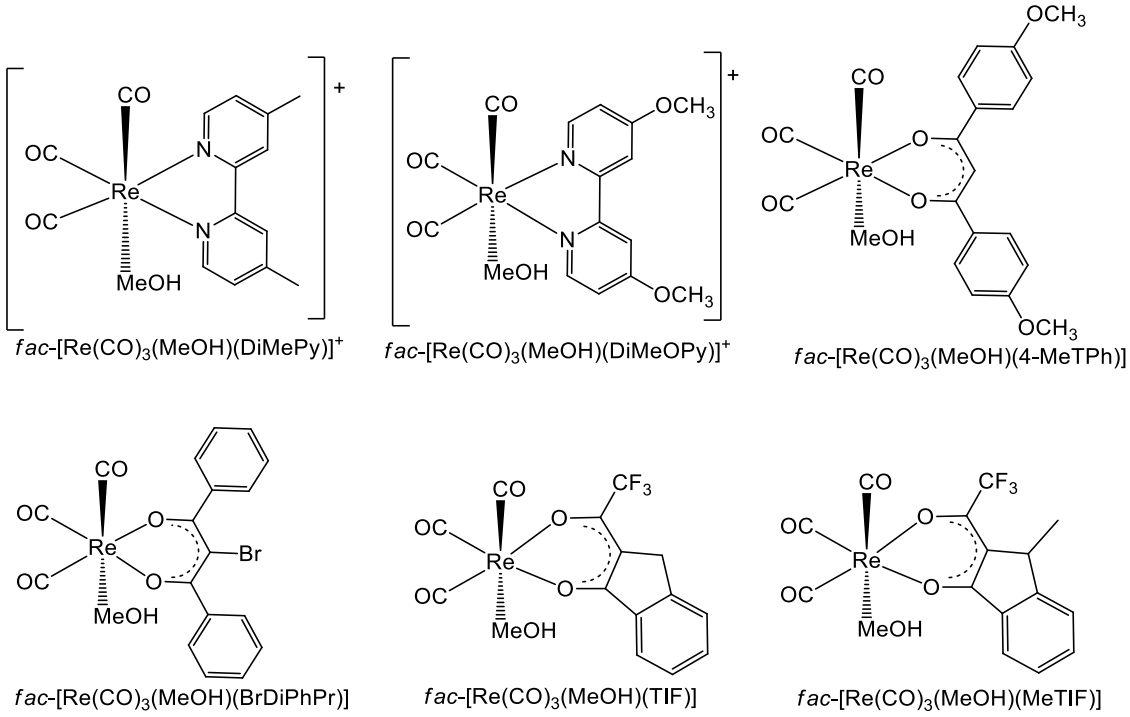

fac-[Re(CO)$_3$(MeOH)(DiMePy)]$^+$ *fac*-[Re(CO)$_3$(MeOH)(DiMeOPy)]$^+$ *fac*-[Re(CO)$_3$(MeOH)(4-MeTPh)]

fac-[Re(CO)$_3$(MeOH)(BrDiPhPr)] *fac*-[Re(CO)$_3$(MeOH)(TIF)] *fac*-[Re(CO)$_3$(MeOH)(MeTIF)]

Scheme 5-2: Rhenium(I) tricarbonyl complexes investigated in this kinetic study.

All the reactions were studied at different temperatures (15 ˚C, 25 ˚C, 35 ˚C and 45 ˚C). Since the complexes were not soluble in water, all the kinetic studies were carried out in methanol as a suitable solvent. This was an unfortunate discovery since we anticipated that at least the TIF and/or MeTIF complexes would be water soluble to be able to evaluate the *p*K$_a$ values and behaviour in water at ~ pH7 (human blood pH).[8,9]

It was preliminary assumed that the bromido complexes form the corresponding methanol substituted complexes over a certain period of time when it is dissolved in

8 Li, J., Li, H., Yan, P., Chen, P., Hou, G., Li, G. *Inorg. Chem*. **51** (2012) 5050-5057.
9 Li, W., Yan, P., Hou, G., Li, H., Li, W. *Dalton Trans*. **42** (2013) 11537-11548.

methanol.[5,10,11] This assumption was confirmed and verified by infrared spectroscopy and UV/Vis studies. The methanol complexes were stable after 24 hours and the end products were characterized as described in Chapter 3.

The kinetic reactions were performed under *pseudo* first-order conditions with [X] >> *fac*-[Re(CO)$_3$(MeOH)(*L,L'*-Bid)]^n. It was expected that the Br$^-$ counter ion in *fac*-[Re(CO)$_3$(MeOH)(DiMePy)][Br] and *fac*-[Re(CO)$_3$(MeOH)(DiMeOPy)][Br] would not have an influence (or compete) in the methanol substitution reaction because [X] >> *fac*-[Re(CO)$_3$(MeOH)(*L,L'*-Bid)]^n. But to exclude the possible effect of the Br$^-$ ions on the reaction, one equivalent of $AgNO_3$ was added to the metal complex solution and the AgBr was filtered off. Therefore the possibility of any 'competition' with regards to the entering ligand was excluded. Based on the results, the following general mechanism is predicted (Scheme **5-3**):

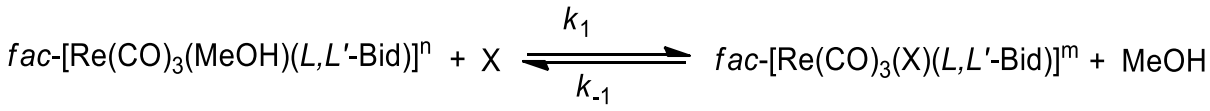

L,L'-Bid = *N,N*'- or *O,O*'- donor bidentate ligand
X = TU, NCS$^-$, PCy_3 or PPh_3, Br$^-$
n = +1, 0
m = +1, 0, -1

Scheme 5-3: The expected reaction mechanism for the methanol substitution reactions of *fac*-[Re(CO)$_3$(MeOH)(*L,L'*-Bid)]^n.

Rate = k_1[*fac*-[Re(CO)$_3$(X)(*L,L'*-Bid)]][X] – k_{-1}[*fac*-[Re(CO)$_3$(X)(*L,L'*-Bid)]] Equation **7**

In Scheme **5-3**, k_1 represents the forward rate constant and k_{-1} represents the reverse rate constant. *fac*-[Re(CO)$_3$(MeOH)(*L,L'*-Bid)]^n is the starting complex, *fac*-[Re(CO)$_3$(X)(*L,L'*-Bid)]^m is the substituted product and X is the entering monodentate ligand. When *pseudo* first-order conditions are used [X] >> *[fac*-[Re(CO)$_3$(MeOH)(*L,L'*-Bid)]], Equation **7** is reduced to:

$k_{obs} = k_1[X] + k_{-1}$ Equation **8**

10 Brink, A., Visser, H.G., Roodt, A. *Inorg. Chem*. **52** (2013) 8950-8961.
11 Brink, A., Visser, H.G., Roodt, A. *Inorg. Chem*. **53** (2014) 12480-12488.

In Equation **8,** k_{obs} represents the observed rate constant. This equation holds for the equilibrium reactions and the equilibrium constant is determined from Equation **5** and **6** as discussed in Paragraph 5.2.2.

The kinetic study of each rhenium complex will be described in detail with the respective entering ligands.

5.3.1 Reaction between *fac*-[Re(CO)$_3$(MeOH)(DiMePy)]$^+$ and entering ligands

The synthesis of *fac*-[Re(CO)$_3$(MeOH)(DiMePy)]$^+$ from the starting synthon [NEt$_4$]$_2$[Re(CO)$_3$(Br)$_3$] has been described in Chapter 3. *fac*-[Re(CO)$_3$(Br)(DiMePy)] was dissolved in methanol and stirred for 24 hours to yield *fac*-[Re(CO)$_3$(MeOH)(DiMePy)]$^+$. The reaction between *fac*-[Re(CO)$_3$(MeOH)(DiMePy)]$^+$ and four different monodentate ligands (thiourea (TU), thiocyanate (NCS$^-$), tricyclohexylphosphine (PCy$_3$) and bromide (Br$^-$)) were monitored with UV/Vis in methanol.

5.3.1.1 fac-[Re(CO)$_3$(MeOH)(DiMePy)]$^+$ + TU

The methanol substitution reaction between *fac*-[Re(CO)$_3$(MeOH)(DiMePy)]$^+$ and thiourea (TU) was performed at 355 nm in methanol and at four different temperatures ranging between 15.1 °C and 44.8 °C, with [TU] varying from 0.05 M to 0.5 M. The rate constant values obtained from these fits are presented in Table **5-1**. The final UV/Vis spectrum of the reaction solution is identical to the one obtained from the synthesized *fac*-[Re(CO)$_3$(TU)(DiMePy)]$^+$ complex in Chapter 3.

The graph of k_{obs} *vs* [TU] at different temperatures is presented in Figure **5-1** below and the Eyring plot is illustrated in Figure **5-2**.

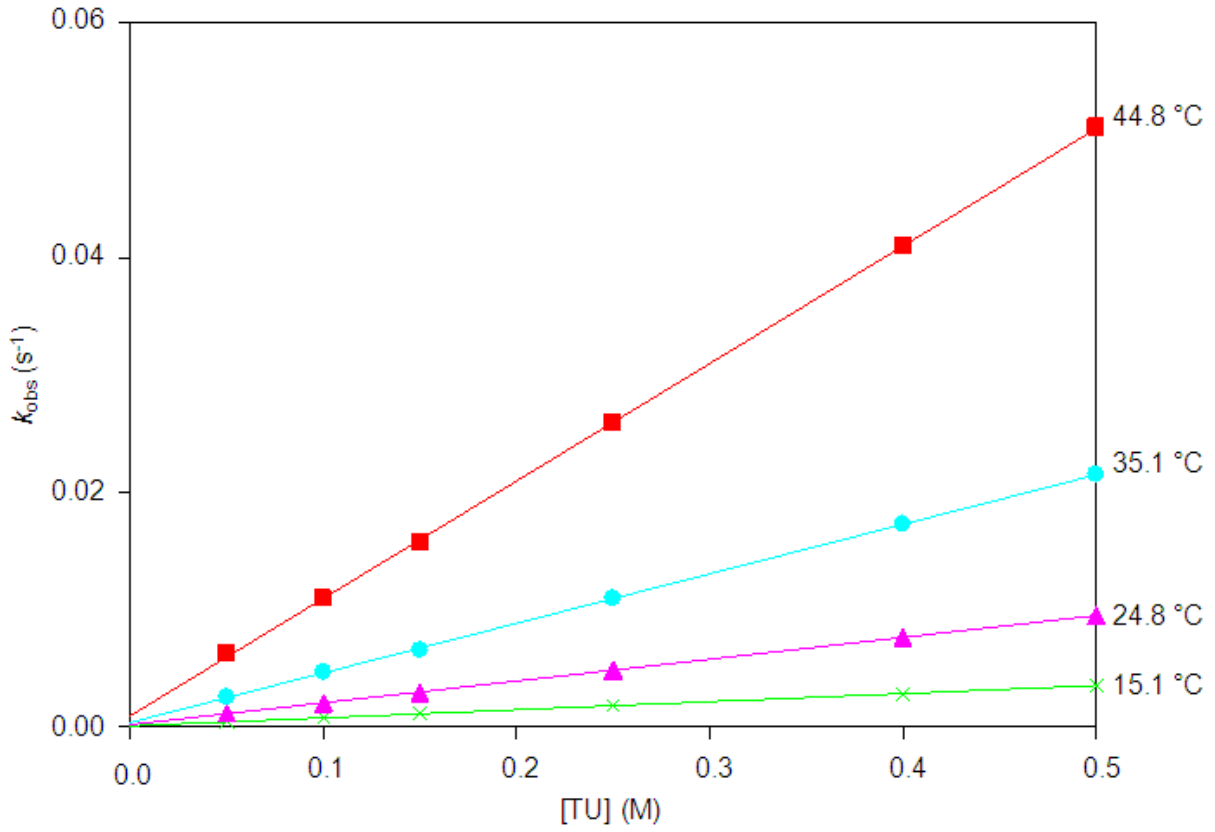

Figure 5-1: Plot of k_{obs} *vs* [TU] for the reaction between *fac*-[Re(CO)$_3$(MeOH)(DiMePy)]$^+$ and thiourea at four different temperatures in methanol, with [TU] = 0.05 M to 0.5 M. [Re] = 1 x 10^{-4} M, λ = 355 nm.

The activation parameters have been calculated from the Eyring plot (Equation **3**) as well as the global fit of temperature *vs* ligand concentration *vs* k_{obs} data (Equation **4**) and it is clear that the traditional Eyring plot yields similar results to the global fit. $\Delta H^{\ddagger}$ = 65 ± 1 kJmol^{-1} and $\Delta S^{\ddagger}$ = -59 ± 5 JK^{-1}mol^{-1} from the Eyring plot and $\Delta H^{\ddagger}$ = 77.5 ± 0.8 kJmol^{-1} and $\Delta S^{\ddagger}$ = -14 ± 2 JK^{-1} mol^{-1} from the global fit.

Table 5-1: Summary of the rate constants for the reaction between *fac*-[Re(CO)$_3$(MeOH)(DiMePy)]$^+$ and thiourea at different temperatures, with [TU] = 0.05 M to 0.5 M. [Re] = 1 x 10^{-4} M, λ = 355 nm.

	15.1 °C	**24.8 °C**	**35.1 °C**	**44.8 °C**
$10^3 k_1$ ($M^{-1}s^{-1}$)	6.89 ± 0.03	18.6 ± 0.1	42.3 ± 0.4	100.2 ± 0.5
$10^3 k_{-1}$ (s^{-1})	0.067 ± 0.007	0.19 ± 0.04	0.36 ± 0.08	0.9 ± 0.1
K_1 (M^{-1})[a]	103 ± 11	98 ± 20	118 ± 26	111 ± 12
K_1 (M^{-1})[b]	115 ± 9	100 ± 6	99 ± 12	99 ± 7

[a] $K_1 = k_1/k_{-1}$; [b] $A_{obs} = \frac{A_M + A_{ML}K_1[X]}{1 + K_1[X]}$

The plot of ln(k_1/T) *vs* 1/T is presented in Figure **5-2**. A comparative discussion of the data will be undertaken in Paragraph 5.4.

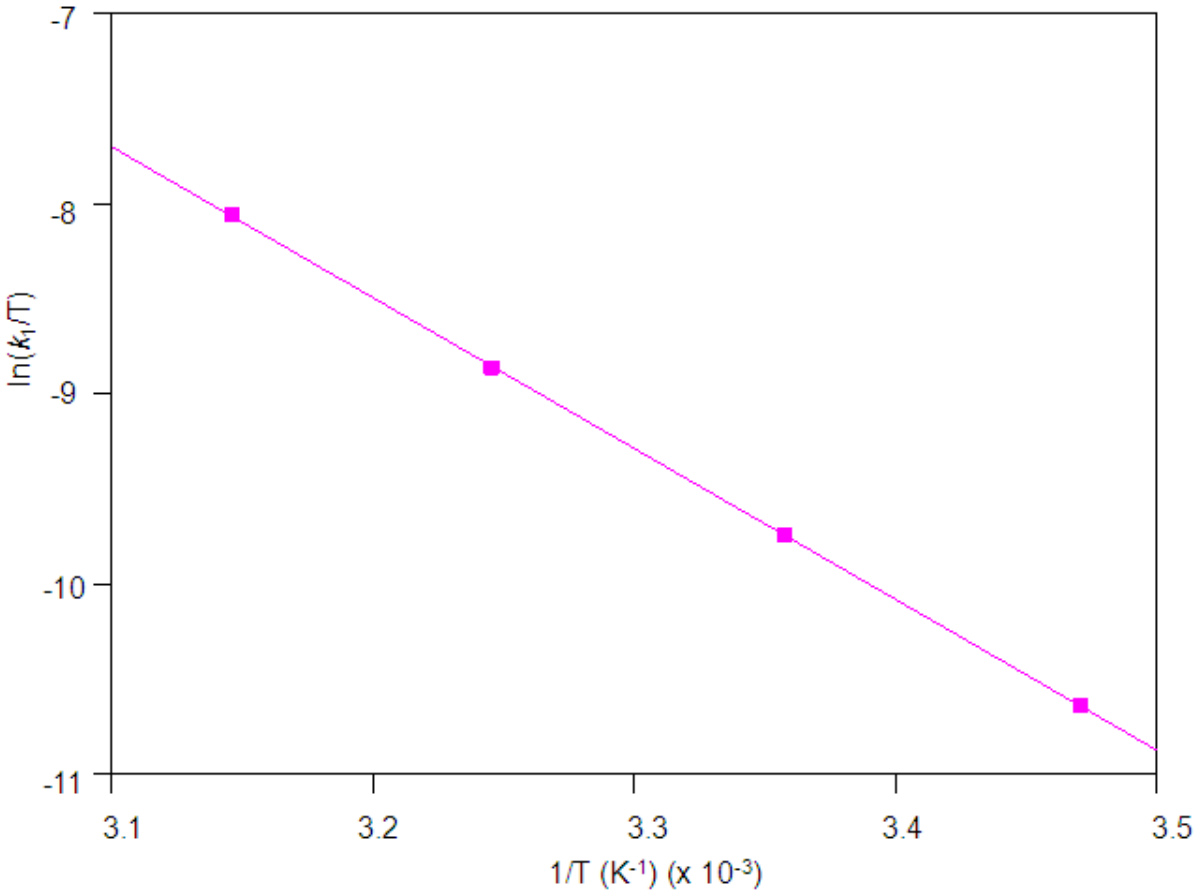

Figure 5-2: Plot of ln(k_1/T) *vs* 1/T for the reaction between *fac*-[Re(CO)$_3$(MeOH)(DiMePy]$^+$ and thiourea for a temperature range of 15.1 °C to 44.8 °C.

5.3.1.2 fac-[Re(CO)$_3$(MeOH)(DiMePy)]$^+$ + NCS$^-$

The methanol substitution reaction between *fac*-[Re(CO)$_3$(MeOH)(DiMePy)]$^+$ and thiocyanate was performed at 360 nm in methanol and at four different temperatures ranging between 14.2 °C and 44.9 °C, with [NCS$^-$] varying between 0.05 M and 0.5 M. The final UV/Vis spectrum of the reaction solution is identical to the one obtained from the synthesized *fac*-[Re(CO)$_3$(NCS)(DiMePy)] complex in Chapter 3. The graph of k_{obs} *vs* [NCS$^-$] at different temperatures is presented in Figure **5-3**, the rate constants for the reaction are reported in Table **5-2** while the Eyring plot is illustrated in Figure **5-4**.

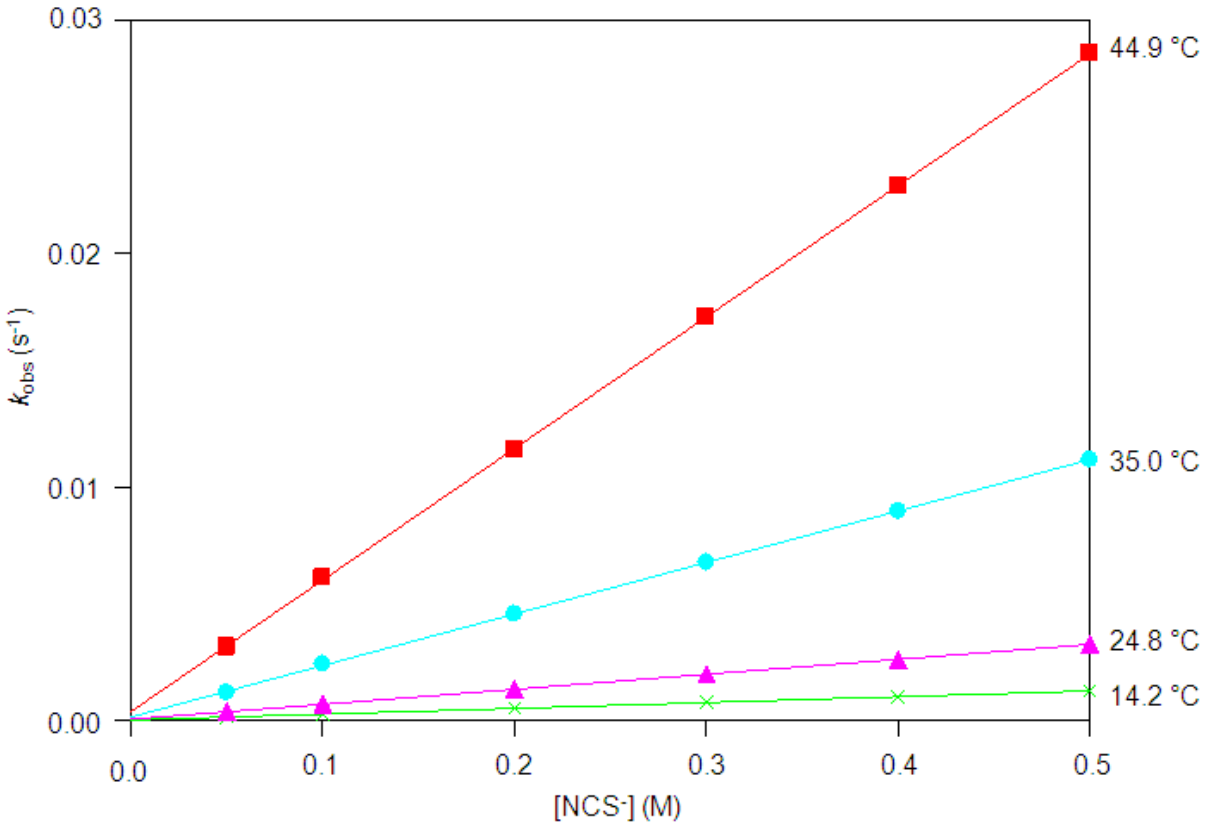

Figure 5-3: Plot of k_{obs} *vs* [NCS$^-$] for the reaction between *fac*-[Re(CO)$_3$(MeOH)(DiMePy)]$^+$ and NCS$^-$ at four different temperatures, with [NCS$^-$] varying between 0.05 M and 0.5 M. [Re] = 1 x 10^{-4} M, λ = 360 nm in methanol.

The activation parameters have been calculated from the Eyring plot (Equation **3**) as well as the global fit of temperature *vs* ligand concentration *vs* k_{obs} data (Equation **4**) and the traditional Eyring plot yields similar results to the global fit. $\Delta H^{\ddagger}$ = 74 ± 2 kJmol^{-1} and $\Delta S^{\ddagger}$ = -34 ± 1 JK^{-1}mol^{-1} from the Eyring plot and $\Delta H^{\ddagger}$ = 77 ± 2 kJmol^{-1} and $\Delta S^{\ddagger}$ = -27 ± 5 JK^{-1}mol^{-1} from the global fit.

Table 5-2: Summary of the rate constants for the reaction between *fac*-[Re(CO)$_3$(MeOH)(DiMePy)]$^+$ and thiocyanate at different temperatures, with [NCS$^-$] varying between 0.05 M and 0.5 M. [Re] = 1 x 10^{-4} M, λ = 360 nm.

	14.2 °C	**24.8 °C**	**35.0 °C**	**44.9 °C**
$10^3 k_1$ ($M^{-1}s^{-1}$)	2.482 ± 0.009	6.42 ± 0.02	22.1 ± 0.1	56.3 ± 0.2
$10^3 k_{-1}$ (s^{-1})	0.016 ± 0.003	0.044 ± 0.005	0.14 ± 0.03	0.38 ± 0.05
K_1 (M^{-1})[a]	155 ± 29	146 ± 17	158 ± 34	148 ± 20
K_1 (M^{-1})[b]	118 ± 3	118 ± 4	119 ± 7	121 ± 5

[a] $K_1 = k_1/k_{-1}$; [b] $A_{obs} = \frac{A_M + A_{ML}K_1[X]}{1 + K_1[X]}$

The plot of ln(k_1/T) *vs* 1/T is presented in Figure **5-4**. A comparative discussion of the data will be undertaken in Paragraph 5.4.

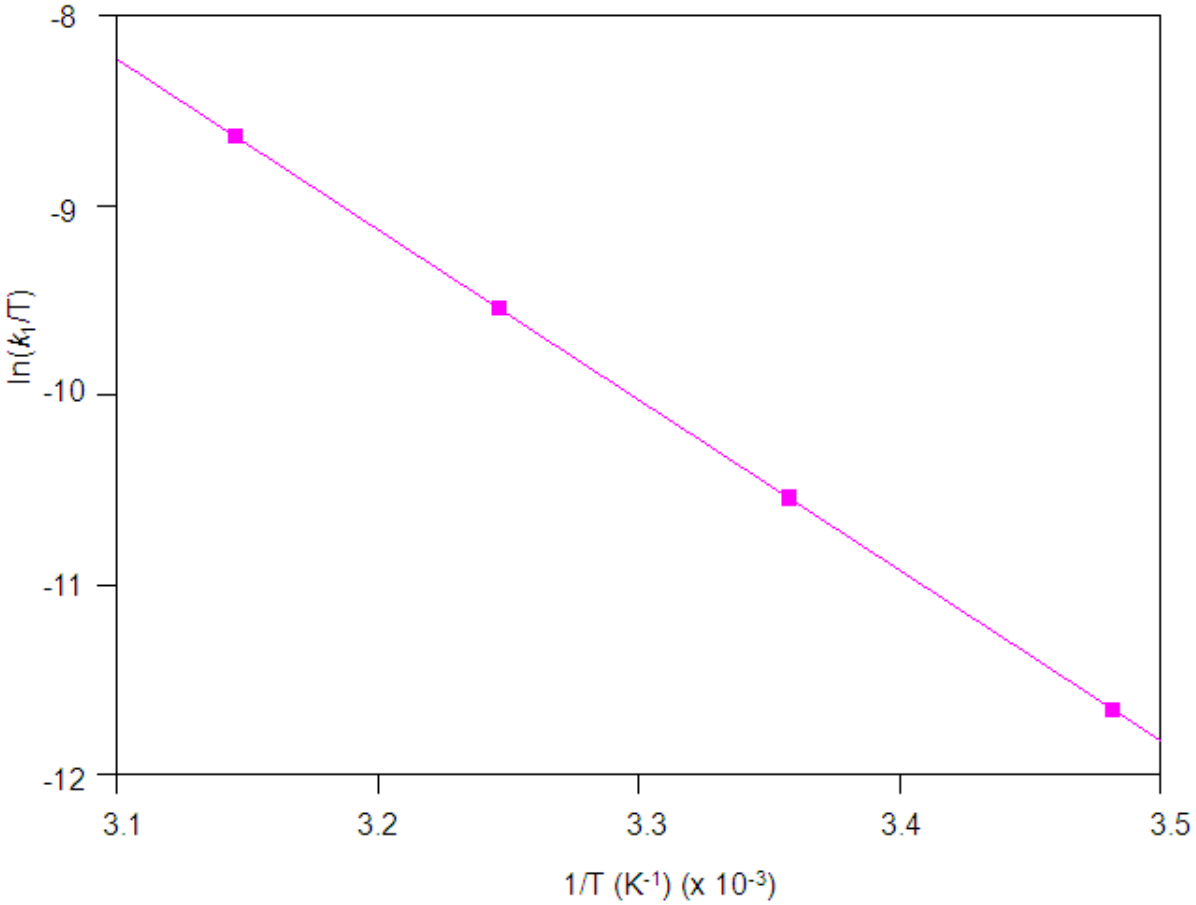

Figure 5-4: Plot of ln(k_1/T) *vs* 1/T for the reaction between *fac*-[Re(CO)$_3$(MeOH)(DiMePy)]$^+$ and thiocyanate ions for a temperature range of 14.2 °C to 44.9 °C.

5.3.1.3 fac-[Re(CO)$_3$(MeOH)(DiMePy)]$^+$ + PCy$_3$

The methanol substitution reaction between *fac*-[Re(CO)$_3$(MeOH)(DiMePy)]$^+$ and tricyclohexylphosphine was performed at 350 nm in methanol and at four different temperatures ranging between 15.5 °C and 44.5 °C, with [PCy$_3$] varying between 0.01 M and 0.05 M. The concentration of PCy$_3$ could not be increased since the solution was saturated at 0.05 M in methanol. At concentrations lower than 0.01 M the absorbance change is too small; thus the smaller concentration range of 0.01 M to 0.05 M was used. The final UV/Vis spectrum of the reaction solution is identical to the one obtained from the synthesized *fac*-[Re(CO)$_3$(PCy$_3$)(DiMePy)]$^+$ complex in

Chapter 3. The graph of k_{obs} *vs* [PCy_3] at different temperatures is presented in Figure **5-5**, the rate constants for the reactions are reported in Table **5-3** and the Eyring plot is illustrated in Figure **5-6**.

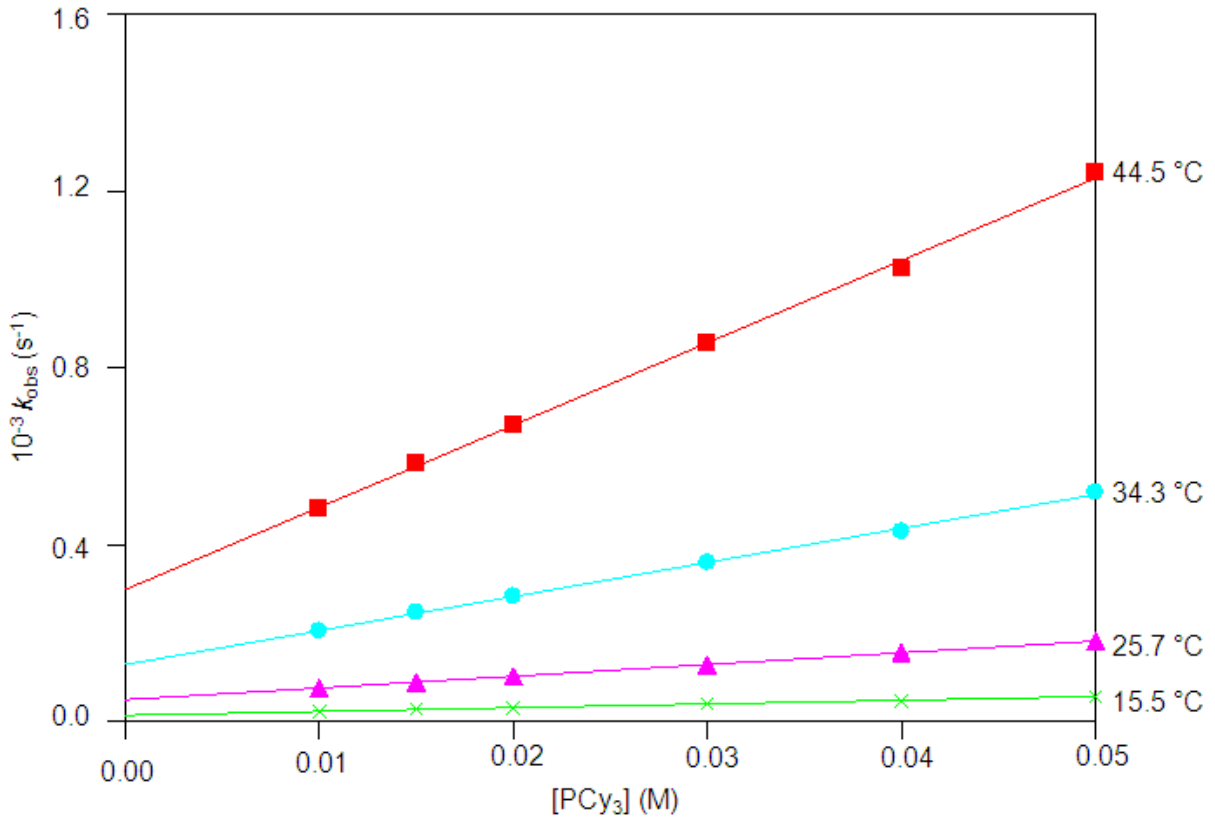

Figure 5-5: Plot of k_{obs} *vs* [PCy_3] for the reaction between *fac*-[$Re(CO)_3(MeOH)(DiMePy)]^+$ and PCy_3 at four different temperatures, with [PCy_3] varying between 0.01 M and 0.05 M. [Re] = 1 x 10^{-4} M, λ = 350 nm in methanol.

The activation parameters have been calculated from the Eyring plot (Equation **3**) as well as the global fit of temperature *vs* ligand concentration *vs* k_{obs} data (Equation **4**) and it is clear that the traditional Eyring plot yields similar results to the global fit. $\Delta H^{\ddagger}$ = 79 ± 1 $kJmol^{-1}$ and $\Delta S^{\ddagger}$ = -26 ± 2 $JK^{-1}mol^{-1}$ from the Eyring plot and $\Delta H^{\ddagger}$ = 72 ± 4 $kJmol^{-1}$ and $\Delta S^{\ddagger}$ = -51 ± 14 JK^{-1} mol^{-1} from the global fit.

Table 5-3: Summary of the rate constants of the reaction between *fac*-[Re(CO)$_3$(MeOH)(DiMePy)]$^+$ and PCy$_3$ at different temperatures, with [PCy$_3$] varying between 0.01 M and 0.05 M. [Re] = 1 x 10^{-4} M, λ = 350 nm.

	15.5 °C	25.7 °C	34.3 °C	44.5 °C
$10^3 k_1$ ($M^{-1}s^{-1}$)	0.850 ± 0.02	2.66 ± 0.01	7.7 ± 0.1	18.6 ± 0.3
$10^3 k_{-1}$ (s^{-1})	0.0141 ± 0.0006	0.0490 ± 0.0004	0.129 ± 0.004	0.30 ± 0.01
K_1 (M^{-1})[a]	60 ± 3	54 ± 0.5	60 ± 2	62 ± 2
K_1 (M^{-1})[b]	65 ± 4	55 ± 12	69 ± 4	64 ± 4

[a] $K_1 = k_1/k_{-1}$; [b] $A_{obs} = \frac{A_M + A_{ML}K_1[X]}{1 + K_1[X]}$

The plot of ln(k_1/T) *vs* 1/T is presented in Figure **5-6**. A comparative discussion of the data will be undertaken in the discussion in Paragraph 5.4

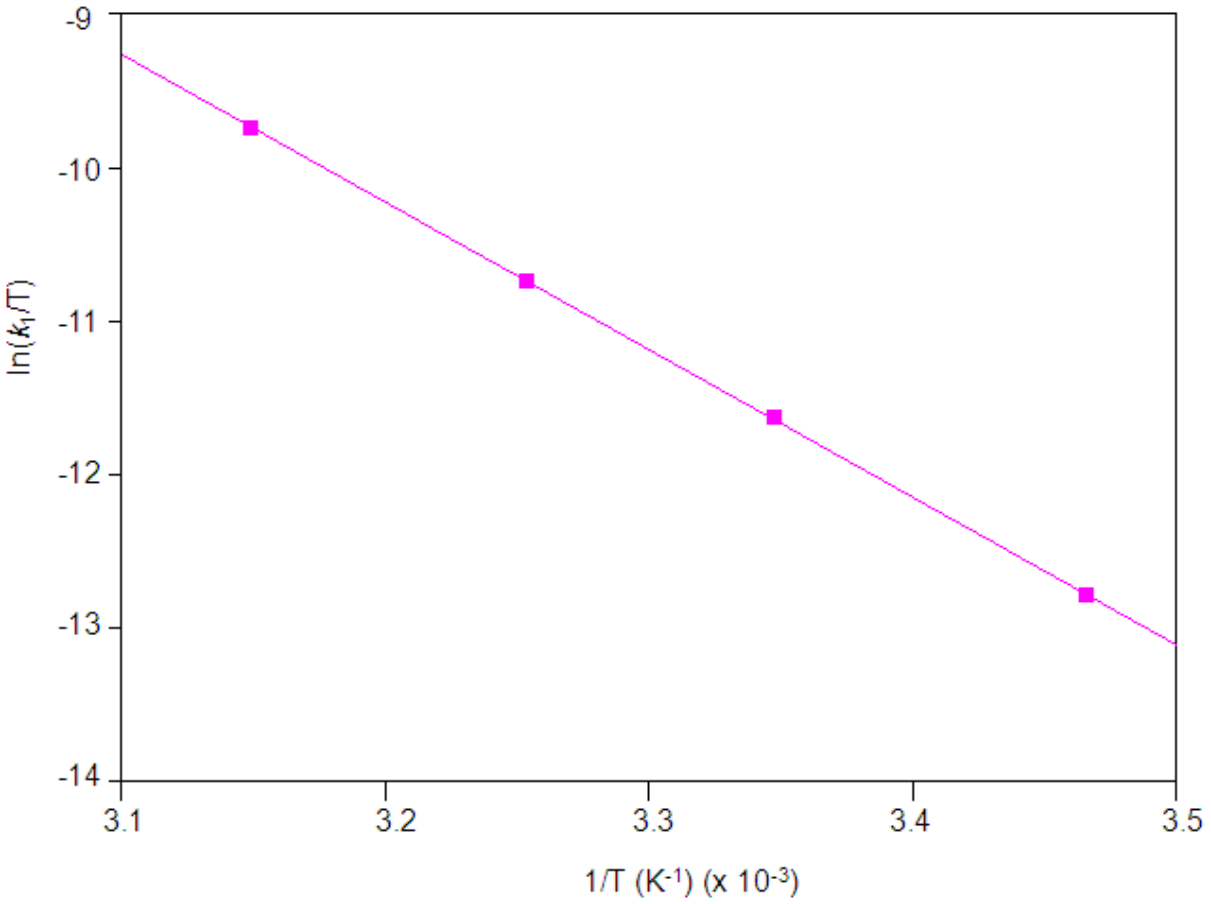

Figure 5-6: Plot of ln(k_1/T) *vs* 1/T for the reaction between *fac*-[Re(CO)$_3$(MeOH)(DiMePy]$^+$ and tricyclohexylphosphine for a temperature range of 15.5 °C to 44.5 °C.

5.3.1.4 fac-[Re(CO)$_3$(MeOH)(DiMePy)]$^+$ + Br$^-$

The methanol substitution reaction between *fac*-[Re(CO)$_3$(MeOH)(DiMePy)]$^+$ and bromide (Br$^-$) was performed at 340 nm in methanol and at four different temperatures ranging between 15.3 °C and 45.0 °C, with [Br$^-$] varying between 0.05 M and 0.5 M. The final UV/Vis spectrum of the reaction solution is identical to the one obtained from the synthesized *fac*-[Re(CO)$_3$(Br)(DiMePy)] complex in Chapter 3. The graph of k_{obs} *vs* [Br$^-$] at different temperatures is presented in Figure **5-7**. An illustration of the A_{obs} *vs* [Br$^-$], for the thermodynamically calculated equilibrium constant at 24.8 °C, is presented in Figure **5-8**. The rate constants for the reactions are reported in Table **5-4** and the Eyring plot is illustrated in Figure **5-9**.

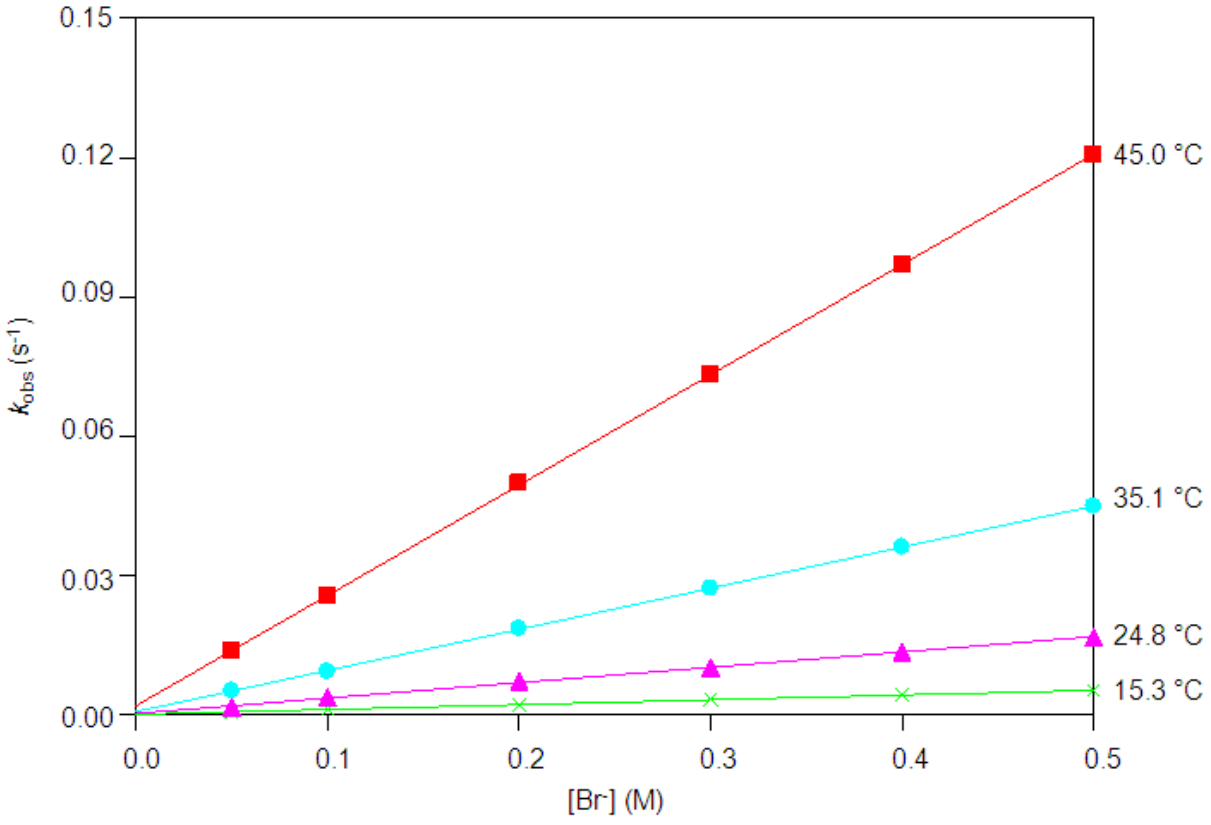

Figure 5-7: Plot of k_{obs} *vs* [Br$^-$] for the reaction between *fac*-[Re(CO)$_3$(MeOH)(DiMePy)]$^+$ and bromide ions at four different temperatures, with [Br$^-$] varying between 0.05 M and 0.5 M. [Re] = 1 x 10^{-4} M, λ = 340 nm, methanol.

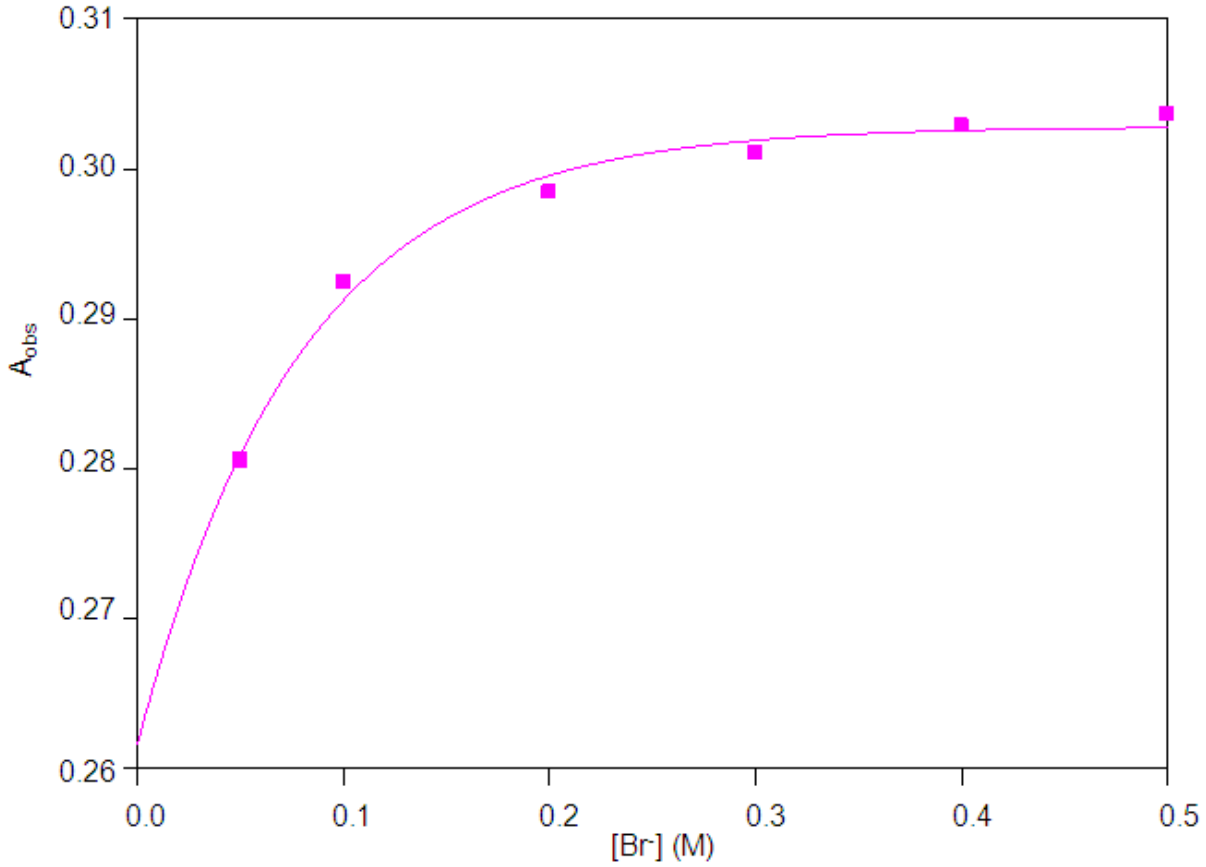

Figure 5-8: Plot of A_{obs} *vs* $[Br^-]$ for the reaction of *fac*-$[Re(CO)_3(MeOH)(DiMePy)]^+$ with Br^- ions at 24.8 °C, [Re] = 1 x 10^{-4} M, λ = 340 nm.

The activation parameters have been calculated from the Eyring plot (Equation **3**) as well as the global fit of tempertature *vs* ligand concentration *vs* k_{obs} data (Equation **4**) and it is clear that the traditional Eyring plot yields similar results to the global fit. $\Delta H^{\ddagger}$ = 77 ± 1 kJmol^{-1} and $\Delta S^{\ddagger}$ = -13 ± 1 JK^{-1}mol^{-1} from the Eyring plot and $\Delta H^{\ddagger}$ = 78 ± 1 kJmol^{-1} and $\Delta S^{\ddagger}$ = -13 ± 3 JK^{-1}mol^{-1} from the global fit.

Table 5-4: Summary of the rate constants of the reaction between *fac*-$[Re(CO)_3(MeOH)(DiMePy)]^+$ and bromide ions at different temperatures, with $[Br^-]$ varying between 0.05 M and 0.5 M. [Re] = 1 x 10^{-4} M, λ = 340 nm.

	15.3 °C	**24.8 °C**	**35.1 °C**	**45.0 °C**
$10^3 k_1$ ($M^{-1}s^{-1}$)	10.39 ± 0.02	33.1 ± 0.6	88.6 ± 0.4	237.7 ± 0.6
$10^3 k_{-1}$ (s^{-1})	0.079 ± 0.006	0.28 ± 0.02	0.7 ± 0.1	1.9 ± 0.2
K_1 (M^{-1})[a]	132 ± 10	118 ± 9	127 ± 18	125 ± 13
K_1 (M^{-1})[b]	103 ± 4	120 ± 2	101 ± 6	104 ± 5

[a] $K_1 = k_1/k_{-1}$; [b] $A_{obs} = \frac{A_M + A_{ML}K_1[X]}{1 + K_1[X]}$

The plot of ln(k_1/T) *vs* 1/T is presented in Figure **5-9**. A comparative discussion of the data will be undertaken in Paragraph 5.4.

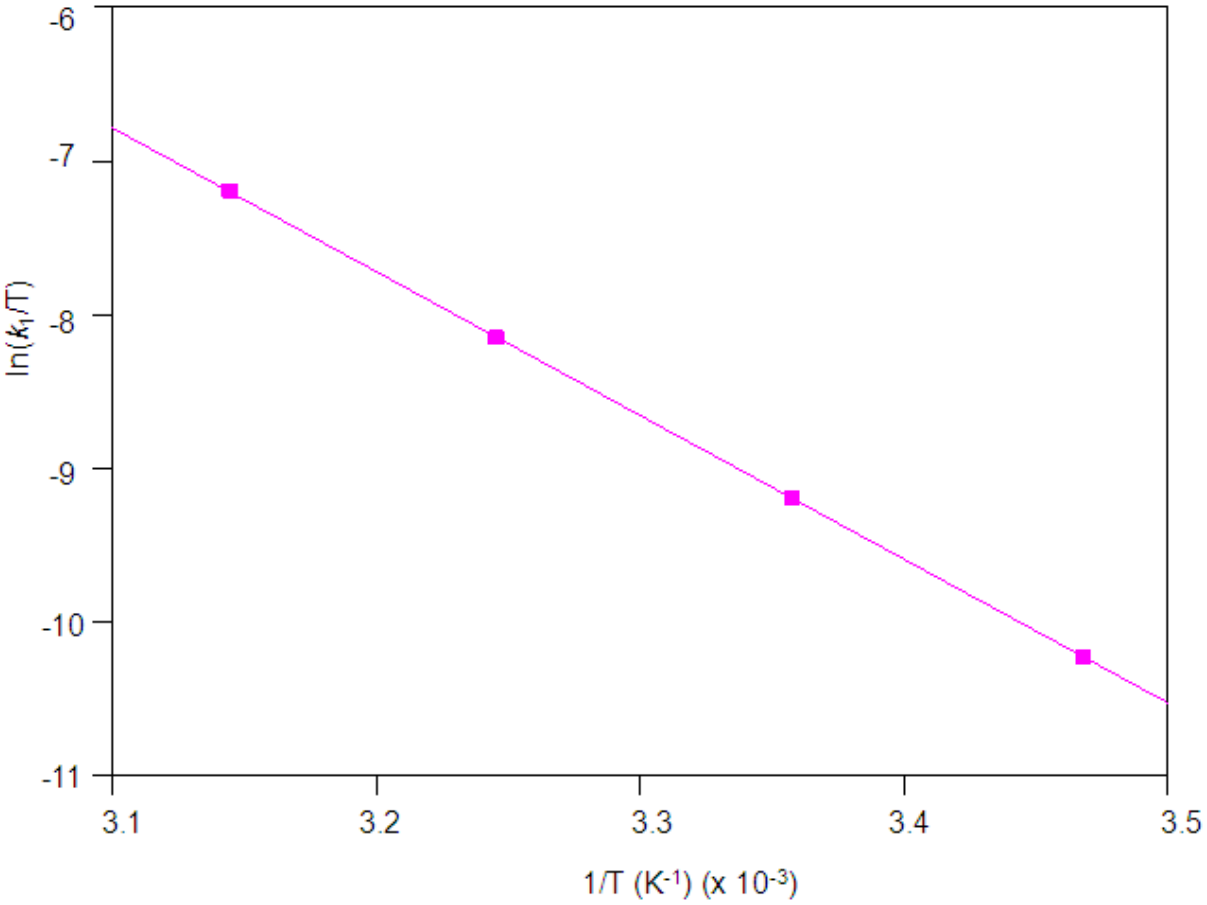

Figure 5-9: Plot of ln(k_1/T) *vs* 1/T for the reaction between *fac*-[Re(CO)$_3$(MeOH)(DiMePy]$^+$ and bromide ions for the temperature range of 15.3 °C to 45.0 °C.

5.3.1.5 Summary of the results of the methanol substitution reactions of fac-[Re(CO)$_3$(MeOH)(DiMePy)]$^+$

The substitution reactions between *fac*-[Re(CO)$_3$(MeOH)(DiMePy)]$^+$ and four different mondentate ligands have been studied (Paragraph 5.3.1.1 to 5.3.1.4, thiourea (TU), thiocyanate ions (NCS$^-$), tricyclohexylphosphine (PCy$_3$) and bromide ions (Br$^-$)).

The k_1 values (Table **5-5**) for the substitution reactions with different entering ligands are comparable to each other, with k_1 (Br) > k_1 (TU) > k_1 (NCS$^-$) > k_1 (PCy$_3$). A graph to illustrate the rates of the different entering ligands at ~ 25 °C is illustrated in Figure **5-10**. The reverse reaction rate constant, k_{-1} decreases in the following order Br$^-$ >

TU > NCS^- ≈ PCy_3 while the stability constant, K_1, for these reactions are similar within experimental error for NCS^-, Br^- and TU while K_1 for the reaction with PCy_3 is at least two times smaller than the other three reactions. K_1 varies between 54.3 ± 0.5 and 146 ± 17. Generally a good agreement exists between the stability constants, K_1, determined kinetically and those determined thermodynamically. The enthalpy of activation, $\Delta H^{\ddagger}$ values for all the reactions are similar while the small negative values of $\Delta S^{\ddagger}$ for all the reactions (with TU, NCS^-, PCy_3 and Br^-) suggest an interchange associative type of activation. The $\Delta H^{\ddagger}$ values for all the reactions determined from the Eyring equation and from the global fit, are all similar within experimental error, while the $\Delta S^{\ddagger}$ values differ significantly but when considering the large esd's of these values, it is still similar within experimental error, except for the reaction with TU.

Table 5-5: Rate constants of the different reactions between *fac*-$[Re(CO)_3(MeOH)(DiMePy)]^+$ and different entering ligands at ~ 25 °C.

	$10^3 k_1$ ($M^{-1}s^{-1}$)	$10^3 k_{-1}$ (s^{-1})	K_1 (M^{-1})	$\Delta H^{\ddagger}$ ($kJmol^{-1}$)	$\Delta S^{\ddagger}$ ($JK^{-1}mol^{-1}$)
TU	18.6 ± 0.1	0.19 ± 0.04	98 ± 20[a], 100 ± 6[b]	65 ± 1[c], 77.5 ± 0.8[d]	-59 ± 5[c], -14 ± 2[d]
NCS^-	6.42 ± 0.02	0.044 ± 0.005	146 ± 17[a], 118 ± 4[b]	74 ± 2[c], 77 ± 2[d]	-34 ± 1[c], -27 ±5[d]
PCy_3	2.66 ± 0.01	0.0490 ± 0.0004	54.3 ± 0.5 [a], 55 ± 2[b]	79 ± 1[c], 72 ± 4[d]	-26 ± 2[c], -51 ± 14[d]
Br^-	33.1 ± 0.6	0.28 ± 0.02	118 ± 9[a], 120 ± 2[b]	77 ± 1[c], 78 ± 1[d]	-13 ± 1[c], -13 ± 3[d]

[a] $K_1 = k_1/k_{-1}$, [b] $A_{obs} = \frac{A_M + A_{ML}K_1[L]}{1 + K_1[L]}$, [c] Eyring fit, [d] Global fit.

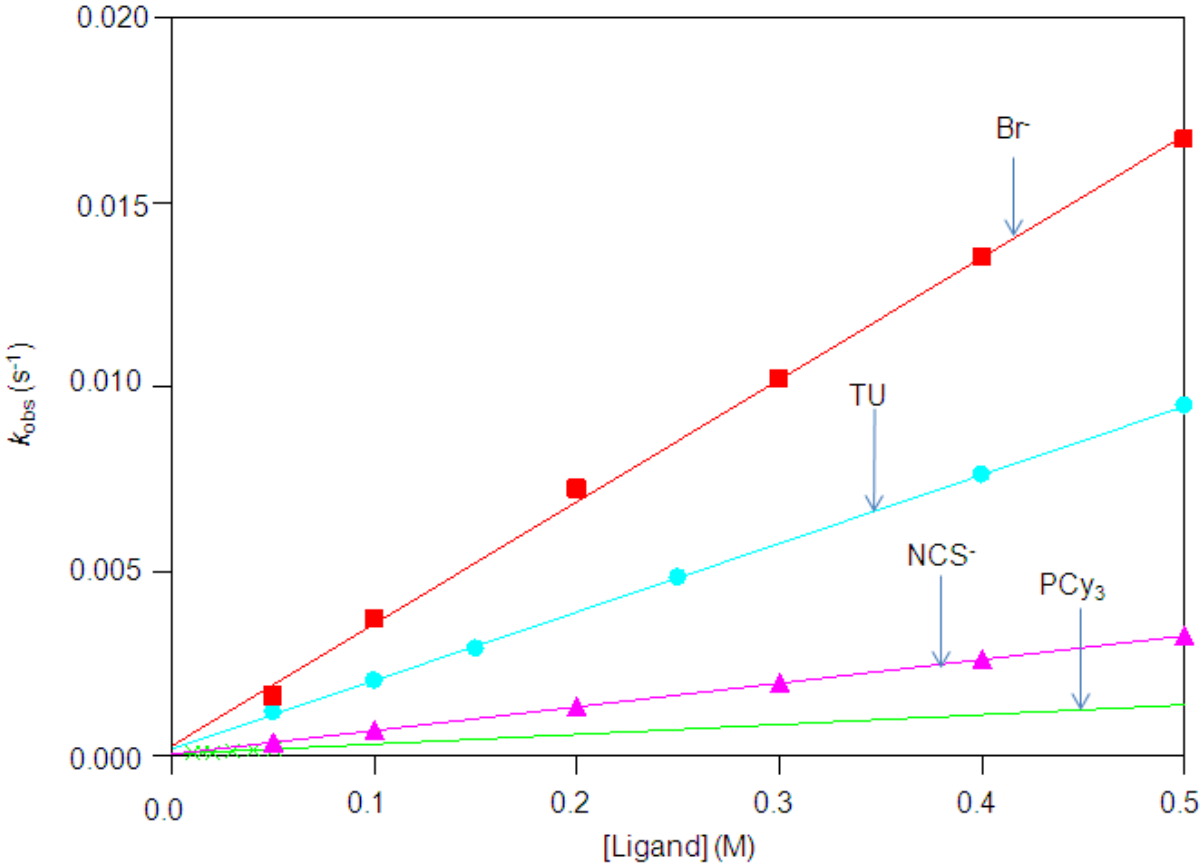

Figure 5-10: Schematic representation of the k_{obs} *vs* [ligand] of the reactions between *fac*-[Re(CO)$_3$(MeOH)(DiMePy)]$^+$ and various entering ligands at ~ 25 °C.

5.3.2 Reaction between *fac*-[Re(CO)$_3$(MeOH)(DiMeOPy)]$^+$ and entering ligands

The synthesis of *fac*-[Re(CO)$_3$(MeOH)(DiMeOPy)]$^+$ from the starting synthon [NEt$_4$]$_2$[Re(CO)$_3$Br$_3$] has been described in Chapter 3. *fac*-[Re(CO)$_3$(Br)(DiMeOPy)] was dissolved in methanol and stirred for 24 hours to yield *fac*-[Re(CO)$_3$(MeOH)(DiMeOPy)]$^+$. The reaction between *fac*-[Re(CO)$_3$(MeOH)(DiMeOPy)]$^+$ and four different monodentate ligands (thiourea (TU), thiocyanate (NCS$^-$), tricyclohexylphosphine (PCy$_3$) and bromide (Br$^-$)) were monitored with UV/Vis in methanol.

5.3.2.1 fac-[Re(CO)$_3$(MeOH)(DiMeOPy)]$^+$ + TU

The methanol substitution reaction between *fac*-[Re(CO)$_3$(MeOH)(DiMeOPy)]$^+$ and thiourea (TU) was performed at 345 nm in methanol and at four different temperatures ranging between 14.7 °C and 45.6 °C, with [TU] varying between 0.05 M and 0.5 M. The final UV/Vis spectrum of the reaction solution is identical to the one obtained from the synthesized *fac*-[Re(CO)$_3$(TU)(DiMeOPy)]$^+$ complex in Chapter 3.

The graph of k_{obs} *vs* [TU] at different temperatures is presented in Figure **5-11** below, the rate constants for the reactions are reported in Table **5-6** and the Eyring plot is illustrated in Figure **5-12**.

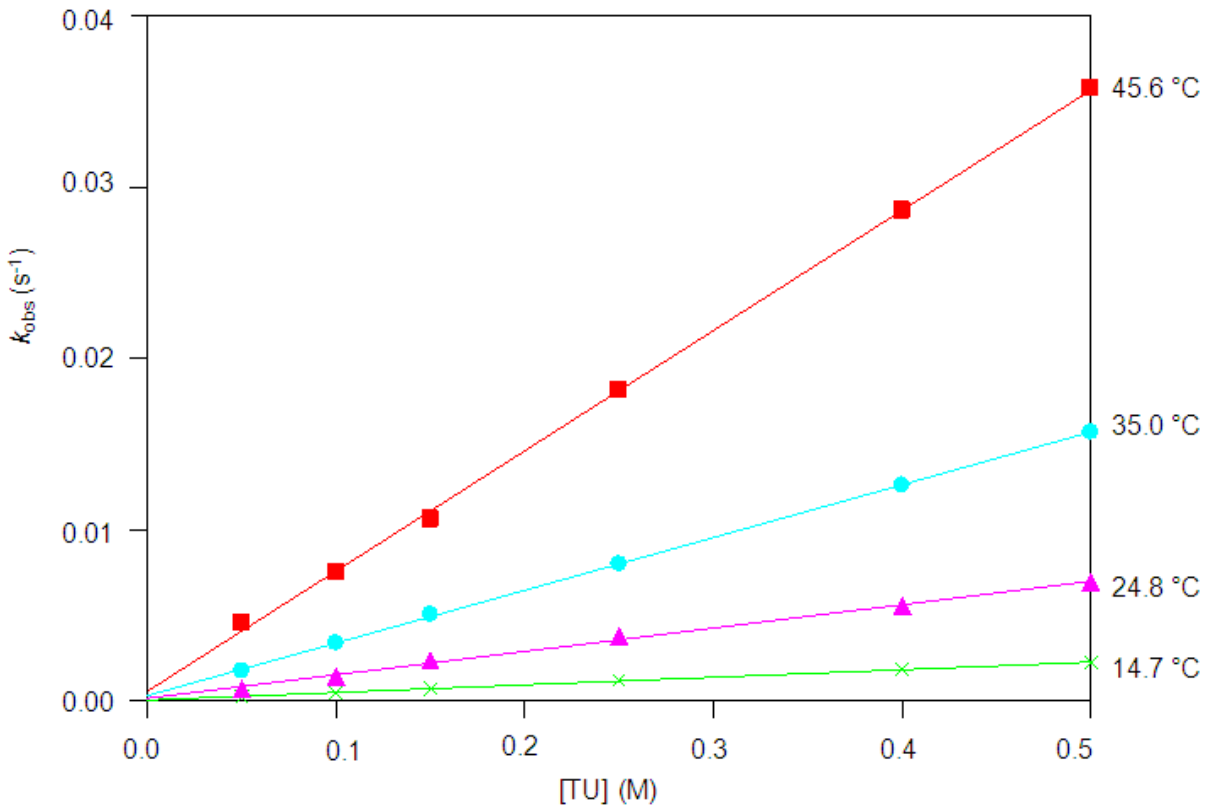

Figure 5-11: Plot of k_{obs} *vs* [TU] for the reaction between *fac*-[Re(CO)$_3$(MeOH)(DiMeOPy)]$^+$ and thiourea at four different temperatures in methanol with [TU] = 0.05 M to 0.5 M. [Re] = 1 x10^{-4} M, λ = 345 nm.

The activation parameters have been calculated by the Eyring plot (Equation **3**) as well as the global fit of tempertature *vs* ligand concentration *vs* k_{obs} data (Equation **4**) and it is clear that the traditional Eyring plot yields similar results to the global fit.

$\Delta H^{\ddagger}$ = 73 ± 1 kJmol^{-1} and $\Delta S^{\ddagger}$ = -35 ± 4 JK^{-1}mol^{-1} from the Eyring plot and $\Delta H^{\ddagger}$ = 61 ± 1 kJmol^{-1} and $\Delta S^{\ddagger}$ = -77 ± 4 JK^{-1}mol^{-1} from the global fit.

Table 5-6: Summary of the rate constants of the reaction between *fac*-[Re(CO)$_3$(MeOH)(DiMeOPy)]$^+$ and thiourea at different temperatures, with [TU] = 0.05 M to 0.5 M. [Re] = 1 x 10^{-4} M, λ = 345 nm.

	14.7 °C	**24.8 °C**	**35.0 °C**	**45.6 °C**
$10^3 k_1$ ($M^{-1}s^{-1}$)	4.44 ± 0.04	13.7 ± 0.4	30.8 ± 0.2	70.3 ± 0.8
$10^3 k_{-1}$ (s^{-1})	0.04 ± 0.01	0.15 ± 0.01	0.30 ± 0.05	0.60 ± 0.02
K_1 (M^{-1})[a]	111 ± 28	91 ± 7	103 ± 17	117 ± 4
K_1 (M^{-1})[b]	85 ± 8	86 ± 4	90 ± 8	90 ± 4

[a] $K_1 = k_1/k_{-1}$; [b] $A_{obs} = \frac{A_M + A_{ML}K_1[X]}{1 + K_1[X]}$

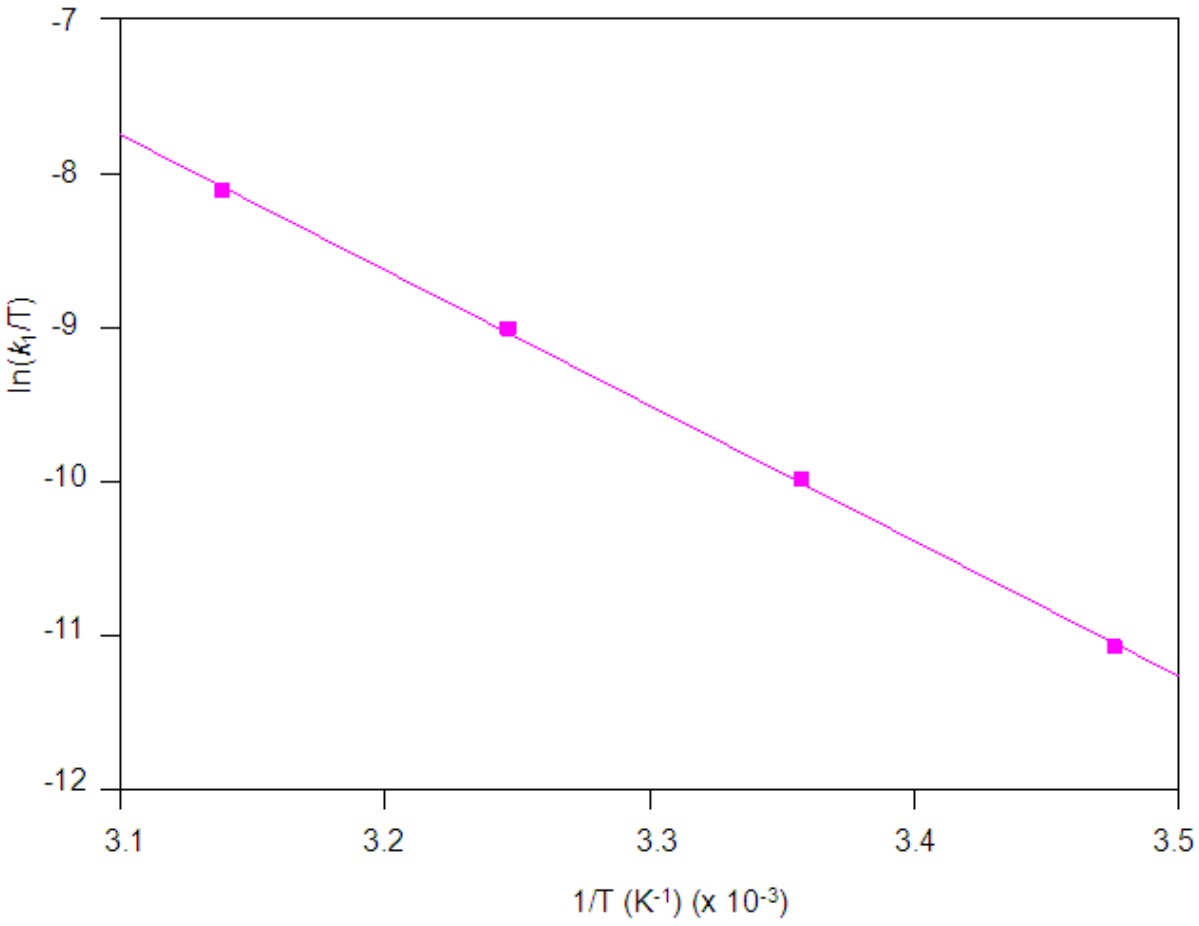

Figure 5-12: Plot of ln(k_1/T) *vs* 1/T for the reaction between *fac*-[Re(CO)$_3$(MeOH)(DiMeOPy)]$^+$ and thiourea for a temperature range of 14.7 °C to 45.6 °C.

The plot of ln(k_1/T) *vs* 1/T is presented in Figure **5-12**. A comparative discussion of the data will be undertaken in Paragraph 5.4.

5.3.2.2 fac-[Re(CO)$_3$(MeOH)(DiMeOPy)]$^+$ + NCS$^-$

The methanol substitution reaction between *fac*-[Re(CO)$_3$(MeOH)(DiMeOPy)]$^+$ and thiocyanate was performed at 345 nm in methanol and at four different temperatures ranging between 14.5 °C and 45.0 °C, with [NCS$^-$] varying between 0.05 M and 0.5 M. The final UV/Vis spectrum of the reaction solution is identical to the one obtained from the synthesized *fac*-[Re(CO)$_3$(NCS)(DiMeOPy)] complex in Chapter 3. The graph of k_{obs} *vs* [NCS$^-$] at different temperatures is presented in Figure **5-13** below, the rate constants for the reaction are reported in Table **5-7** while the Eyring plot is illustrated in Figure **5-14**.

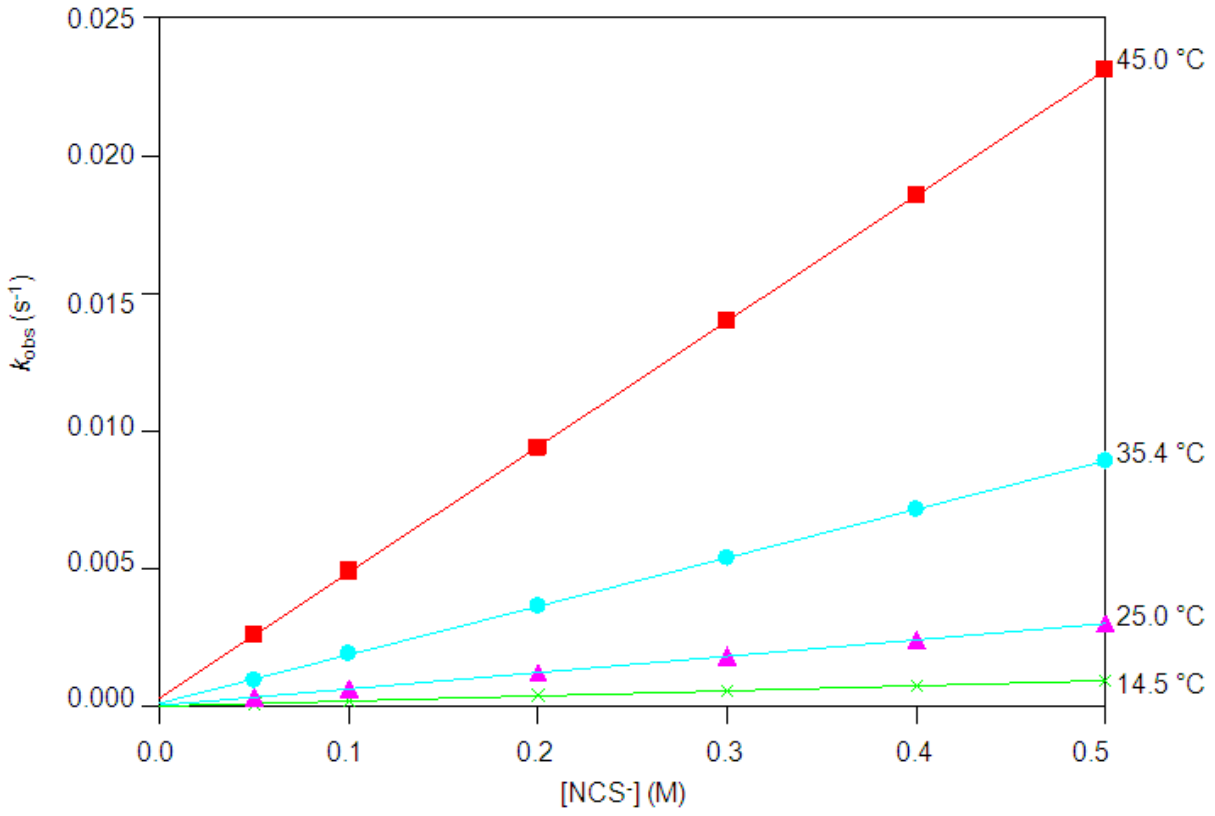

Figure 5-13: Plot of k_{obs} *vs* [NCS$^-$] for the reaction between *fac*-[Re(CO)$_3$(MeOH)(DiMeOPy)]$^+$ and NCS$^-$ at four different temperatures, with [NCS$^-$] varying between 0.05 M and 0.5 M. [Re] = 1 x 10^{-4} M, λ = 345 nm in methanol.

The activation parameters have been calculated by the Eyring plot (Equation **3**) as well as the global fit of tempertature *vs* ligand concentration *vs* k_{obs} data (Equation **4**) and the traditional Eyring plot yields similar results to the global fit. $\Delta H^{\ddagger}$ = 77 ± 1 kJmol^{-1} and $\Delta S^{\ddagger}$ = -27 ± 1 JK^{-1}mol^{-1} from the Eyring plot and $\Delta H^{\ddagger}$ = 78.0 ± 0.3 kJmol^{-1} and $\Delta S^{\ddagger}$ = -26.4 ± 0.8 JK^{-1}mol^{-1} from the global fit.

Table 5-7 Summary of the rate constants of the reaction between *fac*-[Re(CO)$_3$(MeOH)(DiMeOPy)]$^+$ and NCS$^-$ at different temperatures, with [NCS$^-$] = 0.05 M to 0.5 M. [Re] = 1 x 10^{-4} M, λ = 345 nm.

	14.5 °C	**25.0 °C**	**35.4 °C**	**45.0 °C**
$10^3 k_1$ ($M^{-1}s^{-1}$)	1.849 ± 0.009	5.94 ± 0.02	17.62 ± 0.08	45.61 ± 0.07
$10^3 k_{-1}$ (s^{-1})	0.013 ± 0.003	0.043 ± 0.005	0.12 ± 0.02	0.32 ± 0.02
K_1 (M^{-1})[a]	142 ± 33	138 ± 16	147 ± 24	143 ± 9
K_1 (M^{-1})[b]	104 ± 10	103 ± 7	90 ± 4	90 ± 2

a $K_1 = k_1/k_{-1}$; **b** $A_{obs} = \frac{A_M + A_{ML}K_1[X]}{1 + K_1[X]}$

The plot of ln(k_1/T) *vs* 1/T is presented in Figure **5-14**. A comparative discussion of the data will be undertaken in Paragraph 5.4.

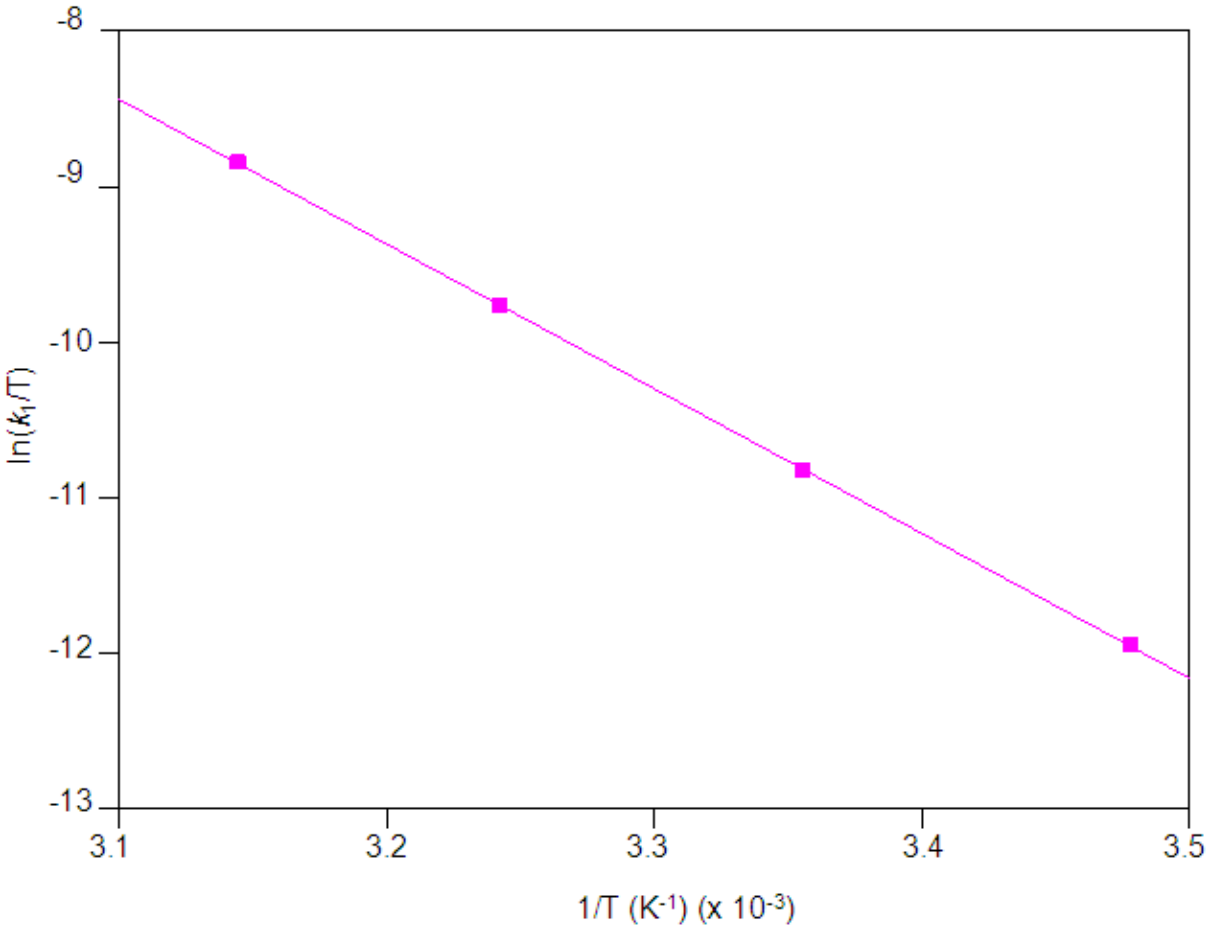

Figure 5-14: Plot of ln(k_1/T) *vs* 1/T for the reaction between *fac*-[Re(CO)$_3$(MeOH)(DiMeOPy)]$^+$ and thiocyanate for the temperature range of 14.5 °C to 45.0 °C.

5.3.2.3 fac-[Re(CO)$_3$(MeOH)(DiMeOPy)]$^+$ + PCy$_3$

The methanol substitution reaction between *fac*-[Re(CO)$_3$(MeOH)(DiMeOPy)]$^+$ and tricyclohexylphosphine was performed at 340 nm in methanol and at four different temperatures ranging between 14.9 °C and 45.3 °C, with [PCy$_3$] varying between 0.01 M and 0.05 M. The concentration of PCy$_3$ could not be increased since the solution was saturated at 0.05 M in methanol. At concentrations lower than 0.01 M the absorbance change is too small; thus the smaller concentration range of 0.01 M to 0.05 M was used. The final UV/Vis spectrum of the reaction solution is identical to the one obtained from the synthesized *fac*-[Re(CO)$_3$(PCy$_3$)(DiMeOPy)]$^+$ complex in Chapter 3. The graph of k_{obs} *vs* [PCy$_3$] at different temperatures is presented in

Figure **5-15** below, the rate constants for the reactions are reported in Table **5-8** and the Eyring plot is illustrated in Figure **5-16**.

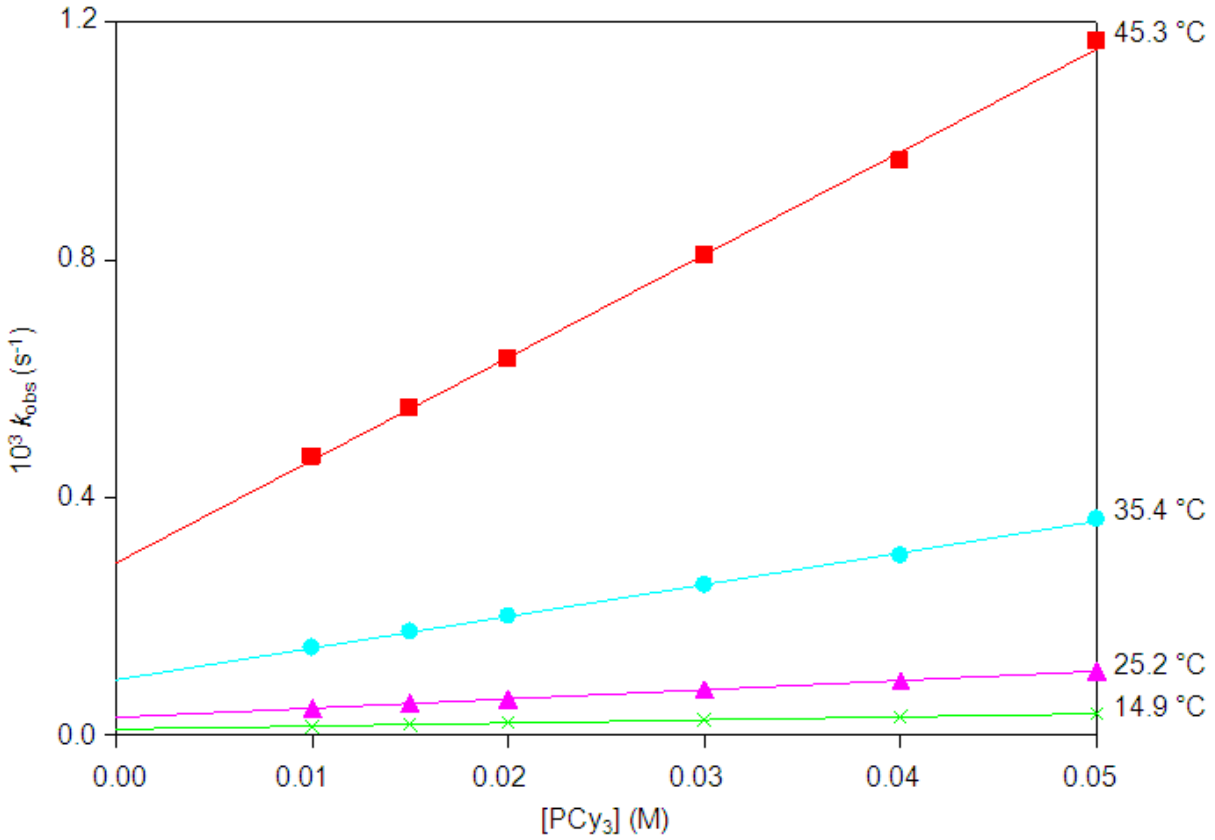

Figure 5-15: Plot of k_{obs} *vs* $[PCy_3]$ for the reaction between *fac*-$[Re(CO)_3(MeOH)(DiMeOPy)]^+$ and tricyclohexylphosphine at four different temperatures, with $[PCy_3]$ varying between 0.01 M and 0.05 M. [Re] = 1 x 10^{-4} M, λ = 340 nm in methanol.

Table 5-8: Summary of the rate constants of the reaction between *fac*-$[Re(CO)_3(MeOH)(DiMeOPy)]^+$ and PCy_3 at different temperatures, with $[PCy_3]$ = 0.01 M to 0.05 M. [Re] = 1 x 10^{-4} M, λ = 340 nm.

	14.9 °C	25.2 °C	35.4 °C	45.3 °C
$10^3 k_1$ ($M^{-1}s^{-1}$)	0.52 ± 0.01	1.56 ± 0.02	5.35 ± 0.09	17.3 ± 0.3
$10^3 k_{-1}$ (s^{-1})	0.0098 ± 0.0003	0.0295 ± 0.0006	0.093 ± 0.003	0.290 ± 0.009
K_1 (M^{-1})[a]	53 ± 2	53 ± 1	58 ± 2	60 ± 2
K_1 (M^{-1})[b]	59 ± 8	59 ± 4	55 ± 3	59 ± 5

[a] $K_1 = k_1/k_{-1}$; [b] $A_{obs} = \frac{A_M + A_{ML}K_1[X]}{1 + K_1[X]}$

The activation parameters have been calculated by the Eyring plot (Equation **3**) as well as the global fit of temperature *vs* ligand concentration *vs* k_{obs} data (Equation **4**) and it is clear that the traditional Eyring plot yields similar results to the global fit.

$\Delta H^{\ddagger}$ = 80 ± 2 kJmol^{-1} and $\Delta S^{\ddagger}$ = -27 ± 2 JK^{-1}mol^{-1} from the Eyring plot and $\Delta H^{\ddagger}$ = 94 ± 1 kJmol^{-1} and $\Delta S^{\ddagger}$ = 15 ± 4 JK^{-1}mol^{-1} from the global fit.

The plot of ln(k_1/T) *vs* 1/T is presented in Figure **5-16**. A comparative discussion of the data will be undertaken in Paragraph 5.4.

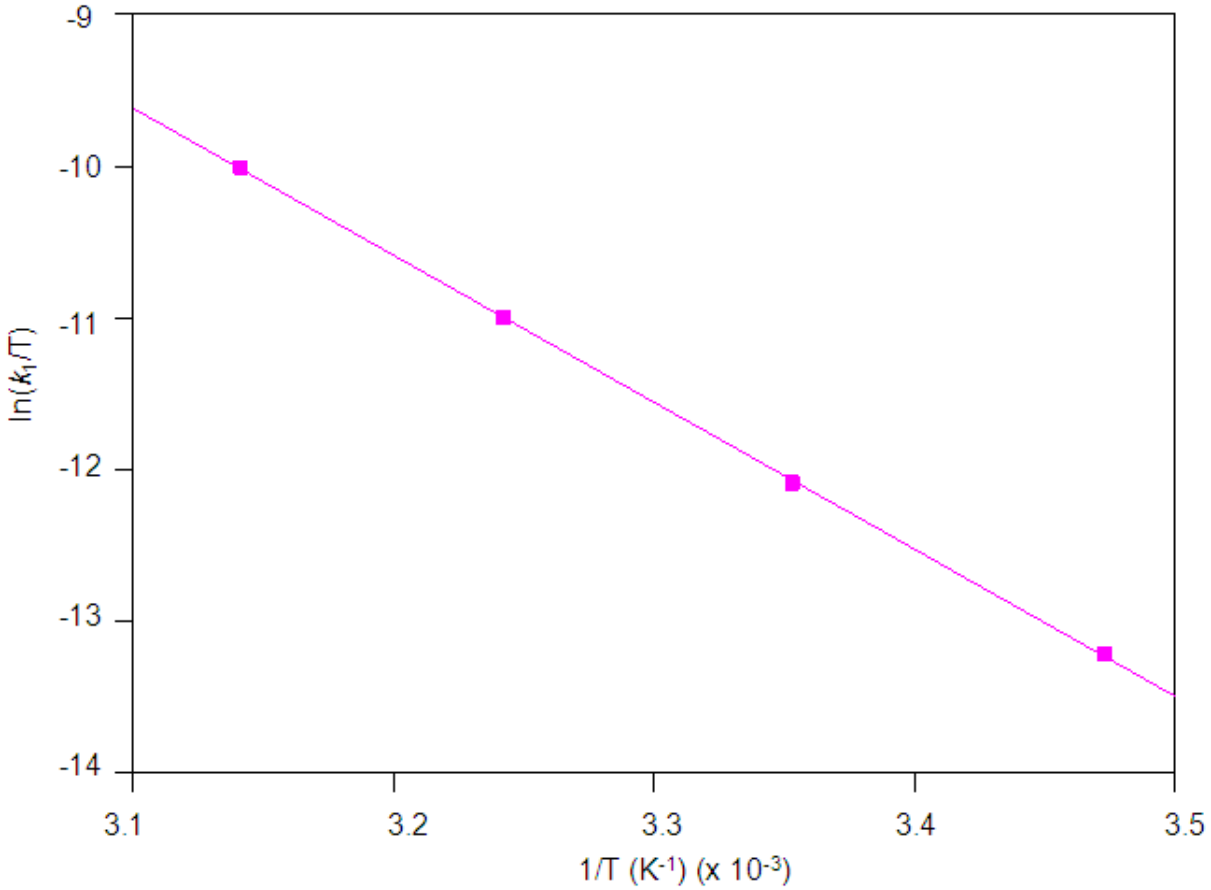

Figure 5-16: Plot of ln(k_1/T) *vs* 1/T for the reaction between *fac*-[Re(CO)$_3$(MeOH)(DiMeOPy)]$^+$ and tricyclohexylphosphine for a temperature range of 14.9 °C to 45.3 °C.

5.3.2.4 fac-[Re(CO)$_3$(MeOH)(DiMeOPy)]$^+$ + Br$^-$

The methanol substitution reaction between *fac*-[Re(CO)$_3$(MeOH)(DiMeOPy)]$^+$ and bromide (Br$^-$) was performed at 342 nm in methanol and at four different temperatures ranging between 15.6 °C and 45.6 °C, with [Br$^-$] varying between 0.05 M and 0.5 M. The final UV/Vis spectrum of the reaction solution is identical to the one obtained from the synthesized *fac*-[Re(CO)$_3$(Br)(DiMeOPy)] complex in Chapter 3. The graph of k_{obs} *vs* [Br$^-$] at different temperatures is presented in Figure **5-17**. An illustration of the A_{obs} *vs* [Br$^-$], for the thermodynamically calculated

equilibrium constant at 24.7 °C, is presented in Figure **5-18**.The rate constants for the reactions are reported in Table **5-9** and the Eyring plot is illustrated in Figure **5-19**.

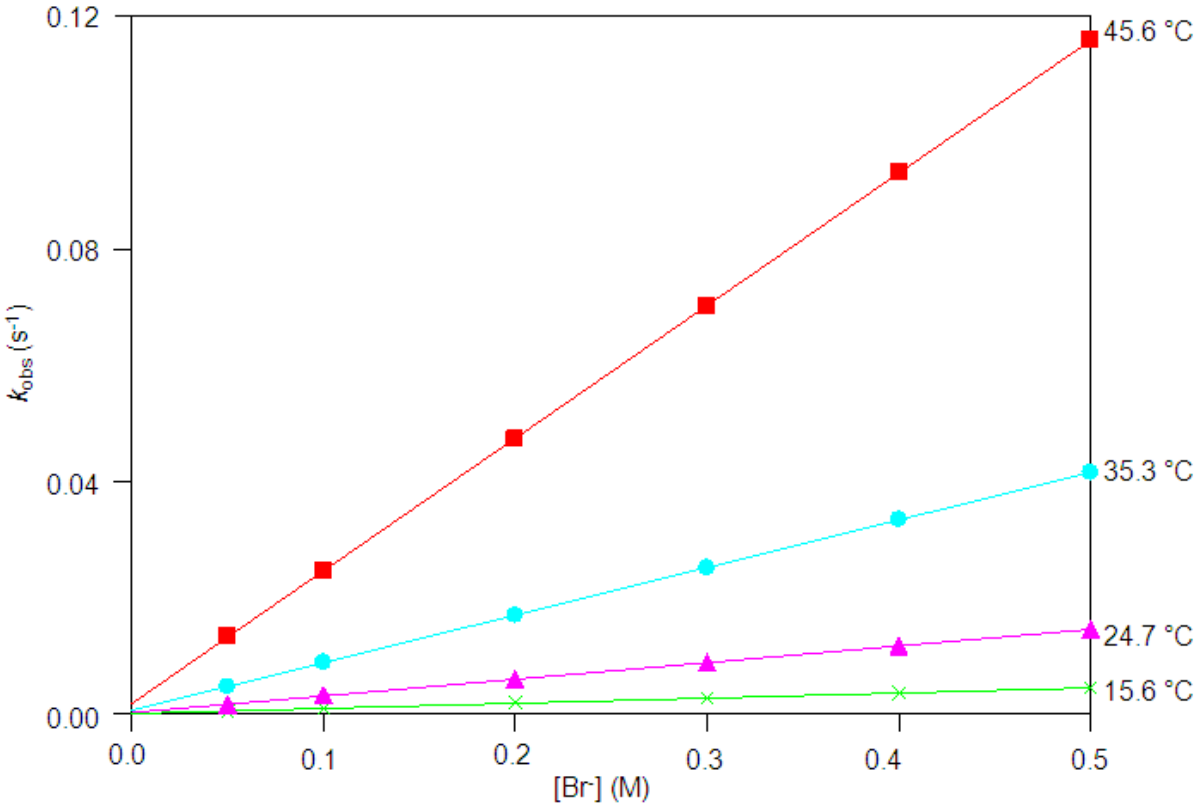

Figure 5-17: Plot of k_{obs} *vs* [Br$^-$] for the reaction between *fac*-[Re(CO)$_3$(MeOH)(DiMeOPy)]$^+$ and bromide ions at four different temperatures, with [Br$^-$] varying between 0.05 M and 0.5 M. [Re] = 1 x 10^{-4} M, λ = 342 nm, methanol.

The activation parameters have been calculated by the Eyring plot (Equation **3**) as well as the global fit of tempertature *vs* ligand concentration *vs* k_{obs} data (Equation **4**) and it is clear that the traditional Eyring plot yields similar results to the global fit. $\Delta H^{\ddagger}$ = 78 ± 1 kJmol^{-1} and $\Delta S^{\ddagger}$ = -10 ± 1 JK^{-1}mol^{-1} from the Eyring plot and $\Delta H^{\ddagger}$ = 77.9 ± 0.8 kJmol^{-1} and $\Delta S^{\ddagger}$ = -14 ± 2 JK^{-1}mol^{-1} from the global fit.

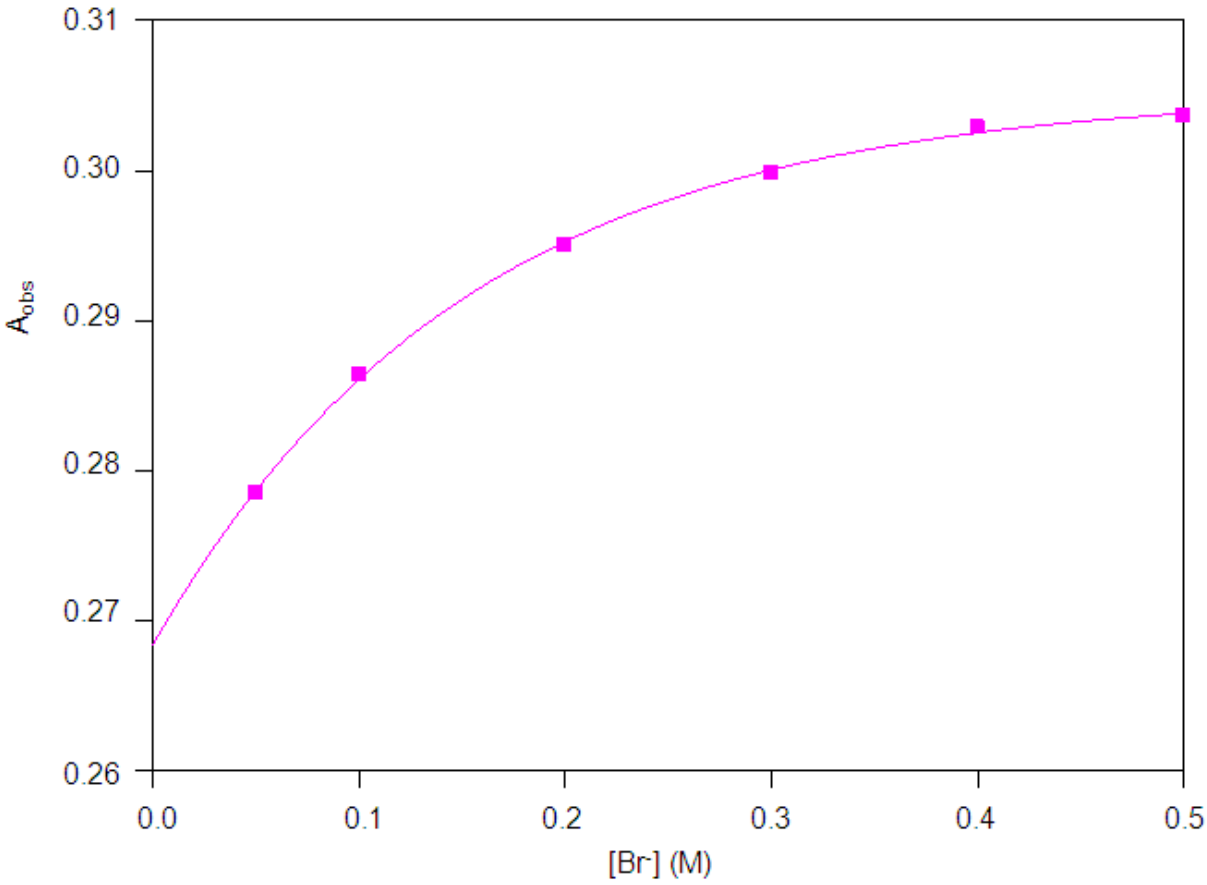

Figure 5-18: Plot of A_{obs} *vs* [Br^-] for the reaction of *fac*-[$Re(CO)_3(MeOH)(DiMeOPy)]^+$ with Br^- ions at 24.7 °C. [Re] = 1 x 10^{-4} M, λ = 342 nm.

Table 5-9: Summary of the rate constants of the reaction between *fac*-[$Re(CO)_3(MeOH)(DiMeOPy)]^+$ and Br^- ions at different temperatures, with [Br^-] = 0.05 M to 0.5 M. [Re] = 1 x 10^{-4} M, λ = 342 nm.

	15.6 °C	**24.7 °C**	**35.3 °C**	**45.6 °C**
$10^3 k_1$ ($M^{-1}s^{-1}$)	8.81 ± 0.04	28.7 ± 0.1	81.91 ± 0.09	228.3 ± 0.4
$10^3 k_{-1}$ (s^{-1})	0.07 ± 0.01	0.23 ± 0.04	0.62 ± 0.03	1.8 ± 0.1
K_1 (M^{-1})[a]	126 ± 18	125 ± 22	132 ± 6	127 ± 7
K_1 (M^{-1})[b]	103 ± 5	102 ± 8	102 ± 7	98 ± 8

a $K_1 = k_1/k_{-1}$; **b** $A_{obs} = \frac{A_M + A_{ML}K_1[X]}{1 + K_1[X]}$

The plot of ln(k_1/T) *vs* 1/T is presented in Figure **5-19**. A comparative discussion of the data will be undertaken in Paragraph 5.4.

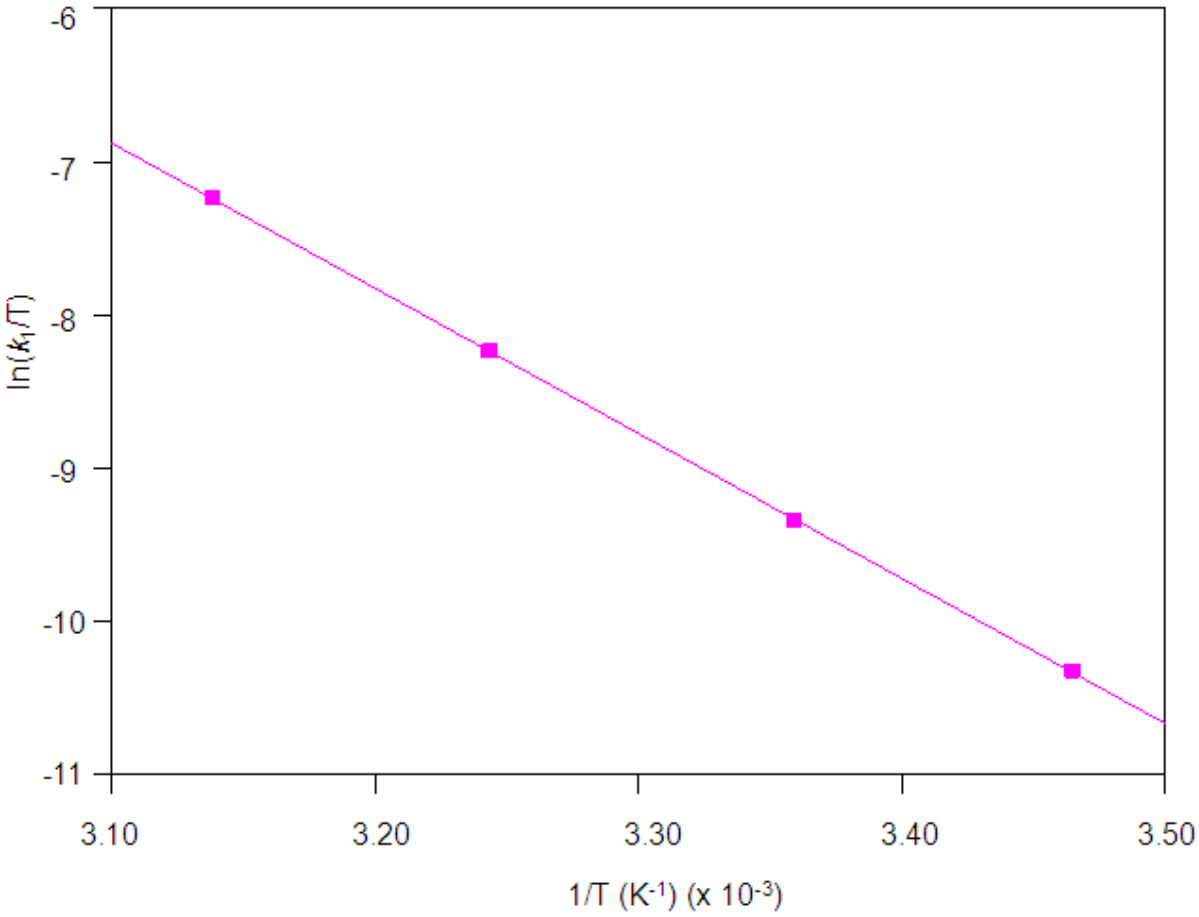

Figure 5-19: Plot of ln(k_1/T) *vs* 1/T for the reaction between *fac*-[Re(CO)$_3$(MeOH)(DiMeOPy]$^+$ and bromide ions for a temperature range of 15.6 °C to 45.6 °C.

5.3.2.5 Summary of the results of the methanol substitution reactions of fac-[Re(CO)$_3$(MeOH)(DiMeOPy)]$^+$

The substitution reactions between *fac*-[Re(CO)$_3$(MeOH)(DiMeOPy)]$^+$ and four different mondentate ligands have been studied (Paragraph 5.3.2.1 to 5.3.2.4, thiourea (TU), thiocyanate ions (NCS$^-$), tricyclohexylphosphine (PCy$_3$) and bromide ions (Br$^-$)).

The k_1 values (Table **5-10**) for the substitution reactions with different entering ligands are comparable to each other, with k_1 (Br$^-$) > k_1 (TU) > k_1 (NCS$^-$) > k_1 (PCy$_3$). A graph to illustrate the effect of the entering ligand on the rate of the reaction is given in Figure **5-20**. The reverse reaction rate constant, k_{-1} decreases in the following order Br$^-$ > TU > NCS$^-$ > PCy$_3$ while the stability constant, K_1, for these

reactions shows the following trend K_1 (Br^-) ≈ K_1 (NCS^-) > K_1 (TU) > K_1 (PCy_3) and fall within the range of 53 ± 1 to 138 ± 16 M^{-1}. A reasonably good agreement exists between the stability constants, K_1, determined kinetically and those determined thermodynamically. The enthalpy of activation ($\Delta H^{\ddagger}$) values for all the reactions are similar within experimental error and the small negative values of $\Delta S^{\ddagger}$ for the reactions with TU, NCS^-, PCy_3 and Br^- suggest an interchange associative type of activation, however the global fit value of the reaction with PCy_3 suggests an interchange dissociative type of activation. The $\Delta H^{\ddagger}$ and $\Delta S^{\ddagger}$ values calculated from the Eyring equation and the global fit are in reasonably good agreement except for the reaction with TU and PCy_3 (for $\Delta H^{\ddagger}$) and for the reaction with TU ($\Delta S^{\ddagger}$).

Table 5-10: Rate constants of the different reactions between *fac*-[Re(CO)$_3$(MeOH)(DiMeOPy)]$^+$ and different entering ligands at ~ 25 °C.

	$10^3 k_1$ ($M^{-1}s^{-1}$)	$10^3 k_{-1}$ (s^{-1})	K_1 (M^{-1})	$\Delta H^{\ddagger}$ ($kJmol^{-1}$)	$\Delta S^{\ddagger}$ ($JK^{-1}mol^{-1}$)
TU	13.7 ± 0.4	0.15 ± 0.01	91 ± 7[a], 86 ± 4[b]	73 ± 1[c], 61 ± 1[d]	-35 ± 4[c], -77 ± 4[d]
NCS^-	5.94 ± 0.02	0.043 ± 0.005	138 ± 16[a], 103 ± 7[b]	77 ± 1[c], 78.0 ± 0.3[d]	-27 ± 1[c], -26.4 ± 0.8[d]
PCy_3	1.56 ± 0.02	0.0295 ± 0.0006	53 ± 1[a], 59 ± 4[b]	80 ± 2[c], 94 ± 1[d]	-27 ± 2[c], 15 ± 4[d]
Br^-	28.7 ± 0.1	0.23 ± 0.04	125 ± 22[a], 102 ± 8[b]	78 ± 1[c], 77.9 ± 0.8[d]	-10 ± 1[c], -14 ± 2[d]

[a] $K_1 = k_1/k_{-1}$, [b] $A_{obs} = \frac{A_M + A_{ML}K_1[X]}{1 + K_1[X]}$; [c] Eyring fit, [d] Global fit.

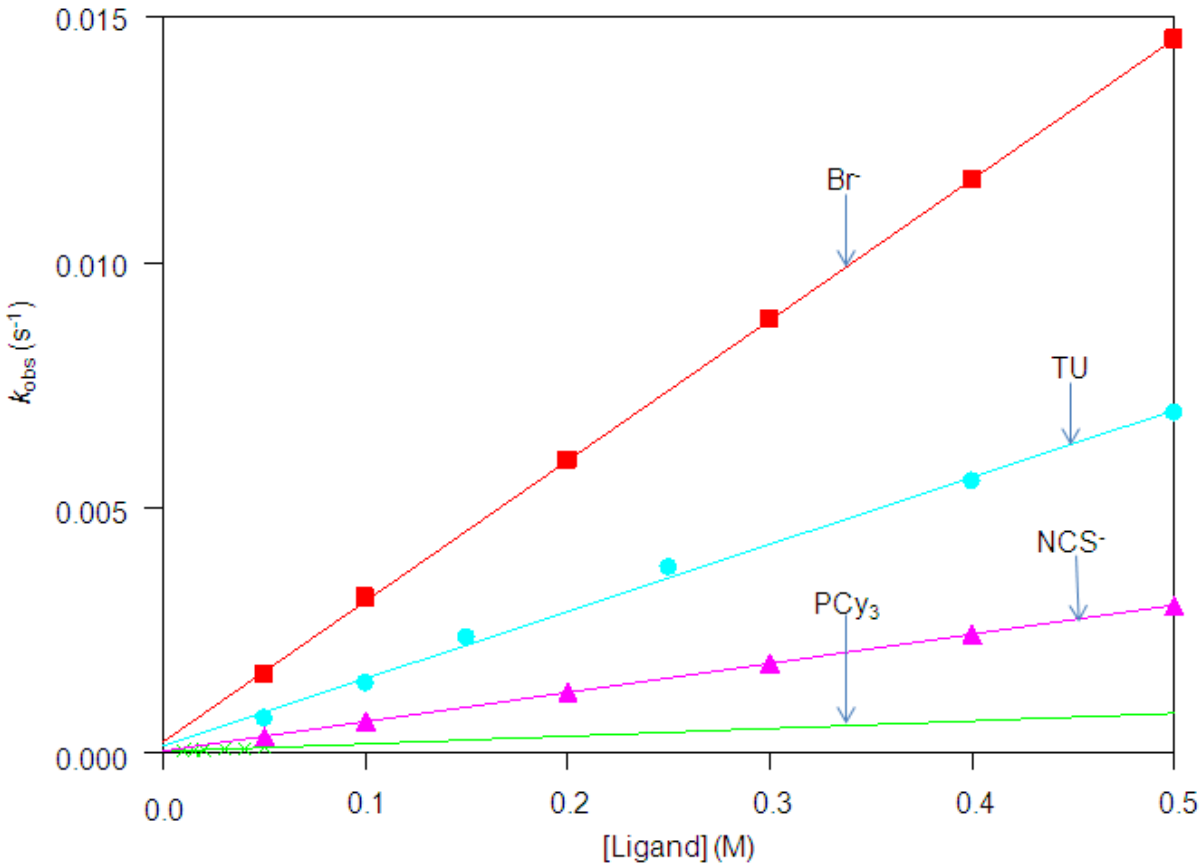

Figure 5-20: Schematic representation of k_{obs} *vs* [ligand] of the reactions between *fac*-[Re(CO)$_3$(MeOH)(DiMeOPy)]$^+$ and various entering ligands at ~ 25 °C.

5.3.3 Reaction between *fac*-[Re(CO)$_3$(MeOH)(4-MeTPh)] and entering ligands

The synthesis of *fac*-[Re(CO)$_3$(MeOH)(4-MeTPh)] from the starting synthon [NEt$_4$]$_2$[Re(CO)$_3$Br$_3$] has been described in Chapter 3. *fac*-[NEt$_4$][Re(CO)$_3$(Br)(4-MeTPh)] was dissolved in methanol and stirred for 24 hours to yield *fac*-[Re(CO)$_3$(MeOH)(4-MeTPh)]. The reaction between *fac*-[Re(CO)$_3$(MeOH)(4-MeTPh)] and four different monodentate ligands (thiourea (TU), thiocyanate (NCS$^-$), tricyclohexylphosphine (PCy$_3$) and bromide (Br$^-$)) were monitored with UV/Vis in methanol.

5.3.3.1 fac-[Re(CO)$_3$(MeOH)(4-MeTPh)] + TU

The methanol substitution reaction between *fac*-[Re(CO)$_3$(MeOH)(4-MeTPh)] and thiourea (TU) was performed 345 nm in methanol and at four different temperatures ranging between 14.3 °C and 45.7 °C, with [TU] varying from 0.05 M to 0.5 M. The final UV/Vis spectrum of the reaction solution is identical to the one obtained from the synthesized *fac*-[Re(CO)$_3$(TU)(4-MeTPh)] complex in Chapter 3.

The graph of k_{obs} *vs* [TU] at different temperatures is presented in Figure **5-21** below, the rate constants for the reactions are reported in Table **5-11** and the Eyring plot is illustrated in Figure **5-22**.

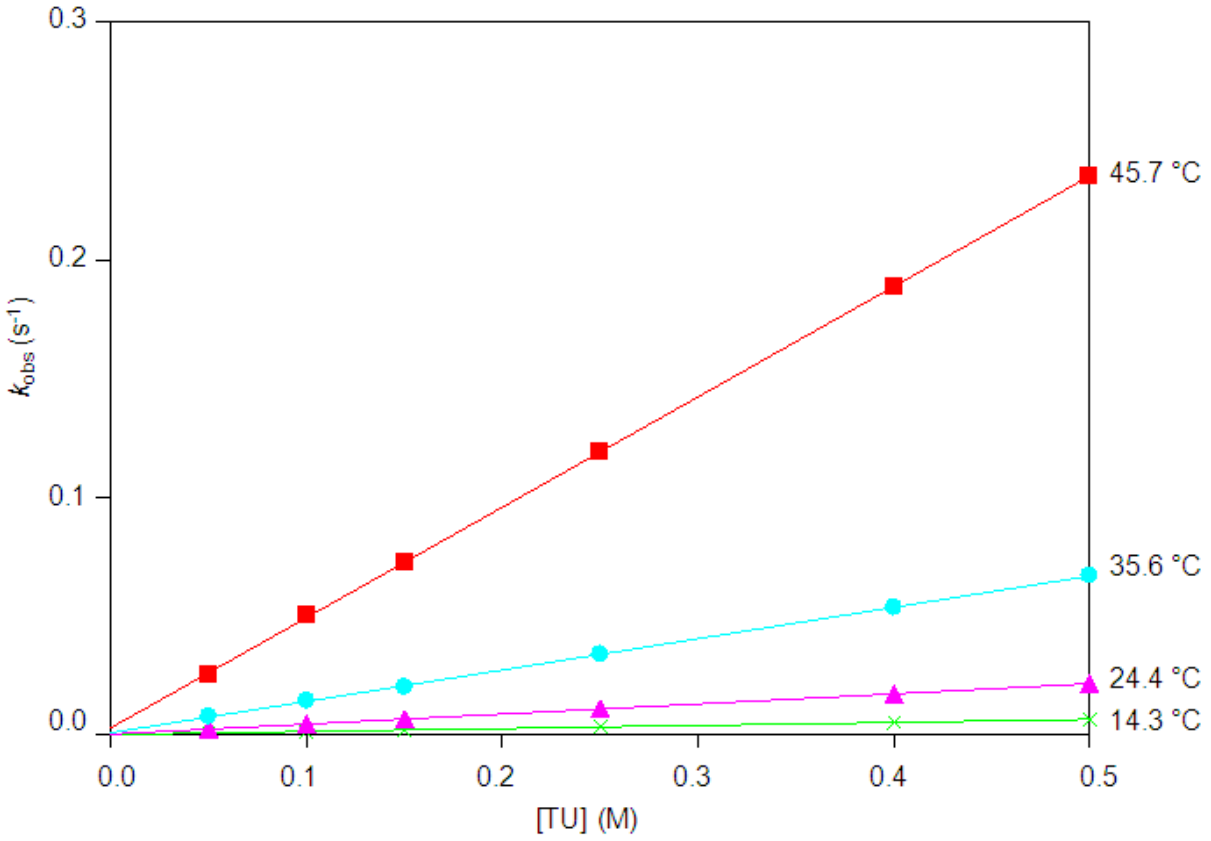

Figure 5-21: Plot of k_{obs} *vs* [TU] for the reaction between *fac*-[Re(CO)$_3$(MeOH)(4-MeTPh)] and thiourea at four different temperatures in methanol, with [TU] = 0.05 M to 0.5 M. [Re] = 3 x 10^{-4} M, λ = 345 nm.

The activation parameters have been calculated by the Eyring plot (Equation **3**) as well as the global fit of temperature *vs* ligand concentration *vs* k_{obs} data (Equation **4**) and the traditional Eyring plot yields similar results to the global fit. $\Delta H^{\ddagger}$ = 78 ± 1 kJmol^{-1} and $\Delta S^{\ddagger}$ = -7 ± 2 JK^{-1}mol^{-1} from the Eyring plot and $\Delta H^{\ddagger}$ = 99 ± 2 kJmol^{-1} and $\Delta S^{\ddagger}$ = 59 ± 5 JK^{-1}mol^{-1} from the global fit.

Table 5-11: Summary of the rate constants of the reaction between *fac*-[Re(CO)$_3$(MeOH)(4-MeTPh)] and TU at different temperatures, with [TU] = 0.05 M to 0.5 M. [Re] = 3 x 10^{-4} M, λ = 345 nm.

	14.3 °C	**24.4 °C**	**35.6 °C**	**45.7 °C**
$10^3 k_1$ ($M^{-1}s^{-1}$)	12.85 ± 0.06	42.5 ± 0.1	132.1 ± 0.8	465 ± 2
$10^3 k_{-1}$ (s^{-1})	0.09 ± 0.02	0.29 ± 0.04	0.88 ± 0.03	3.0 ± 0.6
K_1 (M^{-1})[a]	143 ± 32	147 ± 20	150 ± 5	155 ± 31
K_1 (M^{-1})[b]	136 ± 7	138 ± 4	135 ± 3	121 ± 7

[a] $K_1 = k_1/k_{-1}$; [b] $A_{obs} = \frac{A_M + A_{ML}K_1[X]}{1 + K_1[X]}$

The plot of ln(k_1/T) *vs* 1/T is presented in Figure **5-22**. A comparative discussion of the data will be undertaken in Paragraph 5.4.

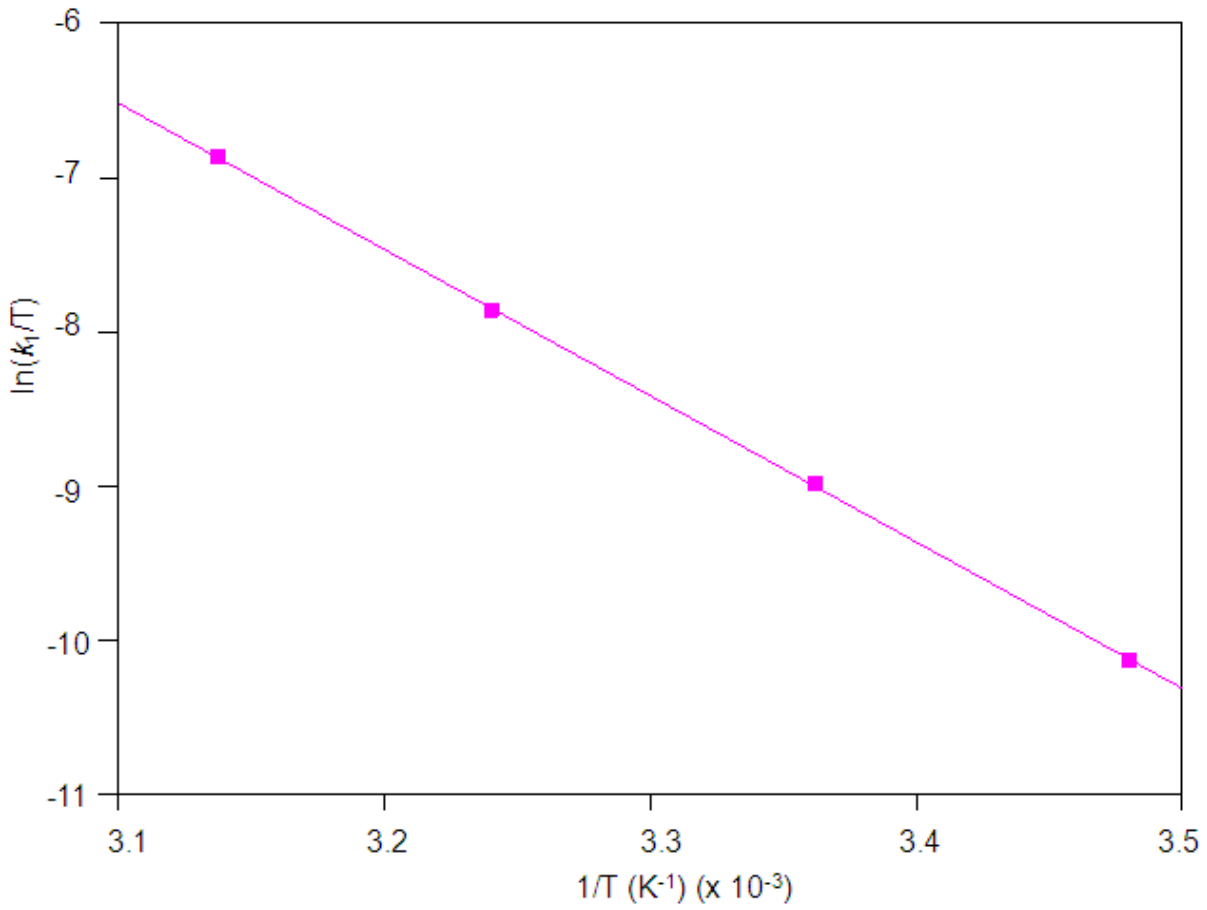

Figure 5-22: Plot of ln(k_1/T) *vs* 1/T for the reaction between *fac*-[Re(CO)$_3$(MeOH)(4-MeTPh)] and thiourea for a temperature range of 14.3 °C to 45.7 °C.

5.3.3.2 fac-[Re(CO)$_3$(MeOH)(4-MeTPh)] + NCS$^-$

The methanol substitution reaction between *fac*-[Re(CO)$_3$(MeOH)(4-MeTPh)] and thiocyanate was performed at 335 nm in methanol and at four different temperatures ranging between 15.4 °C and 44.9 °C, with [NCS$^-$] varying between 0.05 M and 0.5 M. The final UV/Vis spectrum of the reaction solution is identical to the one obtained from the synthesized *fac*-[Re(CO)$_3$(NCS)(4-MeTPh)]$^-$ complex in Chapter 3.

The graph of k_{obs} *vs* [NCS$^-$] at different temperatures is presented in Figure **5-23** below, the rate constants for the reaction are reported in Table **5-12** while the Eyring plot is illustrated in Figure **5-24**.

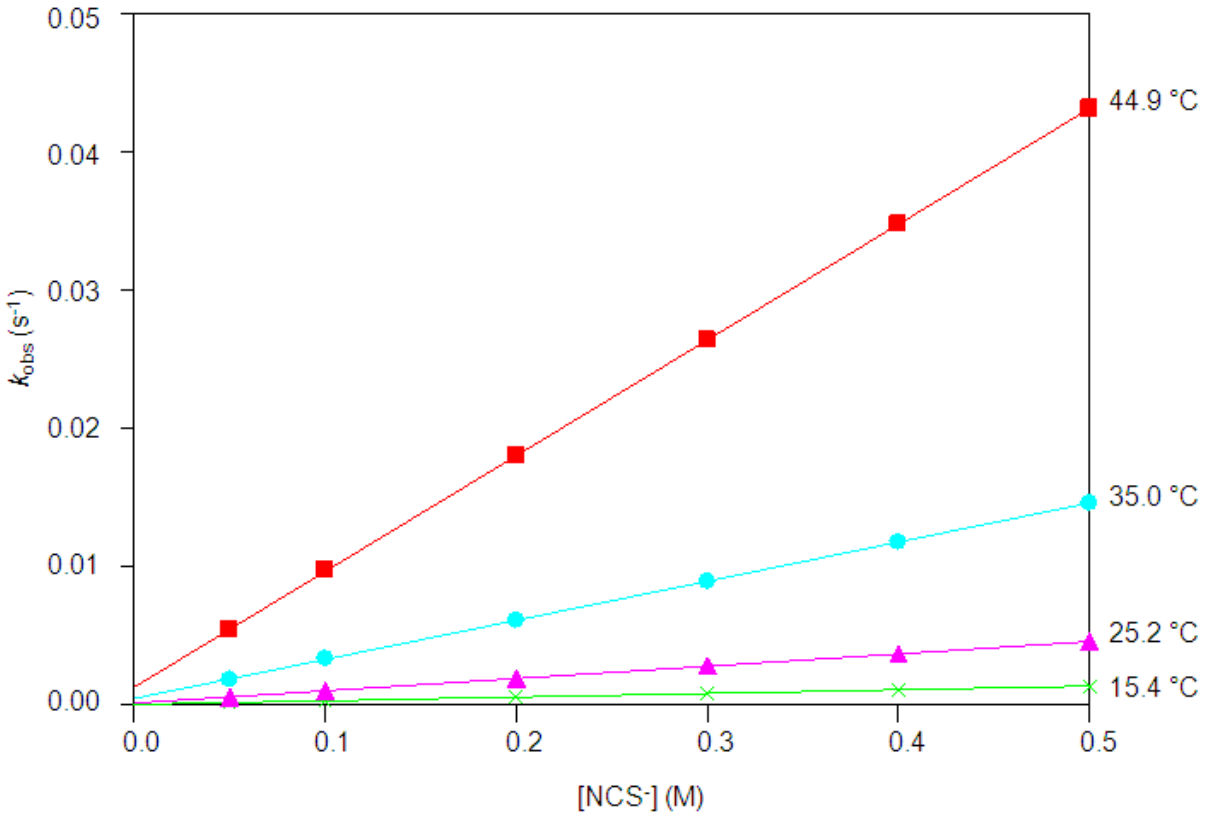

Figure 5-23: Plot of k_{obs} *vs* [NCS$^-$] for the reaction between *fac*-[Re(CO)$_3$(MeOH)(4-MeTPh)] and thiocyanate ions at four different temperatures in methanol, with [NCS$^-$] = 0.05 M to 0.5 M. [Re] = 3 x 10^{-4} M, λ = 335 nm.

The activation parameters have been calculated by the Eyring plot (Equation **3**) as well as the global fit of temperature *vs* ligand concentration *vs* k_{obs} data (Equation **4**) and it is clear that the traditional Eyring plot yields similar results to the global fit.

$\Delta H^{\ddagger}$ = 86 ± 1 kJmol^{-1} and $\Delta S^{\ddagger}$ = 7 ± 1 JK^{-1}mol^{-1} from the Eyring plot and $\Delta H^{\ddagger}$ = 86.8 ± 0.2 kJmol^{-1} and $\Delta S^{\ddagger}$ = 6.5 ± 0.7 JK^{-1}mol^{-1} from the global fit.

Table 5-12: Summary of the rate constants of the reaction between *fac*-[Re(CO)$_3$(MeOH)(4-MeTPh)] and NCS$^-$ ions at different temperatures, with [NCS$^-$] = 0.05 M to 0.5 M. [Re] = 3 x 10^{-4} M, λ = 335 nm.

	15.4 °C	**25.2 °C**	**35.0 °C**	**44.9 °C**
$10^3 k_1$ ($M^{-1}s^{-1}$)	2.66 ± 0.02	8.90 ± 0.04	28.3 ± 0.1	83.8 ± 0.1
$10^3 k_{-1}$ (s^{-1})	0.043 ± 0.007	0.15 ± 0.01	0.48 ± 0.03	1.30 ± 0.03
K_1 (M^{-1})[a]	62 ± 10	59 ± 4	59 ± 4	64 ± 1
K_1 (M^{-1})[b]	44 ± 4	50 ± 1	49.9 ± 0.8	49 ± 2

[a] $K_1 = k_1/k_{-1}$; [b] $A_{obs} = \frac{A_M + A_{ML}K_1[X]}{1 + K_1[X]}$

The plot of ln(k_1/T) *vs* 1/T is presented in Figure **5-24**. A comparative discussion of the data will be undertaken in Paragraph 5.4.

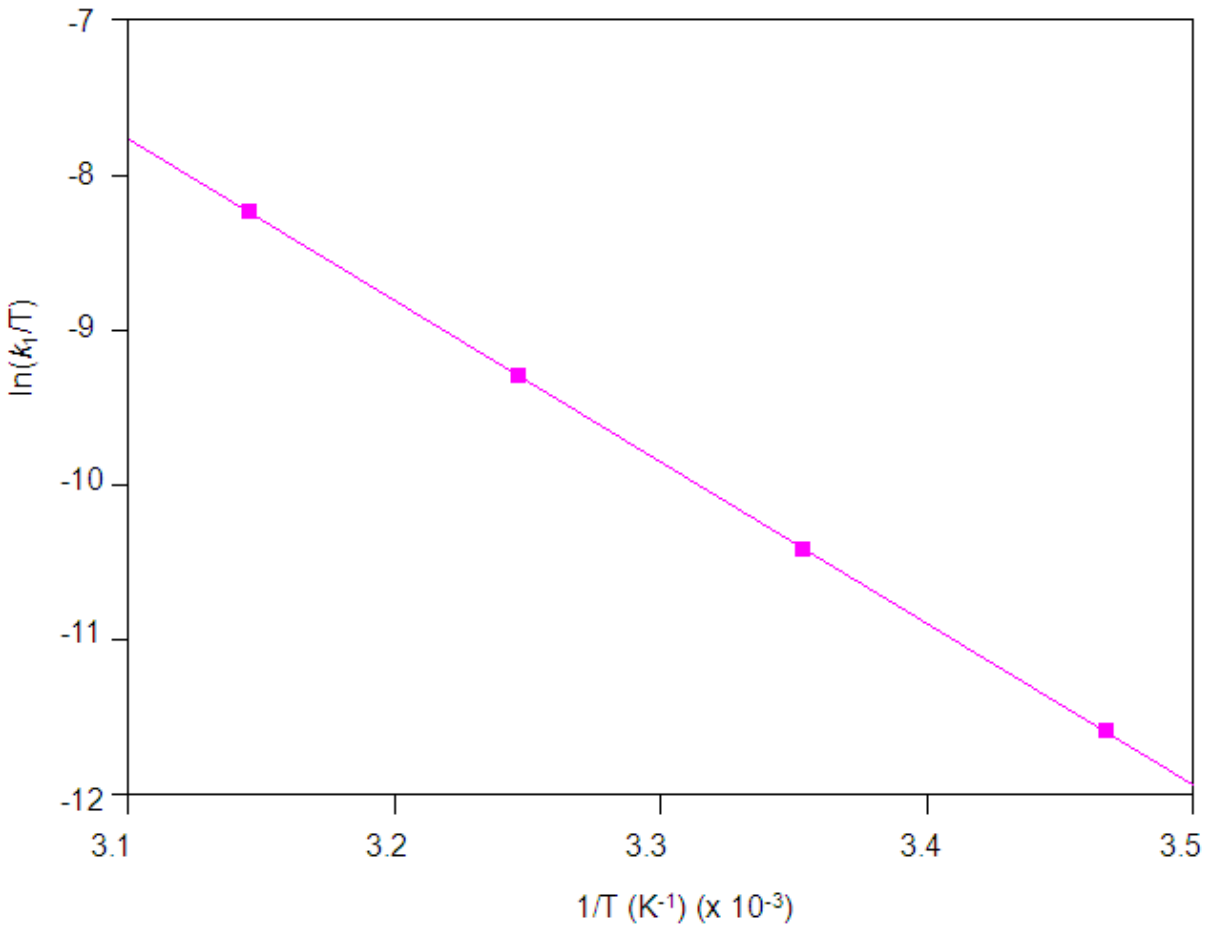

Figure 5-24: Plot of ln(k_1/T) *vs* 1/T for the reaction between *fac*-[Re(CO)$_3$(MeOH)(4-MeTPh)] and thiocyanate ions for a temperature range of 15.4 °C to 44.9 °C.

5.3.3.3 fac-[Re(CO)$_3$(MeOH)(4-MeTPh)] + PCy$_3$

The methanol substitution reaction between *fac*-[Re(CO)$_3$(MeOH)(4-MeTPh)] and tricyclohexylphosphine was performed at 335 nm in methanol and at four different temperatures ranging between 14.6 °C and 45.3 °C, with [PCy$_3$] varying between 0.01 M and 0.05 M. The concentration of PCy$_3$ could not be increased since the solution was saturated at 0.05 M in methanol. At concentrations lower than 0.01 M the absorbance change is too small; thus the smaller concentration range of 0.01 M to 0.05 M was used. The final UV/Vis spectrum of the reaction solution is identical to the one obtained from the synthesized *fac*-[Re(CO)$_3$(PCy$_3$)(4-MeTPh)] complex in Chapter 3.

The graph of k_{obs} *vs* [PCy$_3$] at different temperatures is presented in Figure **5-25** below, the rate constants for the reactions are reported in Table **5-13** and the Eyring plot is illustrated in Figure **5-26**.

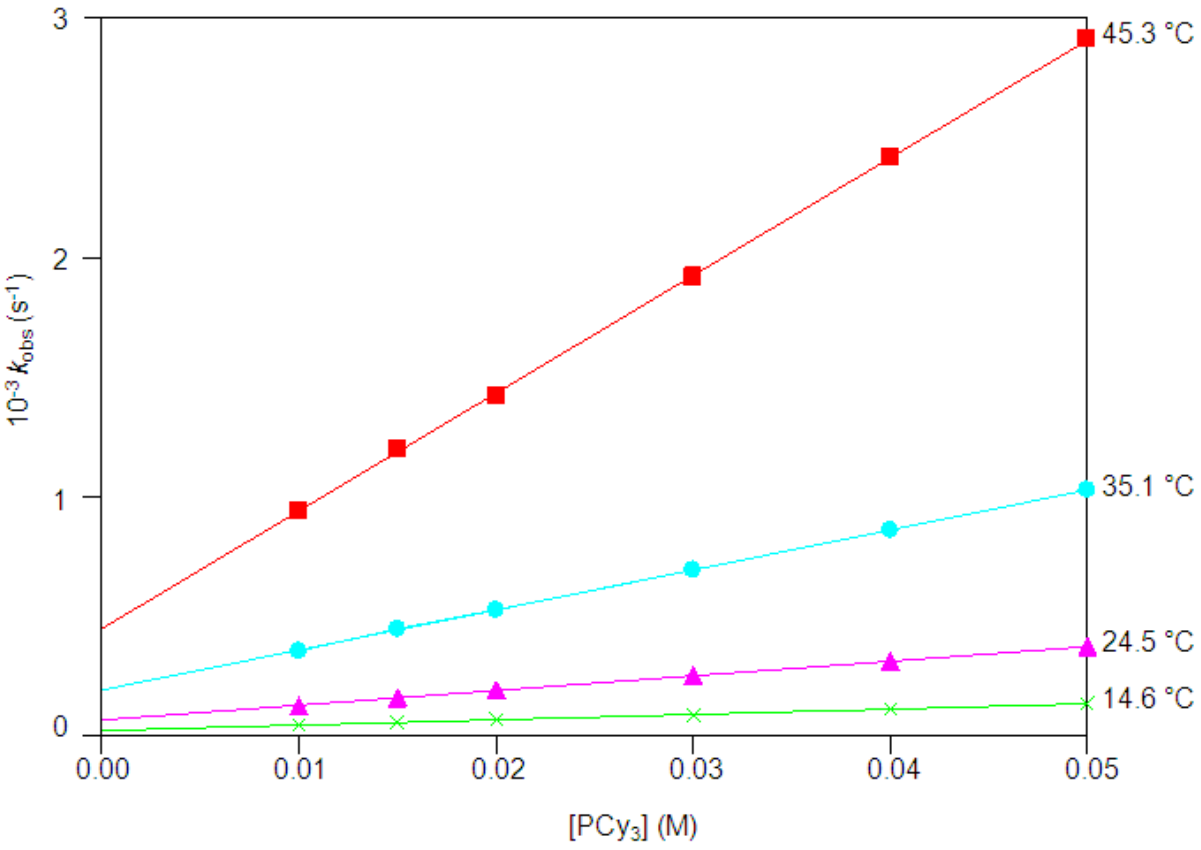

Figure 5-25: Plot of k_{obs} *vs* [PCy$_3$] for the reaction between *fac*-[Re(CO)$_3$(MeOH)(4-MeTPh)] and tricyclohexylphosphine at four different temperatures in methanol, with [PCy$_3$] = 0.01 M to 0.05 M. [Re] = 3 x 10^{-4} M, λ = 335 nm.

The activation parameters have been calculated by the Eyring plot (Equation **3**) as well as the global fit of temperature *vs* ligand concentration *vs* k_{obs} data (Equation **4**) and the traditional Eyring plot yields similar results to the global fit. $\Delta H^{\ddagger}$ = 75 ± 1 kJmol^{-1} and $\Delta S^{\ddagger}$ = -35 ± 3 JK^{-1}mol^{-1} from the Eyring plot and $\Delta H^{\ddagger}$ = 82.7 ± 0.8 kJmol^{-1} and $\Delta S^{\ddagger}$ = -11 ± 3 JK^{-1}mol^{-1} from the global fit.

Table 5-13: Summary of the rate constants of the reaction between *fac*-[Re(CO)$_3$(MeOH)(4-MeTPh)] and tricyclohexylphosphine at different temperatures, with [PCy$_3$] = 0.01 M to 0.05 M. [Re] = 3 x 10^{-4} M, λ = 335 nm.

	14.6 ˚C	**24.5 ˚C**	**35.1 ˚C**	**45.3 ˚C**
$10^3 k_1$ ($M^{-1}s^{-1}$)	2.23 ± 0.02	6.14 ± 0.08	16.73 ± 0.09	49.2 ± 0.3
$10^3 k_{-1}$ (s^{-1})	0.0231 ± 0.0006	0.064 ± 0.003	0.192 ± 0.003	0.449 ± 0.009
K_1 (M^{-1})[a]	97 ± 3	96 ± 5	87 ± 1	110 ± 2
K_1 (M^{-1})[b]	91 ± 6	94 ± 8	101 ± 9	93 ± 10

[a] $K_1 = k_1/k_{-1}$; [b] $A_{obs} = \frac{A_M + A_{ML}K_1[X]}{1 + K_1[X]}$

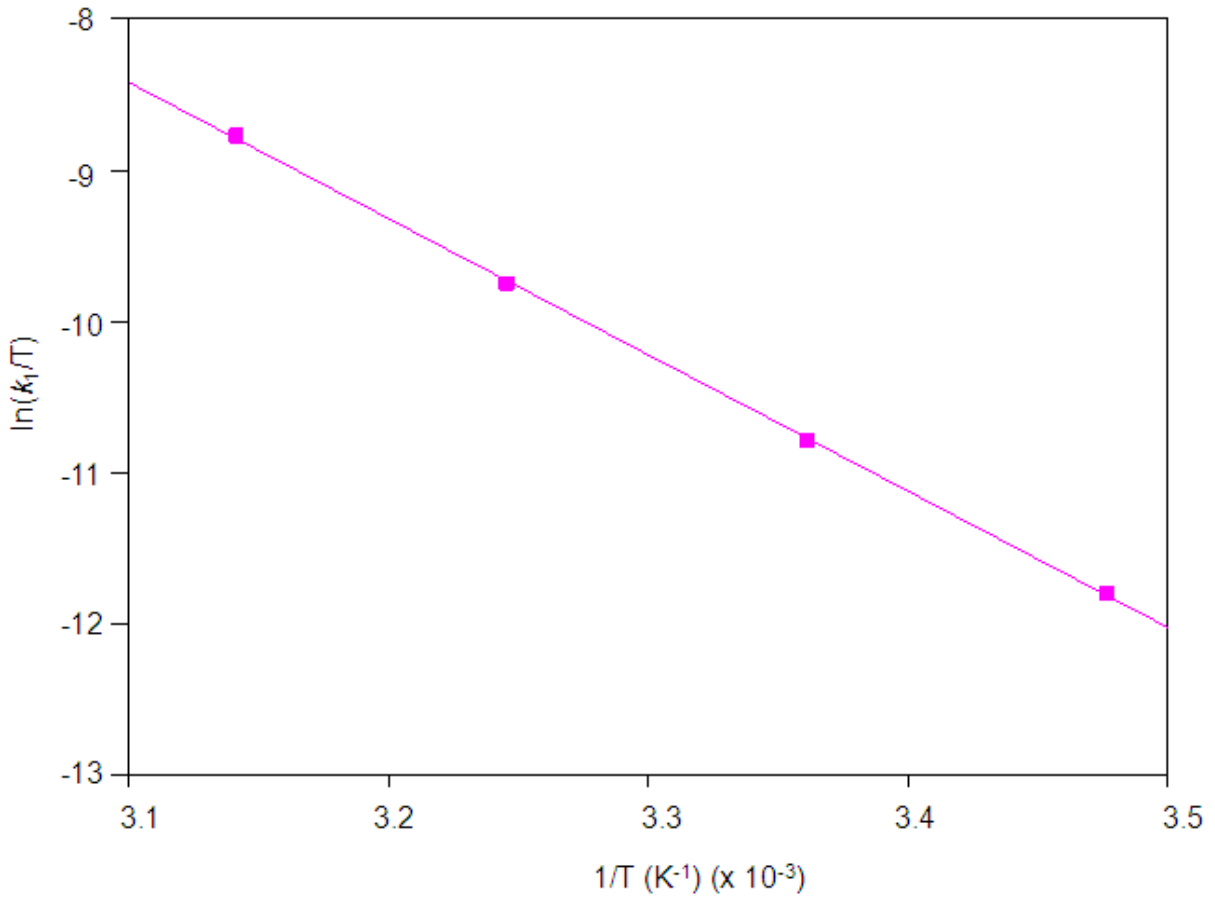

Figure 5-26: Plot of ln(k_1/T) *vs* 1/T for the reaction between *fac*-[Re(CO)$_3$(MeOH)(4-MeTPh)] and tricyclohexylphosphine for a temperature range of 14.6 °C to 45.3 °C.

The plot of $\ln(k_1/T)$ *vs* 1/T is presented in Figure **5-26**. A comparative discussion of the data will be undertaken in Paragraph 5.4.

5.3.3.4 fac-[Re(CO)$_3$(MeOH)(4-MeTPh)] + Br$^-$

The methanol substitution reaction between *fac*-[Re(CO)$_3$(MeOH)(4-MeTPh)] and bromide (Br^-) was performed at 330 nm in methanol and at four different temperatures ranging between 14.4 °C and 45.5 °C, with [Br^-] varying between 0.05 M and 0.5 M. The final UV/Vis spectrum of the reaction solution is identical to the one obtained from the synthesized *fac*-[Re(CO)$_3$(Br)(4-MeTPh)]$^-$ complex in Chapter 3.

The graph of k_{obs} *vs* [Br^-] at different temperatures is presented in Figure **5-27**. An illustration of the A_{obs} vs [Br^-], for the thermodynamically calculated equilibrium constant at 24.9 °C, is presented in Figure **5-28**. The rate constants for the reactions are reported in Table **5-14** and the Eyring plot is illustrated in Figure **5-29**.

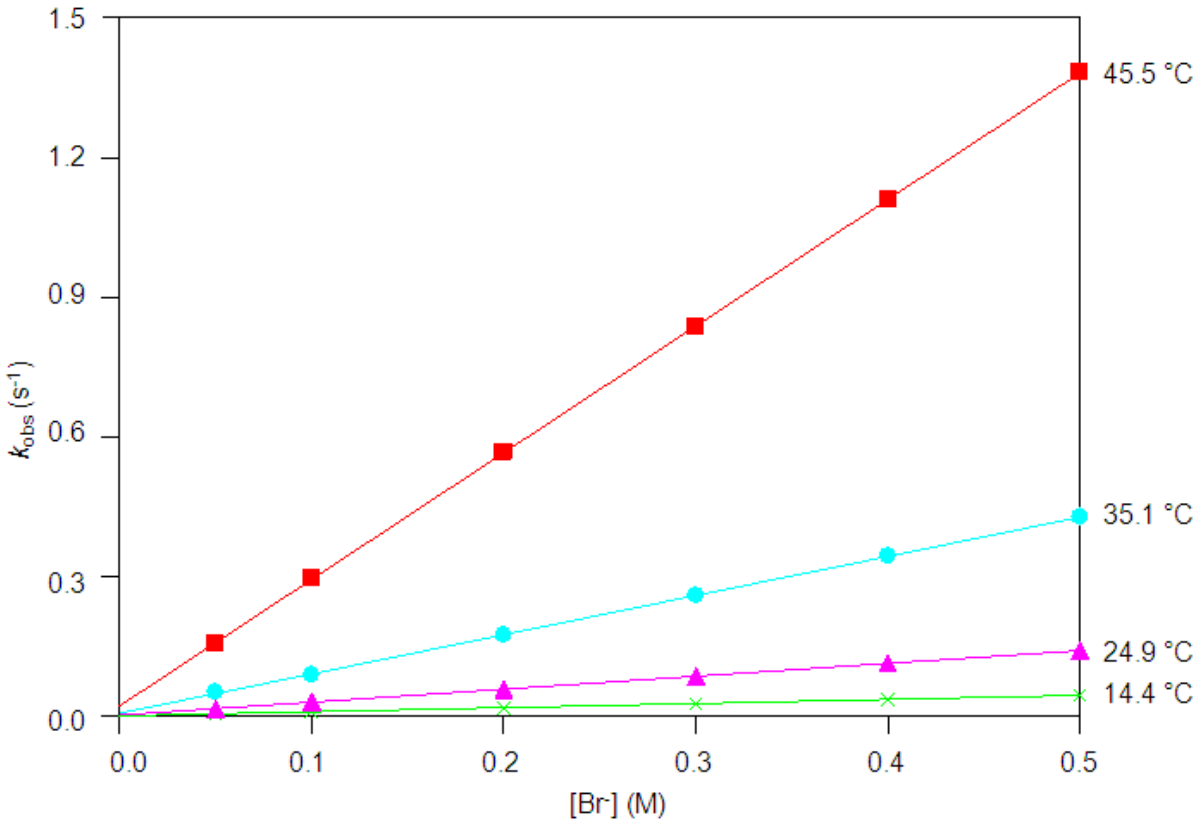

Figure 5-27: Plot of k_{obs} *vs* [Br^-] for the reaction between *fac*-[Re(CO)$_3$(MeOH)(4-MeTPh)] and bromide ions at four different temperatures in methanol, with [Br^-] = 0.05 M to 0.5 M. [Re] = 3 x 10^{-4} M, λ = 330 nm.

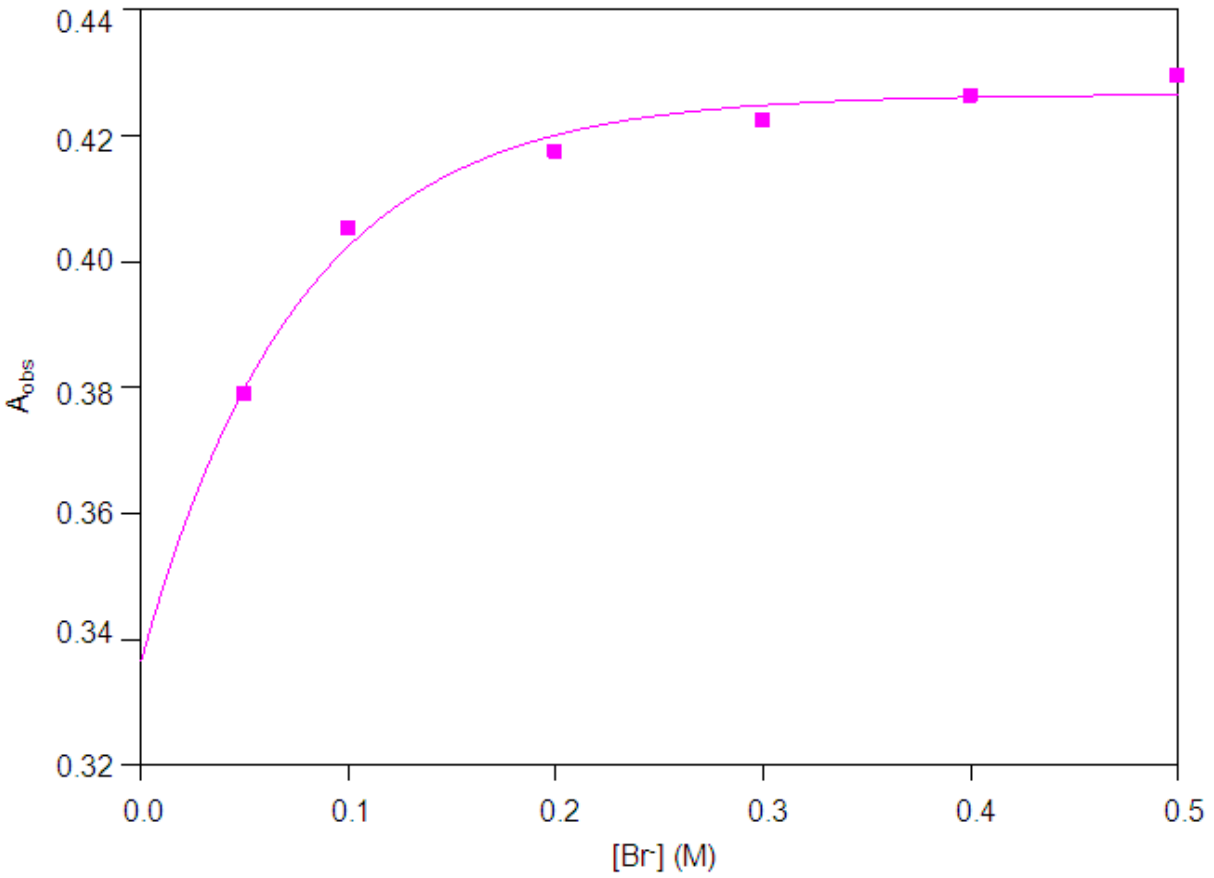

Figure 5-28: Plot of A_{obs} *vs* [Br^-] for the reaction of *fac*-[$Re(CO)_3$(MeOH)(4-MeTPh] with Br^- ions at 24.9 °C. [Re] = 3 x 10^{-4} M, 330 nm.

The activation parameters have been calculated by the Eyring plot (Equation **3**) as well as the global fit of temperature *vs* ligand concentration vs k_{obs} data (Equation **4**) and the traditional Eyring plot yields similar results to the global fit. $\Delta H^{\ddagger}$ = 81 ± 1 kJmol^{-1} and $\Delta S^{\ddagger}$ = 18 ± 3 JK^{-1}mol^{-1} from the Eyring plot and $\Delta H^{\ddagger}$ = 90.4 ± 0.8 kJmol^{-1} and $\Delta S^{\ddagger}$ = 46 ± 2 JK^{-1}mol^{-1} from the global fit.

Table 5-14: Summary of the rate constants of the reaction between *fac*-[$Re(CO)_3$(MeOH)(4-MeTPh)] and bromide ions at different temperatures, with [Br^-] = 0.05 M to 0.5 M. [Re] = 3 x 10^{-4} M, λ = 330 nm.

	14.4 °C	**24.9 °C**	**35.1 °C**	**45.5 °C**
$10^3 k_1$ ($M^{-1}s^{-1}$)	88.4 ± 0.4	277 ± 2	842 ± 5	2721 ± 6
$10^3 k_{-1}$ (s^{-1})	0.8 ± 0.1	2.6 ± 0.6	7 ± 1	22 ± 2
K_1 (M^{-1})[a]	111 ± 14	107 ± 25	120 ± 17	124 ± 11
K_1 (M^{-1})[b]	98 ± 3	100 ± 2	198 ± 5	100 ± 4

[a] $K_1 = k_1/k_{-1}$; [b] $A_{obs} = \frac{A_M + A_{ML}K_1[X]}{1 + K_1[X]}$

The plot of ln(k_1/T) *vs* 1/T is presented in Figure **5-29**. A comparative discussion of the data will be undertaken in Paragraph 5.4.

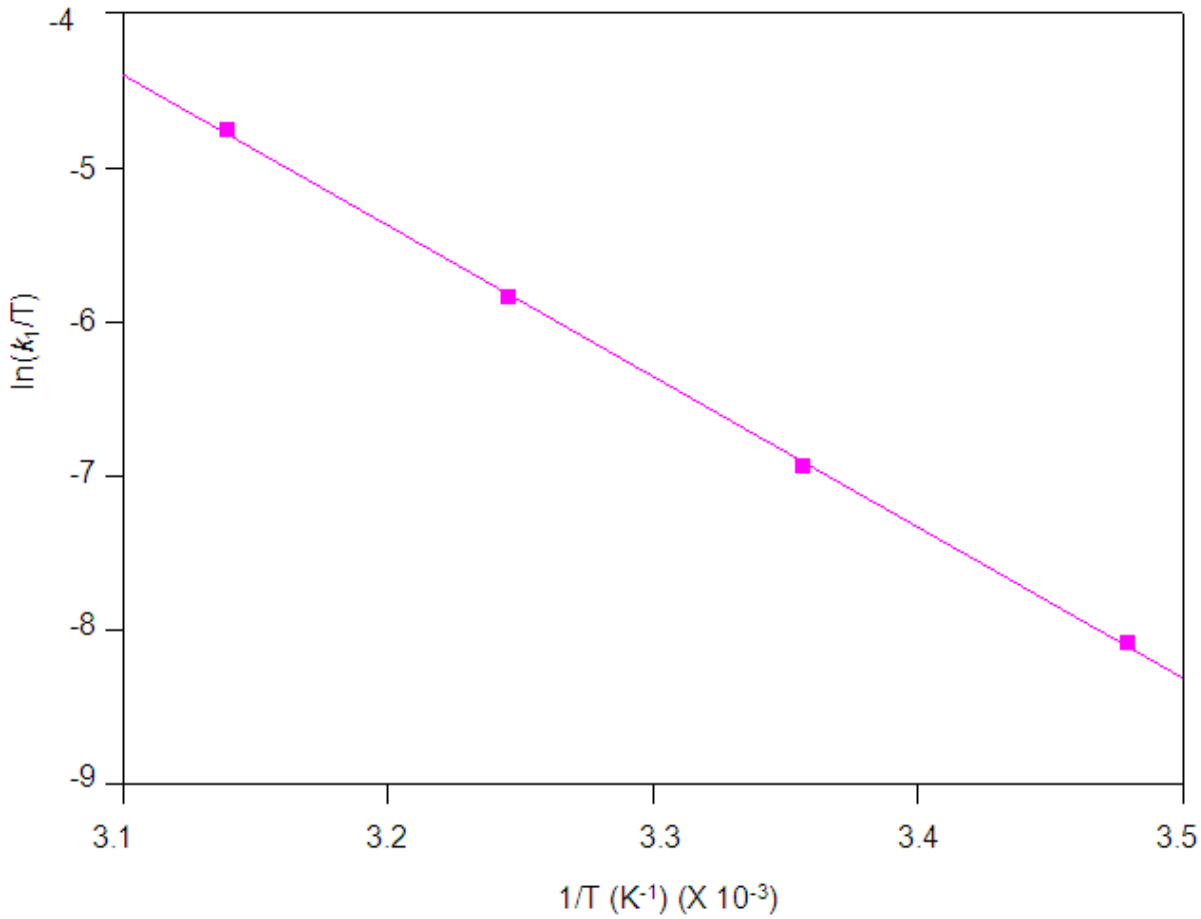

Figure 5-29: Plot of ln(k_1/T) *vs* 1/T for the reaction between *fac*-[Re(CO)$_3$(MeOH)(4-MeTPh] and bromide ions for a temperature range of 14.4 °C to 45.5 °C.

5.3.3.5 Summary of the results of the methanol substitution reactions of fac-[Re(CO)$_3$(MeOH)(4-MeTPh)]

The substitution reactions between *fac*-[Re(CO)$_3$(MeOH)(4-MeTPh)] and four different mondentate ligands have been studied (Paragraph 5.3.3.1 to 5.3.3.4, thiourea (TU), thiocyanate ions (NCS^-), tricyclohexylphosphine (PCy_3) and bromide ions (Br^-)).

The k_1 values (Table **5-15**) for the substitution reactions with different entering ligands form the following trend: $k_1(Br^-) > k_1$ (TU) > k_1 (NCS^-) > k_1 (PCy_3). A graph to illustrate the rates of the different entering ligands at ~ 25 °C is given in

Figure **5-30**. The reverse reaction rate constant, k_{-1} decreases in the following order Br^- > TU > NCS^- > PCy_3 while the stability constant for these reactions decreases in the following order K_1 (TU) > K_1 (Br^-) > K_1 (PCy_3) > K_1 (NCS^-) and fall within the range of 50 ± 1 to 147 ± 20 with the thiourea and bromide complexes being the most stable. A good agreement exists between the stability constants, K_1, determined kinetically and those determined thermodynamically. The enthalpy of activation ($\Delta H^{\ddagger}$) values for all the reactions are similar and a relatively good agreement is seen between the values obtained from the Eyring fit compared to the values obtained from the global fit. The small negative and small positive values for $\Delta S^{\ddagger}$ for all the reactions (with TU, NCS^-, PCy_3 and Br^-) suggest an interchange associative and/or interchange dissociative activation. The Eyring and global fit data do not correspond well and again emphasizes the large error in the $\Delta S^{\ddagger}$ values and the need for high pressure studies to confirm the mechanism of activation.

Table 5-15: Rate constants of the different reactions between *fac*-[Re(CO)$_3$(MeOH)(4-MeTPh)] and different entering ligands at ~ 25 °C.

	$10^3 k_1$ ($M^{-1}s^{-1}$)	$10^3 k_{-1}$ (s^{-1})	K_1 (M^{-1})	$\Delta H^{\ddagger}$ ($kJmol^{-1}$)	$\Delta S^{\ddagger}$ ($JK^{-1}mol^{-1}$)
TU	42.5 ± 0.1	0.29 ± 0.04	147 ± 20[a], 138 ± 4[b]	78 ± 1[c], 99 ± 2[d]	-7 ± 2[c], 59 ± 5[d]
NCS^-	8.90 ± 0.04	0.15 ± 0.01	59 ± 4[a], 50 ± 1[b]	86 ± 1[c], 86.8 ± 0.2[d]	-7 ± 1[c], 6.5 ± 0.7[d]
PCy_3	6.14 ± 0.08	0.064 ± 0.003	96 ± 5[a], 94 ± 8[b]	75 ± 1[c], 82.7 ± 0.8[d]	-35 ± 3[c], -11 ± 3[d]
Br^-	277 ± 2	2.6 ± 0.6	107 ± 25[a], 100 ± 2[b]	81 ± 1[c], 90.4 ± 0.8[d]	-18 ± 3[c], 46 ± 2[d]

[a] $K_1 = k_1/k_{-1}$; [b] $A_{obs} = \frac{A_M + A_{ML}K_1[X]}{1 + K_1[X]}$; [c] Eyring fit; [d] Global fit.

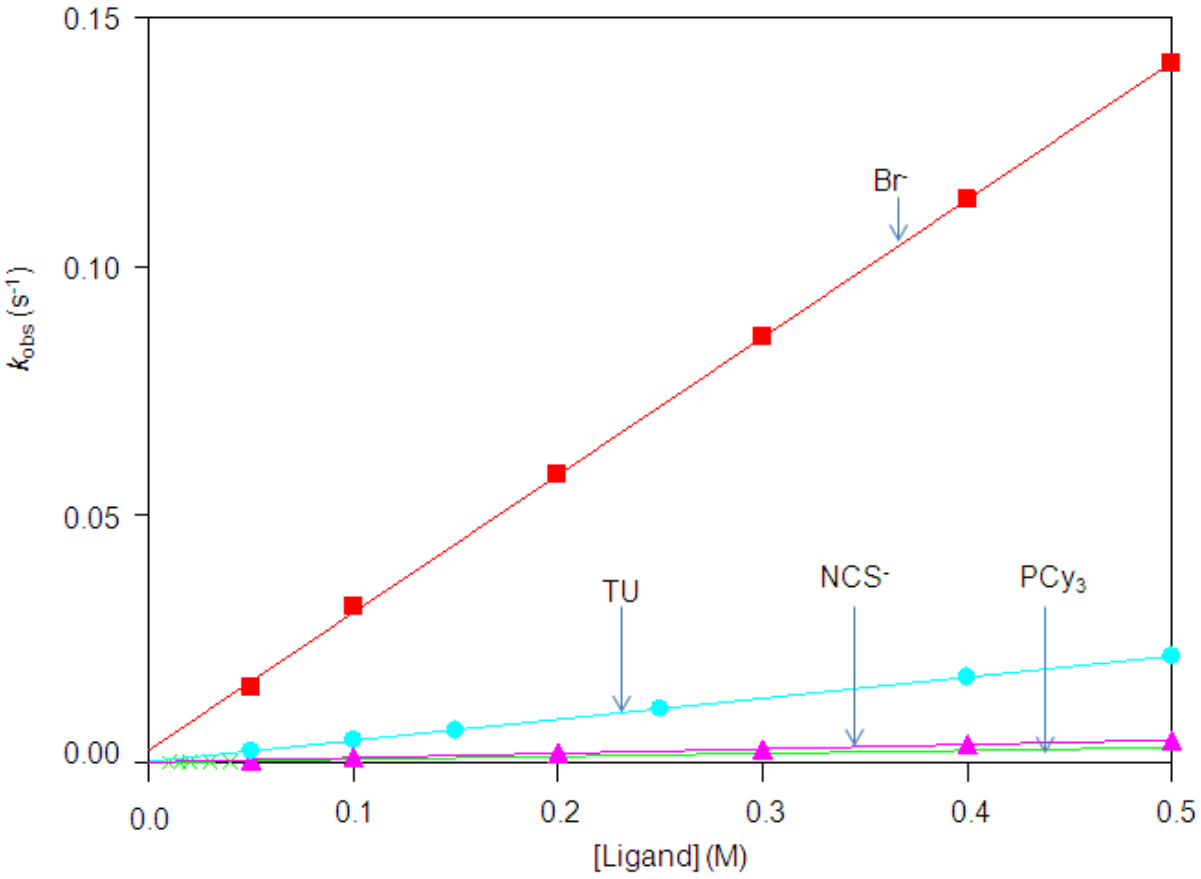

Figure 5-30: Schematic representation of k_{obs} *vs* [ligand] of the reactions between *fac*-[Re(CO)$_3$(MeOH)(4-MeTPh)] and various entering ligands at ~ 25 °C.

5.3.4 Reaction between *fac*-[Re(CO)$_3$(MeOH)(BrDiPhPr)] and entering ligands

The synthesis of *fac*[Re(CO)$_3$(MeOH)(BrDiPhPr)] from the starting synthon [NEt$_4$]$_2$[Re(CO)$_3$Br$_3$] has been described in Chapter 3. *fac*-[NEt$_4$][Re(CO)$_3$(Br)(BrDiPhPr)] was dissolved in methanol and stirred for 24 hours to yield *fac*-[Re(CO)$_3$(MeOH)(BrDiPhPr)]. The reaction between *fac*-[Re(CO)$_3$(MeOH)(BrDiPhPr)] and four different monodentate ligands (thiourea (TU), thiocyanate (NCS^-), triphenylphosphine (PPh_3) and bromide (Br^-)) were monitored with UV/Vis in methanol.

5.3.4.1 fac-[Re(CO)$_3$(MeOH)(BrDiPhPr)] + TU

The methanol substitution reaction between *fac*-[Re(CO)$_3$(MeOH)(BrDiPhPr)] and thiourea (TU) was performed at 345 nm in methanol and at four different temperatures ranging between 14.6 °C and 45.3 °C, with [TU] varying between 0.05 M and 0.5 M. The final UV/Vis spectrum of the reaction solution is identical to the one obtained from the synthesized *fac*-[Re(CO)$_3$(TU)(BrDiPhPr)] complex in Chapter 3.

The graph of k_{obs} *vs* [TU] at different temperatures is presented in Figure **5-31** below, the rate constants for the reactions are reported in Table **5-16** and the Eyring plot is illustrated in Figure **5-32**.

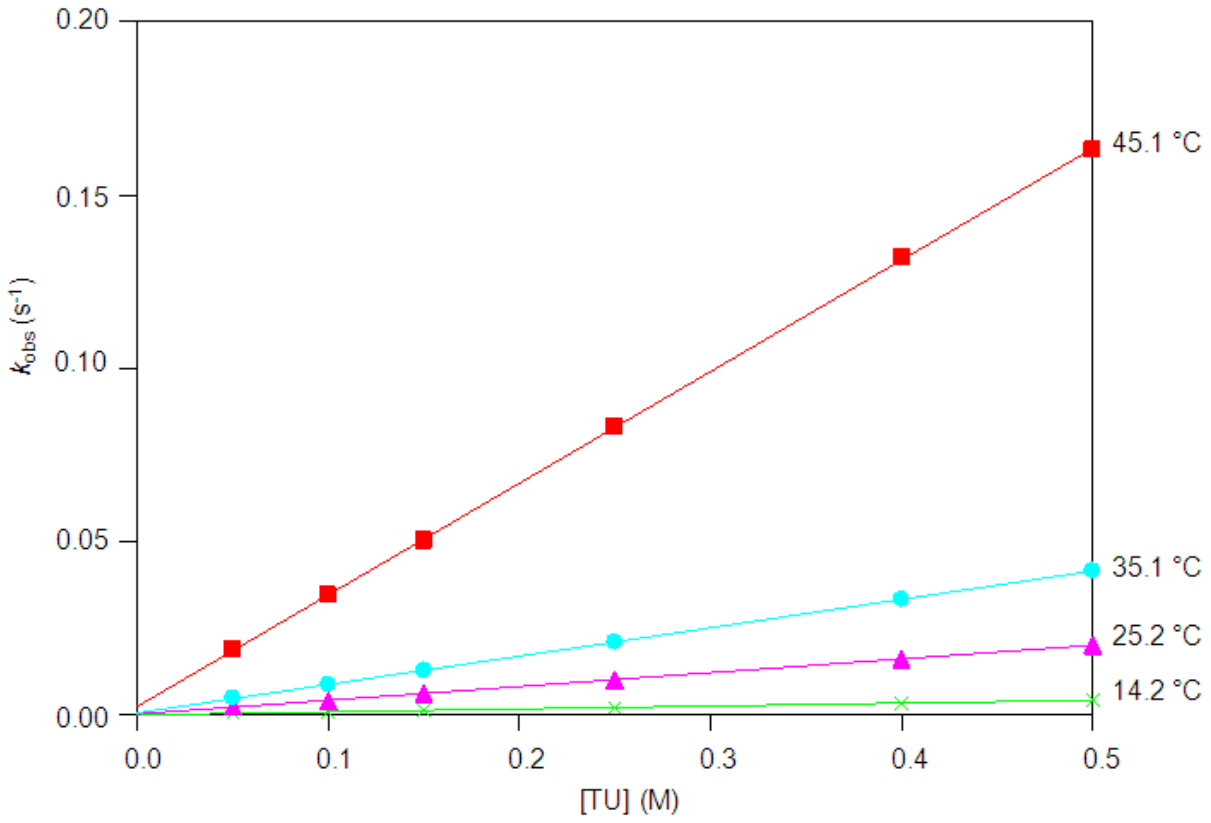

Figure 5-31: Plot of k_{obs} *vs* [TU] for the reaction between *fac*-[Re(CO)$_3$(MeOH)(BrDiPhPr)] and thiourea at four different temperatures in methanol, with [TU] = 0.05 M to 0.5 M. [Re] = 3 x10^{-4} M, λ = 345 nm.

The activation parameters have been calculated by the Eyring plot (Equation **3**) as well as the global fit of temperature *vs* ligand concentration *vs* k_{obs} data (Equation **4**): $\Delta H^{\ddagger}$ = 79 ± 1 kJmol^{-1} and $\Delta S^{\ddagger}$ = -4 ± 1 JK^{-1}mol^{-1} from the Eyring plot and $\Delta H^{\ddagger}$ = 101 ± 3 kJmol^{-1} and $\Delta S^{\ddagger}$ = 61 ± 11 JK^{-1}mol^{-1} from the global fit.

Table 5-16: Summary of the rate constants of the reaction between *fac*-[Re(CO)$_3$(MeOH)(BrDiPhPr)] and thiourea at different temperatures in methanol, with [TU] = 0.05 M to 0.5 M. [Re] = 3 x10^{-4} M, λ = 345 nm.

	14.6 °C	**24.5** °C	**35.1** °C	**45.3** °C
$10^3 k_1$ ($M^{-1}s^{-1}$)	8.52 ± 0.04	39.6 ± 0.2	81.8 ± 0.2	322 ± 1
$10^3 k_{-1}$ (s^{-1})	0.07 ± 0.01	0.33 ± 0.06	0.67 ± 0.07	2.5 ± 0.4
K_1 (M^{-1})[a]	122 ± 17	120 ± 22	122 ± 13	129 ± 21
K_1 (M^{-1})[b]	116 ± 8	112 ± 3	104 ± 6	106 ± 6

[a] $K_1 = k_1/k_{-1}$; [b] $A_{obs} = \frac{A_M + A_{ML}K_1[X]}{1 + K_1[X]}$

The plot of ln(k_1/T) *vs* 1/T is presented in Figure **5-32**. A comparative discussion of the data will be undertaken in Paragraph 5.4.

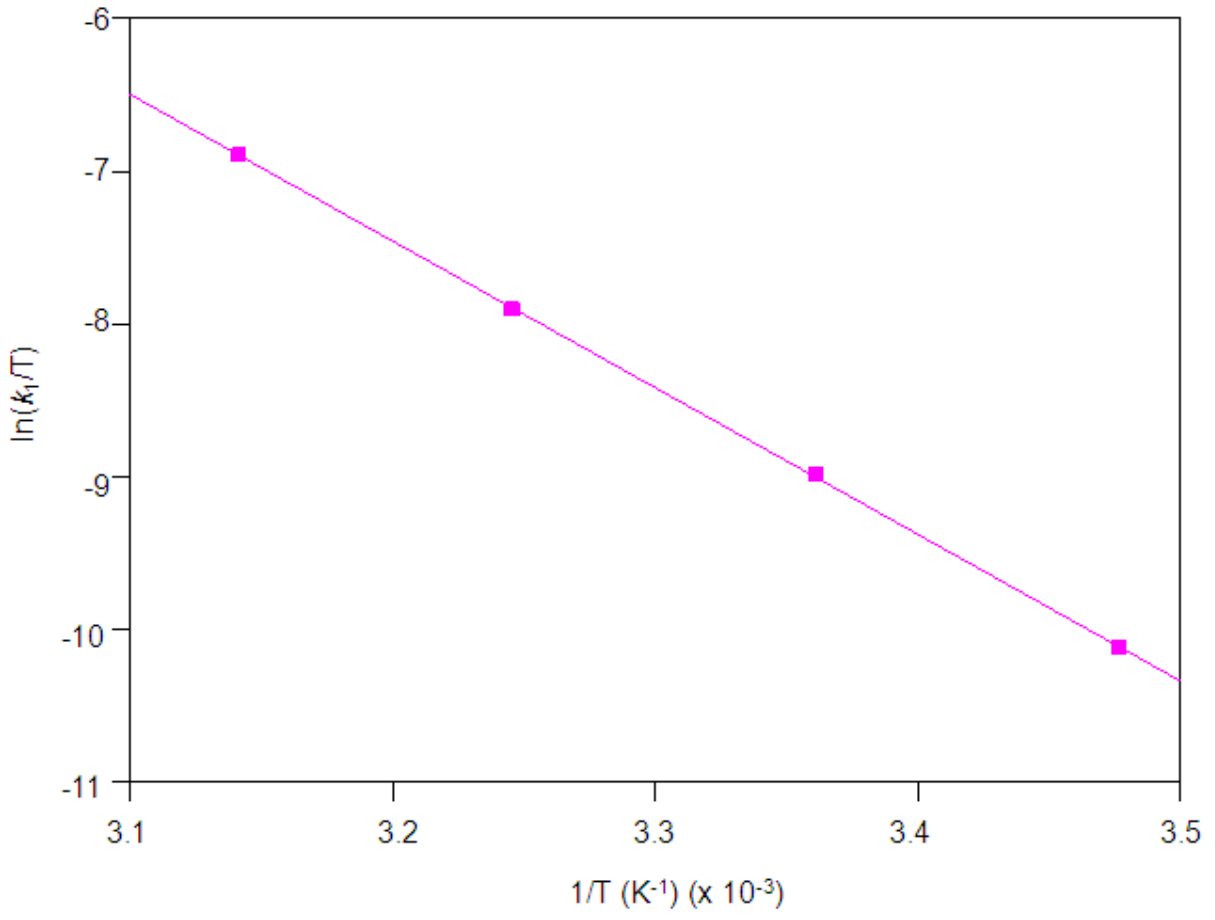

Figure 5-32: Plot of ln(k_1/T) *vs* 1/T for the reaction between *fac*-[Re(CO)$_3$(MeOH)(BrDiPhPr] and thiourea for a temperature range of 14.6 °C to 45.3 °C.

5.3.4.2 fac-[Re(CO)$_3$(MeOH)(BrDiPhPr)] + NCS$^-$

The methanol substitution reaction between *fac*-[Re(CO)$_3$(MeOH)(BrDiPhPr)] and thiocyanate was performed at 340 nm in methanol and at four different temperatures ranging between 14.5 °C and 45.3 °C, with [NCS$^-$] varying between 0.05 M and 0.5 M. The final UV/Vis spectrum of the reaction solution is identical to the one obtained from the synthesized *fac*-[Re(CO)$_3$(NCS)(BrDiPhPr)]$^-$ complex in Chapter 3. The graph of k_{obs} *vs* [NCS$^-$] at different temperatures is presented in Figure **5-33** below, the rate constants for the reaction are reported in Table **5-17** while the Eyring plot is illustrated in Figure **5-34**.

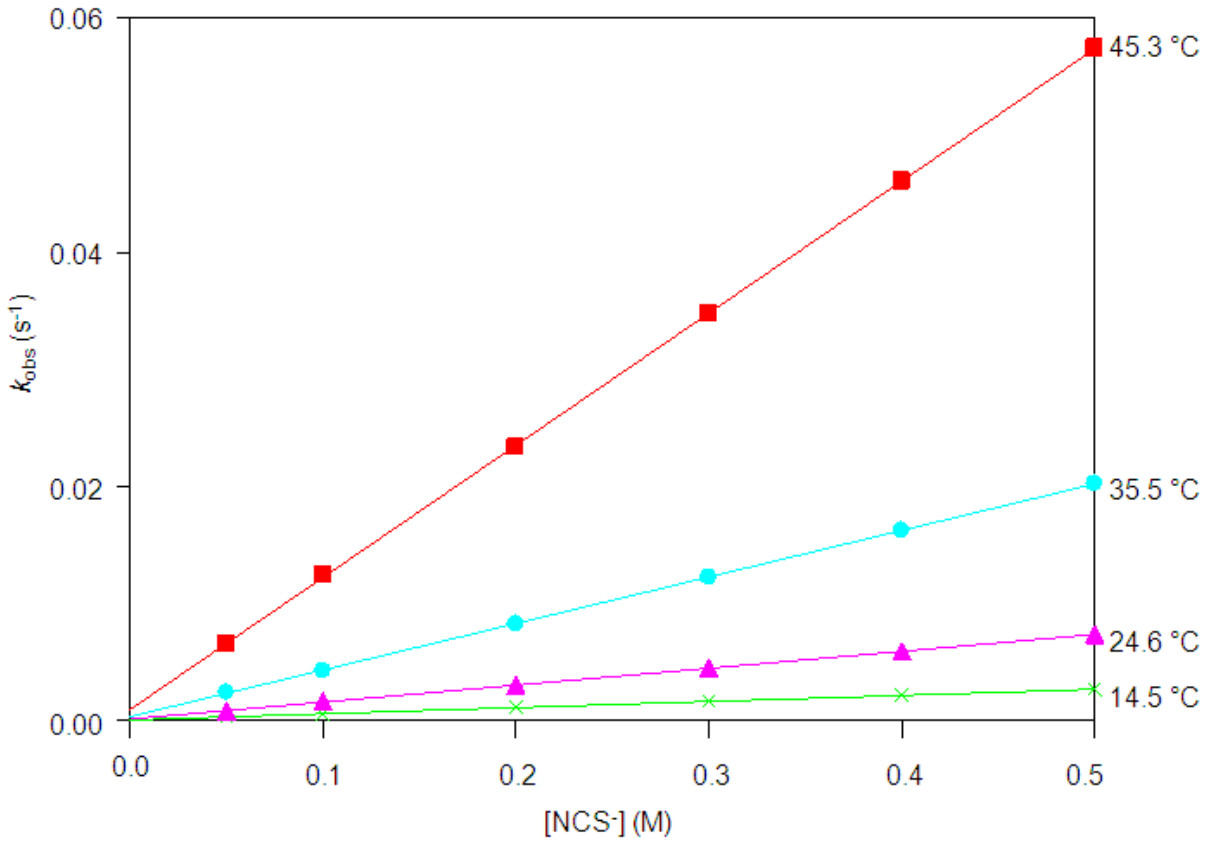

Figure 5-33: Plot of k_{obs} *vs* [NCS$^-$] for the reaction between *fac*-[Re(CO)$_3$(MeOH)(BrDiPhPr] and thiocyanate ions at four different temperatures in methanol, with [NCS$^-$] = 0.05 M to 0.5 M. [Re] = 3 x10^{-4} M, λ = 340 nm.

The activation parameters have been calculated by the Eyring plot (Equation **3**) as well as the global fit of temperature *vs* ligand concentration *vs* k_{obs} data (Equation **4**) and the traditional Eyring plot yields similar results to the global fit. $\Delta H^{\ddagger}$ = 73 ± 1 kJmol^{-1} and $\Delta S^{\ddagger}$ = -33 ± 4 JK^{-1}mol^{-1} from the Eyring plot and $\Delta H^{\ddagger}$ = 81 ± 1 kJmol^{-1} and $\Delta S^{\ddagger}$ = -11 ± 3 JK^{-1} mol^{-1} from the global fit.

Table 5-17: Summary of the rate constants of the reaction between *fac*-[Re(CO)$_3$(MeOH)(BrDiPhPr)] and NCS$^-$ at different temperatures in methanol, with [NCS$^-$] = 0.05 M to 0.5 M. [Re] = 3 x10^{-4} M, λ = 340 nm.

	14.5 °C	**24.6 °C**	**35.5 °C**	**45.3 °C**
$10^3 k_1$ ($M^{-1}s^{-1}$)	5.23 ± 0.01	14.466 ± 0.006	39.8 ± 0.2	113.0 ± 0.5
$10^3 k_{-1}$ (s^{-1})	0.041 ± 0.004	0.121 ± 0.002	0.33 ± 0.05	0.9 ± 0.1
K_1 (M^{-1})[a]	128 ± 12	120 ± 2	121 ± 18	126 ± 14
K_1(M^{-1})[b]	120 ± 5	120 ± 4	116 ± 9	115 ± 2

a $K_1 = k_1/k_{-1}$; **b** $A_{obs} = \frac{A_M + A_{ML}K_1[X]}{1 + K_1[X]}$

The plot of ln(k_1/T) *vs* 1/T is presented in Figure **5-34**. A comparative discussion of the data will be undertaken in Paragraph 5.4.

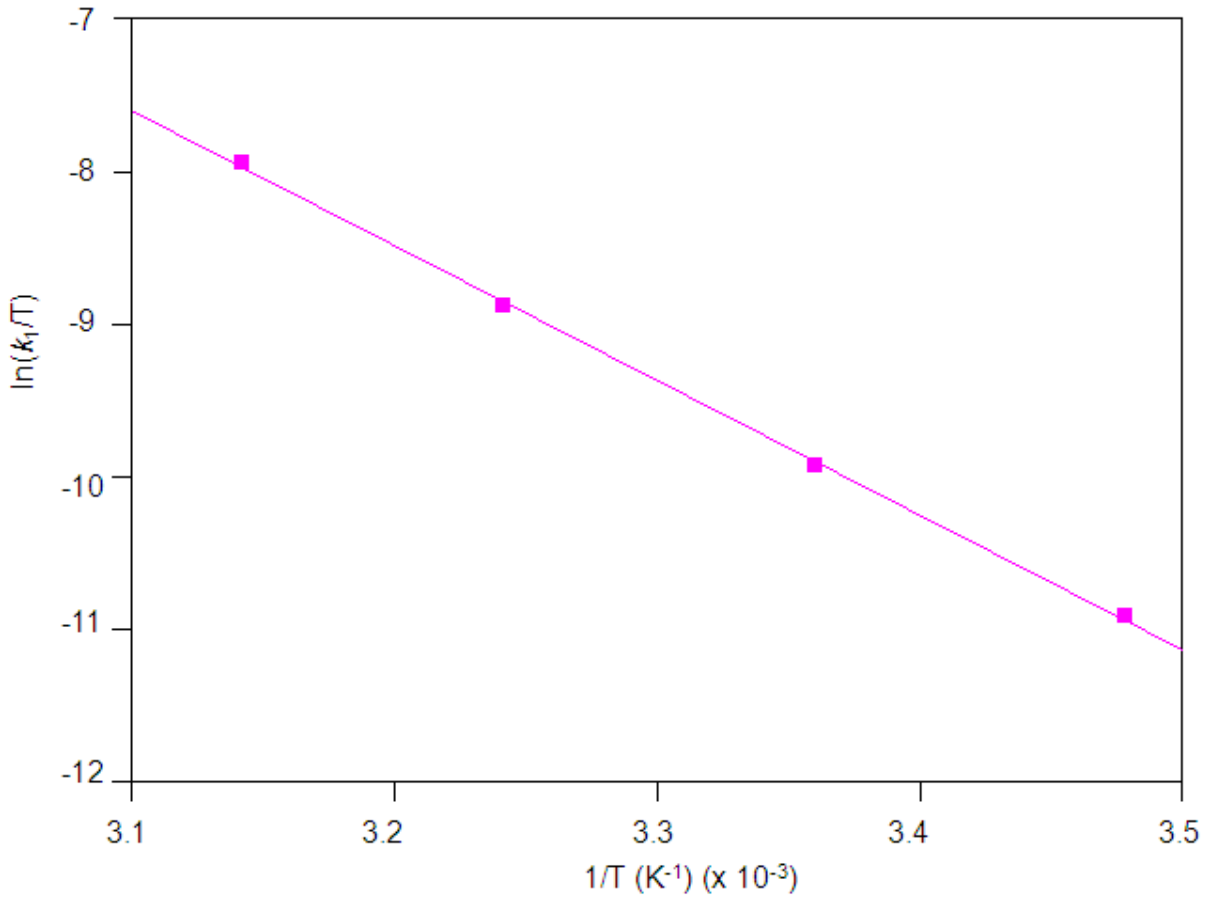

Figure 5-34: Plot of ln(k_1/T) *vs* 1/T for the reaction between *fac*-[Re(CO)$_3$(MeOH)(BrDiPhPr)] and thiocyanate ions for a temperature range of 14.5 °C to 45.3 °C.

5.3.4.3 fac-[Re(CO)$_3$(MeOH)(BrDiPhPr)] + PPh$_3$

The methanol substitution reaction between *fac*-[Re(CO)$_3$(MeOH)(BrDiPhPr)] and triphenylphosphine (PPh$_3$) was performed at 330 nm in methanol and at four different temperatures ranging between 14.6 °C to 45.3 °C, with [PPh$_3$] varying between 0.005 M and 0.05 M. The concentration of PPh$_3$ could not be increased since the solution was saturated at 0.05 M in methanol. At concentrations lower than 0.005 M the absorbance change is too small; thus the smaller concentration range of 0.005 M to 0.05 M was used. The final UV/Vis spectrum of the reaction solution is identical to the one obtained from the synthesized *fac*-[Re(CO)$_3$(PPh$_3$)(BrDiPhPr)] complex in Chapter 3. The graph of k_{obs} *vs* [PPh$_3$] at different temperatures is presented in Figure **5-35** below, the rate constants for the reaction are reported in Table **5-18** while the Eyring plot is illustrated in Figure **5-36**.

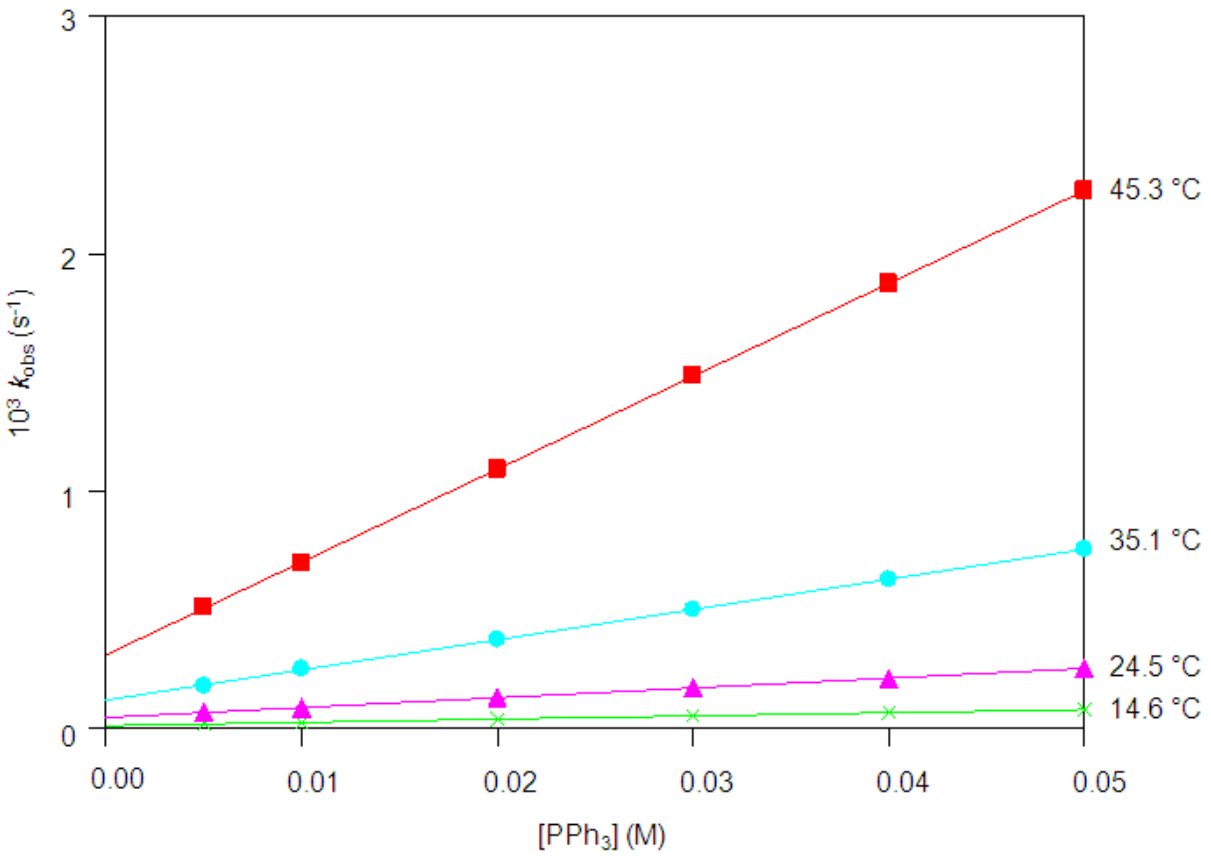

Figure 5-35: Plot of k_{obs} vs [PPh$_3$] for the reaction between *fac*-[Re(CO)$_3$(MeOH)(BrDiPhPr)] and triphenylphosphine at four different temperatures in methanol, with [PPh$_3$] = 0.005 M to 0.05 M. [Re] = 3 x10^{-4} M, λ = 330 nm.

The activation parameters have been calculated by the Eyring plot (Equation **3**) as well as the global fit of temperature *vs* ligand concentration *vs* k_{obs} data (Equation **4**) and the traditional Eyring plot yields similar results to the global fit. $\Delta H^{\ddagger}$ = 80 ± 2 kJmol^{-1} and $\Delta S^{\ddagger}$ = -20 ± 5 JK^{-1}mol^{-1} from the Eyring plot and $\Delta H^{\ddagger}$ = 87 ± 1 kJmol^{-1} and $\Delta S^{\ddagger}$ = 9 ± 3 JK^{-1}mol^{-1} from the global fit.

Table 5-18: Summary of the rate constants of the reaction between *fac*-[Re(CO)$_3$(MeOH)(BrDiPhPr)] and triphenylphosphine at four different temperatures, with [PPh$_3$] = 0.005 M to 0.05 M. [Re] = 3 x10^{-4} M, λ = 330 nm.

	14.6 ˚C	**24.5 ˚C**	**35.1 ˚C**	**45.3 ˚C**
$10^3 k_1$ ($M^{-1}s^{-1}$)	1.364 ± 0.008	4.30 ± 0.05	12.72 ± 0.07	39.2 ± 0.1
$10^3 k_{-1}$ (s^{-1})	0.0114 ± 0.0002	0.039 ± 0.001	0.119 ± 0.002	0.310 ± 0.004
K_1 (M^{-1})[a]	120 ± 21	110 ± 3	107 ± 2	126 ± 2
K_1 (M^{-1})[b]	120 ± 9	110 ± 14	114 ± 8	112 ± 3

a $K_1 = k_1/k_{-1}$; **b** $A_{obs} = \frac{A_M + A_{ML}K_1[X]}{1 + K_1[X]}$

The plot of ln(k_1/T) *vs* 1/T is presented in Figure **5-36**. A comparative discussion of the data will be undertaken in Paragraph 5.4.

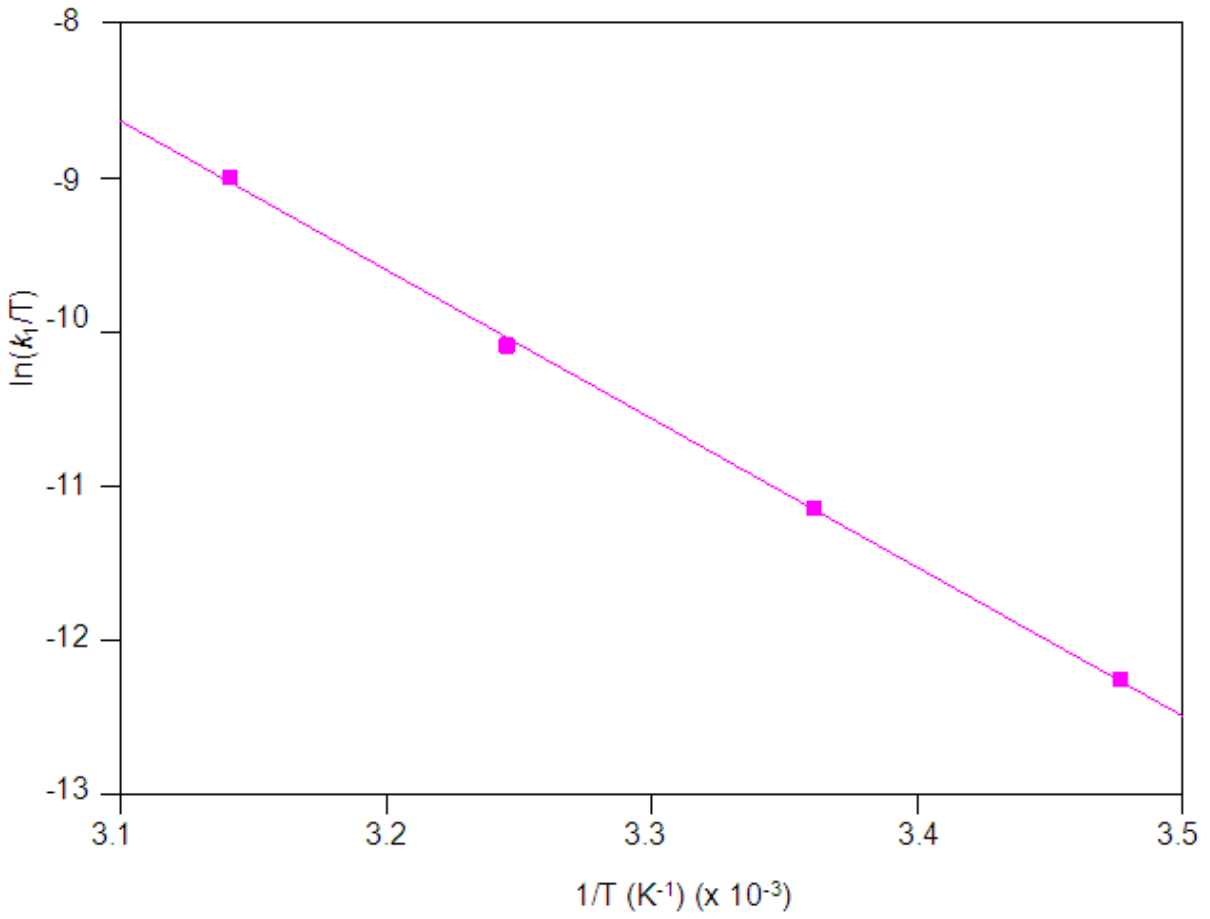

Figure 5-36: Plot of ln(k_1/T) *vs* 1/T for the reaction between *fac*-[Re(CO)$_3$(MeOH)(BrDiPhPr)] and triphenylphosphine for a temperature range of 14.6 °C to 45.3 °C.

5.3.4.4 fac-[Re(CO)$_3$(MeOH)(BrDiPhPr)] + Br$^-$

The methanol substitution reaction between *fac*-[Re(CO)$_3$(MeOH)(BrDiPhPr)] and bromide (Br^-) was performed at 340 nm in methanol and at four different temperatures ranging between 15.3 °C and 45.1 °C, with [Br^-] varying between 0.05 M and 0.5 M. The final UV/Vis spectrum of the reaction solution is identical to the one obtained from the synthesized *fac*-[Re(CO)$_3$(Br)(BrDiPhPr)]$^-$ complex in Chapter 3. The graph of k_{obs} *vs* [Br^-] at different temperatures is presented in Figure **5-37**. An illustration of the A_{obs} vs [Br^-], for the thermodynamically calculated equilibrium constant at 25.5 °C, is presented in Figure **5-38**. The rate constants for the reactions are reported in Table **5-19** and the Eyring plot is illustrated in Figure **5-39**.

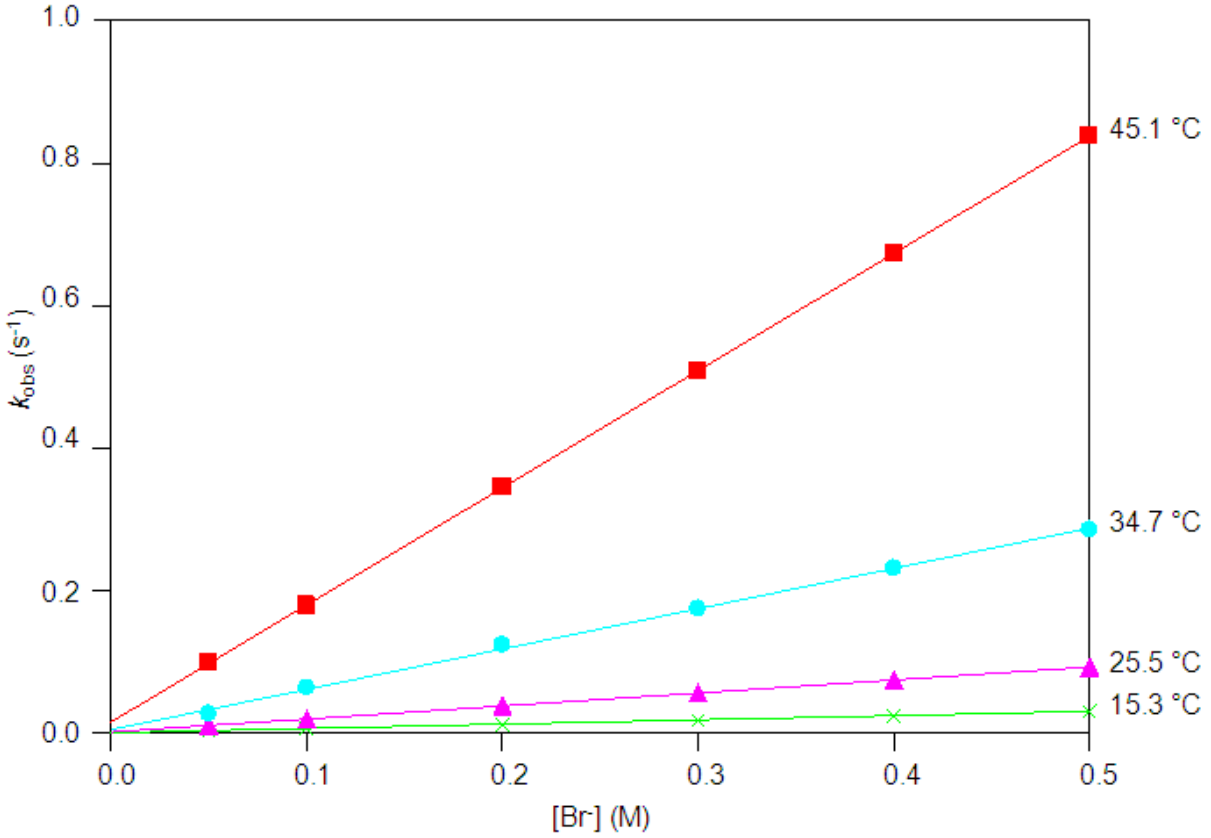

Figure 5-37: Plot k_{obs} *vs* [Br^-] for the reaction between *fac*-[$Re(CO)_3(MeOH)(BrDiPhPr)$] and bromide ions at four different temperatures in methanol, with [Br^-] = 0.05 M to 0.5 M. [Re] = 3 x 10^{-4} M, λ = 340 nm.

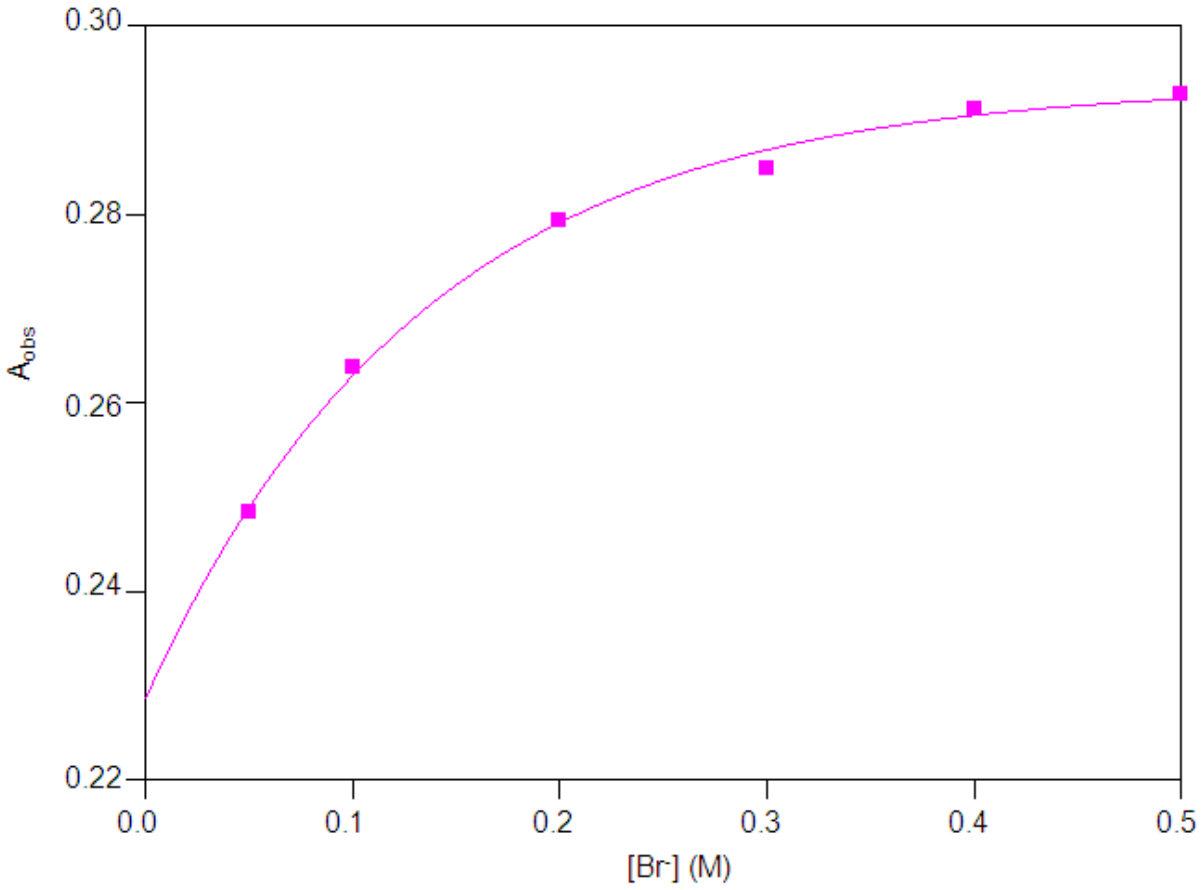

Figure 5-38: Plot of A_{obs} *vs* [Br^-] for the reaction of *fac*-[$Re(CO)_3$(MeOH)(BrDiPhPr] with Br^- ions at 25.5 °C. [Re] = 3 x 10^{-4} M, λ = 340 nm.

The activation parameters have been calculated by the Eyring plot (Equation **3**) as well as the global fit (Equation **4**) and it is clear that the traditional Eyring plot yields similar results than the global fit. $\Delta H^{\ddagger}$ = 83 ± 1 kJmol^{-1} and $\Delta S^{\ddagger}$ = 18 ± 2 JK^{-1}mol^{-1} from the Eyring plot and $\Delta H^{\ddagger}$ = 83 ± 1 kJmol^{-1} and $\Delta S^{\ddagger}$ = 18 ± 4 JK^{-1}mol^{-1} from the global fit.

Table 5-19: Summary of the rate constants of the reaction between *fac*-[$Re(CO)_3$(MeOH)(BrDiPhPr)] and bromide ions at different temperatures in methanol, with [Br^-] = 0.05 M to 0.5 M. [Re] = 3 x 10^{-4} M, λ = 340 nm.

	15.3 °C	**25.5 °C**	**34.7 °C**	**45.1 °C**
$10^3 k_1$ ($M^{-1}s^{-1}$)	60.0 ± 0.2	182 ± 1	566 ± 1	1645 ± 3
$10^3 k_{-1}$ (s^{-1})	0.54 ± 0.05	1.6 ± 0.3	4.7 ± 0.3	15.6 ± 0.9
K_1 (M^{-1})[a]	111 ± 10	114 ± 21	120 ± 8	105 ± 6
K_1 (M^{-1})[b]	101 ± 6	97 ± 6	105 ± 6	96 ± 6

[a] $K_1 = k_1/k_{-1}$; [b] $A_{obs} = \frac{A_M + A_{ML}K_1[X]}{1 + K_1[X]}$

The plot of ln(k_1/T) vis 1/T is presented in Figure **5-39**. A comparative discussion of the data will be undertaken in Paragraph 5.4.

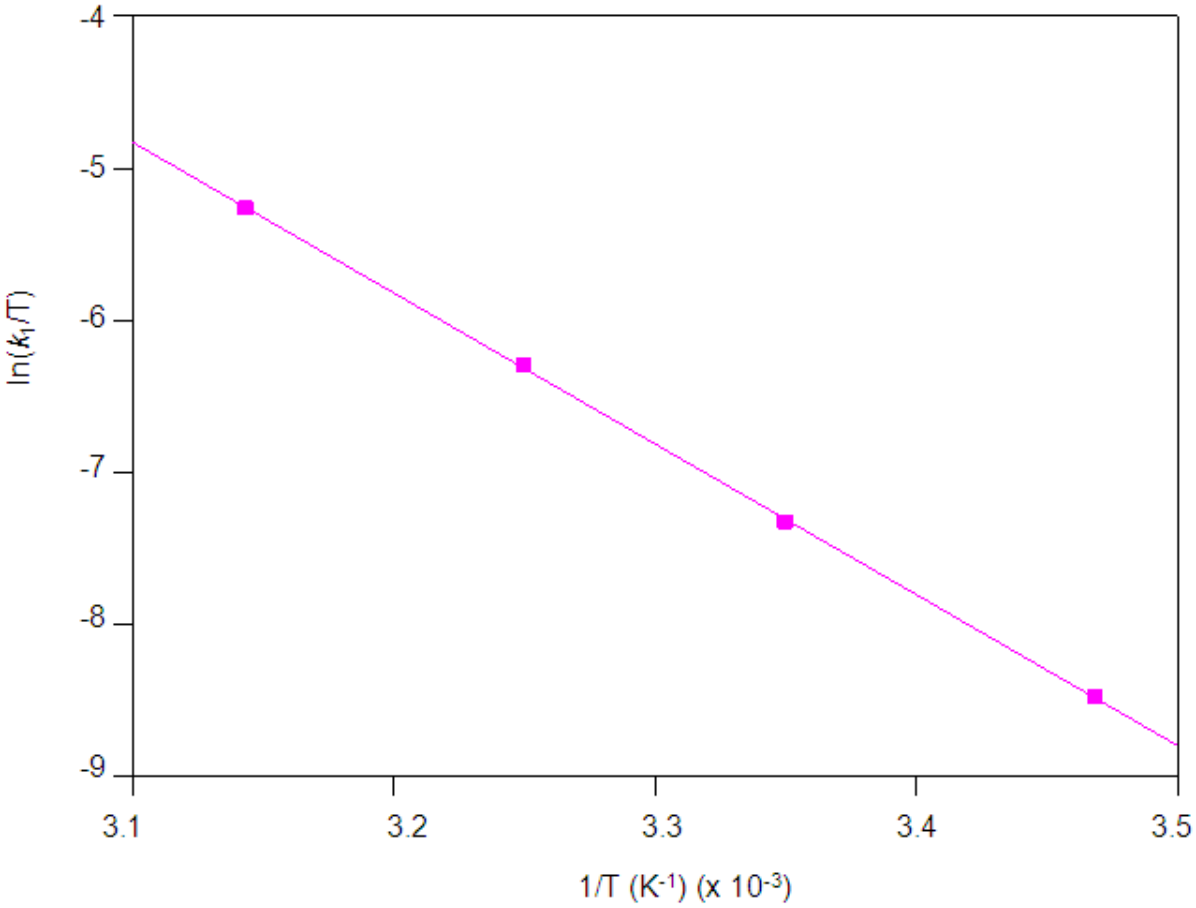

Figure 5-39: Plot of ln(k_1/T) *vs* 1/T for the reaction between *fac*-[Re(CO)$_3$(MeOH)(BrDiPhPr)] and bromide ions for a temperature range of 15.3 °C to 45.1 °C.

5.3.4.5 Summary of the results of the methanol substitution reactions of fac-[Re(CO)$_3$(MeOH)(BrDiPhPr)]

The substitution reactions between *fac*-[Re(CO)$_3$(MeOH)(BrDiPhPr)] and four different mondentate ligands have been studied (Paragraph 5.3.4.1 to 5.3.4.4, thiourea (TU), thiocyanate ions (NCS^-), triphenylphosphine (PPh_3) and bromide ions (Br^-)).

The k_1 values (Table **5-20**) for the substitution reactions with different entering ligands follow the trend k_1 (Br^-) > k_1 (TU) > k_1 (NCS^-) > k_1 (PPh_3). A graph to illustrate the effect of the entering ligand on the rate of the reaction is illustrated in Figure **5-40**. The reverse reaction rate constant, k_{-1} decreases in the following order Br^- > TU >

NCS^- > PPh_3 while the stability constant, K_1, for all these reactions are relatively similar and fall within the range of 97 ± 6 to 120 ± 22. A good agreement exists between the stability constants, K_1, determined kinetically and those determined thermodynamically. The enthalpy of activation ($\Delta H^‡$) values from the Eyring and global fit for all the reactions are similar except for the reaction with TU. The small negative and small positive values of $\Delta S^‡$ for all the reactions (with TU, NCS^-, PPh_3 and Br^-) suggest an interchange associative/dissociative type activation. Again, the data from the Eyring and global fit do not agree well and the $\Delta S^‡$ values have large esd's, emphasizing the need for high pressure studies to determine the mechanism of activation.

Table 5-20: Rate constants of the different reactions between *fac*-[Re(CO)$_3$(MeOH)(BrDiPhPr)] and different entering ligands at ~ 25 °C.

	$10^3 k_1$ ($M^{-1}s^{-1}$)	$10^3 k_{-1}$ (s^{-1})	K_1 (M^{-1})	$\Delta H^‡$ ($kJmol^{-1}$)	$\Delta S^‡$ ($JK^{-1}mol^{-1}$)
TU	39.6 ± 0.2	0.33 ± 0.06	120 ± 22[a], 112 ± 3[b]	79 ± 1[c], 101 ± 3[d]	-4 ± 1[c], 61 ± 11[d]
NCS^-	14.466 ± 0.006	0.121 ± 0.002	120 ± 2[a], 120 ± 4[b]	73 ± 1[c], 81 ± 1[d]	-33 ± 4[c], -11 ± 3[d]
PPh_3	4.30 ± 0.05	0.039 ± 0.001	110 ± 3[a], 110 ± 14[b]	80 ± 2[c], 87 ± 1[d]	-20 ± 5[c], 9 ± 3[d]
Br^-	182 ± 1	1.6 ± 0.3	114 ± 21[a], 97 ± 6[b]	83 ± 1[c], 83 ± 1[d]	-18 ± 2[c], 18 ± 4[d]

[a] $K_1 = k_1/k_{-1}$, [b] $A_{obs} = \frac{A_M + A_{ML}K_1[L]}{1 + K_1[L]}$, [c] Eyring fit, [d] Global fit.

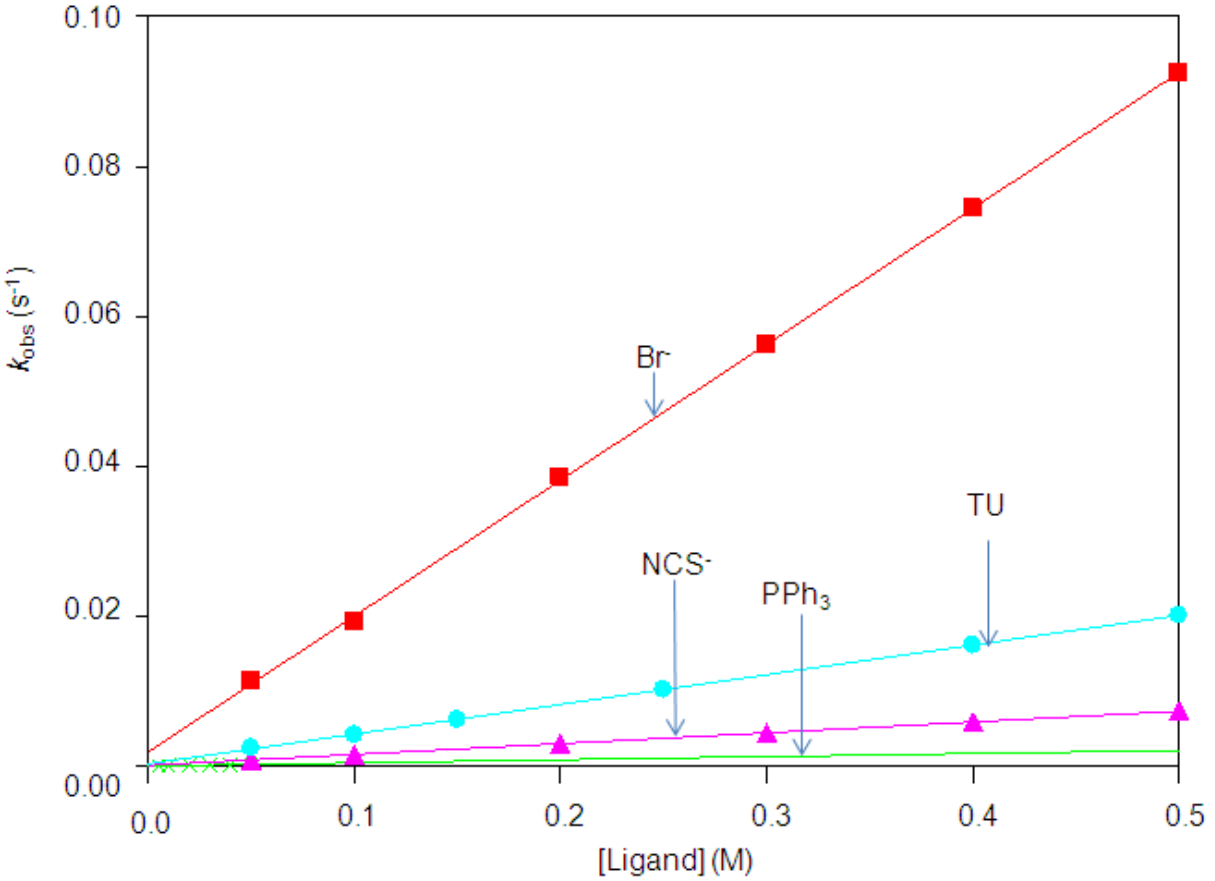

Figure 5-40: Schematic representation of k_{obs} *vs* [ligand] of the reactions between *fac*-[Re(CO)$_3$(MeOH)(BrDiPhPr)] and various entering ligands at ~ 25 °C.

5.3.5 Reaction between *fac*-[Re(CO)$_3$(MeOH)(TIF)] and entering ligands

The synthesis of *fac*-[Re(CO)$_3$(MeOH)(TIF)] from the starting synthon [NEt$_4$]$_2$[Re(CO)$_3$Br$_3$] has been described in Chapter 3. *fac*-[Re(CO)$_3$(Br)(TIF)]$^-$ was dissolved in methanol and stirred for 24 hours to yield *fac*-[Re(CO)$_3$(MeOH)(TIF)]. The reaction between *fac*-[Re(CO)$_3$(MeOH)(TIF)] and four different monodentate ligands (thiourea (TU), thiocyanate (NCS$^-$), tricyclohexylphosphine (PCy$_3$) and bromide (Br$^-$)) were monitored with UV/Vis in methanol.

5.3.5.1 fac-[Re(CO)$_3$(MeOH)(TIF)] + TU

The methanol substitution reaction between *fac*-[Re(CO)$_3$(MeOH)(TIF)] and thiourea (TU) was performed at 345 nm in methanol and at four different temperatures ranging between 15.4 °C and 45.0 °C, with [TU] varying between 0.05 M and 0.5 M. The final UV/Vis spectrum of the reaction solution is identical to the one obtained from the synthesized *fac*-[Re(CO)$_3$(TU)(TIF)] complex in Chapter 3.

The graph of k_{obs} *vs* [TU] at different temperatures is presented in Figure **5-41** below, the rate constants for the reactions are reported in Table **5-21** and the Eyring plot is illustrated in Figure **5-42**.

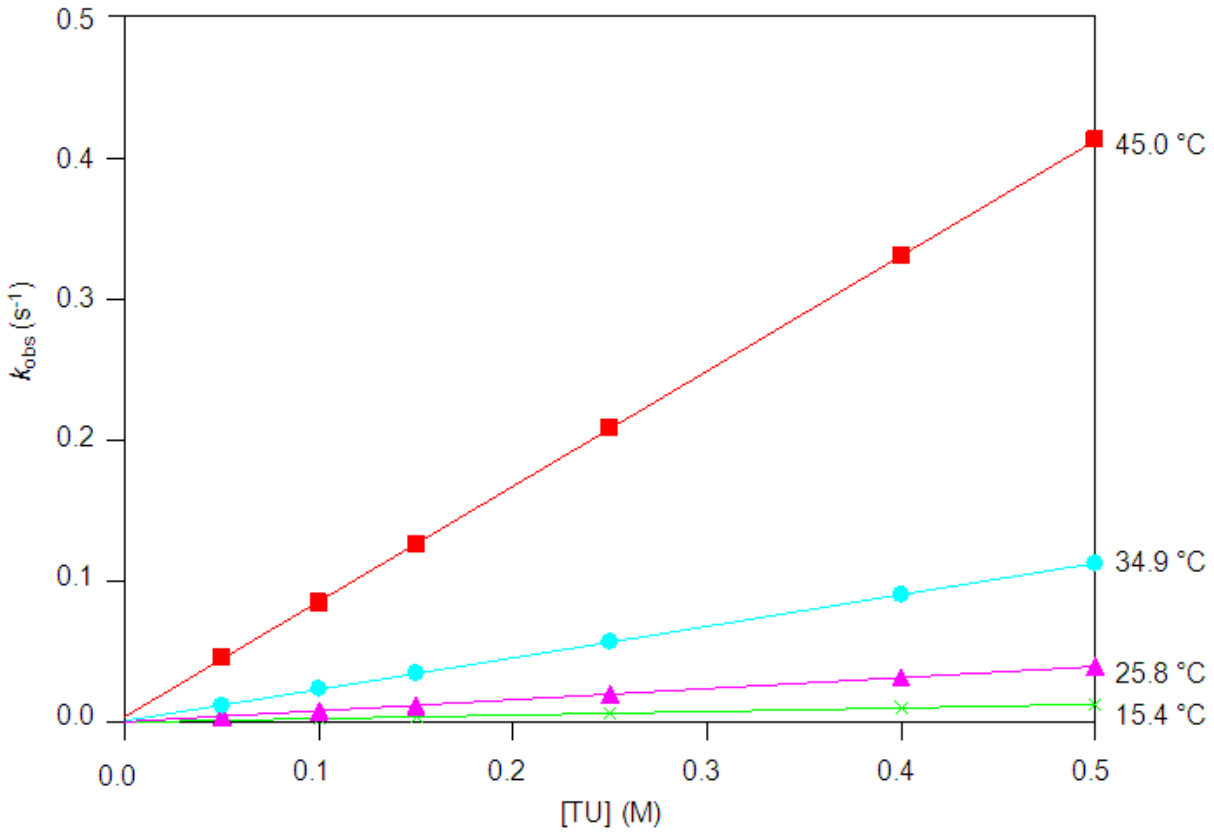

Figure 5-41: Plot of k_{obs} *vs* [TU] for the reaction between *fac*-[Re(CO)$_3$(MeOH)(TIF)] and thiourea at different temperatures in methanol, with [TU] = 0.05 M to 0.5 M. [Re] = 3 x10^{-4} M, λ = 345 nm.

The activation parameters have been calculated by the Eyring plot (Equation **3**) as well as the global fit of temperature *vs* ligand concentration *vs* k_{obs} data (Equation **4**) and the traditional Eyring plot yields similar results than the global fit.

$\Delta H^{\ddagger}$ = 77 ± 1 kJmol^{-1} and $\Delta S^{\ddagger}$ = -8 ± 2 JK^{-1}mol^{-1} from the Eyring plot and $\Delta H^{\ddagger}$ = 109 ± 2 kJmol^{-1} and $\Delta S^{\ddagger}$ = 94 ± 8 JK^{-1}mol^{-1} from the global fit.

Table 5-21: Summary of the rate constants of the reaction between *fac*-[Re(CO)$_3$(MeOH)(TIF)] and thiourea at four different temperatures in methanol, with [TU] = 0.05 M to 0.5 M. [Re] = 3 x10^{-4} M, λ = 345 nm.

	15.4 °C	**25.8 °C**	**34.9 °C**	**45.0 °C**
$10^3 k_1$ ($M^{-1}s^{-1}$)	25.21 ± 0.09	78.3 ± 0.5	223.4 ± 0.9	816 ± 2
$10^3 k_{-1}$ (s^{-1})	0.12 ± 0.03	0.4 ± 0.1	1.1 ± 0.3	4.2 ± 0.7
K_1 (M^{-1})[a]	210 ± 53	196 ± 49	203 ± 55	194 ± 32
K_1 (M^{-1})[b]	182 ± 9	190 ± 10	180 ± 13	177 ± 15

[a] $K_1 = k_1/k_{-1}$; [b] $A_{obs} = \frac{A_M + A_{ML}K_1[X]}{1 + K_1[X]}$

The plot of ln(k_1/T) *vs* 1/T is presented in Figure **5-42**. A comparative discussion of the data will be undertaken in Paragraph 5.4.

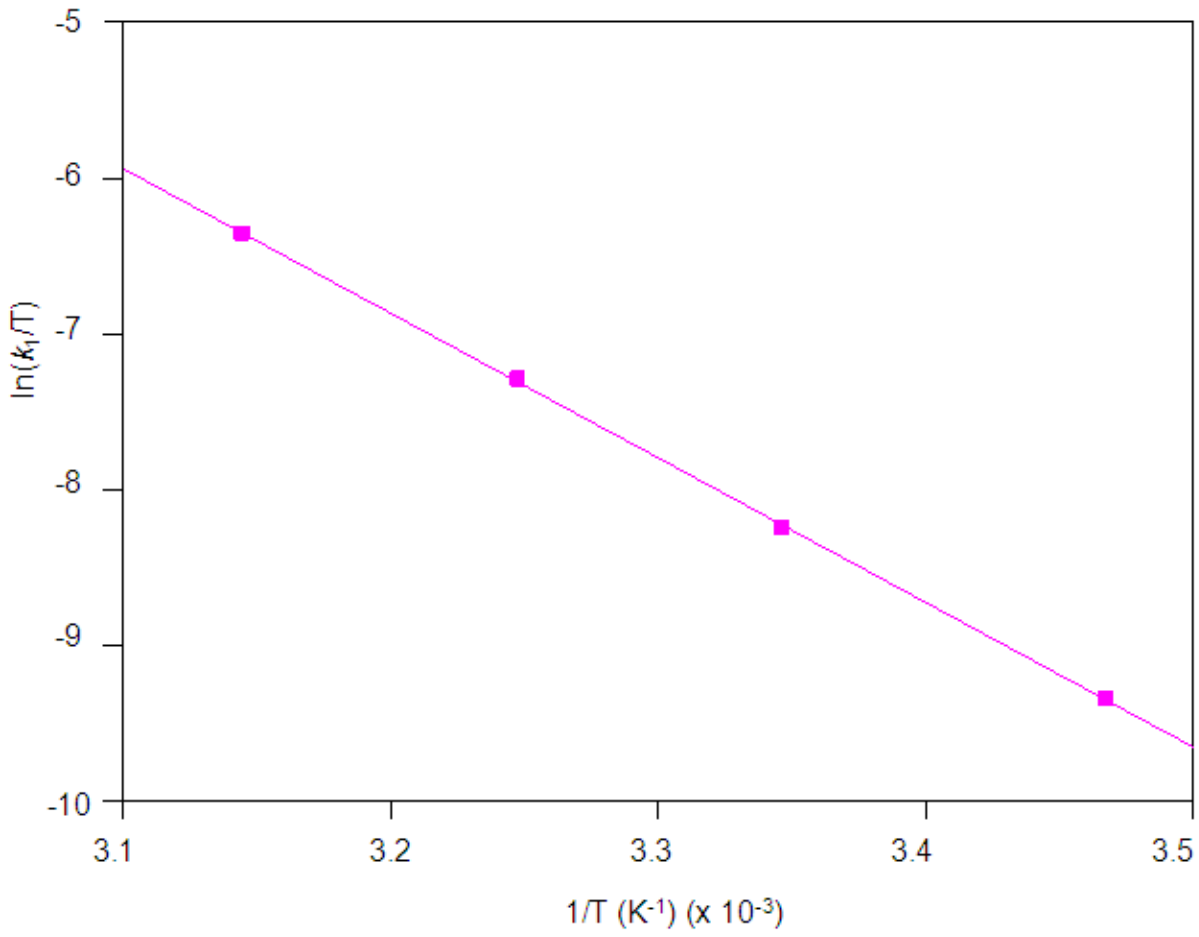

Figure 5-42: Plot of ln(k_1/T) *vs* 1/T for the reaction between *fac*-[Re(CO)$_3$(MeOH)(TIF)] and thiourea for a temperature range of 15.4 °C to 45.0 °C.

5.3.5.2 fac-[Re(CO)$_3$(MeOH)(TIF)] + NCS$^-$

The methanol substitution reaction between *fac*-[Re(CO)$_3$(MeOH)(TIF)] and thiocyanate was performed at 345 nm in methanol and at four different temperatures ranging between 15.8 °C and 45.1 °C, with [NCS$^-$] varying between 0.05 M and 0.5 M. The final UV/Vis spectrum of the reaction solution is identical to the one obtained from the synthesized *fac*-[Re(CO)$_3$(NCS)(TIF)]$^-$ complex in Chapter 3.

The graph of k_{obs} *vs* [NCS$^-$] at different temperatures is presented in Figure **5-43** below, the rate constants for the reaction are reported in Table **5-22** while the Eyring plot is illustrated in Figure **5-44**.

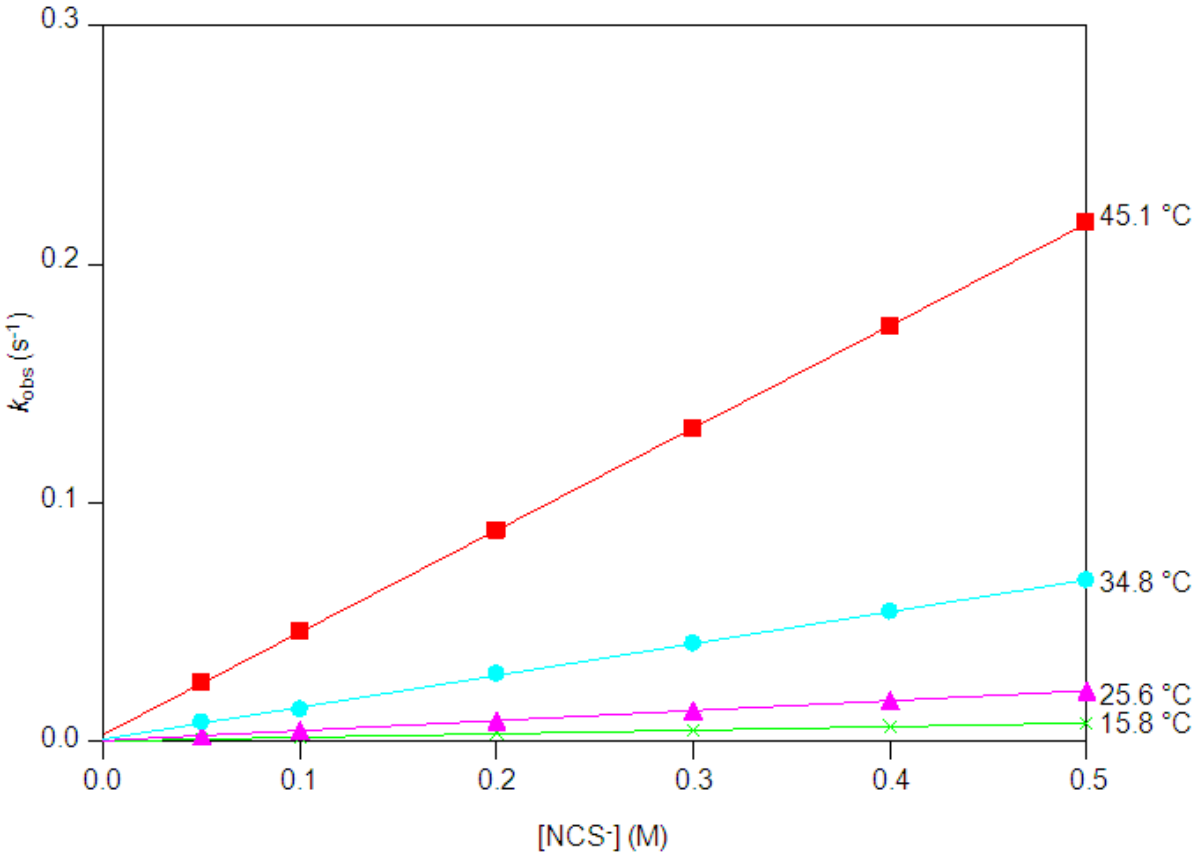

Figure 5-43: Plot of k_{obs} *vs* [NCS$^-$] for the reaction between *fac*-[Re(CO)$_3$(MeOH)(TIF)] and thiocyanate ions at four different temperatures in methanol, with [NCS$^-$] = 0.05 M to 0.5 M. [Re] = 3 x10^{-4} M, λ = 345 nm.

The activation parameters have been calculated by the Eyring plot (Equation **3**) as well as the global fit of temperature *vs* ligand concentration *vs* k_{obs} data (Equation **4**) and the traditional Eyring plot yields similar results to the global fit.

$\Delta H^{\ddagger}$ = 77 ± 1 kJmol^{-1} and $\Delta S^{\ddagger}$ = -11 ± 2 JK^{-1}mol^{-1} from the Eyring plot and $\Delta H^{\ddagger}$ = 89.8 ± 0.9 kJmol^{-1} and $\Delta S^{\ddagger}$ = 29 ± 3 JK^{-1}mol^{-1} from the global fit.

Table 5-22: Summary of the rate constants of the reaction between *fac*-[Re(CO)$_3$(MeOH)(TIF)] and NCS$^-$ at different temperatures, with [NCS$^-$] = 0.05 M to 0.5 M. [Re] = 3 x10^{-4} M, λ = 345 nm.

	15.8 °C	25.6 °C	34.8 °C	45.1 °C
$10^2 k_1$ ($M^{-1}s^{-1}$)	15.15 ± 0.05	42.0 ± 0.4	133.7 ± 0.2	428.4 ± 0.6
$10^2 k_{-1}$ (s^{-1})	0.10 ± 0.01	0.3 ± 0.1	0.88 ± 0.05	2.9 ± 0.2
K_1 (M^{-1})[a]	152 ± 15	140 ± 47	152 ± 9	148 ± 10
K_1 (M^{-1})[b]	136 ± 6	138 ± 6	140 ± 5	132 ± 6

[a] $K_1 = k_1/k_{-1}$; [b] $A_{obs} = \frac{A_M + A_{ML}K_1[X]}{1 + K_1[X]}$

The plot of ln(k_1/T) *vs* 1/T is presented in Figure **5-44**. A comparative discussion of the data will be undertaken in Paragraph 5.4.

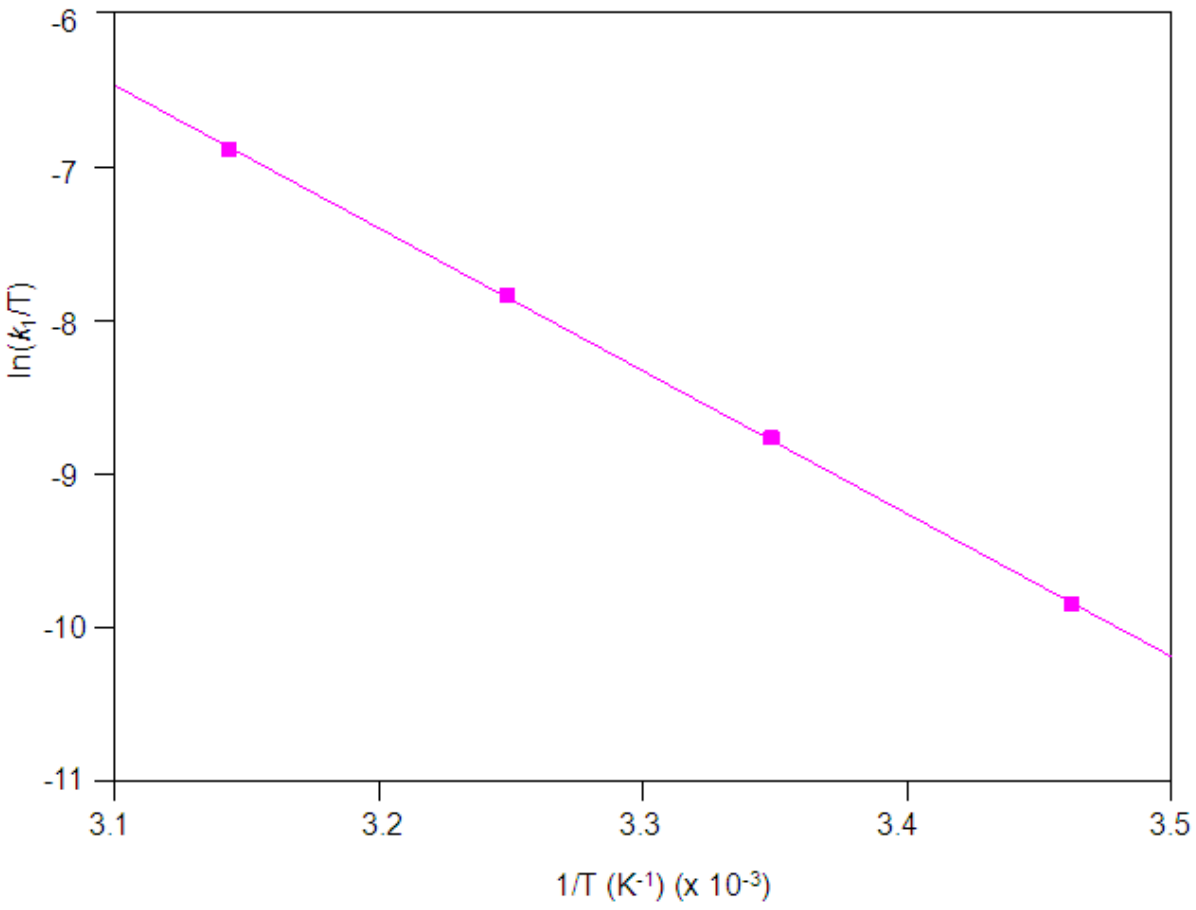

Figure 5-44: Plot of ln(k_1/T) *vs* 1/T for the reaction between *fac*-[Re(CO)$_3$(MeOH)(TIF)] and thiocyanate ions for a temperature range of 15.8 °C to 45.1 °C.

5.3.5.3 fac-[Re(CO)$_3$(MeOH)(TIF)] + PCy$_3$

The methanol substitution reaction between *fac*-[Re(CO)$_3$(MeOH)(TIF)] and tricyclohexylphosphine was performed at 345 nm in methanol and at four different temperatures ranging between 15.6 °C and 45.3 °C, with [PCy$_3$] varying between 0.01 M and 0.05 M. The concentration of PCy$_3$ could not be increased since the solution was saturated at 0.01 M in methanol. At concentrations lower than 0.01 M the absorbance change is too small; thus the smaller concentration range of 0.01 M to 0.05 M was used. The final UV/Vis spectrum of the reaction solution is identical to the one obtained from the synthesized *fac*-[Re(CO)$_3$(PCy$_3$)(TIF)] complex in Chapter 3.

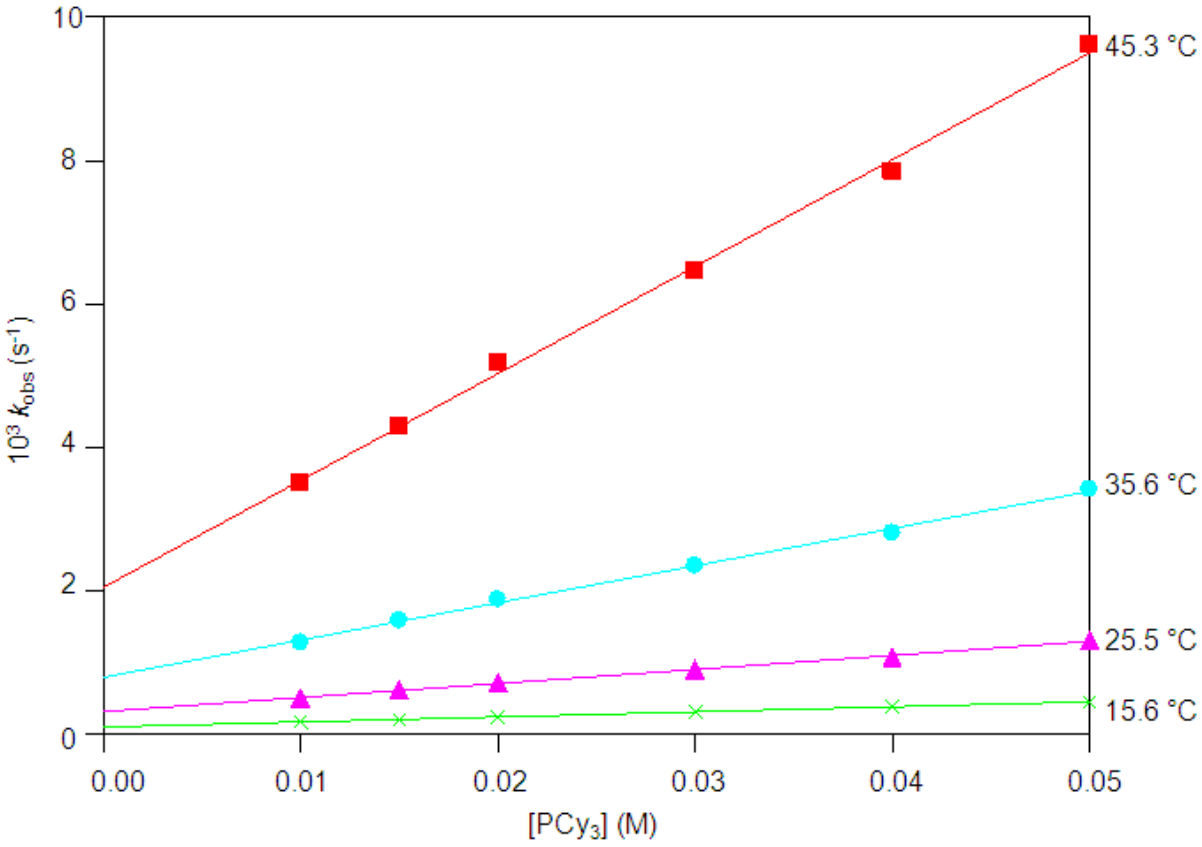

Figure 5-45: Plot of k_{obs} *vs* [PCy$_3$] for the reaction between *fac*-[Re(CO)$_3$(MeOH)(TIF)] and tricyclohexylphosphine at four different temperatures in methanol, with [PCy$_3$] = 0.01 M to 0.05 M. [Re] = 3 x 10^{-4} M, λ = 345 nm.

The graph of k_{obs} *vs* [PCy$_3$] at different temperatures is presented in Figure **5-45** below, the rate constants for the reaction are reported in Table **5-23** while the Eyring

plot is illustrated in Figure **5-46**. The activation parameters have been calculated by the Eyring plot (Equation **3**) as well as the global fit of temperature *vs* ligand concentration *vs* k_{obs} data (Equation **4**) and it is clear that the data from the Eyring plot and global fit is similar: $\Delta H^{\ddagger}$ = 74 ± 2 kJmol^{-1} and $\Delta S^{\ddagger}$ = -28 ± 5 JK^{-1}mol^{-1} from the Eyring plot and $\Delta H^{\ddagger}$ = 80 ± 1 kJmol^{-1} and $\Delta S^{\ddagger}$ = -12 ± 3 JK^{-1}mol^{-1} from the global fit.

Table 5-23: Summary of the rate constants of the reaction between *fac*-[Re(CO)$_3$(MeOH)(TIF)] and tricyclohexylphosphine at different temperatures, with [PCy$_3$] = 0.01 M to 0.05 M. [Re] = 3 x10^{-4} M, λ = 345 nm.

	15.6 °C	**25.5 °C**	**35.6 °C**	**45.3 °C**
$10^2 k_1$ ($M^{-1}s^{-1}$)	7.0 ± 0.2	19.6 ± 0.4	52 ± 1	149 ± 4
$10^2 k_{-1}$ (s^{-1})	0.101 ± 0.005	0.32 ± 0.01	0.80 ± 0.04	2.0 ± 0.1
K_1 (M^{-1})[a]	69 ± 4	61 ± 2	65 ± 3	75 ± 4
K_1 (M^{-1})[b]	71 ± 3	69 ± 4	71 ± 3	71 ± 5

a $K_1 = k_1/k_{-1}$; **b** $A_{obs} = \frac{A_M + A_{ML}K_1[L]}{1 + K_1[L]}$

The plot of ln(k_1/T) *vs* 1/T is presented in Figure **5-46**. A comparative discussion of the data will be undertaken in Paragraph 5.4.

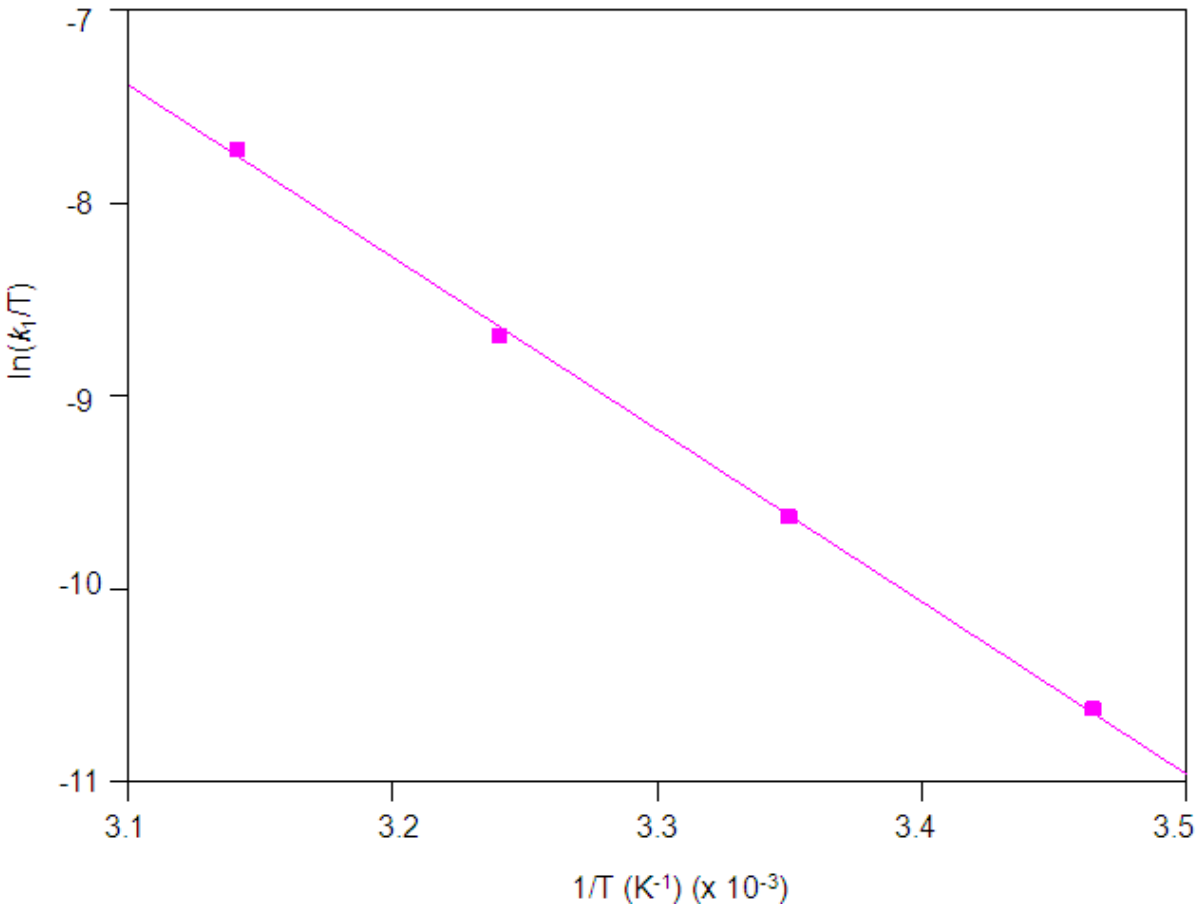

Figure 5-46: Plot of ln(k_1/T) *vs* 1/T for the reaction between *fac*-[Re(CO)$_3$(MeOH)(TIF)] and tricyclohexylphosphine for a temperature range of 15.6 °C to 45.3 °C.

5.3.5.4 fac-[Re(CO)$_3$(MeOH)(TIF)] + Br$^-$

The methanol substitution reaction between *fac*-[Re(CO)$_3$(MeOH)(TIF)] and bromide (Br$^-$) was performed at 343 nm in methanol and at four different temperatures ranging between 15.8 °C and 45.0 °C, with [Br$^-$] varying between 0.05 M and 0.5 M. The final UV/Vis spectrum of the reaction solution is identical to the one obtained from the synthesized *fac*-[Re(CO)$_3$(Br)(TIF)]$^-$ complex in Chapter 3.

The graph of k_{obs} *vs* [Br$^-$] at different temperatures is presented in Figure **5-47**. An illustration of the A_{obs} *vs* [Br$^-$], for the thermodynamically calculated equilibrium constant at 25.7 °C, is presented in Figure **5-48**. The rate constants for the reactions are reported in Table **5-24** and the Eyring plot is illustrated in Figure **5-49**.

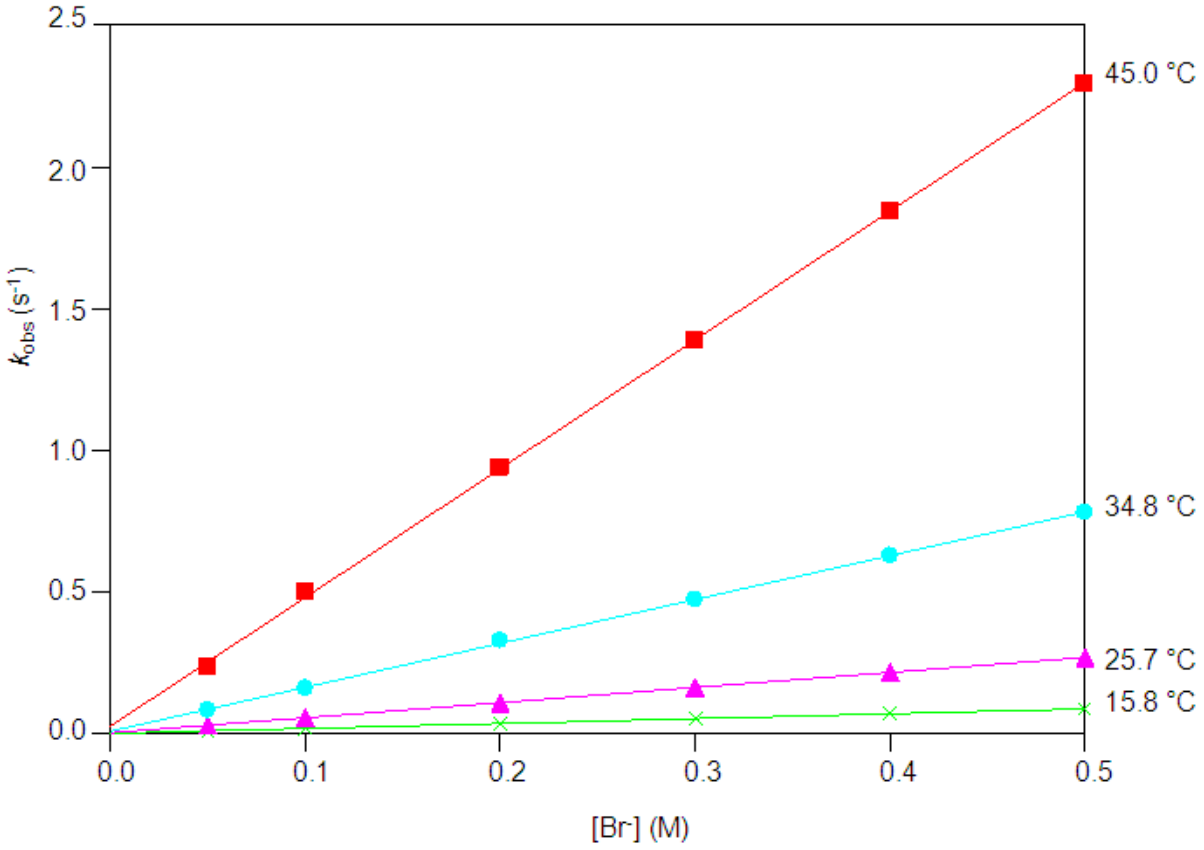

Figure 5-47: Plot of k_{obs} *vs* [Br^-] for the reaction between *fac*-[$Re(CO)_3(MeOH)(TIF)$] and bromide ions at four different temperatures in methanol, with [Br^-] = 0.05 M to 0.5 M. [Re] = 3 x 10^{-4} M, λ = 343 nm.

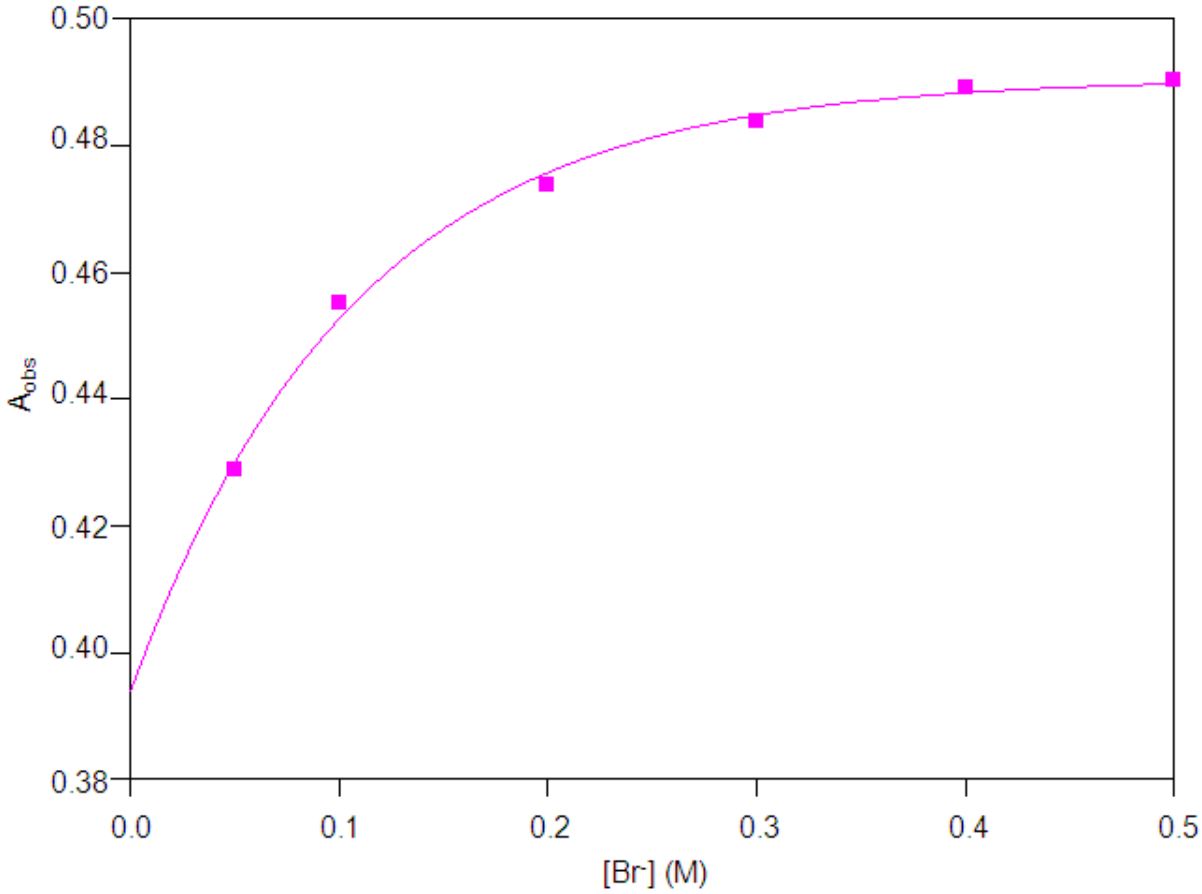

Figure 5-48: Plot of A_{obs} *vs* [Br^-] for the reaction of *fac*-[$Re(CO)_3(MeOH)(TIF)$] with Br^- ions at 25.7 °C. [Re] = 3 x 10^{-4} M, λ = 343 nm.

The activation parameters have been calculated by the Eyring plot (Equation **3**) as well as the global fit of temperature *vs* ligand concentration *vs* k_{obs} data (Equation **4**) and the traditional Eyring plot yields similar results to the global fit. $\Delta H^{\ddagger}$ = 83 ± 1 kJmol^{-1} and $\Delta S^{\ddagger}$ = 29 ± 4 JK^{-1}mol^{-1} from the Eyring plot and $\Delta H^{\ddagger}$ = 83.9 ± 0.9 kJmol^{-1} and $\Delta S^{\ddagger}$ = 30 ± 3 JK^{-1}mol^{-1} from the global fit.

Table 5-24: Summary of the rate constants of the reaction between *fac*-[$Re(CO)_3(MeOH)(TIF)$] and bromide ions at different temperatures in methanol, with [Br^-] = 0.05 M to 0.5 M. [Re] = 3 x 10^{-4} M, λ = 343 nm.

	15.8 °C	**25.7 °C**	**34.8 °C**	**45.0 °C**
$10^3 k_1$ ($M^{-1}s^{-1}$)	173 ± 0.7	533 ± 1	1546 ± 3	4558 ± 4
$10^3 k_{-1}$ (s^{-1})	1.0 ± 0.2	3.1 ± 0.4	9.2 ± 0.8	21 ± 1
K_1 (M^{-1})[a]	173 ± 35	172 ± 22	168 ± 15	217 ± 10
K_1 (M^{-1})[b]	165 ± 6	162 ± 6	163 ± 12	158 ± 3

[a] $K_1 = k_1/k_{-1}$; [b] $A_{obs} = \frac{A_M + A_{ML}K_1[X]}{1 + K_1[X]}$

The plot of ln(k_1/T) *vs* 1/T is presented in Figure **5-49**. A comparative discussion of the data will be undertaken in Paragraph 5.4.

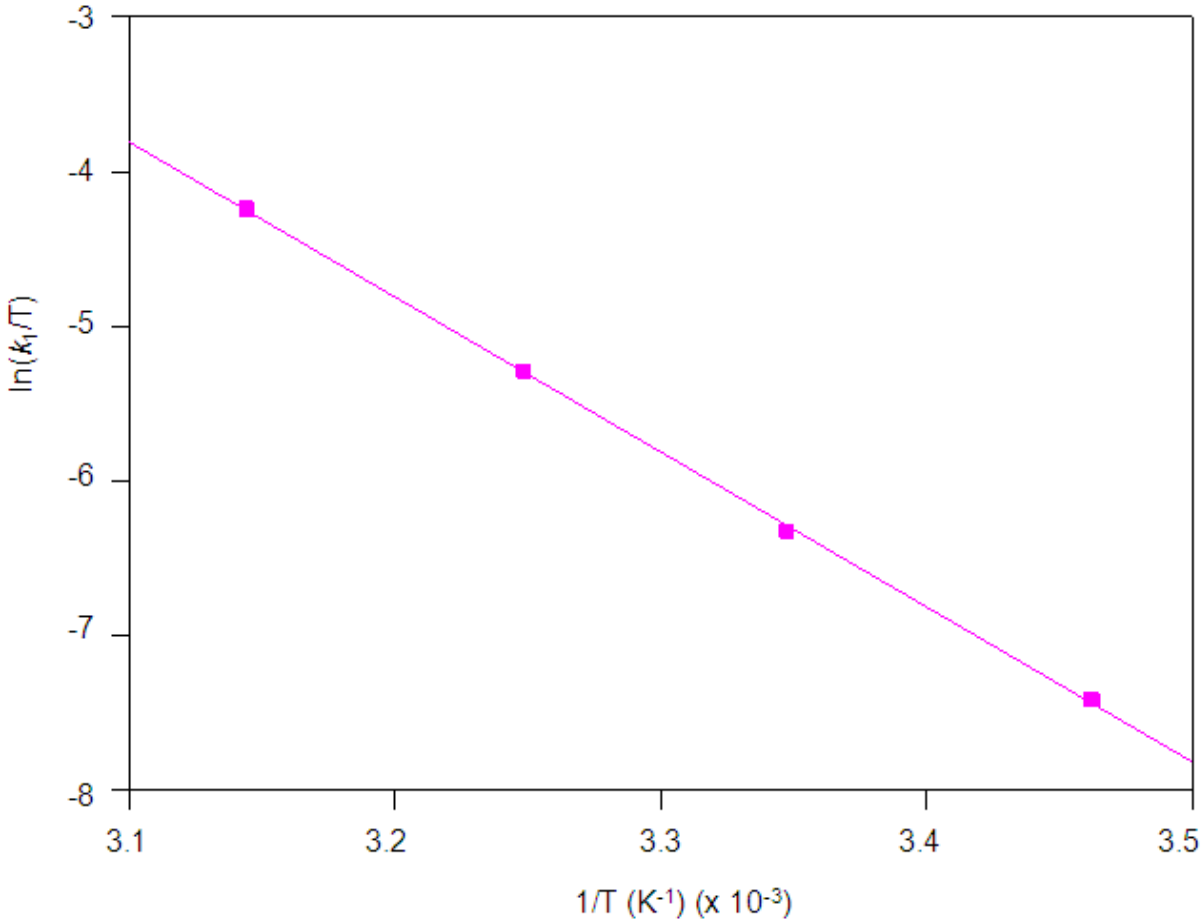

Figure 5-49: Plot of ln(k_1/T) *vs* 1/T for the reaction between *fac*-[Re(CO)$_3$(MeOH)(TIF)] and bromide ions for a temperature range of 15.8 °C to 45.0 °C.

5.3.5.5 Summary of the results of the methanol substitution reactions of fac-[Re(CO)$_3$(MeOH)(TIF)]

The substitution reactions between *fac*-[Re(CO)$_3$(MeOH)(TIF)] and four different mondentate ligands have been studied (Paragraph 5.3.5.1 to 5.3.5.4, thiourea (TU), thiocyanate (NCS^-), tricyclohexylphosphine (PCy_3) and bromide ions (Br^-)).

The k_1 values (Table **5-25**) for the substitution reactions with different entering ligands decrease as follows: k_1 (Br^-) > k_1 (TU) > k_1 (NCS^-) > k_1 (PCy_3). A graph to illustrate the effect of the entering ligands on the rate of the reaction is illustrated in Figure **5-50**. The reverse reaction rate constant, k_{-1} decreases in the following order Br^- > TU > NCS^- ≈ PCy_3 and the stability constant, (K_1) for these reactions decrease

as follows: K_1(TU) > K_1(Br^-) > K_1(NCS^-) > K_1(PCy_3) with the PCy_3 complex being the least stable of the four complexes; K_1 range from 61 ± 2 to 196 ± 49. A good agreement exists between the stability constants determined kinetically and those determined thermodynamically. The enthalpy of activation ($\Delta H^{\ddagger}$) values for all the reactions are similar and within normal range while the small negative to small positive values of $\Delta S^{\ddagger}$ for all the reactions (with TU, NCS^-, PCy_3 and Br^-) suggest an interchange associative/dissociative type of activation. The $\Delta H^{\ddagger}$ and $\Delta S^{\ddagger}$ values for all the reactions, calculated from the Eyring equation as well as the global fit, differ significantly and again stresses the need to do high pressure experiments to confirm the type of activation.

Table 5-25: Rate constants of the different reactions between *fac*-[$Re(CO)_3$(MeOH)(TIF)] and different entering ligands at ~ 25 °C.

	$10^3 k_1$ ($M^{-1}s^{-1}$)	$10^3 k_{-1}$ (s^{-1})	K_1 (M^{-1})	$\Delta H^{\ddagger}$ ($kJmol^{-1}$)	$\Delta S^{\ddagger}$ ($JK^{-1}mol^{-1}$)
TU	78.3 ± 0.5	0.4 ± 0.1	196 ± 49[a], 190 ± 10[b]	77 ± 1[c], 109 ± 2[d]	-8 ± 2[c], 94 ± 8[d]
NCS^-	42.0 ± 0.4	0.3 ± 0.1	140 ± 47[a], 138 ± 6[b]	77 ± 1[c], 89.8 ± 0.9[d]	-11 ± 2[c], 29 ± 3
PCy_3	19.6 ± 0.4	0.32 ± 0.01	61 ± 2[a], 69 ± 4[b]	74 ± 2[c], 80 ± 1[d]	-28 ± 5[c], -12 ± 3[d]
Br^-	533 ± 1	3.1 ± 0.4	172 ± 22[a], 162 ± 6[b]	83 ± 1[c], 83.9 ± 0.9[d]	-29 ± 4[c], 30 ± 3[d]

[a] $K_1 = k_1/k_{-1}$, [b] $A_{obs} = \frac{A_M + A_{ML}K_1[X]}{1 + K_1[X]}$, [c] Eyring fit, [d] Global fit.

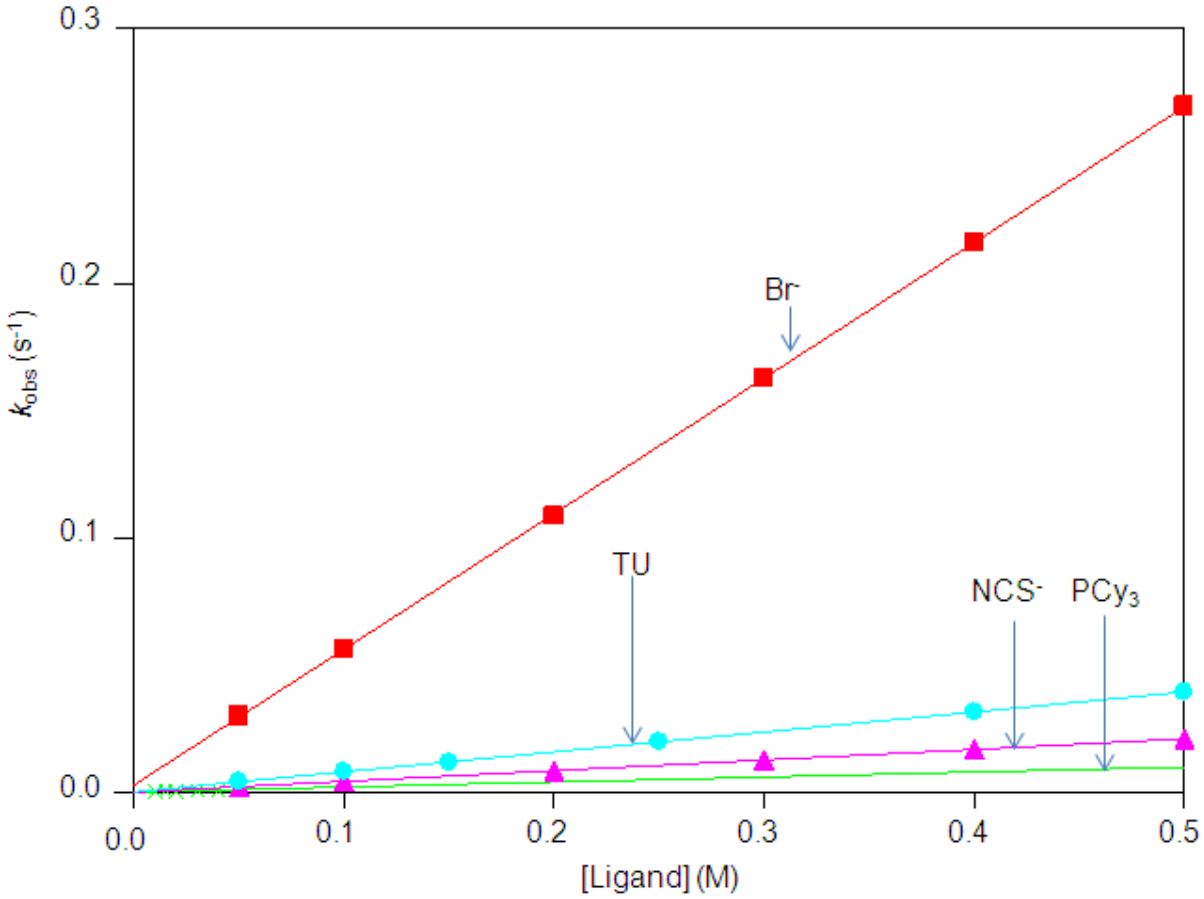

Figure 5-50: Schematic representation k_{obs} *vs* [ligand] of the reactions between *fac*-[Re(CO)$_3$(MeOH)(TIF)] and various entering ligands at ~ 25 °C.

5.3.6 Reaction between *fac*-[Re(CO)$_3$(MeOH)(MeTIF)] and entering ligands

The synthesis of *fac*-[Re(CO)$_3$(MeOH)(MeTIF)] from the starting synthon [NEt$_4$]$_2$[Re(CO)$_3$Br$_3$] has been described in Chapter 3. *fac*-[Re(CO)$_3$(Br)(MeTIF)]$^-$ was dissolved in methanol and stirred for 24 hours to yield *fac*-[Re(CO)$_3$(MeOH)(MeTIF)]. The reaction between *fac*-[Re(CO)$_3$(MeOH)(MeTIF)] and four different monodentate ligands (thiourea (TU), thiocyanate (NCS$^-$), tricyclohexylphosphine (PCy_3) and bromide (Br$^-$)) were monitored with UV/Vis in methanol.

5.3.6.1 fac-[Re(CO)$_3$(MeOH)(MeTIF)] + TU

The methanol substitution reaction between *fac*-[Re(CO)$_3$(MeOH)(MeTIF)] and thiourea (TU) was performed at 345 nm in methanol and at four different

temperatures ranging between 15.1 °C and 45.3 °C, with [TU] varying from 0.05 M to 0.5 M. The final UV/Vis spectrum of the reaction solution is identical to the one obtained from the synthesized *fac*-[Re(CO)$_3$(TU)(MeTIF)] complex in Chapter 3.

The graph of k_{obs} *vs* [TU] at different temperatures is presented in Figure **5-51** below, the rate constants for the reactions are reported in Table **5-26** and the Eyring plot is illustrated in Figure **5-52**.

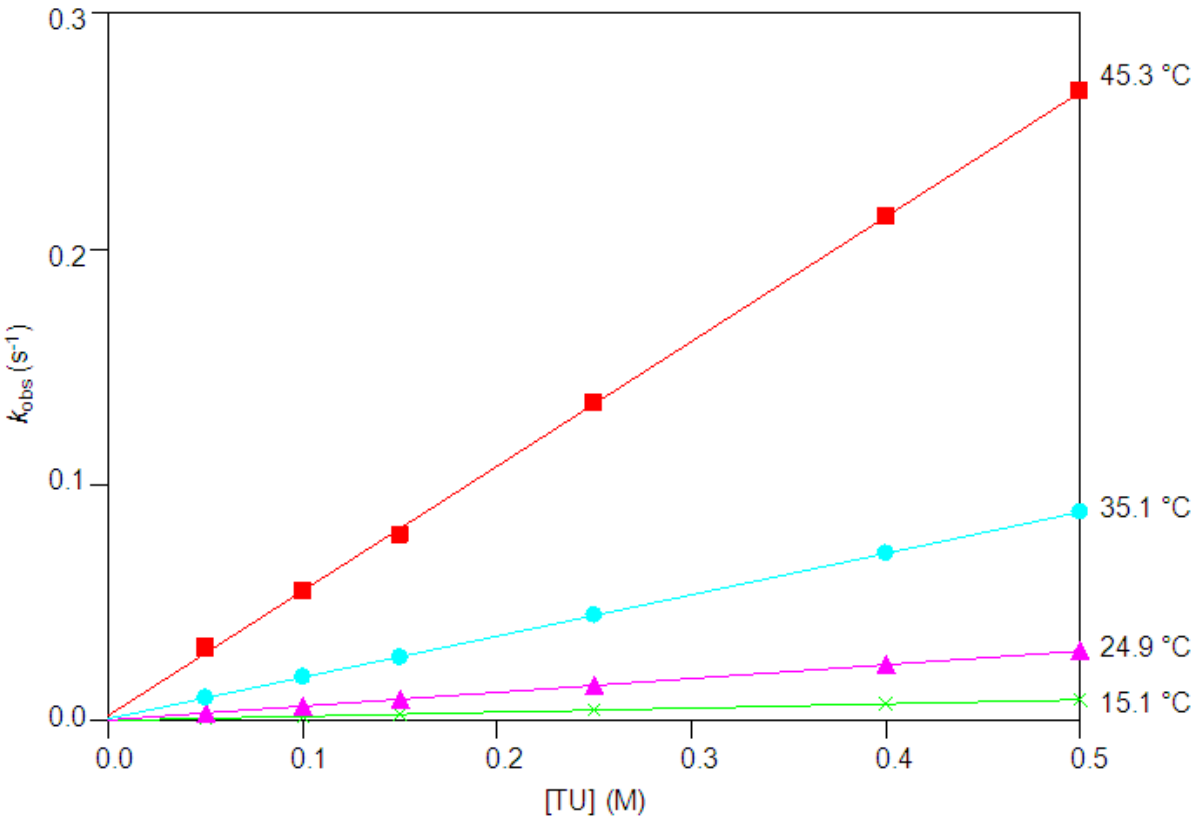

Figure 5-51: Plot of k_{obs} *vs* [TU] for the reaction between *fac*-[Re(CO)$_3$(MeOH)(MeTIF)] and thiourea at four different temperatures in methanol, with [TU] = 0.05 M to 0.5 M. [Re] = 3 x10^{-4} M, λ = 345 nm.

The activation parameters have been calculated by the Eyring plot (Equation **3**) as well as the global fit of temperature *vs* ligand concentration vs k_{obs} data (Equation **4**) and it is clear that the traditional Eyring plot yields similar results to the global fit. $\Delta H^{\ddagger}$ = 83 ± 1 kJmol^{-1} and $\Delta S^{\ddagger}$ = 10 ± 2 JK^{-1}mol^{-1} from the Eyring plot and $\Delta H^{\ddagger}$ = 85 ± 1 kJmol^{-1} and $\Delta S^{\ddagger}$ = 14 ± 3 JK^{-1}mol^{-1} from the global fit.

Table 5-26: Summary of the rate constants of the reaction between *fac*-[Re(CO)$_3$(MeOH)(MeTIF)] and thiourea at different temperatures in methanol, with [TU] = 0.05 M to 0.5 M. [Re] = 3 x10^{-4} M, λ = 345 nm.

	15.1 °C	24.9 °C	35.1 °C	45.3 °C
$10^3 k_1$ ($M^{-1}s^{-1}$)	17.50 ± 0.08	58.6 ± 0.2	175.4 ± 0.5	528.9 ± 0.5
$10^3 k_{-1}$ (s^{-1})	0.07 ± 0.02	0.26 ± 0.06	0.8 ± 0.1	2.2 ± 0.1
K_1 (M^{-1})[a]	250 ± 71	225 ± 52	219 ± 27	240 ± 11
K_1 (M^{-1})[b]	205 ± 11	200 ± 8	205 ± 4	210 ± 7

[a] $K_1 = k_1/k_{-1}$; [b] $A_{obs} = \frac{A_M + A_{ML}K_1[X]}{1 + K_1[X]}$

The plot of ln(k_1/T) *vs* 1/T is presented in Figure **5-52**. A comparative discussion of the data will be undertaken in Paragraph 5.4.

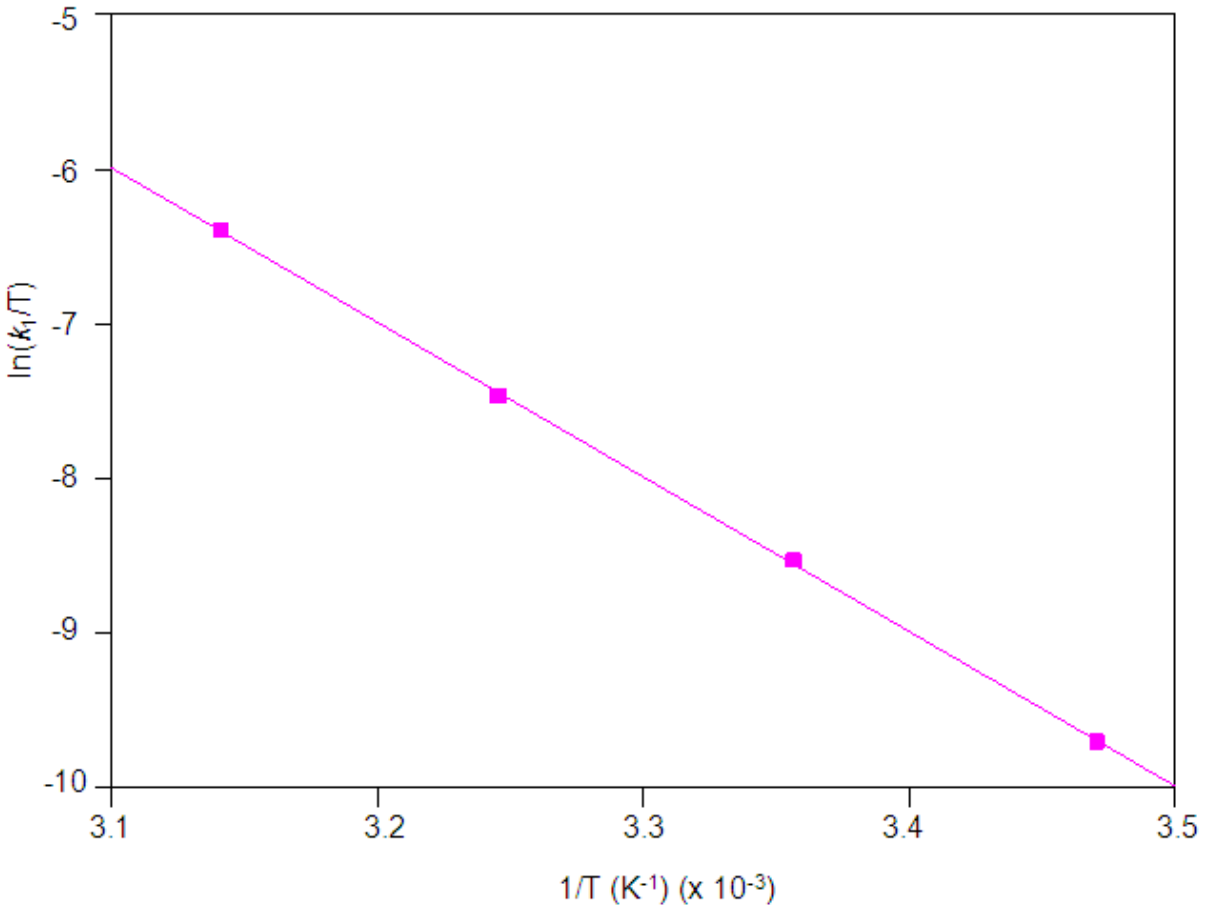

Figure 5-52: Plot of ln(k_1/T) *vs* 1/T for the reaction between *fac*-[Re(CO)$_3$(MeOH)(MeTIF)] and thiourea for a temperature range of 15.1 °C to 45.3 °C.

5.3.6.2 fac-[Re(CO)$_3$(MeOH)(MeTIF)] + NCS$^-$

The methanol substitution reaction between *fac*-[Re(CO)$_3$(MeOH)(MeTIF)] and thiocyanate was performed at 340 nm in methanol and at four different temperatures ranging between 14.8 °C and 45.1 °C, with [NCS$^-$] varying between 0.05 M and 0.5 M. The final UV/Vis spectrum of the reaction solution is identical to the one obtained from the synthesized *fac*-[Re(CO)$_3$(NCS)(MeTIF)]$^-$ complex in Chapter 3.

The graph of k_{obs} *vs* [NCS$^-$] at different temperatures is presented in Figure **5-53** below, the rate constants for the reaction are reported in Table **5-27** while the Eyring plot is illustrated in Figure **5-54**.

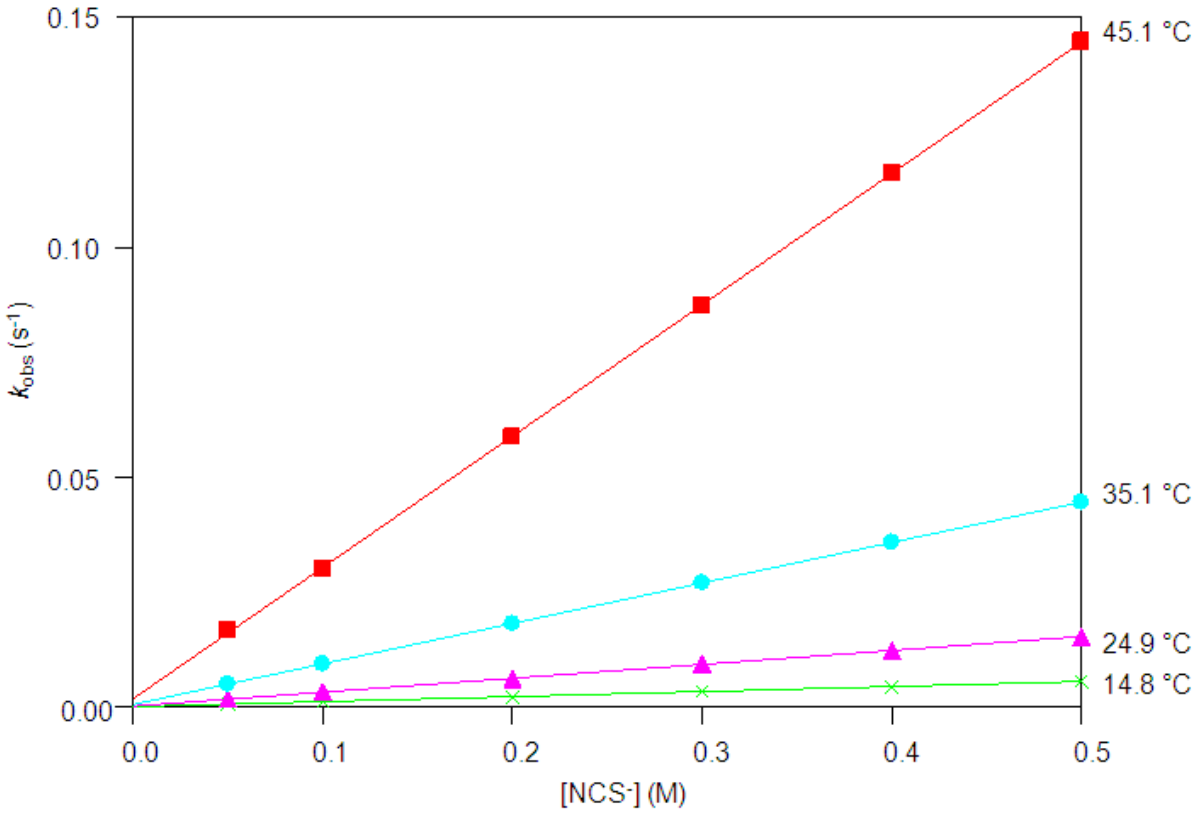

Figure 5-53: Plot of k_{obs} *vs* [NCS$^-$] for the reaction between *fac*-[Re(CO)$_3$(MeOH)(MeTIF)] and thiocyanate ions at four different temperatures in methanol, with [NCS$^-$] = 0.05 M to 0.5 M. [Re] = 3 x10^{-4} M, λ = 340 nm.

The activation parameters have been calculated by the Eyring plot (Equation **3**) as well as the global fit of temperature *vs* ligand concentration *vs* k_{obs} data (Equation **4**): $\Delta H^{\ddagger}$ = 73 ± 1 kJmol^{-1} and $\Delta S^{\ddagger}$ = -28 ± 3 JK^{-1}mol^{-1} from the Eyring plot and $\Delta H^{\ddagger}$ = 90 ± 1 kJmol^{-1} and $\Delta S^{\ddagger}$ = 28 ± 4 JK^{-1}mol^{-1} from the global fit.

Table 5-27: Summary of the rate constants of the reaction between *fac*-[Re(CO)$_3$(MeOH)(MeTIF)] and NCS$^-$ at different temperatures, with [NCS$^-$] = 0.05 M to 0.5 M. [Re] = 3 x10^{-4} M, λ = 340 nm.

	14.8 °C	**24.9 °C**	**35.1 °C**	**45.1 °C**
$10^3 k_1$ ($M^{-1}s^{-1}$)	10.95 ± 0.07	30.3 ± 0.2	88.0 ± 0.3	285.7 ± 0.9
$10^3 k_{-1}$ (s^{-1})	0.07 ± 0.02	0.19 ± 0.06	0.57 ± 0.09	1.8 ± 0.3
K_1 (M^{-1})[a]	156 ± 45	159 ± 50	154 ± 24	159 ± 26
K_1 (M^{-1})[b]	124 ± 3	120 ± 5	132 ± 4	128 ± 7

[a] $K_1 = k_1/k_{-1}$; [b] $A_{obs} = \frac{A_M + A_{ML}K_1[X]}{1 + K_1[X]}$

The plot of ln(k_1/T) *vs* 1/T is presented in Figure **5-54**. A comparative discussion of the data will be undertaken in Paragraph 5.4.

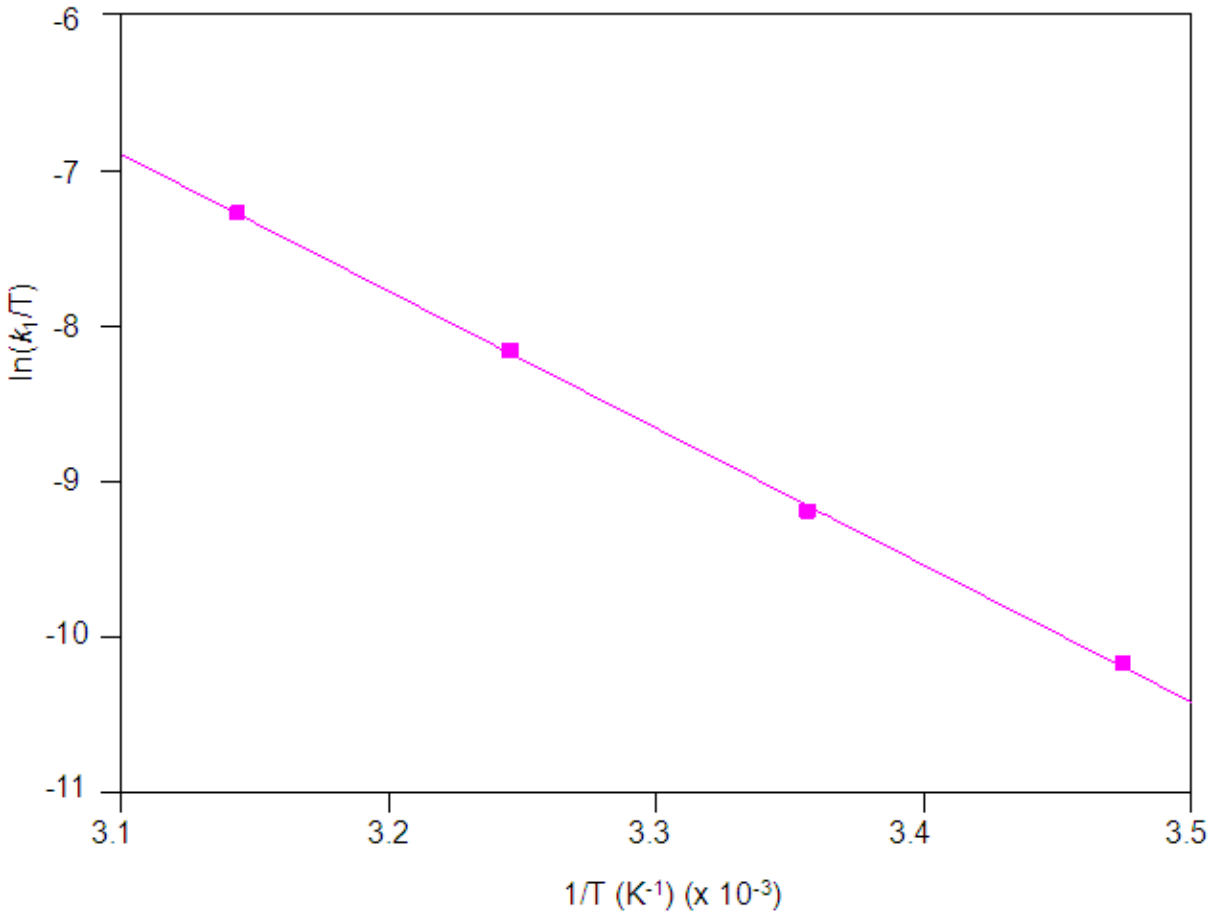

Figure 5-54: Plot of ln(k_1/T) *vs* 1/T for the reaction between *fac*-[Re(CO)$_3$(MeOH)(MeTIF)] and thiocyanate for a temperature range of 14.8°C to 45.1 °C.

5.3.6.3 fac-[Re(CO)$_3$(MeOH)(MeTIF)] + PCy$_3$

The methanol substitution reaction between *fac*-[Re(CO)$_3$(MeOH)(MeTIF)] and tricyclohexylphosphine was performed at 345 nm in methanol and at four different temperatures ranging between 14.7 °C and 45.7 °C, with [PCy$_3$] varying between 0.01 M and 0.05 M. The concentration of PCy$_3$ could not be increased since the solution was saturated at 0.05 M in methanol. At concentrations lower than 0.01 M the absorbance change is too small; thus the smaller concentration range of 0.01 M to 0.05 M was used. The final UV/Vis spectrum of the reaction solution is identical to the one obtained from the synthesized *fac*-[Re(CO)$_3$(PCy$_3$)(MeTIF)] complex in Chapter 3.

The graph of k_{obs} *vs* [PCy$_3$] at different temperatures is presented in Figure **5-55** below, the rate constants for the reaction are reported in Table **5-28** while the Eyring plot is illustrated in Figure **5-56**.

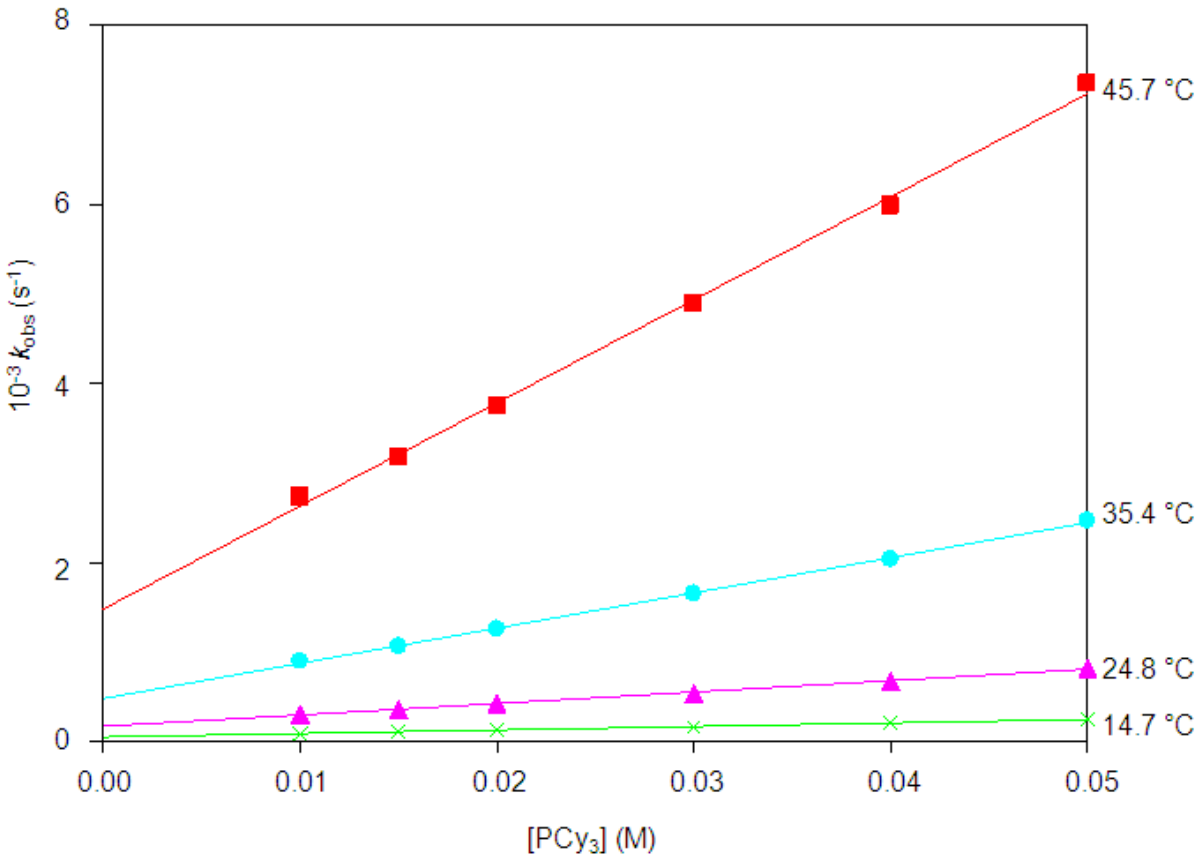

Figure 5-55: Plot of k_{obs} *vs* [PCy$_3$] for the reaction between *fac*-[Re(CO)$_3$(MeOH)(MeTIF)] and tricyclohexylphosphine at four different temperatures in methanol, with [PCy$_3$] = 0.01 M to 0.05 M. [Re] = 3 x10^{-4} M, λ = 345 nm.

The activation parameters have been calculated by the Eyring plot (Equation **3**) as well as the global fit of temperature *vs* ligand concentration *vs* k_{obs} data (Equation **4**) and it is clear that the traditional Eyring plot yields similar results to the global fit. $\Delta H^{\ddagger}$ = 80 ± 1 kJmol^{-1} and $\Delta S^{\ddagger}$ = -11 ± 2 JK^{-1}mol^{-1} from the Eyring plot and $\Delta H^{\ddagger}$ = 82 ± 1 kJmol^{-1} and $\Delta S^{\ddagger}$ = -8 ± 3 JK^{-1}mol^{-1} from the global fit.

Table 5-28: Summary of the rate constants of the reaction between *fac*-[Re(CO)$_3$(MeOH)(MeTIF)] and tricyclohexylphosphine at different temperatures in methanol, with [PCy$_3$] = 0.01 M to 0.05 M. [Re] = 3 x10^{-4} M, λ = 345 nm.

	14.7 °C	**24.8 °C**	**35.4 °C**	**45.7 °C**
$10^3 k_1$ ($M^{-1}s^{-1}$)	3.93 ± 0.07	12.8 ± 0.3	39.3 ± 0.6	115 ± 3
$10^3 k_{-1}$ (s^{-1})	0.052 ± 0.002	0.17 ± 0.01	0.48 ± 0.02	1.48 ± 0.09
K_1 (M^{-1})[a]	76 ± 3	75 ± 5	82 ± 4	78 ± 5
K_1 (M^{-1})[b]	86 ± 5	83 ± 7	75 ± 4	80 ± 4

a $K_1 = k_1/k_{-1}$; **b** $A_{obs} = \frac{A_M + A_{ML}K_1[X]}{1 + K_1[X]}$

The plot of ln(k_1/T) *vs* 1/T is presented in Figure **5-56**. A comparative discussion of the data will be undertaken in Paragraph 5.4.

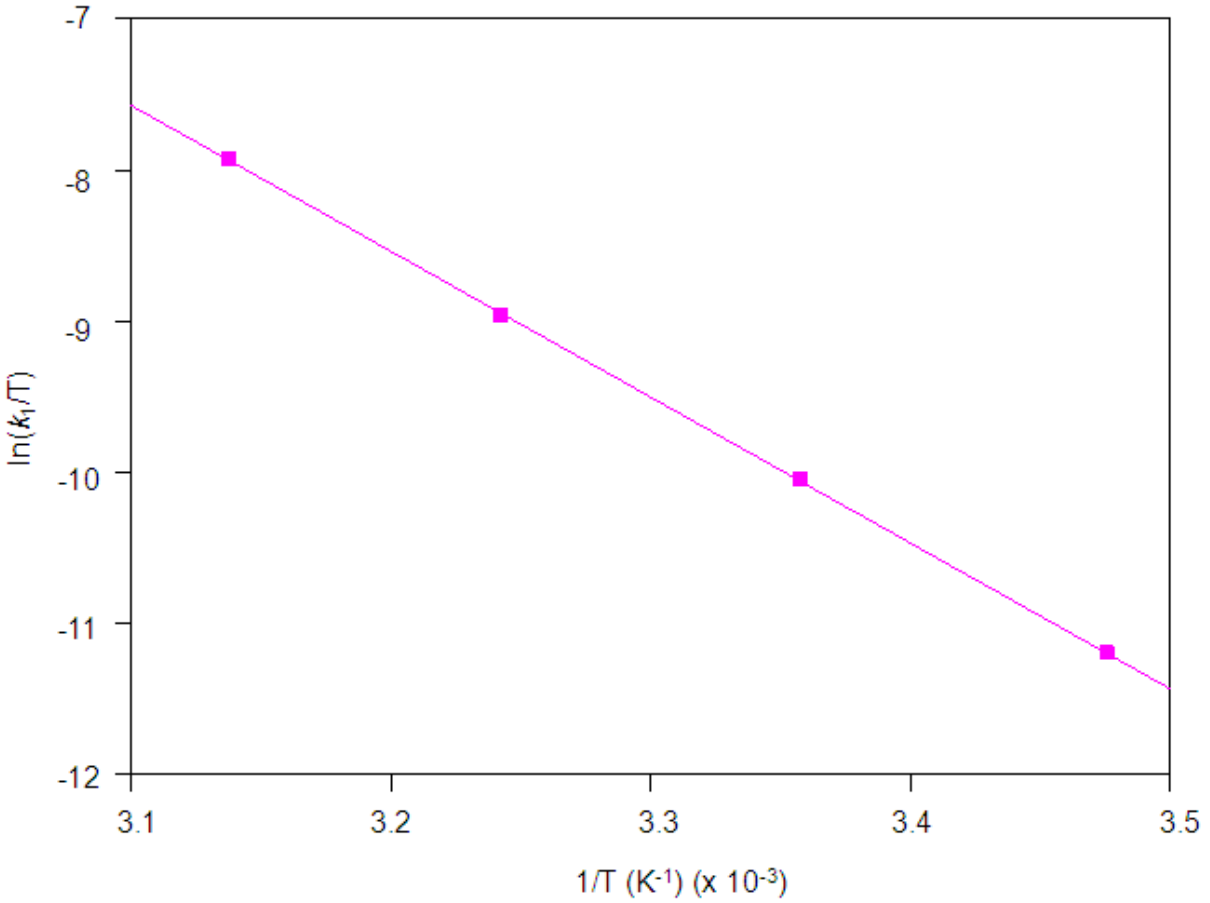

Figure 5-56: Plot of ln(k_1/T) *vs* 1/T for the reaction between *fac*-[Re(CO)$_3$(MeOH)(MeTIF)] and tricyclohexylphosphine for a temperature range of 14.7 °C to 45.7 °C.

5.3.6.4 fac-[Re(CO)$_3$(MeOH)(MeTIF)] + Br$^-$

The methanol substitution reaction between *fac*-[Re(CO)$_3$(MeOH)(MeTIF)] and bromide ions (Br$^-$) was performed at 340 nm in methanol and at four different temperatures ranging between 14.6 °C and 45.0 °C, with [Br$^-$] varying between 0.05 M and 0.5 M. The final UV/Vis spectrum of the reaction solution is identical to the one obtained from the synthesized *fac*-[Re(CO)$_3$(Br)(MeTIF)]$^-$ complex in Chapter 3.

The graph of k_{obs} *vs* [Br$^-$] at different temperatures is presented in Figure **5-57**. An illustration of A_{obs} *vs* [Br$^-$], for the thermodynamically calculated equilibrium constant at 24.5 °C, is presented in Figure **5-58**. The rate constants for the reactions are reported in Table **5-29** and the Eyring plot is illustrated in Figure **5-59**.

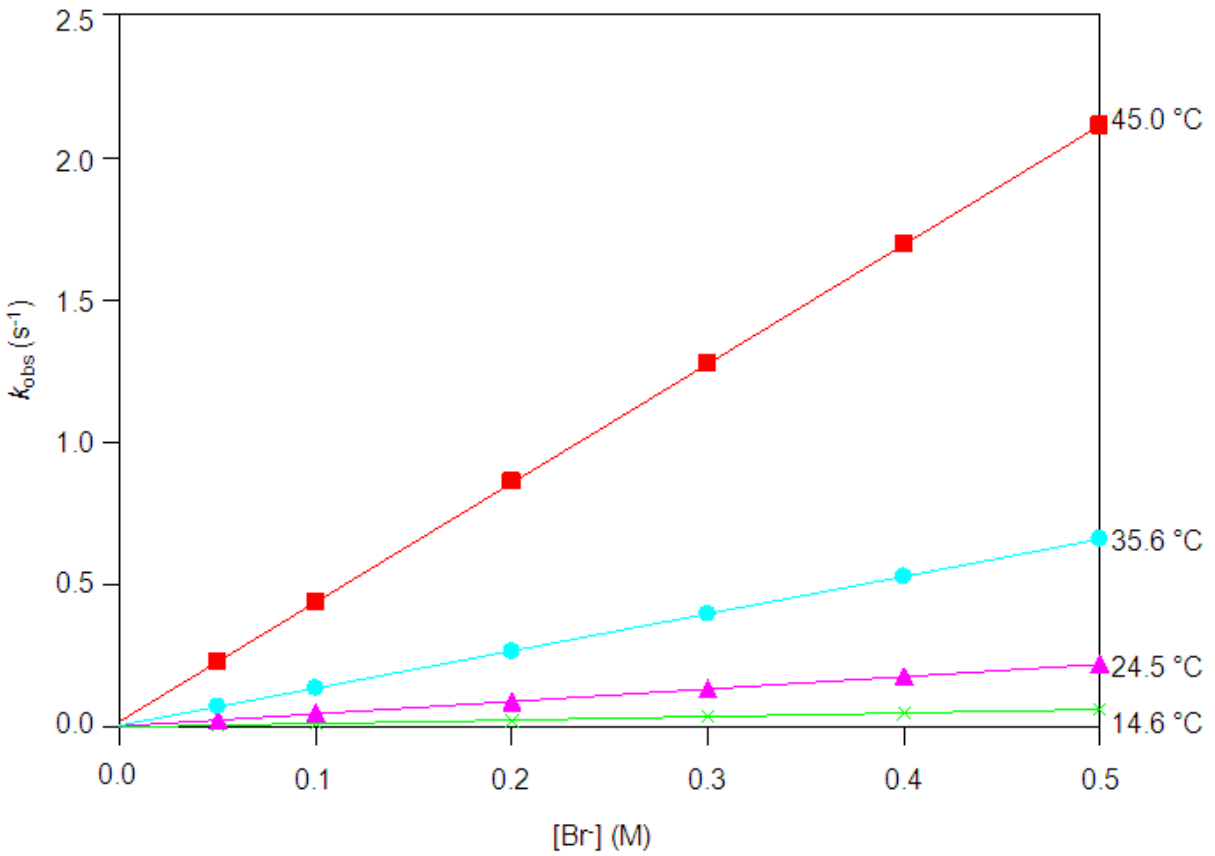

Figure 5-57: Plot of k_{obs} *vs* [Br$^-$] for the reaction between *fac*-[Re(CO)$_3$(MeOH)(MeTIF)] and bromide ions at four different temperatures in methanol, with [Br$^-$] = 0.05 M to 0.5 M. [Re] = 3 x 10^{-4} M, λ = 340 nm.

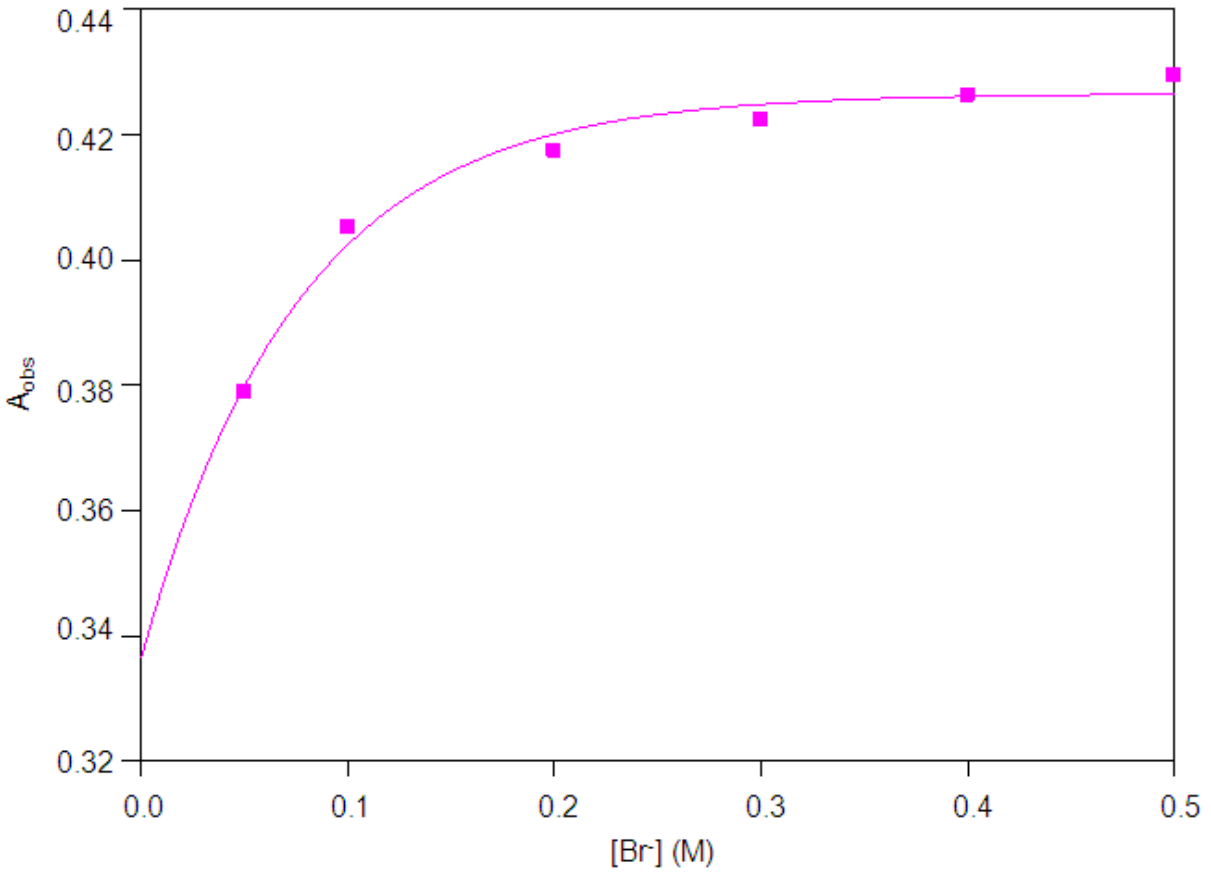

Figure 5-58: Plot of A_{obs} *vs* [Br^-] of the reaction of *fac*-[$Re(CO)_3$(MeOH)(MeTIF)] with Br^- ions at 24.5 °C. [Re] = 3 x 10^{-4} M, λ = 340 nm.

The activation parameters have been calculated by the Eyring plot (Equation **3**) as well as the global fit of temperature *vs* ligand concentration *vs* k_{obs} data (Equation **4**) and it is clear that the traditional Eyring plot yields similar results to the global fit. $\Delta H^{\ddagger}$ = 83 ± 1 kJmol^{-1} and $\Delta S^{\ddagger}$ = 27 ± 2 JK^{-1}mol^{-1} from the Eyring plot and $\Delta H^{\ddagger}$ = 94 ± 2 kJmol^{-1} and $\Delta S^{\ddagger}$ = 62 ± 5 JK^{-1}mol^{-1} from the global fit.

Table 5-29: Summary of the rate constants of the reaction between *fac*-[$Re(CO)_3$(MeOH)(MeTIF)] and bromide ions at different temperatures in methanol, with [Br^-] = 0.05 M to 0.5 M. [Re] = 3 x 10^{-4} M, λ = 340 nm.

	14.6 °C	**24.5 °C**	**35.6 °C**	**45.0 °C**
$10^2 k_1$ ($M^{-1}s^{-1}$)	124.0 ± 0.5	438 ± 1	1308 ± 3	4182 ± 6
$10^2 k_{-1}$ (s^{-1})	0.7 ± 0.2	2.4 ± 0.4	6.6 ± 0.8	21 ± 2
K_1 (M^{-1})[a]	177 ± 51	183 ± 30	198 ± 24	199 ± 19
K_1 (M^{-1})[b]	156 ± 3	165 ± 5	160 ± 6	164 ± 3

[a] $K_1 = k_1/k_{-1}$; [b] $A_{obs} = \frac{A_M + A_{ML}K_1[X]}{1 + K_1[X]}$

The plot of ln(k_1/T) *vs* 1/T is presented in Figure **5-59**. A comparative discussion of the data will be undertaken in Paragraph 5.4.

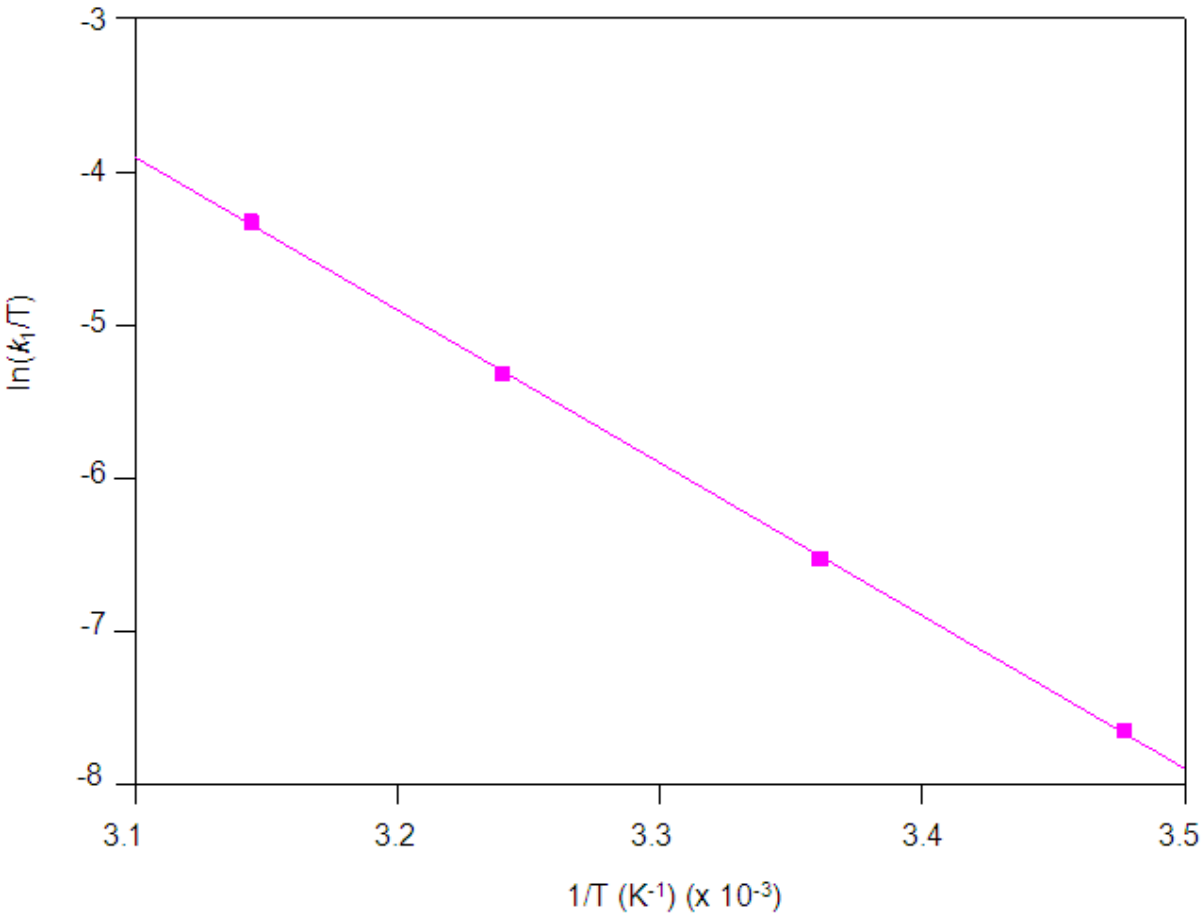

Figure 5-59: Plot of ln(k_1/T) *vs* 1/T for the reaction between *fac*-[Re(CO)$_3$(MeOH)(MeTIF)] and bromide ions for a temperature range of 14.6 °C to 45.0 °C.

5.3.6.5 Summary of the results of the methanol substitution reactions of fac-[Re(CO)$_3$(MeOH)(MeTIF)]

The substitution reactions between *fac*-[Re(CO)$_3$(MeOH)(MeTIF)] and four different mondentate ligands have been studied (Paragraph 5.3.6.1 to 5.3.6.4, thiourea (TU), thiocyanate (NCS^-), tricyclohexylphosphine (PCy_3) and bromide ions (Br^-)).

The k_1 values for the substitution reactions with different entering ligands follow the trend k_1 (Br^-) > k_1 (TU) > k_1 (NCS^-) > k_1 (PCy_3). A graph to illustrate the effect of the entering ligand on the rate of the reaction is illustrated in Figure **5-60**. The reverse

reaction rate constant (k_{-1}) decreases in the following order Br^- > TU > NCS^- > PCy_3 and the stability constant, K_1, for these reactions follow the trend: K1(TU) > K1(Br-) > K1(NCS-) > K1(PCy3) with the PCy3 being the least stable complex. K_1 range between 75 ± 5 and 225 ± 52. A reasonably good agreement exists between the stability constants determined kinetically and those determined thermodynamically. The enthalpy of activation ($\Delta H^{\ddagger}$) values for all the reactions are similar while the small negative to small positive values of $\Delta S^{\ddagger}$ for all the reactions (with TU, NCS^-, PCy_3 and Br^-) suggest an interchange associative to interchange dissociative type of activation. Generally the $\Delta H^{\ddagger}$ and $\Delta S^{\ddagger}$ values calculated from the Eyring equation and the global fit differ significantly. A large variation in the $\Delta S^{\ddagger}$ values again highlights the need for high pressure studies to confirm the mechanism of activation.

Table 5-30: Rate constants of the different reactions between *fac*-[Re(CO)$_3$(MeOH)(MeTIF)] and different entering ligands at ~ 25 °C.

	$10^3 k_1$ ($M^{-1}s^{-1}$)	$10^3 k_{-1}$ (s^{-1})	K_1 (M^{-1})	$\Delta H^{\ddagger}$ ($kJmol^{-1}$)	$\Delta S^{\ddagger}$ ($JK^{-1}mol^{-1}$)
TU	58.6 ± 0.2	0.26 ± 0.06	225 ± 52[a], 200 ± 8[b]	83 ± 1[c], 85 ± 1[d]	10 ± 2[c], 14 ± 3[d]
NCS^-	30.3 ± 0.2	0.19 ± 0.06	159 ± 50[a], 120 ± 5[b]	73 ± 1[c], 90 ± 1[d]	-28± 3[c], 28 ± 4[d]
PCy_3	12.8 ± 0.3	0.17 ± 0.01	75 ± 5[a], 83 ± 7[b]	80 ± 1[c], 82 ± 1[d]	28 ± 3[c], -8 ± 3[d]
Br^-	438 ± 1	2.4 ± 0.4	183 ± 30[a], 165 ± 5[b]	83 ± 1[c], 94 ± 2[d]	27 ± 2[c], 62± 5[d]

[a] $K_1 = k_1/k_{-1}$, [b] $A_{obs} = \frac{A_M + A_{ML}K_1[X]}{1 + K_1[X]}$, [c] Eyring fit, [d] Global fit.

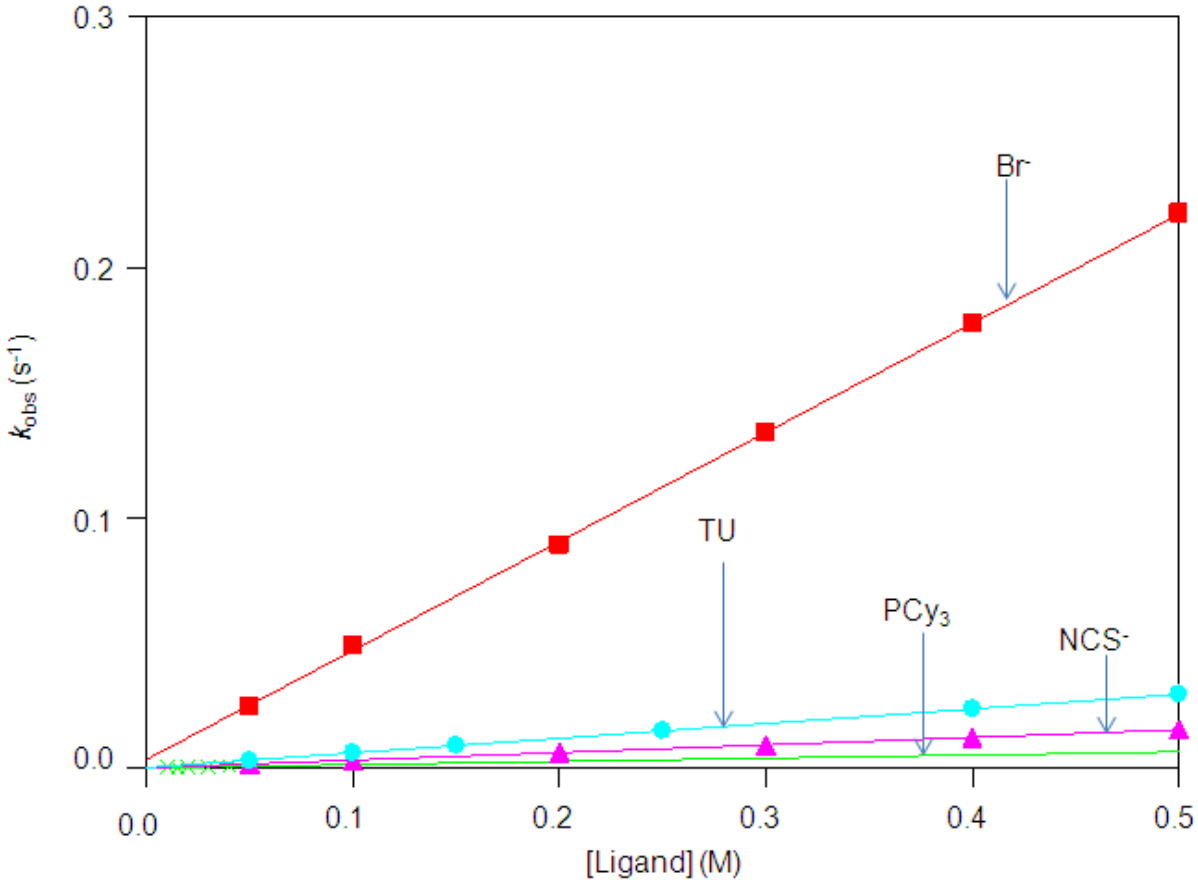

Figure 5-60: Schematic representation of k_{obs} *vs* [ligand] of the reactions between *fac*-[Re(CO)$_3$(MeOH)(MeTIF)] and various entering ligands at ~ 25 °C.

5.4 Discussion

The six rhenium(I) tricarbonyl complexes selected for this methanol substitution study were *fac*-[Re(CO)$_3$(MeOH)(DiMePy)]$^+$ (**1**) and *fac*-[Re(CO)$_3$(MeOH)(DiMeOPy)]$^+$ (**2**) representing the complexes with *N,N'*-bidentate ligands and the four complexes with *O,O'*-bidentate ligands were *fac*-[Re(CO)$_3$(MeOH)(4-MeTPh)] (**3**), *fac*-[Re(CO)$_3$(MeOH)(BrDiPhPr)], (**4**) *fac*-[Re(CO)$_3$(MeOH)(TIF)] (**5**) and *fac*-[Re(CO)$_3$(MeOH)(MeTIF)] (**6**). A methanol ligand is available for substitution by monodentate ligands in these complexes. The rate constants for these methanol substitution reactions, discussed in detail in Paragraph 5.3 are summarized in Table **5-31** and Table **5-32**.

5.4.1 Rhenium(I) tricarbonyl complexes with *N,N'*-bidentate ligands

A schematic diagram of *fac*-$[Re(CO)_3(MeOH)(DiMePy)]^+$ (**1**) and *fac*-$[Re(CO)_3(MeOH)(DiMeOPy)]^+$ (**2**) is given in Figure **5-61**.

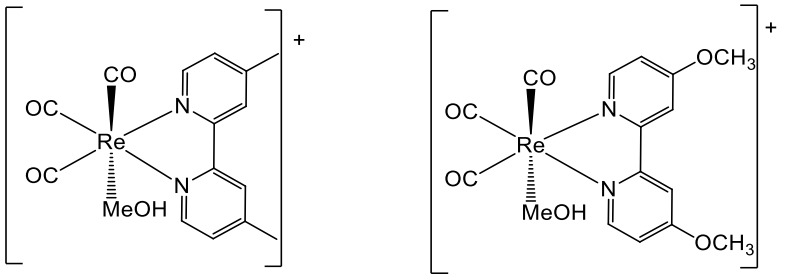

fac-$[Re(CO)_3(MeOH)(DiMePy)]^+$ (**1**) *fac*-$[Re(CO)_3(MeOH)(DiMeOPy)]^+$ (**2**)

Figure 5-61: Schematic illustration of *fac*-$[Re(CO)_3(MeOH)(DiMePy)]^+$ (1) and *fac*-$[Re(CO)_3(MeOH)(DiMeOPy)]^+$ (2).

A comparison of the kinetic data of **1** and **2** (Table **5-31**), revealed the following:

- There is a slight increase in k_1 for the substitution reactions from **2** to **1** for every entering ligand as shown in Table **5-31**. The reason for this is unclear since the only difference between **1** and **2** is the extra oxygen atoms on the backbone of **2** and it is unexpected to have an influence on the electron density on the metal centre. It might be due to the steric effect, but we cannot confirm this at this stage.
- The forward rate constants of **1** and **2** follow the same trend of Br^- > TU > NCS^- > PCy_3, while the reverse rate constants of **1** and **2** also follow the same trend: $k_{-1}(Br^-) > k_{-1}(TU) > k_{-1}(NCS^-) \approx k_{-1}(PCy_3)$.
- The forward rate constant for **1** and **2** with the neutral TU and PCy_3 as entering monodentate ligands clearly shows that the S donor TU is ~ 7/8 times faster than the P donor PCy_3; with NCS^- and Br^- as negatively charged entering ligands, Br^- is ~ 5 times faster than NCS^-. No systematic variation in k_1 values is observed between the reactions with neutral monodentate ligands and charged monodentate ligands, although it is expected that the negatively charged entering ligands will have an electrostatic effect that influence the rate in a positive way, compared to the absence thereof with the neutral entering ligands. The reactions with TU are faster than the reactions with NCS^-, illustrating the affinity of Re(I) for S donor ligands.

- For **1** the total difference in k_1 values from PCy_3 to Br^- is ~ 12 fold and for **2** ~ 18 fold while the k_{-1} values of **1** differs by a factor of ~ 5.7 and for **2** it differs by a factor of ~ 7.8.
- The K_1 values for the reaction with NCS^- and Br^- for **1** and **2** are the highest, suggesting the most stable products followed by the TU complexes, with the PCy_3 complexes being the least stable.
- A reasonably good agreement between the kinetically *vs* thermodynamically determined K_1 values is observed.
- Generally, the $\Delta H^{\ddagger}$ values for all the reactions for both complexes (**1** and **2**) are similar and also in the same range as other reactions of this type.[1,5,10,11,12]
- The small negative and small positive values of $\Delta S^{\ddagger}$ for the reactions of **1** and **2** suggests an interchange associative to interchange dissociative type of activation.
- A reasonably good agreement is seen in the traditional Eyring plot and Global fit determined $\Delta H^{\ddagger}$ values, however larger variations are seen in the $\Delta S^{\ddagger}$ values.
- With regards to the mechanism of the reactions of **1** and **2**, the $\Delta S^{\ddagger}$ values mainly suggest an I_a mechanism (small negative values) while it is not clear whether a larger dependence on the Re-MeOH bond breaking (dependent on k_1) or Re-X bond breaking (dependent on k_{-1}) is more prominent with a total difference in k_1 for **1** and **2** of ~12 and ~18 and in k_{-1} for **1** and **2** of ~6 and ~8 respectively.
- The k_1 values obtained for the substitution reactions of **1** and **2** with Br^- are (33.1 ± 0.6) x 10^{-3} $M^{-1}s^{-1}$ and (28.7 ± 0.1) x 10^{-3} $M^{-1}s^{-1}$ respectively, while in literature a value of (42 ± 7) x 10^{-3} $M^{-1}s^{-1}$ and (50 ± 3) x 10^{-3} $M^{-1}s^{-1}$ is reported for the reaction of *fac*-$[Re(CO)_3(MeOH)(Bipy)]^+$ and *fac*-$[Re(CO)_3(MeOH)(Phen)]^+$ with Br^- (Bipy = 2,2'-bipyridine, Phen = phenanthroline).[5] To compare phosphorus donor ligands, the reaction of **1** and **2** with PCy_3 yield k_1 values of (2.66 ± 0.01) x 10^{-3} $M^{-1}s^{-1}$ and (1.56 ± 0.02) x 10^{-3} $M^{-1}s^{-1}$ while for *fac*-$[Re(CO)_3(MeOH)(Bipy)]^+$ and *fac*-$[Re(CO)_3(MeOH)(Phen)]^+$ values of (12.3 ± 0.1) x 10^{-3} $M^{-1}s^{-1}$ and (7.9 ± 0.1) x 10^{-3} $M^{-1}s^{-1}$ for 1,3,5-triaza-7-phospha-adamantane (PTA) as entering ligand are reported. For S donor ligands, the reaction of **1** and **2** with thiourea yielded

k_1 values of (18.6 ± 0.1) x 10^{-3} $M^{-1}s^{-1}$ and (13.7 ± 0.4) x 10^{-3} $M^{-1}s^{-1}$ while for *fac*-$[Re(CO)_3(MeOH)(Bipy)]^+$ and *fac*-$[Re(CO)_3(MeOH)(Phen)]^+$ values of (17.3 ± 0.1) x 10^{-3} $M^{-1}s^{-1}$ and (13.7 ± 0.1) x 10^{-3} $M^{-1}s^{-1}$ for methylthiourea (MeTU) as entering ligand are reported. All in all the rate constants reported here for **1** and **2** are comparable to other Re-*N,N'* complexes in literature.[1,5,12]

Table 5-31: Summary of the results of the methanol substitution reactions of *fac*-$[Re(CO)_3(MeOH)(DiMePy)]^+$ (1) and *fac*-$[Re(CO)_3(MeOH)(DiMeOPy)]^+$ (2) with different entering ligands at ~ 25 °C.

	Constant	(1)	(2)
TU	10^3k_1 ($M^{-1}s^{-1}$)	18.6 ± 0.1	13.7 ± 0.4
	10^3k_{-1} (s^{-1})	0.19 ± 0.04	0.15 ± 0.01
	K_1 (M^{-1})	98 ± 20[a], 100 ± 6[b]	91 ± 7[a], 86 ± 4[b]
	$\Delta H^{\ddagger}$ (kJmol^{-1})	65 ± 1[c], 77.5 ± 0.8[d]	73 ± 1[c], 61 ± 1[d]
	$\Delta S^{\ddagger}$ ($JK^{-1}mol^{-1}$)	-59 ± 5[c], -14 ± 2[d]	-35 ± 4[c], -77 ± 4[d]
NCS^-	10^3k_1 ($M^{-1}s^{-1}$)	6.42 ± 0.02	5.94 ± 0.02
	10^3k_{-1} (s^{-1})	0.044 ± 0.005	0.043 ± 0.005
	K_1 (M^{-1})	146 ± 17[a], 118 ± 4[b]	138 ± 16[a], 103 ± 7[b]
	$\Delta H^{\ddagger}$ (kJmol^{-1})	74 ± 2[c], 77 ± 2[d]	77 ± 1[c], 78.0 ± 0.3[d]
	$\Delta S^{\ddagger}$ ($JK^{-1}mol^{-1}$)	-34 ± 1[c], -27 ± 5[d]	-27 ± 1[c], -26.4 ± 0.8[d]
PCy_3	10^3k_1 ($M^{-1}s^{-1}$)	2.66 ± 0.01	1.56 ± 0.02
	10^3k_{-1} (s^{-1})	0.0490 ± 0.0004	0.0295 ± 0.0006
	K_1 (M^{-1})	54.3 ± 0.5 [a], 55 ± 12[b]	53 ± 1[a], 59 ± 4[b]
	$\Delta H^{\ddagger}$ (kJmol^{-1})	79 ± 1[c], 72 ± 4[d]	80 ± 2[c], 94 ± 1[d]
	$\Delta S^{\ddagger}$ ($JK^{-1}mol^{-1}$)	-26 ± 2[c], -51 ± 14[d]	-27 ± 2[c], 15 ± 4[d]
Br^-	10^3k_1 ($M^{-1}s^{-1}$)	33.1 ± 0.6	28.7 ± 0.1
	10^3k_{-1} (s^{-1})	0.28 ± 0.02	0.23 ± 0.04
	K_1 (M^{-1})	118 ± 9[a], 120 ± 2[b]	125 ± 22[a], 102 ± 8[b]
	$\Delta H^{\ddagger}$ (kJmol^{-1})	77 ± 1[c], 78 ± 1	78 ± 1[c], 77.9 ± 0.8[d]
	$\Delta S^{\ddagger}$ ($JK^{-1}mol^{-1}$)	-13 ± 1[c], -13 ± 3[d]	-10 ± 1[c], -14 ± 2[d]

[a] Kinetically calculated, [b] Thermodynamically calculated, [c] from Eyring plot, [d] from Global fit.

[12] Twala, T.N., Schutte-Smith, Roodt, A., Visser, H.G. *Dalton Trans*. **44(7)** (2015) 3278-3288.

5.4.2 Rhenium(I) tricarbonyl complexes with *O,O'*-bidentate ligands

Schematic diagram of *fac*-[Re(CO)$_3$(MeOH)(4-MeTPh)] (**3**), *fac*-[Re(CO)$_3$(MeOH)(BrDPhPr)] (**4**), *fac*-[Re(CO)$_3$(MeOH)(TIF)] (**5**) and *fac* [Re(CO)$_3$(MeOH)(MeTIF)] (**6**) is given in Figure **5-62**.

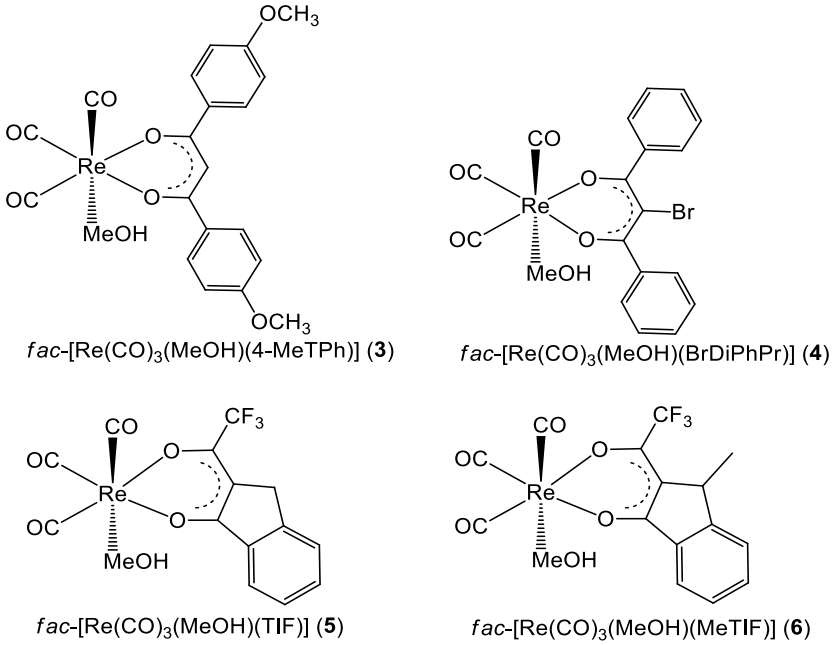

Figure 5-62: Schematic illustrations of *fac*-[Re(CO)$_3$(MeOH)(4-MeTPh)] (3), *fac*-[Re(CO)$_3$(MeOH)(BrDiPhPr)] (4), *fac*-[Re(CO)$_3$(MeOH)(TIF)] (5) and *fac*-[Re(CO)$_3$(MeOH)(MeTIF)] (6).

A comparison of *fac*-[Re(CO)$_3$(MeOH)(4-MeTPh)] (**3**), *fac*-[Re(CO)$_3$(MeOH)(BrDiPhPr)] (**4**), *fac*-[Re(CO)$_3$(MeOH)(TIF)] (**5**) and *fac*-[Re(CO)$_3$(MeOH)(MeTIF)] (**6**) (Table **5-32**), revealed the following:

- The forward rate constants of **3**, **4**, **5** and **6** follows the same trend of Br^- > TU > NCS^- > PCy_3/PPh_3.
- When comparing the k_1 values of **3** and **4**, **3** is slightly faster than **4** for all the reactions except for the reaction with NCS^-. The reason for this might be the electron withdrawing Br atom attached to the backbone of the acac moiety of BrDiPhPr, decreasing the electron density on the metal centre, shortening the Re-MeOH bond, which makes it more difficult to substitute.

- When comparing the k_1 values of **5** and **6**, **5** is slightly faster than **6** for all four reactions. The reason for this is unclear but it could possibly be due to a small steric effect of the extra methyl group on the backbone of **6** or the electron withdrawing effect of the methyl group shortening the Re-MeOH bond and therefore slowing down the methanol substitution.
- A comparison of the forward rate constant for **3** and **4** with TU and PCy_3/PPh_3 as neutral entering monodentate ligands shows that TU is ~7 to ~9 times faster than PCy_3/PPh_3; with NCS^- and Br^- as negatively charged entering ligands, Br^- is ~12.5 to ~31 times faster than NCS^-. In total, k_1 for **3** varies with a factor of ~45 while for **4** it varies with a factor of ~42.
- For the reactions with the neutral ligands TU and PCy_3 of **5** and **6**, TU is ~4 times faster than PCy_3; for the negatively charged ligands NCS^- and Br^-, Br^- is ~12.7 to ~14.5 times faster than NCS^-. In total k_1 varies with a factor of ~27 for **5** and a factor of ~34 for **6**.
- The k_{-1} values of **3**, **4**, **5** and **6** for the four reactions follow the same trend: $k_{-1}(Br^-) > k_{-1}(TU) > k_{-1}(NCS^-) \approx k_{-1}(PCy_3/PPh_3)$ with a total variation in k_{-1} of ~40 (for **3**), ~41 (for **4**), ~10 (for **5**), and ~14 (for **6**).
- The stability constants of **3**, **4**, **5** and **6** vary significantly but it is safe to say that the PCy_3/PPh_3 complexes are the least stable for **3**, **4**, **5** and **6**.
- Interestingly, **5** and **6** form relatively more stable products with TU and Br^- compared to **3** and **4**, while **3** and **4** form more stable products with the phosphorous donors PCy_3/PPh_3 compared to **5** and **6**.
- A reasonably good agreement of kinetically *vs* thermodynamically determined K_1 values are observed for **3**, **4**, **5** and **6**.
- The $\Delta H^{\ddagger}$ values for all the reactions of **3**, **4**, **5** and **6** are similar and also compare well to other reaction of this type.[5,13,14,18,19]
- The small negative to small positive values of $\Delta S^{\ddagger}$ for the reactions of **3**, **4**, **5** and **6** suggests an interchange associative to interchange dissociative type of activation.

[13] Manicum, A., Schutte-Smith, M., Kemp, G., Visser, H.G. *Polyhedron*. **85** (2015) 190-195.

[14] Schutte, M., Roodt, A., Visser, H.G. *Inorg. Chem*. **51**(21) (2012) 11996-12006.

- Generally, a reasonably good agreement is observed between the traditional Eyring plot and Global fit data of $\Delta H^{\ddagger}$ and $\Delta S^{\ddagger}$. In most cases, the $\Delta S^{\ddagger}$ values differ significantly, emphasizing once again the large errors in the $\Delta S^{\ddagger}$ values and the need for high pressure studies.
- When considering the mechanism of the reactions of **3**, **4**, **5** and **6**, it is unclear from the $\Delta S^{\ddagger}$ values whether the reactions proceed *via* an I_a (small negative) or I_d mechanism (small positive). It is also not clear whether a larger dependence on the Re-MeOH bond breaking (dependent on k_1) or Re-X bond breaking (dependent on k_{-1}) is more prominent with a total difference in k_1 for **3**, **4**, **5** and **6** of ~45, ~42, ~27, ~37 and in k_{-1} for **3**, **4**, **5** and **6** of ~40, ~41, ~10 and ~14 respectively.
- The k_1 values obtained for the reaction of **3**, **4**, **5** and **6** with PCy_3/PPh_3 are reported as (6.14 ± 0.08) x 10^{-3} $M^{-1}s^{-1}$, (4.30 ± 0.05) x 10^{-3} $M^{-1}s^{-1}$, (19.6 ± 0.4) x10^{-3} $M^{-1}s^{-1}$ and (12.8 ± 0.3) x 10^{-3} $M^{-1}s^{-1}$ respectively, while in literature a value of (1.04 ± 0.02) x 10^{-3} $M^{-1}s^{-1}$ and (20.30 ± 0.04) x 10^{-3} $M^{-1}s^{-1}$ are reported for the reaction between *fac*-[$Re(CO)_3$(MeOH)(Acac)] and PCy_3 and PPh_3 respectively (Acac = acetylacetone).[13] The reaction of **3**, **4**, **5** and **6** with bromide ions yielded k_1 values of (227 ± 2) x 10^{-3} $M^{-1}s^{-1}$, (182 ± 1) x 10^{-3} $M^{-1}s^{-1}$, (533 ± 1) x 10^{-3} $M^{-1}s^{-1}$ and (438 ± 1) x 10^{-3} $M^{-1}s^{-1}$, while in literature values of (70.6 ± 0.4) x 10^{-3} $M^{-1}s^{-1}$ and (7200 ± 300) x 10^{-3} $M^{-1}s^{-1}$ are reported for *fac*-[$Re(CO)_3$(MeOH)($TropBr_3$)] and *fac*-[$Re(CO)_3$(MeOH)(Flav)] respectively ($TropBr_3$ = tribromotropolonato , Flav = hydroxyflavonato).[5] For S donor ligands, the reaction of **3**, **4**, **5** and **6** with thiourea yielded k_1 values of (42.5 ± 0.1) x 10^{-3} $M^{-1}s^{-1}$, (39.6 ± 0.2) x 10^{-3} $M^{-1}s^{-1}$, (78.3 ± 0.5) x 10^{-3} $M^{-1}s^{-1}$ and (58.6 ± 0.2) x 10^{-3} $M^{-1}s^{-1}$, respectively, while for *fac*-[$Re(CO)_3$(MeOH)(Trop)] (Trop = tropolone) a k_1 value of (556 ± 3) x 10^{-3} $M^{-1}s^{-1}$ and for *fac*-[$Re(CO)_3$(MeOH)(Isa)] (Isa = isatin) a k_1 value of (36.5 ± 0.2) x 10^{-3} $M^{-1}s^{-1}$ is reported. [15,18] To compare N donor entering ligands, the reaction of **3**, **4**, **5** and **6** with NCS^- yielded k_1 values of (8.90 ± 0.04) x 10^{-3} $M^{-1}s^{-1}$, (14.466 ± 0.006) x 10^{-3} $M^{-1}s^{-1}$, (42.0 ± 0.4) x 10^{-3} $M^{-1}s^{-1}$ and (30.3 ± 0.2) x 10^{-3} $M^{-1}s^{-1}$ respectively, while for *fac*-[$Re(CO)_3$(MeOH)(Trop)] a value of (268 ± 2) x 10^{-3} $M^{-1}s^{-1}$ is reported and for *fac*-[$Re(CO)_3$(MeOH)(Isa)] a value of (18.7 ± 0.1) x

[15] Schutte, M., Ph.D. Thesis, University of the Free State, Bloemfontein, South Africa, 2011.

10^{-3} $M^{-1}s^{-1}$ is reported.[15,17] There is a significant and unclear difference between the data reported here and data from the literature of Re-*O,O'* complexes, especially when compared to the Trop, TropBr3 and Flav complexes. It is important to note that a small change in the bidentate ligand yield significantly different kinetic results as reported earlier.[5,18] Therefore the comparison done here with Br^- and the S and N donor entering ligands is not really reliable since the *O,O'* bidentate ligands in this study and referenced above differ significantly with regards to structures, steric and electron donating ability.

Table 5-32: Summary of the results of the reactions of *fac*-[Re(CO)$_3$(MeOH)(4-MeTPh)] (3) *fac*-[Re(CO)$_3$(MeOH)(BrDPhPr)] (4), *fac*-[Re(CO)$_3$(MeOH)(TIF)] (5) and *fac*-[Re(CO)$_3$(MeOH)(MeTIF)] (6) with different entering ligands at ~ 25 °C.

	Constant	(3)	(4)	(5)	(6)
TU	10^3k_1 ($M^{-1}s^{-1}$)	42.5 ± 0.1	39.6 ± 0.2	78.3 ± 0.5	58.6 ± 0.2
	10^3k_{-1} (s^{-1})	0.29 ± 0.04	0.33 ± 0.06	0.4 ± 0.1	0.26 ± 0.06
	K_1 (M^{-1})	147 ± 20[a], 138 ± 4[b]	120 ± 22[a], 112 ± 3[b]	196 ± 49[a],190 ± 10[b]	225 ± 52[a],200 ± 8[b]
	$\Delta H^‡$ (kJmol^{-1})	78 ± 1[c], 77.5 ± 0.8[d]	79 ± 1[c], 101 ± 3[d]	77 ± 1[c], 109 ± 2[d]	83 ± 1[c], 85 ± 1[d]
	$\Delta S^‡$ ($JK^{-1}mol^{-1}$)	-7 ± 2[c], -14 ± 2[d]	-4 ± 1[c], 61 ± 11[d]	-8 ± 2[c], 94 ± 8[d]	10 ± 2[c], 14 ± 3[d]
NCS^-	10^3k_1 ($M^{-1}s^{-1}$)	8.90 ± 0.04	14.466 ± 0.006	42.0 ± 0.4	30.3 ± 0.2
	10^3k_{-1} (s^{-1})	0.15 ± 0.01	0.121 ± 0.002	0.3 ± 0.1	0.19 ± 0.06
	K_1 (M^{-1})	59 ± 4[a], 50 ± 1[b]	120 ± 2[a], 120 ± 4[b]	140 ± 47[a],138 ± 6[b]	159 ± 50[a],120 ± 5[b]
	$\Delta H^‡$ (kJmol^{-1})	86 ± 1[c], 77 ± 2[d]	73 ± 1[c], 81 ± 1[d]	77 ± 1[c], 89.8 ± 0.9[d]	73 ± 1[c], 90 ± 1[d]
	$\Delta S^‡$ ($JK^{-1}mol^{-1}$)	7 ± 1[c], -27 ± 5[d]	-33 ± 4[c], -11 ± 3[d]	-11 ± 2[c], 29 ± 3	-28 ± 3[c], 28 ± 4[d]
PCy_3/PPh_3	10^3k_1 ($M^{-1}s^{-1}$)	6.14 ± 0.08[e]	4.30 ± 0.05[f]	19.6 ± 0.4[e]	12.8 ± 0.3[e]
	10^3k_{-1} (s^{-1})	0.064 ± 0.003	0.039 ± 0.001	0.32 ± 0.01	0.17 ± 0.01
	K_1 (M^{-1})	96 ± 5[a], 94 ± 8[b]	110 ± 3[a], 110 ± 14[b]	61 ± 2[a], 69 ± 4[b]	75 ± 5[a], 83 ± 7[b]
	$\Delta H^‡$ (kJmol^{-1})	75 ± 1[c], 72 ± 4[d]	80 ± 2[c], 87 ± 1[d]	74 ± 2[c], 80 ± 1[d]	80 ± 1[c], 82 ± 1[d]
	$\Delta S^‡$ ($JK^{-1}mol^{-1}$)	-35 ± 3[c], -51 ± 14[d]	-20 ± 5[c], 9 ± 3[d]	-28 ± 5[c], -12 ± 3[d]	-11 ± 2[c], -8 ± 3[d]
Br^-	10^3k_1 ($M^{-1}s^{-1}$)	277 ± 2	182 ± 1	533 ± 1	438 ± 1
	10^3k_{-1} (s^{-1})	2.6 ± 0.6	1.6 ± 0.3	3.1 ± 0.4	2.4 ± 0.4
	K_1 (M^{-1})	107 ± 25[a], 100 ± 2[b]	114 ± 21[a], 97 ± 6[b]	172 ± 22[a],162 ± 6[b]	183 ± 30[a],165 ± 5[b]
	$\Delta H^‡$ (kJmol^{-1})	81 ± 1[c], 78 ± 1[d]	83 ± 1[c], 83 ± 1[d]	83 ± 1[c], 83.9 ± 0.9[d]	83 ± 1[c], 94 ± 2[d]
	$\Delta S^‡$ ($JK^{-1}mol^{-1}$)	18 ± 3[c], -13 ± 3[d]	18 ± 2[c], 18 ± 4[d]	29 ± 4[c], 30 ± 3[d]	27 ± 2[c], 62 ± 5[d]

[a] Kinetically calculated, [b] Thermodynamically calculated, [c] from Eyring plot, [d] from Global fit, [e] PCy_3, [f] PPh_3.

5.5 Conclusion

fac-[Re(CO)$_3$(Br)(DiMePy)], *fac*-[Re(CO)$_3$(Br)(DiMeOPy)], *fac*-[Re(CO)$_3$(Br)(4-MeTPh)]$^-$, *fac*-[Re(CO)$_3$(Br)(BrDiPhPr)]$^-$, *fac*-[Re(CO)$_3$(Br)(TIF)]$^-$ and *fac*-[Re(CO)$_3$(Br)(MeTIF)]$^-$ were dissolved in methanol for 24 hours to form the methanol solvento species *fac*-[Re(CO)$_3$(MeOH)(DiMePy)]$^+$, *fac*-[Re(CO)$_3$(MeOH)(DiMeOPy)]$^+$, *fac*-[Re(CO)$_3$(MeOH)(4-MeTPh)], *fac*-[Re(CO)$_3$(MeOH)(BrDiPhBr)], *fac*-[Re(CO)$_3$(MeOH)(TIF)] and *fac*-[Re(CO)$_3$(MeOH)(MeTIF)] as confirmed by IR and NMR (Chapter 3). The methanol ligand in the axial position was available for substitution with different monodentate ligands (TU, NCS$^-$, PCy$_3$/PPh$_3$ and Br$^-$). In conclusion:

- All k_1 values increases as the temperature increases in all complexes and in all reactions.
- Complexes with *N,N'* bidentate ligands reacted slower than the complexes with *O,O'* bidentate ligands and this correspond to the work reported in literature.[5,16,17,18,19]
- The complexes with the β-diketone ligands coordinated to the metal centre (**3** and **4**) reacted slower than the complexes with the β-hydroxyketone ligands coordinated to the metal centre (**5** and **6**) with all four monodentate ligands.
- All the reactions of **3**, **4**, **5** and **6** with the corresponding entering ligands are faster than the reactions of **1** and **2** respectively, therefore k_1 (*O,O'*-Bid) > k_1 (*N,N'*-Bid). On average, k_1(TU)(**1** and **2**) < k_1(TU)(**3** and 4) < k_1(TU)(**5** and **6**); k_1(NCS$^-$)(**1** and **2**) < k_1(NCS$^-$)(**3** and **4**) < k_1(NCS$^-$)(**5** and **5**); k_1(PCy$_3$/PPh$_3$)(**1** and **2**) < k_1(PCy$_3$/PPh$_3$)(**3** and **4**) < k_1(PCy$_3$/PPh$_3$)(**5** and **6**); k_1(Br$^-$)(**1** and **2**) < k_1(Br$^-$)(**3** and **4**) < k_1(Br$^-$)(**5** and **6**).
- The $\Delta H^{\ddagger}$ values for all the reactions are within the same range and correspond well to similar reactions in literature.

[16] Brink, A., Visser, H.G., Roodt, A. *Inorg. Chem*. **53**(23) (2014) 12480-12488.
[17] Brink, A., Visser, H.G., Roodt, A. *Inorg. Chem*. **52**(15) (2013) 8950-8961.
[18] Schutte-Smith, M., Roodt, A., Visser, H.G. *Dalton Trans*. **48** (2019) 9984-9997.
[19] Gantsho, V.L., Dotou, M., Jakubaszek, M., Goud, B., Gasser, G., Visser, H.G., Schutte-Smith, M. *Dalton Trans*. **49** (2020) 35-46.

- An illustration of the Eyring plots of all six complexes' four reactions (Figure **5-63**) shows the increase in rate as you move from **1** / **2** to **3** / **4** and to **5** / **6**.
- Considering the type of activation of these reactions: (1) A relative independence of k_1 and k_{-1} values for all the entering ligands were observed. (2) Therefore it is unclear whether the Re-X bond breaking or Re-MeOH bond breaking are more significant. (3) The methanol substitution reactions for these 6 metal complexes (per entering ligand), with increasing electron donating ability, do not have a significant impact on the rate constant (factor of ~45 at most), however a definite increase is observed moving from the Re-*N,N'* to Re-*O,O'* complexes. (4) The fact that **5** and **6** yield larger k_1 values compared to **3** and **4** possibly suggests an I_a mechanism, since the F atoms will decreases the electron density on the Re centre, promoting an associative activation mechanism. (5) The small negative to small positive $\Delta S^{\ddagger}$ values obtained for all 24 reactions, although most have large esd's, are in the same range and suggest the same type of mechanism, and is indicative of an I_a to I_d type of activation.
- All in all we are hesitant to propose a mechanism of activation for these complexes, although the data at hand suggest an I_a or I_d mechanism, and it is clear that high pressure studies are imperative to confirm the type of mechanism.

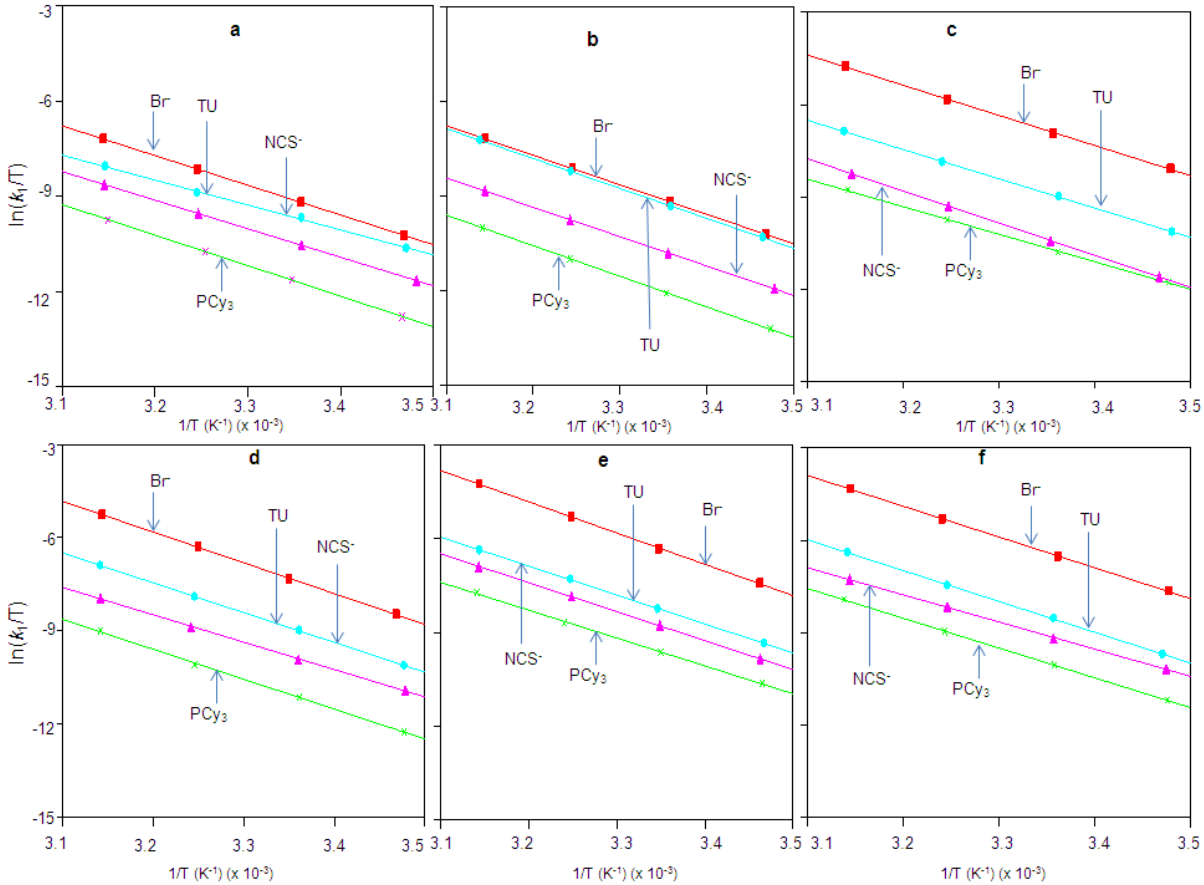

Figure 5-63: Eyring plots of the reactions between (a) *fac*-[Re(CO)$_3$(MeOH)(DiMePy)]$^+$, (b) *fac*-[Re(CO)$_3$(MeOH)(DiMeOPy)]$^+$, (c) *fac*-[Re(CO)$_3$(MeOH)(4-MeTPh)], (d) *fac*-[Re(CO)$_3$(MeOH)(BrDiPhBr)], (e) *fac*-[Re(CO)$_3$(MeOH)(TIF)] and (f) *fac*-[Re(CO)$_3$(MeOH)(MeTIF)] with different entering ligands.

Some of this Re(I) tricarbonyl complexes and bidentate ligands reported in Chapter 3 are analysed by photoluminescence and will be discussed in Chapter 6.

6 PHOTOLUMINESCENCE STUDY OF LIGANDS AND RHENIUM(I) TRICARBONYL COMPLEXES

6.1 Introduction

Luminescence is the emission of electromagnetic radiation from a substance upon excitation; the material is often called a phosphor, which means “light bearer”.[1] The substances (mostly inorganic complexes) absorb radiant energy of a certain wavelength range and reradiate it at a longer wavelength. Luminescent emission occurs as a result of a photo effect inside the complicated discrete luminescence centres. The process generally involves two stages; (a) excitation, where the system temporarily attains a higher energy level and (b) emission, where absorbed energy is released by radiative or non-radiative transitions.[2]

The 2,2’-bipyridine ligand has been extensively used as a metal chelating ligand due to its ease of functionalization and robust redox stability.[4] It is a neutral ligand that forms a charged complex with metal cations. This ligand sensitizes the organic scaffolds and therefore potentially makes the Re(I) tricarbonyl complexes photoluminescent. The idea is to use the bipyridine ligand framework in this study since it can be readily functionalized.[3,4,5,6,7]

---

[1] van Leeuwen, F. B., Hardwick, J. C. H., van Erkel, A. R. *Radiology*. **276** (2015) 12-29.

[2] Taboada, C. T., Brunetti, A. E., Pedron, F. N., Neto, F. C., Estrin, D. A., Bari, S. E., Chemes, L. B., Lopes, N. P., Lagorio, M. G., Faivovch, J. *Proc. Natl. Acad. Sci. U.S.A.* **114** (2017) 3672-3677.

[3] Dawid, U., Pruchnik, F. P., Starosta, R. *Dalton Trans.* **17** (2009) 3348-3353.

[4] Kaes, C., Katz, A., Hosseini, M. W. *Chem. Rev*. **100** (2000) 3553-3590.

[5] Schumacher, J. N., Green, C. R., Best, F. W., Newell, M. P. *J. Agric. Food Chem*. **25** (1977) 310-320.

[6] Jacob, P., Benowitz, N., Yu, L., Duan, M. J., Liang. *G. Addiction*. **92** (1997) 626-632.

β-Diketone ligands have many interesting properties such as strong absorption bands in a wide range of wavelengths for its π-π* transition, and therefore has been targeted for its ability to sensitize luminescence.[8] The *β*-diketone systems are valuable substrates in chemical synthesis with transition metals due to the two carbonyl substituents. The aromaticity plays a large role in the photoluminescence of complexes; hence many photoluminescent ligands contain aromatic systems.[8] It has been reported that *β*-diketone ligands tend to undergo tautomerism between the enol and keto form. The enol- form is the more preferred tautomer in the solid state.[9]

β-Hydroxyketones are also widely utilised for luminescence purposes because they form stable adducts with metal ions and strongly absorb in a large wavelength range, resulting in them being 'antennas' that sensitize the luminescence of the metal ions.[10,11] The *β*-hydroxyketone ligands contain high energy oscillators like O-H and C-H bonds that enables them to quench the metal excited states non-radiatively, resulting in lower luminescence intensities and shorter excited state life-times. Replacing C-H bonds with C-F bonds is important because it results in a more efficient emission and also the heavy-atom effect, which facilitate intersystem crossing and enhance the metal-centered luminescence.[12,13] High value luminescence quantum yields are generally associated with ligands that possess an extensive delocalized system of conjugate double bonds and leads to a relative rigid structure.[14] However, the rigid ligand restricts the thermal vibration of the complexes and reduces the loss of energy by nonradioactive decay.[15,16,17]

---

7 Foder, G. B., Colasanti, B. *InAlkaloids:Chemical and Biological Perspectives*. Pelletier, S. W. Ed.; Wiley: New York, 1985; Vol.3, Chapter 1.

8 Bilge, S., Kiliç, Z., Hayvali, Z., Hökelek, T., Safran, S. *J. Chem. Sci*. **121** (2009) 989-1001.

9 Mohanan, K., Subhadrambika, N., Selwin Joseyphus, R.; Swathy, S. S., Nisha, V. P., *J.Saudi Chem. Soc*. **20** (2016) 379-390.

10 Shen, L., Shi, M., Li, F. Y., Zhang, D. Q., Li, X. H., Shi, E. X., Yi, T., Do, Y. K., Huang, C. H. *Inorg. Chem*. **45** (2006) 6188-6197.

11 Ambili Raj, D. B., Bijiu, S., Reddy, M. L. P. *Inorg. Chem*. **47** (2008) 8091-8100.

12 He, P., Wang, H. H., Liu, S. G., Shi, J. X., Wang, G., Gong, M. L. *Inorg. Chem*. **48** (2009) 11382-11387.

13 Zheng, Y. X., Lin, J., Lin, Q., Yu, Y. N., Meng, Q. G., Zhou, Y. H., Wang, S. B., Wang, H. Y., Zhang, J. *J. Mater. Chem*. **11** (2001) 2615-2619.

14 Wang, D., Kang, Y., Fan, L., Hu, Y., Zheng, J. *Opt. Mater*. **36** (2013) 357-361.

15 Yan, B. *Mater. Lett*. **57** (2003) 2535-2539.

16 Bassett, A. P., Magennis, S. W., Glover, P. B., Lewis, D. J.,Spencer, N., Parsons, S., Williams, R. M., Cola, L. D., Pikramenou, Z. *J. Am. Chem. Soc*. **126** (2004) 9413-9424.

17 Jenekhe, S. A., Osaheni, *J. A. Chem. Mater*. **6** (1994) 1906-1909.

Li *et al.*[18] investigated the photoluminescence properties of rhenium(I) complexes based on bipyridine derivatives with carbazole moieties and observed that at room temperature, in chloroform solution, the complexes display intense absorption bands at *ca*. 220 nm – 350 nm which can be assigned to a spin-allowed intraligand π→π* transition, and the low energy broad bands in the 360 nm – 480 nm region are attributed to the metal to ligand charge-transfer (MLCT) dπ(Re) → π* (diimine). When carbazole moieties were introduced, the MLCT absorption and molar extinction coefficient of all the complexes improved. All complexes show the strong emission around 620 nm from the maximum excitation peak, which are assigned to dπ(Re) → π* (diimine) MLCT phosphorescence.

Sacksteder *et al.*[19] studied the luminescence of *fac*-[ReL(CO)$_3$X] (L = 2,2'-bipyridine, 1,10-phenanthroline, and 5-phenyl-1,10-phenanthroline, X = substituted pyridine or quinoline) type complexes. It was found that the relatively small but useful variations in the state energies can be affected by altering the Hammett σ value of substituents on the pyridines. Complexes exhibited a metal to ligand charge-transfer (MLCT) phosphorescence at room temperature. By choice of suitable ligands, the emission can be switched to ligand-localized phosphorescence on cooling to 77 K. This explains, on the basis of the proximity of the lowest temperature, that the MLCT state can equilibrate to an energy that is lower than that of the π→π* state and give MLCT luminescence. At low temperature, the MLCT state cannot relax during the excited-state decay and emission is from the lowest MLCT and π→π* triplet states.

Bertrand *et al*.[20] developed Re(I) tricarbonyl complexes prepared from different ancillary ligands. Complexes with benzothiadiazole−triazole ligands show interesting luminescent quantum yields in acetonitrile and constitute valuable luminescent metal complexes in organic media. A series of complexes with bidentate 1-(2-quinolinyl)-1,2,3-triazole (Taquin) and 1-(2-pyridyl)-1,2,3-triazole (Tapy) ligands bearing various 4-substituted alkyl side chains designed and synthesized with efficient procedures. Their photophysical properties are characterized in acetonitrile and in a H_2O/DMSO (98/2) mixture and compared to those of the parent Quinta- and Pyta-based

[18] Li, H., Wu, J., Zhou, X., Kang, L., Li, D., Sui, Y., Zhou, Y., You-Xuan Zheng, Y., Zuo, J., You, X. *DaltonTrans*. **47** (2009) 10563-10569.
[19] Sacksteder, A., Zipp, A. P., Brown, E. A., Streich, J., Demas. J. N., DeGraff, B. A. *Inog. Chem*. **29**(21) (1990) 4335-4340.
[20] Bertrand, H. C., Slede, S., Guillot, R., Lambert, F., Polocar, C. *Inorg. Chem.* **53**(12) (2014) 6204-6223.

complexes (where Quinta = quinoline ring) and Pyta = 4-(2-pyridyl)-1,2,3-triazole)). Tapy complexes bearing long alkyl chains show impressive enhancement of its luminescent properties relative to the parent Pyta complex. Preliminary cellular imaging studies in MDAMB231 breast cancer cells reveal a strong increase in the luminescence signal in cells incubated with the Tapy complex substituted with a C12 alkyl chain. This study points out the interesting potential of the Tapy ligand in coordination chemistry, which has been largely unexplored.

In this chapter, the photoluminescence of an array of the synthesised rhenium tricarbonyl complexes with *O,O'* β-diketone, β-hydroxyketone as well as *N,N'* bipyridine ligand systems are investigated. From the above mentioned literature, the ligands and complexes synthesized in this study could provide valuable luminescent properties which may potentially be applied in photodynamic therapy as discussed in Chapter 2.The photoluminescence studies are carried out in the solid state supported by a few solution state studies, in addition to the UV/Vis experiments of the selected ligands and complexes which were carried out in solution to investigate their relative absorption nature. Scheme **6-1** illustrates the ligands and Re(I) tricarbonyl complexes that were investigated in this chapter.

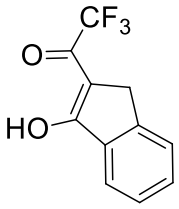

2,2,2-Trifluoro-1-(3-hydroxy-1H-inden-2-yl)ethan-1-one (TIFH)

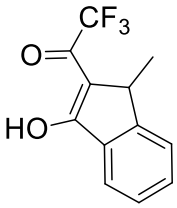

2,2,2-Trifluoro-1-(3-hydroxy-1-methyl-1H-inden-2-yl)ethan-1-one (MeTIFH)

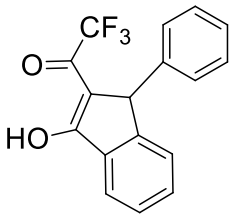

2,2,2-Trifluoro-1-(3-hydroxy-1-phenyl-1H-inden-2-yl)ethan-1-one (PhTIFH)

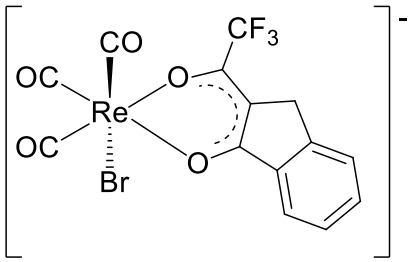

fac-[Re(CO)$_3$(Br)(TIF)]$^-$

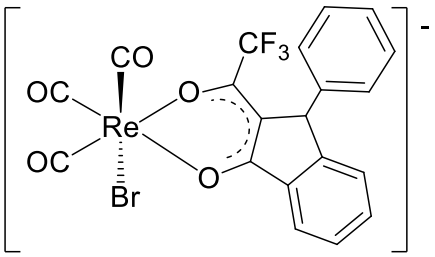

fac-[Re(CO)$_3$(Br)(PhTIF)]$^-$

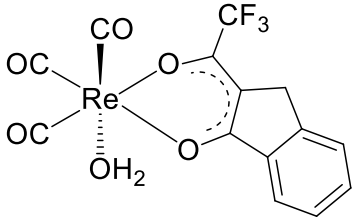

fac-[Re(CO)$_3$(H$_2$O)(TIF)]

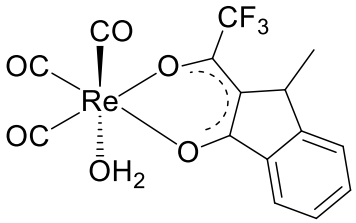

fac-[Re(CO)$_3$(H$_2$O)(MeTIF)]

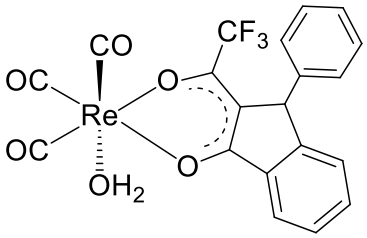

fac-[Re(CO)$_3$(H$_2$O)(PhTIF)]

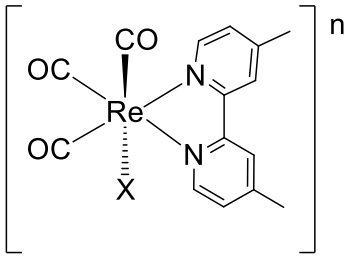

fac-[Re(CO)$_3$(X)(DiMePy)]^n

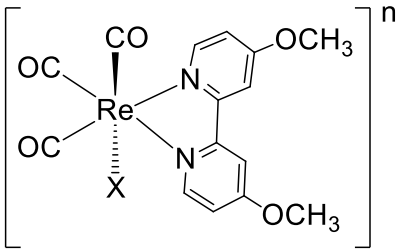

fac-[Re(CO)$_3$(X)(DiMeOPy)]^n

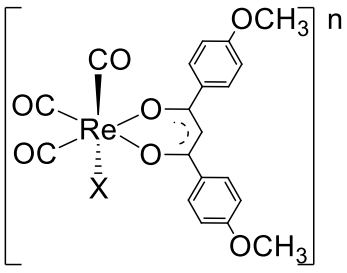

fac-[Re(CO)$_3$(X)(4-MeTPh)]^n

Where X = Br, MeOH, H_2O, TU, NCS^-, PCy_3,PPh_3

n = +1, 0, DiMePy = 4,4'-dimethyl-2,2'-bipyridine, DiMeOPy = 4,4'-dimethoxy-2,2'-bipyridine

4-MeTPy = 1,3-bis(4-methoxyphenyl)propane-1,3-dione

Scheme 6-1: Illustration of the ligands and Re(I) tricarbonyl complexes used in this photoluminescence study.

6.2 Experimental procedure

All the chemicals and reagents used for the synthetic procedures were purchased from Sigma-Aldrich, and were used without any further purification. All UV/Vis spectra were collected on a Varian Cary 50 Conc. Spectrophotometer, equipped with a Julabo F12-mV temperature cell regulator accurate within 0.1 °C, using a 1.000(1) cm tandem quartz cuvette. All reported absorption, excitation and emission wavelength (λ_{max}) values were collected at room temperature (25.0 °C).

An Edinburgh Instruments FLS980 photoluminescence spectrometer with double monochromators was used to do the photoluminescence measurements. A 450 W xenon lamp was used to excite the samples and a Hammamatsu R928P photomultiplier tube was used to measure the luminescence. The spectra were corrected for the spectral response of the system. The integrating sphere was used to measure the quantum yield of samples. The total excitation light was recorded using a reflective spectralon sample, after which the excitation light reflected from the sample. The samples were not all uniform in physical appearance. Therefore, the samples were compared based on their measurement settings. Table **6-1** illustrates the comparison by colour grouping. All complexes highlighted with the same colour were evaluated under the same measurement settings.

The luminescence output (integrated area under the emission curve) was divided by the absorbed light (integrated difference of the reflection from the spectralon and the sample) to give the quantum yield. All the complexes were analysed in the solid state form with two complexes which were repeated in the liquid state. The results of these two solution state experiments compared well with the solid state results. For comparison reasons, a specific excitation wavelength for some of the complexes was chosen so that these complexes could be compared. The chosen excitation wavelength falls within the excitation range of each complex.

6.3 Solid state photoluminescence results and discussion

The results obtained from the photoluminescence evaluation of the three ligand systems and the twenty two Re(I) complexes are presented in Figure **6-1** to Figure **6-25** below. Some of the photoluminescence measurements were measured in variable conditions due to the physical properties of the compounds. Each figure consists of two graphs; an excitation graph (blue) and an emission graph (red) at different wavelengths as indicated on each graph for each complex. The quantum yields of specific complexes were not measured due to low intensities and some could not be compared due to the non-ideal physical properties.

6.3.1 2,2,2-Trifluoro-1-(3-hydroxy-1H-inden-2-yl)ethan-1-one (TIFH)

The luminescence spectra in Figure **6-1** is a spectroscopic representation of the excitation and emission of the TIFH ligand. This ligand is a multi-emitter with multiple excitation wavelengths from 500 nm to 725 nm with the most prominent excitation peak at 650 nm that gives rise to the maximum emission at 740 nm. The complex emits from 665 nm to 835 nm. The quantum yield was not measured due to the quality of the sample (amount of the sample in the sample holder and a sticky product).

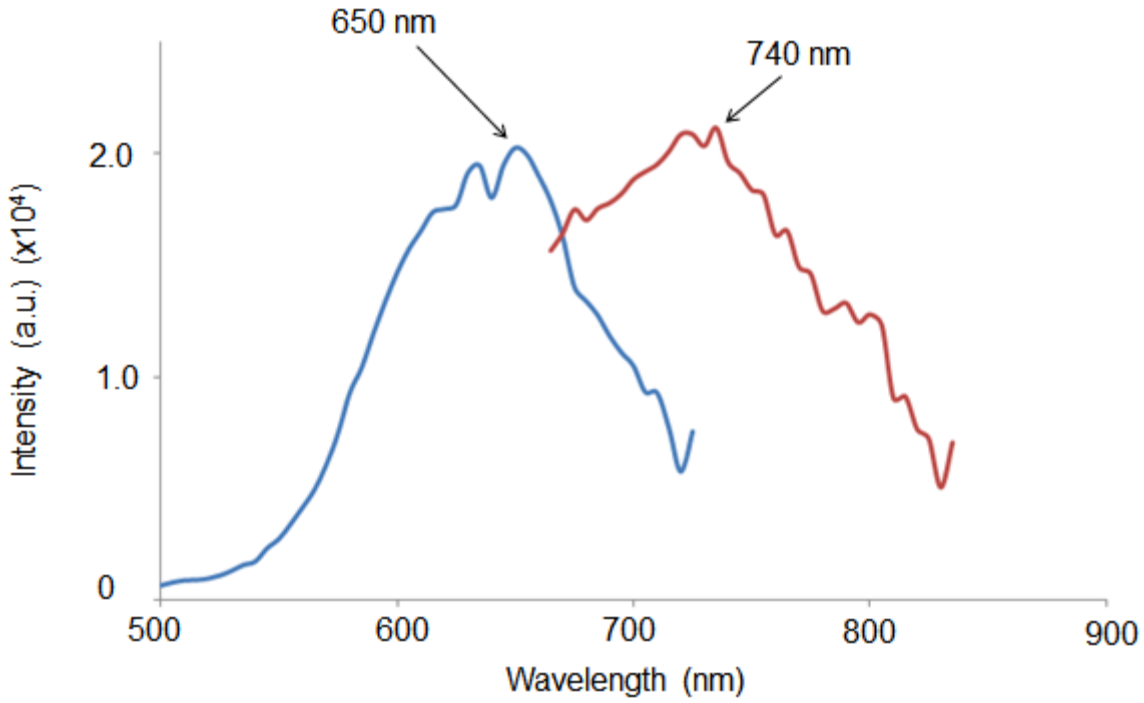

Figure 6-1: Excitation (blue) and emission (red) spectra of 2,2,2-trifluoro-1-(3-hydroxy-1H-inden-2-yl)ethan-1-one recorded in solid state.

6.3.2 *fac*-[Re(CO)$_3$(Br)(TIF)]$^-$

The luminescence spectra in Figure **6-2** is a spectroscopic representation of the excitation and emission of *fac*-[Re(CO)$_3$(Br)(TIF)]$^-$. This complex is a multi-emitter with multiple excitation wavelengths from 500 nm to 725 nm and the most prominent excitation peak is at 705 nm that gives rise to the maximum emission at 740 nm. The complex emits from 720 nm to 835 nm. Unfortunately the quantum yield could not be calculated as an insufficient amount of product was synthesised. Time restraints with regards to this thesis prevented the recalculation of the quantum yield. Obtaining the quantum yield will form part of future work.

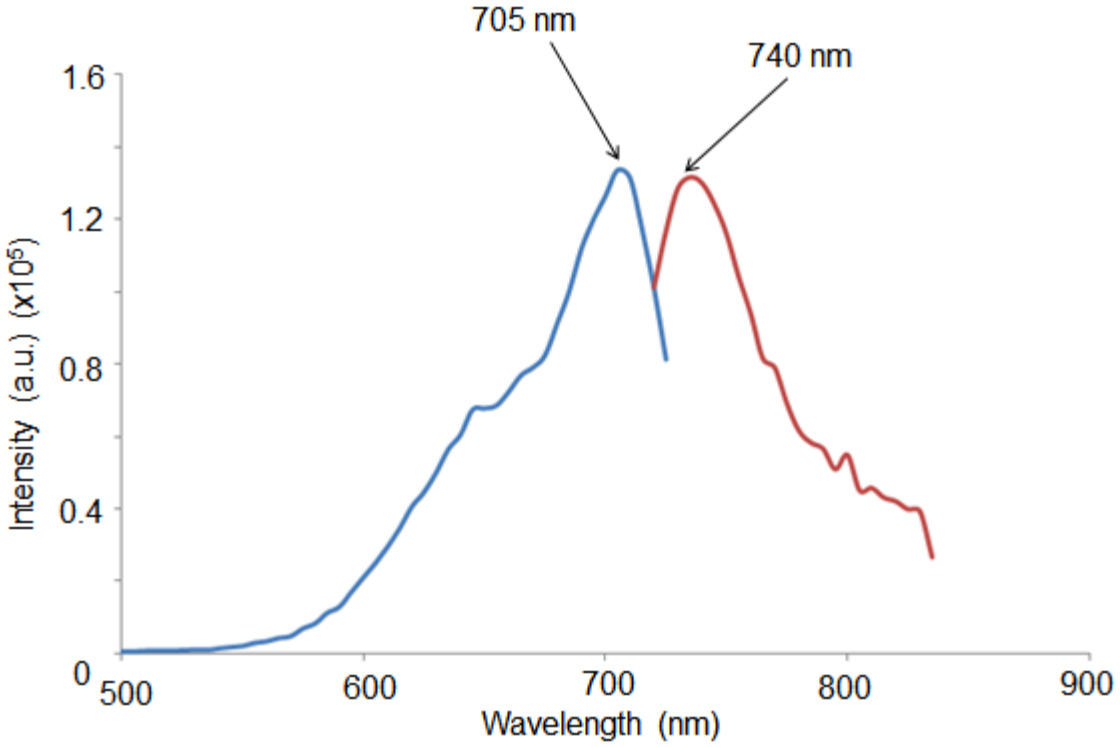

Figure 6-2: Excitation (blue) and emission (red) spectra of *fac*-[Re(CO)$_3$(Br)(TIF)]$^-$ recorded in solid state.

6.3.3 *fac*-[Re(CO)$_3$(H$_2$O)(TIF)]

The luminescence spectra in Figure **6-3** is a spectroscopic representation of the excitation and emission of *fac*-[Re(CO)$_3$(H$_2$O)(TIF)]. The complex is a multi-emitter complex with multiple excitation wavelengths from 500 nm to 725 nm and the most prominent excitation peak is at 705 nm that gives rise to the maximum emission at 740 nm. The complex emits from 720 nm to 835 nm. Unfortunately the quantum yield was not calculated because of a shortage of product. The calculation of the quantum yield will form part of future work.

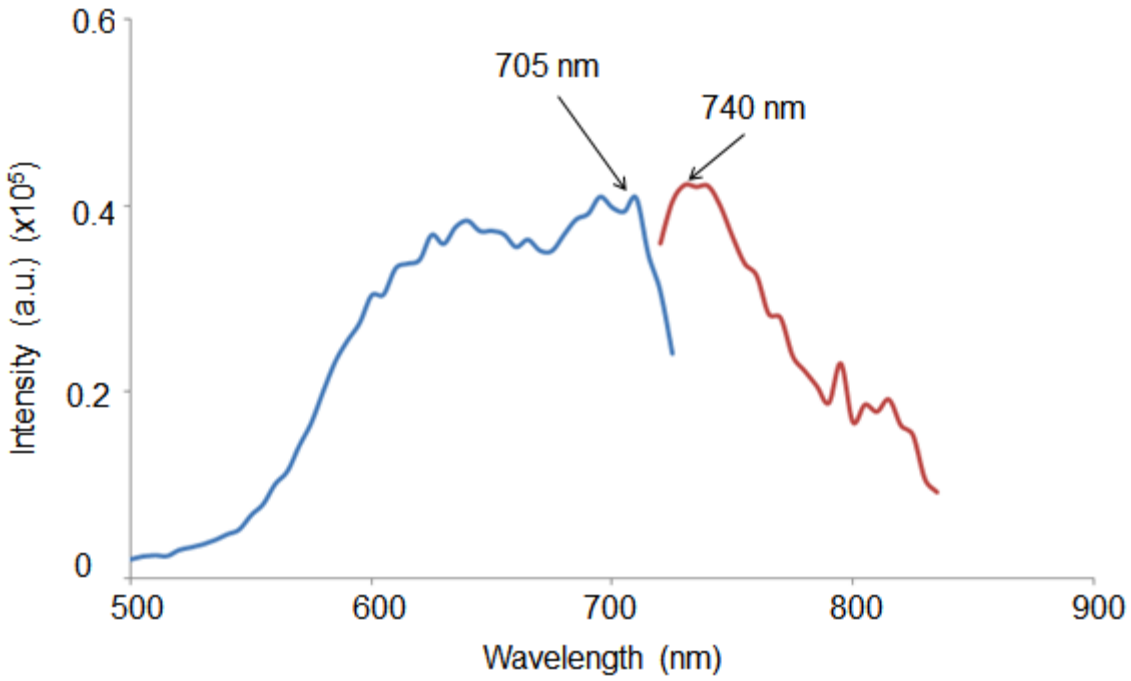

Figure 6-3: Excitation (blue) and emission (red) spectra of *fac*-[Re(CO)$_3$(H$_2$O)(TIF)] recorded in solid state.

6.3.4 2,2,2-Trifluoro-1-(3-hydroxy-1-methyl-1H-inden-2-yl)ethan-1-one (MeTIFH)

The luminescence spectra in Figure **6-4** is a spectroscopic representation of the excitation and emission of the MeTIFH ligand. This ligand is a multi-emitter with multiple excitation wavelengths from 300 nm to 585 nm and the most prominent excitation peak is at 534 nm that gives rise to the maximum emission at 595 nm. The ligand emits from 544 nm to 835 nm. The quantum yield was not measured due to the quality of the sample (amount of the sample in the sample holder and a sticky product), but will form part of future work.

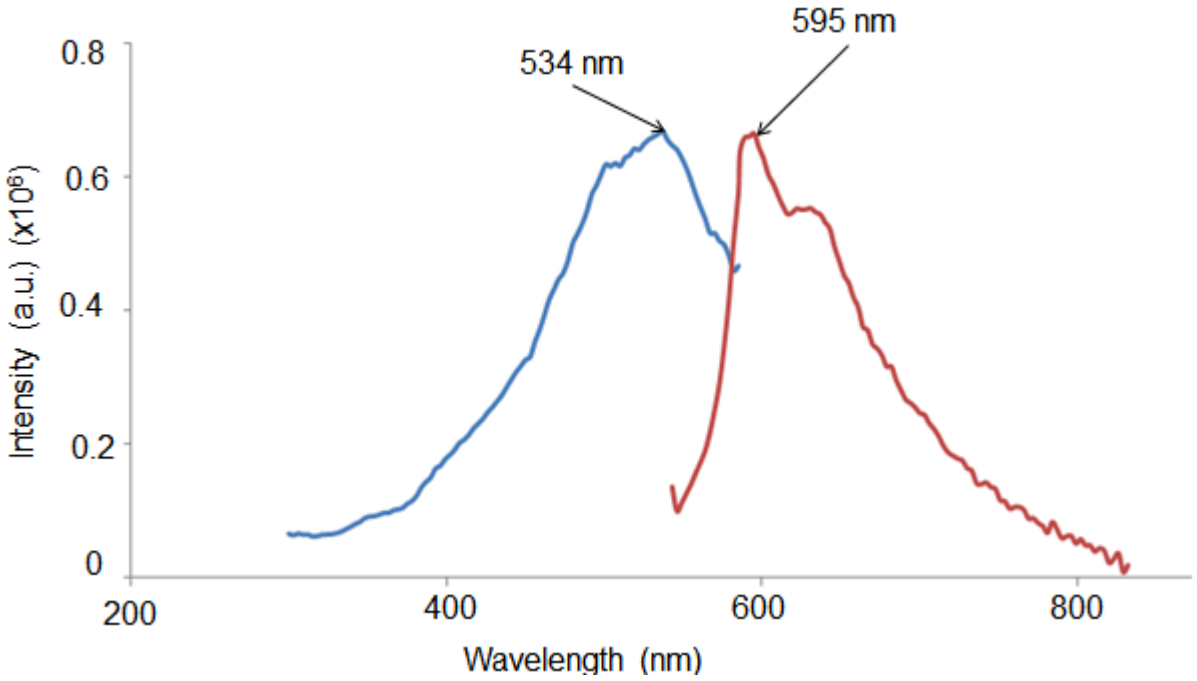

Figure 6-4: Excitation (blue) and emission (red) spectra of 2,2,2-trifluoro-1-(3-hydroxy-1-methyl-1H-inden-2-yl)ethan-1-one recorded in solid state.

6.3.5 *fac*-[Re(CO)$_3$(H$_2$O)(MeTIF)]

The luminescence spectra in Figure **6-5** is a spectroscopic representation of the excitation and emission of *fac*-[Re(CO)$_3$(H$_2$O)(MeTIF)]. The complex is a multi-emitter with multiple excitation wavelengths from 300 nm to 699 nm and the most prominent excitation peak is at 600 nm that gives rise to the maximum emission at 720 nm. The complex emits from 620 nm to 836 nm. Unfortunately the quantum yield was not calculated due to a shortage of product, but will form part of future work.

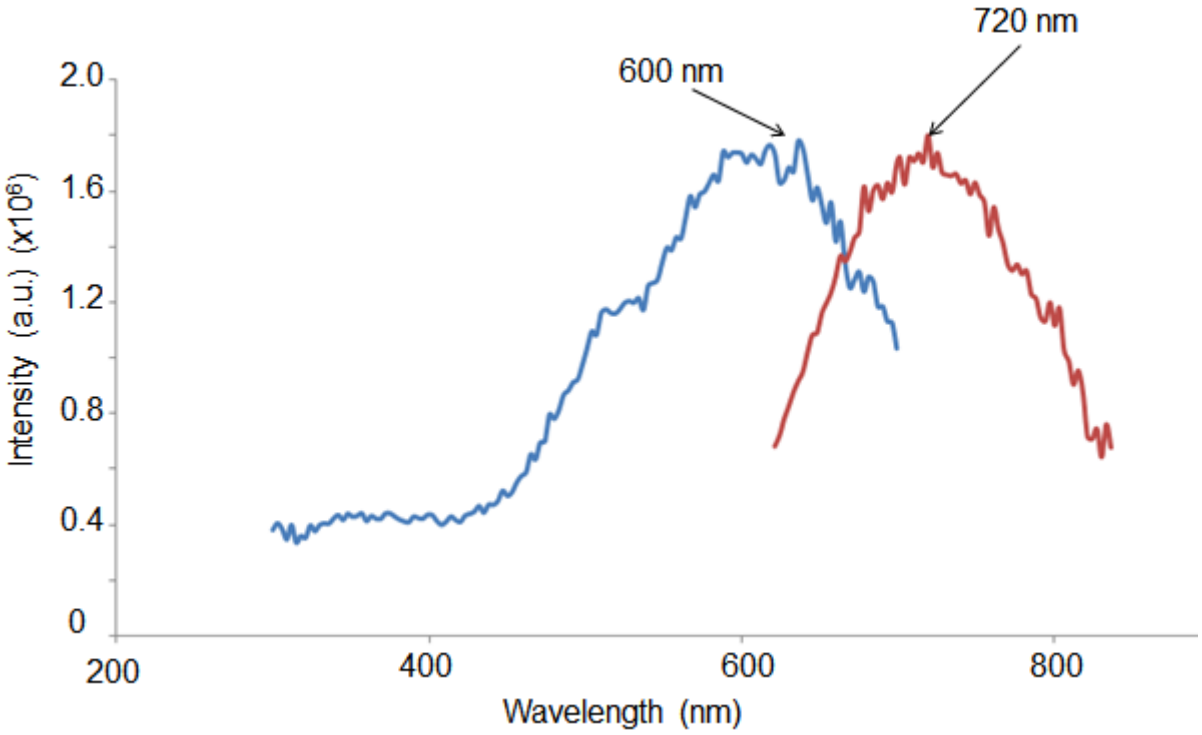

Figure 6-5: Excitation (blue) and emission (red) spectra of *fac*-[Re(CO)$_3$(H$_2$O)(MeTIF)] recorded in solid state.

6.3.6 2,2,2-Trifluoro-1-(3-hydroxy-1-phenyl-1H-inden-2-yl)ethan-1-one (PhTIFH)

The luminescence spectra in Figure **6-6** is a spectroscopic representation of the excitation and emission of the PhTIFH ligand. This ligand is a multi-emitter with multiple excitation wavelengths from 300 nm to 585 nm with the most prominent excitation peak at 550 nm that gives rise to the maximum emission at 595 nm. The ligand emits from 585 nm to 836 nm. The quantum yield was not measured due to the quality of the sample (amount of the sample in the sample holder and a sticky product), but will form part of future work.

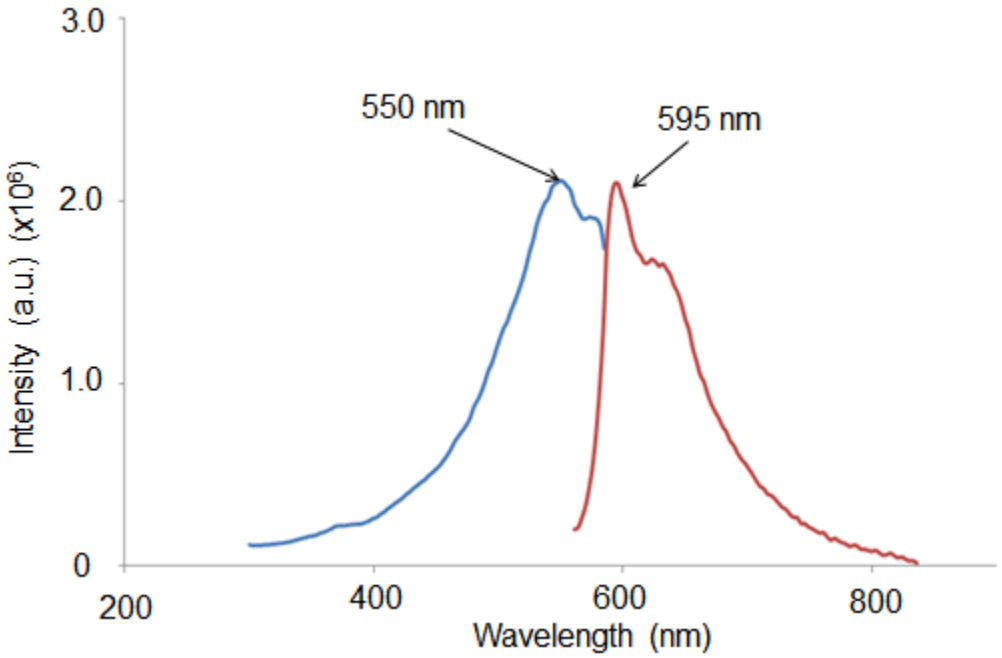

Figure 6-6: Excitation (blue) and emission (red) spectra of 2,2,2-trifluoro-1-(3-hydroxy-1-phenyl-1H-inden-2-yl)ethan-1-one recorded in solid state.

6.3.7 *fac*-[Re(CO)$_3$(Br)(PhTIF)]$^-$

The luminescence spectra in Figure **6-7** is a spectroscopic representation of the excitation and emission of *fac*-[Re(CO)$_3$(Br)(PhTIF)]$^-$. This complex is a multi-emitter with multiple excitation wavelengths from 300 nm to 576 nm and the most prominent excitation peak is at 540 nm that gives rise to the maximum emission at 592 nm. The complex emits from 556 nm to 835 nm. Unfortunately the quantum yield was not calculated due to time constraints, but will form part of future work.

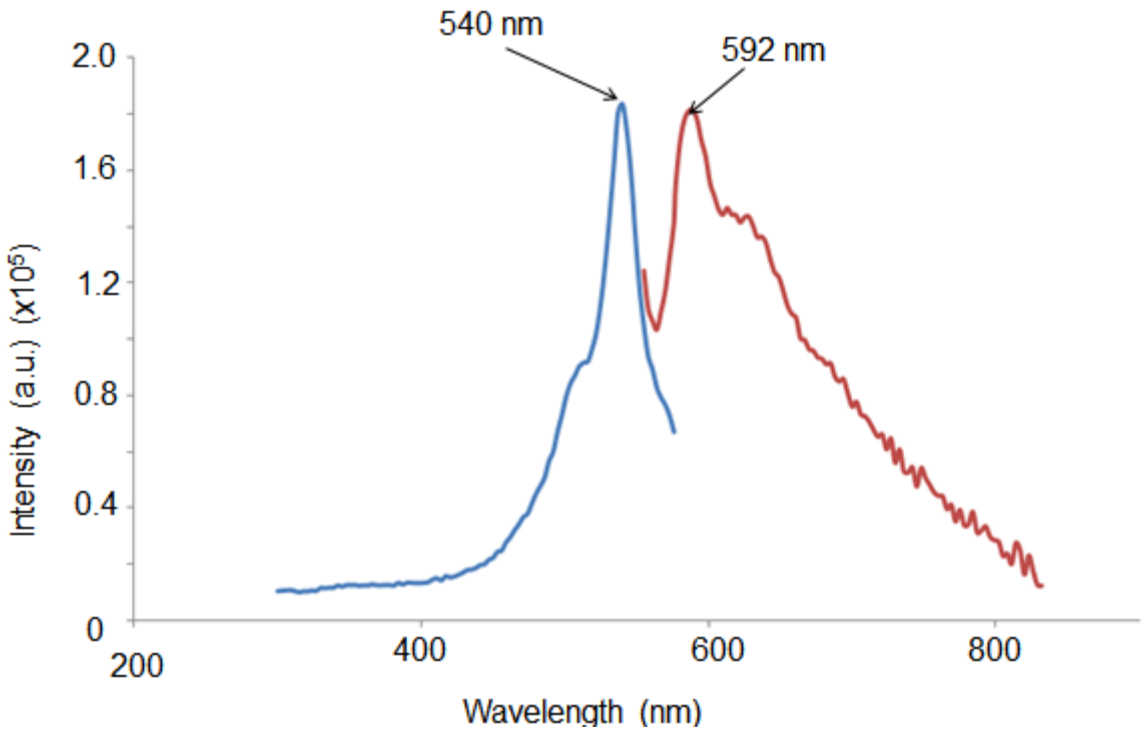

Figure 6-7: Excitation (blue) and emission (red) spectra of *fac*-[Re(CO)$_3$(Br)(PhTIF)]$^-$ recorded in solid state.

6.3.8 *fac*-[Re(CO)$_3$(H$_2$O)(PhTIF)]

The luminescence spectra in Figure **6-8** is a spectroscopic representation of the excitation and emission of *fac*-[Re(CO)$_3$(H$_2$O)(PhTIF)]. The complex is a multi-emitter with multiple excitation wavelengths from 300 nm to 636 nm and the most prominent excitation peak is at 550 nm that gives rise to the maximum emission at 650 nm. The complex emits from 565 nm to 835 nm. Unfortunately the quantum yield was not calculated due to time constraints, but will form part of future work.

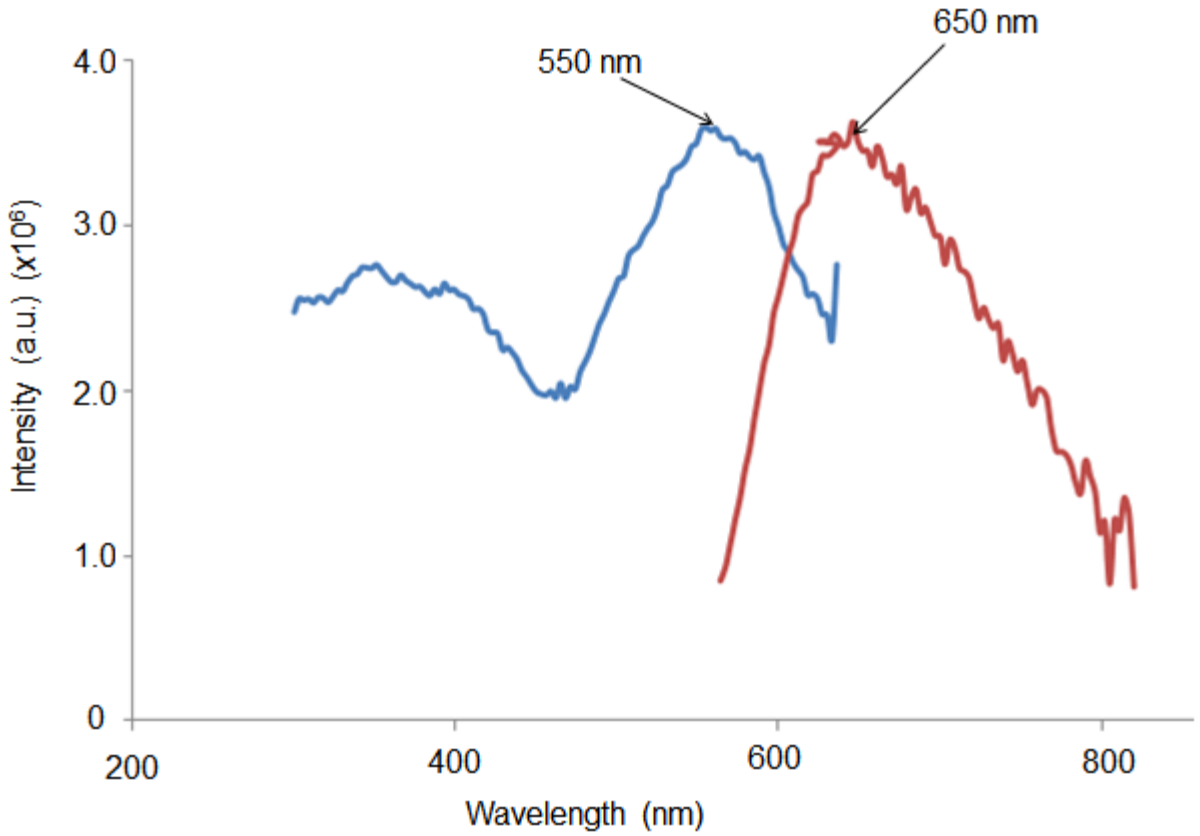

Figure 6-8: Excitation (blue) and emission (red) spectra of *fac*-[Re(CO)$_3$(H$_2$O)(PhTIF)] recorded in solid state.

6.3.9 *fac*-[Re(CO)$_3$(Br)(DiMePy)]

The luminescence spectra in Figure **6-9** is a spectroscopic representation of the excitation and emission of *fac*-[Re(CO)$_3$(Br)(DiMePy)]. This complex is a multi-emitter with multiple excitation wavelengths from 230 nm to 500 nm with the most prominent excitation peak at 370 nm that gives rise to the maximum emission at 545 nm. The complex emits from 470 nm to 800 nm and has a quantum yield of 56 %.

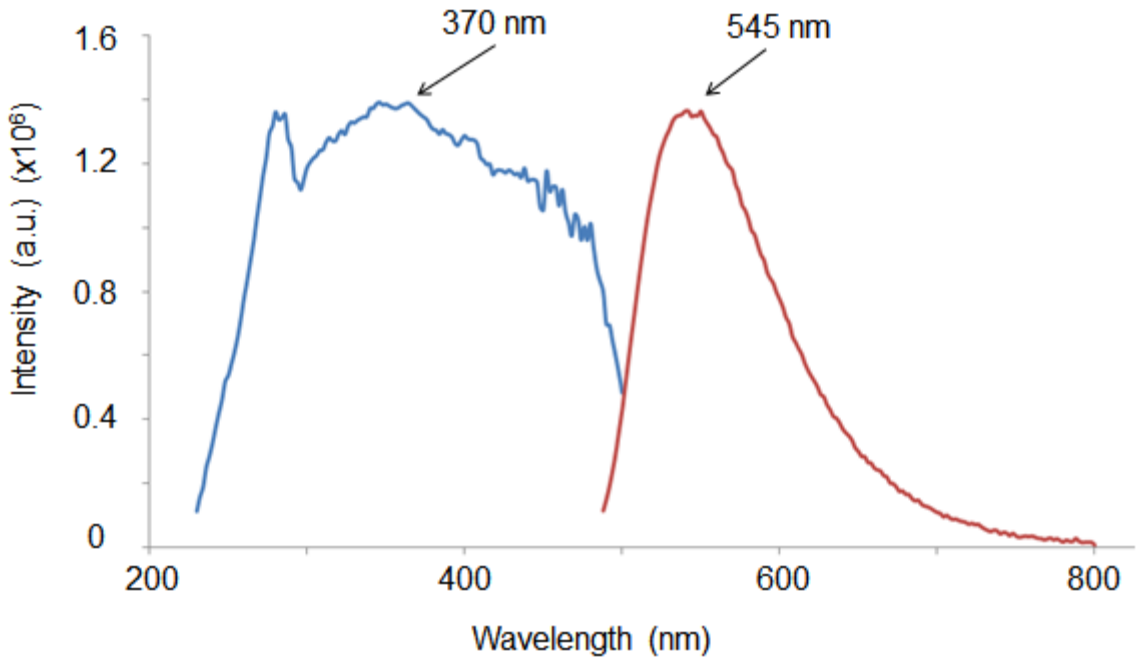

Figure 6-9 Excitation (blue) and emission (red) spectra of *fac*-[Re(CO)$_3$(Br)(DiMePy)] recorded in solid state.

6.3.10 *fac*-[Re(CO)$_3$(H$_2$O)(DiMePy)]$^+$

The luminescence spectra in Figure **6-10** is a spectroscopic representation of the excitation and emission of *fac*-[Re(CO)$_3$(H$_2$O)(DiMePy)]$^+$. The complex is also a multi-emitter with multiple excitation wavelengths from 230 nm to 500 nm and the most prominent excitation peak is at 370 nm that gives rise to the maximum emission at 545 nm. The complex emits from 460 nm to 800 nm and has a quantum yield of 23 %.

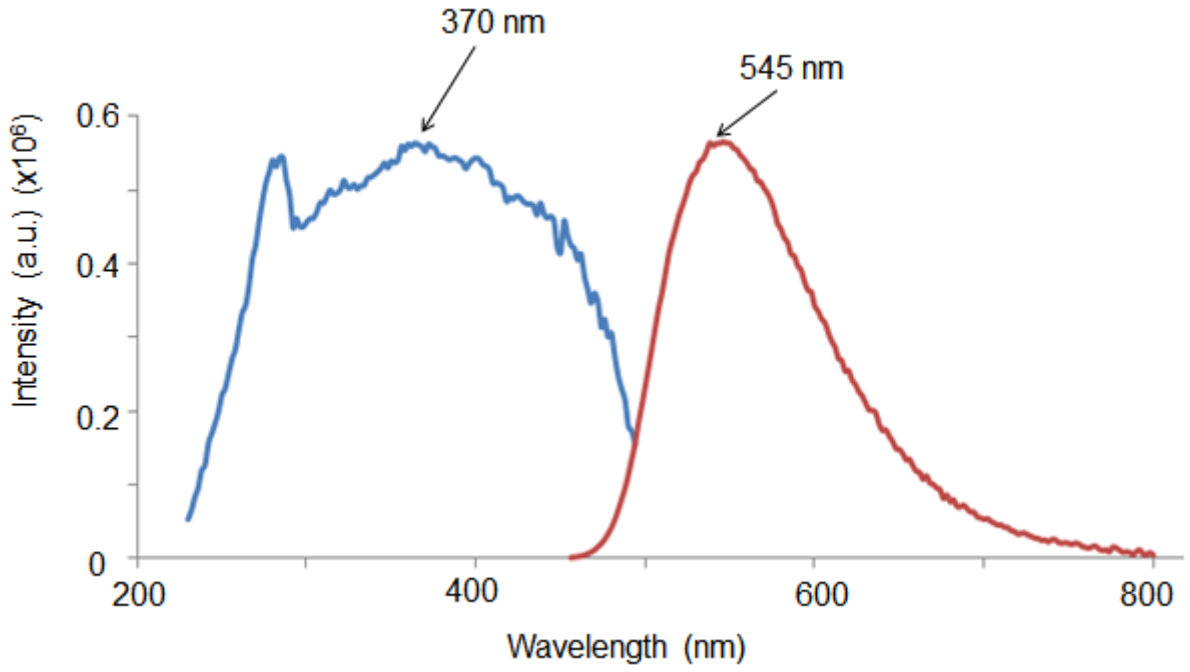

Figure 6-10: Excitation (blue) and emission (red) spectra of *fac*-[Re(CO)$_3$(H$_2$O)(DiMePy)]$^+$ recorded in solid state.

6.3.11 *fac*-[Re(CO)$_3$(MeOH)(DiMePy)]$^+$

The luminescence spectra in Figure **6-11** is a spectroscopic representation of the excitation and emission of *fac*-[Re(CO)$_3$(MeOH)(DiMePy)]$^+$, where the bromido ligand in *fac*-[Re(CO)$_3$(Br)(DiMePy)] is substituted by a methanol solvent molecule. *fac*-[Re(CO)$_3$(MeOH)(DiMePy)]$^+$ is a multi-emitter with multiple excitation wavelengths from 250 nm to 500 nm with a prominent excitation peak at 370 nm (chosen for comparison reasons) that gives rise to the maximum emission at 520 nm. The complex emits from 445 nm to 800 nm and has a quantum yield of 8.8 %.

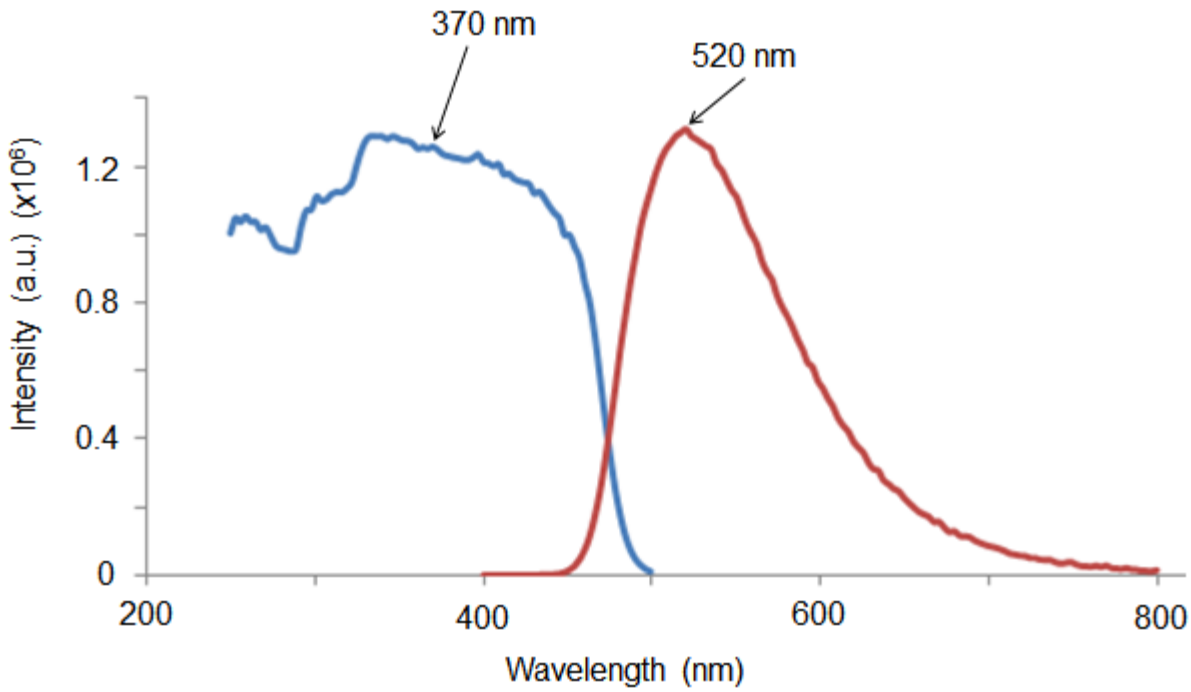

Figure 6-11: Excitation (blue) and emission (red) spectra of *fac*-[Re(CO)$_3$(MeOH)(DiMePy)]$^+$ recorded in solid state.

6.3.12 *fac*-[Re(CO)$_3$(TU)(DiMePy)]$^+$

The luminescence spectra in Figure **6-12** is a spectroscopic representation of the excitation and emission of *fac*-[Re(CO)$_3$(TU)(DiMePy)]$^+$, where the methanol ligand in *fac*-[Re(CO)$_3$(MeOH)(DiMePy)]$^+$ is substituted by a thiourea monodentate ligand. *fac*-[Re(CO)$_3$(TU)(DiMePy)]$^+$ a multi-emitter with multiple excitation wavelengths from 250 nm to 553 nm with the most prominent excitation peak at 370 nm that gives rise to the maximum emission at 574 nm. The complex emits from 470 nm to 800 nm and has a quantum yield of 3.0 %.

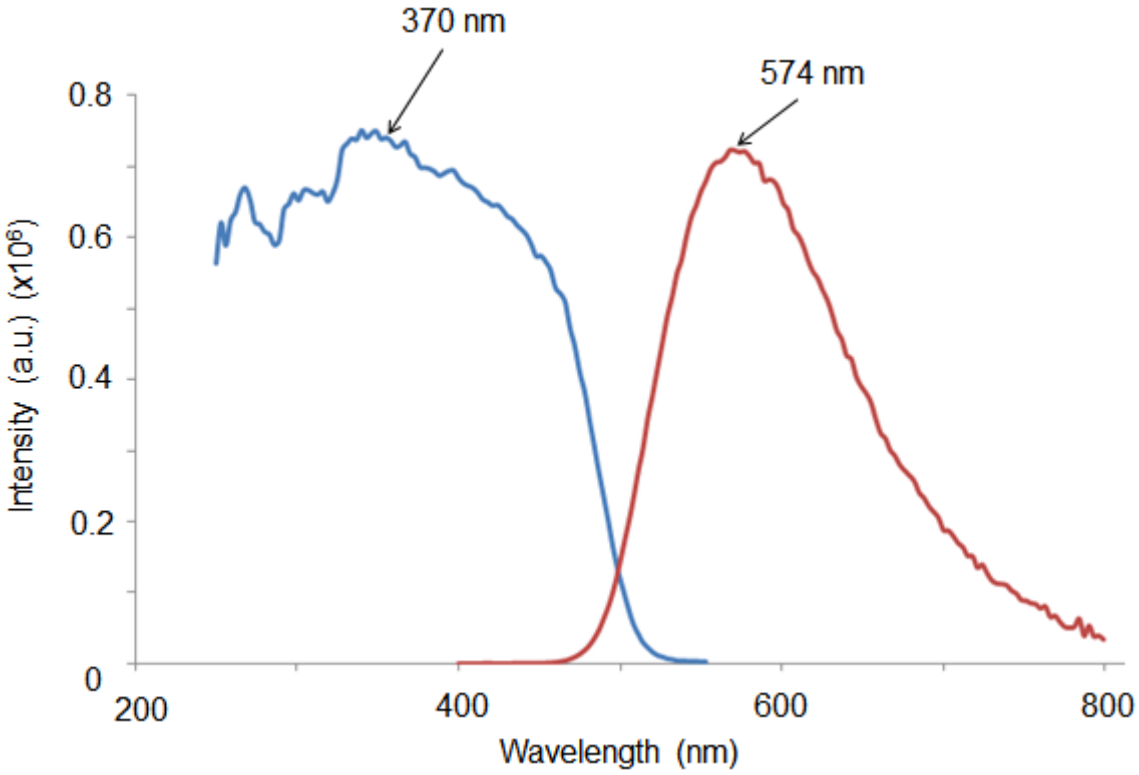

Figure 6-12: Excitation (blue) and emission (red) spectra of *fac*-[Re(CO)$_3$(TU)(DiMePy)]$^+$ recorded in solid state.

6.3.13 *fac*-[Re(CO)$_3$(NCS)(DiMePy)]

The luminescence spectra in Figure **6-13** is a spectroscopic representation of the excitation and emission of *fac*-[Re(CO)$_3$(NCS)(DiMePy)], where the methanol ligand in *fac*-[Re(CO)$_3$(MeOH)(DiMePy)]$^+$ is substituted by a thiocyanate monodentate ligand. *fac*-[Re(CO)$_3$(NCS)(DiMePy)] is a multi-emitter with multiple excitation wavelengths from 250 nm to 535 nm and a prominent excitation peak at 370 nm (chosen for comparison reasons) that gives rise to the maximum emission at 556 nm. The complex emits from 480 nm to 800 nm and has a quantum yield of 4.9 %.

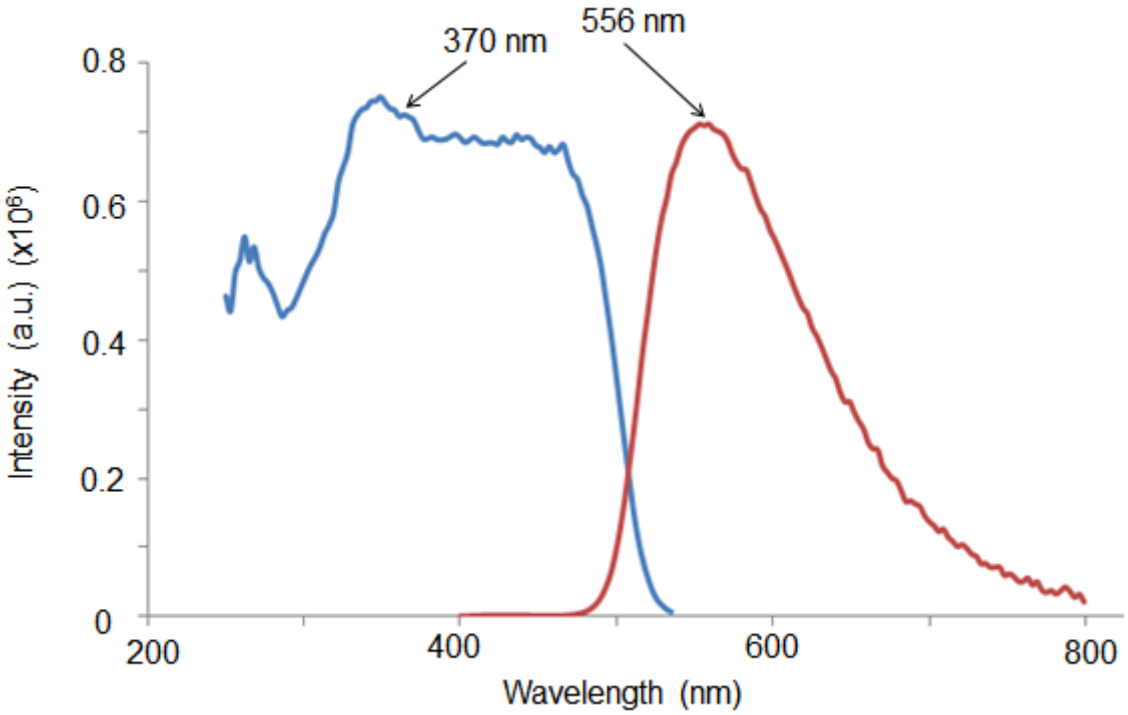

Figure 6-13: Excitation (blue) and emission (red) spectra of *fac*-[Re(CO)$_3$(NCS)(DiMePy)] recorded in solid state.

6.3.14 *fac*-[Re(CO)$_3$(PCy$_3$)(DiMePy)]$^+$

The luminescence spectra in Figure **6-14** is a spectroscopic representation of the excitation and emission of *fac*-[Re(CO)$_3$(PCy$_3$)(DiMePy)]$^+$, where the methanol ligand in *fac*-[Re(CO)$_3$(MeOH)(DiMePy)]$^+$ is substituted by a tricyclohexylphosphine monodentate ligand. *fac*-[Re(CO)$_3$(PCy$_3$)(DiMePy)]$^+$ is a multi-emitter with multiple excitation wavelengths from 250 nm to 535 nm and a prominent excitation peak (chosen for comparison reasons) at 370 nm that gives rise to the maximum emission at 556 nm. The complex emits from 400 nm to 799 nm and has a quantum yield of 2.8 %.

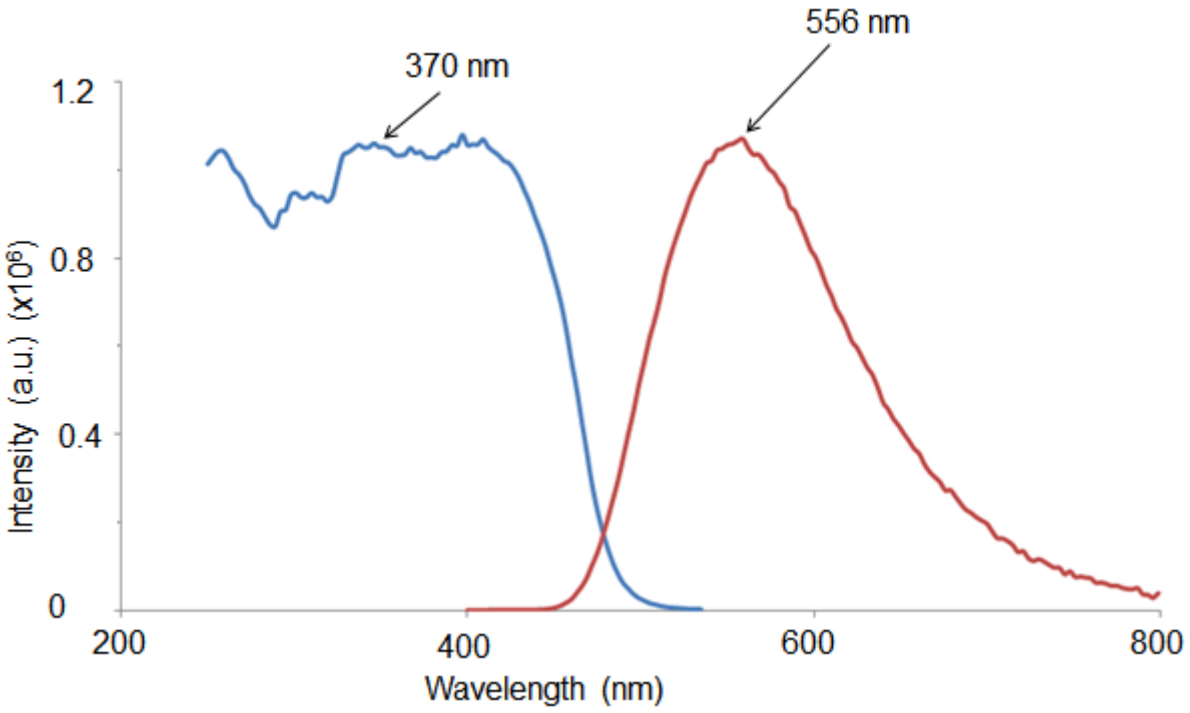

Figure 6-14: Excitation (blue) and emission (red) spectra of *fac*-[Re(CO)$_3$(PCy$_3$)(DiMePy)]$^+$ recorded in solid state.

6.3.15 *fac*-[Re(CO)$_3$(Br)(DiMeOPy)]

The luminescence spectra in Figure **6-15** is a spectroscopic representation of the excitation and emission of *fac*-[Re(CO)$_3$(Br)(DiMeOPy)]. This complex is a multi-emitter with multiple excitation wavelengths from 230 nm to 500 nm and the most prominent excitation peak is at 370 nm that gives rise to the maximum emission at 545 nm. The complex emits from 450 nm to 800 nm and has a quantum yield of 48 %.

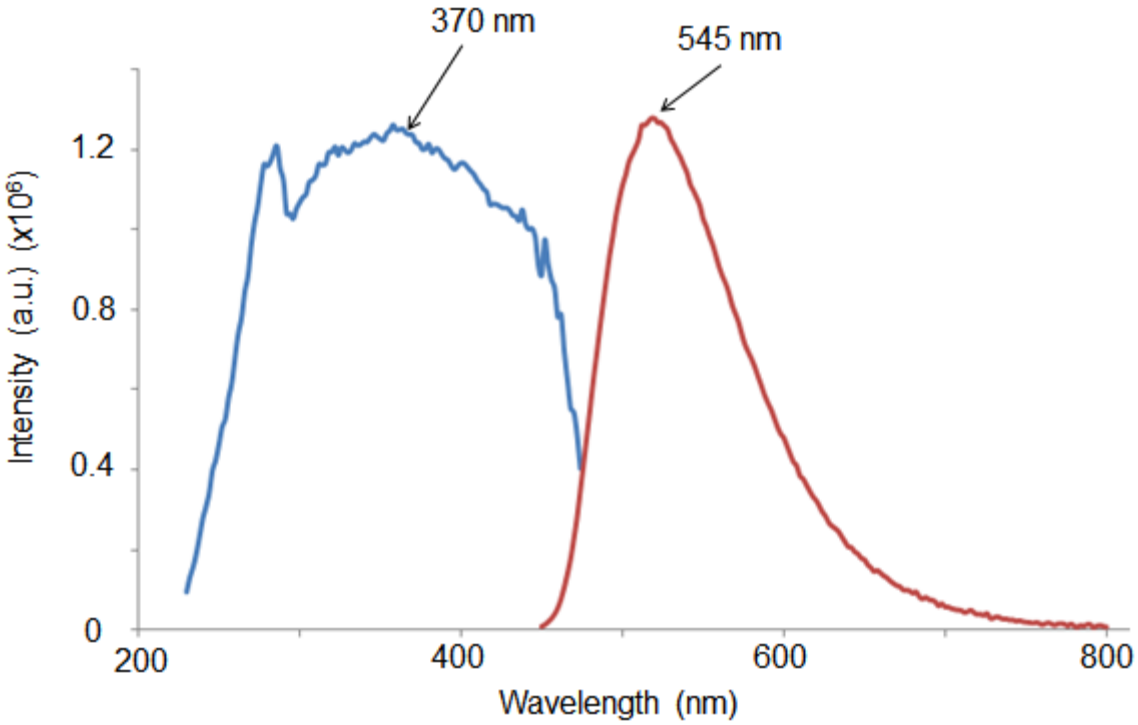

Figure 6-15: Excitation (blue) and emission (red) spectra of *fac*-[Re(CO)$_3$(Br)(DiMeOPy)] recorded in solid state.

6.3.16 *fac*-[Re(CO)$_3$(H$_2$O)(DiMeOPy)]$^+$

The luminescence spectra in Figure **6-16** is a spectroscopic representation of the excitation and emission of *fac*-[Re(CO)$_3$(H$_2$O)(DiMeOPy)]$^+$. The complex is also a multi-emitter with multiple excitation wavelengths from 230 nm to 500 nm and the most prominent excitation peak is at 370 nm that gives rise to the maximum emission at 545 nm. The complex emits from 460 nm to 800 nm and has a quantum yield of 22 %.

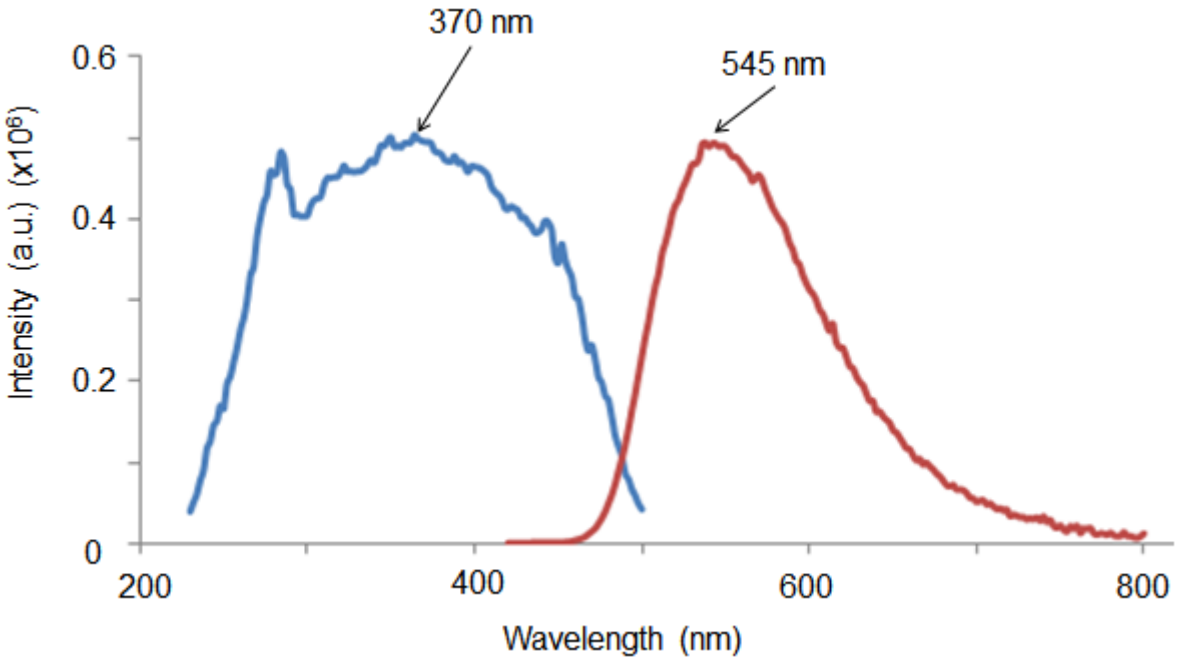

Figure 6-16: Excitation (blue) and emission (red) spectra of *fac*-[Re(CO)$_3$(H$_2$O)(DiMeOPy)]$^+$ recorded in solid state.

6.3.17 *fac*-[Re(CO)$_3$(MeOH)(DiMeOPy)]$^+$

The luminescence spectra in Figure **6-17** is a spectroscopic representation of the excitation and emission of *fac*-[Re(CO)$_3$(MeOH)(DiMeOPy)]$^+$, where the bromido ligand in *fac*-[Re(CO)$_3$(Br)(DiMeOPy)] is substituted by a methanol solvent molecule. This multi-emitter has multiple excitation wavelengths from 250 nm to 500 nm and the most prominent excitation peak is at 415 nm that gives rise to the maximum emission at 530 nm. The complex emits from 495 nm to 800 nm and has a quantum yield of 2.8 %.

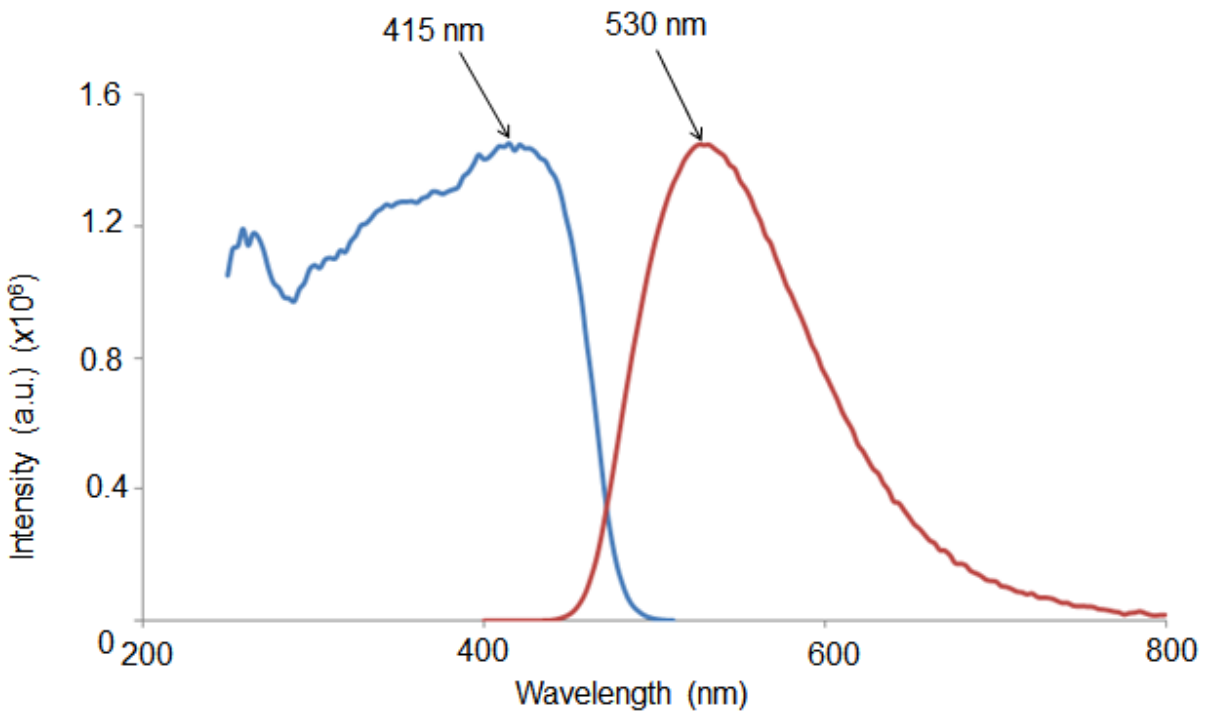

Figure 6-17: Excitation (blue) and emission (red) spectra of *fac*-[Re(CO)$_3$(MeOH)(DiMeOPy)]$^+$ recorded in solid state.

6.3.18 *fac*-[Re(CO)$_3$(TU)(DiMeOPy)]$^+$

The luminescence spectra in Figure **6-18** is a spectroscopic representation of the excitation and emission of *fac*-[Re(CO)$_3$(TU)(DiMeOPy)]$^+$, where the methanol ligand in *fac*-[Re(CO)$_3$(MeOH)(DiMeOPy)]$^+$ is substituted by a thiourea monodentate ligand. This multi-emitter has multiple excitation wavelengths from 250 nm to 553 nm and a prominent excitation peak (chosen for comparison reasons) at 370 nm that gives rise to the maximum emission at 600 nm. The complex emits from 466 nm to 800 nm and has a quantum yield of 1.4 %.

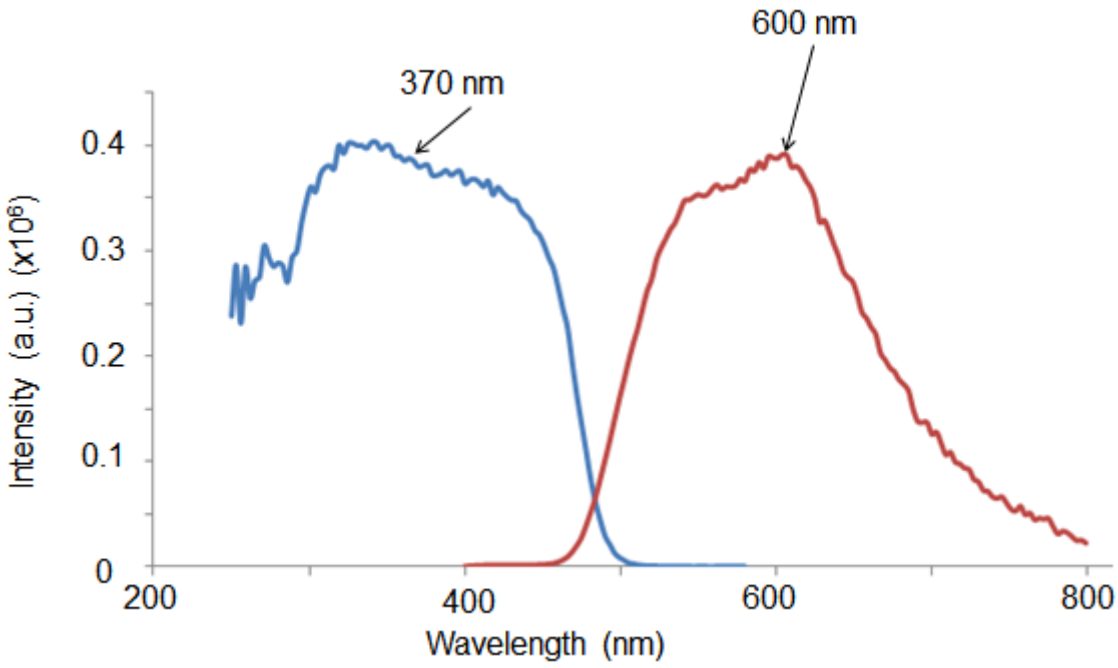

Figure 6-18: Excitation (blue) and emission (red) spectra of *fac*-[Re(CO)$_3$(TU)(DiMeOPy)]$^+$ recorded in solid state.

6.3.19 *fac*-[Re(CO)$_3$(NCS)(DiMeOPy)]

The luminescence spectra in Figure **6-19** is a spectroscopic representation of the excitation and emission of *fac*-[Re(CO)$_3$(NCS)(DiMeOPy)], where the methanol ligand in *fac*-[Re(CO)$_3$(MeOH)(DiMeOPy)]$^+$ is substituted by a thiocyanate monodentate ligand. *fac*-[Re(CO)$_3$(NCS)(DiMeOPy)] is a multi-emitter with multiple excitation wavelengths from 250 nm to 532 nm and a prominent excitation peak (chosen for comparison reasons) at 370 nm that gives rise to the maximum emission at 553 nm. The complex emits from 470 nm to 800 nm and has a quantum yield of 4.3 %.

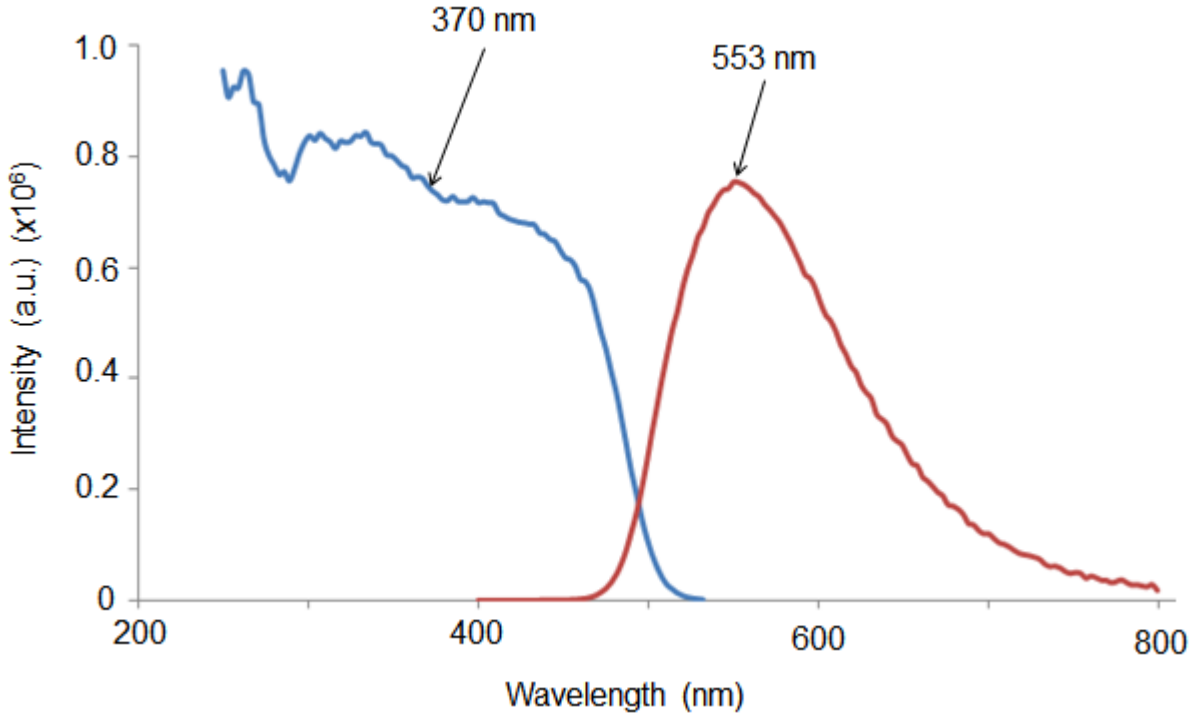

Figure 6-19: Excitation (blue) and emission (red) spectra of *fac*-[Re(CO)$_3$(NCS)(DiMeOPy)] recorded in solid state.

6.3.20 *fac*-[Re(CO)$_3$(PCy$_3$)(DiMeOPy)]$^+$

The luminescence spectra in Figure **6-20** is a spectroscopic representation of the excitation and emission of *fac*-[Re(CO)$_3$(PCy$_3$)(DiMeOPy)]$^+$, where the methanol ligand in *fac*-[Re(CO)$_3$(MeOH)(DiMePy)]$^+$ is substituted by a tricyclohexylphosphine monodentate ligand. *fac*-[Re(CO)$_3$(PCy$_3$)(DiMeOPy)]$^+$ is a multi-emitter with multiple excitation wavelengths from 250 nm to 517 nm and a prominent excitation peak at 370 nm (chosen for comparison reasons) that gives rise to the maximum emission at 538 nm. The complex emits from 445 nm to 800 nm and has a quantum yield of 2.1 %.

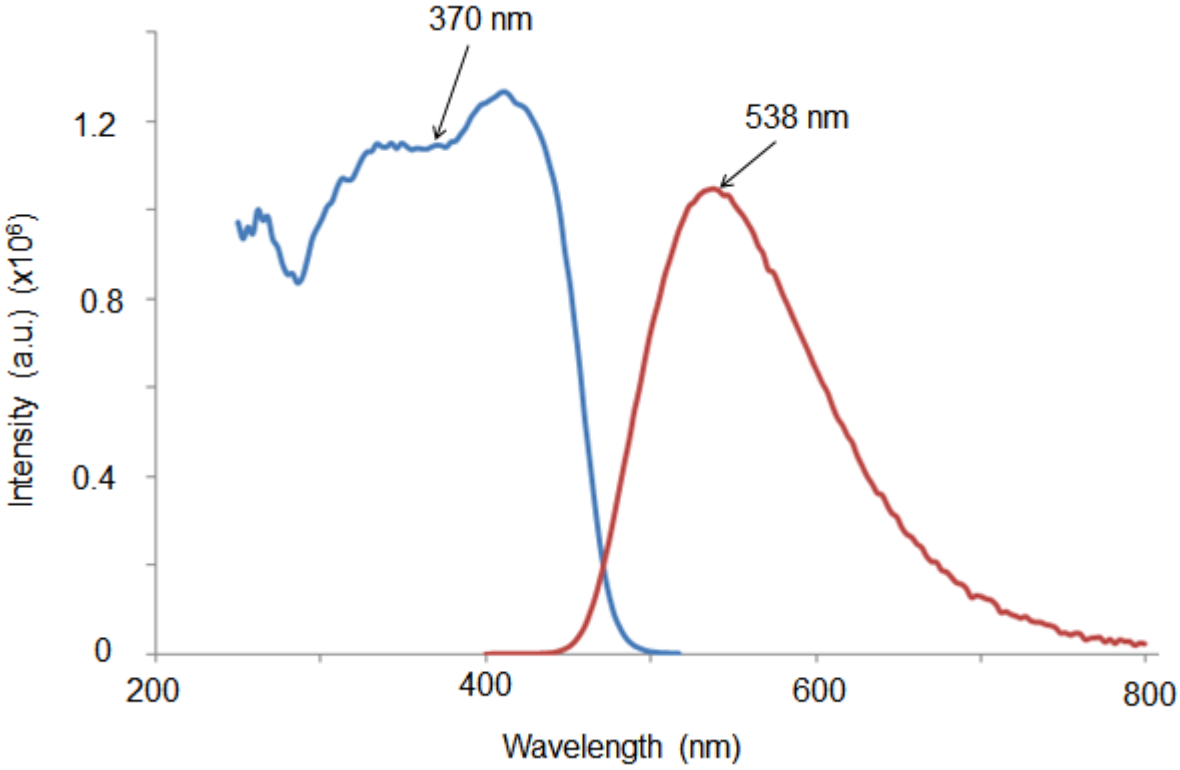

Figure 6-20: Excitation (blue) and emission (red) spectra of *fac*-[Re(CO)$_3$(PCy$_3$)(DiMeOPy)]$^+$ recorded in solid state.

6.3.21 *fac*-[Re(CO)$_3$(Br)(4-MeTPh)]$^-$

The luminescence spectra in Figure **6-21** is a spectroscopic representation of the excitation and emission of *fac*-[Re(CO)$_3$(Br)(4-MeTPh)]$^-$. This complex is a multi-emitter with multiple excitation wavelengths from 230 nm to 440 nm and the prominent excitation peak at 415 nm gives rise to the maximum emission at 450 nm. The complex emits from 400 nm to 550 nm and has a quantum yield of 21 %.

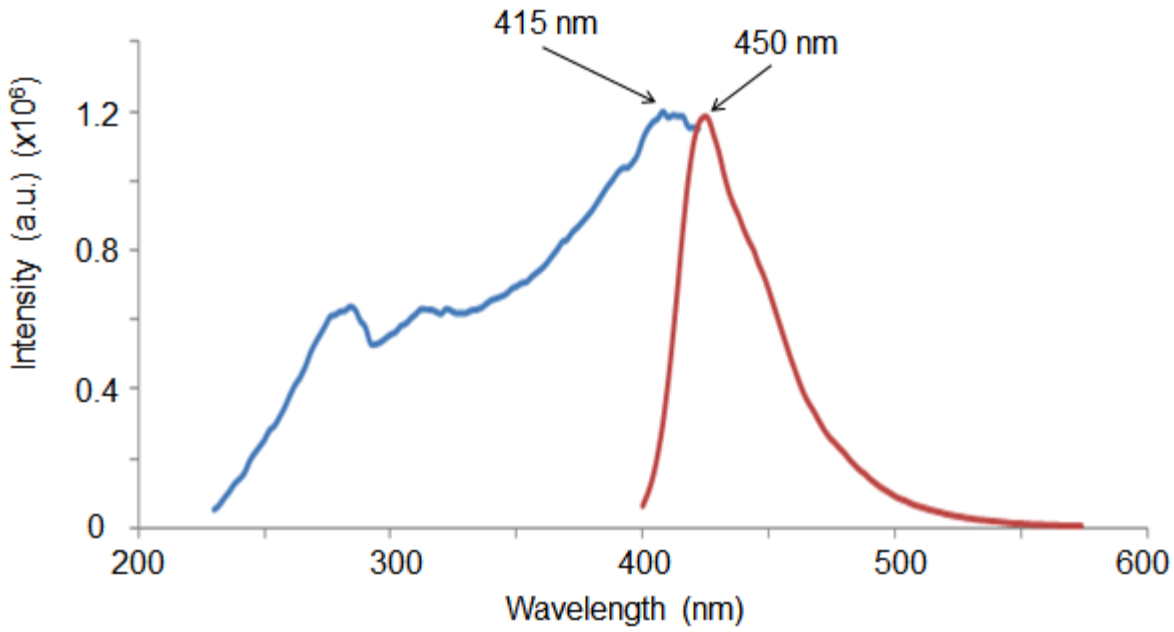

Figure 6-21: Excitation (blue) and emission (red) spectra of *fac*-[Re(CO)$_3$(Br)(4-MeTPh)]$^-$ recorded in solid state.

6.3.22 *fac*-[Re(CO)$_3$(H$_2$O)(4-MeTPh)]

The luminescence spectra in Figure **6-22** is a spectroscopic representation of the excitation and emission of *fac*-[Re(CO)$_3$(H$_2$O)(4-MeTPh)]. The complex is a multi-emitter with multiple excitation wavelengths from 230 nm to 440 nm and the most prominent excitation peak is at 415 nm that gives rise to the maximum emission at 450 nm. The complex emits from 420 nm to 600 nm and has a quantum yield of 13 %.

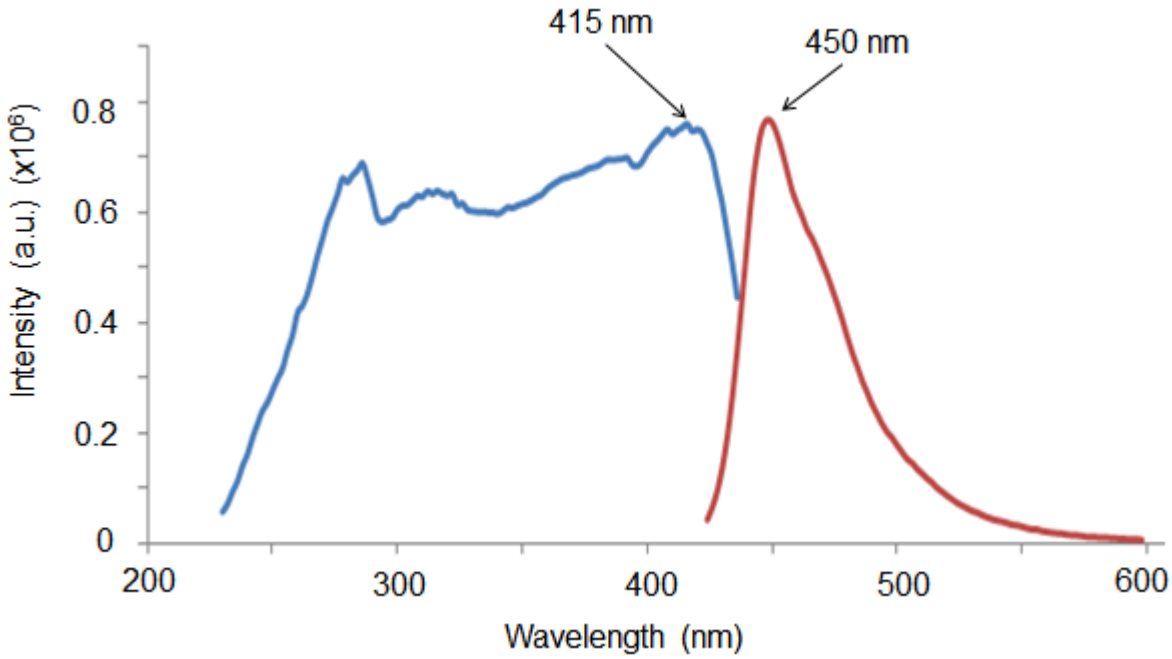

Figure 6-22: Excitation (blue) and emission (red) spectra of *fac*-[Re(CO)$_3$(H$_2$O)(4-MeTPh)] recorded in solid state.

6.3.23 *fac*-[Re(CO)$_3$(TU)(4-MeTPh)]

The luminescence spectra in Figure **6-23** is a spectroscopic representation of the excitation and emission of *fac*-[Re(CO)$_3$(TU)(4-MeTPh)], where the bromido ligand in *fac*-[Re(CO)$_3$(Br)(4-MeTPh)]$^-$ is substituted by a thiourea monodentate ligand. This is a multi-emitter with multiple excitation wavelengths from 250 nm to 535 nm and a prominent excitation peak at 370 nm (chosen for comparison reasons) that gives rise to the maximum emission at 556 nm. The complex emits from 470 nm to 800 nm and has a quantum yield of 3.4 %.

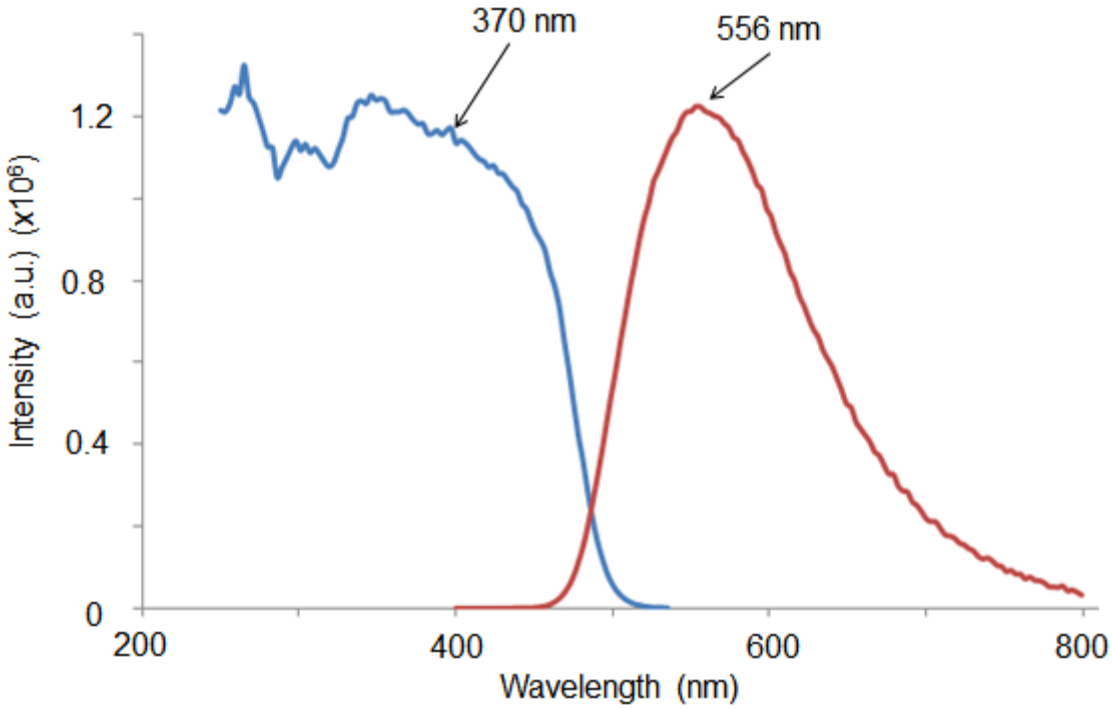

Figure 6-23: Excitation (blue) and emission (red) spectra of *fac*-[Re(CO)$_3$(TU)(4-MeTPh)] recorded in solid state.

6.3.24 *fac*-[Re(CO)$_3$(NCS)(4-MeTPh)]$^-$

The luminescence spectra in Figure **6-24** is a spectroscopic representation of the excitation and emission of *fac*-[Re(CO)$_3$(NCS)(4-MeTPh)]$^-$, where the bromido ligand in *fac*-[Re(CO)$_3$(Br)(4-MeTPh)]$^-$ is substituted by a thiocyanate monodentate ligand. *fac*-[Re(CO)$_3$(NCS)(4-MeTPh)]$^-$ is a multi-emitter with multiple excitation wavelengths from 250 nm to 535 nm and a prominent excitation peak at 370 nm (chosen for comparison reasons) that gives rise to the maximum emission at 556 nm. The complex emits from 475 nm to 800 nm and has a quantum yield of 9.8 %.

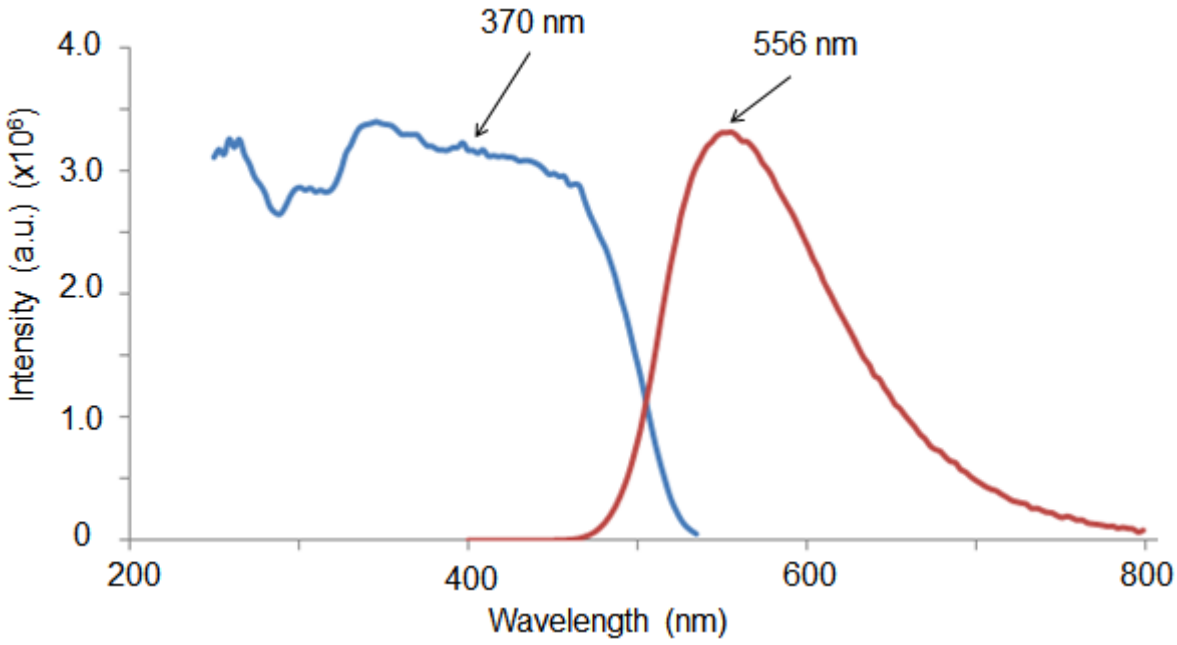

Figure 6-24: Excitation (blue) and emission (red) spectra of *fac*-[Re(CO)$_3$(NCS)(4-MeTPh)]$^-$ recorded in solid state.

6.3.25 *fac*-[Re(CO)$_3$(PCy$_3$)(4-MeTPh)]

The luminescence spectra in Figure **6-25** is a spectroscopic representation of the excitation and emission of *fac*-[Re(CO)$_3$(PCy$_3$)(4-MeTPh)], where the bromido ligand in *fac*-[Re(CO)$_3$(Br)(4-MeTPh)]$^-$ is substituted by a tricyclohexylphosphine monodentate ligand. *fac*-[Re(CO)$_3$(PCy$_3$)(4-MeTPh)] is a multi-emitter with multiple excitation wavelengths from 250 nm to 535 nm and the excitation peak at 370 nm (chosen for comparison reasons) gives rise to the maximum emission at 556 nm. The complex emits from 470 nm to 800 nm and has a quantum yield of 4.2 %.

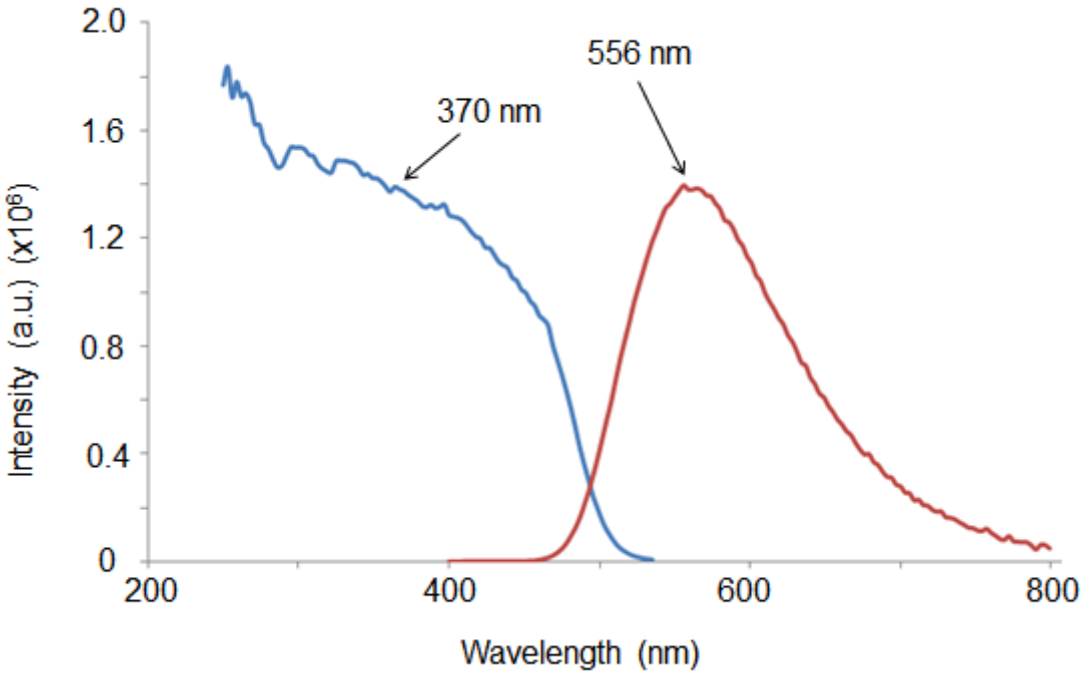

Figure 6-25: Excitation (blue) and emission (red) spectra of *fac*-[Re(CO)$_3$(PCy$_3$)(4-MeTPh)] recorded in solid state.

6.4 Solution state photoluminescence results and discussion

The results obtained from the photoluminescence evaluation using chloroform as solvent for the two Re(I) tricarbonyl complexes *fac*-$[Re(CO)_3(H_2O)(DiMePy)]^+$ and *fac*-$[Re(CO)_3(H_2O)(DiMeOPy]^+$ are presented in Figure **6-26** and **6-27**. Each figure consists of three graphs; chloroform solvent (light green), an excitation graph (blue) and an emission graph (red) at the same wavelengths as indicated on each graph for each complex. The quantum yields of these complexes were not calculated due to time constraints, but will form part of future work.

6.4.1 *fac*-[Re(CO)$_3$(H$_2$O)(DiMePy)]$^+$

The luminescence spectra in Figure **6-26** is a spectroscopic representation of chloroform solvent and the excitation and emission of *fac*-[Re(CO)$_3$(H$_2$O)(DiMePy)]$^+$. The complex is a multi-emitter with multiple excitation wavelengths from 250 nm to 550 nm and the excitation peak at 285 nm gives rise to the maximum emission at 610 nm. The complex emits from 430 nm to 830 nm.

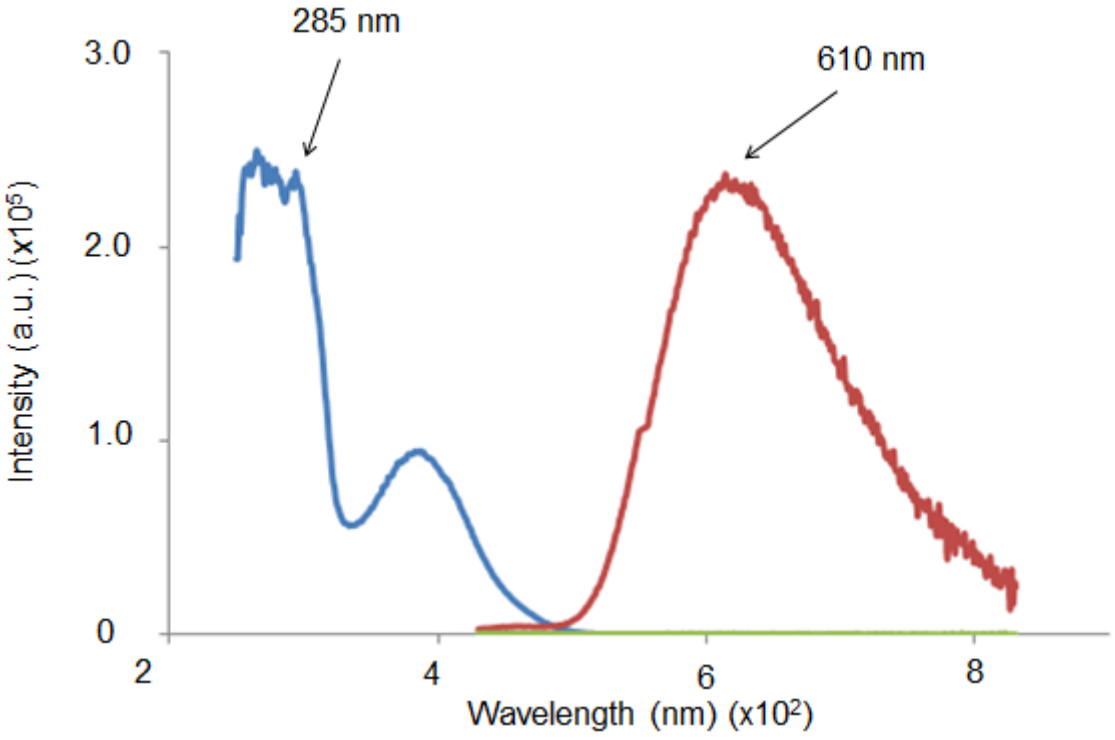

Figure 6-26: Excitation (blue) and emission (red) spectra of *fac*-[Re(CO)$_3$(H$_2$O)(DiMePy)]$^+$ recorded in solution state.

6.4.2 *fac*-[Re(CO)$_3$(H$_2$O)(DiMeOPy)]$^+$

The luminescence spectra in Figure **6-27** is a spectroscopic representation of chloroform solvent (green graph) and the excitation and emission of *fac*-[Re(CO)$_3$(H$_2$O)(DiMeOPy)]$^+$. The complex is also a multi-emitter with multiple excitation wavelengths from 250 nm to 550 nm and the excitation peak at 285 nm (chosen for comparison reason) gives rise to the maximum emission at 625 nm. The complex emits from 430 nm to 830 nm.

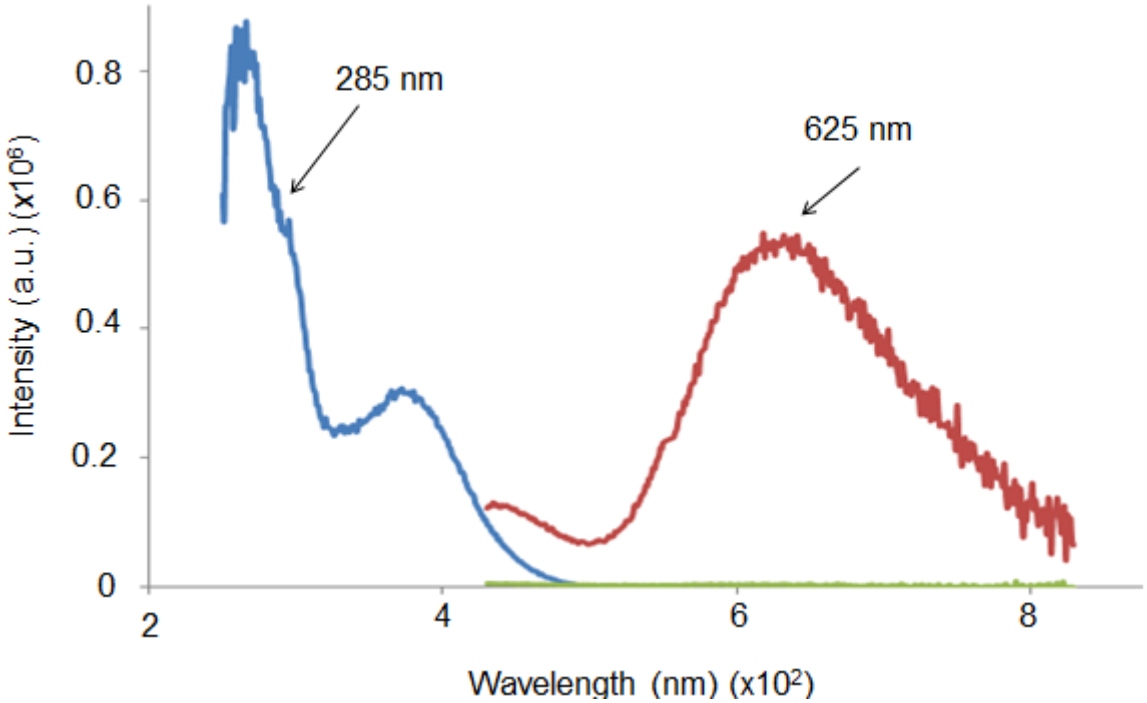

Figure 6-27: Excitation (blue) and emission (red) spectra of *fac*-[Re(CO)$_3$(H$_2$O)(DiMeOPy)]$^+$ recorded in solution state.

6.5 Conclusion

The solid state luminescence spectra of the β-hydroxyketones ligands and twenty two complexes were successfully measured. For some samples the quantum yields could not be calculated due to the sample quality (insufficient amount of sample in the sample holder or challenges with sticky or oily products) and quantity (low yields and time constraints). Additionally the liquid state luminescence spectra of

fac-[Re(CO)$_3$(H$_2$O)(DiMePy)]$^+$ and *fac*-[Re(CO)$_3$(H$_2$O)(DiMeOPy)]$^+$ were calculated. A summary of the absorption, excitation, emission wavelengths and quantum yields are given in Table **6.1** below. All complexes highlighted with the same colour were evaluated under identical measurement settings and the data obtained for these complexes are therefore comparable.

Table 6-1: The absorbance, excitation and emission range; the maximum peak for excitation, emission and quantum yields (where available) for the ligands and Re(I) tricarbonyl complexes evaluated.

Complexes and ligands	Absorbance (nm)	Excitation range (nm)	Excitation peak$_{max}$ (nm)	Emission range (nm)	Emission peak$_{max}$ (nm)	Quantum yield (%)
Solid state luminescence results						
TIFH ligand	280, 350, 580	500 - 725	650	665 – 835	740	-
fac-[Re(CO)$_3$(Br)(TIF)]$^-$	284, 348	500 - 725	705	720 – 835	740	-
fac-[Re(CO)$_3$(H$_2$O)(TIF)]	355, 486	500 - 725	705	720 – 835	740	-
MeTIFH ligand	350, 525	300 - 585	534	544 – 835	595	-
fac-[Re(CO)$_3$(H$_2$O)(MeTIF)]	353, 530	300 - 699	600	620 – 836	720	-
PhTIFH ligand	450, 520	300 - 585	550	620 – 836	595	-
fac-[Re(CO)$_3$(Br)(PhTIF)]$^-$	455, 525	300 - 576	540	556 – 835	592	-
fac-[Re(CO)$_3$(H$_2$O)(PhTIF)]	454, 523	300 - 636	550	565 – 835	650	-
fac-[Re(CO)$_3$(Br)(DiMePy)]	345	230 - 500	370	470- 800	545	56
fac-[Re(CO)$_3$(H$_2$O)(DiMePy)]$^+$	364	230 - 500	370	460 – 800	545	23
fac-Re(CO)$_3$(MeOH)(DiMePy)]$^+$	364	250 - 500	370	445 – 800	520	8.8
fac-[Re(CO)$_3$(TU)(DiMePy)]$^+$	355	250 - 553	370	470 – 800	574	3.0
fac-[Re(CO)$_3$(NCS)(DiMePy)]	360	250 - 535	370	480 – 800	556	4.9
fac-[Re(CO)$_3$(PCy$_3$)(DiMePy)]$^+$	362	250 - 535	370	460 – 800	556	2.8
fac-[Re(CO)$_3$(Br)(DiMeOPy)]	346	230 - 500	370	450 – 800	545	48
fac-[Re(CO)$_3$(H$_2$O)(DiMeOPy)]$^+$	360	230 - 500	370	460 – 800	545	22
fac-Re(CO)$_3$(MeOH)(DiMeOPy)]$^+$	365	250 - 500	415	495 – 800	530	2.8
fac-[Re(CO)$_3$(TU)(DiMeOPy)]$^+$	353	250 - 553	370	466 – 800	600	1.4
fac-[Re(CO)$_3$(NCS)(DiMeOPy)]	350	250 - 532	370	470 – 800	553	4.3
fac-[Re(CO)$_3$(PCy$_3$)(DiMeOPy)]$^+$	349	250 - 517	370	445 – 800	538	2.1
fac-[Re(CO)$_3$(Br)(4-MeTPh)]$^-$	388	230 - 440	415	425 – 550	450	21
fac-[Re(CO)$_3$(H$_2$O)(4-MeTPh)]	360	230 - 440	415	420 – 600	450	13
fac-[Re(CO)$_3$(TU)(4-MeTPh)]	350	250 - 535	370	470 – 800	556	3.4
fac-[Re(CO)$_3$(NCS)(4-MeTPh)]$^-$	338	250 - 535	370	475 – 800	556	9.8
fac-[Re(CO)$_3$(PCy$_3$)(4-MeTPh)]	340	250 - 535	370	470 – 800	556	4.2
Solution state luminescence results						
fac-[Re(CO)$_3$(H$_2$O)(DiMePy)]$^+$	364	250-550	285	430–830	610	-
fac-[Re(CO)$_3$(H$_2$O)(DiMeOPy)]$^+$	360	250-550	285	430–830	625	-

The absorption wavelength of the ligands and complexes are in the same range as its excitation wavelength as expected. All the complexes with bromido ligands in the

6th position were synthesized from *fac*-$[NEt_4]_2[(Re(CO)_3(Br)_3]$ (ReAA). The ReAA used, has no photoluminescent properties on its own but when it is coordinated to a ligand that has promising photoluminescence properties, it is usually affected. All the selected ligands that were coordinated to the Re(I) tricarbonyl core yielded photoluminescent complexes. Some of the complexes and ligands were not measured at exactly the same conditions due to their physical properties. Photoluminescence is a very sensitive measurement type that can be affected by, for instance, the quantity of the sample (amount of sample in the sample holder) or whether it is a powder or a sticky product. This is the reason that some samples have higher intensities than others, therefore the intensity comparisons were not discussed for all complexes and ligands as a whole. All complexes and ligands were compared based on the group colours as illustrated in Table **6-1**; the measurement settings per colour coded group were the same therefore those complexes could safely be compared.

The TIFH ligand has a broad excitation wavelength from 500 nm to 725 nm and two excitation peaks at 630 nm and 650 nm; the maximum peak at 650 nm gives rise to the maximum emission peak at 740 nm. When TIFH is coordinated to the Re(I) tricarbonyl core the excitation peak at 650 nm became dominant and red-shifted to 705 nm, with *fac*-$[Re(CO)_3(Br)(TIF)]^-$ having only one excitation peak compared to two for the free ligand. The photoluminescence of *fac*-$[Re(CO)_3(Br)(TIF)]^-$ and *fac*-$[Re(CO)_3(H_2O)(TIF)]$ were measured at the same conditions, both have the same maximum excitation peaks at 705 nm that gives rise to the maximum emission peak at 740 nm. The emission peak of *fac*-$[Re(CO)_3(Br)(TIF)]^-$ is prominent and better defined than the aqua specie. Unfortunately the quantum yield of these two complexes could not be calculated, due to an insufficient amount of product and time constraints.

The MeTIFH ligand is derived from TIFH. The methyl group that is added to the back bone of TIFH will be used to investigate the potential influence it might have. The excitation of MeTIFH is found to be at a higher energy than TIFH, the maximum excitation peak shifted to 534 nm from 650 nm for the free TIFH ligand and gave rise to a maximum emission peak at 595 nm compared to 740 nm for TIFH indicating a blue-shift. When MeTIFH is coordinated to the Re(I) tricarbonyl core with water in the 6th position (*fac*-$[Re(CO)_3(H_2O)(MeTIF)]$), the physical property of the complex

changes, the excitation wavelength increases from 534 nm for MeTIH to 600 nm for *fac*-[Re(CO)$_3$(H$_2$O)(MeTIF)], while the emission wavelength increases from 595 nm for MeTIH to 720 nm for *fac*-[Re(CO)$_3$(H$_2$O)(MeTIF)].

The PhTIFH ligand is also derived from TIFH. The phenyl ring on the indanone shifted the excitation range from 500 nm to 725 nm for TIFH to 300 nm to 585 nm for PhTIFH and the maximum excitation peak moved to 550 nm for PhTIFH compared to 650 nm for the TIFH ligand. The maximum emission also blue-shifted from 740 nm for TIFH to 595 nm for PhTIFH. When PhTIFH is coordinated to the Re(I) tricarbonyl core (bromido complex) and is excited at 540 nm, the maximum emission peak are found at 592 nm. Substituting the bromido ligand with a water ligand, excitation at 550 nm obtains a maximum emission at 650 nm which is red-shifted. Unfortunately we were unable to obtain *fac*-[Re(CO)$_3$(Br)(PhTIF)] in a uniform crystalline form for comparison, however it yields good photoluminescence results with a very high intensity. Two broad peaks were formed during the excitation state and a maximum peak at 550 nm gave rise to a maximum emission peak at 650 nm.

fac-[Re(CO)$_3$(Br)(DiMePy)] and *fac*-[Re(CO)$_3$(Br)(DiMeOPy)] have been derivatized by substituting the bromido ligands in the 6th position by a range of other monodentate ligands namely; methanol (MeOH), water (H$_2$O), thiourea (TU), thiocyanate (NCS$^-$) and tricyclohexylphosphine (PCy$_3$). The photoluminescence of *fac*-[Re(CO)$_3$(Br)(DiMePy)] and *fac*-[Re(CO)$_3$(Br)(DiMeOPy)] were measured under identical conditions, both were excited at 370 nm and both gave rise to a maximum emission peak at 545 nm. The bromide ion is a heavy atom that increases the spin-orbit coupling and promotes the reverse intersystem crossing which endow the molecules with more distinct delayed fluorescence.[18,21] When the bromido ligands are substituted by a water ligand in *fac*-[Re(CO)$_3$(Br)(DiMePy)] and *fac*-[Re(CO)$_3$(Br)(DiMeOPy)] to form *fac*-[Re(CO)$_3$(H$_2$O)(DiMePy)]$^+$ and *fac*-[Re(CO)$_3$(H$_2$O)(DiMeOPy)]$^+$ the identical excitation and emission results are observed, 370 nm and 545 nm for the excitation and emission respectively. However, the water molecule is found to quench the photoluminescence of both complexes and a lower intensity is observed for the aqua complexes compared to the bromido complexes. The quantum yield of *fac*-[Re(CO)$_3$(Br)(DiMePy)] and *fac*-[Re(CO)$_3$(Br)(DiMeOPy)] are 56 % and 48 % respectively while for the aqua

[21] Najbar, J., Mac, M. *J. Chem. Soc. Faraday Trans*. **87(10)** (1991) 1523-1529.

complexes, *fac*-[Re(CO)$_3$(H$_2$O)(DiMePy)] and *fac*-[Re(CO)$_3$(H$_2$O)(DiMeOPy)] the quantum yields are 23 % and 22 % respectively. This observation follows the trend reported in literature which indicates that the addition of an oxygen atom in a complex quenches the photoluminescence.[22,23] *fac*-[Re(CO)$_3$(Br)(DiMeOPy)] has a lower quantum yield than *fac*-[Re(CO)$_3$(Br)(DiMePy)] possibly due to the oxygen on the periphery of the ligand backbone.

With the substitution of the bromido ligand in *fac*-[Re(CO)$_3$(Br)(DiMePy)] with the various monodentate ligands MeOH, TU, NCS$^-$ and PCy$_3$, different maximum emissions are observed. Three of the complexes are red-shifted with maximum emission wavelengths of 574 nm, 556 nm and 556 nm for *fac*-[Re(CO)$_3$(TU)(DiMePy)]$^+$, *fac*-[Re(CO)$_3$(NCS)(DiMePy)] and *fac*-[Re(CO)$_3$(PCy$_3$)(DiMePy)]$^+$ respectively while *fac*-[Re(CO)$_3$(MeOH)(DiMePy)]$^+$ is blue shifted with a maximum emission at 520 nm. The thiourea complex is found to be the most red-shifted followed by identical values for the thiocyanate and tricyclohexylphosphine complexes. The quantum yields of the complexes when substituting the bromido ligand with MeOH, TU, NCS$^-$ and PCy$_3$ are 8.8, 3.0, 4.9 and 2.8 % respectively, all remarkably lower than the bromido complex's quantum yield of 56 %. No absolute conclusions can be made with regards to the quantum yield due to the variation of the physical properties.

When substituting the bromido ligand in *fac*-[Re(CO)$_3$(Br)(DiMeOPy)] with the identical range of monodentate ligands (MeOH, TU, NCS$^-$ and PCy$_3$), different maximum emissions are also observed. *fac*-[Re(CO)$_3$(TU)(DiMeOPy)]$^+$ and *fac*-[Re(CO)$_3$(NCS)(DiMeOPy)] are red-shifted with maximum emission wavelengths of 600 nm and 553 nm, while *fac*-[Re(CO)$_3$(MeOH)(DiMeOPy)]$^+$ and *fac*-[Re(CO)$_3$(PCy$_3$)(DiMeOPy)]$^+$ are blue-shifted with maximum emissions at 556 nm and 538 nm respectively. A similar trend is observed in the case of DiMePy complexes with the thiourea complex being the most red-shifted complex followed by the thiocyanate complex. The quantum yield of *fac*-[Re(CO)$_3$(X)(DiMeOPy)] when substituting the bromido ligand with the following monodentate ligands MeOH, TU, NCS$^-$ and PCy$_3$ also drops significantly from 48 % to 2.8, 1.4, 4.3 and 2.1 %

[22] Green, S. *Environ. Sci. Technol*. **30** (1996) 1400-1407.
[23] Conrow, P. D., M.Sc. Dissertation, Rochester Institute of Technology, Henrietta, New York. 2001.

respectively. The quantum yields could not be further evaluated due to the variation of physical properties.

fac-$[Re(CO)_3(Br)(4\text{-}MeTPh)]^-$ has similarly been derivatized via the substitution of the bromido ligand for MeOH, H_2O, TU, NCS^- or PCy_3. *fac*-$[Re(CO)_3(Br)(4\text{-}MeTPh)]^-$ and *fac*-$[Re(CO)_3(H_2O)(4\text{-}MeTPh)]$ were measured under identical conditions, excitation occurred at 415 nm, both give rise to a maximum emission peak at 450 nm. However, as previously observed in the DiMePy and DiMeOPy system, the presence of oxygen in the water molecule possibly quenched the photoluminescence in *fac*-$[Re(CO)_3(Br)(4\text{-}MeTPh)]^-$ lowering the quantum yield from 21.1 % to 13 % for *fac*-$[Re(CO)_3(H_2O)(4\text{-}MeTPh)]$.

Similar maximum emissions are observed with the substitution of the bromido ligand in *fac*-$[Re(CO)_3(Br)(4\text{-}MeTPh)]^-$ with the monodentate ligand range. *fac*-$[Re(CO)_3(TU)(4\text{-}MeTPh)]$, *fac*-$[Re(CO)_3(NCS)(4\text{-}MeTPh)]^-$ and *fac*-$[Re(CO)_3(PCy_3)(4\text{-}MeTPh)]$ were excited at 370 nm and maximum emissions at 556 nm were observed for all three complexes. All were red-shifted from the maximum emission of the bromido complex of 450 nm to 556 nm. The quantum yield of the complexes when substituting the bromido ligand with TU, NCS^- and PCy_3 were 3.4, 9.8 and 4.2 % respectively, all lower than the bromido complex of 21 %.

Table **6-2** below illustrates the effect of substituting the bromido ligand with a water ligand in each of the complexes listed. The compared complexes are measured under identical settings and conditions. Scheme **6-2** illustrates the structures of the three complexes that are compared.

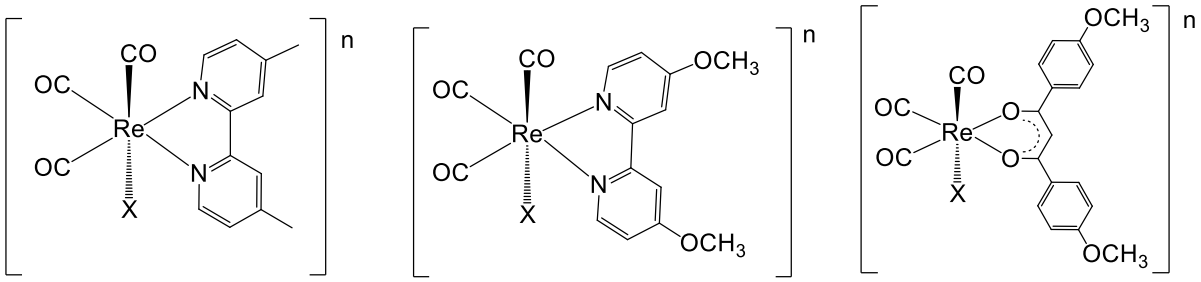

fac-$[Re(CO)_3(X)(DiMePy)]^n$ *fac*-$[Re(CO)_3(X)(DiMeOPy)]^n$ *fac*-$[Re(CO)_3(X)(4\text{-}MeTPh)]^n$

where X = Br/H_2O
n = +1, 0

Scheme 6-2: Illustration of the *N,N'* and *O,O'* Re(I) tricarbonyl structures indicating the effect of bromido / aqua substitution on the quantum yield.

Table 6-2: Summary of quantum yields obtained for the six Re(I) complexes.

Complexes	Quantum yield (%)
fac-[Re(CO)$_3$(Br)(DiMePy)]	56
fac-[Re(CO)$_3$(H$_2$O)(DiMePy)]$^+$	23
fac-[Re(CO)$_3$(Br)(DiMeOPy)]	48
fac-[Re(CO)$_3$(H$_2$O)(DiMeOPy)]$^+$	22
fac-[Re(CO)$_3$(Br)(4-MeTPh)]$^-$	21
fac-[Re(CO)$_3$(H$_2$O)(4-MeTPh)]	13

In the comparison of the bromido complexes: *fac*-[Re(CO)$_3$(Br)(DiMePy)] has the highest quantum yield of 56 % followed by *fac*-[Re(CO)$_3$(Br)(DiMeOPy)] and *fac*-[Re(CO)$_3$(Br)(4-MeTPh)]$^-$ with 48% and 21 % respectively. *fac*-[Re(CO)$_3$(Br)(DiMePy)] is structurally symmetrical and chemically similar to *fac*-[Re(CO)$_3$(Br)(DiMeOPy)], differing only by the methyl and methoxy group on the back bone of the structure. It is likely that the oxygen atom of the methoxy group is the cause for the quenching of the photoluminescence from the quantum yield of 56 % to 48 %. From *fac*-[Re(CO)$_3$(Br)(DiMePy)] to *fac*-[Re(CO)$_3$(Br)(4-MeTPh)]$^-$ the quantum yield decreases significantly from 56 % to 21%, also considered to be associated with the four oxygen atoms in the 4-MeTPh bidentate ligand containing the coordinate *O,O'* atoms and methoxy functionality on the backbone.

For the aqua complexes: *fac*-[Re(CO)$_3$(H$_2$O)(DiMePy)] has the highest quantum yield of 23 % followed by *fac*-[Re(CO)$_3$(H$_2$O)(DiMeOPy)] and *fac*-[Re(CO)$_3$(H$_2$O)(4-MeTPh)] with 22 % and 13 % respectively. *fac*-[Re(CO)$_3$(H$_2$O)(DiMePy)] is similar to *fac*-[Re(CO)$_3$(H$_2$O)(DiMeOPy)] as the differences lie primary with the methyl and methoxy groups (again more oxygen atoms quenching the photoluminescence). The quantum yield decreases significantly from *fac*-[Re(CO)$_3$(H$_2$O)(DiMePy)] to *fac*-[Re(CO)$_3$(H$_2$O)(4-MeTPh)] (23 % to 13%).

The effect on the quantum yield when substituting the bromido ligand with the aqua ligand in the 6th position is prominet, with an average decrease ranging from ~ 59 to 38 %. On the other hand, altering the ligand backbone from methyl to methoxy functionalities has minimal effect with a ~ 5-10 % decrease in quantum yield for the complexes containing the DiMePy and DiMeOPy ligands.

The ligands and complexes; TIFH, MeTIFH, PhTIFH, *fac*-[Re(CO)$_3$(Br)(TIF)], *fac*-[Re(CO)$_3$(H$_2$O)(TIF)], *fac*-[Re(CO)$_3$(Br)(MeTIF)], *fac*-[Re(CO)$_3$(Br)(PhTIF)] and *fac*-[Re(CO)$_3$(H$_2$O)(PhTIF)] have the highest excitation and emission wavelengths in

total, similar to promising complexes in literature.[24,Error! Bookmark not defined.] Cheung *et al*. compared light-induced fluorescence (LIF) and nominal injected drug dose in order to predict the depth of necrosis response to photodynamic therapy (PDT) in a murine tumor model. Photofrin's fluorescence excitation and emission were measured at 545 nm and 628 nm from the tumor which are classified as a good wavelength and they were in the same range as the results obtained here.[24] Taboada *et al.* investigated the natural occurring fluorescence in frogs. The excitation and emission ranges were also similar to the results obtained for the complexes in this study.**Error! Bookmark not defined.**

The ligands and complexes investigated in this study gave good results with maximum excitation and emission wavelengths that are in the recommended range of 534 nm to 705 nm and 595 nm to 740 nm respectively and can potentially be used as PDT agents.**Error! Bookmark not defined.**

The behaviour of *fac*-$[Re(CO)_3(H_2O)(DiMePy)]^+$ and *fac*-$[Re(CO)_3(H_2O)(DiMeOPy)]^+$ were further investigated in solution state. The photoluminescence were measured under identical conditions, both excited at 285 nm and gave rise to a maximum emission peak at 610 nm for *fac*-$[Re(CO)_3(H_2O)(DiMePy)]$ and 625 nm for *fac*-$[Re(CO)_3(H_2O)(DiMeOPy)]$. The solution state results (when compared to the solid state results), indicate the maximum emission is red-shifted for both the aqua species. The longer wavelength is potentially more appropriate for model PDT agents than the solid state results.

The results obtained in this study, even though it was not one of the main objectives, indicate the potential use of these ligands and complexes as OLEDs. For its potential application in PDT, it is however imperative to expand the variation in ligands and more importantly to repeat the photoluminescence experiments of all the complexes in solution state. Since the solvent plays an extremely important role in the photoluminescence results, it must also be considered to use different solvents. The results obtained in this study is fundamental for future work in this regard, especially the red-shift found for the *O,O'* bidentate ligands and its complexes.

[24] Cheung, R., Solonenko, M., Busch, T. M., Piero, F. D., Put. M. E., Hahn, S. M., Yodh, A. G. *J. Biomed. Opt.* **8**(2) (2003)248-252.

7 EVALUATION OF THIS STUDY

7.1 Results obtained

The aim of this study was to investigate the ability of the chosen bipyridine bidentate ligands, β-diketone bidentate ligands and synthesized β-hydroxyketone bidentate ligands to coordinate to the *fac*-$[Re(CO)_3]^+$ core and to evaluated its photoluminescence, potential chemotherapeutic and kinetic behaviour.

Three β-hydroxyketone bidentate ligands and fourty eight Re(I) tricarbonyl complexes were synthesized and characterized successfully, including the kinetic end products of six of the complexes, which confirmed the structure of the substituted products. The crystal structure of one ligand, 4-MeTPh and five Re(I) tricarbonyl complexes (*fac*-$[Re(CO)_3(Br)(DiMePy)]$, *fac*-$[Re(CO)_3(Act)(DiMePy)][NO_3]$, *fac*-$[Re(CO)_3(NO_3)(DiMePy)]$, *fac*-$[Re(CO)_3(Br)(DiMeOPy)]$, *fac*-$[Re(CO)_3(NO_3)(DiMePy)]$) are reported. Unfortunately, we were unable to grow suitable crystals for single crystal x-ray diffraction of the kinetic end products. All the reported complexes in this study contributes significantly to the already available database of Re(I) tricarbonyl complexes.

The methanol substitution reactions between *fac*-$[Re(CO)_3(MeOH)(L,L'\text{-Bid})]^n$ (where *L,L'*-Bid = DiMePy, DiMeOPy, 4-MeTPhH, BrDiPhPrH, TIFH, MeTIFH, n = +1, 0) and different monodentate entering ligands, thiourea (TU), sodium thiocyanate (NCS^-), triphenylphosphine (PPh_3) or tricyclohexylphosphine (PCy_3) and sodium bromide (Br^-) were evaluated at different temperatures. Excellent results were obtained and the available knowledge on the methanol substitution kinetics of Re(I) complexes have been expanded to a great extent and should be of good use in future studies.

The solid state photoluminescence spectra of three β-hydroxyketone ligands and twenty two Re(I) complexes (with *O,O'* β-diketone, β-hydroxyketone as well as *N,N'*-bipyridine ligand systems) are reported in this study. Due to differences in physical properties, some of the complexes and ligands were not measured under the same

conditions. The quantum yields could not be calculated due to challenges regarding the sample quality; these challenges include insufficient amount of sample for the sample holder, challenges with sticky or oily products and time and financial constraints. Additionally the liquid state luminescence spectra of *fac*-$[Re(CO)_3(H_2O)(DiMePy)]^+$ and *fac*-$[Re(CO)_3(H_2O)(DiMeOPy)]^+$ were obtained. The excitation and emission wavelengths of all the samples were measured. All absorption wavelengths reported fall within the expected excitation range. The ligands and complexes TIFH, MeTIFH, PhTIFH, *fac*-$[Re(CO)_3(Br)(TIF)]$, *fac*-$[Re(CO)_3(H_2O)(TIF)]$, *fac*-$[Re(CO)_3(Br)(MeTIF)]$, *fac*-$[Re(CO)_3(Br)(PhTIF)]$ and *fac*-$[Re(CO)_3(H_2O)(PhTIF)]$ have the highest excitation and emission wavelengths. The ligands and complexes investigated in this study showed promising results with maximum excitation and emission wavelengths ranging from 534 nm to 705 nm and 595 nm to 740 nm, respectively. This falls within the range of the required properties needed for PDT agents. The solution state photoluminescence results of *fac*-$[Re(CO)_3(H_2O)(DiMePy)]^+$ and *fac*-$[Re(CO)_3(H_2O)(DiMeOPy)]^+$ (when compared to the solid state results), indicate the maximum emission is red-shifted for both the aqua species and the bromido species. The longer wavelength found in the solution state studies is potentially more appropriate for model PDT agents than the solid state results.

Unfortunately, due to time constraints and Covid-19 related restrictions and protocols, we were unable to send these complexes for cytotoxic evaluation in Paris, France.

7.2 Future work

Although a great contribution was made to the available knowledge of the coordination behaviour of Re(I) tricarbonyl complexes, the kinetic behaviour and photoluminescent properties of Re(I) complexes with *N,N'* and *O,O"* bidentate ligands, the following should form part of future research:

1. Cytotoxic evaluation of *N,N'*-, β-hydroxyketone ligands and 4-MeTPh, and their respective rhenium(I) tricarbonyl complexes. We were unable to send the samples to France due to the Covid-19 pandemic. Due to time constraints (six months were lost in the lab) to finish the thesis in time, we decided to evaluate these complexes at a later stage.

2. High pressure kinetic study of all the Re(I) tricarbonyl complexes investigated in Chapter 5 using different entering monodentate ligands in order to unambiguously determine the mechanism.
3. An effort should be made to functionalise the existing Re(I) tricarbonyl complexes to make it (more) water soluble, in order to do aqueous kinetic studies and to determine the *p*Ka values, stability and reaction mechanisms in water.
4. The *O,O'* bidentate ligand range must be expanded to form a more concise picture of the photoluminescence, cytotoxicity and kinetic behaviour of these complexes. It is clear that the structure of the *O,O'* ligand plays an important role on the electrondonating ability and substitution rate of the complexes.
5. The complexes that have emission wavelengths that are within range for potential PDT agents, should be investigated further by evaluating its photoactivity.

APPENDIX A

Table A-1: Atomic coordinates (x 10^4) and equivalent isotropic displacement parameters ($Å^2$ x 10^3) for 4-MeTPhH. U(eq) is defined as one third of the trace of the orthogonalized U^{ij} tensor.

	x	y	z	U(eq)
C(1)	5452(11)	10733(5)	1354(1)	68(1)
C(1')	12218(12)	18513(5)	-254(1)	79(2)
C(2)	5797(8)	9741(4)	2012(1)	45(1)
C(2')	9959(10)	17752(4)	385(1)	53(1)
C(3')	8745(10)	16638(4)	207(1)	58(1)
C(3)	6907(9)	8709(4)	2243(1)	54(1)
C(4)	6117(9)	8616(4)	2647(1)	51(1)
C(4')	6987(10)	15772(4)	448(1)	56(1)
C(5')	9429(10)	17990(4)	797(1)	56(1)
C(5)	3885(9)	10678(4)	2194(1)	47(1)
C(6)	3090(9)	10563(4)	2604(1)	47(1)
C(6')	7700(9)	17138(4)	1030(1)	53(1)
C(7')	6411(9)	16003(4)	862(1)	47(1)
C(7)	4146(8)	9547(3)	2839(1)	43(1)
C(8')	4491(9)	15079(4)	1102(1)	50(1)
C(8)	3218(9)	9369(4)	3274(1)	50(1)
C(9)	1377(9)	10281(4)	3491(1)	50(1)
C(9')	3626(9)	15280(4)	1510(1)	50(1)
C(10)	485(9)	10080(4)	3901(1)	49(1)
C(10')	1781(9)	14368(4)	1726(1)	48(1)
C(11')	845(8)	14538(3)	2160(1)	42(1)
C(11)	-1402(9)	11002(4)	4138(1)	47(1)
C(12')	-1092(9)	13615(4)	2353(1)	51(1)
C(12)	-1982(10)	10766(4)	4550(1)	57(1)
C(13')	-1906(9)	13713(4)	2759(1)	53(1)
C(13)	-3727(10)	11638(4)	4791(1)	58(1)
C(14')	1906(9)	15559(4)	2396(1)	47(1)
C(14)	-2687(10)	12139(4)	3972(1)	55(1)
C(15')	1117(9)	15681(4)	2805(1)	47(1)
C(15)	-4421(10)	12997(4)	4204(1)	56(1)
C(16)	-4973(10)	12754(4)	4618(1)	53(1)
C(16')	-786(9)	14740(4)	2989(1)	47(1)
C(17)	-7231(12)	13517(5)	5254(1)	79(2)
C(17')	-440(11)	15730(5)	3643(1)	68(1)
O(1')	3575(7)	14015(3)	919(1)	67(1)
O(1)	4154(7)	8320(3)	3455(1)	67(1)
O(2')	843(7)	13319(3)	1547(1)	67(1)
O(3')	11701(7)	18662(3)	181(1)	70(1)
O(3)	6712(7)	9745(3)	1612(1)	62(1)

O(4')	-1698(7)	14747(3)	3388(1)	62(1)
O(2)	1406(7)	9015(3)	4081(1)	67(1)
O(4)	-6717(8)	13665(3)	4819(1)	69(1)

Table A-2: Bond distances (Å) and angles (°) for 4-MeTPh.

Bond	Bond Distance	Bond Angle	Angle
O(1)-C(2)	1.302(2)	C(7)-O(3)-C(8)	118.8(2)
O(2)-C(3)	1.319(3)	C(14)-O(4)-C(15)	118.39(16)
O(3)-C(7)	1.369(3)	C(2)-C(1)-C(3)	121.9(2)
O(3)-C(8)	1.448(3)	O(1)-C(2)-C(1)	119.7(2)
O(4)-C(14)	1.381(2)	O(1)-C(2)-C(11)	116.6(2)
O(4)-C(15)	1.442(3)	C(1)-C(2)-C(11)	123.6(2)
C(1)-C(2)	1.402(3)	O(2)-C(3)-C(1)	119.8(2)
C(1)-C(3)	1.410(3)	O(2)-C(3)-C(4)	116.77(19)
C(2)-C(11)	1.494(3)	C(1)-C(3)-C(4)	123.5(2)
C(3)-C(4)	1.472(3)	C(10)-C(4)-C(5)	117.8(2)
C(4)-C(10)	1.401(3)	C(10)-C(4)-C(3)	120.0(2)
C(4)-C(5)	1.406(3)	C(5)-C(4)-C(3)	122.29(19)
C(5)-C(6)	1.374(3)	C(6)-C(5)-C(4)	121.1(2)
C(6)-C(7)	1.405(3)	C(5)-C(6)-C(7)	120.2(2)
C(7)-C(9)	1.393(3)	O(3)-C(7)-C(9)	124.6(2)
C(9)-C(10)	1.389(3)	O(3)-C(7)-C(6)	115.4(2)
C(11)-C(17)	1.397(3)	C(9)-C(7)-C(6)	119.9(2)
C(11)-C(12)	1.397(3)	C(10)-C(9)-C(7)	119.1(2)
C(12)-C(13)	1.394(3)	C(9)-C(10)-C(4)	121.9(2)
C(13)-C(14)	1.387(3)	C(17)-C(11)-C(12)	116.82(19)
C(14)-C(16)	1.396(3)	C(17)-C(11)-C(2)	120.0(2)
C(16)-C(17)	1.382(3)	C(12)-C(11)-C(2)	123.17(19)
		C(13)-C(12)-C(11)	122.73(19)
		C(14)-C(13)-C(12)	119.0(2)
		O(4)-C(14)-C(13)	124.2(2)
		O(4)-C(14)-C(16)	116.52(19)
		C(13)-C(14)-C(16)	119.3(2)
		C(17)-C(16)-C(14)	120.8(2)
		C(16)-C(17)-C(11)	121.3(2

Table A-3: Anisotropic displacement parameters ($Å^2$ x 10^3) for 4-MeTPh.The anisotropic displacement factor exponent takes the form: $-2\pi^2[h2a^{*2}U^{11} + \ldots\ldots + 2hka^*b^*U^{12}]$.

	U_{11}	U_{22}	U_{33}	U_{23}	U_{13}	U_{12}
O(1)	94(1)	54(1)	66(1)	-15(1)	2(1)	-7(1)
O(2)	94(1)	57(1)	59(1)	-21(1)	-4(1)	2(1)
O(3)	94(1)	69(1)	55(1)	6(1)	17(1)	14(1)
O(4)	79(1)	61(1)	55(1)	8(1)	11(1)	-8(1)
C(1)	61(1)	44(1)	48(1)	-4(1)	-5(1)	5(1)

C(2)	54(1)	41(1)	58(2)	-7(1)	-10(1)	10(1)
C(3)	56(1)	52(1)	46(1)	-6(1)	-10(1)	16(1)
C(4)	56(1)	52(1)	38(1)	-6(1)	-8(1)	15(1)
C(5)	72(2)	58(2)	40(1)	-7(1)	2(1)	12(1)
C(6)	76(2)	54(2)	49(1)	-7(1)	5(1)	7(1)
C(7)	62(1)	58(2)	48(1)	5(1)	6(1)	21(1)
C(8)	95(2)	97(2)	58(2)	12(2)	21(1)	22(2)
C(9)	71(2)	72(2)	39(1)	-8(1)	2(1)	21(1)
C(10)	67(1)	60(2)	48(1)	-10(1)	-7(1)	15(1)
C(11)	46(1)	37(1)	50(1)	0(1)	-4(1)	7(1)
C(12)	54(1)	40(1)	53(1)	2(1)	4(1)	-1(1)
C(13)	58(1)	40(1)	49(1)	2(1)	2(1)	0(1)
C(14)	51(1)	45(1)	50(1)	8(1)	4(1)	5(1)
C(15)	87(2)	75(2)	49(1)	0(1)	7(1)	-9(1)
C(16)	58(1)	45(1)	67(2)	7(1)	5(1)	-6(1)
C(17)	53(1)	40(1)	65(2)	-3(1)	-5(1)	2(1)

Table A-4: Hydrogen bond distances (Å) and angles (º) for 4-MeTPh.

D-H…A	d(D-H)	d(H…A)	d(D…A)	D-H…A angle
C4-H4…O1[a]	0.93	2.49	2.804(6)	100
C12-H12…O12[a]	0.93	2.46	2.781(5)	101

Symmetry code, transformations used to generate equivalent atoms: [a] x, y, z.

APPENDIX B

Table B-1: Atomic coordinates (x 10^4) and equivalent isotropic displacement parameters (Å^2 x 10^3) for *fac*-[Re(CO)$_3$(Br)(DiMePy)]. U(eq) is defined as one third of the trace of the orthogonalized U^{ij} tensor.

	x	y	z	U(eq)
C(1)	7759(10)	-1908(10)	5570(20)	28(3)
C(2)	6451(9)	-1113(9)	3278(19)	25(3)
C(3)	6337(9)	-1088(9)	6826(19)	26(3)
C(4)	5911(8)	1233(9)	5568(16)	17(2)
C(5)	5688(8)	2246(10)	5596(17)	21(2)
C(6)	6245(8)	2957(9)	5090(16)	19(2)
C(7)	7018(8)	2620(9)	4484(17)	20(2)
C(8)	7211(8)	1585(9)	4414(16)	19(2)
C(9)	7982(8)	1188(9)	3738(16)	19(2)
C(10)	8581(8)	1790(10)	2944(17)	22(2)
C(11)	9305(9)	1350(10)	2300(18)	26(3)
C(12)	9379(9)	307(11)	2429(19)	27(3)
C(13)	8769(9)	-269(12)	3218(17)	27(3)
C(14)	6051(10)	4062(9)	5229(19)	25(3)
C(15)	9943(10)	1970(12)	1470(20)	34(3)
N(1)	8086(7)	172(7)	3847(13)	17(2)
N(2)	6664(7)	923(8)	5048(14)	18(2)
O(1)	8103(8)	-2676(8)	5749(17)	40(3)
O(2)	6011(7)	-1417(7)	2079(13)	32(2)
O(3)	5840(8)	-1322(8)	7728(15)	37(2)
Br(1)	8197(1)	125(1)	8019(2)	24(1)
Re(1)	7170(1)	-616(1)	5314(1)	19(1)

Table B-2: Bond distances (Å) and angles (°) for *fac*-[Re(CO)$_3$(Br)(DiMePy)].

Bond	Bond Distance	Bond Angle	Angle
C(1)-O(1)	1.147(17)	O(1)-C(1)-Re(1)	178.9(14)
C(1)-Re(1)	1.938(14)	O(2)-C(2)-Re(1)	178.8(13)
C(2)-O(2)	1.144(17)	O(3)-C(3)-Re(1)	177.0(12)
C(2)-Re(1)	1.913(15)	N(2)-C(4)-C(5)	121.8(11)
C(3)-O(3)	1.136(18)	C(6)-C(5)-C(4)	120.2(12)
C(3)-Re(1)	1.936(15)	C(5)-C(6)-C(7)	117.4(11)
C(4)-N(2)	1.333(16)	C(5)-C(6)-C(14)	121.4(12)
C(4)-C(5)	1.391(17)	C(7)-C(6)-C(14)	121.2(12)
C(5)-C(6)	1.362(18)	C(6)-C(7)-C(8)	121.0(11)
C(6)-C(7)	1.400(17)	N(2)-C(8)-C(7)	118.7(11)
C(6)-C(14)	1.504(16)	N(2)-C(8)-C(9)	117.7(11)
C(7)-C(8)	1.409(16)	C(7)-C(8)-C(9)	123.6(12)
C(8)-N(2)	1.347(16)	N(1)-C(9)-C(10)	120.8(11)
C(8)-C(9)	1.448(17)	N(1)-C(9)-C(8)	115.6(11)

C(9)-N(1)	1.360(16)	C(10)-C(9)-C(8)	123.5(11)
C(9)-C(10)	1.412(18)	C(11)-C(10)-C(9)	120.2(12)
C(10)-C(11)	1.398(19)	C(12)-C(11)-C(10)	116.9(13)
C(11)-C(12)	1.39(2)	C(12)-C(11)-C(15)	122.1(13)
C(11)-C(15)	1.48(2)	C(10)-C(11)-C(15)	121.0(13)
C(12)-C(13)	1.403(19)	C(11)-C(12)-C(13)	121.4(13)
C(13)-N(1)	1.342(16)	N(1)-C(13)-C(12)	120.6(13)
N(1)-Re(1)	2.175(10)	C(13)-N(1)-C(9)	120.1(11)
N(2)-Re(1)	2.187(10)	C(13)-N(1)-Re(1)	124.0(9)
Br(1)-Re(1)	2.6325(17)	C(9)-N(1)-Re(1)	115.6(8)
		C(4)-N(2)-C(8)	120.5(11)
		C(4)-N(2)-Re(1)	124.7(8)
		C(8)-N(2)-Re(1)	114.5(8)
		C(2)-Re(1)-C(3)	91.4(6)
		C(2)-Re(1)-C(1)	89.4(6)
		C(3)-Re(1)-C(1)	89.1(6)
		C(2)-Re(1)-N(1)	94.8(5)
		C(3)-Re(1)-N(1)	169.7(5)
		C(1)-Re(1)-N(1)	99.1(5)
		C(2)-Re(1)-N(2)	95.0(5)
		C(3)-Re(1)-N(2)	96.1(5)
		C(1)-Re(1)-N(2)	173.1(5)
		N(1)-Re(1)-N(2)	75.2(4)
		C(2)-Re(1)-Br(1)	177.3(4)
		C(3)-Re(1)-Br(1)	91.1(4)
		C(1)-Re(1)-Br(1)	91.6(4)
		N(1)-Re(1)-Br(1)	82.6(3)
		N(2)-Re(1)-Br(1)	83.9(3)

Table B-3: Anisotropic displacement parameters ($Å^2$ x 10^3) for *fac*-$[Re(CO)_3(Br)(DiMePy)]$.The anisotropic displacement factor exponent takes the form: $-2\pi^2[h2a^{*2}U^{11} + ... + 2hka^*b^*U^{12}]$.

	U11	U22	U33	U23	U13	U12
C(1)	33(7)	22(6)	31(7)	-2(5)	9(6)	-3(6)
C(2)	31(7)	17(6)	28(7)	3(5)	10(6)	0(5)
C(3)	34(7)	14(5)	28(7)	-2(5)	1(6)	-4(5)
C(4)	19(5)	17(5)	16(6)	5(4)	1(4)	5(4)
C(5)	20(6)	25(6)	19(6)	-2(5)	5(5)	-1(5)
C(6)	23(6)	18(5)	18(6)	1(4)	3(5)	7(5)
C(7)	24(6)	15(5)	21(6)	-3(4)	7(5)	-3(5)
C(8)	24(6)	19(6)	15(6)	-2(4)	2(5)	3(5)
C(9)	24(6)	20(6)	13(5)	-1(4)	4(4)	2(5)
C(10)	24(6)	21(6)	18(6)	3(5)	-1(5)	0(5)
C(11)	28(7)	25(6)	24(7)	-4(5)	-3(5)	-3(5)
C(12)	21(6)	31(7)	29(7)	5(6)	7(5)	2(5)

C(13)	30(7)	37(7)	15(6)	-4(5)	14(5)	4(6)
C(14)	35(7)	15(5)	26(7)	-1(5)	2(6)	2(5)
C(15)	31(7)	37(8)	38(9)	11(7)	15(6)	7(6)
O(1)	43(6)	25(5)	51(7)	-3(5)	3(5)	12(5)
O(2)	42(6)	24(5)	27(5)	0(4)	-8(4)	-2(4)
O(3)	46(6)	31(5)	37(6)	6(5)	17(5)	-7(5)
Br(1)	26(1)	22(1)	25(1)	-3(1)	1(1)	4(1)
Re(1)	22(1)	13(1)	22(1)	0(1)	4(1)	0(1)

Table B-4: Hydrogen coordinates (x 10^4) and isotropic displacement parameters (Å^2 x 10^3) for *fac*-[Re(CO)$_3$(Br)(DiMePy)].

	x	y	z	U(eq)
H(4)	5523	757	5921	21
H(5)	5156	2440	5961	25
H(7)	7411	3086	4121	23
H(10)	8493	2482	2849	26
H(12)	9842	-15	1982	32
H(13)	8839	-963	3306	32
H(14A)	6515	4445	4815	38
H(14B)	6012	4231	6431	38
H(14C)	5503	4215	4528	38
H(15A)	9779	2666	1508	51
H(15B)	9941	1766	272	51
H(15C)	10522	1880	2093	51

Table B-5: Hydrogen bond distances (Å) and angles (º) for *fac*-[Re(CO)$_3$(Br)(DiMePy)].

D-H…A	d (D-H)	d (H…A)	d (D…A)	D-H…A angle
C5-H5…O3[a]	0.93	2.54	3.393(17)	153
C7-H7…Br1[b]	0.93	2.84	3.744(12)	164

Symmetry code, transformations used to generate equivalent atoms: [a]1-x, ½+y, -½-z; [b]x, $\frac{3}{2}$-y, ½+z.

Table B-6: π-ring bond distances (Å) and angles (º) for *fac*-[Re(CO)$_3$(Br)(DiMePy)].

Y-X(I)	Res(I) → Cg(J)	X…Cg (Å)	Y-X…Cg (º)	Y…Cg (Å)
Re1-Br1[a]	[1] → Cg1	2.914(4)	39	1.858
Re1-Br1[b]	[1] → Cg2	3.955(6)	151	6.387
C14-H14[C]	[1] → Cg1	2.97(2)	130	3.673

Symmetry code, transformations used to generate equivalent atoms: [a] x, y, z; [b] x, y, -1+z; Cg1; [c] x, $\frac{3}{2}$-y, -½+z; Cg1= centroid atoms of Re1-N1-C9-C8-N2; Cg2 = N1-C9-C10-C11-C12-C13.

Table B-7: The intermolecular O…π interactions observed in the structure of *fac*-[Re(CO)$_3$(Br)(DiMePy)].

Torsion Angles	Angle	Torsion Angles	Angle
N(2)-C(4)-C(5)-C(6)	-0.2(19)	C(10)-C(11)-C(12)-C(13)	-2(2)
C(4)-C(5)-C(6)-C(7)	2.6(19)	C(15)-C(11)-C(12)-C(13)	-180.0(14)
C(4)-C(5)-C(6)-C(14)	-175.6(12)	C(11)-C(12)-C(13)-N(1)	1(2)

C(5)-C(6)-C(7)-C(8)	-0.4(19)	C(12)-C(13)-N(1)-C(9)	-0.6(19)
C(14)-C(6)-C(7)-C(8)	177.8(12)	C(12)-C(13)-N(1)-Re(1)	-173.9(10)
C(6)-C(7)-C(8)-N(2)	-4.2(19)	C(10)-C(9)-N(1)-C(13)	0.9(18)
C(6)-C(7)-C(8)-C(9)	177.6(12)	C(8)-C(9)-N(1)-C(13)	178.4(11)
N(2)-C(8)-C(9)-N(1)	-1.3(17)	C(10)-C(9)-N(1)-Re(1)	174.8(9)
C(7)-C(8)-C(9)-N(1)	177.0(11)	C(8)-C(9)-N(1)-Re(1)	-7.7(13)
N(2)-C(8)-C(9)-C(10)	176.2(11)	C(5)-C(4)-N(2)-C(8)	-4.6(18)
C(7)-C(8)-C(9)-C(10)	-6(2)	C(5)-C(4)-N(2)-Re(1)	170.5(9)
N(1)-C(9)-C(10)-C(11)	-1.8(19)	C(7)-C(8)-N(2)-C(4)	6.7(18)
C(8)-C(9)-C(10)-C(11)	-179.1(12)	C(9)-C(8)-N(2)-C(4)	-175.0(11)
C(9)-C(10)-C(11)-C(12)	2.2(19)	C(7)-C(8)-N(2)-Re(1)	-168.9(9)
C(9)-C(10)-C(11)-C(15)	-179.7(13)	C(9)-C(8)-N(2)-Re(1)	9.4(14)

APPENDIX C

Table C-1: Atomic coordinates (x 10^4) and equivalent isotropic displacement parameters (Å^2 x 10^3) for *fac*-[R(CO)$_3$(Act)(DiMePy)][NO$_3$]. U(eq) is defined as one third of the trace of the orthogonalized U^{ij} tensor.

	x	y	z	U(eq)
Re(1)	6070(1)	6748(1)	7185(1)	22(1)
O(1)	5246(4)	8396(6)	5513(6)	68(1)
O(2)	4722(3)	5625(5)	6431(4)	40(1)
O(3)	6139(3)	5243(5)	5799(4)	45(1)
O(6)	7046(2)	7530(4)	7831(3)	32(1)
N(1)	6129(3)	7743(5)	8293(4)	30(1)
N(2)	6691(3)	5796(5)	8525(4)	30(1)
C(1)	5556(3)	7776(6)	6130(5)	30(1)
C(2)	5233(3)	6051(6)	6734(4)	26(1)
C(3)	6120(3)	5798(6)	6321(5)	29(1)
C(4)	6992(3)	4828(5)	8619(5)	26(1)
C(5)	7383(4)	4247(6)	9496(5)	30(1)
C(6)	7462(3)	4675(6)	10317(5)	28(1)
C(7)	7163(3)	5681(5)	10229(5)	25(1)
C(8)	6781(3)	6221(5)	9330(4)	21(1)
C(10)	6515(3)	7859(6)	9957(5)	27(1)
C(11)	6217(3)	8898(6)	9791(5)	30(1)
C(12)	5885(4)	9338(6)	8858(6)	35(2)
C(13)	5850(3)	8754(6)	8137(5)	30(1)
C(14)	7873(4)	4065(6)	11285(6)	40(2)
C(15)	6270(4)	9503(7)	10607(6)	43(2)
C(16)	7245(3)	7892(5)	7346(4)	16(1)
C(17)	7820(3)	8353(6)	7822(4)	27(1)
C(18)	6904(3)	7825(5)	6456(4)	18(1)
C(9)	6464(3)	7314(5)	9200(4)	22(1)
O(7)	5620(4)	7376(7)	3966(6)	68(1)
O(8)	4730(4)	8695(7)	3216(6)	68(1)
O(9)	4440(4)	6881(6)	3454(6)	68(1)
N(3)	4911(3)	7760(5)	3513(4)	30(1)

Table C-2: Bond distances (Å) and angles (°) for *fac*-[R(CO)$_3$(Act)(DiMePy)][NO$_3$].

Bond	Bond Distance	Bond Angle	Angle
Re(1)-C(2)	1.899(7)	C(2)-Re(1)-C(1)	88.0(3)
Re(1)-C(1)	1.915(7)	C(2)-Re(1)-C(3)	88.1(3)
Re(1)-C(3)	1.926(7)	C(1)-Re(1)-C(3)	88.7(3)
Re(1)-O(6)	2.157(5)	C(2)-Re(1)-O(6)	174.7(2)
Re(1)-N(1)	2.170(6)	C(1)-Re(1)-O(6)	95.8(3)
Re(1)-N(2)	2.172(6)	C(3)-Re(1)-O(6)	95.8(2)
O(1)-C(1)	1.137(10)	C(2)-Re(1)-N(1)	95.6(2)

O(2)-C(2)	1.149(8)	C(1)-Re(1)-N(1)	96.9(3)
O(3)-C(3)	1.138(8)	C(3)-Re(1)-N(1)	173.3(3)
O(6)-C(16)	1.259(7)	O(6)-Re(1)-N(1)	80.2(2)
N(1)-C(13)	1.349(10)	C(2)-Re(1)-N(2)	95.6(2)
N(1)-C(9)	1.349(8)	C(1)-Re(1)-N(2)	171.3(3)
N(2)-C(4)	1.343(9)	C(3)-Re(1)-N(2)	99.3(3)
N(2)-C(8)	1.352(8)	O(6)-Re(1)-N(2)	80.2(2)
C(4)-C(5)	1.392(9)	N(1)-Re(1)-N(2)	74.8(2)
C(5)-C(6)	1.392(9)	C(16)-O(6)-Re(1)	123.9(4)
C(6)-C(7)	1.381(9)	C(13)-N(1)-C(9)	117.9(6)
C(6)-C(14)	1.516(9)	C(13)-N(1)-Re(1)	124.6(5)
C(7)-C(8)	1.393(9)	C(9)-N(1)-Re(1)	117.5(5)
C(8)-C(9)	1.483(9)	C(4)-N(2)-C(8)	117.7(6)
C(10)-C(9)	1.385(8)	C(4)-N(2)-Re(1)	125.4(5)
C(10)-C(11)	1.396(10)	C(8)-N(2)-Re(1)	116.9(5)
C(11)-C(12)	1.389(11)	O(1)-C(1)-Re(1)	178.6(7)
C(11)-C(15)	1.506(9)	O(2)-C(2)-Re(1)	177.6(5)
C(12)-C(13)	1.374(10)	O(3)-C(3)-Re(1)	178.8(7)
C(16)-C(18)	1.221(8)	N(2)-C(4)-C(5)	123.1(6)
C(16)-C(17)	1.256(8)	C(6)-C(5)-C(4)	118.9(6)
O(7)-N(3)	1.487(10)	C(7)-C(6)-C(5)	118.1(6)
O(8)-N(3)	1.212(10)	C(7)-C(6)-C(14)	120.9(6)
O(9)-N(3)	1.527(9)	C(5)-C(6)-C(14)	120.9(6)

Table C-3: Anisotropic displacement parameters ($Å^2$ x 10^3) for *fac*-$[R(CO)_3(Act)(DiMePy)][NO_3]$.The anisotropic displacement factor exponent takes the form: $-2\pi^2[h2a^{*2}U^{11} + \ldots\ldots + 2hka^*b^*U^{12}]$.

U11	U22	U33	U23	U13	U12	
Re(1)	20(1)	28(1)	18(1)	-2(1)	12(1)	-1(1)
O(1)	67(2)	67(2)	67(2)	8(2)	38(2)	-5(2)
O(2)	27(3)	56(3)	36(3)	-13(2)	18(2)	-10(2)
O(3)	58(4)	51(3)	32(3)	-7(2)	31(3)	7(3)
O(6)	27(2)	46(3)	22(2)	-2(2)	14(2)	-8(2)
N(1)	30(2)	31(2)	29(2)	-1(1)	17(2)	-4(1)
N(2)	30(2)	31(2)	29(2)	-1(1)	17(2)	-4(1)
C(1)	27(3)	41(4)	19(3)	2(3)	12(3)	1(3)
C(2)	25(3)	30(3)	19(3)	-5(2)	11(3)	2(3)
C(3)	29(3)	33(4)	23(3)	0(3)	15(3)	-2(3)
C(4)	28(3)	23(3)	32(3)	-4(3)	20(3)	1(3)
C(5)	32(3)	25(3)	37(4)	1(3)	23(3)	3(3)
C(6)	29(3)	25(3)	30(3)	5(3)	18(3)	1(3)
C(7)	24(3)	26(3)	24(3)	-1(2)	14(3)	-4(2)
C(8)	19(3)	21(3)	24(3)	-3(2)	14(2)	-5(2)
C(10)	26(3)	29(3)	25(3)	-7(3)	15(3)	-2(3)
C(11)	29(3)	29(3)	39(4)	-10(3)	25(3)	-4(3)

C(12)	31(3)	25(3)	45(4)	-5(3)	22(3)	2(3)
C(13)	26(3)	31(4)	30(3)	1(3)	15(3)	0(3)
C(14)	48(4)	30(4)	38(4)	10(3)	24(4)	5(3)
C(15)	48(4)	40(4)	48(4)	-23(4)	32(4)	-6(3)
C(16)	15(2)	14(2)	16(2)	2(2)	8(2)	1(2)
C(17)	19(3)	40(4)	19(3)	6(2)	10(2)	-13(3)
C(18)	21(3)	24(3)	13(2)	1(2)	13(2)	-5(2)
C(9)	20(3)	23(3)	26(3)	-4(2)	15(2)	-4(2)
O(7)	67(2)	67(2)	67(2)	8(2)	38(2)	-5(2)
O(8)	67(2)	67(2)	67(2)	8(2)	38(2)	-5(2)
O(9)	67(2)	67(2)	67(2)	8(2)	38(2)	-5(2)
N(3)	30(2)	31(2)	29(2)	-1(1)	17(2)	-4(1)

Table C-4: Hydrogen bond distances (Å) and angles (º) for fac-[R(CO)$_3$(Act)(DiMePy)][NO$_3$]

D-H…A	d(D-H)	d(H…A)	d(D…A)	D-H…A angle
C5-H5…O8[a]	0.95	2.47	3.343(10)	153
C7-H7…O6[b]	0.95	2.54	3.317(7)	139

Symmetry code, transformations used to generate equivalent atoms: [a] ½+x,- ½+ y, z; [b] ½-x, ½y,-z.

Table C-5: The intermolecular O…π interactions observed in the structure of *fac*-[Re(CO)$_3$NO$_3$(DiMeOPy)].

Y-X(I)	Res(I) → Cg(J)	X…Cg	Y-X…Cg	Y…Cg
C2-O2[a]	[1] → Cg1	3.180(9)	122	3.913(9)

Symmetry code, transformations used to generate equivalent atoms: [a] 1-x, y, ½-z Cg1 = centroid atoms of Re1-N1-C9-C8-N2.

APPENDIX D

Table D-1: Atomic coordinates (x 10^4) and equivalent isotropic displacement parameters ($Å^2$ x 10^3) for *fac*-[$Re(CO)_3NO_3$(DiMePy)]. U(eq) is defined as one third of the trace of the orthogonalized U^{ij} tensor.

	x	y	z	U(eq)
C(1)	5171(8)	3943(5)	8058(3)	35(1)
C(2)	2016(8)	3821(6)	7501(3)	43(2)
C(3)	3397(7)	5704(5)	7931(3)	38(1)
C(4)	1802(7)	6253(5)	6163(4)	37(1)
C(5)	1151(7)	6717(5)	5494(4)	38(1)
C(6)	1393(7)	6243(5)	4808(3)	32(1)
C(7)	2248(6)	5263(4)	4839(3)	28(1)
C(8)	2856(6)	4829(4)	5530(3)	22(1)
C(9)	3751(6)	3787(4)	5594(3)	21(1)
C(10)	3939(7)	3127(4)	4979(3)	27(1)
C(11)	4765(7)	2156(5)	5081(3)	30(1)
C(12)	5377(7)	1878(4)	5813(3)	29(1)
C(13)	5142(7)	2567(4)	6408(3)	27(1)
C(14)	710(8)	6712(5)	4065(4)	45(2)
C(15)	4985(9)	1428(5)	4421(4)	48(2)
N(1)	4335(5)	3499(3)	6312(2)	21(1)
N(2)	2652(5)	5321(4)	6192(2)	26(1)
N(3)	7174(6)	5839(4)	7197(3)	39(1)
O(1)	5924(7)	3558(4)	8576(3)	57(1)
O(2)	889(6)	3356(5)	7686(3)	64(2)
O(3)	3090(6)	6338(4)	8371(3)	56(1)
O(6)	5943(5)	5407(3)	6773(2)	33(1)
O(7)	7131(7)	5873(5)	7880(3)	69(2)
O(8)	8297(6)	6226(5)	6864(3)	61(2)
Re(01)	3872(1)	4604(1)	7220(1)	24(1)

Table D-2: Bond distances (Å) and angles (°) for *fac*-[$Re(CO)_3NO_3$(DiMePy)].

Bond	Bond Distance	Bond Angle	Angle
C(1)-O(1)	1.153(7)	O(1)-C(1)-Re(01)	178.0(6)
C(1)-Re(01)	1.913(6)	O(2)-C(2)-Re(01)	178.5(6)
C(2)-O(2)	1.149(7)	O(3)-C(3)-Re(01)	177.8(6)
C(2)-Re(01)	1.889(6)	N(2)-C(4)-C(5)	123.0(6)
C(3)-O(3)	1.150(7)	C(4)-C(5)-C(6)	120.3(6)
C(3)-Re(01)	1.919(6)	C(5)-C(6)-C(7)	116.6(5)
C(4)-N(2)	1.342(7)	C(5)-C(6)-C(14)	122.4(6)
C(4)-C(5)	1.373(8)	C(7)-C(6)-C(14)	120.8(6)
C(5)-C(6)	1.379(8)	C(8)-C(7)-C(6)	120.4(5)
C(6)-C(7)	1.396(8)	N(2)-C(8)-C(7)	122.0(5)
C(6)-C(14)	1.492(8)	N(2)-C(8)-C(9)	115.4(4)
C(7)-C(8)	1.380(7)	C(7)-C(8)-C(9)	122.5(5)

C(8)-N(2)	1.345(6)	N(1)-C(9)-C(10)	121.6(5)
C(8)-C(9)	1.479(7)	N(1)-C(9)-C(8)	115.1(4)
C(9)-N(1)	1.357(6)	C(10)-C(9)-C(8)	123.2(4)
C(9)-C(10)	1.381(7)	C(11)-C(10)-C(9)	120.2(5)
C(10)-C(11)	1.380(8)	C(10)-C(11)-C(12)	117.6(5)
C(11)-C(12)	1.383(7)	C(10)-C(11)-C(15)	121.1(5)
C(11)-C(15)	1.499(8)	C(12)-C(11)-C(15)	121.3(5)
C(12)-C(13)	1.382(7)	C(13)-C(12)-C(11)	119.7(5)
C(13)-N(1)	1.330(7)	N(1)-C(13)-C(12)	122.8(5)
N(1)-Re(01)	2.170(4)	C(13)-N(1)-C(9)	118.0(4)
N(2)-Re(01)	2.170(4)	C(13)-N(1)-Re(01)	124.9(3)
N(3)-O(7)	1.212(6)	C(9)-N(1)-Re(01)	117.1(3)
N(3)-O(8)	1.224(6)	C(4)-N(2)-C(8)	117.6(5)
N(3)-O(6)	1.299(6)	C(4)-N(2)-Re(01)	125.0(4)
O(6)-Re(01)	2.156(4)	C(8)-N(2)-Re(01)	117.3(3)
		O(7)-N(3)-O(8)	124.0(5)
		O(7)-N(3)-O(6)	119.7(5)
		O(8)-N(3)-O(6)	116.3(5)
		N(3)-O(6)-Re(01)	123.6(3)
		C(2)-Re(01)-C(1)	87.9(3)
		C(2)-Re(01)-C(3)	88.9(3)
		C(1)-Re(01)-C(3)	85.8(3)
		C(2)-Re(01)-O(6)	173.4(2)
		C(1)-Re(01)-N(2)	173.1(2)
		C(3)-Re(01)-N(2)	98.8(2)
		O(6)-Re(01)-N(2)	78.90(15)
		N(1)-Re(01)-N(2)	74.73(16)

Table D-3: Anisotropic displacement parameters ($Å^2$ x 10^3) for *fac*-$[Re(CO)_3NO_3(DiMePy)]$.The anisotropic displacement factor exponent takes the form: $-2\pi^2[h2a^{*2}U^{11} + \ldots\ldots + 2hka^*b^*U^{12}]$.

	U11	U22	U33	U23	U13	U12
C(1)	47(4)	32(3)	27(3)	-7(2)	3(3)	-11(3)
C(2)	46(4)	59(4)	24(3)	-7(3)	7(3)	-16(3)
C(3)	33(3)	44(4)	35(3)	-9(3)	-1(2)	0(3)
C(4)	36(3)	33(3)	41(4)	-3(3)	-2(3)	1(3)
C(5)	33(3)	26(3)	54(4)	2(3)	-5(3)	5(2)
C(6)	21(3)	37(3)	37(3)	9(3)	-4(2)	-5(2)
C(7)	26(3)	30(3)	29(3)	1(2)	1(2)	-5(2)
C(8)	20(2)	26(3)	20(2)	1(2)	2(2)	-7(2)
C(9)	20(2)	26(3)	18(2)	4(2)	0(2)	-6(2)
C(10)	30(3)	33(3)	17(3)	-2(2)	-1(2)	-5(2)
C(11)	33(3)	34(3)	23(3)	-3(2)	4(2)	-1(2)
C(12)	32(3)	26(3)	29(3)	1(2)	0(2)	-3(2)

C(13)	29(3)	32(3)	20(3)	4(2)	-4(2)	-1(2)
C(14)	40(4)	44(4)	48(4)	19(3)	-7(3)	-5(3)
C(15)	64(5)	47(4)	32(3)	-14(3)	5(3)	6(3)
N(1)	20(2)	27(2)	17(2)	0(2)	0(2)	-4(2)
N(2)	23(2)	26(2)	28(2)	-5(2)	-2(2)	-4(2)
N(3)	40(3)	48(3)	28(3)	-5(2)	0(2)	-23(2)
O(1)	78(4)	57(3)	32(3)	17(2)	-11(2)	0(3)
O(2)	68(4)	90(4)	35(3)	-9(3)	15(2)	-46(3)
O(3)	56(3)	62(3)	52(3)	-30(3)	7(2)	6(2)
O(6)	35(2)	40(2)	23(2)	-3(2)	-1(2)	-16(2)
O(7)	68(4)	111(5)	26(3)	-6(3)	-5(2)	-57(3)
O(8)	55(3)	86(4)	44(3)	-4(3)	8(2)	-47(3)
Re(01)	27(1)	29(1)	18(1)	-3(1)	2(1)	-5(1)

Table D-4: Hydrogen bond distances (Å) and angles (º) for *fac*-[Re(CO)$_3$NO$_3$(DiMePy)].

D-H…A	d(D-H)	d(H…A)	d(D…A)	D-H…A angle
C5-H5…O1[a]	0.95	2.56	3.352(8)	141
C7-H7…O6[b]	0.95	2.56	3.425(6)	151
C12-H12…O7[c]	0.95	2.55	3.165(8)	123
C15-H15B…O2[d]	0.98	2.46	3.230(8)	135
C15-H15C…O1[e]	0.98	2.53	3.460(9)	158

Symmetry code, transformations used to generate equivalent atoms: [a] $\frac{3}{2}$-x,-½-y,½-z; [b] 2-x,-y,-z; [c] $\frac{5}{2}$+x,-½-y,-½+z; [d] ½+x,-½-y,-½+z; ½+x, ½+y,-½+z.

APPENDIX E

Table E-1: Atomic coordinates (x 10^4) and equivalent isotropic displacement parameters ($Å^2$ x 10^3) for *fac*-[$Re(CO)_3(Br)(DiMeOPy)$]. U(eq) is defined as one third of the trace of the orthogonalized U^{ij} tensor.

	x	y	z	U(eq)
Re(1)	8146(1)	881(1)	833(1)	16(1)
Br(1)	6500(1)	643(1)	1521(1)	29(1)
O(1)	7575(3)	-468(3)	-499(3)	30(1)
O(2)	10074(3)	1127(3)	40(3)	29(1)
O(3)	7335(4)	2541(3)	-134(3)	36(1)
O(4)	8957(3)	-1968(3)	3586(2)	28(1)
O(5)	9271(3)	3114(3)	3879(3)	31(1)
N(1)	8612(3)	-159(3)	1701(3)	16(1)
N(2)	8524(3)	1733(3)	1846(3)	16(1)
C(1)	7791(4)	29(4)	7(3)	22(1)
C(2)	9348(4)	1040(4)	345(3)	22(1)
C(3)	7642(4)	1913(4)	215(3)	22(1)
C(4)	8548(4)	2704(4)	1876(3)	20(1)
C(5)	8774(4)	3221(4)	2524(4)	21(1)
C(6)	8999(4)	2721(4)	3202(3)	21(1)
C(7)	8963(4)	1710(4)	3188(3)	20(1)
C(8)	8733(4)	1240(4)	2511(3)	18(1)
C(9)	8736(3)	181(4)	2436(3)	16(1)
C(10)	8872(4)	-431(4)	3061(3)	19(1)
C(11)	8856(4)	-1424(4)	2941(3)	19(1)
C(12)	8761(4)	-1775(4)	2186(3)	18(1)
C(13)	8644(4)	-1113(4)	1594(3)	17(1)
C(14)	9273(6)	4158(5)	3930(5)	42(2)
C(15)	8940(5)	-2997(4)	3496(4)	31(1)

Table E-2: Bond distances (Å) and angles (°) for *fac*-[$Re(CO)_3(Br)(DiMeOPy)$].

Bond	Bond Distance	Bond Angle	Angle
Re(1)-C(2)	1.900(6)	C(2)-Re(1)-C(1)	88.6(2)
Re(1)-C(1)	1.916(6)	C(2)-Re(1)-C(3)	89.8(2)
Re(1)-C(3)	1.921(6)	C(1)-Re(1)-C(3)	87.4(2)
Re(1)-N(2)	2.173(4)	C(2)-Re(1)-N(2)	94.2(2)
Re(1)-N(1)	2.178(4)	C(1)-Re(1)-N(2)	174.6(2)
Re(1)-Br(1)	2.6194(6)	C(3)-Re(1)-N(2)	97.3(2)
O(1)-C(1)	1.152(7)	C(2)-Re(1)-N(1)	96.5(2)
O(2)-C(2)	1.154(7)	C(1)-Re(1)-N(1)	100.3(2)
O(3)-C(3)	1.144(7)	C(3)-Re(1)-N(1)	170.3(2)
O(4)-C(11)	1.349(7)	N(2)-Re(1)-N(1)	74.81(17)
O(4)-C(15)	1.438(7)	C(2)-Re(1)-Br(1)	179.13(17)
O(5)-C(6)	1.343(7)	C(1)-Re(1)-Br(1)	91.62(18)

O(5)-C(14)	1.453(7)	C(3)-Re(1)-Br(1)	91.10(17)
N(1)-C(13)	1.339(7)	N(2)-Re(1)-Br(1)	85.55(12)
N(1)-C(9)	1.362(7)	N(1)-Re(1)-Br(1)	82.67(11)
N(2)-C(4)	1.349(7)	C(11)-O(4)-C(15)	117.8(5)
N(2)-C(8)	1.366(7)	C(6)-O(5)-C(14)	117.3(6)
C(4)-C(5)	1.365(8)	C(13)-N(1)-C(9)	117.8(4)
C(5)-C(6)	1.393(9)	C(13)-N(1)-Re(1)	124.9(4)
C(6)-C(7)	1.406(8)	C(9)-N(1)-Re(1)	116.4(3)
C(7)-C(8)	1.375(8)	C(4)-N(2)-C(8)	117.6(5)
C(8)-C(9)	1.477(7)	C(4)-N(2)-Re(1)	125.6(4)
C(9)-C(10)	1.384(8)	C(8)-N(2)-Re(1)	116.8(3)
C(10)-C(11)	1.395(8)	O(1)-C(1)-Re(1)	178.7(5)
C(11)-C(12)	1.395(8)	O(2)-C(2)-Re(1)	178.9(5)
C(12)-C(13)	1.382(7)	O(3)-C(3)-Re(1)	178.0(6)
		N(2)-C(4)-C(5)	124.3(5)
		C(4)-C(5)-C(6)	118.4(5)
		O(5)-C(6)-C(5)	126.1(5)
		O(5)-C(6)-C(7)	115.5(5)
		C(5)-C(6)-C(7)	118.4(5)
		C(8)-C(7)-C(6)	119.8(6)
		N(2)-C(8)-C(7)	121.6(5)
		N(2)-C(8)-C(9)	115.3(5)
		C(7)-C(8)-C(9)	123.1(5)
		N(1)-C(9)-C(10)	121.7(5)
		N(1)-C(9)-C(8)	115.2(5)
		C(10)-C(9)-C(8)	123.0(5)
		C(9)-C(10)-C(11)	119.5(5)
		O(4)-C(11)-C(10)	115.6(5)
		O(4)-C(11)-C(12)	125.5(5)
		C(10)-C(11)-C(12)	118.9(5)
		C(13)-C(12)-C(11)	117.7(5)
		N(1)-C(13)-C(12)	124.2(5)

Table E-3: Anisotropic displacement parameters ($Å^2$ x 10^3) for *fac*-$[Re(CO)_3(Br)(DiMeOPy)]$.The anisotropic displacement factor exponent takes the form: $-2\pi^2[h2a^{*2}U^{11} + \ldots\ldots + 2hka^*b^*U^{12}]$.

U11	U22	U33	U23	U13	U12	
Re(1)	16(1)	14(1)	18(1)	1(1)	-3(1)	0(1)
Br(1)	22(1)	24(1)	42(1)	0(1)	2(1)	-1(1)
O(1)	42(3)	21(2)	27(2)	-3(2)	-10(2)	3(2)
O(2)	23(2)	37(2)	27(2)	1(2)	5(2)	-5(2)
O(3)	45(3)	22(2)	42(3)	11(2)	-17(2)	4(2)
O(4)	39(2)	22(2)	24(2)	6(2)	-3(2)	-1(2)
O(5)	37(2)	26(2)	28(2)	-13(2)	5(2)	-13(2)
N(1)	14(2)	13(2)	19(2)	2(2)	-1(2)	-1(2)

N(2)	13(2)	14(2)	21(2)	-4(2)	1(2)	-2(2)
C(1)	24(3)	15(2)	25(3)	6(2)	-2(2)	3(2)
C(2)	28(3)	21(3)	17(3)	0(2)	-6(2)	4(2)
C(3)	22(3)	16(2)	27(3)	1(2)	-6(2)	-2(2)
C(4)	15(2)	20(3)	24(3)	1(2)	2(2)	1(2)
C(5)	18(2)	13(2)	32(3)	-5(2)	4(2)	-2(2)
C(6)	16(2)	20(3)	29(3)	-6(2)	6(2)	-6(2)
C(7)	18(2)	19(3)	23(3)	-3(2)	1(2)	-2(2)
C(8)	13(2)	18(2)	22(3)	-3(2)	2(2)	0(2)
C(9)	11(2)	18(2)	18(2)	-2(2)	-1(2)	0(2)
C(10)	20(3)	20(3)	18(3)	-1(2)	0(2)	0(2)
C(11)	16(2)	18(2)	23(3)	4(2)	2(2)	0(2)
C(12)	16(2)	16(2)	24(3)	1(2)	1(2)	2(2)
C(13)	16(2)	18(2)	18(2)	1(2)	-3(2)	1(2)
C(14)	49(4)	26(3)	52(4)	-20(3)	8(4)	-9(3)
C(15)	41(4)	19(3)	32(3)	7(2)	7(3)	1(3)

Table E-6: Hydrogen bond distances (Å) and angles (º) for *fac*-[Re(CO)$_3$(Br)(DiMeOPy)].

D-H…A	d(D-H) (Å)	d(H…A) (Å)	d(D…A) (Å)	D-H…A angle (º)
C7-H7…O2[a]	0.93	2.58	3.430(11)	152
C12-H12…Br1[b]	0.93	2.87	3.779(7)	167
C14-H12B…O1[c]	0.96	2.54	3.325(13)	139

Symmetry code, transformations used to generate equivalent atoms: [a] -x, y, ½-z; [b] ½-x, -½+y, z; [c] ½-x, ½-y, -½+z

Table E-7: π-ring bond distances (Å) and angles (º) for fac-[Re(CO)$_3$(Br)(DiMeOPy)].

Y-X(I)	Res(I) → Cg(J)	X…Cg (Å)	Y-X…Cg (º)	Y…Cg (Å)
Re1-Br1	[1] → Cg1	2.947(18)	38.7	1.871(2)

Symmetry code, transformations used to generate equivalent atoms: [a] x, y, z Cg1 = centroid atoms of Re1-N1-C9-C8-N2

APPENDIX F

Table F-1: Atomic coordinates (x 10^4) and equivalent isotropic displacement parameters (Å^2 x 10^3) for *fac*-[Re(CO)$_3$(NO$_3$)(DiMeOPy)]. U(eq) is defined as one third of the trace of the orthogonalized U^{ij} tensor.

	x	y	z	U(eq)
C(1)	6106(4)	7933(5)	7790(3)	35(1)
C(2)	7111(5)	5708(5)	8193(3)	39(1)
C(3)	4715(5)	6187(4)	8347(3)	42(1)
C(4)	4481(5)	3708(4)	7089(3)	35(1)
C(5)	4207(4)	2618(4)	6686(3)	33(1)
C(6)	4745(4)	2358(4)	5955(3)	28(1)
C(7)	5554(4)	3219(4)	5661(3)	26(1)
C(8)	5794(4)	4294(4)	6101(3)	24(1)
C(9)	6641(4)	5248(4)	5834(3)	24(1)
C(10)	7323(4)	5096(4)	5154(3)	26(1)
C(11)	8138(4)	6020(4)	4959(3)	31(1)
C(12)	8229(5)	7066(4)	5462(3)	39(1)
C(13)	7498(4)	7155(4)	6112(3)	35(1)
C(14)	3886(6)	354(4)	5812(4)	50(1)
C(15)	8791(5)	4897(5)	3808(3)	46(1)
N(1)	6720(3)	6275(3)	6321(2)	28(1)
N(2)	5262(3)	4551(3)	6822(2)	27(1)
N(3)	3242(4)	7581(4)	6527(3)	37(1)
O(1)	6355(4)	8912(3)	7996(3)	50(1)
O(2)	7951(4)	5345(4)	8669(3)	63(1)
O(3)	4155(5)	6079(4)	8927(3)	72(1)
O(4)	8877(3)	5966(3)	4338(2)	43(1)
O(5)	4562(3)	1342(3)	5483(2)	36(1)
O(6)	4145(3)	6816(3)	6429(2)	37(1)
O(7)	3231(4)	8074(4)	7221(3)	64(1)
O(8)	2449(4)	7777(3)	5893(3)	53(1)
Re(1)	5696(1)	6307(1)	7421(1)	28(1)

Table F-2: Bond distances (Å) and angles (°) for *fac*-[Re(CO)$_3$(NO$_3$)(DiMeOPy)].

Bond	Bond Distance	Bond Angle	Angle
C(1)-O(1)	1.142(5)	O(1)-C(1)-Re(1)	178.8(4)
C(1)-Re(1)	1.908(5)	O(2)-C(2)-Re(1)	178.8(5)
C(2)-O(2)	1.145(6)	O(3)-C(3)-Re(1)	177.2(5)
C(2)-Re(1)	1.898(6)	N(2)-C(4)-C(5)	123.8(4)
C(3)-O(3)	1.159(6)	C(4)-C(5)-C(6)	118.8(4)
C(3)-Re(1)	1.906(5)	O(5)-C(6)-C(5)	126.0(4)
C(4)-N(2)	1.346(5)	O(5)-C(6)-C(7)	115.4(4)
C(4)-C(5)	1.366(6)	C(5)-C(6)-C(7)	118.6(4)
C(5)-C(6)	1.379(6)	C(8)-C(7)-C(6)	119.6(4)

C(6)-O(5)	1.338(5)	N(2)-C(8)-C(7)	121.8(4)
C(6)-C(7)	1.396(6)	N(2)-C(8)-C(9)	115.2(4)
C(7)-C(8)	1.372(6)	C(7)-C(8)-C(9)	123.0(4)
C(8)-N(2)	1.362(5)	N(1)-C(9)-C(10)	122.6(4)
C(8)-C(9)	1.476(6)	N(1)-C(9)-C(8)	114.9(4)
C(9)-N(1)	1.357(5)	C(10)-C(9)-C(8)	122.5(4)
C(9)-C(10)	1.379(6)	C(9)-C(10)-C(11)	119.3(4)
C(10)-C(11)	1.392(6)	O(4)-C(11)-C(12)	116.8(4)
C(11)-O(4)	1.333(5)	O(4)-C(11)-C(10)	124.9(4)
C(11)-C(12)	1.389(6)	C(12)-C(11)-C(10)	118.2(4)
C(12)-C(13)	1.367(7)	C(13)-C(12)-C(11)	118.8(4)
C(13)-N(1)	1.339(6)	N(1)-C(13)-C(12)	124.2(4)
C(14)-O(5)	1.434(6)	C(13)-N(1)-C(9)	116.9(4)
C(15)-O(4)	1.433(6)	C(13)-N(1)-Re(1)	125.2(3)
N(1)-Re(1)	2.163(4)	C(9)-N(1)-Re(1)	117.7(3)
N(2)-Re(1)	2.165(3)	C(4)-N(2)-C(8)	117.4(4)
N(3)-O(7)	1.216(5)	C(4)-N(2)-Re(1)	125.3(3)
N(3)-O(8)	1.222(5)	C(8)-N(2)-Re(1)	117.3(3)
N(3)-O(6)	1.296(5)	O(7)-N(3)-O(8)	123.7(4)
O(6)-Re(1)	2.161(3)	O(7)-N(3)-O(6)	119.8(4)
		O(8)-N(3)-O(6)	116.5(4)
		C(11)-O(4)-C(15)	117.7(4)
		C(6)-O(5)-C(14)	118.2(4)
		N(3)-O(6)-Re(1)	125.1(3)
		C(2)-Re(1)-C(3)	87.3(2)
		C(2)-Re(1)-C(1)	90.5(2)
		C(3)-Re(1)-C(1)	87.6(2)
		C(2)-Re(1)-O(6)	172.75(16)
		C(3)-Re(1)-O(6)	97.34(19)
		C(1)-Re(1)-O(6)	95.22(17)
		C(2)-Re(1)-N(1)	93.75(18)
		C(3)-Re(1)-N(1)	174.23(16)
		C(1)-Re(1)-N(1)	98.05(17)
		O(6)-Re(1)-N(1)	81.04(13)
		C(2)-Re(1)-N(2)	93.73(17)
		C(3)-Re(1)-N(2)	99.46(17)
		C(1)-Re(1)-N(2)	171.92(17)
		O(6)-Re(1)-N(2)	80.07(13)
		N(1)-Re(1)-N(2)	74.82(13)

Table F-3: Anisotropic displacement parameters ($Å^2$ x 10^3) for *fac*-[$Re(CO)_3(NO_3)$(DiMeOPy)].The anisotropic displacement factor exponent takes the form: $-2\pi^2[h2a^{*2}U^{11} + \ldots\ldots + 2hka^*b^*U^{12}]$.

U11	U22	U33	U23	U13	U12	
C(1)	28(2)	39(3)	37(3)	-9(2)	7(2)	-2(2)
C(2)	45(3)	34(3)	39(3)	-7(2)	6(2)	-6(2)
C(3)	48(3)	34(3)	47(3)	-19(2)	15(3)	-9(2)
C(4)	37(3)	34(3)	37(2)	-4(2)	16(2)	-5(2)
C(5)	32(2)	27(2)	41(3)	-1(2)	14(2)	-9(2)
C(6)	26(2)	22(2)	36(2)	-2(2)	3(2)	1(2)
C(7)	26(2)	25(2)	29(2)	-1(2)	8(2)	1(2)
C(8)	23(2)	24(2)	25(2)	-2(2)	4(2)	1(2)
C(9)	22(2)	22(2)	29(2)	2(2)	4(2)	3(2)
C(10)	25(2)	26(2)	28(2)	-2(2)	5(2)	1(2)
C(11)	31(2)	32(2)	32(2)	5(2)	13(2)	0(2)
C(12)	41(3)	29(2)	50(3)	-1(2)	19(2)	-8(2)
C(13)	34(3)	25(2)	45(3)	-7(2)	9(2)	-3(2)
C(14)	59(4)	26(3)	70(4)	-10(2)	27(3)	-16(2)
C(15)	50(3)	47(3)	48(3)	-7(2)	28(3)	-6(2)
N(1)	26(2)	24(2)	34(2)	-1(2)	9(2)	-3(1)
N(2)	26(2)	26(2)	30(2)	-4(2)	8(2)	-3(1)
N(3)	30(2)	31(2)	52(3)	2(2)	14(2)	1(2)
O(1)	51(2)	36(2)	65(2)	-21(2)	12(2)	-11(2)
O(2)	60(3)	59(3)	63(3)	1(2)	-17(2)	8(2)
O(3)	92(3)	73(3)	62(3)	-19(2)	51(3)	-22(3)
O(4)	47(2)	39(2)	48(2)	-4(2)	27(2)	-12(2)
O(5)	41(2)	23(2)	47(2)	-9(1)	17(2)	-6(1)
O(6)	34(2)	36(2)	40(2)	-9(2)	6(2)	6(1)
O(7)	65(3)	74(3)	55(2)	-19(2)	20(2)	26(2)
O(8)	42(2)	43(2)	71(3)	6(2)	-5(2)	9(2)
Re(1)	27(1)	27(1)	30(1)	-8(1)	7(1)	-3(1)

Table F-4: Hydrogen bond distances (Å) and angles (º) for *fac*-[$Re(CO)_3(NO_3)$(DiMePy)].

D-H…A	d(D-H)	d(H…A)	d(D…A)	D-H…A angle
C7-H7…O6[a]	0.95	2.48	3.337(6)	150
C14-H14B…O3[b]	0.98	2.41	3.386(8)	174
C15-H15A…O1	0.98	2.56	3.412(7)	145

Symmetry code, transformations used to generate equivalent atoms: [a] -x,-y,-z; [b] -½-x, ½+y, ½-z; [c] ½+x,- ½-y,-½+z

Table F-5: The intermolecular O…π interactions observed in the structure of *fac*-[$Re(CO)_3(NO_3)$(DiMeOPy)].

Y-X(I)	Res(I) → Cg(J)	X…Cg	Y-X…Cg	Y…Cg
C1-O1 [a]	[1] → Cg1	3.176(8)	134	4.048
C1-O1 [a]	[1] → Cg2	3.383(9)	156	4.448

Symmetry code, transformations used to generate equivalent atoms: [a] ½-x, -½+y, ½-z; Cg1 = centroid atoms of Re1-N1-C9-C8-N2; Cg1 = N1-C9-C10-C11-C12-C13

APPENDIX G

The methanol substitution reactions between *fac*-[Re(CO)$_3$(MeOH)(DiMePy]$^+$ and thiourea (TU), sodium thiocyanate (NCS$^-$), tricyclohexylphosphine (PCy$_3$) and sodium bromide (Br$^-$) as entering ligands were followed. Each reaction was investigated at four temperatures and the rhenium concentration was kept constant at 1 x 10^{-4} M throughout.

Table G-1: Temperature and [TU] dependence of the *pseudo* first-order reaction between *fac*-[Re(CO)$_3$(MeOH)(DiMePy)]$^+$ and thiourea. [Re] = 1 x 10^{-4} M, λ = 355 nm, MeOH.

k_{obs} (s^{-1})				
[TU] (M)	**15.1 °C**	**24.8 °C**	**35.1 °C**	**44.8 °C**
0.05	0.00040	0.001186	0.002542	0.006213
0.1	0.00076	0.002029	0.00467	0.0109
0.15	0.001099	0.002899	0.006524	0.015711
0.25	0.001804	0.004831	0.01093	0.025918
0.4	0.00282	0.007619	0.017271	0.041003
0.5	0.003505	0.009495	0.02153	0.05113

Table G-2: Temperature and [NCS$^-$] dependence of the *pseudo* first-order reaction between *fac*-[Re(CO)$_3$(MeOH)(DiMePy)]$^+$ and thiocyanate ions. [Re] = 1 x 10^{-4} M, λ = 360 nm, MeOH.

k_{obs} (s^{-1})				
[NCS$^-$] (M)	**14.2 °C**	**24.8 °C**	**35.0 °C**	**44.9 °C**
0.05	0.000140	0.0003566	0.00119	0.00314
0.1	0.0002592	0.00069	0.00241	0.006113
0.2	0.0005168	0.0013329	0.004554	0.0116
0.3	0.0007624	0.0019722	0.00676	0.017256
0.4	0.001008	0.0026115	0.008965	0.022912
0.5	0.0012549	0.0032487	0.011164	0.028549

Table G-3: Temperature and [PCy_3] dependence of the *pseudo* first-order reaction between *fac*-[$Re(CO)_3(MeOH)(DiMePy)]^+$ and tricyclohexylphosphine. [Re] = 1 x 10^{-4} M, λ = 350 nm, MeOH.

k_{obs} (s^{-1})				
[PCy_3] (M)	15.5 °C	25.7 °C	34.3 °C	44.5 °C
0.01	2.2E-05	7.62E-05	0.000205	0.000483
0.015	2.7E-05	8.88E-05	0.000247	0.000585
0.02	3.1E-05	0.000102	0.000283	0.000671
0.03	4.07E-05	0.000129	0.00036	0.000857
0.04	4.75E-05	0.000156	0.00043	0.001025
0.05	5.62E-05	0.000182	0.000519	0.001243

Table G-4: A_{obs} *vs* [Br^-] for the reaction of *fac*-[$Re(CO)_3(MeOH)(DiMePy)]^+$ with Br^- ions. [Re] = 1 x 10^{-4} M, 25 °C, [Br^-] = 0.05M to 0.5M, MeOH.

[Br^-] (M)	A_{obs}
0.05	0.213
0.1	0.268
0.2	0.361425
0.3	0.394537
0.4	0.416037
0.5	0.435

Table G-5: Temperature and [Br^-] dependence of the *pseudo* first-order reaction between *fac*-[$Re(CO)_3(MeOH)(DiMePy)]^+$ and bromide ions. [Re] = 1 x 10^{-4} M, λ = 340 nm, MeOH.

k_{obs} (s^{-1})				
[Br^-] (M)	15.3 °C	24.8 °C	35.1 °C	45.0 °C
0.05	0.00060	0.001605	0.005168	0.01363
0.1	0.00112	0.003696	0.009301	0.02563
0.2	0.002148	0.007232	0.018552	0.049836
0.3	0.003207	0.010204	0.027238	0.073135
0.4	0.004236	0.013513	0.036097	0.097014
0.5	0.005274	0.016698	0.044923	0.120672

The methanol substitution reactions between *fac*-[$Re(CO)_3(MeOH)(DiMeOPy)]^+$ and thiourea (TU), sodium thiocyanate (NCS^-), tricyclohexylphosphine (PCy_3) and sodium bromide (Br^-) as entering ligands were followed. Each reaction was investigated at four temperatures and the rhenium concentration was kept constant at 1 x 10^{-4} M throughout.

Table G-6: Temperature and [TU] dependence of the *pseudo* first-order reaction between *fac*-[Re(CO)$_3$(MeOH)(DiMeOPy)]$^+$ and thiourea. [Re] = 1 x 10^{-4} M, λ = 345 nm, MeOH.

k_{obs} (s^{-1})				
[TU] (M)	**14.7 °C**	**24.8 °C**	**35.0 °C**	**45.6 °C**
0.05	0.000261	0.0007	0.001748	0.004527
0.1	0.00047	0.001426	0.00339	0.0075
0.15	0.00071	0.002354	0.005035	0.010623
0.25	0.00117746	0.003784	0.008005	0.018128
0.4	0.001818564	0.005542	0.012604	0.028668
0.5	0.0022479	0.006937	0.015706	0.035811

Table G-7: Temperature and [NCS$^-$] dependence of the *pseudo* first-order reaction between *fac*-[Re(CO)$_3$(MeOH)(DiMeOPy)]$^+$ and thiocyanate ions. [Re] = 1 x 10^{-4} M, λ = 345 nm, MeOH.

k_{obs} (s^{-1})				
[NCS$^-$] (M)	**14.5 °C**	**25.0 °C**	**35.4 °C**	**45.0 °C**
0.05	0.000101	0.00033	0.000956	0.00259
0.1	0.000200	0.000645	0.001926	0.004915
0.2	0.0003876	0.001236	0.003641	0.009403
0.3	0.0005702	0.001829	0.005402	0.013983
0.4	0.0007528	0.002421	0.007164	0.018563
0.5	0.0009359	0.003012	0.008921	0.023133

Table G-8: Temperature and [PCy$_3$] dependence of the *pseudo* first-order reaction between *fac*-[Re(CO)$_3$(MeOH)(DiMeOPy)]$^+$ and tricyclohexylphosphine. [Re] = 1 x 10^{-4} M, λ = 345 nm, MeOH.

k_{obs} (s^{-1})				
[PCy$_3$] (M)	**14.9 °C**	**25.2 °C**	**35.4 °C**	**45.3 °C**
0.01	1.45E-05	4.48E-05	0.000147	0.000469
0.015	1.79E-05	5.36E-05	0.000174	0.00055
0.02	2.06E-05	6.08E-05	0.0002	0.000633
0.03	2.56E-05	7.64E-05	0.000253	0.000808
0.04	3.04E-05	9.1E-05	0.000302	0.000967
0.05	3.57E-05	0.000108	0.000364	0.001168

Table G-9: A_{obs} *vs* [Br^-] for the reaction of *fac*-[$Re(CO)_3(MeOH)(DiMeOPy)]^+$ with Br^- ions. [Re] = 1 x 10^{-4} M, 25 °C, [Br^-] = 0.05M to 0.5M, MeOH.

[Br^-] (M)	A_{obs}
0.05	0.241
0.1	0.314
0.2	0.362958
0.3	0.397
0.4	0.405
0.5	0.418

Table G-10: Temperature and [Br^-] dependence of the *pseudo* first-order reaction between *fac*-[$Re(CO)_3(MeOH)(DiMeOPy)]^+$ and bromide ions. [Re] = 1 x 10^{-4} M, λ = 342 nm, MeOH.

k_{obs} (s^{-1})				
[Br] (M)	**15.6 °C**	**24.7 °C**	**35.3 °C**	**45.6 °C**
0.05	0.000489	0.001603	0.00469	0.01335
0.1	0.00095	0.003166	0.008862	0.024632
0.2	0.001847	0.005965	0.016978	0.047238
0.3	0.002719	0.008831	0.025183	0.070184
0.4	0.003592	0.011704	0.033406	0.093172
0.5	0.004461	0.014553	0.04157	0.116007

The methanol substitution reactions between *fac*-[$Re(CO)_3$(MeOH)(4-MeTPh)] and thiourea (TU), sodium thiocyanate (NCS^-), tricyclohexylphosphine (PCy_3) and sodium bromide (Br^-) as entering ligands were followed. Each reaction was investigated at four temperatures and the rhenium concentration was kept constant at 3 x 10^{-4} M throughout.

Table G-11: Temperature and [TU] dependence of the *pseudo* first-order reaction between *fac*-[$Re(CO)_3$(MeOH)(4-MeTPh)] and thiourea. [Re] = 3 x 10^{-4} M, λ = 345 nm, MeOH.

k_{obs} (s^{-1})				
[TU] (M)	**14.3 °C**	**24.4 °C**	**35.6 °C**	**45.7 °C**
0.05	0.00075	0.00242	0.007666	0.025166
0.1	0.001338	0.004599	0.014385	0.050604
0.15	0.002039	0.006568	0.020125	0.072677
0.25	0.003315	0.010919	0.033904	0.119152
0.4	0.00523	0.017273	0.053718	0.188864
0.5	0.006513	0.021531	0.067021	0.23521

Table G-12: Temperature and [NCS^-] dependence of the *pseudo* first-order reaction between *fac*-[$Re(CO)_3$(MeOH)(4-MeTPh)] and thiocyanate. [Re] = 3 x 10^{-4} M, λ = 335 nm, MeOH.

k_{obs} (s^{-1})				
[NCS^-] (M)	15.4 °C	25.2 °C	35.0 °C	44.9 °C
0.05	0.000169	0.00057	0.001837	0.00545
0.1	0.000304	0.001044	0.003367	0.009743
0.2	0.000589	0.00194	0.006136	0.018023
0.3	0.000848	0.002821	0.008966	0.026415
0.4	0.001108	0.003703	0.011795	0.034807
0.5	0.001367	0.004586	0.014619	0.043186

Table G-13: Temperature and [PCy_3] dependence of the *pseudo* first-order reaction between *fac*-[$Re(CO)_3$(MeOH)(4-MeTPh)] and tricyclohexylphosphine. [Re] = 3 x 10^{-4} M, λ = 335 nm, MeOH.

k_{obs} (s^{-1})				
[PCy_3] (M)	14.6 °C	24.5 °C	35.1 °C	45.3 °C
0.01	4.5E-05	0.000125	0.000355	0.00094
0.015	5.65E-05	0.00016	0.000448	0.001201
0.02	6.85E-05	0.000192	0.000527	0.001421
0.03	8.63E-05	0.000252	0.000694	0.00192
0.04	0.000113	0.000311	0.000861	0.002418
0.05	0.000135	0.0003735	0.001028	0.002913

Table G-14: A_{obs} *vs* [Br^-] for the reaction of *fac*-[$Re(CO)_3$(MeOH)(4-MeTPh)] with Br^- ions. [Re] = 3 x 10^{-4} M, 25 °C, [Br^-] = 0.05M to 0.5M, MeOH.

[Br^-] (M)	A_{obs}
0.05	0.3232
0.1	0.382
0.2	0.486
0.3	0.533
0.4	0.555
0.5	0.587

Table G-15: Temperature and [Br] dependence of the *pseudo* first-order reaction between *fac*-[Re(CO)$_3$(MeOH)(4-MeTPh)] and bromide ions. [Re] = 3 x 10^{-4} M, λ = 330 nm, MeOH.

k_{obs} (s^{-1})				
[Br$^-$] (M)	**14.4 °C**	**24.9 °C**	**35.1 °C**	**45.5 °C**
0.05	0.00521	0.015366	0.051755	0.1550
0.1	0.009753	0.0314	0.088328	0.297328
0.2	0.018187	0.058187	0.173989	0.567593
0.3	0.027342	0.085742	0.25949	0.83639
0.4	0.036102	0.11346	0.343856	1.109933
0.5	0.045002	0.141002	0.428002	1.382852

The methanol substitution reactions between *fac*-[Re(CO)$_3$(MeOH)(BrDiPhPr)] and thiourea (TU), sodium thiocyanate (NCS$^-$), tricyclohexylphosphine (PCy$_3$) and sodium bromide (Br$^-$) as entering ligands were followed. Each reaction was investigated at four temperatures and the rhenium concentration was kept constant at 3 x 10^{-4} M throughout.

Table G-16: Temperature and [TU] dependence of the *pseudo* first-order reaction between *fac*-[Re(CO)$_3$(MeOH)(BrDiPhPr)] and thiourea. [Re] = 3 x 10^{-4} M, λ = 345 nm, MeOH.

k_{obs} (s^{-1})				
[TU] (M)	**14.2 °C**	**25.2 °C**	**35.1 °C**	**45.1 °C**
0.05	0.0004956	0.002426	0.004909	0.018961
0.1	0.000936	0.004175	0.008788	0.034478
0.15	0.001327	0.006257	0.012852	0.050262
0.25	0.002215	0.010233	0.02109	0.08319
0.4	0.003476	0.016175	0.033391	0.13201
0.5	0.00433	0.020153	0.041624	0.16296

Table G-17: Temperature and [NCS^-] dependence of the *pseudo* first-order reaction between *fac*-[$Re(CO)_3$(MeOH)(BrDiPhPr)] and thiocyanate. [Re] = 3 x 10^{-4} M, λ = 340 nm, MeOH.

k_{obs} (s^{-1})				
[NCS^-] (M)	14.5 °C	24.6 °C	35.5 °C	45.3 °C
0.05	0.0003025	0.000815	0.002405436	0.0064937
0.1	0.000559	0.0016	0.00424	0.0125
0.2	0.001094	0.003014	0.008248772	0.023351689
0.3	0.001614	0.00446	0.012243013	0.034725982
0.4	0.002134	0.005907	0.016237255	0.046100275
0.5	0.002655	0.00735	0.02025	0.0575

Table G-18: Temperature and [PPh_3] dependence of the *pseudo* first-order reaction between *fac*-[$Re(CO)_3$(MeOH)(BrDiPhPr)] and triphenylphosphine. [Re] = 3 x 10^{-4} M, λ = 330 nm, MeOH.

k_{obs} (s^{-1})				
[PPh_3] (M)	14.8 °C	24.9 °C	35.4 °C	44.9 °C
0.005	0.0000184	0.0000676	0.000179	0.000512
0.01	0.0000252	0.0000864	0.000251	0.000693
0.02	0.0000385	0.000129	0.000374	0.001093
0.03	0.0000519	0.00017	0.000501	0.001484
0.04	0.000066	0.000211	0.000628	0.001876
0.05	0.0000799	0.000253	0.000755	0.002268

Table G-19: A_{obs} *vs* [Br^-] for the reaction of *fac*-[$Re(CO)_3$(MeOH)(BrDiPhPr)] with Br^- ions. [Re] = 1 x 10^{-4} M, 25 °C, [Br^-] = 0.05M to 0.5M, MeOH.

[Br^-] (M)	A_{obs}
0.05	0.581
0.1	0.642
0.2	0.705
0.3	0.729169
0.4	0.748
0.5	0.758

Table G-20: Temperature and [Br^-] dependence of the *pseudo* first-order reaction between *fac*-[$Re(CO)_3(MeOH)(BrDiPhPr)$] and bromide ions. [Re] = 3 x 10^{-4} M, λ = 340 nm, MeOH.

k_{obs} (s^{-1})				
[Br^-] (M)	15.3 °C	25.5 °C	34.7 °C	45.1 °C
0.05	0.00357	0.0108	0.027195	0.0985
0.1	0.00651	0.019218	0.063384	0.179
0.2	0.012454	0.0386	0.12396	0.346
0.3	0.018611	0.056298	0.17458	0.50789
0.4	0.024539	0.074426	0.2312	0.67356
0.5	0.030502	0.092502	0.2856	0.8385

The methanol substitution reactions between *fac*-[$Re(CO)_3(MeOH)(TIF)$] and thiourea (TU), sodium thiocyanate (NCS^-), tricyclohexylphosphine (PCy_3) and sodium bromide (Br^-) as entering ligands were followed. Each reaction was investigated at four temperatures and the rhenium concentration was kept constant at 3 x 10^{-4} M throughout.

Table G-21: Temperature and [TU] dependence of the *pseudo* first-order reaction between *fac*-[$Re(CO)_3(MeOH)(TIF)$] and thiourea. [Re] = 3 x 10^{-4} M, λ = 345 nm, MeOH.

k_{obs} (s^{-1})				
[TU] (M)	15.4 °C	25.8 °C	35.9 °C	45.0 °C
0.05	0.00138	0.00448	0.011702	0.046402
0.1	0.00264	0.008293	0.0237	0.084575
0.15	0.003868	0.011841	0.034841	0.126235
0.25	0.006482	0.02005	0.057064	0.208278
0.4	0.010205	0.031726	0.090459	0.330743
0.5	0.012713	0.039613	0.112613	0.412613

Table G-22: Temperature and [NCS^-] dependence of the *pseudo* first-order reaction between *fac*-[$Re(CO)_3(MeOH)(TIF)$] and thiocyanate. [Re] = 3 x 10^{-4} M, λ = 345 nm, MeOH.

k_{obs} (s^{-1})				
[NCS^-] (M)	15.8 °C	25.6 °C	34.8 °C	45.1 °C
0.05	0.00087	0.00230	0.0079429	0.0245612
0.1	0.0015912	0.00470	0.01330958	0.0458
0.2	0.00315	0.0085187	0.0283014	0.0883014
0.3	0.0046654	0.012880	0.040987	0.1312446
0.4	0.0061683	0.0170607	0.0543563	0.1742399
0.5	0.0076602	0.0212602	0.067602	0.2173228

Table G-23: Temperature and [PCy_3] dependence of the *pseudo* first-order reaction between *fac*-[$Re(CO)_3(MeOH)(TIF)$] and tricyclohexylphosphine. [Re] = 3 x 10^{-4} M, λ = 345 nm, MeOH.

k_{obs} (s^{-1})				
[PCy_3] (M)	15.3 °C	25.5 °C	34.7 °C	45.1 °C
0.01	0.00017	0.000505	0.001277	0.003497
0.015	0.000207	0.000619	0.00159	0.00429
0.02	0.000244	0.000715	0.001882	0.005182
0.03	0.000313	0.000904	0.002351	0.006458
0.04	0.000381	0.001076	0.002807	0.007848
0.05	0.0004538	0.00131	0.00342	0.00962

Table G-24: A_{obs} *vs* [Br^-] for the reaction of *fac*-[$Re(CO)_3(MeOH)(TIF)$] with Br^- ions. [Re] = 1 x 10^{-4} M, 25 °C, [Br^-] = 0.05M to 0.5M, MeOH.

[Br^-] (M)	A_{obs}
0.05	0.128
0.1	0.204303
0.2	0.263
0.3	0.293587
0.4	0.299428
0.5	0.32

Table G-25: Temperature and [Br^-] dependence of the *pseudo* first-order reaction between *fac*-[$Re(CO)_3(MeOH)(TIF)$] and bromide ions. [Re] = 3 x 10^{-4} M, λ = 343 nm, MeOH.

k_{obs} (s^{-1})				
[Br^-] (M)	15.8 °C	25.7 °C	34.8 °C	45.0 °C
0.05	0.0095	0.0301	0.083136	0.235
0.1	0.0184	0.0566	0.15993	0.49993
0.2	0.036027	0.108627	0.328863	0.939316
0.3	0.053007	0.163123	0.473232	1.388623
0.4	0.069987	0.216166	0.627917	1.844482
0.5	0.0876	0.2696	0.7806	2.2956

The methanol substitution reactions between *fac*-[$Re(CO)_3(MeOH)(MeTIF)$] and thiourea (TU), sodium thiocyanate (NCS^-), tricyclohexylphosphine (PCy_3) and sodium bromide (Br^-) as entering ligands were followed. Each reaction was investigated at four temperatures and the rhenium concentration was kept constant at 3 x 10^{-4} M throughout.

Table G-26: Temperature and [TU] dependence of the *pseudo* first-order reaction between *fac*-[Re(CO)$_3$(MeOH)(MeTIF)] and thiourea. [Re] = 3 x 10^{-4} M, λ = 345 nm, MeOH.

k_{obs} (s^{-1})				
[TU] (M)	**15.1 °C**	**24.9 °C**	**35.1 °C**	**45.3 °C**
0.05	0.00094	0.00310	0.00970	0.030922
0.1	0.00182	0.006093	0.0184	0.055043
0.15	0.002668	0.009147	0.026764	0.078764
0.25	0.004496	0.014983	0.044798	0.134456
0.4	0.007069	0.023684	0.070977	0.213791
0.5	0.008813	0.029513	0.088513	0.267313

Table G-27: Temperature and [NCS$^-$] dependence of the *pseudo* first-order reaction between *fac*-[Re(CO)$_3$(MeOH)(MeTIF)] and thiocyanate ions. [Re] = 3 x 10^{-4} M, λ = 340 nm, MeOH.

k_{obs} (s^{-1})				
[NCS$^-$] (M)	**14.8 °C**	**24.9 °C**	**35.1 °C**	**45.1 °C**
0.05	0.00063	0.00175	0.004999	0.016622
0.1	0.001191	0.00325	0.009378	0.030
0.2	0.002219	0.006119	0.01811	0.058697
0.3	0.00337	0.009296	0.027046	0.087461
0.4	0.004453	0.012306	0.0358	0.116088
0.5	0.00556	0.01537	0.0446	0.14484

Table G-28: Temperature and [PCy$_3$] dependence of the *pseudo* first-order reaction between *fac*-[Re(CO)$_3$(MeOH)(MeTIF)] and tricyclohexylphosphine. [Re] = 3 x 10^{-4} M, λ = 345 nm, MeOH.

k_{obs} (s^{-1})				
[PCy$_3$] (M)	**14.7 °C**	**24.8 °C**	**35.4 °C**	**45.7 °C**
0.01	9.22E-05	0.000308	0.000898	0.002737
0.015	0.00011	0.000363	0.001064	0.003177
0.02	0.000133	0.000427	0.00126	0.00375
0.03	0.000166	0.000536	0.001652	0.004896
0.04	0.000209	0.00068	0.002037	0.005988
0.05	0.00025	0.00082	0.00247	0.00735

Table G-29: A_{obs} *vs* $[Br^-]$ for the reaction of *fac*-$[Re(CO)_3(MeOH)(MeTIF)]$ with Br^- ions. [Re] = 1 x 10^{-4} M, 25 °C, $[Br^-]$ = 0.05M to 0.5M, MeOH

$[Br^-]$ (M)	A_{obs}
0.05	0.436
0.1	0.486
0.2	0.578
0.3	0.59
0.4	0.5981
0.5	0.616

Table G-30: Temperature and $[Br^-]$ dependence of the *pseudo* first-order reaction between *fac*-$[Re(CO)_3(MeOH)(MeTIF)]$ and bromide ions. [Re] = 3 x 10^{-4} M, λ = 340 nm, MeOH.

k_{obs} (s^{-1})				
$[Br^-]$ (M)	14.6 °C	24.5 °C	35.6 °C	45.0 °C
0.05	0.00680	0.024636	0.0730	0.2310
0.1	0.0132	0.04888	0.1375	0.4368
0.2	0.025182	0.089182	0.2670	0.861039
0.3	0.038074	0.134192	0.39861	1.275656
0.4	0.050217	0.177756	0.528794	1.694178
0.5	0.0626	0.2216	0.6616	2.1116

APPENDIX H

CheckCIF report of 4-MeTPh

checkCIF/PLATON report

Structure factors have been supplied for datablock(s) shelx

THIS REPORT IS FOR GUIDANCE ONLY. IF USED AS PART OF A REVIEW PROCEDURE FOR PUBLICATION, IT SHOULD NOT REPLACE THE EXPERTISE OF AN EXPERIENCED CRYSTALLOGRAPHIC REFEREE.

No syntax errors found. CIF dictionary Interpreting this report

Datablock: shelx

Bond precision: C-C = 0.0076 A Wavelength=0.71073

Cell: a=4.185(3) b=10.358(7) c=33.09(2)
alpha=89.43(2) beta=89.56(2) gamma=89.99(2)
Temperature: 293 K

	Calculated	Reported
Volume	1434.3(17)	1434.0(16)
Space group	P -1	P -1
Hall group	-P 1	-P 1
Moiety formula	C17 H22 O4, C17 H21 O4	C17 H22 O4, C17 H21 O4
Sum formula	C34 H43 O8	C34 H43 O8
Mr	579.68	579.68
Dx,g cm-3	1.342	2.685
Z	2	4
Mu (mm-1)	0.095	0.189
F000	622.0	622.3
F000’	622.33	
h,k,lmax	5,13,44	5,13,43
Nref	7161	7161
Tmin,Tmax		
Tmin’		

Correction method= Not given

Data completeness= 1.000 Theta(max)= 28.316

R(reflections)= 0.1231(2652) wR2(reflections)= 0.4262(6997)

S = 1.209 Npar= 379

The following ALERTS were generated. Each ALERT has the format
test-name_ALERT_alert-type_alert-level.
Click on the hyperlinks for more details of the test.

Alert level A

PLAT043_ALERT_1_A Calculated and Reported Mol. Weight Differ by .. 579.68 Check
PLAT051_ALERT_1_A Mu(calc) and Mu(CIF) Ratio Differs from 1.0 by . 49.99 %

Alert level B

PLAT026_ALERT_3_B Ratio Observed / Unique Reflections (too) Low .. 37% Check
PLAT084_ALERT_3_B High wR2 Value (i.e. > 0.25) ..... 0.43 Report
PLAT112_ALERT_2_B ADDSYM Detects New (Pseudo) Symm. Elem n 100 %Fit
PLAT113_ALERT_2_B ADDSYM Suggests Possible Pseudo/New Space Group P21/n Check
PLAT315_ALERT_2_B Singly Bonded Carbon Detected (H-atoms Missing). C18 Check
PLAT411_ALERT_2_B Short Inter H...H Contact H9B ..H14A . 1.88 Ang.
1+x,y,z = 1_655 Check
PLAT411_ALERT_2_B Short Inter H...H Contact H23B ..H26B . 1.89 Ang.
1+x,y,z = 1_655 Check
PLAT939_ALERT_3_B Large Value of Not (SHELXL) Weight Optimized S . 214.65 Check

---

Alert level C

DIFMN02_ALERT_2_C The minimum difference density is < -0.1*ZMAX*0.75
_refine_diff_density_min given = -0.680
Test value = -0.600
DIFMN03_ALERT_1_C The minimum difference density is < -0.1*ZMAX*0.75
The relevant atom site should be identified.
DIFMX02_ALERT_1_C The maximum difference density is > 0.1*ZMAX*0.75
The relevant atom site should be identified.
PLAT041_ALERT_1_C Calc. and Reported SumFormula Strings Differ Please Check
PLAT052_ALERT_1_C Info on Absorption Correction Method Not Given Please Do !
PLAT053_ALERT_1_C Minimum Crystal Dimension Missing (or Error) ... Please Check
PLAT054_ALERT_1_C Medium Crystal Dimension Missing (or Error) ... Please Check
PLAT055_ALERT_1_C Maximum Crystal Dimension Missing (or Error) ... Please Check
PLAT082_ALERT_2_C High R1 Value ..... 0.12 Report
PLAT097_ALERT_2_C Large Reported Max. (Positive) Residual Density 0.71 eA-3
PLAT098_ALERT_2_C Large Reported Min. (Negative) Residual Density -0.68 eA-3
PLAT309_ALERT_2_C Single Bonded Oxygen (C-O > 1.3 Ang) ..... O2 Check
PLAT309_ALERT_2_C Single Bonded Oxygen (C-O > 1.3 Ang) ..... O5 Check
PLAT340_ALERT_3_C Low Bond Precision on C-C Bonds ..... 0.00756 Ang.
PLAT360_ALERT_2_C Short C(sp3)-C(sp3) Bond C3 - C4 . 1.42 Ang.
PLAT360_ALERT_2_C Short C(sp3)-C(sp3) Bond C5 - C6 . 1.41 Ang.
PLAT360_ALERT_2_C Short C(sp3)-C(sp3) Bond C14 - C15 . 1.40 Ang.
PLAT360_ALERT_2_C Short C(sp3)-C(sp3) Bond C20 - C21 . 1.38 Ang.
PLAT360_ALERT_2_C Short C(sp3)-C(sp3) Bond C22 - C23 . 1.36 Ang.
PLAT360_ALERT_2_C Short C(sp3)-C(sp3) Bond C29 - C30 . 1.41 Ang.
PLAT360_ALERT_2_C Short C(sp3)-C(sp3) Bond C31 - C32 . 1.42 Ang.
PLAT362_ALERT_2_C Short C(sp3)-C(sp2) Bond C2 - C3 . 1.39 Ang.
PLAT362_ALERT_2_C Short C(sp3)-C(sp2) Bond C2 - C5 . 1.40 Ang.
PLAT362_ALERT_2_C Short C(sp3)-C(sp2) Bond C4 - C7 . 1.40 Ang.
PLAT362_ALERT_2_C Short C(sp3)-C(sp2) Bond C6 - C7 . 1.38 Ang.
PLAT362_ALERT_2_C Short C(sp3)-C(sp2) Bond C8 - C9 . 1.41 Ang.
PLAT362_ALERT_2_C Short C(sp3)-C(sp2) Bond C11 - C14 . 1.39 Ang.
PLAT362_ALERT_2_C Short C(sp3)-C(sp2) Bond C19 - C20 . 1.41 Ang.
PLAT362_ALERT_2_C Short C(sp3)-C(sp2) Bond C19 - C22 . 1.40 Ang.
PLAT362_ALERT_2_C Short C(sp3)-C(sp2) Bond C26 - C27 . 1.41 Ang.
PLAT362_ALERT_2_C Short C(sp3)-C(sp2) Bond C28 - C29 . 1.40 Ang.
PLAT362_ALERT_2_C Short C(sp3)-C(sp2) Bond C28 - C31 . 1.40 Ang.
PLAT362_ALERT_2_C Short C(sp3)-C(sp2) Bond C32 - C33 . 1.39 Ang.
PLAT410_ALERT_2_C Short Intra H...H Contact H3A ..H4B . 1.99 Ang.
x,y,z = 1_555 Check
PLAT410_ALERT_2_C Short Intra H...H Contact H3B ..H4A . 1.99 Ang.
x,y,z = 1_555 Check
PLAT410_ALERT_2_C Short Intra H...H Contact H5A ..H6B . 1.98 Ang.

```
                                                  x,y,z  =      1_555 Check
PLAT410_ALERT_2_C Short Intra H...H Contact  H5B      ..H6A      .       1.98 Ang.
                                                  x,y,z  =      1_555 Check
PLAT410_ALERT_2_C Short Intra H...H Contact  H14A     ..H15A     .       1.97 Ang.
                                                  x,y,z  =      1_555 Check
PLAT410_ALERT_2_C Short Intra H...H Contact  H14B     ..H15B     .       1.97 Ang.
                                                  x,y,z  =      1_555 Check
PLAT410_ALERT_2_C Short Intra H...H Contact  H20A     ..H21B     .       1.95 Ang.
                                                  x,y,z  =      1_555 Check
PLAT410_ALERT_2_C Short Intra H...H Contact  H20B     ..H21A     .       1.96 Ang.
                                                  x,y,z  =      1_555 Check
PLAT410_ALERT_2_C Short Intra H...H Contact  H22A     ..H23B     .       1.93 Ang.
                                                  x,y,z  =      1_555 Check
PLAT410_ALERT_2_C Short Intra H...H Contact  H22B     ..H23A     .       1.93 Ang.
                                                  x,y,z  =      1_555 Check
PLAT410_ALERT_2_C Short Intra H...H Contact  H29A     ..H30A     .       1.98 Ang.
                                                  x,y,z  =      1_555 Check
PLAT410_ALERT_2_C Short Intra H...H Contact  H29B     ..H30B     .       1.98 Ang.
                                                  x,y,z  =      1_555 Check
PLAT410_ALERT_2_C Short Intra H...H Contact  H31A     ..H32B     .       1.99 Ang.
                                                  x,y,z  =      1_555 Check
PLAT410_ALERT_2_C Short Intra H...H Contact  H31B     ..H32A     .       1.99 Ang.
                                                  x,y,z  =      1_555 Check
PLAT411_ALERT_2_C Short Inter H...H Contact  H14B     ..H15A     .       2.06 Ang.
                                                1+x,y,z  =      1_655 Check
PLAT411_ALERT_2_C Short Inter H...H Contact  H20B     ..H21B     .       2.05 Ang.
                                                1+x,y,z  =      1_655 Check
PLAT411_ALERT_2_C Short Inter H...H Contact  H20B     ..H21A     .       2.14 Ang.
                                              2-x,3-y,-z  =      2_785 Check
PLAT411_ALERT_2_C Short Inter H...H Contact  H22A     ..H23A     .       2.04 Ang.
                                                1+x,y,z  =      1_655 Check
PLAT906_ALERT_3_C Large K Value in the Analysis of Variance ......     21.105 Check
PLAT906_ALERT_3_C Large K Value in the Analysis of Variance ......      2.114 Check
PLAT911_ALERT_3_C Missing FCF Refl Between Thmin & STh/L=    0.600          3 Report
PLAT918_ALERT_3_C Reflection(s) with I(obs) much Smaller I(calc) .         12 Check
PLAT975_ALERT_2_C Check Calcd Resid. Dens.  0.93A   From C18             0.70 eA-3
PLAT975_ALERT_2_C Check Calcd Resid. Dens.  0.82A   From C13             0.60 eA-3
PLAT975_ALERT_2_C Check Calcd Resid. Dens.  0.97A   From C18             0.51 eA-3
PLAT977_ALERT_2_C Check Negative Difference Density on H3A              -0.45 eA-3
PLAT977_ALERT_2_C Check Negative Difference Density on H4A              -0.47 eA-3
PLAT977_ALERT_2_C Check Negative Difference Density on H4B              -0.42 eA-3
PLAT977_ALERT_2_C Check Negative Difference Density on H5A              -0.54 eA-3
PLAT977_ALERT_2_C Check Negative Difference Density on H5B              -0.58 eA-3
PLAT977_ALERT_2_C Check Negative Difference Density on H6B              -0.33 eA-3
PLAT977_ALERT_2_C Check Negative Difference Density on H9A              -0.46 eA-3
PLAT977_ALERT_2_C Check Negative Difference Density on H9B              -0.39 eA-3
PLAT977_ALERT_2_C Check Negative Difference Density on H12A             -0.43 eA-3
PLAT977_ALERT_2_C Check Negative Difference Density on H12B             -0.47 eA-3
PLAT977_ALERT_2_C Check Negative Difference Density on H14A             -0.43 eA-3
PLAT977_ALERT_2_C Check Negative Difference Density on H14B             -0.38 eA-3
PLAT977_ALERT_2_C Check Negative Difference Density on H15A             -0.33 eA-3
PLAT977_ALERT_2_C Check Negative Difference Density on H15B             -0.38 eA-3
PLAT977_ALERT_2_C Check Negative Difference Density on H20B             -0.34 eA-3
PLAT977_ALERT_2_C Check Negative Difference Density on H21A             -0.35 eA-3
PLAT977_ALERT_2_C Check Negative Difference Density on H21B             -0.50 eA-3
PLAT977_ALERT_2_C Check Negative Difference Density on H22B             -0.38 eA-3
PLAT977_ALERT_2_C Check Negative Difference Density on H23A             -0.38 eA-3
PLAT977_ALERT_2_C Check Negative Difference Density on H23B             -0.39 eA-3
PLAT977_ALERT_2_C Check Negative Difference Density on H26A             -0.46 eA-3
PLAT977_ALERT_2_C Check Negative Difference Density on H26B             -0.37 eA-3
PLAT977_ALERT_2_C Check Negative Difference Density on H29A             -0.63 eA-3
PLAT977_ALERT_2_C Check Negative Difference Density on H29B             -0.47 eA-3
```

```
PLAT977_ALERT_2_C Check Negative Difference Density on H30B            -0.42 eA-3
PLAT977_ALERT_2_C Check Negative Difference Density on H31B            -0.36 eA-3
PLAT977_ALERT_2_C Check Negative Difference Density on H32A            -0.61 eA-3
PLAT977_ALERT_2_C Check Negative Difference Density on H32B            -0.66 eA-3
```

Alert level G

```
FORMU01_ALERT_2_G  There is a discrepancy between the atom counts in the
           _chemical_formula_sum and the formula from the _atom_site* data.
           Atom count from _chemical_formula_sum:C34 H43 O8
           Atom count from the _atom_site data:  C17 H21.5 O4
CELLZ01_ALERT_1_G Difference between formula and atom_site contents detected.
CELLZ01_ALERT_1_G ALERT: Large difference may be due to a
           symmetry error - see SYMMG tests
          From the CIF: _cell_formula_units_Z    4
          From the CIF: _chemical_formula_sum  C34 H43 O8
          TEST: Compare cell contents of formula and atom_site data

          atom    Z*formula  cif sites diff
          C        136.00     68.00   68.00
          H        172.00     86.00   86.00
          O         32.00     16.00   16.00
PLAT045_ALERT_1_G Calculated and Reported Z Differ by a Factor ...       0.50 Check
PLAT154_ALERT_1_G The s.u.'s on the Cell Angles are Equal ..(Note)       0.02 Degree
PLAT199_ALERT_1_G Reported _cell_measurement_temperature ..... (K)        293 Check
PLAT200_ALERT_1_G Reported   _diffrn_ambient_temperature ..... (K)        293 Check
PLAT343_ALERT_2_G Unusual sp?      Angle Range in Main Residue for        C13 Check
PLAT343_ALERT_2_G Unusual sp?      Angle Range in Main Residue for        C18 Check
PLAT790_ALERT_4_G Centre of Gravity not Within Unit Cell: Resd.  #          2 Note
             C17 H21 O4
PLAT883_ALERT_1_G No Info/Value for _atom_sites_solution_primary .     Please Do !
PLAT912_ALERT_4_G Missing # of FCF Reflections Above STh/L=  0.600        157 Note
PLAT941_ALERT_3_G Average HKL Measurement Multiplicity ...........        3.6 Low
PLAT978_ALERT_2_G Number C-C Bonds with Positive Residual Density.          0 Info
```

```
   2 ALERT level A = Most likely a serious problem - resolve or explain
   8 ALERT level B = A potentially serious problem, consider carefully
  86 ALERT level C = Check. Ensure it is not caused by an omission or oversight
  14 ALERT level G = General information/check it is not something unexpected

  16 ALERT type 1 CIF construction/syntax error, inconsistent or missing data
  83 ALERT type 2 Indicator that the structure model may be wrong or deficient
   9 ALERT type 3 Indicator that the structure quality may be low
   2 ALERT type 4 Improvement, methodology, query or suggestion
   0 ALERT type 5 Informative message, check
```

It is advisable to attempt to resolve as many as possible of the alerts in all categories. Often the minor alerts point to easily fixed oversights, errors and omissions in your CIF or refinement strategy, so attention to these fine details can be worthwhile. In order to resolve some of the more serious problems it may be necessary to carry out additional measurements or structure refinements. However, the purpose of your study may justify the reported deviations and the more serious of these should normally be commented upon in the discussion or experimental section of a paper or in the "special_details" fields of the CIF. checkCIF was carefully designed to identify outliers and unusual parameters, but every test has its limitations and alerts that are not important in a particular case may appear. Conversely, the absence of alerts does not guarantee there are no aspects of the results needing attention. It is up to the individual to critically assess their own results and, if necessary, seek expert advice.

Publication of your CIF in IUCr journals

A basic structural check has been run on your CIF. These basic checks will be run on all CIFs submitted for publication in IUCr journals (*Acta Crystallographica, Journal of Applied Crystallography, Journal of Synchrotron Radiation*); however, if you intend to submit to *Acta Crystallographica Section C* or *E* or *IUCrData*, you should make sure that full publication checks are run on the final version of your CIF prior to submission.

Publication of your CIF in other journals

Please refer to the *Notes for Authors* of the relevant journal for any special instructions relating to CIF submission.

PLATON version of 22/03/2021; check.def file version of 19/03/2021

Datablock shelx - ellipsoid plot

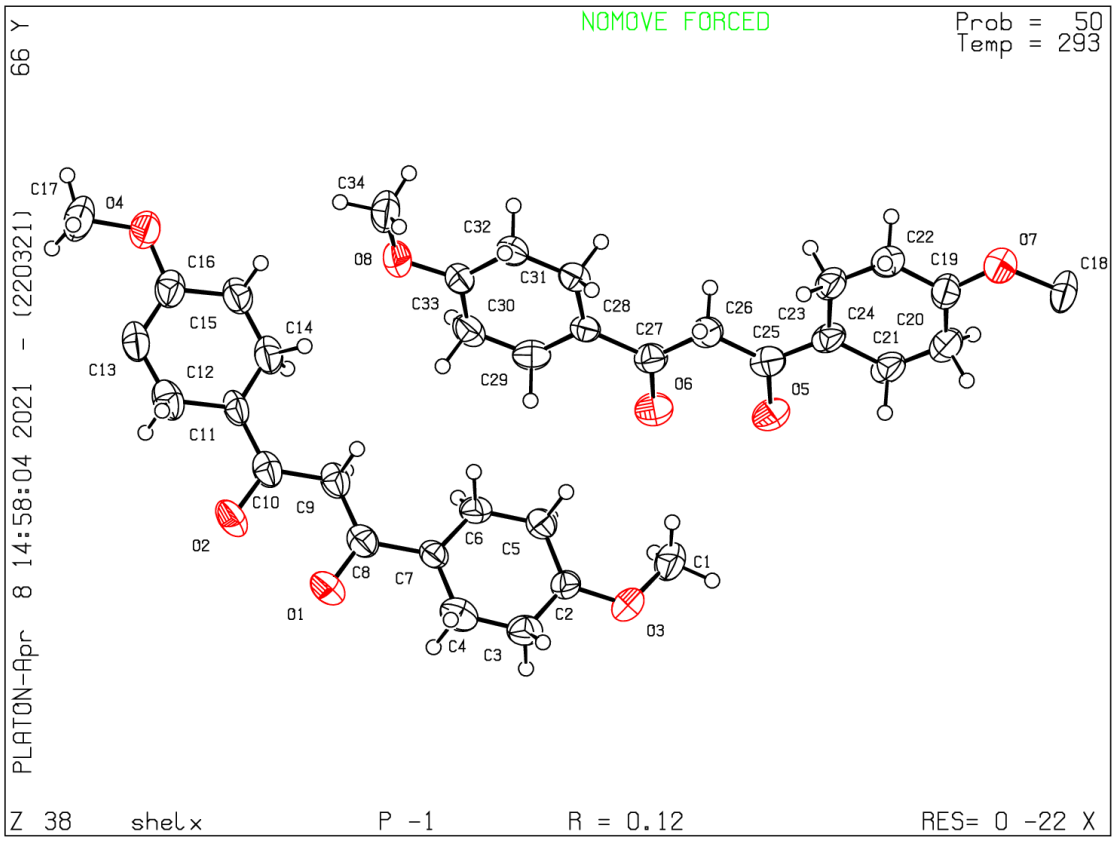

APPENDIX I

CheckCIF report of *fac*-[$Re(CO)_3(Br)(DiMePY)$]

checkCIF/PLATON report

Structure factors have been supplied for datablock(s) 16rpn3_0ma

THIS REPORT IS FOR GUIDANCE ONLY. IF USED AS PART OF A REVIEW PROCEDURE FOR PUBLICATION, IT SHOULD NOT REPLACE THE EXPERTISE OF AN EXPERIENCED CRYSTALLOGRAPHIC REFEREE.

No syntax errors found. CIF dictionary Interpreting this report

Datablock: 16rpn3_0ma

```
Bond precision:  C-C = 0.0152 A          Wavelength=0.71073

Cell:             a=15.306(5)     b=13.289(5)         c=7.687(5)
                  alpha=90        beta=97.299(5)      gamma=90
Temperature:      100 K
```

	Calculated	Reported
Volume	1550.9(13)	1550.9(13)
Space group	P 21/c	P 1 21/c 1
Hall group	-P 2ybc	-P 2ybc
Moiety formula	C15 H12 Br N2 O3 Re	C15 H12 Br N2 O3 Re
Sum formula	C15 H12 Br N2 O3 Re	C15 H12 Br N2 O3 Re
Mr	534.38	534.38
Dx,g cm-3	2.289	2.289
Z	4	4
Mu (mm-1)	10.424	10.424
F000	1000.0	1000.0
F000’	995.58	
h,k,lmax	20,17,10	20,17,10
Nref	3747	3738
Tmin,Tmax	0.301,0.387	0.649,0.745
Tmin’	0.072	

```
Correction method= # Reported T Limits: Tmin=0.649 Tmax=0.745
AbsCorr = MULTI-SCAN

Data completeness= 0.998          Theta(max)= 27.998

R(reflections)= 0.0490( 3158)     wR2(reflections)= 0.1305( 3738)

S = 1.218                 Npar= 199
```

The following ALERTS were generated. Each ALERT has the format
test-name_ALERT_alert-type_alert-level.
Click on the hyperlinks for more details of the test.

Alert level B

PLAT930_ALERT_2_B FCF-based Twin Law (1 0 0)[4 0 1] Est.d BASF 0.06 Check

Alert level C

ABSTY02_ALERT_1_C An _exptl_absorpt_correction_type has been given without a literature citation. This should be contained in the _exptl_absorpt_process_details field. Absorption correction given as multi-scan

PLAT342_ALERT_3_C Low Bond Precision on C-C Bonds ..... 0.01518 Ang.
PLAT906_ALERT_3_C Large K Value in the Analysis of Variance ..... 2.194 Check
PLAT911_ALERT_3_C Missing FCF Refl Between Thmin & STh/L= 0.600 8 Report
PLAT918_ALERT_3_C Reflection(s) with I(obs) much Smaller I(calc) . 5 Check
PLAT939_ALERT_3_C Large Value of Not (SHELXL) Weight Optimized S . 40.91 Check

Alert level G

PLAT083_ALERT_2_G SHELXL Second Parameter in WGHT Unusually Large 47.22 Why ?
PLAT153_ALERT_1_G The s.u.’s on the Cell Axes are Equal ..(Note) 0.005 Ang.
PLAT380_ALERT_4_G Incorrectly? Oriented X(sp2)-Methyl Moiety ..... C14 Check
PLAT380_ALERT_4_G Incorrectly? Oriented X(sp2)-Methyl Moiety ..... C15 Check
PLAT870_ALERT_4_G ALERTS Related to Twinning Effects Suppressed .. ! Info
PLAT883_ALERT_1_G No Info/Value for _atom_sites_solution_primary . Please Do !
PLAT912_ALERT_4_G Missing # of FCF Reflections Above STh/L= 0.600 1 Note
PLAT931_ALERT_5_G CIFcalcFCF Twin Law (1 0 0) Est.d BASF 0.06 Check
PLAT933_ALERT_2_G Number of OMIT Records in Embedded .res File ... 4 Note
PLAT960_ALERT_3_G Number of Intensities with I < - 2*sig(I) ... 3 Check

---

0 **ALERT level A** = Most likely a serious problem - resolve or explain
1 **ALERT level B** = A potentially serious problem, consider carefully
6 **ALERT level C** = Check. Ensure it is not caused by an omission or oversight
10 **ALERT level G** = General information/check it is not something unexpected

3 ALERT type 1 CIF construction/syntax error, inconsistent or missing data
3 ALERT type 2 Indicator that the structure model may be wrong or deficient
6 ALERT type 3 Indicator that the structure quality may be low
4 ALERT type 4 Improvement, methodology, query or suggestion
1 ALERT type 5 Informative message, check

It is advisable to attempt to resolve as many as possible of the alerts in all categories. Often the minor alerts point to easily fixed oversights, errors and omissions in your CIF or refinement strategy, so attention to these fine details can be worthwhile. In order to resolve some of the more serious problems it may be necessary to carry out additional measurements or structure refinements. However, the purpose of your study may justify the reported deviations and the more serious of these should normally be commented upon in the discussion or experimental section of a paper or in the "special_details" fields of the CIF. checkCIF was carefully designed to identify outliers and unusual parameters, but every test has its limitations and alerts that are not important in a particular case may appear. Conversely, the absence of alerts does not guarantee there are no aspects of the results needing attention. It is up to the individual to critically assess their own results and, if necessary, seek expert advice.

Publication of your CIF in IUCr journals

A basic structural check has been run on your CIF. These basic checks will be run on all CIFs submitted for publication in IUCr journals (*Acta Crystallographica, Journal of Applied Crystallography, Journal of Synchrotron Radiation*); however, if you intend to submit to *Acta Crystallographica Section C* or *E* or *IUCrData*, you should make sure that full publication checks are run on the final version of your CIF prior to submission.

Publication of your CIF in other journals

Please refer to the *Notes for Authors* of the relevant journal for any special instructions relating to CIF submission.

PLATON version of 22/03/2021; check.def file version of 19/03/2021

Datablock 16rpn3_0ma - ellipsoid plot

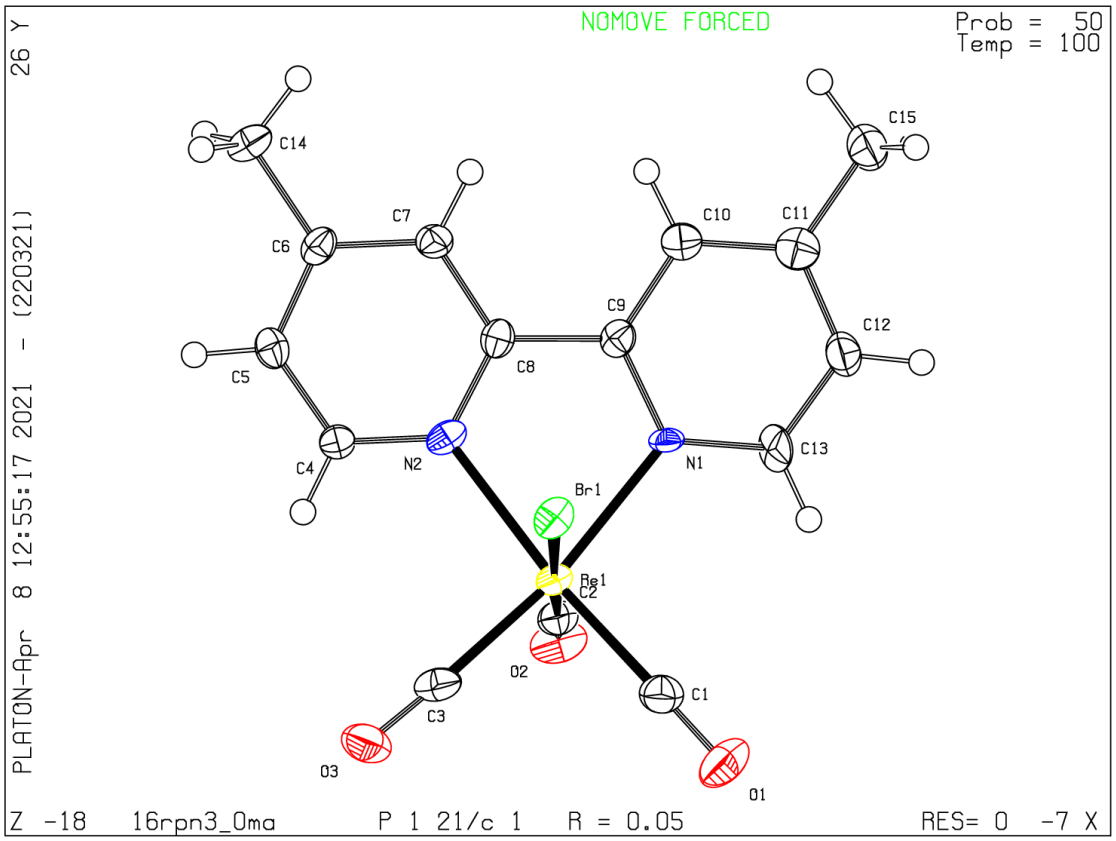

APPENDIX J

CheckCIF report of *fac*-[$Re(CO)_3(ACT)(DiMePY)(NO_3)$]

checkCIF/PLATON report

Structure factors have been supplied for datablock(s) shelx

THIS REPORT IS FOR GUIDANCE ONLY. IF USED AS PART OF A REVIEW PROCEDURE FOR PUBLICATION, IT SHOULD NOT REPLACE THE EXPERTISE OF AN EXPERIENCED CRYSTALLOGRAPHIC REFEREE.

No syntax errors found. CIF dictionary Interpreting this report

Datablock: shelx

```
Bond precision:  C-C = 0.0103 A          Wavelength=0.71073

Cell:            a=24.369(3)    b=12.1227(15)       c=17.004(4)
                 alpha=90       beta=126.477(3)     gamma=90
Temperature:     100 K
```

	Calculated	Reported
Volume	4039.2(12)	4039.2(11)
Space group	C 2/c	C 2/c
Hall group	-C 2yc	-C 2yc
Moiety formula	C18 H18 N2 O4 Re, N O3	?
Sum formula	C18 H18 N3 O7 Re	C18 H18 N3 O7 Re
Mr	574.56	574.55
Dx,g cm-3	1.890	1.890
Z	8	8
Mu (mm-1)	6.062	6.061
F000	2224.0	2224.0
F000’	2217.16	
h,k,lmax	32,16,22	32,16,22
Nref	4864	4857
Tmin,Tmax	0.380,0.662	
Tmin’	0.352	

```
Correction method= Not given

Data completeness= 0.999          Theta(max)= 27.998

R(reflections)= 0.0432( 4171)     wR2(reflections)= 0.1216( 4857)

S = 1.044                 Npar= 232
```

The following ALERTS were generated. Each ALERT has the format
test-name_ALERT_alert-type_alert-level.
Click on the hyperlinks for more details of the test.

Alert level A

```
PLAT057_ALERT_3_A Correction for Absorption Required   RT(exp) ...       1.74 Do !
PLAT413_ALERT_2_A Short Inter XH3 .. XHn     H4       ..H17B     .       1.74 Ang.
                                    3/2-x,-1/2+y,3/2-z  =      4_646 Check
PLAT413_ALERT_2_A Short Inter XH3 .. XHn     H7       ..H17A     .       1.79 Ang.
                                      3/2-x,3/2-y,2-z  =      7_667 Check
PLAT413_ALERT_2_A Short Inter XH3 .. XHn     H10      ..H17A     .       1.64 Ang.
                                      3/2-x,3/2-y,2-z  =      7_667 Check
PLAT413_ALERT_2_A Short Inter XH3 .. XHn     H14B     ..H18B     .       1.82 Ang.
                                         x,1-y,1/2+z  =      6_566 Check
PLAT413_ALERT_2_A Short Inter XH3 .. XHn     H15C     ..H18C     .       1.63 Ang.
                                         x,2-y,1/2+z  =      6_576 Check
```

Alert level B

```
PLAT362_ALERT_2_B Short  C(sp3)-C(sp2) Bond  C16      - C17      .       1.26 Ang.
PLAT362_ALERT_2_B Short  C(sp3)-C(sp2) Bond  C16      - C18      .       1.22 Ang.
PLAT972_ALERT_2_B Check Calcd Resid. Dens.  0.24A   From N3            -2.81 eA-3
PLAT972_ALERT_2_B Check Calcd Resid. Dens.  0.31A   From O9            -2.67 eA-3
```

Alert level C

```
PLAT244_ALERT_4_C Low    'Solvent' Ueq as Compared to Neighbors of        N3 Check
PLAT342_ALERT_3_C Low Bond Precision on  C-C Bonds ..............   0.01031 Ang.
PLAT911_ALERT_3_C Missing FCF Refl Between Thmin & STh/L=    0.600         2 Report
PLAT971_ALERT_2_C Check Calcd Resid. Dens.  0.03A   From O1            2.16 eA-3
PLAT971_ALERT_2_C Check Calcd Resid. Dens.  0.10A   From O8            1.52 eA-3
PLAT975_ALERT_2_C Check Calcd Resid. Dens.  0.80A   From O9            0.64 eA-3
PLAT977_ALERT_2_C Check Negative Difference Density on H14A           -0.78 eA-3
PLAT977_ALERT_2_C Check Negative Difference Density on H14B           -0.33 eA-3
PLAT977_ALERT_2_C Check Negative Difference Density on H17A           -1.04 eA-3
PLAT977_ALERT_2_C Check Negative Difference Density on H17B           -0.41 eA-3
PLAT977_ALERT_2_C Check Negative Difference Density on H17C           -0.54 eA-3
PLAT977_ALERT_2_C Check Negative Difference Density on H18A           -0.58 eA-3
PLAT977_ALERT_2_C Check Negative Difference Density on H18B           -1.04 eA-3
PLAT977_ALERT_2_C Check Negative Difference Density on H18C           -0.82 eA-3
```

Alert level G

```
PLAT083_ALERT_2_G SHELXL Second Parameter in WGHT  Unusually Large     57.57 Why ?
PLAT128_ALERT_4_G Alternate Setting for Input Space Group     C2/c      I2/a Note
PLAT171_ALERT_4_G The CIF-Embedded .res File Contains EADP Records        2 Report
PLAT230_ALERT_2_G Hirshfeld Test Diff for    O1       --C1       .       8.3 s.u.
PLAT232_ALERT_2_G Hirshfeld Test Diff (M-X)  Re1      --N1       .       6.9 s.u.
PLAT380_ALERT_4_G Incorrectly? Oriented X(sp2)-Methyl Moiety .....       C14 Check
PLAT380_ALERT_4_G Incorrectly? Oriented X(sp2)-Methyl Moiety .....       C15 Check
PLAT380_ALERT_4_G Incorrectly? Oriented X(sp2)-Methyl Moiety .....       C17 Check
PLAT380_ALERT_4_G Incorrectly? Oriented X(sp2)-Methyl Moiety .....       C18 Check
PLAT883_ALERT_1_G No Info/Value for _atom_sites_solution_primary .    Please Do !
PLAT910_ALERT_3_G Missing # of FCF Reflection(s) Below Theta(Min).        4 Note
PLAT912_ALERT_4_G Missing # of FCF Reflections Above STh/L=  0.600        2 Note
PLAT960_ALERT_3_G Number of Intensities with I  <   - 2*sig(I) ...        1 Check
PLAT965_ALERT_2_G The SHELXL WEIGHT Optimisation has not Converged    Please Check
PLAT978_ALERT_2_G Number C-C Bonds with Positive Residual Density.        2 Info
```

---

6 **ALERT level A** = Most likely a serious problem - resolve or explain
4 **ALERT level B** = A potentially serious problem, consider carefully
14 **ALERT level C** = Check. Ensure it is not caused by an omission or oversight
15 **ALERT level G** = General information/check it is not something unexpected

```
  1 ALERT type 1 CIF construction/syntax error, inconsistent or missing data
 25 ALERT type 2 Indicator that the structure model may be wrong or deficient
  5 ALERT type 3 Indicator that the structure quality may be low
  8 ALERT type 4 Improvement, methodology, query or suggestion
  0 ALERT type 5 Informative message, check
```

It is advisable to attempt to resolve as many as possible of the alerts in all categories. Often the minor alerts point to easily fixed oversights, errors and omissions in your CIF or refinement strategy, so attention to these fine details can be worthwhile. In order to resolve some of the more serious problems it may be necessary to carry out additional measurements or structure refinements. However, the purpose of your study may justify the reported deviations and the more serious of these should normally be commented upon in the discussion or experimental section of a paper or in the "special_details" fields of the CIF. checkCIF was carefully designed to identify outliers and unusual parameters, but every test has its limitations and alerts that are not important in a particular case may appear. Conversely, the absence of alerts does not guarantee there are no aspects of the results needing attention. It is up to the individual to critically assess their own results and, if necessary, seek expert advice.

Publication of your CIF in IUCr journals

A basic structural check has been run on your CIF. These basic checks will be run on all CIFs submitted for publication in IUCr journals (*Acta Crystallographica*, *Journal of Applied Crystallography*, *Journal of Synchrotron Radiation*); however, if you intend to submit to *Acta Crystallographica Section C* or *E* or *IUCrData*, you should make sure that full publication checks are run on the final version of your CIF prior to submission.

Publication of your CIF in other journals

Please refer to the *Notes for Authors* of the relevant journal for any special instructions relating to CIF submission.

PLATON version of 22/03/2021; check.def file version of 19/03/2021

Datablock shelx - ellipsoid plot

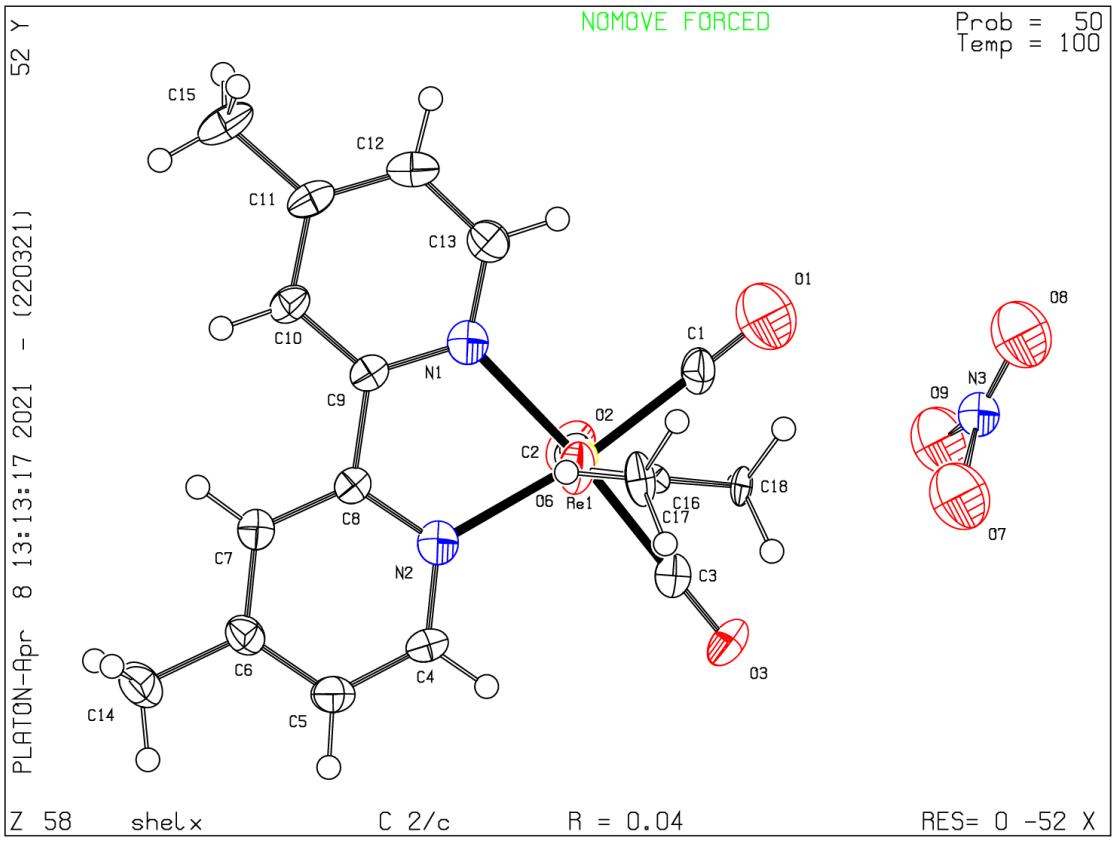

APPENDIX K

CheckCIF report of *fac*-[$Re(CO)_3(NO_3)$(DiMePY)]

checkCIF/PLATON report

Structure factors have been supplied for datablock(s) q1_19pn4_0m

THIS REPORT IS FOR GUIDANCE ONLY. IF USED AS PART OF A REVIEW PROCEDURE FOR PUBLICATION, IT SHOULD NOT REPLACE THE EXPERTISE OF AN EXPERIENCED CRYSTALLOGRAPHIC REFEREE.

No syntax errors found. CIF dictionary Interpreting this report

Datablock: q1_19pn4_0m

Bond precision: C-C = 0.0099 A Wavelength=0.71073

Cell: a=8.0498(6) b=12.4089(10) c=17.6719(14)
alpha=90 beta=95.542(3) gamma=90
Temperature: 100 K

	Calculated	Reported
Volume	1757.0(2)	1757.0(2)
Space group	P 21/n	P 1 21/n 1
Hall group	-P 2yn	-P 2yn
Moiety formula	C15 H12 N3 O6 Re	C15 H12 N3 O6 Re
Sum formula	C15 H12 N3 O6 Re	C15 H12 N3 O6 Re
Mr	516.49	516.48
Dx,g cm-3	1.952	1.953
Z	4	4
Mu (mm-1)	6.951	6.951
F000	984.0	984.0
F000’	980.56	
h,k,lmax	10,16,23	10,16,23
Nref	4401	4378
Tmin,Tmax	0.597,0.795	0.659,0.745
Tmin’	0.207	

Correction method= # Reported T Limits: Tmin=0.659 Tmax=0.745
AbsCorr = MULTI-SCAN

Data completeness= 0.995 Theta(max)= 28.376

R(reflections)= 0.0428(3659) wR2(reflections)= 0.0859(4378)

S = 1.069 Npar= 196

The following ALERTS were generated. Each ALERT has the format
test-name_ALERT_alert-type_alert-level.
Click on the hyperlinks for more details of the test.

Alert level B

PLAT971_ALERT_2_B Check Calcd Resid. Dens. 0.02A   From O6 2.61 eA-3

Alert level C

ABSTY02_ALERT_1_C An _exptl_absorpt_correction_type has been given without
a literature citation. This should be contained in the
_exptl_absorpt_process_details field.
Absorption correction given as multi-scan

PLAT241_ALERT_2_C High 'MainMol' Ueq as Compared to Neighbors of O6 Check
PLAT342_ALERT_3_C Low Bond Precision on C-C Bonds ..... 0.00991 Ang.
PLAT601_ALERT_2_C Unit Cell Contains Solvent Accessible VOIDS of . 66 Ang**3
PLAT906_ALERT_3_C Large K Value in the Analysis of Variance ..... 4.526 Check
PLAT972_ALERT_2_C Check Calcd Resid. Dens. 1.43A   From C3 -2.33 eA-3
PLAT977_ALERT_2_C Check Negative Difference Density on H14A -0.44 eA-3
PLAT977_ALERT_2_C Check Negative Difference Density on H15C -0.52 eA-3

Alert level G

PLAT083_ALERT_2_G SHELXL Second Parameter in WGHT Unusually Large 15.32 Why ?
PLAT171_ALERT_4_G The CIF-Embedded .res File Contains EADP Records 1 Report
PLAT230_ALERT_2_G Hirshfeld Test Diff for O1 --C1 . 5.7 s.u.
PLAT230_ALERT_2_G Hirshfeld Test Diff for O3 --C3 . 7.7 s.u.
PLAT232_ALERT_2_G Hirshfeld Test Diff (M-X) Re1 --O6 . 11.4 s.u.
PLAT380_ALERT_4_G Incorrectly? Oriented X(sp2)-Methyl Moiety ..... C14 Check
PLAT380_ALERT_4_G Incorrectly? Oriented X(sp2)-Methyl Moiety ..... C15 Check
PLAT883_ALERT_1_G No Info/Value for _atom_sites_solution_primary . Please Do !
PLAT910_ALERT_3_G Missing # of FCF Reflection(s) Below Theta(Min). 2 Note
PLAT912_ALERT_4_G Missing # of FCF Reflections Above STh/L= 0.600 23 Note
PLAT978_ALERT_2_G Number C-C Bonds with Positive Residual Density. 0 Info

0 **ALERT level A** = Most likely a serious problem - resolve or explain
1 **ALERT level B** = A potentially serious problem, consider carefully
8 **ALERT level C** = Check. Ensure it is not caused by an omission or oversight
11 **ALERT level G** = General information/check it is not something unexpected

2 ALERT type 1 CIF construction/syntax error, inconsistent or missing data
11 ALERT type 2 Indicator that the structure model may be wrong or deficient
3 ALERT type 3 Indicator that the structure quality may be low
4 ALERT type 4 Improvement, methodology, query or suggestion
0 ALERT type 5 Informative message, check

It is advisable to attempt to resolve as many as possible of the alerts in all categories. Often the minor alerts point to easily fixed oversights, errors and omissions in your CIF or refinement strategy, so attention to these fine details can be worthwhile. In order to resolve some of the more serious problems it may be necessary to carry out additional measurements or structure refinements. However, the purpose of your study may justify the reported deviations and the more serious of these should normally be commented upon in the discussion or experimental section of a paper or in the "special_details" fields of the CIF. checkCIF was carefully designed to identify outliers and unusual parameters, but every test has its limitations and alerts that are not important in a particular case may appear. Conversely, the absence of alerts does not guarantee there are no aspects of the results needing attention. It is up to the individual to critically assess their own results and, if necessary, seek expert advice.

Publication of your CIF in IUCr journals

A basic structural check has been run on your CIF. These basic checks will be run on all CIFs submitted for publication in IUCr journals (*Acta Crystallographica, Journal of Applied Crystallography, Journal of Synchrotron Radiation*); however, if you intend to submit to *Acta Crystallographica Section C* or *E* or *IUCrData*, you should make sure that full publication checks are run on the final version of your CIF prior to submission.

Publication of your CIF in other journals

Please refer to the *Notes for Authors* of the relevant journal for any special instructions relating to CIF submission.

PLATON version of 22/03/2021; check.def file version of 19/03/2021

Datablock q1_19pn4_0m - ellipsoid plot

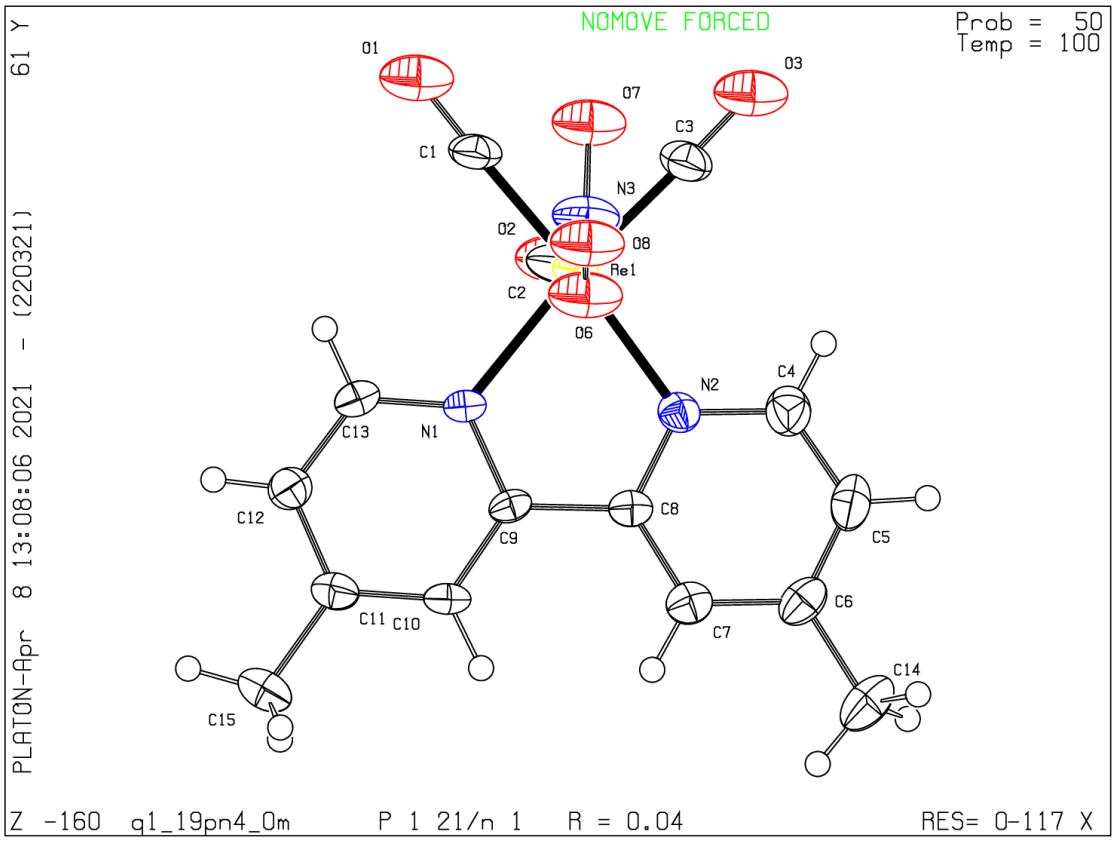

APPENDIX L

CheckCIF report of *fac*-[$Re(CO)_3(Br)(DiMeOPY)$]

checkCIF/PLATON report

Structure factors have been supplied for datablock(s) shelx

THIS REPORT IS FOR GUIDANCE ONLY. IF USED AS PART OF A REVIEW PROCEDURE FOR PUBLICATION, IT SHOULD NOT REPLACE THE EXPERTISE OF AN EXPERIENCED CRYSTALLOGRAPHIC REFEREE.

No syntax errors found. CIF dictionary Interpreting this report

Datablock: shelx

Bond precision: C-C = 0.0078 A Wavelength=0.71073

Cell: a=14.05100 b=13.89300 c=17.21000
alpha=90 beta=90 gamma=90
Temperature: 100 K

	Calculated	Reported
Volume	3359.573	3360
Space group	P b c n	P b c n
Hall group	-P 2n 2ab	-P 2n 2ab
Moiety formula	C15 H12 Br N2 O5 Re	?
Sum formula	C15 H12 Br N2 O5 Re	C15 H12 Br N2 O5 Re
Mr	566.38	566.38
Dx,g cm-3	2.240	2.240
Z	8	8
Mu (mm-1)	9.640	9.640
F000	2128.0	2128.0
F000’	2119.23	
h,k,lmax	18,18,22	18,18,22
Nref	4066	4055
Tmin,Tmax		
Tmin’		

Correction method= Not given

Data completeness= 0.997 Theta(max)= 27.999

R(reflections)= 0.0302(3528) wR2(reflections)= 0.0815(4055)

S = 1.110 Npar= 217

The following ALERTS were generated. Each ALERT has the format
test-name_ALERT_alert-type_alert-level.
Click on the hyperlinks for more details of the test.

Alert level B

```
PLAT430_ALERT_2_B Short Inter D...A Contact  O1       ..O3       .       2.84 Ang.
                                             3/2-x,-1/2+y,z  =      7_755 Check
PLAT910_ALERT_3_B Missing # of FCF Reflection(s) Below Theta(Min).         12 Note
```

Alert level C

```
PLAT052_ALERT_1_C Info on Absorption Correction Method   Not Given     Please Do !
PLAT053_ALERT_1_C Minimum Crystal Dimension Missing (or Error) ...     Please Check
PLAT054_ALERT_1_C Medium  Crystal Dimension Missing (or Error) ...     Please Check
PLAT055_ALERT_1_C Maximum Crystal Dimension Missing (or Error) ...     Please Check
PLAT141_ALERT_4_C s.u. on a - Axis Small or Missing ..............    0.00000 Ang.
PLAT142_ALERT_4_C s.u. on b - Axis Small or Missing ..............    0.00000 Ang.
PLAT143_ALERT_4_C s.u. on c - Axis Small or Missing ..............    0.00000 Ang.
PLAT151_ALERT_1_C No s.u. (esd) Given on Volume ..................     Please Do !
PLAT906_ALERT_3_C Large K Value in the Analysis of Variance ......      2.173 Check
PLAT934_ALERT_3_C Number of (Iobs-Icalc)/Sigma(W) > 10 Outliers ..          1 Check
PLAT971_ALERT_2_C Check Calcd Resid. Dens.  1.92A   From C13            2.41 eA-3
PLAT971_ALERT_2_C Check Calcd Resid. Dens.  0.82A   From Re1            2.07 eA-3
PLAT972_ALERT_2_C Check Calcd Resid. Dens.  0.46A   From Br1           -1.66 eA-3
PLAT972_ALERT_2_C Check Calcd Resid. Dens.  0.50A   From Br1           -1.64 eA-3
PLAT972_ALERT_2_C Check Calcd Resid. Dens.  0.39A   From Br1           -1.63 eA-3
PLAT972_ALERT_2_C Check Calcd Resid. Dens.  0.43A   From Br1           -1.58 eA-3
```

Alert level G

```
PLAT083_ALERT_2_G SHELXL Second Parameter in WGHT  Unusually Large      32.08 Why ?
PLAT232_ALERT_2_G Hirshfeld Test Diff (M-X)  Re1      --Br1      .       14.3 s.u.
PLAT883_ALERT_1_G No Info/Value for _atom_sites_solution_primary .     Please Do !
PLAT913_ALERT_3_G Missing # of Very Strong Reflections in FCF ....          1 Note
PLAT933_ALERT_2_G Number of OMIT Records in Embedded .res File ...         10 Note
PLAT960_ALERT_3_G Number of Intensities with I  <   - 2*sig(I) ...          2 Check
PLAT965_ALERT_2_G The SHELXL WEIGHT Optimisation has not Converged     Please Check
PLAT978_ALERT_2_G Number C-C Bonds with Positive Residual Density.          1 Info
```

```
  0 ALERT level A = Most likely a serious problem - resolve or explain
  2 ALERT level B = A potentially serious problem, consider carefully
 16 ALERT level C = Check. Ensure it is not caused by an omission or oversight
  8 ALERT level G = General information/check it is not something unexpected

  6 ALERT type 1 CIF construction/syntax error, inconsistent or missing data
 12 ALERT type 2 Indicator that the structure model may be wrong or deficient
  5 ALERT type 3 Indicator that the structure quality may be low
  3 ALERT type 4 Improvement, methodology, query or suggestion
  0 ALERT type 5 Informative message, check
```

It is advisable to attempt to resolve as many as possible of the alerts in all categories. Often the minor alerts point to easily fixed oversights, errors and omissions in your CIF or refinement strategy, so attention to these fine details can be worthwhile. In order to resolve some of the more serious problems it may be necessary to carry out additional measurements or structure refinements. However, the purpose of your study may justify the reported deviations and the more serious of these should normally be commented upon in the discussion or experimental section of a paper or in the "special_details" fields of the CIF. checkCIF was carefully designed to identify outliers and unusual parameters, but every test has its limitations and alerts that are not important in a particular case may appear. Conversely, the absence of alerts does not guarantee there are no aspects of the results needing attention. It is up to the individual to critically assess their own results and, if necessary, seek expert advice.

Publication of your CIF in IUCr journals

A basic structural check has been run on your CIF. These basic checks will be run on all CIFs submitted for publication in IUCr journals (*Acta Crystallographica, Journal of Applied Crystallography, Journal of Synchrotron Radiation*); however, if you intend to submit to *Acta Crystallographica Section C* or *E* or *IUCrData*, you should make sure that full publication checks are run on the final version of your CIF prior to submission.

Publication of your CIF in other journals

Please refer to the *Notes for Authors* of the relevant journal for any special instructions relating to CIF submission.

PLATON version of 22/03/2021; check.def file version of 19/03/2021

Datablock shelx - ellipsoid plot

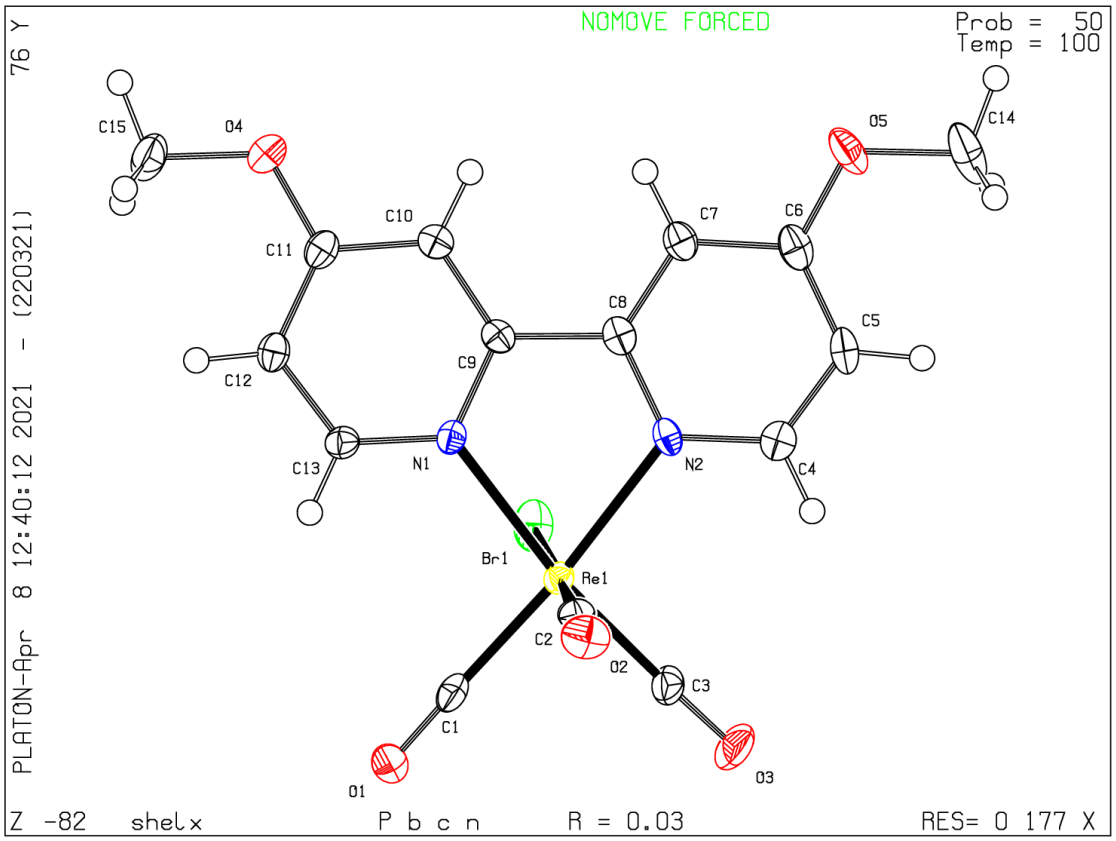

APPENDIX M

CheckCIF report of *fac*-[$Re(CO)_3(NO_3)$(DiMeOPY)]

checkCIF/PLATON report

Structure factors have been supplied for datablock(s) q1_19opn1_0m

THIS REPORT IS FOR GUIDANCE ONLY. IF USED AS PART OF A REVIEW PROCEDURE FOR PUBLICATION, IT SHOULD NOT REPLACE THE EXPERTISE OF AN EXPERIENCED CRYSTALLOGRAPHIC REFEREE.

No syntax errors found. CIF dictionary Interpreting this report

Datablock: q1_19opn1_0m

```
Bond precision:  C-C = 0.0061 A          Wavelength=0.71073

Cell:            a=10.5469(15)     b=10.9844(18)      c=15.674(2)
                 alpha=90          beta=98.306(4)     gamma=90
Temperature:     100 K

                Calculated                Reported
Volume          1796.8(5)                 1796.8(5)
Space group     P 21/n                    P 1 21/n 1
Hall group      -P 2yn                    -P 2yn
Moiety formula  C15 H12 N3 O8 Re          C15 H12 N3 O8 Re
Sum formula     C15 H12 N3 O8 Re          C15 H12 N3 O8 Re
Mr              548.49                    548.48
Dx,g cm-3       2.028                     2.028
Z               4                         4
Mu (mm-1)       6.812                     6.812
F000            1048.0                    1048.0
F000'           1044.62
h,k,lmax        14,14,20                  14,14,20
Nref            4505                      4471
Tmin,Tmax       0.245,0.286               0.645,0.746
Tmin'           0.206

Correction method= # Reported T Limits: Tmin=0.645 Tmax=0.746
AbsCorr = MULTI-SCAN

Data completeness= 0.992          Theta(max)= 28.371

R(reflections)= 0.0307( 3747)     wR2(reflections)= 0.0641( 4471)

S = 1.055                 Npar= 244
```

The following ALERTS were generated. Each ALERT has the format
test-name_ALERT_alert-type_alert-level.
Click on the hyperlinks for more details of the test.

Alert level C

```
ABSTY02_ALERT_1_C  An _exptl_absorpt_correction_type has been given without
           a literature citation. This should be contained in the
           _exptl_absorpt_process_details field.
           Absorption correction given as multi-scan
PLAT910_ALERT_3_C Missing # of FCF Reflection(s) Below Theta(Min).          5 Note
PLAT911_ALERT_3_C Missing FCF Refl Between Thmin & STh/L=    0.600          6 Report
```

Alert level G

```
PLAT432_ALERT_2_G Short Inter X...Y Contact  O1       ..C9              2.98 Ang.
                                    3/2-x,1/2+y,3/2-z  =      2_656 Check
PLAT883_ALERT_1_G No Info/Value for _atom_sites_solution_primary .     Please Do !
PLAT912_ALERT_4_G Missing # of FCF Reflections Above STh/L=  0.600         24 Note
PLAT933_ALERT_2_G Number of OMIT Records in Embedded .res File ...          2 Note
PLAT941_ALERT_3_G Average HKL Measurement Multiplicity ...........        4.4 Low
PLAT978_ALERT_2_G Number C-C Bonds with Positive Residual Density.          3 Info
```

```
   0 ALERT level A = Most likely a serious problem - resolve or explain
   0 ALERT level B = A potentially serious problem, consider carefully
   3 ALERT level C = Check. Ensure it is not caused by an omission or oversight
   6 ALERT level G = General information/check it is not something unexpected

   2 ALERT type 1 CIF construction/syntax error, inconsistent or missing data
   3 ALERT type 2 Indicator that the structure model may be wrong or deficient
   3 ALERT type 3 Indicator that the structure quality may be low
   1 ALERT type 4 Improvement, methodology, query or suggestion
   0 ALERT type 5 Informative message, check
```

It is advisable to attempt to resolve as many as possible of the alerts in all categories. Often the minor alerts point to easily fixed oversights, errors and omissions in your CIF or refinement strategy, so attention to these fine details can be worthwhile. In order to resolve some of the more serious problems it may be necessary to carry out additional measurements or structure refinements. However, the purpose of your study may justify the reported deviations and the more serious of these should normally be commented upon in the discussion or experimental section of a paper or in the "special_details" fields of the CIF. checkCIF was carefully designed to identify outliers and unusual parameters, but every test has its limitations and alerts that are not important in a particular case may appear. Conversely, the absence of alerts does not guarantee there are no aspects of the results needing attention. It is up to the individual to critically assess their own results and, if necessary, seek expert advice.

Publication of your CIF in IUCr journals

A basic structural check has been run on your CIF. These basic checks will be run on all CIFs submitted for publication in IUCr journals (*Acta Crystallographica*, *Journal of Applied Crystallography*, *Journal of Synchrotron Radiation*); however, if you intend to submit to *Acta Crystallographica Section C* or *E* or *IUCrData*, you should make sure that full publication checks are run on the final version of your CIF prior to submission.

Publication of your CIF in other journals

Please refer to the *Notes for Authors* of the relevant journal for any special instructions relating to CIF submission.

PLATON version of 22/03/2021; check.def file version of 19/03/2021

Datablock q1_19opn1_0m - ellipsoid plot